Durham University

Durham E-Theses

Genesis of collision-related volcanism on the Erzurum-kars plateau, North eastern turkey

Mehmet Keskin

How to cite:

Keskin, Mehmet (1994) Genesis of collision-related volcanism on the Erzurum-kars plateau, North eastern turkey. Doctoral thesis, Durham University.

Use policy

The full-text may be used and/or reproduced, and given to third parties in any format or medium, without prior permission or charge, for personal research or study, educational, or not-for-profit purposes provided that:

- a full bibliographic reference is made to the original source
- a https://etheses.durham.ac.uk/id/eprint/5883/ is made to the metadata record in Durham E-Theses
- the full-text is not changed in any way

The full-text must not be sold in any format or medium without the formal permission of the copyright holders.

Please consult the full Durham E-Theses policy for further details.

Academic Support Office, The Palatine Centre, Durham University, Stockton Road, Durham, DH1 3LE
e-mail: e-theses.admin@durham.ac.uk Tel: +44 0191 334 6107
https://etheses.durham.ac.uk

The copyright of this thesis rests with the author.
No quotation from it should be published without
his prior written consent and information derived
from it should be acknowledged.

Genesis of Collision-Related Volcanism on the Erzurum-Kars Plateau, Northeastern Turkey

by

Mehmet Keskin

A thesis submitted in partial fulfilment of the requirements for the degree of Doctor of Philosophy

Department of Geological Sciences

University of Durham

September 1994

2 1 FEB 1995

This work is dedicated to my parents,
Sema and Yavuz Keskin for their love
and understanding, and
to Belma for her love

ABSTRACT

Genesis of Collision-Related Volcanism on the Erzurum-Kars Plateau, Northeastern Turkey

Mehmet Keskin, University of Durham, 1994

The Eastern Anatolia Region exhibits one of the world's best exposed and most complete transects across a volcanic province related to continent-continent collision. Within this region, the Erzurum-Kars Plateau is of particular importance since it contains the full record of post-collision volcanism from 11 to 1.5 Ma.

The volcanics of the Erzurum-Kars Plateau cover a broad compositional range from basalts to rhyolites displaying a calc-alkaline character. They show a distinctive subduction signature represented by selective enrichment of the large ion lithophile and light rare earth elements. Among trace elements, Y behaves in a quite different way forming two distinct trends against silica named as the low- and high-Y series. Lavas of the high-Y series are characterised by a distinct bimodal volcanism (from basalt to rhyolite), in contrast to the low-Y series which comprises an unimodal andesitic volcanism. Trace element systematics together with modelling of theoretical Rayleigh fractionation vectors suggest that the low-Y series underwent a hydrous crystallisation dominated by amphibole as the mafic phase, whereas the high-Y series was dominated by anhydrous (POAM) crystallisation. Al-in-amphibole geobarometer calculations on the plateau volcanics reveal that the low-Y series evolved in magma chambers located between 20 and 28 km. In contrast, magma chambers of the high-Y series were much shallower, around 14-22 km. The high-Y series dominates early and late stages of the volcanic activity, whereas the low-Y series dominates the middle (between 7.5 and 5 Ma) stage, probably coinciding with the most intensive stage of crustal thickening.

Sr, Pb, Nd and $\delta^{18}O$ isotopic systematics also show significant differences between the high- and low-Y series. Lavas of the high-Y series are always more radiogenic with respect to the lavas of low-Y series. Results of assimilation combined with crystallisation (AFC) modelling suggests that the low-Y series assimilated a lower crustal material which is compositionally similar to the granulitic xenoliths from the Pannonian Basin in Hungary and from Central Europe. In contrast, the high-Y series assimilated two different upper crustal materials. In both the low- and high-Y series, the maximum assimilation rate was around 40% of the fractional crystallisation rate.

Trace element and isotopic differences between the low- and high-Y series are not significantly dependent upon variations in the source. These differences appear to have been extensively controlled by the AFC processes.

Declaration

I declare that this thesis, which I submit for the degree of Doctor of Philosophy at the University of Durham, is my own work and is not substantially the same as any which has previously been submitted for a degree at this or another university.

Mehmet Keskin

University of Durham

Department of Geological Sciences
September 1994

Copyright © by Mehmet Keskin
The copyright of this thesis rests with the author. No quotation or data from it should be published without Mehmet Keskin's prior written consent and any information derived from it should be acknowledged.

Acknowledgements

First, my deepest thanks to my supervisor, Dr. Julian Pearce for his helpful comments, criticisms and patience. Needless to say, this work would never have been finished without his constant help and encouragement. He painstakingly went through each chapter as it was completed and offered many invaluable suggestions. I have benefited greatly from our discussions on every aspect.

Special thanks are due to my second supervisor Dr. Dave Hirst for his very pertinent and detailed comments on the manuscript. He provided detailed comments at length on most of the chapters which improved the work significantly.

I should like to express my gratitude to the Turkish Ministry of Education for providing me with a generous grant to carry out my research.

I would like to express my thanks to Natural Environment Research Council (NERC), Isotope Geoscience Laboratory in Keyworth, Nottingham, for the laboratory facilities in which I was privileged to carry out my isotopic analyses. I owe much to Dr. Pamela Kempton and Dr. Peter Greenwood for their invaluable help and unfailing support.

I owe a special depth of gratitude to Dr. Gill Foulger, my adviser, for all her support, encouragement and help.

I would like to express my appreciation to Dr. Andrew Peckett for generously allowing me to use Durham electron microprobe.

I am very grateful to the people in the Exploration Division of the Turkish Petroleum Company (TPAO) in Ankara that supported me financially and logistically in my research on the Erzurum-Kars Plateau Volcanics. The situation TPAO arranged and maintained made a great amount of productive fieldwork possible that otherwise could have easily never been done, and I am only one of many who has benefited from their support. I also wish to thank my colleagues in TPAO, Ayhan Üngör, Ömer Şahintürk for their encouragement and help during the course of my fieldwork.

I wish to thank MTA geologists; Dr. Evren Yazgan, Dr. Jerf Asutay, Ali Arbas, Latif Gök, Mehmet İmik for allowing me to stay in their field camp based in Horasan during my first fieldwork.

I owe much to several people of DSI, including Cavit Bulut, Erdoğan Cimili and Behman Turan who have provided me with an accommodation during the first field season.

Particular thanks must go to Ron Hardy for his patience and help during the acquisition of my rather large data set. Not only did he make all the arrangements for my XRF work, but also he gave much-needed encouragement during those stressful days when it seemed the sample preparation and analytical work would never be finished.

There are many other people to whom thanks are due for their help and assistance. Here are some that stand out in my mind: George Randall, Ron Lambert and Julia Harrison for their production of about 200 thin and polished probe sections, Gerry Dresser and Alan Carr for providing photographic services of excellent quality, Dave Asbury for his assistence, Dave Stevenson and Neville Hallam for their support to solve computing problems and George Ruth for solving my computer hardware problems.

I wish to express my gratitude to the driver of the Land Rover, Nevzat Akbaba, working well away from geology. Well what more can I say, this 65 years old young fellow who became one of my best friends in my life was the most energetic, brave person and the best field driver I have ever seen. His company was much appreciated. I also thank to Halil Toprak, who was my driver during the second field season, for his great performance.

I would like to thank those geochemist friends including Ian Parkinson, Mark Wharton, Kate Lawson, Sarah Acland and Victoria Hards to whom I owe a large personal debt; because of their constant intellectual interest and personal encouragement of my work.

The continued love of my parents, Yavuz and Sema Keskin and my brother Mustafa, has been a source of constant encouragement to me. I owe a special debt of gratitude to them for their continued support throughout the course of my education.

Finally, my deepest thanks must go to Belma Haznedar, for her unfailing support and love. The task of writing this thesis was made much easier by her constant encouragement and understanding.

CONTENTS

Chapter 1: INTRODUCTION Page

1.1. Tectonic setting of the Eastern Anatolia Region 1

1.2. Previous studies in Eastern Anatolia 2

1.2.1. Previous studies on the collision-related volcanics of Eastern Anatolia 3

1.3. Objectives of this thesis 9

1.4. Source of the analytical data used in this thesis 10

1.4.1. XRF analysis 10

1.4.2. Electron Microprobe analysis 11

1.4.3. K-Ar dating 11

1.4.4. ICP-MS analysis 11

1.4.5. Radiogenic isotope analysis 11

1.4.6. Oxygen ($\delta^{18}O$) isotope analysis 12

1.5. Description of thesis 12

Chapter 2: STRATIGRAPHY

Introduction 14

2.1. THE Mt. DUMLU AREA 18

2.1.1. The Lower tuff (Ltl) 21

2.1.2. The Arzutu amphibole dacite (Amd) 23

2.1.3. The Güngörmez andesite/dacite (Gad) 23

2.1.4. The Girekösek dacite (Gpd) 25

2.1.5. The Dumlu amphibole dacite/andesite (Dpad) 25

2.2. THE Mt. KARGAPAZARI AREA 26

2.2.1. The Basal tuff (Btl) 31

2.2.2. The Köşk pyroxene andesite (Kpa) 32

2.2.3. The Güngörmez andesite/dacite (Gad) 33

2.2.4. The Çobandede dacite (Çpd) 34

2.2.5. The Girekösek dacite (Gpd) 34

2.2.6. The Karapınar basalt (Kb) 35

2.2.7. The Göllerdüzü amphibole dacite (Gpaa) 36

2.2.8. The Kargapazarı volcanics (Kv) 36

2.3. THE PASINLER AREA 39
2.3.1. NORTH OF PASINLER 39
2.3.1.1. Harabedere and Sansordere sections 42
2.3.1.1.1. Harabedere Gorge 42
2.3.1.1.1.1. The basement units 42
2.3.1.1.1.1.1. The Upper Eocene Narman Group 42
2.3.1.1.1.1.1.1. The Kışlaköy Volcanic member (En_1) 44
2.3.1.1.1.1.1.2. The Narman formation (En_2) 46
2.3.1.1.1.2. THE PASINLER PLATEAU UNITS 46
2.3.1.1.1.2.1. The Black andesite/dacite (Baad) 46
2.3.1.1.1.2.2. The Lower tuff (Ltl) 47
2.3.1.1.1.2.3. The Kızılveren amphibole dacite/andesite (Kpd) 47
2.3.1.1.1.2.4. The Middle Tuff (Mtl) 48
2.3.1.1.1.2.5. The Black ignimbrite (Bign) 48
2.3.1.1.1.2.6. The Kargapazarı volcanics (Kv) 51
2.3.1.1.1.2.7. The Upper Tuff (Utl) 53
2.3.1.1.1.2.8. The Ardıçlıdağ volcanite 53
2.3.1.1.1.2.8.1. The Ardıçlıdağ rhyolitic lava unit (Ard) 54
2.3.1.1.1.2.8.2. The Ardıçlıdağ ignimbrite unit (Aign) 55
2.3.1.2. The Büyükdere Gorge Section 56
2.3.1.3. The Pasinler Town-Hasandağ Section 66
2.3.1.4. The Tımar Gorge Section 68
2.3.2. SOUTH OF PASINLER 69
2.3.2.1. The East Anatolian Accretionary Complex (EAAC) 72
2.3.2.2. The Bulkasım formation (Eb) 72
2.3.2.3. The Narman Group (En) 73
2.3.2.4. The Güllüce formation (Mg) 73
2.3.2.5. The Hündül limestone (Mh) 74
2.3.2.6. The Tuzluyolları dacite (Mtd) 74

2.4. THE HORASAN AREA 74
2.4.1. NORTH OF HORASAN TOWN 75
2.4.1.1. Basement Units 75
2.4.1.1.1. Metamorphic basement rocks 75
2.4.1.1.2. The East Anatolian Accretionary Complex (EAAC) 76
2.4.1.1.3. The Eocene Bulkasım formation (Eb) 77
2.4.1.1.4. The Eocene Narman formation (En) 77
2.4.1.1.5. The Akveren dacite (Mad) 79
2.4.1.2. The Erzurum-Kars Plateau Volcanics 80

2.4.1.2.1. The Kötek basalt (Köb)....80
2.4.1.2.2. Pyroclastic basal unit (Pblh)....82
2.4.1.2.3. The Köroğlu dacite/andesite (Kpad)....83
2.4.1.2.4. The Horasan plateau unit (Hpl)....85
2.4.2. SOUTH OF HORASAN TOWN....87
2.4.2.1. Basement units....88
2.4.2.1.1. The Upper Cretaceous Çatköse formation (Küç)....88
2.4.2.1.2. The Middle Eocene Bulkasım formation (Eb)....88
2.4.2.1.3. The Oligo-Miocene Güllüce formation (Mg)....88
2.4.2.2. Volcanic units....89
2.4.2.2.1. The Saçdağ dacite (Sd)....89
2.4.2.3. The Pliocene Aras formation (Pla)....90

2.5. Mt. ALADAĞ AREA....92
2.5.1. West of Mt. Aladağ....93
2.5.2. South of Mt. Aladağ....96

2.6. KAĞIZMAN AND EAST OF Mt. ALADAĞ....97
2.6.1. THE BASEMENT UNITS....97
2.6.1.1. The East Anatolian Accretionary Complex (EAAC)....97
2.6.1.2. The Late Cretaceous Kötek limestone (Ckl)....98
2.6.1.3. The Eocene Camuşlu formation (Ec)....98
2.6.1.4. The Late Miocene Güllüce formation (Mg)....100
2.6.2. THE ERZURUM-KARS PLATEAU VOLCANICS....101
2.6.2.1. Pyroclastic basal unit (Pblk)....101
2.6.2.2. The Çukurayva rhyolite (Çr)....101
2.6.2.3. The Paslı trachydacite (Ptd)....103
2.6.2.4. The Kars plateau unit (Kpl)....104
2.7. SUMMARY....105

Chapter 3: MAJOR AND TRACE ELEMENT GEOCHEMISTRY

Introduction....107
3.1. Classification of the volcanic units using major element geochemistry....108
3.1.1. Harker diagrams of major elements....115
3.2. Classification of the volcanic units using trace element geochemistry....115
3.2.1. Interpretation of trace element fractionation trends....131
3.3. Rare earth element patterns....147

3.3.1. REE patterns of the high-Y series 149
3.3.2. REE patterns of the low-Y series 150
3.3.3. Multi-element patterns 152
3.4. Trace element bivariate diagrams 163

Chapter 4: MINERAL GEOCHEMISTRY

Introduction 166
4.1. Classification of Minerals 167
4.1.1. Distribution of the composition of plagioclases 167
4.1.1.1. Composition of plagioclases and their glass inclusions as evidence of magma mixing 169
4.1.2. Distribution of the composition of pyroxenes and their classification 180
4.1.2.1. Calculations of pyroxene end-members 180
4.1.2.2. Distribution of the compositions of pyroxenes on the Erzurum-Kars Plateau 181
4.1.3. Classification and distribution of the composition of amphiboles 187
4.1.4. Olivine 196
4.2. Calculation of solidus pressures and temperatures using the chemical composition of minerals 199
4.2.1. The two-pyroxene thermometry 199
4.2.2. Amphibole-plagioclase geothermometer and geobarometer 206
4.2.2.1. Al-in-hornblende barometer 206
4.2.2.2. Amphibole-plagioclase geothermometer 209
4.2.3. Feldspar geothermometers 213
4.2.3.1. Calculations based on the temperature dependence of Eu and Sr distribution coefficients in plagioclases 213
4.2.3.2. Plagioclase thermometer of Kudo and Weill 214
4.2.3.3. Two feldspar thermometers 216
4.2.4. $\delta^{18}O$ isotope geothermometer 219
4.2.5. Comparison of geothermometer results gathered using different methods 222
4.3. Partition Coefficients 225
4.3.1. Calculation of partition coefficients 226
4.3.1.1. Amphibole 238
4.3.1.2. Plagioclase 238
4.3.1.3. Anorthoclase 239
4.3.1.4. Orthopyroxene 242

4.3.1.5. Clinopyroxene....242
4.3.1.6. Biotite....242
4.3.2. Compilation of partition coefficient values....242
4.3.3. Onuma diagrams....250

Chapter 5: ISOTOPE GEOCHEMISTRY AND PETROLOGIC MODELLING

Introduction....263
5.1. Isotope systematics....266
5.2. Assimilation combined with fractional crystallisation (AFC) modelling of the isotopic data....270
5.2.1. Theory....270
5.2.2. Estimation of end-member compositions....274
5.2.3. AFC modelling of the high- and low-Y series....289
5.3. Summary....300

Chapter 6: PETROGRAPHY

6.1. Textural and mineralogic differences between the high- and low-Y series....301
6.1.1. Lavas of the low-Y series....301
6.1.1.1. The aphyric lavas....301
6.1.1.2. Amphibole bearing porphyritic domes....304
6.1.2. Lavas of the high-Y series....307
6.1.2.1. Basic to intermediate lavas....307
6.1.2.2. Acidic domes, pyroclastic falls and flow (ignimbrite) deposits....307

Chapter 7: CONCLUSION AND DISCUSSION

Introduction....311
7.1. Volcanostratigraphy....311
7.2. Tectonic....313
7.3. K-Ar dating results....315
7.4. Results of trace element and isotope systematics....316
7.4.1. Geochemical characteristics of the volcanism and classification of volcanic units using trace elements....316
7.4.2. The petrologic model for collision related volcanics of the Erzurum-Kars Plateau:

magma generation, fractionation and assimilation history.....318

7.4.2.1. Model for magma generation..... 318
7.4.2.2. Fractionation and assimilation history of the volcanics..... 319
7.4.2.2.1. Zone I: a probable MASH zone.....321
7.4.2.2.2. Zone II: processes in the lower crust and transition between lower and upper crust.....324
7.4.2.2.3. Zone III: processes in the upper crustal basic to intermediate magma chambers..... 325
7.4.2.2.4. Zone IV: processes in the shallow level upper crustal acidic magma chambers..... 327

7.5. Results of this thesis in comparison with Previous studies on the collision-related volcanics of Eastern Anatolia..... 330

REFERENCES.....335

APPENDIX

A. Table of K-Ar dating

B. Sample preparation and analytical method

C. Accuracy and precision of the data

D. XRF whole-rock major and trace element dataset

E. ICP-MS whole-rock dataset

F. Electron microprobe dataset (diskette 1; data format: Microsoft Excel 4.0)

F.1. Amphiboles (hardcopy and file: amphibol.xls)
F.2. Pyroxenes (file: pyroxene.xls)
F.3. Plagioclase and alkali feldspar (file: plagiocl.xls)

G. AFC-Wizard program (diskette 2; data format: Microsoft Excel 4.0)

Chapter 1
INTRODUCTION

Collision volcanism is one of the least studied types of continental volcanism, even though it is a common phenomenon in orogenic systems. A systematic geochemical approach to collision volcanism can provide a better understanding of magma genesis, the evolution of the magma plumbing system and the extent of crustal assimilation and fractional crystallisation in collision systems. Another prime objective in attempting to understand the nature of collision volcanism is to explain the relationship between the chemistry of the magmatism and the compressional tectonic setting in which it occurs.

Recent examples of collision-related volcanism are located in two main regions in the world: the Tibetan Plateau in the Himalayas and Eastern Anatolia. Compared to the Tibetan Plateau, Eastern Anatolia offers an easily accessible and well exposed traverse of large volumes of collision-related volcanics.

1.1. Tectonic setting of the Eastern Anatolia Region

Eastern Anatolia offers the world's most complete transect across a volcanic province related to continent-continent collision. The region lies between the Pontides to the North, the Fold and Thrust belt of the Arabian foreland to the south and extends as far as the Turkish-Iranian and Turkish-Russia state boundary. The collision took place in the Eocene time (Robertson and Aktaş, 1984), between the Arabian and Eurasian plates giving rise to an extensive crustal shortening. As a result of this shortening, in the Middle Miocene, the region was uplifted to form a plateau, Eastern Anatolia Plateau, over half of which lies 2 km above sea level. According to Canıtez and Toksöz (1980), the thickness of continental crust reached 45 km. Collision-related volcanism began at about 11 Ma ago, immediately after the rapid uplift of the area and continued up to the historical times covering almost two third of the region and reaching up to 1 km in thickness in places.

After a certain amount of crustal uplift, thickening slowed down because of excessive lithostathic pressure, and this event gave way to the formation of a pair of transform faults which take up westward lateral movement. Since the Middle-Late Miocene, some of the compressional stress in the region has been converted into the extensional movement in the west by means of right-lateral strike-slip along the North Anatolian Transform Fault (NATF) combined with left-lateral strike-slip along

the East Anatolian Transform Fault (EATF). Formation of these faults in the Mid-Late Miocene was the manifestation of the last major wholesale change in the tectonic style of Turkey, namely "the neotectonic episode" as defined by Şengör and Yılmaz (1981). The palaeotectonic episode includes all the tectonic elements formed before the neotectonic episode, namely structures older than the Mid-Late Miocene. The NATF and EATF are termed "transforms" because they transform compressional deformation in Eastern Anatolia into the extensional deformation in the Aegean Region of western Turkey through the "Ova regime" (Şengör, 1980) in the Central Anatolia Region by means of strike-slip movement. The area bounded by these two faults is called "the Anatolian Wedge". It is driven westwards to override the oceanic lithosphere of the Mediterranean along subduction zones. Lateral displacement along these faults (throws) are calculated as 85±5 km for the NATF and 22±5 km for the EATF (Seymen, 1975; Arpat and Şaroğlu, 1972; Seymen and Aydın, 1972). The current rates of slip calculated from geophysical studies are about 0.9 cm a^{-1} for the NATF and 0.2 cm a^{-1} for the EATF. These rates give the Anatolia Wedge a westward escape rate of 0.5 cm a^{-1} (McKenzie, 1976). Tectonic escape along these faults can only remove a small part of the strain induced by the convergence of the Arabian plate about 1.4 cm a^{-1} (Dewey et al., 1986). Thus, the rest of the strain has been accommodated in the Eastern Anatolian crust via crustal shortening. Diffuse and complex strike-slip faulting (Şaroğlu et al., 1980, Yılmaz et al., 1987) provides evidence for continuing shortening across the region. These faults are either SE-trending with a dominantly right-lateral strike-slip displacement (e.g., Varto, Çaldıran and Balık Gölü faults) or NE- to NNE trending with dominantly left-lateral strike-slip displacement (e.g., Malazgirt and Kağızman fault) (Pearce et al., 1990).

1.2. Previous studies in Eastern Anatolia

Most of the previous work carried out in the Eastern Anatolia region has concentrated on the stratigraphy and neotectonism. Only a small number of studies have focused on the geochemistry and petrology of the neovolcanic rocks in the region. Studies related to the stratigraphy of the region have been listed in Figure 1.1. together with the generalised stratigraphic columns from different parts of Eastern Anatolia and a N-S cross section interpreted by Şahitürk and Kasar (1980) which cut through all the region from the Pontides in the north to the Arabian foreland in the south. It is beyond the scope of this thesis to discuss the details of the stratigraphic division of the older formations and the evolution of the basins in which these formations were deposited. Some researchers who worked in different parts of the region gave the same formations different names. In order to overcome this confusion, a correlation table for some of these formations is presented in Table 1.1.

Table: 1.1. Correlation table showing the names and lithologies of the Oligocene and the Early Miocene formations in the Eastern Anatolia Region.

ERZURUM-KARS BASIN		TEKMAN BASIN		MURAT BASIN				
Area	Erzurum-Pasinler-Horasan	Kagızman -Tuzluca	Tekman-Karayazı	Bingöl-Karlıova	Hınıs Area	Zırnak Area	Muş Area	Ahlat-Adilcevaz
Early Miocene	Haneşdüzü *limestone* (1)	-	Haneşdüzü *limestone* (2)	Adilcevaz *limestone* (3)	Güzelbaba *limestone*, Aktuzla fm: *gypsum, limestone, sandstone* (4)	Güzelbaba *limestone*, Aktuzla fm: *gypsum, limestone, sandstone* (5)	Adilcevaz *limestone*, Ebulbahar fm: *Cleyey limestone & marl* (6)	Adilcevaz *limestone* (7)
Oligocene	Çığılgan fm: *marl, sandstone, conglomer.* (1)	-	Çığılgan fm: *marl, sandstone, conglomer.* (2)	-	-	-	-	Ahlat *conglomer.* (7)

Researchers: (1) *Akkuş (1965); Toker (1965); Rathur (1966) and Tütüncü (1966),* (2) *İlker (1966b); Erdoğan (1966) and Tanrıverdi (1977),* (3) *Şaroğlu and Yılmaz (1987),* (4) *Tütüncü (1967); Özcan, (1967); Erdoğan (1967) and Sungurlu (1967),* (5) *Birgili (1968); Şenalp (1966) and İlker (1966a),* (6) *Yılmaz et al. (1987a),* (7) *Demirtaşlı and Pisoni (1965)*

1.2.1. Previous studies on the collision-related volcanics of Eastern Anatolia

The first geochemical study in the Eastern Anatolia region was carried out by Lambert et al. (1974) on a suit of lavas from Mt. Ararat. Their study involves a number of important petrologic results on the collision-related volcanism of North-eastern Anatolia, which were supported by later studies including that of Pearce et al. (1990). They recognised two distinct series, the high- and low-Y series, each consisting of andesite, dacite and rhyodacite of calc-alkaline character. Lambert et al. (1974) suggested that a multi-stage evolution of primitive upper mantle material has occurred, involving equilibration of a liquid containing about 2-5% H_2O with garnet and amphibole followed by subsequent fractionation of anhydrous phases in shallower depth. They pointed out that the parental magma was andesitic in composition and that differentiation of this magma led to the more silicic types. According to these authors, the low-Y series were generated under more hydrous and deeper conditions than the high-Y series. They maintain that the source of water could be the former subduction zone, or a slow moving and seismically undetectable modern subduction zone. On the basis of the geotectonic setting of Mt. Ararat, they argued that subduction zone theory could not be applied to this area. In their geotectonic model they suggested the presence of a lithospheric shear-zone at a complex plate junction. They also inferred that, pre-Mesozoic sialic crust could not be a parental material, because Sr isotopic ratios are much lower than that can be expected from the partial fusion of crustal material.

Bingol - Karliova area 10

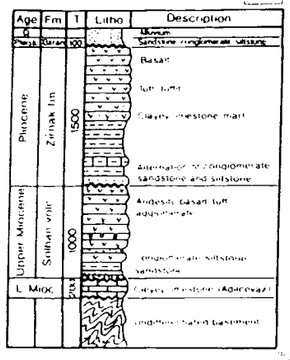

(Saroglu and Yilmaz 1987)

North of Erzurum 1

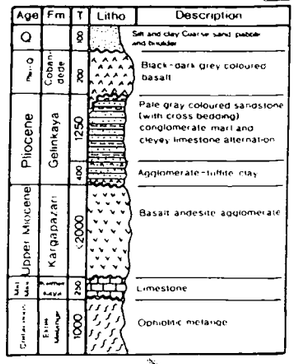

(Inan 1987)

Erzurum - Pasinler - Horasan Area

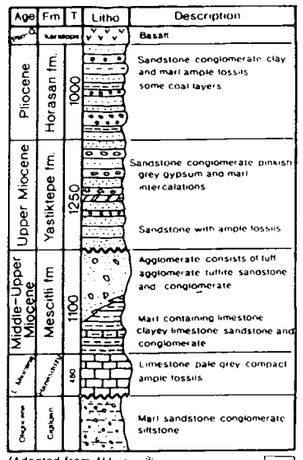

(Adapted from Akkus, 1965, Toker, 1965, Rathur, 1966 and Tutuncu, 1966)

2

North of Horasan 3

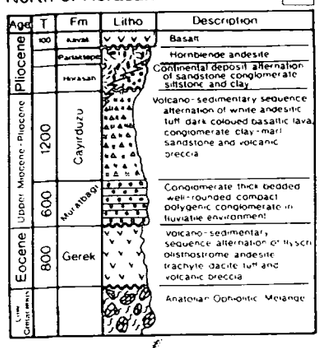

(Kocyigit 1985)

Kagizman - Tuzluca Area 4

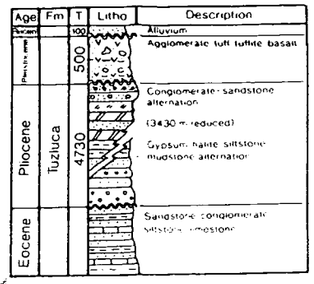

(Havur 1968, Senalp 1968 and Yurdakul 1971)

Hinis Area 9

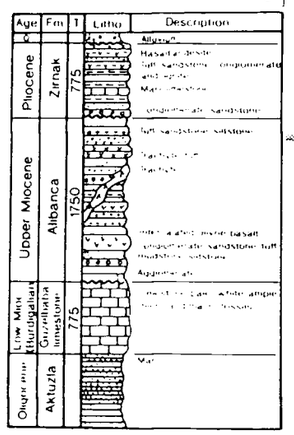

(Adapted from Tuluca 1967, Ozcan 1967, Erdogan 1967 and Sungurlu 1967)

Mus Area 8

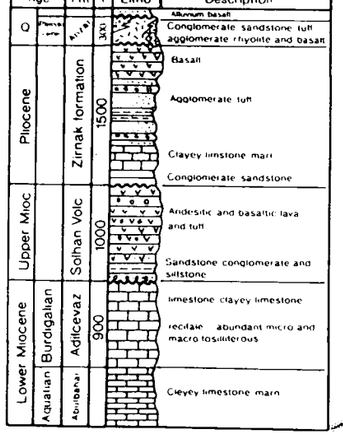

(adapted from Yilmaz et al.1986)

Karayazi - Tekman Area 5

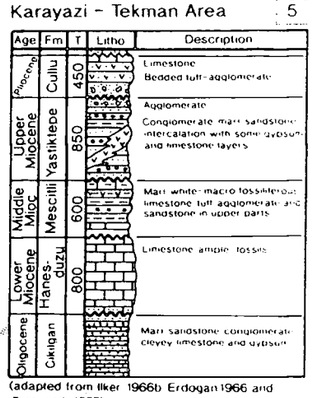

(adapted from Ilker 1966b, Erdogan 1966 and Tanriverdi 1977)

Ahlat - Adilcevaz Area 7

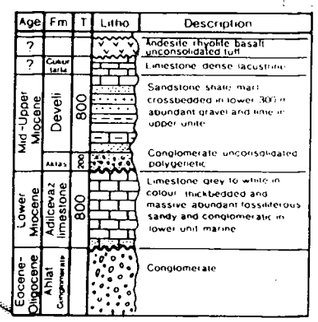

(adapted from Demirtasli and Pisoni 1965)

Zirnak Area 6

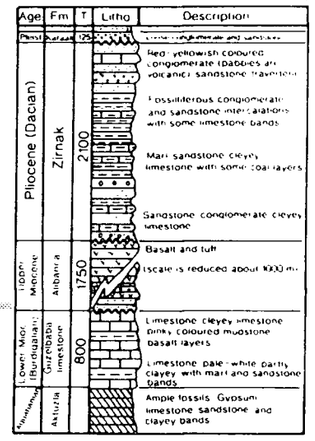

(adapted from Bilgili 1968, Senalp 1966 and Ilker 1966a)

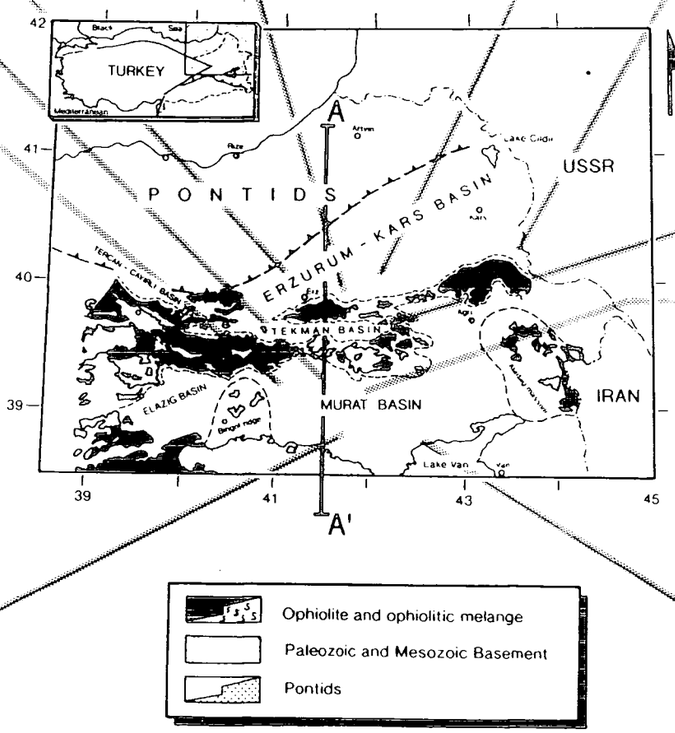

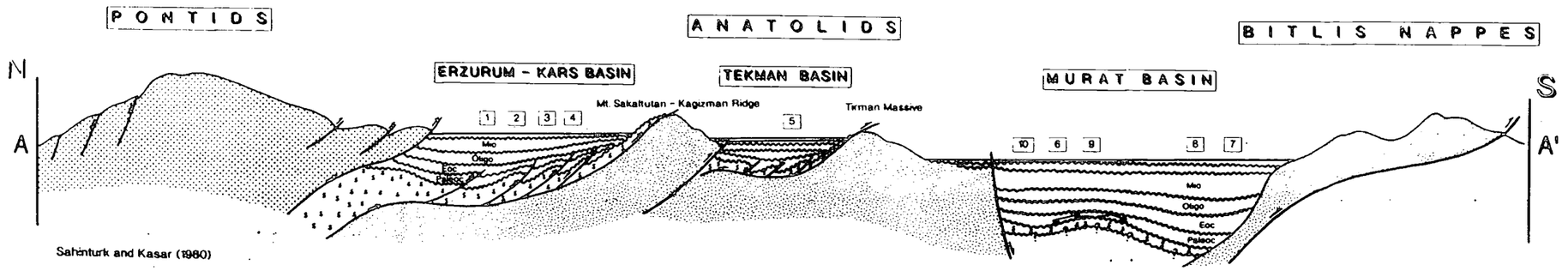

Sahinturk and Kasar (1980)

Figure 1.1.

Figure: 1.2.

The map showing the locations and correlations of the drill- wells from the Eastern Anatolia Region, Turkey.

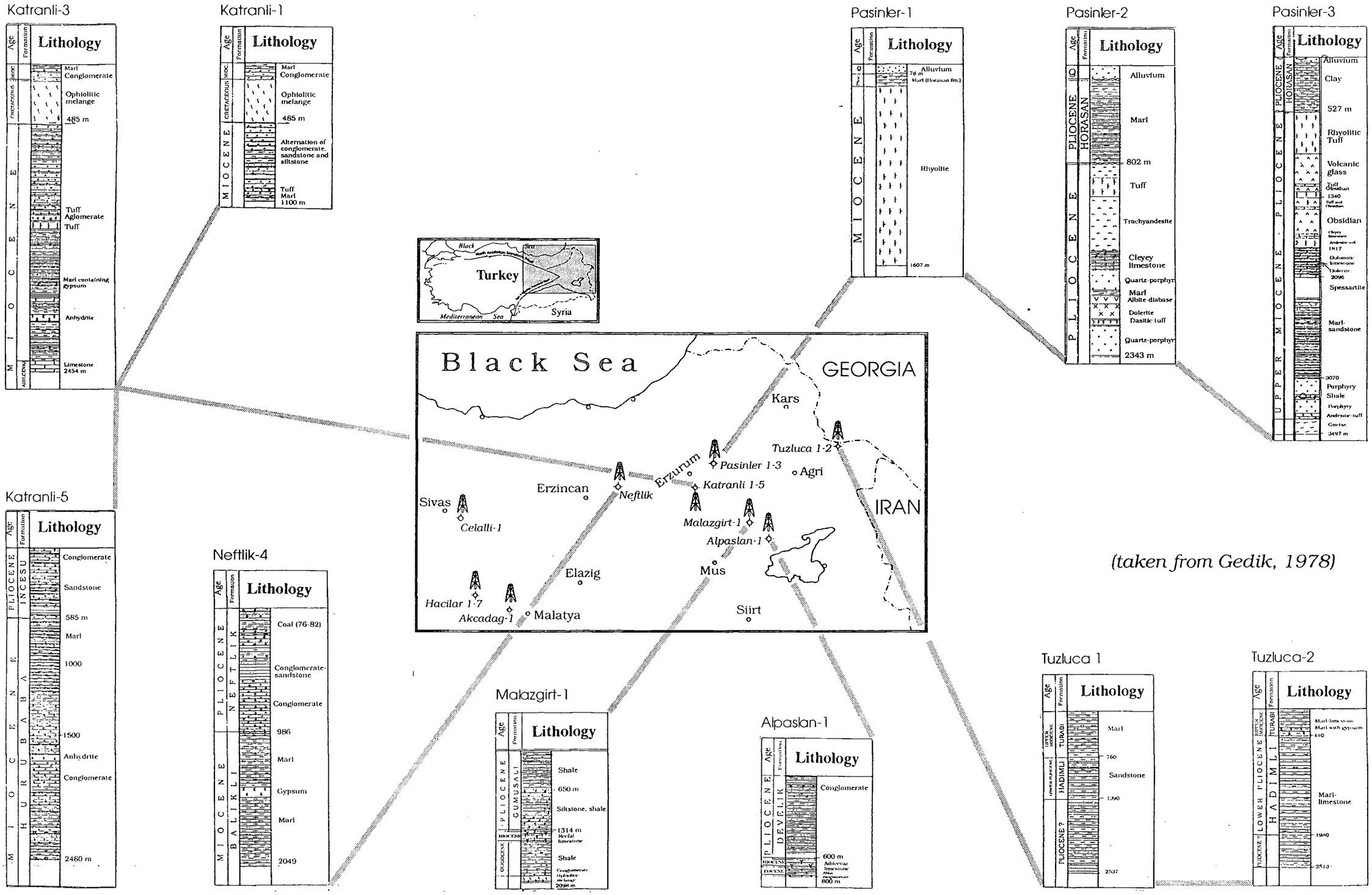

(taken from Gedik, 1978)

Mehmet Keskin

The studies of Innocenti et al. (1976, 1980, 1982b) showed that the volcanic products erupted in the Kars-Ararat area belong to calc-alkaline series and are dominated by andesitic members. These authors suggested that the earliest volcanism was calc-alkaline and that this was followed by alkaline volcanism. However, the results of Pearce et al. (1990) show that this is not true for the collision-related volcanism of Eastern Anatolia. Innocenti et al. (1982a) argued that, even though the data they had were inadequate to draw a conclusion about the petrogenesis of the volcanism, the rare earth elements (REE) and Sr isotope ratios suggested magma genesis by partial melting of mantle anomalously enriched in large ion lithophile elements (LIL). They suggested on the basis of their dating that the andesitic volcanic front migrated northward for 150-200 km during the Pliocene. They interpreted this observation as an evidence of the detachment of the subducted slab immediately after continental collision and argued that this detachment continued to induce magma generation of progressively lower intensity beneath an area corresponding to the Erzurum-Kars Plateau, located progressively further from the continental suture. However, as Pearce et al. (1990) pointed out, there are no intermediate or deep-focus earthquakes that are indicative of a subducting lithospheric slab.

Gülen (1980) argued that alkaline and calc-alkaline volcanism spatially and temporally coexisted in the Tertiary to Quaternary volcanic province in Eastern Turkey. According to Gülen, the low values of $^{87}Sr/^{86}Sr$, the constancy of these ratios over a wide range of SiO_2, and the lack of correlation between the Sr isotopic composition may imply that Ararat lavas have not been modified by crustal contamination. In 1982, he presented an abstract in EOS where he argued that $^{143}Nd/^{144}Nd$ and $^{87}Sr/^{86}Sr$ data for all Ararat suites fall within the Nd-Sr mantle array without any significant crustal contamination whereas data from Süphan volcano fall on a trend towards low $^{143}Nd/^{144}Nd$ and high $^{87}Sr/^{86}Sr$ values indicating a strong evidence for crustal contamination. His $^{207}Pb/^{204}Pb$ ratio for Ararat volcano varies in a wider range with respect to $^{206}Pb/^{204}Pb$ and $^{208}Pb/^{204}Pb$ ratios. About half the data plot within the normal oceanic mantle array while the other half is more radiogenic in $^{207}Pb/^{204}Pb$ extending toward the alkaline suite. He also mentioned the presence of systematic variations between isotopic ratios and major and trace element contents of lavas from Mt. Ararat such as that of $^{87}Sr/^{86}Sr$ and MgO. He interpreted his results as an indication of mixing of MORB-type mantle with an alkali-basalt magma in the Mt. Ararat province. According to him, crustal contamination of this mixture generated Süphan volcanics.

Tokel (1984) suggested that the data from drilling cores in the Eastern Anatolia region indicated the presence of E-W oriented Upper Miocene-Pliocene basins which are bounded by gravity faults and filled by at least 2000 m of limnic and fluvial

deposits. He believes that these depressions could be much deeper than 2000 m and related to a rifting event generated by local tensional forces that could be much larger than the regional compressional forces. He used the mathematical model of Turcotte (1983), which quantitatively showed the possibility of a tensional regime in a collision zone, and argued that such tensional forces could cause pressure release in the crust and shallow mantle. On the basis of his major element database, he argued that these Upper Miocene to Pliocene basins were filled by voluminous tholeiitic and alkaline volcanics which are related to the rifting. He also pointed out that incompatible element (such as Rb, Sr, Nb and Ti) contents of the collision-related volcanics show close resemblance to oceanic tholeiites generated from depleted mantle. Since he has not presented his trace element data in any of his papers, the feasibility of this interpretation seems to be in question. The area he studied (Tokel, 1985) overlaps with the area studied in this thesis (between Erzurum and Kars).

According to Şengör et al. (1985), during the early stages of neotectonic episode, the region underwent an extensive folding phase as a result of crustal shortening. During this period, the early Miocene shallow-water limestone (the Adilcevaz limestone) acted as a buckling layer above the soft flysch-melange lithologies of the Eastern Anatolia Accretionary Complex resulting in the formation of the E-W oriented basins.

Yılmaz et al. (1987) argued that the earliest manifestation of the young volcanism of Eastern Anatolia occurred in the Solhan area around Muş. Their interpretation is based on the stratigraphic relationship of the volcanic units with interbedded and underlying sedimentary formations. They named this volcanic activity the Solhan cycle. Flows of hawaiite dominate the basal part of the volcanic sequence with some mugearitic interlayers. They argued that the parental magma should have been of alkali-olivine basalt composition. On the basis of their major element and electron microprobe data, they claimed that there is no clear petrographic and geochemical evidence indicating crustal contamination in the magmatic evolution of this early volcanic series. According to Yılmaz et al. (1987), the chemical variations in the volcanic rocks may be explained by fractional crystallisation under low to moderate pressure. In their model for magma genesis, they claimed that the partial melting that gave rise to the generation of a mildly alkaline magma occurred at shallow level in the early stages of the crustal thickening due to pressure release, with the development of N-S tension cracks. They argued that mildly alkaline activity changed into calc-alkaline during the initiation of westward escape of the Anatolian scholle from the east Anatolian convergent zone. Yılmaz et al. (1987) explained the formation of this extensive calc-alkaline volcanism in terms of Dewey et al.'s (1986) model which emphasises possible zones of different rheologic properties in a

compressionally deforming continental crust at different levels. Their model involves true crustal magma generation at a zone of detachment around 15 km deep in the crust below which the crust behaves in a ductile manner. In this model, all conditions required for magma generation, such as high heat flow and high-grade metamorphism, were present in the crust. They also cited the widespread ignimbritic eruptions as evidence of crustal melting, because, as they described, they represented a water-saturated granitic magma. According to the authors, the thickened crust began to return to normal with the beginning of the westward escape tectonism along the North and East Anatolian Transform Faults. This period corresponds to a steady change in the nature of volcanism from calc-alkaline to Na-rich alkaline. Yılmaz et al. (1987) claimed that the Erzurum-Kars region in the north was covered predominantly with alkaline basaltic lavas which were genetically related to this period.

Nagao et al. (1989) carried out research on the noble gas and carbon isotopic compositions of gas samples from the Quaternary volcanic area around Nemrut, Çaldıran and Diyadin. They reported the presence of mantle-derived He in all their samples. Their highest $^{3}He/^{4}He$ ratio is around $1.06x10^{-5}$ which resembles to the He isotopic ratios of arc-volcanics in general. Their carbon isotopic ratios showed that CO_2 in these areas does not have an organic origin but a marine carbonate and/or volcanic origin. According to these authors, volatile gases including subduction-related He were originally derived from mantle. En route to the surface these magmas were contaminated by marine carbonate units as a result of interaction with the crust. They argued that the evolved gases came to the surface through faults. Samples from Çaldıran show around 50% He contribution from the continental crust which appears to include carbonate rocks while the samples from Diyadin show up to 71% crustal contribution. Nagao et al. (1989) favour of the model put forward by Innocenti et al. (1982) which assumes the presence of a remnant slab detached from Arabian plate or a renewed subduction of limited intensity beneath the volcanic area.

Ercan et al. (1990) reviewed the previous studies on the collision-related young volcanism of the Eastern Anatolia and contributed to the geology of the area with new K/Ar dating, $^{87}Sr/^{86}Sr$ isotopes and REE analysis. They argued on the basis of their Sr isotopic ratios that the magmas that produced the collision-related volcanism in the Eastern Anatolia region had been contaminated by the Arabian crust which was partly subducted beneath Eastern Anatolia. In their opinion, almost all the volcanic units in the region resemble the upper crustal composition proposed by Taylor and McClennan (1985) in their Li, V, Sc, Co, Ni, Ba, Ga, Y, Rb, Zr, Hf, Ta and Pb contents. They also argued that the Sr, Nb, Cs, Th, and U contents of these volcanics are similar to that of lower and upper crustal compositions.

Pearce et al. (1990) suggested that the character of the neovolcanic activity in the Eastern Anatolia region depended on the tectonic history of the underlying lithosphere and the thermal evolution of the crust. According to them, the calc-alkaline volcanoes of Bingöl, Süphan, Ararat and volcanics of the Erzurum-Kars Plateau were derived from lithosphere carrying a subduction signature associated with pre-collision subduction events. They also maintain that combined assimilation and fractional crystallisation was operational in the thickening continental crust. They argued that there might be two possible mechanisms which could explain the production of great volumes of magmatism: thermal perturbation of metasomatised subcontinental lithosphere and the delamination of the thermal boundary layer. In addition, localised extension could contribute to former mechanisms. Pearce et al. (1990) suggest that the region is characterised by a set of mantle domains running parallel to the collision zone, each of which has yielded magmas of a particular composition since the start of magmatism in the region. Another important inference is that of polybaric crystallisation in the Kars-Mt. Ararat province. In accordance with the Lambert et al.'s (1974) findings from Mt. Ararat, Pearce et al. (1990) demonstrated the presence of extensive amphibole crystallisation on the Erzurum-Kars Plateau during the early stages of fractionation.

Tokel and Ercan (1992) pointed out that the voluminous volcanics associated with collision tectonism in Anatolia display distinctive geochemical characteristics that do not coincide with the three basic tectonic settings in which magma generation occur, namely mid ocean ridges, subduction zones and intraplate settings. The main characteristic feature of this volcanism is the enrichment of high field strength (HFS) elements such as Ti, Nb, Ta and Hf. Therefore, they believe that the source region is different from that of calc-alkaline rocks. They argued that post-collision, in their words, should be considered as a specific tectonic setting in which magma is generated with distinctive characteristics and hence the Neogene volcanics of Anatolia should be cited in literature as the type example of a post-collision magmatism. They claim that the lavas which have previously been considered as being of the calc-alkaline association are not "true calc-alkalic rocks". The data from their database plot into the fields of within plate, low K tholeiite and calc-alkali basalts. They maintain that, moderate concentrations of large ion lithophile (LIL) and light rare earth (LREE) elements cannot be considered as an indicative feature of any of the tectonic settings listed above. They argue that, although HFS elements are retained during slab-mantle interactions in subduction zones, at greater depths they are transferred from slab into sub-continental mantle which will be the source region of the future post-collision volcanism.

1.3. Objectives of this thesis

This study can be considered to be a continuation of the study of Eastern Anatolian volcanism by Pearce et al. (1990) which concentrated on neovolcanism in Eastern Anatolia in a regional scale. In this study, the Erzurum-Kars Plateau has been selected for a detailed work because it is the area on the plateau that provides the most complete record of collision-related volcanism in the form of complete lava and pyroclastic sections. The aim of this project is to study the spatial and temporal variations in magma genesis on the plateau through volcano-stratigraphic traverses to investigate the relative importance of different processes such as fractional crystallisation, assimilation and magma mixing during collision-volcanism. Recognition of lithospheric and asthenospheric sources in the volcanic units, identification of the composition of the mantle source or sources and the evolution of extent of crustal assimilation in the evolution of these units can provide invaluable data on the temporal evolutionary steps of this collision-related volcanic system. It may also provide indirect information for the theoretical tectonic models (e.g. delamination of lithosphere) proposed by several authors for collision terrains. This kind of study has been previously successfully applied to the other types of intra-continental volcanism such as flood basalts (e.g. Columbia River volcanics in the USA), but not to the collision-related volcanism.

During the first two years of my study, with the field assistance from Turkish Petroleum and with the financial support of the Ministry of Education in Turkey, I studied an area of about 3000 km^2 of the Erzurum-Kars Plateau at a reconnaissance scale, collected a total of 350 representative samples and constructed a generalised volcano-stratigraphy of the plateau (see Figure 5.1, p. 264) by correlation of distinctive lavas and pyroclastic units between several traverses. I also mapped 800 km^2 of the western part of the plateau (see Figure 2.1).

This study includes a number of original contributions to the geology of Eastern Anatolia:

- ◊ Collision-related volcanics have been mapped in detail using the volcanic facies concept defined by Cas and Wright (1988). The area mapped covers about 800 km^2 area and comprises the western part of the Erzurum-Kars Plateau including Mt. Dumlu, Mt. Kargapazarı and the town of Pasinler.
- ◊ Eighteen K-Ar age determinations were carried out on some key samples from the representative levels of the traverses mentioned above, especially from the bottom and top of the volcanic sequence. These results provide a good age control over the initiation and cessation of the collision-related volcanism on the plateau.

- ◊ The electron microprobe technique has been applied to the collision-related volcanics of Erzurum-Kars Plateau for the first time. This is also the biggest (888 point analyses) probe database from the Eastern Anatolia region.
- ◊ For the first time in the region, partition coefficients of amphibole, plagioclase, pyroxene, biotite and alkali feldspar have been determined using the mineral separates from the collision-related volcanics of the region.
- ◊ Samples from the western part of the plateau around Mt. Dumlu, Kargapazarı and the Pasinler area were analysed by ICP-MS (Inductively Coupled Plasma Mass Spectrometry) technique for the first time in this study.
- ◊ This is one of the first attempts to utilise oxygen isotopes ($\delta^{18}O$) in a collision volcanic terrain. Apart from Gülen's (1982) unpublished preliminary results from Mt. Ararat, lead (Pb) isotopes were also analysed for the first time on the collision-related volcanics in the region. These two isotopes have the potential of providing invaluable information about the extent of crustal assimilation. The contamination of mantle-derived magma can produce crustal Pb isotopic signatures even for low degrees of contamination due to strong depletion in Pb of mantle-derived melts with respect to crustal materials. It is also the case for $\delta^{18}O$ that show a considerable contrast between mantle-derived magma and crust.

The geochemical whole-rock and mineral database accumulated in this study is one of the largest database on collision-related volcanics in the world. Table 1.2 lists the analytical techniques, number of samples analysed, names of the laboratories and laboratory equipment used in the construction of the database in this study.

1.4. Source of the analytical data used in this thesis

The analytical techniques used in this thesis are summarised below while a more detailed description of techniques together with sample preparations, analytical conditions, and calculations of precision and accuracy of the data, are presented in Appendix A to F.

1.4.1. XRF analysis

A total of about 350 samples from the Erzurum-Kars Plateau were first mechanically crushed and then powdered using an agate ball mill. Then, their trace elements including Ba, Nb, Zr, Y, Sr, Rb, V, Ga, Zn, Ni, Cr, Sc, Co and LREEs (La, Ce and Nd) were analysed on pressed powder pellets using an automated Philips PW1400 XRF spectrometer with a Rh anode tube. The major element contents of the samples were also analysed on fusion-disks.

1.4.2. Electron Microprobe analysis

Electron microprobe analyses of minerals from a total of 70 representative samples were performed by a Cambridge Instruments Geoscan using a focused electron beam and an operation condition of 15 kV gun potential with 70-75 μa beam current. A Co standard was used to calibrate the system. A total of 887 mineral grains (points) were analysed. Ortho and clino pyroxenes (309 points), plagioclase and alkali feldspars (354), olivines (63), amphiboles (57), Biotites (11), opaque minerals (26) and volcanic glass (67) were analysed. Some zoned phenocrysts were analysed at cores and the rims to reveal their chemical zonation.

1.4.3. K-Ar dating

18 samples selected from the key levels of the volcanic succession were dated by Dr. J.G. Mitchell in the Department of Physics at the University of Newcastle.

1.4.4. ICP-MS analysis

A sub-set of 40 samples from the key levels of the stratigraphic sections on the Erzurum-Kars Plateau were selected for analysis by the inductively-coupled-plasma-mass-spectrometer (ICP-MS). Powdered rock samples were dissolved by HF and HNO_3 followed by a series of acid digestion and evaporation steps. Dissolved samples were analysed by ICP-MS on a VG Elemental PlasmaQuad at the University of Durham, Industrial Research Laboratories. A data reduction process involving drift, blank and isotopic overlap corrections and calibration was carried out.

In addition to whole-rock samples, a total of 24 mineral separates (9 amphiboles, 8 plagioclases, 1 sanidine, 3 orthopyroxenes, 1 clinopyroxene, 1 biotite and 1 olivine) were hand picked from a subset of 12 samples showing porphyritic texture. They were then analysed by ICP-MS by the same procedure.

1.4.5. Radiogenic isotope analysis

A subset of 26 samples, including 3 additional samples from the Central Anatolia region, was prepared for radiogenic isotope analysis. These samples are the most representative ones of the key levels of the volcanic succession on the Erzurum-Kars Plateau. Sr and Pb isotopic ratios were determined by using a Finnegan MAT 262 multicollector mass spectrometer at the Natural Environment Research Council (NERC) Isotope Geoscience Laboratory (NIGL). Nd was analysed by a VG354 multicollector mass spectrometer, also located at NIGL.

1.4.6. Oxygen ($\delta^{18}O$) isotope analysis

Oxygen isotopes ($\delta^{18}O$) on 11 of the whole rock and 22 of the mineral samples analysed for other isotopes were analysed at the NERC Isotope Geoscience Laboratory in Nottingham.

Table: 1.2. Table displaying analytical techniques used to analyse collision-relate volcanics of the Erzurum-Kars plateau, the elements analysed, type of analytical equipment and laboratories used.

Method	No. of samples	Elements analysed	Laboratory	Analytic equipment
Whole rock analyses				
XRF	350	Major elements Sc, Cr, V, Ni, Co, Cu, Zn, Ga, Rb, Sr, Y, Zr, Nb, Ba, La, Ce, Nd, Pb, Th	Durham University	Phillips PW1400
ICP-MS	34	Rb,Sr,Y,Zr,Nb,Ba, La,Ce,Pr,Nd,Sm,Eu,Gd,Tb, Dy,Ho,Er,Tm,Yb,Lu, Hf,Ta,Pb,Th,U	Durham Univ., Industrial Research Centre	VG Plasmaquad
K-Ar dating	18	^{40}Ar	Univ. of Newcastle	
Solid source Mass Spectrometry	26	$^{87}Sr/^{86}Sr$ $^{143}Nd/^{144}Nd$ Pb isotopes	NERC, Isotope Geosciences Laboratory, Keyworth, Nottingham	Finnegan MAT 262
	11	Oxygen isotopes ($\delta^{18}O$)	NERC, Keyworth	Gas-source mass spectrometry
Mineral analyses				
Carried out on the mineral separates				
ICP-MS	22	Rb,Sr,Y,Zr,Nb,Ba, La,Ce,Pr,Nd,Sm,Eu,Gd,Tb, Dy,Ho,Er,Tm,Yb,Lu, Hf,Ta,Pb,Th,U	Durham Univ., Industrial Research Centre	VG Plasmaquad
Solid source Mass Spectrometry	11	Oxygen isotopes ($\delta^{18}O$)	NERC, Isotope Geosciences Laboratory	Gas-source mass spectrometry
Carried out on the polished thin sections				
Electron Microprobe	70 (888 points)	Major elements	Durham University	Cambridge Instruments Geoscan

1.5. Description of thesis

The thesis consists of seven chapters. A brief summary of each of these chapters is presented below.

Chapter 2 presents the volcanic stratigraphy of the collision-related volcanics of the Erzurum-Kars Plateau which has been constructed during the course of 6½ months of fieldwork between Erzurum and Kars cities. During this fieldwork, an

approximately 3000 km^2 area of the Erzurum-Kars was studied and 800 km^2 subset of this area was also mapped. A specific aim was to concentrate on the volcano-stratigraphic divisions of the neovolcanic units and the regional correlations. The information presented in this chapter can be used as a base study for researchers in the future. The length of Chapter 2 has therefore inevitably become longer than all other chapters.

Chapter 3 describes the major, trace and REE variations in the volcanic units. In the first two sections of this chapter, the collision-related volcanics of the Erzurum-Kars Plateau are classified on the basis of their major and trace element contents respectively. In the final sections of the chapter, the interpretation of the trace element fractionation trends, REE patterns, multi element patterns and trace element bivariate diagrams are presented with special reference to their petrologic significance.

Chapter 4 is based on the mineral geochemistry of the Erzurum-Kars plateau lavas. It is subdivided into three sections. The first section deals with the classification of minerals; plagioclase, ortho- and clinopyroxenes, amphibole and olivine. Geothermo-barometer calculations based on mineral composition are the main subject of the second section. Major element data obtained from electron microprobe analysis, REE data from ICP-MS analyses and $\delta^{18}O$ data by gas-source mass-spectrometry are the main sources used in this section. The third section focuses on the calculation of the distribution of trace, rare earth and some major elements between plagioclase, amphibole, ortho- and clinopyroxenes, biotite and alkali feldspars and magma. It also presents the results of an extensive compilation of partition coefficients proposed by other researchers.

Chapter 5 gives detailed descriptions of the isotope systematics of the Erzurum-Kars Plateau volcanics. The chapter is made up of two sections. The first section illustrates the variations in Sr, Pb, Nd and oxygen isotopic ratios of samples from key levels on the plateau. The second section presents petrologic modelling based on assimilation combined with crystallisation (AFC).

In Chapter 6, a brief summary of the petrographic properties of the Erzurum-Kars Plateau Volcanics is presented with special emphasis on the textures indicating magma mixing and early history of fractional crystallisation of the magmas that fed the lavas on the plateau.

Chapter 7 presents a general summary of results from previous chapters with special reference to the plumbing system and the extent of magma-crust interaction in the thickened crust beneath the Erzurum-Kars Plateau.

Chapter 2: STRATIGRAPHY

Introduction

This chapter presents the results of the fieldwork carried out in an approximately 3000 km^2 area of the Erzurum-Kars Plateau. From west to the east, the area includes Mt. Dumlu (Gavurdağları mountain range), the northern part of the Erzurum plain, the Karasu river valley, Mt. Kargapazarı ridge, the Pasinler, Horasan, Mt. Aladağ and their surrounding areas and finally the Kağızman area located to the north of the town of Kağızman (Figure 2.1).

Construction of the volcano-stratigraphic sections on the Erzurum-Kars Plateau was a difficult task not only because of the well-known complexities of the stratigraphic relationships of the volcanic rocks in general but also due to the lack of basic geological information on the stratigraphy of collision-related volcanic rocks of the plateau. To my knowledge, this study is the first attempt in its kind to differentiate and map volcanic units on the plateau. Thus, all the formation names used for the volcanic units on the plateau are the names given in this study except for those of the basement units.

The fieldwork undertaken on the plateau consists of two three month field seasons. During the first field season, the whole area was studied on a reconnaissance scale. In order to reveal vertical and lateral variations in the volcanic succession, a series of representative sections that cut the characteristic parts of the plateau were traversed through which a total of 175 volcanic rock samples were collected. These traverses were supplemented by the observations and samples between these sections. Some lava and pyroclastic units that show distinctive texture, mineral composition, physical appearance, eruptive character, and chemistry were used as key horizons to construct the volcano-stratigraphy of the plateau. Some of these units are very widespread on the plateau covering hundreds of km^2. The Dumlu amphibole andesite and the Güngöremez dacite/andesite in the Mt. Dumlu area and the Black ignimbrite and the Kargapazarı volcanics in the Pasinler area are good examples of these.

During the second field season, based on the first years petrographic, geochemical, K-Ar dating and field results, the western part of the plateau that covers about 800 km^2 and comprises Mt. Dumlu, Mt. Kargapazarı and the town of Pasinler

was mapped following the volcanic facies criteria described by Cas and Wright (1988). A total of 170 samples were collected from the area mapped during the second field season. The main criteria used in the differentiation of the volcanic units from each other are petrographic properties such as their textures and phenocryst contents, their eruptive character (e.g. effusive or explosive), depositional characters (especially for pyroclastic falls and flow units) and general physical or field appearance coupled with results of K-Ar dating and their geochemistry.

Most of the lavas forming the Erzurum-Kars Plateau were chiefly originated from fissure eruptions. There are also some isolated domes and volcanoes (e.g. Mt. Aladağ and Mt. Küçük and Büyük Yağlıca in the Kağızman area) on the plateau representing the site of central eruptions. Each volcanic unit either consists of several lava flows with a similar texture, phenocryst content and eruptive character or more than one rock types that are interbedded and each of which contains distinctive textural and mineralogical properties and depositional structures (e.g. the Lower tuff in the Pasinler area which is composed of the Grey, White ignimbrite, pyroclastic falls and agglomerate). Some of these units are composed of lava or pyroclastic flows which are laterally continuous and homogeneous in their petrography, mineralogy and chemistry over large distances such as the Black ignimbrite and Kargapazarı volcanics in the Pasinler area. On the other hand, some other individual flows exhibit a relatively short horizontal extent even though the volcanic unit they form covers a very large area with great thicknesses (e.g. the Güngörmez andesite/dacite in the Mt. Dumlu and Kargapazarı areas). The latter appears to have formed by several fissure eruptions over a particular period of time. They were located on various parts of the plateau with variable distances from each other and fed by a single or more magma chambers with similar compositions and similar fractional crystallisation histories.

The area will be introduced as six sub-areas, corresponding to six main sections, each showing a unique volcano-stratigraphy. From west to the east these are: 2.1. the Mt. Dumlu area, 2.2. the Mt. Kargapazarı area, 2.3. the Pasinler area, 2.4. the Horasan area, 2.5. the Mt. Aladağ area and 2.6. the Kağızman area.

The area mapped has been divided into 1 km squares to form a coordinate system, whose rows are labelled by letters and columns are by numbers, to enable reader to find a location easily (Figure 2.10). The coordinate of a particular locality will be shown in brackets such as (C:18) in the text. The locations of all basic geological maps used in this chapter are shown in Figure 2.2.

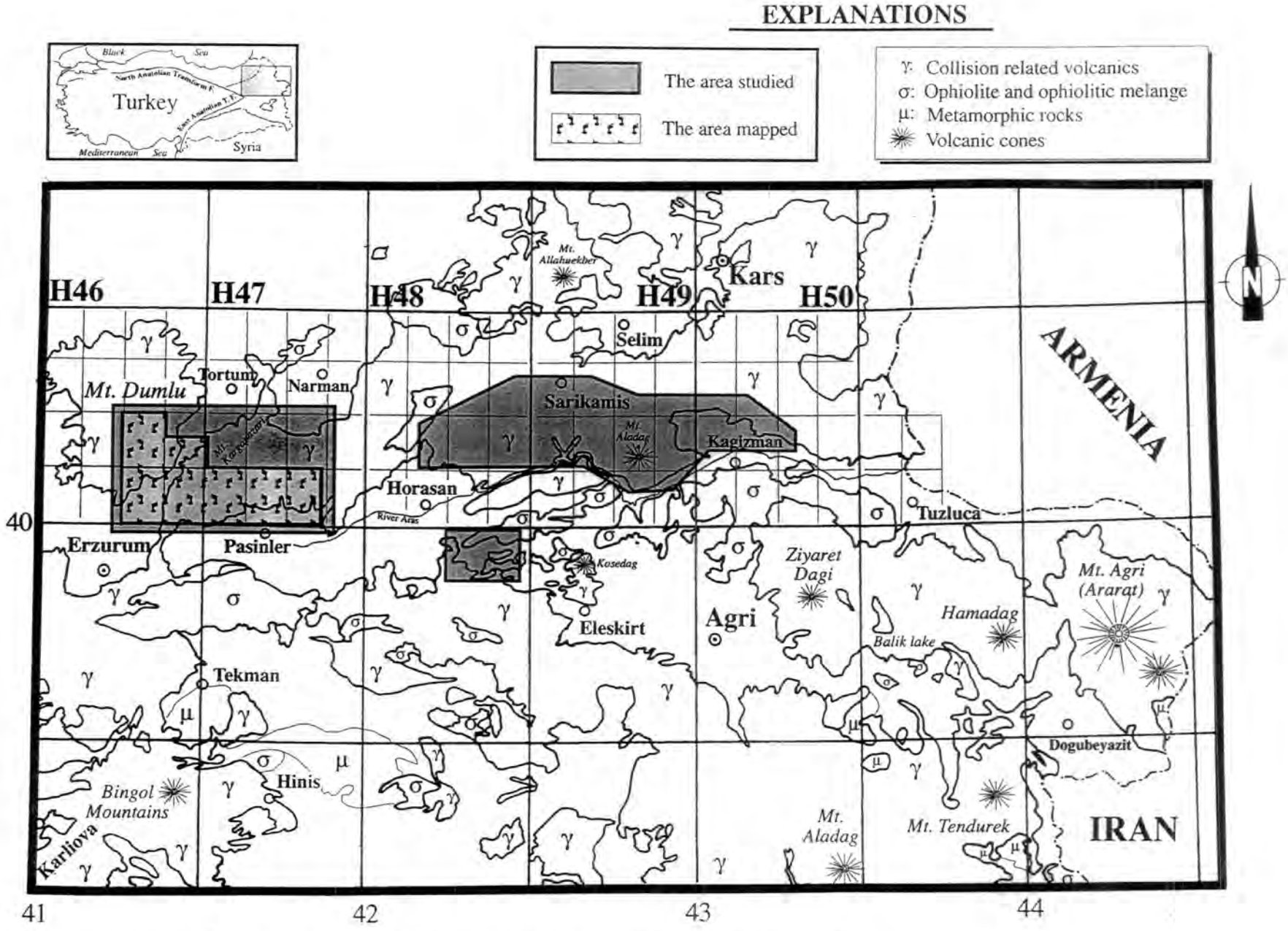

Figure: 2.1. The simplified geological map of northeastern Anatolia region indicating the locations of the collision related volcanics and the areas that have been studied and mapped.

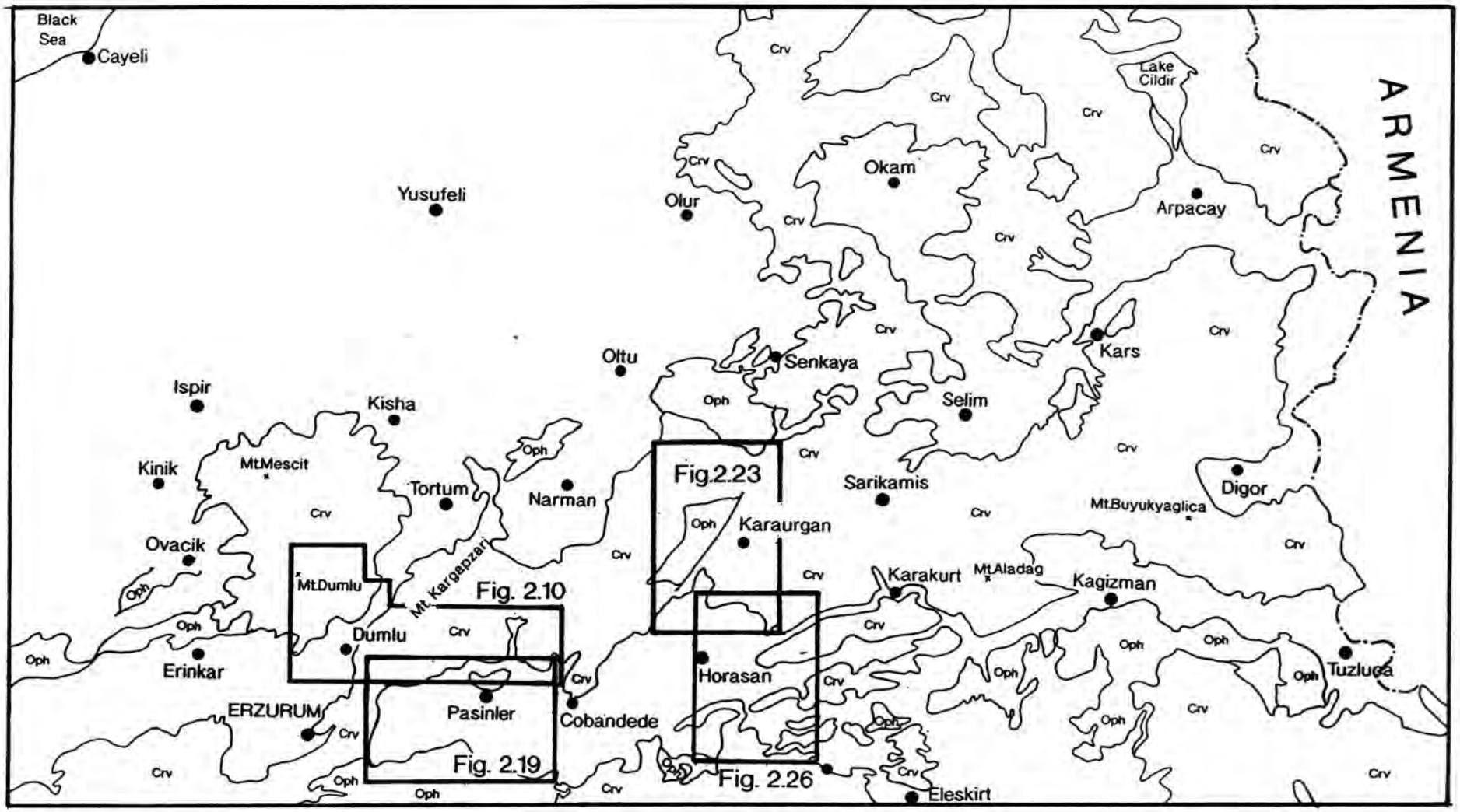

Figure: 2.2. The map showing the locations of maps which are used in this chapter.

Crv: collision-related volcanics, Oph: ophiolitic basement rocks.

2.1. THE Mt. DUMLU AREA

The Mt. Dumlu area comprises the westernmost part of the Erzurum-Kars Plateau. This area in general located within the Gavurdağları Mountain succession that comprise a north-south extending ridge which is composed of a series of high peaks over 3000 m. Among them, Mt. Dumlu is the second highest peak (3200 m) in the Gavurdağları Mountain group after Mt. Mescitdağı (3255 m). Towards the west of a line between the towns of Karahan and Erinkar, the Erzurum-Kars Plateau volcanics almost completely disappear. Eastern border of the volcanics of Mt. Dumlu area with those of adjacent Mt. Kargapazarı area is indicated by the River Karasu Valley in the northeast and the Erzurum Plain in the southwest respectively. This area is named as Mt. Dumlu area after this peak called Mt. Dumlu. In Mt. Dumlu area, the Erzurum-Kars Plateau volcanics cover well over 1000 km^2 area with a thickness reaching over 1 km. In this study, the southeastern part of this area which is located on the eastern slope of Mt. Dumlu and which is adjacent to the Erzurum plain (Karasu Basin) has been studied and mapped. This area covers approximately 245 km^2 (Figure 2.1).

The volcanic succession in the Mt. Dumlu area is quite different from that in the eastern areas, especially that to the east of the Mt. Kargapazarı ridge. The first important difference is that the pyroclastic flows, which are widespread in the east, particularly on the Pasinler plateau, are almost completely absent in the volcanic pile of Mt. Dumlu. The second difference is that, in this area, an amphibole-bearing porphyritic dacite/andesite widely occurs as a very thick unit towards the top of the succession. This unit is only exposed in the east in a small isolated outcrop to the southeast of Köşk village. Another outcrop of a similar lithology is situated further east on the Pasinler Plateau within a 2-3 km^2 area near Kızılveren village (the Kızılveren amphibole dacite/andesite). Unlike the eastern part of the plateau, where pyroclastic falls and reworked products are abundant, Mt. Dumlu is made up mainly of lava flows, which are mainly intermediate to acidic in composition, apart from the relatively common tuff deposits at the base of the succession.

In the north, the River Karasu flows along the middle of the Erzurum-Tbilisi strike-slip fault zone (Westaway, 1990) and acts as a border between the Mt. Dumlu and Mt. Kargapazarı areas. This fault zone is composed of several branches of left-lateral strike-slip faults with NNE strikes (Photos 2.1 and 2.3 and Figure 2.10). In addition to the strike-slip movement, these faults also display significant normal movement. The width of this fault zone between Mt. Dumlu and Kargapazarı is over 20 km. Towards the south, the Karasu river valley widens quickly over a short distance between the

branches of the left-lateral Erzurum-Tbilisi strike-slip fault zone (i.e. between the Arzutu-Kızılkilise and Zağgı-Kızılvank faults) where it changes into an intermontane basin called the Karasu basin or the Erzurum plain (Photos 2.1 and 2.3). In spite of the fact that these faults, together with widespread scree, obscure the stratigraphic correlations in the volcanic succession in most places, the relationship between the volcanic successions of Mt. Dumlu and Mt. Kargapazarı can be clearly observed in the area between the Köşk stream (P:18) and Girekösek village-Karasu valley (K:17) (Figure 2.7).

The volcanic unit in the Mt. Dumlu area unconformably overlies two different tectonic units (see the 1/500000 scale geological map of Eastern Anatolia, Trabzon sheet, Altınlı et. al., 1961):

(1) sedimentary and volcanic units of the Pontides: these include the Lias, Malm and the Cretaceous formations as well as the Eocene volcano-sedimentary units. In the north, between the towns of İspir-Kırık and Pehlivanlı around Mt. Bülanıkdağ, the Erzurum-Kars plateau volcanics are unconformably underlain by Lias and Malm flysch. The Eocene volcano-sedimentary formation, which is called the Narman group is best exposed around the town of Narman. It forms the basement of the volcanic unit over a very large area in the north between the north of Mt. Kargapazarı and Horasan. In the southwest, an imbrication zone containing ophiolitic and sedimentary units of Mesozoic and Tertiary age forms the basement between the towns of Ovacık and Aşkale. This zone also appears to be a part of the Pontides, since it contains slivers of the Malm flysch which is characteristic of the Pontide succession.

(2) the Eastern Anatolian Accretionary Complex: as named by Şengör and Yılmaz (1981) the unit consists of ophiolitic and sedimentary formations which are genetically related to the Neotethys ocean and are trapped between continental blocks resulting from the continental collision which took place about 15 Ma ago. In the south, the basement is generally represented by this unit.

In the area mapped, the base of the Erzurum-Kars Plateau volcanics can be seen neither in the Mt. Dumlu nor in the Mt. Kargapazarı areas, since both are extensively covered by the Erzurum-Kars Plateau Volcanics, the Plio-Quaternary Aras formation and alluvium deposits. The collision-related volcanic sequence reaches its maximum thickness of over 1 km in this area. In this study the three stratigraphic sections (profiles) which have been constructed in the Mt. Dumlu area are as follows:

(I) the Kamber village (R:4)-Kızıldere creek (O:4) section;
(II) the Güngörmez village (J:11)-Mt. Dumlu (G:1) section;
(III) the Kızılkilise village (E:19)-Büyükgüney hill (C:15) section (outside the area mapped).

Photo: 2.1. Panoramic view of the southeastern face of Mt. Dumlu from the east of the town of Dumlu (from V:12). The settlement seen on the right is the town of Dumlu and the plain is the Erzurum-Karasu plain. In the horizon, the peaks which belong to the Mt. Dumlu are over 1 km above the plain form a steep escarpment that lies adjacent to the Erzurum-Karasu plain. This morphology is formed and controlled by the left lateral Arzutu-Kızılkilise strike-slip fault. A large (~10 km^2) alluvial-fan which formed as a result of faulting is seen on the left of the photograph (between Arzutu [V:3] and Kamber villages [S:6]). Two smaller ones are located on the right of the photograph (close to Ağdağ village, [Q:9]) The location of two of the profiles are also indicated on the photograph as I and II (also see Figure 2.4).

(IV) Ağdağ village (Q:9)-Kırkpınar hill (I:9) section (Figure 2.10).

Except for the lower levels of the Kamber Village-Kızıldere stream section, the stratigraphies of these three sections are very similar to each other. In the following paragraphs, the volcanic stratigraphy of the Mt. Dumlu area will be presented with emphasis on the vertical and horizontal variations between and within lava units.

2.1.1. The Lower Tuff (Ltl)

In the Mt. Dumlu area a tuff unit crops out at the apparent base of the volcanic succession. It is mainly composed of consolidated fine ash and lapilli-sized pyroclastic fragments. It varies in thickness reaching over 150-200 m between the villages of Girekösek (M:14) and Karagöbek in the north and in the vicinity of Ümidimyaylası village (R:1). In this study, this epiclastic-reworked pyroclastic sequence is named the Lower tuff after its stratigraphic position in the volcanic succession. In some places, it consists of alternations of fine ash, semi-consolidated or loose siltstone and sandstone beds, all of which are entirely made up of volcanic fragments. In these volcanoclastic beds, soft sediment deformational structures (i.e. slumps) are sometimes present, such as those found to the south of Ümidimyaylası village which is situated to the north of Arzutu village. In this area, small hook-shaped overfolds occur in a zone between undisturbed beds. These folds show no traces of erosion at their upper surfaces and, therefore, are more likely to be related to tectonic deformation, which presumably occurred after the deposition of these beds, rather than sedimentary slumping. If all these sedimentary properties are taken into account, the Lower tuff appears to have been deposited in a shallow water environment, probably a lake.

The lowermost part of the volcanic pile of Mt. Dumlu is also exposed further east in the Mt. Kargapazarı area. To the east of the Karasu river, on the western slopes of Taşlık, Taşlıgüney, Yassı and Kavaklıbaşı hills (O:18), the Lower tuff is underlain by a vitrophyric-porphyritic textured andesite which is named the Köşk pyroxene andesite in this study (Figure 2.6). This unit is, in turn, underlain by a tuff termed the Basal tuff. These two units have a total thickness of 200-250 m. Since this unit is located in the Mt. Kargapazarı area, it will be introduced in the following section of this chapter (i.e. section 2.2, the Mt. Kargapazarı section).

The Lower tuff is overlain by a microporphyritic, amphibole-bearing dacite-andesite in the south, whereas in the north it is overlain by two different volcanic units, namely an aphyric andesite-dacite and quartz-plagioclase bearing porphyritic dacite.

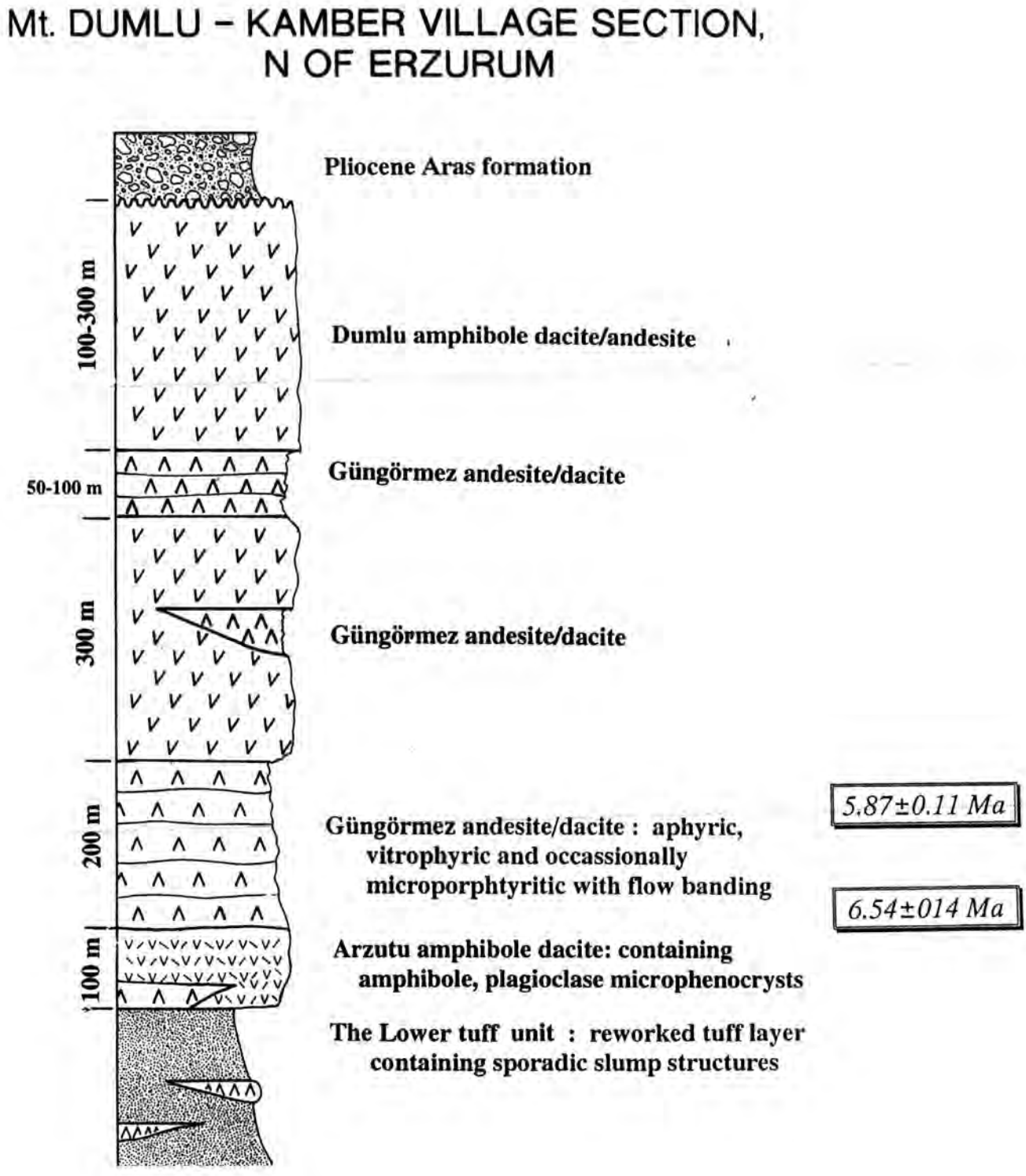

Figure: 2.3. Generalised stratigraphic section of the Mt. Dumlu area.

2.1.2. The Arzutu Amphibole Dacite (Amd)

To the south of Mt. Dumlu, between Arzutu village (V:3) and Kızıldere stream, 1.5 km northwest of Kamber Village (S:6), an amphibole-bearing microporphyritic lava unit overlies the Lower tuff. It forms a 1-2 km wide 7-8 km long strip parallel to the Arzutu-Kızılkilise fault, with a dip to the south-east (Figure 2.4). It consists of massive lava flows, generally showing grey, but sometimes pinkish, colours. Its thickness varies between 50 and 100 m. In this study this unit has been named the Arzutu amphibole dacite after the name of the nearby Arzutu village. It is mainly composed of plagioclase (An_{38-64}), amphibole (magnesio-edenite and tschermakite) and rare ortho- (bronzite and rarely hypersthene) and clinopyroxene (augite) microcrystals. This unit is overlain by the Güngörmez andesite-dacite.

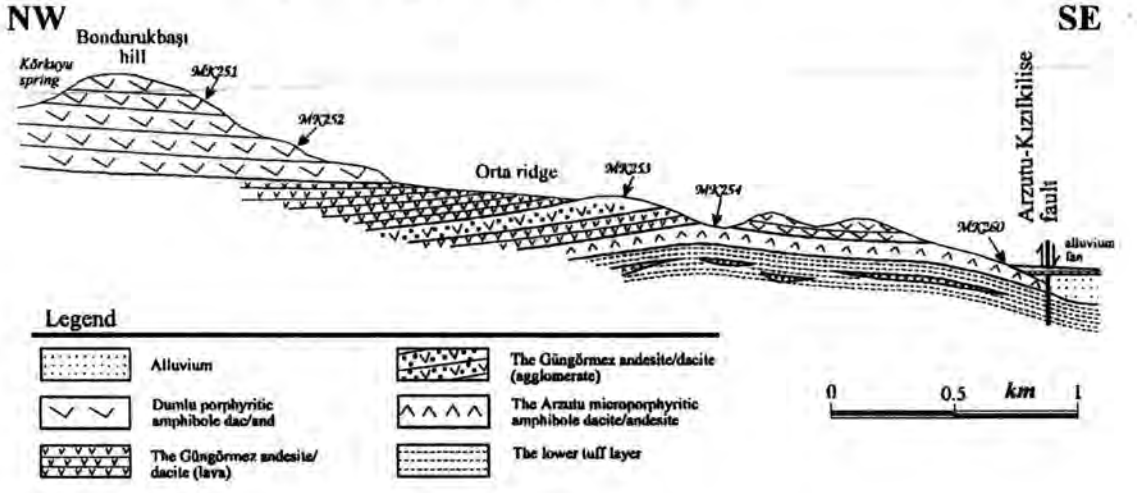

Figure: 2.4. Cross section between Bondurukbaşı hill (O:4) and the Erzurum plain (S:5) showing the relationship between the volcanic units on the SW slope of Mt. Dumlu.

2.1.3. The Güngörmez Andesite / Dacite (Gad)

In the eastern part of the Mt. Dumlu area,. between the villages of Karagöbek in the north and Ağdağ (Q:9) in the south, a volcanic unit composed of aphyric-textured andesitic-dacitic lavas is the first formation overlying the Lower tuff. In this study, a sample collected from its base close to the contact with the Lower tuff in the Kızıldere stream (Q:4) has given a K-Ar age of 6.54±0.14 Ma. Volumetrically, this unit is the most widely exposed in the Mt. Dumlu area, especially in its eastern part. Between Güngörmez village and Közek hill (H:10), close to the Arzutu-Kızılkilise strike-slip fault, it attains a thickness of over 600 m. Its colour varies from black to pale grey and also to different shades of beige and khaki. In this study this unit has been named the Güngörmez dacite-andesite after the area around the Güngörmez village (K:10) where its best outcrops are located.

In some levels, the Güngörmez dacite-andesite contains hard, compact black vitreous dacitic lava flows characteristically displaying vitrophyric textures. In this study, one of these vitrophyric flows almost at the top of the unit has been mapped and named the Black dacite on the basis of its characteristic colour. It is situated 2.5 km north of the Güngörmez village, covering a 3 km² area in the vicinity of Karaçağıldüzü (G:10), Karaçağıl hill and Şehitler hill. It consists of sporadic microphenocrysts to microcrystals of plagioclase (An_{51-52}) and very rare microcrystals of clinopyroxene (augite, endiopside) and orthopyroxene (bronzite) within a glassy groundmass which comprises over 95% of the rock. A sample taken from this unit has been dated by whole-rock K-Ar method at 5.87±0.11 Ma (see Appendix A).

The Güngörmez dacite-andesite also contains highly vesicular zones, which are generally located towards the top of individual lava flows. This kind of lava flow is especially abundant between the vicinity of Çarmakdüzü and the Çerences ridge (O:10), situated to the north of Ağdağ village.

Photo: 2.2. Güngörmez dacite-andesite showing platy-jointing close to the basal surface of an individual lava flow, SE of Zinavuryayla highland, NE of the summit of Mt. Dumlu (C:11).

In general, the Güngörmez dacite-andesite forms massive lava flows showing almost constant texture and colour. It usually does not show any oxidised zones at the top of flows. Therefore, it is generally difficult to recognise individual lava flows within this unit. In some places, lava flows include platy-jointing (related to flow-banding) which has been developed parallel to the basal surface as a result of intensive shear between the channel walls and the coherent central part of lava. Close to the base, the distance between these joints is in the order of centimetres and even millimetres, generally around 1 cm (Photo 2.2). The joint spacing increases upwards and, after a certain limit, it disappears where the lava turns into a massive body. In the field, this platy-jointing is one of the criteria which has been

used to differentiate individual lava flows from each other. On the northern slops of Mt. Dumlu, in the vicinity of Karaçağıl (F:11), the Şehitler hills (E:12) and Karaçağıl ridge, very good examples of this flow structure have been observed.

2.1.4. The Girekösek Dacite (Gpd)

To the north of Girekösek village, near the Petekligüney ridge and Karagöbektabya hill (L:15), a quartz-plagioclase-bearing porphyritic lava unit is located in the upper levels of the Lower tuff (Figure 2.7). This lava unit, which has a lens shaped outcrop exposure, covers just over 1 km^2 area, with a maximum thickness of 70-100 m. Apart from its texture, it displays almost the same colour and composition as the Güngörmez dacite-andesite. It generally contains rounded, magmatically-corroded quartz and euhedral/subhedral plagioclase phenocrysts in a black, glassy groundmass. In this study, this unit is named the Girekösek dacite after the nearby Girekösek village. It also crops out 1 km east of the town of Dumlu, next to the Zağgı-Kızılvank fault in the Mt. Kargapazarı area (W:11). In this area, the unit occupies about 4-4.5 km^2 with a maximum thickness of 50-70 m. Its outcrop pattern is aligned parallel to the east of the Zağgı-Kızılvank fault, dipping to the west and northwest with around 15-20° (Figure 2.8).

2.1.5. The Dumlu Amphibole Dacite / Andesite (Dpad)

The Dumlu amphibole dacite/andesite is the uppermost unit which forms the highest peaks in the area. In the north, Mt. Dumlu (3200 m) (G:1), Mt. Eğerli (3087 m) (B:1), Sarıçağıl (2953 m) (H:4) and Kuşyurdu (2989 m) (F:2) hills are all composed of this unit. In this study, it is named after Mt. Dumlu where its best outcrops are exposed. Its thickness varies widely but reaches over 400-450 m in the vicinity of Mt. Dumlu. Characteristically, it consists of porphyritic dacite/andesite and displays variable shades of grey and pinkish-yellowish colours. Plagioclase (An_{37-65}), amphibole (magnesio-ferri-tschermakite, magnesio-edenite, occasionally magnesio-alumino-kaersutite and magnesio-ferri-taramite), orthopyroxene (mainly bronzite with some hypersthene: clinoenstatite$_{67-80}$) comprise the main phenocryst phases. It also contains microlites of plagioclase and rare clinopyroxene (mainly augite and rarely endiopside).

Between the villages of Zinavuryayla (B:8) in the north and Ağdağ village (Q:9) in the south, the contact between this unit and the underlying Güngörmez dacite-andesite is quite sharp and planar. In this area, the unit is entirely made up of massive porphyritic lava flows, whereas on the south slope of Mt. Dumlu, in the vicinity of the Pokluboyun (M:6) and Mihribat (P:5) hills and Kızıldere stream it is interlayered with the lenses of aphyric lavas of the Güngörmez dacite-andesite. One of them is situated

between Mihribat hill and the Çamurkıran ridge (O:7) as a 3.5 km long, approximately 50-100 m thick lens. The other is located in the upper level of the unit in the vicinity of Pokluboyun (M:6), Sarıbeyin, Körkuyu (N:7), Göller and Kırkgöze (K:7) hills and covers 17-18 km^2 area with a thickness of 100-150 m. The contact between the unit and these lenses is also sharp and planar. Both of these lenses show almost the same composition, field appearance and texture as the Güngörmez dacite-andesite.

2.2. THE Mt. KARGAPAZARI AREA

To the northeast of Erzurum, between the Mt. Dumlu area in the west and the Pasinler Plateau in the east, a series of elongated peaks over 2700-3000 m in altitude form a northeast-southwest (NNE-SSW) trending ridge (Photos 2.3 and 4). This 15-17 km long ridge separates the Erzurum Plain from the Pasinler Plain and the Pasinler Plateau in the east. This ridge as a whole is called Mt. Kargapazarı. In fact, it represents the westernmost and the highest edge of a 15-17 km long and 3-5 km wide high plateau, called the Kargapazarı plateau, which is inclined at 10-15° to the southeast. In this study, the area between the Karasu river valley and the Erzurum plain in the west and the Pertek-Karakale fault in the east is named as the Mt. Kargapazarı area (Figure 2.10). The Mt. Kargapazarı ridge and plateau themselves are situated in the middle of the area.

The volcanic succession in the Kargapazarı area is cut by a series of northeast-southwest striking, left-lateral strike-slip faults which belong to the Erzurum-Tbilisi strike-slip fault zone. In addition to the strike-slip movement, these faults exhibit a normal movement. In general, the eastern or southeastern sides of these faults comprise the upthrown block (Photos 2.3 and 4), although there are some exceptions, e.g. the Karakale Pertek fault. The Kargapazarı plateau is bounded by two of these faults: the Kargapazarı fault in the northwest and the Karakale-Pertek fault in the southeast. The Kargapazarı fault, which lies adjacent to the Mt. Kargapazarı ridge, forms a steep, 300-350 m high escarpment on which a good section of the volcanic succession is exposed (Photo 2.4). This fault appears to be responsible for the general tilting of the plateau to the southeast.

The area located between the River Karasu in the west and the Kargapazarı fault in the east is cut by several strike-slip faults showing southwest-northeast strikes. These are also the branches of the Erzurum-Tbilisi fault zone. Elongation of some streams, such as the Karasu and the Köşk, is caused by these fault lines. Compared to the adjacent Kargapazarı Plateau, this area has completely lost its plateau shape as a result of faulting and intensive erosion (Photo 2.4).

Photo: 2.3. Panoramic view of the area between the Mt. Kargapazarı ridge and the northern entrance of the Erzurum-Karasu plain taken from north of Çipak village (O:11), on the SE skirts of Mt. Dumlu. The white coloured unit which crops out adjacent to the plain is the Pliocene Aras formation (Pla) which is mainly made up of detrital lithologies most of which have been gathered from the Erzurum-Kars Plateau volcanics. In this area, the most significant geomorphologic elements are the NE-SW striking strike-slip faults that belong to the Erzurum-Tbilisi fault zone. They exhibit well-formed linear alignments in the morphology and juxtapose different formations as well as different levels of the same units. Abbreviations: Qal: Quaternary alluvial deposits, Qalo: old alluvium, Pla: the Pliocene Aras formation, Gad: the Güngörmez andesite/dacite, Ltl: the Lower tuff, Kpa: the Köşk pyroxene andesite/dacite. DTF: Dumlu-Tafta fault, ZKF: Zağı-Kızılvank fault, *KF: Kargapazarı Fault. For comparison, see Figure 2.10, the geological map of the area in 1/100000 scale.*

Photo: 2.4. A general view of the northwestern face of Mt. Kargapazarı ridge (~3000-3100m) and the foothills from Sutaşı hill (P:17). In this area, a set of NE-SW striking mostly right-lateral strike-slip faults cut the volcanic units forming an en echelon fault system whose blocks create a step-like morphology. The NE-SW extending valley located between the foothills and the Sutaşı hill from which the photographs were taken is also formed by one of these faults, named in this study the Köşk fault (KF). At the back, one of these major faults, the Kargapazarı fault (KPF), creates a ~500m high escarpment on which a good section of the volcanic succession is exposed (the Karapınar ridge section [KRS]; see Figure 2.9). Blt: the Basal tuff, Gad: the Güngörmez andesite/dacite, Çpd: the Çobandede dacite, Kpa: the Köşk pyroxene andesite.

Mt. KARGAPAZARI SECTION, N OF ERZURUM

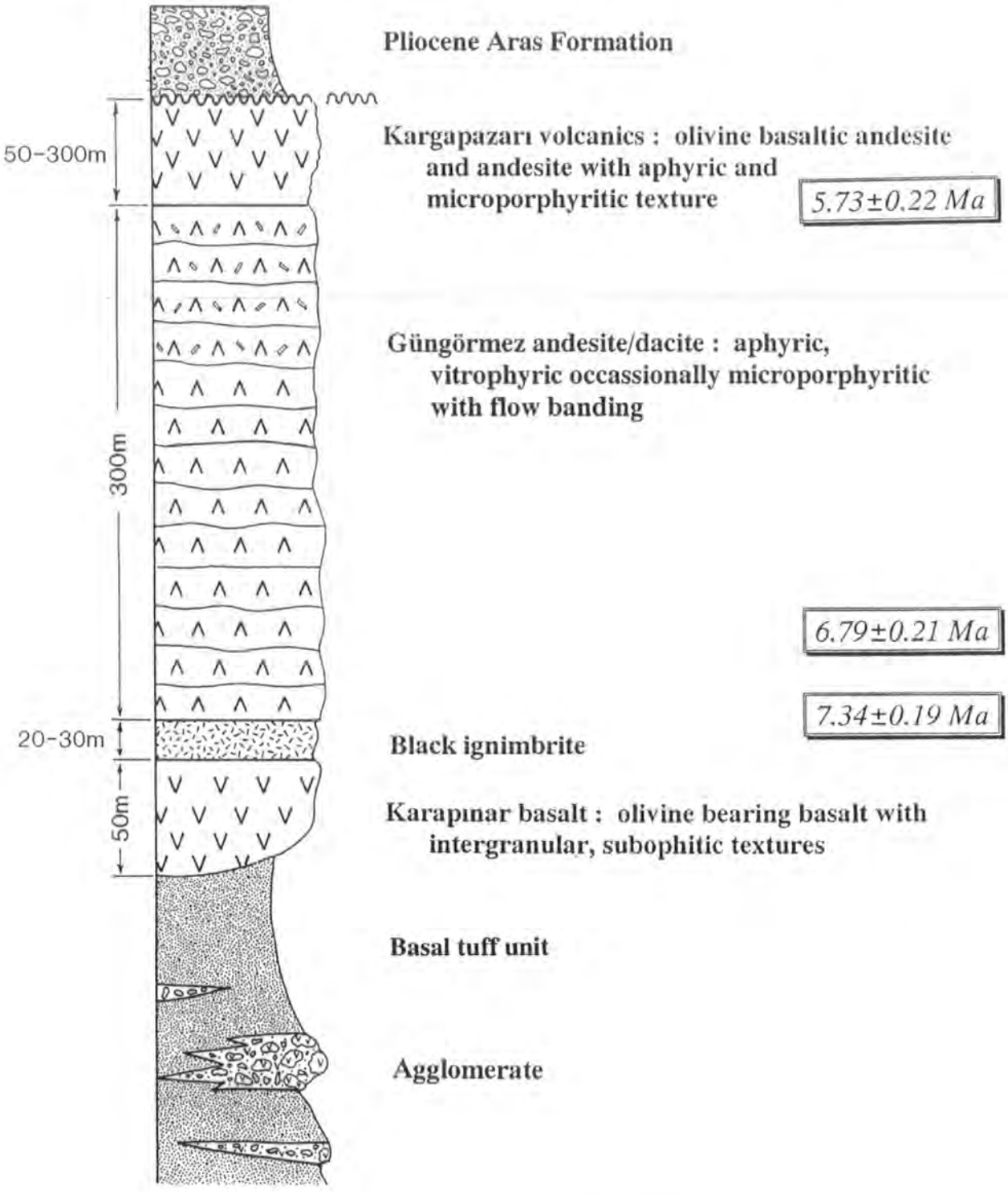

Figure: 2.5. Generalised stratigraphic section of the Mt. Kargapazarı area.

The Erzurum-Kars Plateau Volcanics (EKPV) are brought adjacent to the Erzurum plain by one of these faults, which is called the Zağgı-Kızılvank fault, in the southwest (Photo 2.3). Adjacent to this fault, lava and pyroclastic units of the EKPV dip to the northwest at about 20-25° as a monoclinal flexure. Away from this fault, about 2½-3 km to the east, the dip decreases and the lavas become almost horizontal. In fact, the direction of dip of the lava flows fluctuates because of vertical offset on the strike slip faults that cut this part of the EKPV, and also presumably because of the palaeo-topographical irregularities. The flexure extends parallel to the fault all along the western slopes of the Mt. Kargapazarı area. Together with the Kargapazarı Plateau located to the east, which dips at 10-15° to the SE, the flexure forms the NW limb of a wide antiform, whose axis is located close to and parallel with the Kargapazarı fault with a strike of SW-NE. The NW limb of this antiform is cut, lowered and partly terminated by the faults which have significant vertical offset and left lateral movement.

In the following paragraphs the volcano-stratigraphy of the Kargapazarı area will be introduced from the base to the top.

Photo: 2.5. General view of the Kışlaköy volcanic member of the Upper Eocene Narman Group in the vicinity of Yukarıhinzorik (A:29) village, SE of the town of Tortum. In this location, the unit is composed of the alternations of agglomerate and intermediate lavas that dip to the northwest at about 40-50° .

In the mapped part of the Kargapazarı area, the basement of the Erzurum-Kars Plateau Volcanics (EKPV) is not exposed. This basement crops out further north outside this area in the vicinity of Yukarıhinzorik (A:29) and Hamidiye (C:33) villages, to the southeast of the town of Tortum. In this location, it consists of the Kışlaköy volcanic member of the Late Eocene Narman formation (Photo 2.5).

In the Mt. Kargapazarı area, a tuff unit which contains intercalations of agglomerate forms the base of the volcanic pile. It shows similarities to the Lower tuff exposed at the base of Mt. Dumlu although the Lower tuff represents a higher stratigraphic level. Several strike-slip faults cutting the western part of the Mt. Kargapazarı area complicate the stratigraphic interpretations in this part of the area since they juxtapose different levels of the volcanic sequence. The Basal tuff is overlain by three different lava units: (1) an aphyric andesite-dacite unit showing similarities to the Güngörmez andesite-dacite which covers large areas in the Mt. Dumlu area; (2) a porphyritic clinopyroxene andesite which is named in this study the Köşk pyroxene andesite as its best outcrops are located close to Köşk village; and (3) an intergranular to subophitic-textured basaltic lava flow which outcrops in a small area east of the Kargapazarı fault.

2.2.1. The Basal Tuff (Btl)

The base of the succession is exposed in the vicinity of Köşk village (R:16) and along the Köşk stream valley which is located about 5 km northeast of the town of Dumlu. At the apparent base of the volcanic succession, a reworked tuff unit crops out. In this study this unit is named the Basal tuff owing to its stratigraphic position in the succession. It consists of interbeds of reworked tuff, unconsolidated or slightly consolidated silt and fine sand, agglomerate and ash. It occasionally contains thin basic to intermediate lava lenses. Silt and sand beds are entirely composed of volcanic material and display ripple-mark and cross bedding in places. They are mostly very well sorted. They generally display white and cream colours although the colour varies widely from yellow, beige to red and greenish-grey in places. On the north slope of Horumsuma hill, the Basal tuff is interlayered with the Köşk pyroxene andesite.

The agglomerate crops out as small lenses. Three of these lenses, which are located upward in the Basal tuff close to the contact with the Köşk pyroxene andesite, have been mapped. The first is situated 1 km northwest of Köşk village on the southwest slope of Armutağacıbaşı hill (Q:15) and has a thickness of about 20-30 m. The second reaches over 70-80 m in thickness and is located about 3.5 km northeast of the same village. The third, 2½ km southwest of Köşk village in the Horumsuma valley, is located between Horumsuma hill (S:14) and Kızılvank village (T:12). All three are laterally wedged within the Basal tuff. In general, they are made up of moderately rounded, aphyric intermediate lava fragments varying in size from sand, through pebble to big blocks and boulders reaching up to ½ m in diameter. They generally exhibit a good stratification with lenses of fine-grained volcanoclastics.

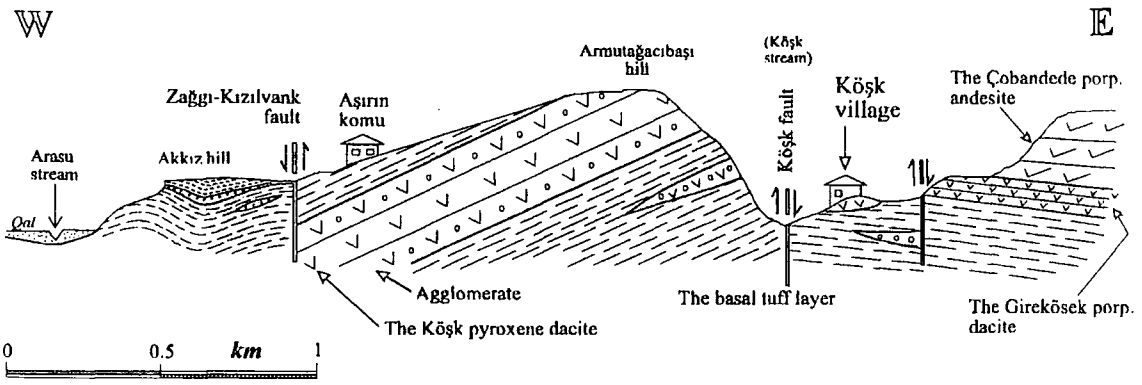

Figure: 2.6. Cross section between Arasu stream (Q:14) and Köşk village (R:16), west of Mt. Kargapazarı.

In the south and southeast of the Mt. Kargapazarı area, the Basal tuff is exposed as isolated patches of outcrops. One of these lies in the Komdere stream valley, to the north of Küçüktüy village. Two others are located adjacent to the Pertek-Karakale fault, north of the Pertek (AB:20) and Haykürt (Z:24) villages respectively. In this area, the Basal tuff displays almost the same properties as in the western areas, except for some pyroclastic fragments derived from pyroclastic falls and flow deposits, e.g. vesicular pumice, obsidian and ignimbrite. The relative abundance of these fragments increases eastward towards the Pasinler area.

2.2.2. The Köşk Pyroxene Andesite (Kpa)

The Köşk pyroxene andesite outcrops in a relatively confined, ridge-shaped area between the Zağgı-Kızılvank and Köşkdere faults which includes the Taşlıgüney, Yassı, Kavaklıkbaşı (O:18), Musruklar, Sutaşı (P:16), Armutağacıbaşı and the Horumsuma (S:14) hills. At its base it lies over the Basal tuff. The Köşk pyroxene-andesite consists of coarse, mostly euhedral clinopyroxene phenocrysts (augite) with minute orthopyroxene (bronzite) and plagioclase ($An_{60-64.4}$) microcrystals and microlites enclosed in a glassy groundmass. It generally has a vitrophyric texture. Since its best outcrops are seen close to the Köşk village, this volcanic unit has been named the Köşk pyroxene-andesite. This unit has a thickness of approximately 100-150 m. Towards the southeast it gets thinner, and to the south of Horumsuma hill (1½ km southwest of the Köşk Village) it wedges out laterally. The Köşk pyroxene-andesite does not outcrop in any other part of the area studied.

The Karasu river valley located to the north of Kelevürt village (O:13) is best displays the relationship between the volcanic successions of the Mt. Kargapazarı and Mt. Dumlu areas, despite the presence of strike-slip faults (Figure 2.7). On the northwest slope of the Sutaşı-Taşlıgüney ridge, the Köşk pyroxene-andesite is overlain by a tuff unit which is laterally equivalent to the Lower tuff in the Mt. Dumlu area. It

contains agglomerate lenses one of which attains a thickness of 15-30 m and outcrops widely on both sides of the southern entrance to the Karasu river valley between Kelevürt and Girekösek (M:14) villages. In the north, the Lower tuff unit is in turn overlain by the Girekösek dacite in the vicinity of Karagöbektabya hill, which is located between the villages of Girekösek and Karagöbek (Figure 2.7). It covers an area of over 1 km^2. The same unit is exposed further southwest in the Mt. Kargapazarı area adjacent to the Zağgı-Kızılvank fault between Kızılvank village and the Tufançyayla ruins (Y:11) (Figure 2.8). The Girekösek dacite is overlain by the aphyric intermediate lava flows of the Güngörmez andesite/dacite i.e. the most abundant volcanic unit of Mt. Dumlu. The Güngörmez andesite/dacite also crops out in a large area to the southwest of Mt. Kargapazarı.

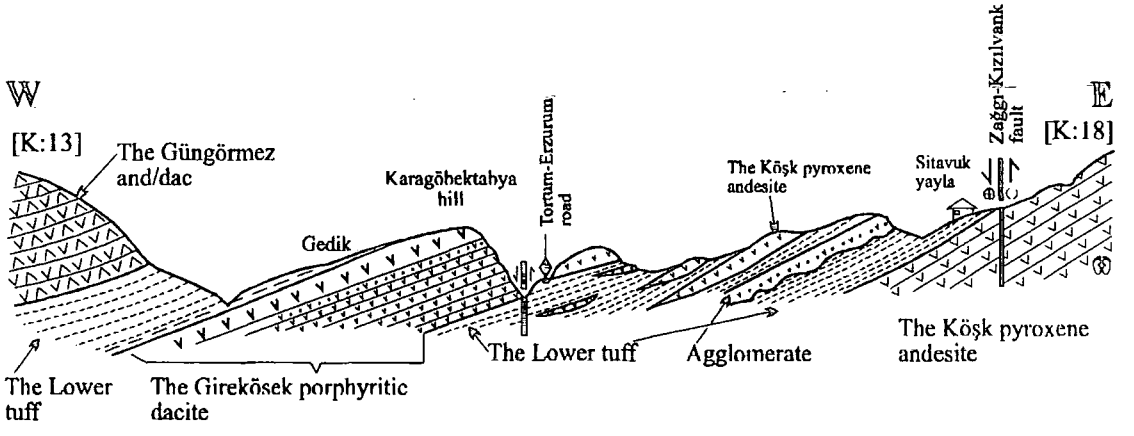

Figure: 2.7. The cross-section showing the relationship between volcanic units of the Mt. Dumlu and the Kargapazarı areas.

2.2.3. The Güngörmez Andesite / Dacite (Gad)

The Güngörmez andesite/dacite has been introduced in detail in the previous section (i.e. the Mt. Dumlu area) and as in the Mt. Dumlu area this unit is mainly composed of aphyric textured, andesitic-dacitic lavas in the Kargapazarı area. It is the most widespread unit exposed between the Kargapazarı and Zağgı-Kızılvank faults where its thickness exceeds 300-350 m, becoming thinner to the east. To the east of the Kargapazarı fault, in the vicinity of Karapınar ridge (S:21) and Haramikaya hill (R:22), its thickness decreases to 200 m and it is overlain by olivine-bearing intermediate to basic lavas of the Kargapazarı volcanics. To the southeast, it appears to have wedged out beneath the Kargapazarı volcanics somewhere close to the middle of the Kargapazarı plateau, since this unit does not outcrop anywhere else on the southeast slope of Mt. Kargapazarı.

A sample taken from the base of the unit 1 km south of Köşk village gives a K-Ar age of 6.79±0.21 Ma. Another sample taken from the summit of Kandil hill (3149m)

(K:26), located about 5 km east of Zağgı village (G:20), outside the area mapped, gives a K-Ar whole rock age of 7.34±0.19 Ma.

2.2.4. The Çobandede Dacite (Çpd)

Between the Köşkdere and Kargapazarı faults, close to its base, the Güngörmez andesite-dacite contains thick lenses of porphyritic pyroxene bearing lava flows whose general appearance and texture are quite similar to those of the Güngörmez andesite-dacite. These lavas are predominantly dacitic and sometimes andesitic in composition and mainly composed of abundant plagioclase (An_{53-29}) ortho (bronzite) and clino-pyroxene (augite) phenocrysts in a glassy matrix. They are generally massive. These

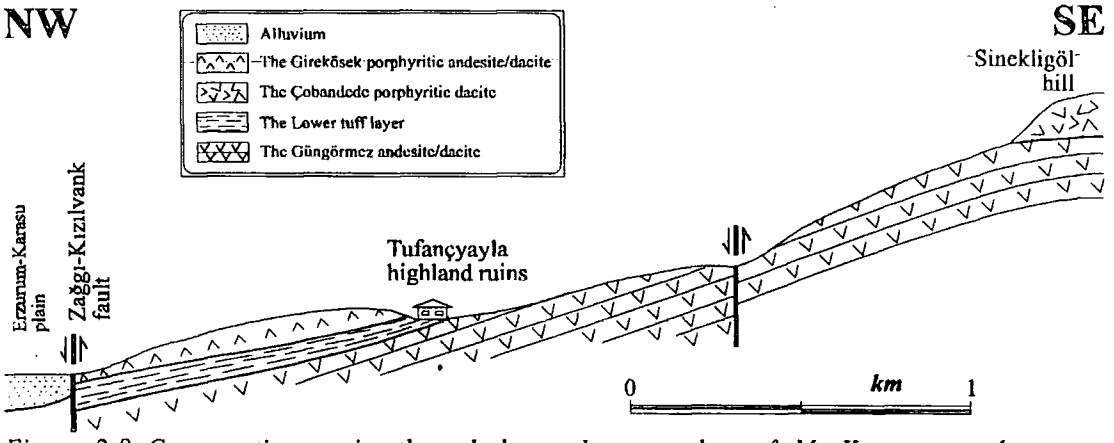

Figure: 2.8. Cross-section passing through the southwestern slope of Mt. Kargapazarı, between the Erzurum plain (V:11) and Sinekligöl hill (W:16).

rocks are named in this study the Çobandede dacites since the best outcrops of this unit are exposed on the Mt. Çobandede (AB:14), 2 km east of Köseahmet village (AB:11). Outcrops of the Çobandede dacite extend parallel to the faults striking southwest-northeast and cross all the area mapped. They crop out from southwest to northwest as three lenses: the first one covers Mt. Çobandede and the Zilligüney (Z:13), Sinekligöl (Y:13), Karanlıkdere (Y:14), Katırcıkellesi (X:15) and Sarp (W:16) hills; the second one is located 1½ km east of the Köşk village and includes the Deveyatağı and Sultanmurat (U:17) hills and the Mezarlıksırtı ridge (S:18); and the last one crops out 2-2½ km north of Köşk village (P:19). This unit does not outcrop anywhere else in the area.

2.2.5. The Girekösek Dacite (Gpd)

The Girekösek dacite unit is named after its best outcrops in the Mt. Dumlu area close to the Girekösek village and is described in Mt. Dumlu section (Section 2.1.4). In

the Mt. Kargapazarı area, the unit is exposed 1 km east of the town of Dumlu (U:10), as a 1 km wide, 4 km long strip adjacent to and east of the Zağgı-Kızılvank fault. This unit displays a petrography and field appearance similar to the Güngörmez andesite/dacite unit which underlies it. The only difference is that it shows a porphyritic texture with plagioclase and quartz megacrysts. Between these two units, a tuff unit outcrops as laterally discontinuous lenses (Figure 2.8). The thickness of the unit ranges from approximately 10 to 50 m.

2.2.6. The Karapınar Basalt (Kb)

To the west of the Kargapazarı ridge, between the Karapınar ridge and Baldırkanlıbaşı hill (Q:22), a 300-350 m thick section of the Kargapazarı Plateau is exposed adjacent to the Kargapazarı fault (Photo 2.4). This is one of the best sections in the Mt. Kargapazarı area and is named the Karapınar section (Figure 2.9). At the apparent base of this section, an intergranular to subophitic textured basalt succession

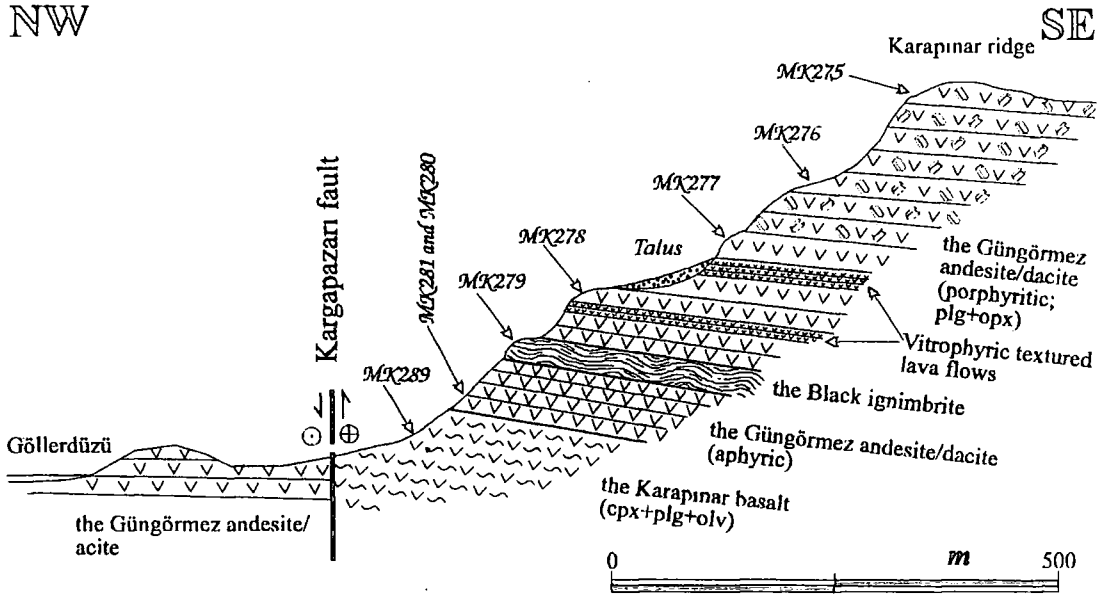

Figure: 2.9. Figure displaying the volcanic succession exposed on the northwestwern face of the Kargapazarı ridge between Göllerdüzü (S:19) and the Karapınar ridge (T:21).

crops out. It is made up of plagioclase (An_{37-38}) and olivine ($Fo_{83.8-85.2}$) phenocrysts and microphenocrysts which are partly surrounded by clinopyroxene phenocrysts (salite) and a glassy matrix. This unit is exposed in a very restricted area between the Bakacak (R:21) and Çingeneyurdu (U:19) hills. Further south, it also outcrops in a very small area in the vicinity of Küçüktüy highland (X:19), which is located 4 km north of Pertek village. This unit is named in this study as the Karapınar basalt since it is located close to the Karapınar ridge. It is one of the most basic lava unit from the studied part of the

Erzurum-Kars Plateau. The apparent thickness of the Karapınar basalt is around 50-80 m. It is restricted to this area of the Erzurum-Kars Plateau.

In the Karapınar section, the Karapınar basalt is overlain by an andesite/dacite lava unit which is aphyric to vitrophyric in texture (Figure 2.9). This unit is very similar to the Güngörmez andesite-dacite and is most probably its lateral equivalent. Its thickness is about 150-170 m. In the middle of this unit a 5-10 m-thick black ignimbrite crops out. It exhibits a well-developed eutaxitic texture with lithic fragments and fiammé, and shows similarities to the Black ignimbrite which outcrops widely in the Pasinler area. Towards the top of the section, a porphyritic andesite/dacite overlies the Güngörmez andesite-dacite, with a thickness of 50-70 m. It contains plagioclase, ortho- and clinopyroxene phenocrysts and shows porphyritic-intersertal and hyalopilitic textures. This unit shows similarities to the Çobandede dacite. In the area mapped, the southwest-northeast elongated peaks on the Kargapazarı ridge are mostly composed of this unit. Finally, an olivine-bearing basaltic to andesitic lava unit, namely the Kargapazarı volcanic unit, overlies all of these units.

2.2.7. The Göllerdüzü Amphibole Dacite (Gpaa)

To the north of Çingeneyurdu hill (U:19), which is located 2½ km southeast of the Köşk Village, a porphyritic amphibole-bearing dacitic lava unit crops out in an area of less than ½ km^2. It forms a dome-shaped body with a thickness of 40-60 m and overlies the Güngörmez andesite-dacite (T:18). It contains plagioclase and amphibole phenocrysts in a glassy groundmass and thus resembles the Dumlu amphibole dacite/andesite which covers large areas in the Mt. Dumlu area. This unit is presumably the product of same volcanism but does not outcrop elsewhere in the Kargapazarı area.

2.2.8. The Kargapazarı Volcanics (Kv)

To the east of the Kargapazarı ridge, at the top of the succession, an olivine-bearing basaltic to andesitic lava unit outcrops widely. It is mainly made up of plagioclase (An_{78-49}), olivine ($Fo_{75.6-84}$) and clinopyroxene (endiopside and augite) microphenocrysts and microcrystals. This unit is named the Kargapazarı volcanics in this study as it forms the best outcrops on the Kargapazarı Plateau. The basal units described earlier completely disappear, presumably by laterally wedging out into the Basal tuff to the east of the Kargapazarı ridge. On the southeast slope of Mt. Kargapazarı, the Kargapazarı volcanics are the only lava unit overlying the Basal tuff. Further east, in the Pasinler area, the Kargapazarı volcanics are exposed as relatively thin patches and overlie the Black ignimbrite.

Photo 2.6. Field photograph of SE face of the Kargapazarı ridge taken from the N of Kotandüzü village, NW of Pasinler (S:33). In this location, the Kargapazarı plateau which is mainly formed by the Kargapazarı volcanics is cut and lowered by the NE-SW striking Karakale-Pertek strike-slip fault. The valley which runs in the middle of the photograph is the Büyükdere stream valley where a magnificent section of pyroclastic flow and fall deposits of the Pasinler area is exposed (see Section 2.3.1.2. the Büyükdere gorge section).

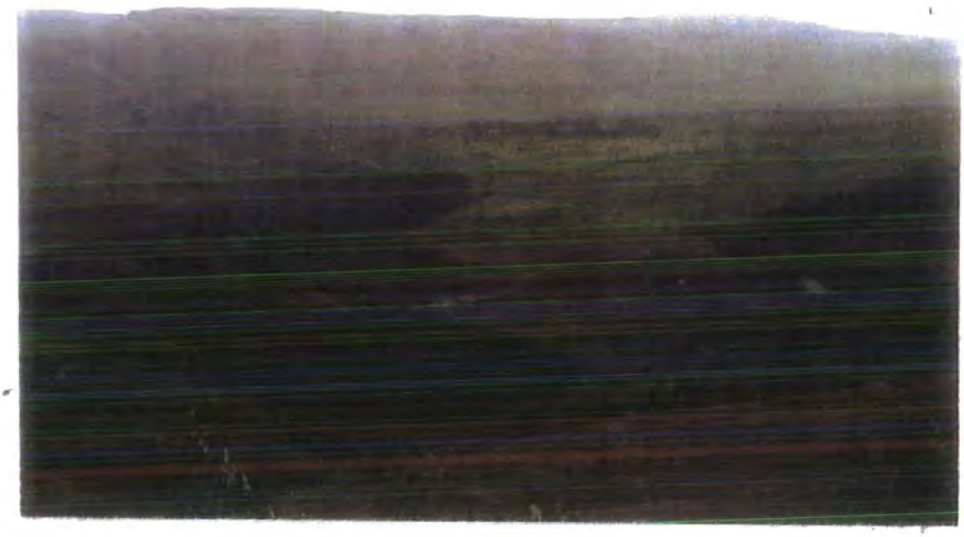

The Kargapazarı volcanics get thicker to the east. On the south slope of the Kargapazarı plateau, the unit attains a thickness of about 250-300 m. To the north of Acıköy village (V:28), in the vicinity of Kurtgüneyibaşı (T:27) and Arpaçukuru (S:28) hills and Mağarasırtı ridge, it is made up of scorious lava flows.

EXPLANATIONS

THE Mt. DUMLU AREA

Qaf	Alluvial fans
Qal	Quaternary alluvium
Qalo	Old alluvium
Pla	Pliocene Aras formation: detrital sediments
Dpad	Dumlu amphibole dacite/ andesite: porphyritic lava domes
Gpd	Girekösek dacite: quartz & plg bearing porphyritic lavas
Gad	Güngörmez andesite/dacite: aphyric lavas
Amd	Arzutu amphibole dacite: microporphyritic lava domes
Ltl	The Lower tuff unit: volcano-sedimentary beds

THE Mt. KARGAPAZARI AREA

Qls	Land-slides
Qal	Quaternary alluvium
Pla	Pliocene Aras formation
Kv	Kargapazari volcanics: olivine bearing basaltic to intermediate lava flows
Gpaa	Göllerdüzü amphibole dacite/andesite: porphyritic lava domes
Krbas	Karapinar basalt: subophitic basaltic lavas containing cpx+plg+olivine
Gpd	Girekösek dacite: quartz and plagioclase bearing porphyritic lavas
Çpd	Çobandede dacite: opx and plg bearing porphyritic lavas
Gad	Güngörmez andesite/dacite: aphyric lava flows
Kpa	Kösk pyroxene andesite: cpx & plg bearing porphyritic lava flows
Btl	Basal tuff unit: pyroclastic fall and reworked deposits, rhyolitic in composition

THE PASINLER AREA

Qls	Land-slides
Qal	Quaternary alluvium
Pla	Pliocene Aras formation
Aign	Ardiçlidag ignimbrite unit: rhyolitic pyroclastic flows
Ard	Ardiçlidag rhyolite: lava domes and flows
Utl	Upper tuff unit: rhyolitic pyroclastic falls
Kv	Kargapazari volcanics
Büan	Büyükdag amphibole andesite: porphyritic domes and lava flows
Bign	Black ignimbrite: crystal rich trachy-dacitic pyroclastic flows
Wign	White ignimbrite: aphyric rhyolitic pyroclastic flows
Mtl	Middle tuff unit: pyroclastic fall deposits of rhyolitic composition
Kpd	Kizilveren amphibole dacite/ andesite: porphyritic lava dome
Ltl	Lower tuff unit: rhyolitic pyroclastic fall deposits
Baa	Black aphyric andesite: lava flows
En1	The Kislaköy volcanic member of the Narman group: andesites & basalts
En	Eocene Narman formation: flysch like fine detritals

GEOLOGICAL MAP OF Mt. DUMLU, Mt. KARGAPAZARI AND PASINLER AREA ERZURUM, NORTHEASTERN TURKEY

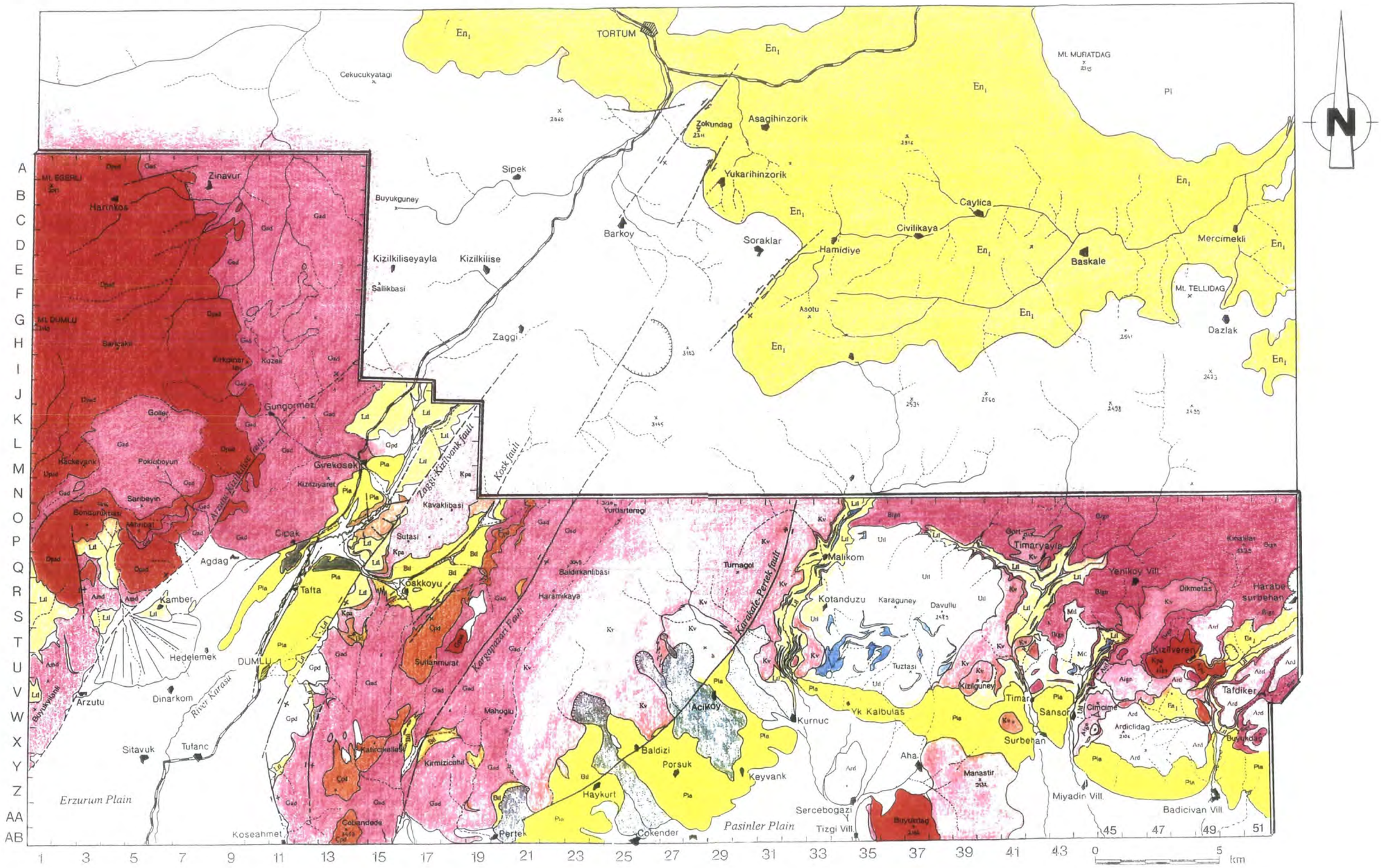

2.3. THE PASINLER AREA

The town of Pasinler, around 25 km east of the city of Erzurum, is located on the south slope of Mt. Hasandağ (2200 m), which is a single cone-shaped topographic irregularity close to the northern edge of the Pasinler plain. The Pasinler plain represents the second biggest W-E extending intermontane basin after the Muş Basin, in Eastern Anatolia. Both of them may have been tectonically controlled by W-E striking reverse faults along their north and south margins. To the north of this basin, the young (Upper Miocene-Pliocene) volcanic rocks of the Erzurum-Kars Plateau are widespread whereas, to the south, they only form small, discrete outcrops with the exception of the Palandöken ridge in further west. In the south they are unconformably underlain by older formations of Late Cretaceous (East Anatolian Accretionary Complex: ophiolitic mélange basement), Eocene (Bulkasım formation and Narman formation: flysch and volcanics) and Early to Middle Miocene age (Hündül limestone: reefal limestone, Güllüce and Aşkale formations). Therefore, only the northern part of the Pasinler area has been chosen to be mapped in detail. In this study, the Pasinler area will be introduced in two sections, as first the northern and then the southern areas.

2.3.1. THE NORTH OF PASINLER

The area located to the north of the Pasinler plain is bounded in the west by the Mt. Kargapazarı Ridge with the left-lateral Pertek-Karakale strike-slip fault acting as the border between the Mt. Kargapazarı ridge and the Pasinler area. This fault juxtaposes two parts of the volcanic succession that differ considerably in terms of their volcano-stratigraphy and topography. To the west of this fault, Mt. Kargapazarı, which is mainly made up of intermediate to basic lava flows with subordinate pyroclastic deposits at the base, forms a high (2700-3150 m), narrow and long plateau shaped morphology. This plateau extends as a long NNE-SSW trending ridge between the Pertek-Karakale and the Mt. Kargapazarı strike-slip faults (SSW-NNE). It forms a steep escarpment adjacent to the latter (Photo 2.6). The plateau in question is slightly inclined (~10°) towards the SE, namely towards the Karakale-Pertek fault. In contrast to Mt. Kargapazarı, the Pasinler Area dominantly consists of pyroclastic flow and fall deposits associated with less voluminous intermediate to acidic lava flows.

The Pasinler Area also has a plateau morphology with an average height of 2200-2300 m from the sea level, about 600-700 m lower than the Mt. Kargapazarı plateau. This plateau is made up of several pyroclastic fall and flow units and less voluminous lava flows, which are more common towards the top of the succession.

Stratigraphically, these units are a lateral continuation of the pyroclastic-rich Basal tuff unit of the Mt. Kargapazarı area. In this study, this plateau has been named the "Pasinler Plateau". The lava and pyroclastic units of the Pasinler Plateau are generally horizontal. However, to the south, close to the Pasinler Plain, they dip southward (~20-30°) as a monoclinal flexure (Photo 2.7) and are unconformably overlain by the subaerial detritals of the Pleistocene Aras formation and Quaternary alluvium deposits. The hinge line of this monoclinal flexure is continuous throughout the southern margin of the Pasinler Plateau with an approximate W-E strike.

The Pasinler area has been studied in more detail than the other areas discussed in this chapter. As well as being easily accessible from several roads, it provides the best exposures throughout the lower parts of the volcanic pile, from lavas and pyroclastics which are in contact with the Eocene basement rocks (in the Harabedere valley) to the plateau-forming lavas that make up the uppermost part of the volcanic succession.

On the Pasinler Plateau, unconsolidated pyroclastic fall and tuff units which are widespread, especially at the base of the succession, are armoured by a relatively erosion-resistant, overlying black pyroclastic flow unit (the Black ignimbrite). The Black-ignimbrite internally consists of several black or reddish coloured pyroclastic flow units which are phenocryst-rich, densely welded and sometimes rheomorphic, with well- developed flow fabrics (Photo 2.10). This pyroclastic flow unit gives the plateau its distinctive topography and covers almost half of the Pasinler Plateau.

The Pasinler Plateau is cut by four deep gorges in which spectacular sections of the volcanic succession are exposed. They are all perpendicular to the Pasinler Plateau (or basin) and represent some of the main drainages feeding the thick alluvium deposits on the plain. From east to west these are the Harabe Dere, the Sansor Dere, the Tımar Çayı and the Büyük Dere valleys.

In this thesis, in the light of field observations coupled with petrographic and geochemical results, the volcano-stratigraphy of the Pasinler Plateau will be presented from base to top by means of three stratigraphic sections which are mainly coincide with these four gorges. Each of these sections will be described in detail in terms of vertical variation within and between eruptive units. Then, subsequent correlation of these sections will be made by using marker lava and pyroclastic units where appropriate. Since the basement of the volcanic succession is exposed only in the Harabedere valley in the east, these sections will be introduced from east to west starting from the Harabedere and Sansordere gorge sections.

Photo: 2.7. Panoramic view of the entrance of Tımar gorge. The photograph is taken from the Sekiler vicinity (T:40) to the SE. On the top-right of the photograph the Pasinler plain (PP) is visible in the distance. The peneplain-like morphology (on the right) is formed by the weakly compacted detrital sediments of the Pliocene Aras formation (Pla) that overlies the volcanic units of the Pasinler Plateau. The cliffs that are located on the both sides of the stream are made up of the Kargapazarı volcanics. On the left of the photo, volcanic units that are mainly composed of pyroclastic flows (the White, Grey and Black ignimbrites) are almost horizontal. To the south, they dip towards the Pasinler plain and again become sub horizontal in a 1.5 km distance forming a monoclinal flexure. In this location the maximum depth of valley from the plateau changes between 250 and 300m. Ltl: the lower tuff, Bign: the Black ignimbrite, Kv: the Kargapazari volcanics. The location of villages and hills are labelled as follows: TM: Timar village, SB: Sürbehan village, HD: Hasandag hill.

2.3.1.1. The Harabedere and Sansordere Sections

Harabedere and Sansordere sections will be presented together here because not only are they close to each other but they also have similar stratigraphic relations.

2.3.1.1.1. Harabedere Gorge

The Harabedere gorge is located in the easternmost part of the area mapped, to the north of Badicivan village. It has a depth of 300-350 m and steep slopes. It is the only place in the mapped area where the basement to the volcanic succession is exposed (Figure 2.11). The basement rocks are predominantly composed of basic to intermediate volcanic rocks (basaltic andesite and basaltic trachy-andesite) associated with subordinate marine sedimentary rocks, both of which are Upper Eocene in age. Compared to the western areas, the thickness of the collision-related volcanic succession on the Pasinler Plateau decreases considerably to ~20m, especially in the vicinity of the Sarıtaş Dere, Kengelli tepe and the Göktepe hills. This basement is unconformably overlain by a set of black, aphyric andesite lava flows about 30-40m in thickness. A thick pyroclastic fall deposit, the Lower tuff, which includes some thin, laterally impersistant intercalations of aphyric-vesicular andesite-dacite unconformably overlies this sequence. This is overlain in turn by a porphyritic amphibole-bearing dacite/andesite, the Kızılveren amphibole dacite/andesite, forming a dome in the vicinity of Kızılveren village and Şalvartap hill. This 2-2½ km^2 area is the only place on the studied part of the Pasinler Plateau where porphyritic amphibole-bearing andesite crops out. This unit in turn is overlain by the relatively thin (10-30 m) Mid-Tuff. A phenocryst-rich black pyroclastic flow unit, the Black ignimbrite, widely covers these units over a large area. The Black ignimbrite is overlain firstly by an olivine-bearing, andesite and basaltic-andesite, the Kargapazarı volcanics, and secondly by a sanidine-bearing porphyritic rhyolite/rhyodacite, the Ardıçlıdağ rhyolite, located at the top of the volcanic succession. In the following pages, the volcano-stratigraphic units of the Harabedere section will be presented starting from the base.

2.3.1.1.1.1. The Basement Units

2.3.1.1.1.1.1. The Upper Eocene Narman Group

In this study, the Upper Eocene formations have been named as the Narman group as it is the equivalent of a group whose best outcrops are located in the vicinity of the Town of Narman, which lies to the north of the study area. The term 'group' has been used here because not only does it contain volcanic units but also flysch-like

HARABEDERE VALLEY - YENIKOY VILLAGE SECTION, NE OF PASINLER

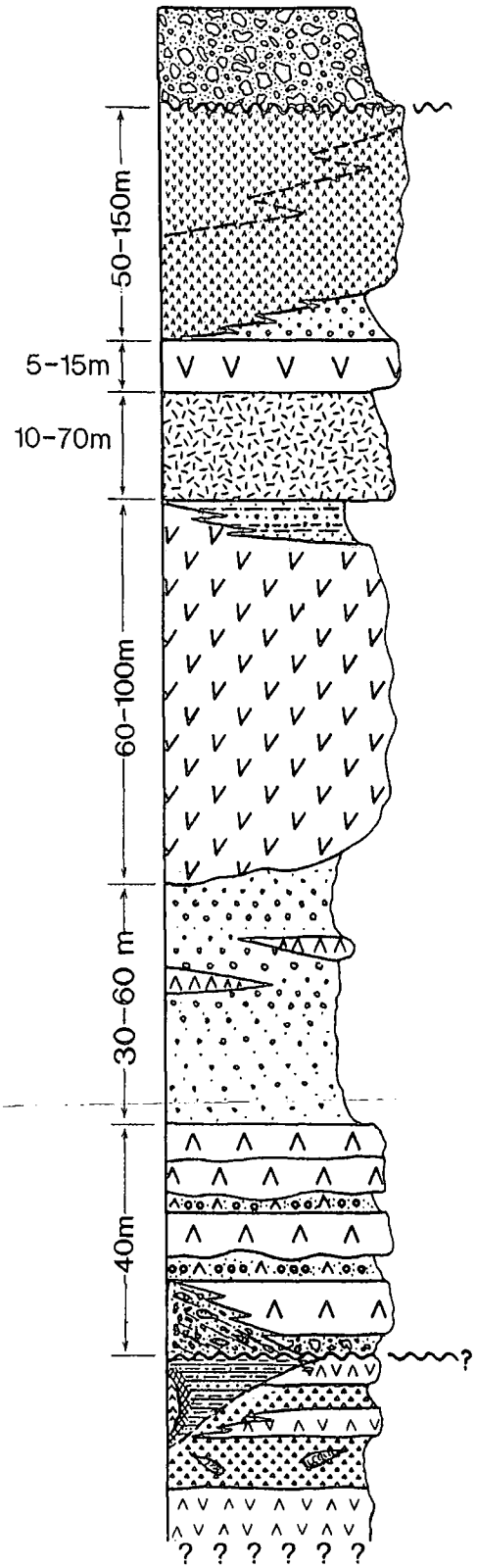

Pliocene Aras formation

Ardıçlıdağ rhyodacitic lava and ignimbrite units

Upper tuff : pumice air fall deposits

Kargapazarı volcanics : olivine basaltic andesite and andesite with aphyric texture

Black ignimbrite : very densely welded, shows eutaxitic texture

Middle tuff

Kızılveren amphibole dacite/andesite: containing amphibole, plagioclase, orthopyroxene phenocrysts

Intercalations of aphyric and vesicular andesite and dacite

Lower tuff unit : pumice air fall deposits occassionally showing grading

Black aphyric andesite

7.83±0.12 Ma

Eocene Narman group

Eocene Narman formation flysch like siltstone-shale alternations

38.5±0.7 Ma

Kıslaköy Volcanic member

Figure: 2.11. Generalised stratigraphic column of the Harabedere valley-Yeniköy village section, NE of Pasinler.

sedimentary beds. To the north of the mapping area, this group covers a very large area. The Narman group has been defined and described by the Turkish Petroleum's geologists in the northern areas around the town of Narman (Sungurlu, 1971). The volcanic part of this group has been given the name of the Kışlaköy volcanic member and in order to avoid confusion and to maintain consistency, these original formation names are retained.

The Narman group contains both volcanic and sedimentary rocks. At its base, a flysch-like detrital sequence occasionally crops out but volcanic rocks are dominant in the group. Even though the relationship between volcanic and sedimentary beds is generally ambiguous in most of the places, some discrete outcrops show sedimentary beds are interlayered with volcanic lava flows.

In the area between the Göktepe-Kengelli hills and the Sarıtaş Dere stream, the stratigraphically uppermost part of the volcanic succession, namely the Ardıçlıdağ rhyolite, unconformably overlies the basement rocks of the Narman group, missing out the other lower volcanic units of the Pasinler Plateau. In other words, hundreds of metres of the thick volcanic pile are laterally wedged out towards this area. This relationship implies the presence of a long lasting palaeo-topographic height made up of the Eocene formations in the area, during the eruption of the volcanic succession on the Pasinler Plateau.

2.3.1.1.1.1.1. The Kışlaköy Volcanic member (En_1)

The Kışlaköy volcanic member has a quite different appearance in the field from the Erzurum-Kars Plateau volcanics on the Pasinler plateau. The unit is recognisable even from a long distance. First of all, in most outcrops it is much more weathered than the fresh lava and pyroclastic rocks of the Upper Miocene-Pliocene volcanics of the Erzurum-Kars Plateau. Secondly, its colour is much darker than these volcanics, displaying greenish dark-grey, i.e. dark-grey on the fresh surface and tones of dark-brown or orange-tan-brown on the altered surface. The Kışlaköy volcanics are composed of alternated lava and agglomerate beds (Photo 2.8). The lava flows are the dominant lithology. They contain virtually no pyroclastic fall deposits such as pumice and ash. The lava is massive in appearance and is cut by several sets of joints in most places. On most outcrops, individual lava flow units within the Eocene volcanics cannot easily be recognised because of the lack of well-preserved structures, e.g. aligned gas pipes at the base of individual lava flows and oxidised surfaces between flows. Where the lava flow units are observed, they are almost horizontal. However, to the north of Mt. Kargapazarı, in the vicinity of Hinzorikülya village (4 km NE of Barköy village), alternations of thick lava flows and agglomerate beds are found

adjacent to the NE-SW trending strike-slip fault. These dip to the north at around 50°-70° (Photo 2.5).

Photo: 2.8. General field view of the Kışlaköy volcanic member of the Eocene Narman Group, Harabedere valley, north of Harabesürbehan village, NE of Pasinler (out of the area mapped).

The Kışlaköy volcanics span a narrow compositional range from basaltic-andesite and basaltic trachy-andesite to andesite, with mainly aphyric or microporphyritic textures. They are all calc-alkaline in character, showing the typical geochemical characteristics of arc volcanism. In general, there are three distinctive rock types, each of which exhibit different phenocryst phases:

1. andesites and basaltic andesites with plagioclase (An_{54-58}) and clinopyroxene (augite) phenocrysts to megacrysts
2. plagioclase and hornblende bearing porphyritic andesites
3. dacite domes

Photo: 2.9. Close-up view of the Eocene Kışlaköy volcanics showing characteristic texture of the unit with plagioclase megacrysts (type 1)

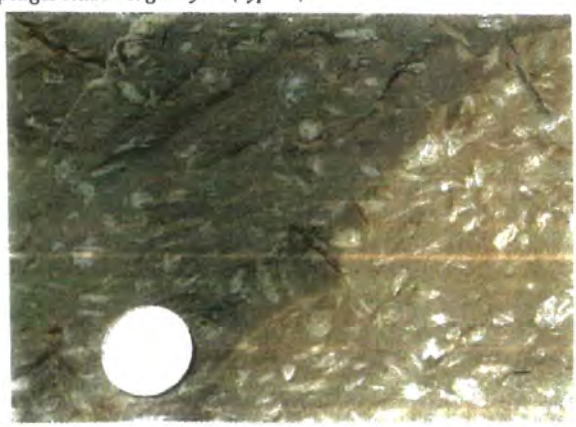

The first type is the dominant lithology in the volcanic unit. Sometimes, as a result of extensive plagioclase crystallisation, it contains megacrysts of plagioclase with diameters of up to 1-2 cm in a pilotaxitic groundmass with intergranular clinopyroxene microcrysts (Photo 2.9). The second type, namely porphyritic hornblende andesite, is much less abundant than

the first. Dacite domes are exposed as small, discrete outcrops. They are the rarest lithology in the Eocene volcanics. They are massive, generally aphyric in texture and white in colour.

Between Harabesürbehan and Kızılveren villages, the Narman group is entirely composed of lava flows, whereas to the south, in a small area situated between Göktepe hill and the Sarıtaşdere stream, flysch-like sedimentary rocks crop out towards the apparent base of the unit.

2.3.1.1.1.1.2. The Narman formation (En_2)

In the area studied, the Narman formation is composed of alternations of thin (5-10 cm) siltstone and shale-mudstone beds. It contains neither sedimentary structures of a deep sea provenance, nor coarse-grained volcanic material characteristic of debris flows. However, it is apparent that it was definitely lain down in the marine environment. The grain size, its distribution in the beds and the geometry of bedding indicate that its original source region was distant from the basin in which it was deposited.

In the area mapped, the Narman formation crops out as a narrow band which extends E-W along the Sarıtaşdere stream. In this location, it is overlain by the Kışlaköy volcanics. Even though its base is not seen in this location, it is presumably underlain again by the Kışlaköy volcanics. To the south of Göktepe hill, sedimentary beds of the Narman formation are cut by the uppermost lava unit, namely the Ardıçlıdağ rhyolite of the Erzurum-Kars Plateau volcanics (Figure 2.12). At the sub-vertical contact with the Ardıçlıdağ rhyolite, in a narrow zone up to 1 meter wide, the colour of sedimentary beds changes into black because of the thermal effect of the Ardıçlıdağ rhyolite (Photo 2.14).

2.3.1.1.1.2. THE PASINLER PLATEAU UNITS

2.3.1.1.1.2.1. The Black andesite / dacite (Baad)

The Black andesite/dacite is the lowermost lava unit in the volcanic succession of the Pasinler Plateau. It unconformably overlies the Upper Eocene basement rocks (the Narman group) and is mainly made up of 4-5 thick (5-15 m) aphyric lava flows. Each lava flow contains a 2-3 m-thick breccia and debris at its base which laterally become lenses between lava flows. These may be the remnants of accretionary levées. Oxidised zones, which have been used as criteria for differentiating individual lava flows in the field, are sometimes present between lava

flows. This unit crops out at the base of Harabedere gorge in a 3 km long, narrow and N-S zone which starts from the entrance of the valley. Each lava flow, at the base, contains platy joints which are almost parallel to the base. The distance between these joints decreases to less than 1 cm at the base. The reason for the formation of these planar joints would be the higher shear between the coherent lava body and the channel walls. Similar flow structures, formed during the solidification of the lava flows, have been described by Cas and Wright (1988, p. 29). The Black andesite is dated at 7.83±0.12 Ma by the K-Ar method.

In this level within the volcanic unit, a discrete scoria cone is also present. It is located on the west slope of Harabedere valley, about 1 km to the east of Göktepe hill. Although its conical shape has not been well preserved, its positive palaeotopographic character can be recognised from its relatively steep contacts to the topographical contours, and also from its faint stratification. It basically contains scoria breccia, lapilli and volcanic bomb fragments with vitrified rims all showing aphyric textures. These are all indicators of an explosive eruption.

2.3.1.1.1.2.2. The Lower tuff (Ltl)

The Lower tuff is the first unit which overlies the black aphyric andesite in the Harabedere gorge. It also blankets the slopes of a scoria cone of the Black andesite. It crops out on the west slope of the Harabedere valley. It is mainly made up of pumice fall beds with alternations of minor reworked pumice and lithic clasts.

It is characteristically white or greyish in colour and composed of pumice fragments of different sizes, from about 2 cm to a few mm. Internally it shows a rather well-developed bedding from 0.5 to 1-1.5 m in thickness with some laminae. Sorting is average to poor and grading is absent in this unit. At some levels, the Lower tuff contains several small-scale channels.

Stratigraphically, this tuff in the Harabedere gorge is the lateral equivalent of the Basal tuff unit which is seen in the Sansordere and Tımar gorges further west. It can be traced further westwards to the Büyükdere gorge. Unlike these areas, the lower tuff in the Harabedere gorge does not contain any ignimbrite flows.

2.3.1.1.1.2.3. The Kızılveren amphibole dacite / andesite (Kpd)

Between Kızılveren Village and Şalvartap hill, in an area of around 2 km^2, a porphyritic, andesite/dacite dome overlies the Lower tuff formation. It is characteristically composed of plagioclase and brown amphibole phenocrysts in a grey-coloured microcrystalline, groundmass. It is named the Kızılveren amphibole

dacite/andesite as its best outcrops are situated close to the Kızılveren village. Apart from the area under discussion, this porphyritic unit is absent in the rest of the Pasinler plateau. It reaches its maximum thickness of over 130 m at Şalvartap hill and is texturally homogeneous throughout its thickness. It is similar to the amphibole-bearing porphyritic dacitic and andesitic lavas cropping out widely to the west in the Mt. Dumlu area (i.e. the Dumlu amphibole andesite/dacite) in terms of its petrography and composition. It is possibly the product of the same volcanic activity which dies out eastwards.

At its upper contact, the Kızılveren amphibole dacite/andesite is covered firstly by a tuff unit, in this study called the Upper tuff, and secondly by the Black ignimbrite where the upper tuff is laterally discontinuous.

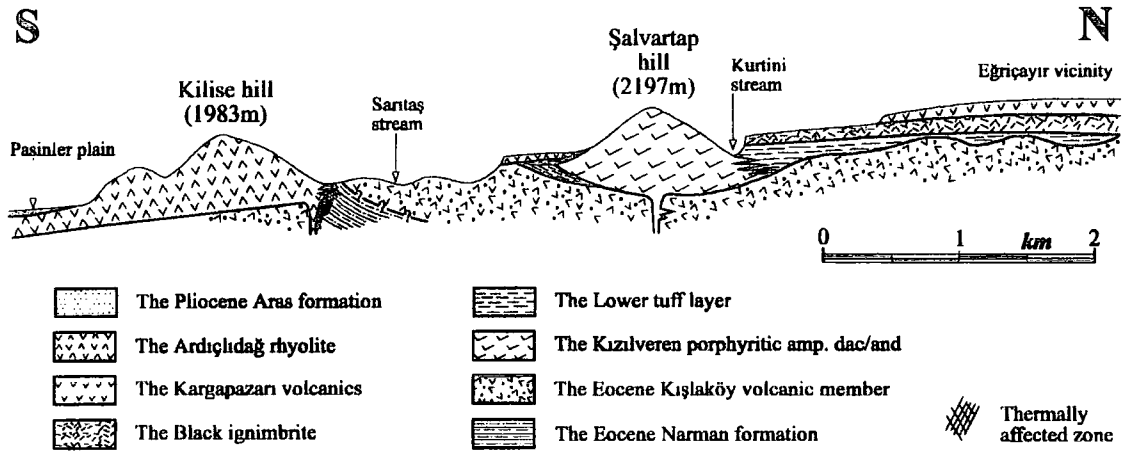

Figure: 2.12. S-N cross section through the volcanic succession between the Kilise hill (Y:47) and the Eğriçayır vicinity (R:47), close to the Harabedere gorge, NE of Pasinler.

2.3.1.1.1.2.4. The Middle Tuff (Mtl)

In this study, the tuff sequence which overlies the Kızılveren amphibole dacite/andesite is named the Middle tuff. This unit consists of relatively fine-grained particles of pumice and felsic ash. Pyroclastic flow products are rare in this unit. Its maximum thickness is around 20-40m. However, it is not laterally continuous to the SW side of the dome of Kızılveren andesite. To the west of this area, in the Sansor Dere gorge, its lateral continuation is exposed in a section where it reaches to a thickness of 150 m with abundant pyroclastic fall beds.

2.3.1.1.1.2.5. The Black ignimbrite (Bign)

The Black ignimbrite covers well over one-third of the area of the Pasinler plateau, with an exposed average thickness of 50 m. Internally, it consists of several densely-welded pyroclastic flow units. Laterally, the total thickness of this unit varies considerably from 3-10 m up to 150-200 m in the Tımar gorge (Photo 2.11). At the

base, it shows a sharp contact with units lower in the succession. The Black ignimbrite performs the function of an armour, which protects the weaker pyroclastic units underneath and gives the plateau its distinctive morphology. It is generally black in colour, although it also exhibits beige, red and pale-purple colours. Characteristically, it shows a well-developed eutaxitic texture, with fiammé which

Photo: 2.10. Close-up photograph of the Black ignimbrite. It displays a well developed eutaxitic texture defined by fiammé. The white fragments are generally white ignimbrite. The coin which is used as a scale is 2 cm in diameter.

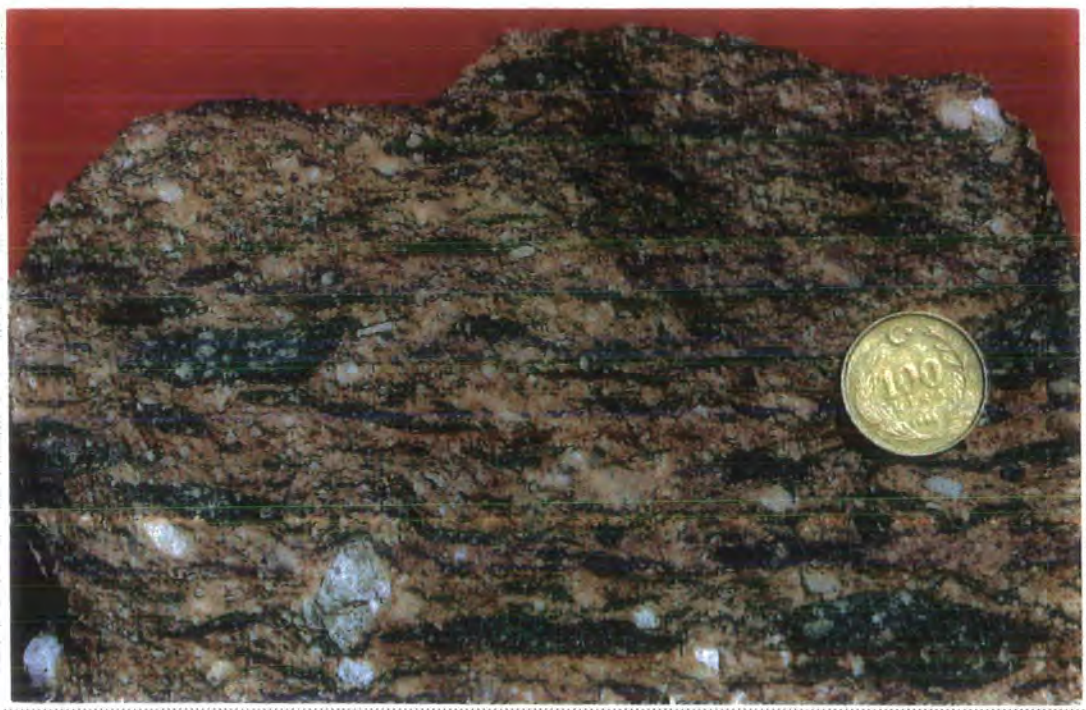

sometimes reach to 5-10 cm in diameter (Photo 2.10). The Black ignimbrite exhibits different stages of rheomorphism, as fiammé are generally stretched to produce a well defined lineation. This may be an indication of secondary mass flowage of the ignimbrite during welding. These fiammé generally consist of black obsidian, containing abundant phenocrysts. The ignimbrite matches the "high grade ignimbrite" as described by Cas & Wright (1988).

Compared to the other pyroclastic formations or facies, the Black ignimbrite contains abundant phenocrysts (up to 40%) of mainly plagioclase. It also includes abundant inclusions from other volcanic units, such as white ignimbrite, pumice and even previously-formed black ignimbrite (Photos 2.10 and 12). According to Sparks and Walker (1977), phenocryst enrichment is a typical feature of ignimbrites and may be due to substantial volumetric loss of the vitric component of the original magma by previous eruptions which gives rise to the deposition of associated air-fall ash deposits.

Photo: 2.11. General field view of the Black ignimbrite, N of the TımarÇayı valley, Kilisedere stream(P:45), NE of Pasinler. In this location, the total thickness of the unit reaches to 200 m.

Photo: 2.12. The black ignimbrite containing inclusions and lithic fragments from other volcanic units which vary in size and lithology. These are, in general, white ignimbrite, pumice (the white big lump in the middle) and previously-formed black ignimbrite (darker coloured fragments). North of Tımaryayla village (N:41), NE of Pasinler.

In the vicinity of Harabesürbehan village, the unit shows well-developed columnar jointing in the more massive parts (Photo 2.13). Extremely stretched

Photo: 2.13. Columnar jointing in densely welded parts of the Black ignimbrite, Harabesürbehan village (R:52), the Harabedere gorge, NE of Pasinler.

fiammé of white pumice (3-5 mm in thickness) reach 30-40 cm in length in places. They exhibit a very good lineation perpendicular to the jointing surface. The Black ignimbrite is overlain by an olivine-bearing andesite-basaltic andesite lava unit, the Kargapazarı volcanics, and then by the Ardıçlıdağ rhyolite.

2.3.1.1.1.2.6. The Kargapazarı Volcanics (Kv)

Despite the fact that olivine-bearing, basaltic-andesite, andesite lava flows of the Kargapazarı volcanics are very widespread as a thick succession in the Mt. Kargapazarı area, they only crop out as relatively thin and small outcrops on the Pasinler Plateau. In the Harabedere gorge section, the Kargapazarı volcanics overlie the Black ignimbrite in the locality of Dikmetaş hill and Buzhane area (north of the village of Kızılveren). They cover an area of 6-6½ km^2 with an average thickness of 5-30 m. In the area between Yertepe and Şalvartap hills, situated close to the east of Sansor Dere gorge, the unit is overlain by the lava and ignimbrite units of Ardıçlıdağ rhyolite.

In the field, the Kargapazarı volcanics have been used as one of the marker horizons for mapping. At the outcrop scale, this unit is very different from the other lava units exposed on the Pasinler Plateau in terms of its general appearance and texture. It exhibits aphyric and microporphyritic textures with occasional vesicular zones. It contains plagioclase micro-phenocrysts and microlites (An_{78-51}) and

TASLIGUNEY VILLAGE - SANSORDERE GORGE SECTION NE OF PASINLER

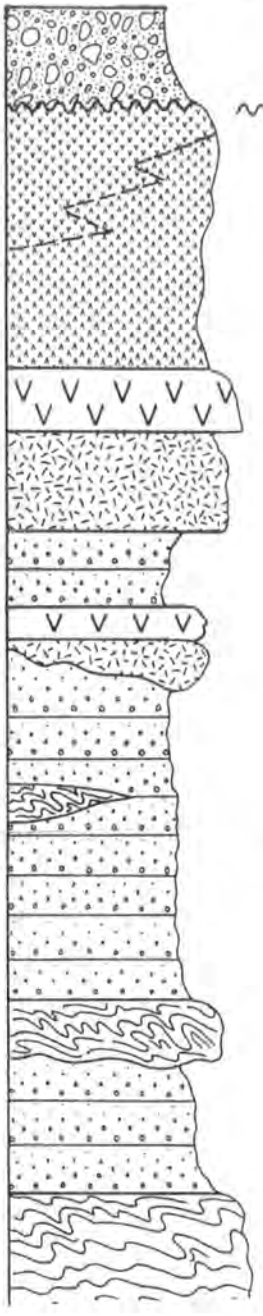

Pliocene Aras formation

Ardıçlıdağ rhyodacitic lava and ignimbrite units

Kargapazarı volcanics : olivine basaltic andesite and andesite with aphyric texture

Black ignimbrite: very densely welded, shows eutaxitic texture

Black ignimbrite

Pumice air-fall deposits

White ignimbrite : showing flow-folds and accretionary lapillies

Figure: 2.13. The stratigraphical section of Taşlıgüney village-Şansordere Gorge section, NE of Pasinler

rarer olivine microcrysts (Fo_{75-84}) in a cryptocryalline or glassy groundmass. On a fresh surface it is greenish-dark grey or dark grey whereas, on the altered surface, it exhibits brownish-yellowish colours.

2.3.1.1.1.2.7. The Upper Tuff (Utl)

In the vicinity Sansor village, around the south entrance of the Sansor Dere gorge, a tuff unit mainly made up of pyroclastic fall deposits overlies the Kargapazarı volcanics. In this area, the volcanic succession has a dip of about 10°-15° to the south, the lateral continuation of the monoclinal flexure mentioned earlier. Towards the south, the Black ignimbrite and the overlying Kargapazarı volcanics become thinner and to the north of Sansor village, their total thickness decreases to 3-5 m. In contrast, the overlying Upper tuff gets thicker to the south, varying from a few metres around Yertepe hill (2.25 km north of Sansor) to over 100 m in the Sansor village area.

The Upper tuff is wedged out to the north, between the olivine-andesite and Ardıçlıdağ rhyolite, and is not seen to the north of Yertepe hill. It mainly consists of pyroclastic fall and tuff deposits. Pumice is the most common detrital material comprising over 90% of the clasts. The unit also contains lithic fragments of the Ardıçlıdağ rhyolite, implying that it is genetically related to the explosive volcanism which formed the Ardıçlıdağ rhyo-dacitic dome. It is creamy-white in colour. Generally it shows a weakly-developed layering with occasional lamination.

2.3.1.1.1.2.8. The Ardıçlıdağ volcanite

At the top of the volcanic succession, a sanidine-bearing rhyolitic and rhyodacitic lava, and a pyroclastic-flow unit, crop out between Kızılveren and Sansor villages, and also in the vicinity of Tafdiker village. It is named the Ardıçlıdağ rhyolite after Ardıçlıdağ hill in 2 km east of Sansor village where its best outcrops are exposed. Even from a distance, it can easily be differentiated from the other volcanic units of the plateau by its distinctive yellowish-white colour and characteristic erosion-surface pattern.

The unit is made up of coarse sanidine phenocrysts with plagioclase, quartz and altered mafic-mineral (amphibole) phenocrysts and subordinate pyroxene microcrystals in a white-glassy groundmass. On most of its outcrops, the unit is severely weathered. This unit is also exposed around Serçeboğazı village, which is located to the northwest of the town of Pasinler.

The Ardıçlıdağ rhyolite can be further subdivided into two members on the basis of their eruptive character and resulting texture:

(1) rhyolitic lava unit;

(2) an ignimbrite which has the same composition as the rhyolitic lava unit.

The Pliocene Aras formation overlies the unit with an angular unconformity to the south.

2.3.1.1.1.2.8.1. The Ardıçlıdağ rhyolitic lava unit (Ard):

In the area around Tafdiker and the north of Kızılveren village (Kavaklıbaşı ridge), the rhyolitic lava unit rests on the Black ignimbrite (Figure 2.14), whereas to the southwest it unconformably overlies the Eocene Narman group (Figure 2.12). It has a massive appearance and does not show any flow structures. Its thickness reaches well over 200 m around Ardıçlıdağ hill. Towards the north and east, this thickness decreases considerably to under 30-50 m.

The unit characteristically shows porphyritic texture with abundant fresh megacrysts and phenocrysts of sanidine, altered amphibole, less abundant plagioclase phenocrysts and occasional clinopyroxene microcrystals surrounded by a glassy groundmass. To the north of the Kızılveren village, in the vicinity of Kavaklıbaşı ridge, it contains biotite micro-phenocrysts in addition to the phenocryst assemblage described above.

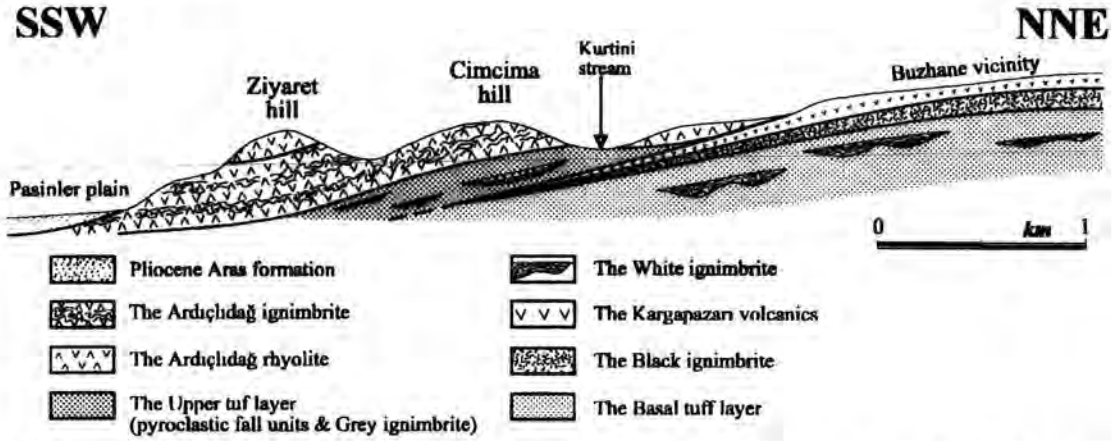

Figure: 2.14. Cross section between the Ziyaret hill (X:44) and Buzhane vicinity (S:47) displaying relationship between volcanic units of the Pasinler plateau, Sansordere gorge, NE of Pasinler.

The Ardıçlıdağ rhyolite, in general, has a truncated dome shape the centre of which is situated roughly between Süleyman hill and Sarıtaş stream. Around Sarıtaş stream, its conduit has been observed, cutting the siltstone/shale beds of the Narman formation (Upper Eocene) (Figure 2.12). A narrow (about 1-1½ m wide), black

thermally-affected zone has developed in the Narman formation in contact with the Ardıçlıdağ rhyolite (Photo 2.14).

2.3.1.1.1.2.8.2. The Ardıçlıdağ ignimbrite unit (Aign):

The Ardıçlıdağ Ignimbrite crops out on the east slope of the Sansordere stream with a NNE-SSW-trending outcrop pattern and conformably covers the west and northwest slope of the rhyo-dacitic dome. It also overlies the Upper tuff which is widely crops out in the vicinity of Sansor village (Figure 2.15). Like the main body of the rhyolitic dome, the ignimbrite unit also has a general southward dip, gradually steeping southward, with an average maximum dip of ≈15°-20°.

Photo: 2.14. Contact zone between the Ardıçlıdağ rhyolite and the Upper Eocene Narman formation. A narrow (about 1-1½ m wide), black thermally-affected zone is present in the Narman formation (on the left). Sarıtaşdere stream (W:47), NE of Pasinler.

The Ardıçlıdağ ignimbrite exhibits the same composition, colour and phenocryst assemblage as the rhyo-dacitic lava dome. However, it has a different, typically eutaxitic, texture which consists of compacted and welded white pumice surrounding the phenocrysts and lithic fragments which are generally a few mm in diameter.

The ignimbrite internally shows variable degrees of welding, represented by the different textures of the various flow units. In the vicinity of Ziyarettepe hill 1 km east of Sansor village, it is overlain by a 7-10 m thick lens of densely-welded, phenocryst-rich ignimbrite which is very similar to the Black ignimbrite. A similar relationship has been observed in Büyükdağ hill situated to the east of Harabedere valley (≈3 km NE of Badicivan village). It shows a well-developed eutaxitic developed eutaxitic texture with abundant flow-oriented laths of plagioclase phenocrysts surrounded by a pale-brown, purple-coloured glassy groundmass.

In the Ardıçlıdağ ignimbrite, perlite also occurs occasionally in the zones of intensive welding, presumably as a result of hydration of obsidian. It is composed of abundant plagioclase and sanidine phenocrysts included in a light grey-coloured glassy matrix with typical perlitic texture. It outcrops around Cimcime and Ziyarettepe hills.

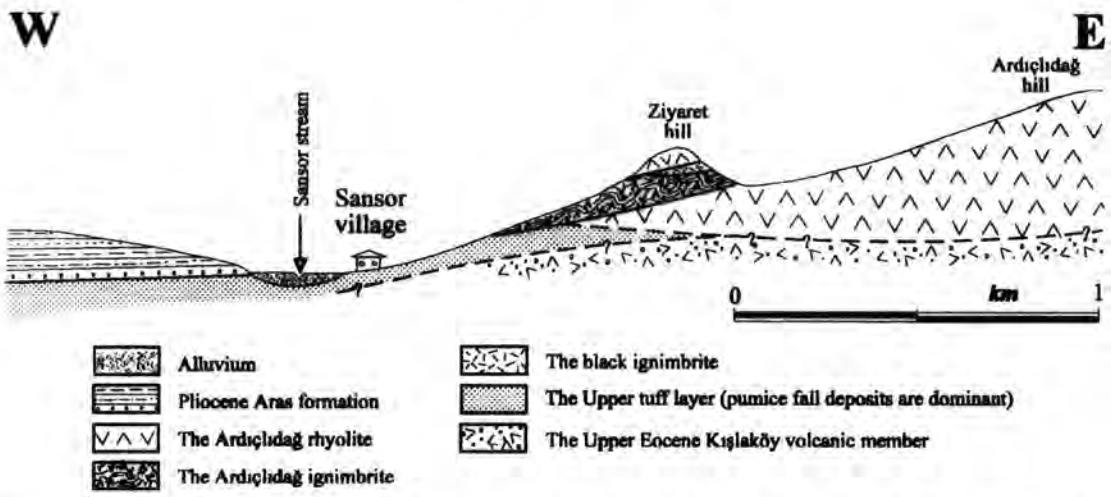

Figure: 2.15. Cross section between Sansor village (W:43) and the Ardıçlıdağ hill (X:46), Sansordere gorge, NE of Pasinler.

2.3.1.2. THE BÜYÜKDERE GORGE SECTION

Büyükdere stream is the biggest of the four streams which cut the Pasinler Plateau. The valley in which it runs is located about 10 km northwest of the town of Pasinler, extending almost parallel to Pertek-Karakale strike-slip fault which trends NNE-SSW. The southern limit of this valley is bounded by the aforementioned major monoclinal fold dipping to the south. The basement of the volcanic succession is not exposed in the Büyükdere gorge. In the southern part, between Terektaşı hill and Açığındağısırtı ridge on the 300 m high eastern slope of the valley, the best outcrops of the Lower tuff are exposed (Photo 2.15). Pyroclastic flows make up almost over 90% of this section (Figure 2.16).

Individual pyroclastic-flow units can be grouped into two facies which primarily differ in terms of colour, the degree of welding, internal structure and general appearance in the field. These facies are named in this study after their outcrop colour: the Grey and White ignimbrites.

The flow units of the white ignimbrite facies account for roughly 25-30% of the lower tuff and occur as three 20-60 m thick flows. They are composed of densely-welded ignimbrite showing rheomorphic structures of variable intensities. In the field, it is easily recognised and differentiated from other flow units on the basis of its distinctive colour and resistant (competent) outcrop pattern (Photo 2.15). The White ignimbrite is almost totally free of crystals and composed entirely of rhyolitic glass (Photo 2.21). Although this unit is massive in places, and seems to be entirely massive from a distance, it is generally inhomogeneous in texture and consists of alternations of variably-welded grey pumice (which still partly retains its vesicular texture) and white ignimbrite (which shows a variable degrees of welding) (Photo 2.18). Furthermore, towards the base, obsidian bands are abundant, where the compaction

Photo: 2.15. Field view of the Açığındağısırtı ridge (U:32), eastern slope of the Büyükdere gorge, NW of Pasinler. The resistant flows (Wign) are the white ignimbrite which occur as 20-60 m thick flows. The Grey ignimbrite (Gign) is characterised by its soft outcrop pattern and its greyish colour while reworked pumice and pyroclastic fall deposits (Pfd) can be recognised by their lighter (pinkish and cream) colours. The thickness of the visible part of the Lower tuff is around 300 m on this photograph. Kvd: dykes of the Kargapazarı volcanics seen in Photo 2.16.

was extremely dense (Photos 2.17 and 18). It also contains accretionary lapilli in different sizes from a few mm up to 7-8 cm (Photo 2.23).

The grey ignimbrite facies is characterised by very thick (≈50 m) flow units which show different tones of grey. It is made up of highly vesicular, massive and very brittle pumice with glassy or sometimes pearly, lustre. In fact, the White ignimbrite comprises the more densely-welded, more basal part of the pyroclastic flow units compared with the Grey ignimbrite. On the outcrop scale, it is clearly seen that the White ignimbrite changes gradually upward into the Grey pumice. Therefore, each white and grey ignimbrite pair together should be considered as a single pyroclastic flow unit, even though the contact between them seems to be sharp from a distance. In the following paragraphs, the Büyükdere section will be described in detail starting from the base.

At the apparent base of the section, a blocky pyroclastic flow crops out. It consists of large pumice blocks of Grey ignimbrite of variable sizes up to 50 cm across. These blocks are surrounded by a matrix which has almost the same composition and texture but is slightly lighter in colour. It is mostly matrix-supported and contains

BUYUKDERE VALLEY SECTION, NW OF PASINLER

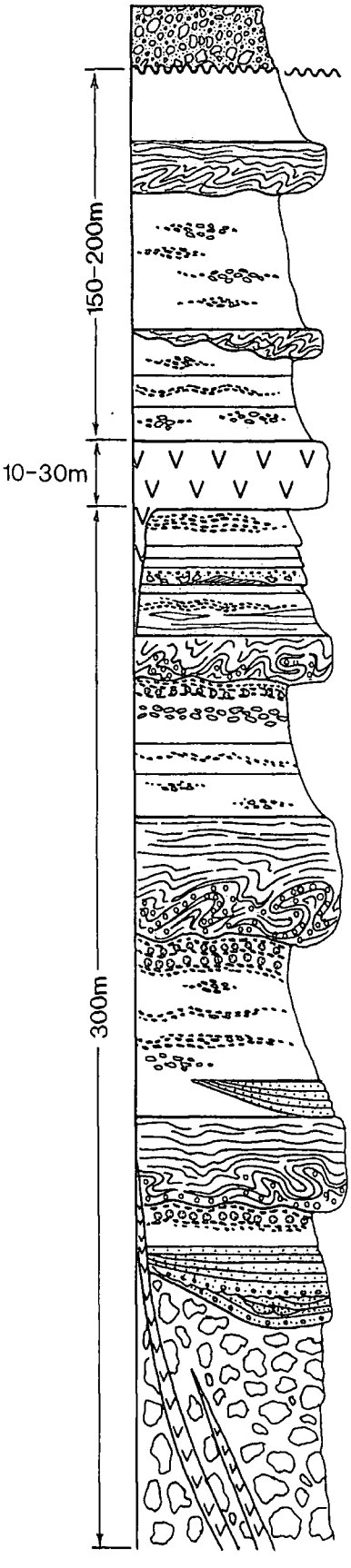

Pliocene Aras formation

White ignimbrite

Grey ignimbrite : coarse vesiculated, containing, accretionary lappies and obsidian bands

Grey ignimbrite

Kargapazarı volcanics : olivine basaltic andesite and andesite with aphyric and microporphyritic texture

White ignimbrite : showing flow-folds and accretionary lapillies

Grey ignimbrite : displays abundant accretionary lapillies, obsidian bands in the contact with the White ignimbrite

Reworked pumice

Reworked pumice with small scaled channels, cream and pink in colour, red in the contact with the White ignimbrite

Grey blocky ignimbrite : pumice flow

Dykes of olivine bearing andesite, basaltic-andesite of Kargapazarı volcanics

Figure: 2.16. Stratigraphic section of Büyükdere valley

occasional sintered obsidian clasts of pebble size. Its apparent thickness is around 100 m.

Blocky, Grey ignimbrite is unconformably overlain by a reworked pumice (Photo 2.19). This unit is composed of ash- to lapilli-sized clasts of scattered and rounded white pumice which were presumably air-fall deposits in their primary depositional environment. It contains around 10-20 % lithic clasts. In general, the unit is pinkish-cream to white in colour. This colour gradually becomes darker and changes into orange within a few metres of the upper contact with the Grey ignimbrite. It has a lens-shaped geometry with a maximum thickness of 15m and a lateral continuation of 100-120m (Photo 2.19). Its upper contact is fairly planar, whereas its lower contact is irregular resembling a small-scale channel-fill. Beds are thicker in the middle becoming thinner towards the sides of the lens.

Photo: 2.16. Dykes of the Kargapazarı volcanics cutting through the basal part of the Lower tuff in the Büyükdere gorge (U:32). They vary in thickness from 30-40 cm to half a metre with a strike of approximately E-W (≈N80E) and dip of 10-20° to the south.

The reworked pumice is composed of two units which are almost identical in their compositions and internal structures but separated by an angular unconformity. The thickness of individual beds varies widely from a few tens of cm up to >1m. They are poorly sorted and have faint normal graded bedding. Reverse grading is also occasionally seen in these beds. Lithic clasts, which are generally a few cm in diameter, up to 20-30 cm, are compositionally homogeneous throughout the unit. The majority are composed of fragments of white-ignimbrite, dark-grey, black aphyric basaltic-andesitic/andesitic lavas, presumably gathered from the basal, aphyric lava flows which are exposed not in this section but further east in the Harabedere Valley.

In this unit, there are some small-scale channel structures in which angular lithic clasts become more abundant.

These basal pyroclastic units are cut by a set of andesitic dykes. In this part of the stratigraphic section, there are three sub parallel dykes (Photo 2.16). Their thickness varies from 30-40 cm to ½ metre. They strike approximately E-W (≈N80E) and dip 10-20° to the south, though the degree of dip changes because of their slightly curved surface. They become thinner and eventually disappear towards the top of the succession. In the Büyükdere gorge, other dykes of similar composition and texture have been observed further north in the valley. One lies at the base of the Büyükdere valley, about 200 m north of the ruin of Kurnuçkomu village. It is vertical with an ≈N-S strike. The other is located on the W slope of the valley, to the east of the Kale (castle) ruin, 1.25 km north of the Kurnuçkomu ruin. This, too, is a vertical dyke showing a N45W strike. Its thickness is about 1-1.5m. They exhibit the same petrography and composition as the Kargapazarı volcanics and are most probably fissures which fed the andesitic and basaltic lavas of the Kargapazarı volcanics outcropping in the upper levels of the succession.

Photo: 2.17. Welded parts of the Grey ignimbrite which is composed of bunches of very thin glass fibres surrounding the sintered obsidian clasts. N of Malikom village (P:33), NW of Pasinler.

The reworked pumice unit is overlain by a 10-15m thick grey pumice flow (Grey ignimbrite) unit. The contact between the reworked pumice and the Grey ignimbrite is sharp and fairly planar. The pumice layer is is greyish-white in colour and quite homogeneous in its composition and texture. It is made up of a massive, highly vesicular pumice which contains thin (a few cm), densely welded zones and occasional obsidian bands and blocks. The size of its vesicles often reach 1 mm in diameter. The grey ignimbrite is quite brittle; it is easily broken when squeezed between the fingers. In some zones, where relatively dense compaction is dominant, it loses its vesicular texture and changes into parallel bunches of very thin glass fibres surrounding the sintered obsidian clasts which are approximately 1-3 cm in diameter.

The Grey ignimbrite unit is conformably overlain by a white ignimbrite unit. The contact between the White and underlying Grey ignimbrite units is sharp but

not planar. The thickness of this unit varies from 15-20 to 50 m. At the base, in a 2-3 m thick zone, it is strongly-welded and changed into an alternation of a few cm thick layers or bands of obsidian and densely welded grey and white pumice. These bands are mostly intensively deformed and folded as a result of rheomorphism (Photo 2.18 and 21). The obsidian bands are black and, in general, broken into small, pebble-sized fragments. This deformation probably took place immediately after the solidification since individual fragments of obsidian show the effects of heat, having sintered surfaces, and are sometimes surrounded by densely welded grey or white pumice, which turns into the fibrous glass in places (Photo 2.17). Towards the top, the degree of welding decreases, and the obsidian-bearing zone gradually changes into white, aphyric, densely welded ignimbrite. There are numerous accretionary lapilli reaching up to 9-10 cm in size in this highly welded zone. They are empty inside and generally cut by three cracks like triple-junctions, joined to each other at an angle of about 120° angles (Photo 2.23). Their interior is a set of convex surfaces and Some of them are filled by fibres of grey pumice. They are generally light grey to cream in colour. Their outer surface is generally grey in colour, smooth and sometimes slightly rough. Accretionary lapilli are also very abundant in the upper zones of the White ignimbrite. However, they are relatively smaller in size and some of them are cored.

Photo: 2.18. Field view of the basal part of an individual ignimbrite flow displaying the densely welded obsidian-rich basal part. This is overlain by the White ignimbrite which exhibits complex rheomorphic folds. Both the obsidian-banded zone and White ignimbrite contains numerous accretionary lapilli. Açığmdağısırtı ridge (U:32), eastern slope of the Büyükdere gorge, NW of Pasinler.

Photo: 2.19. Field photograph of reworked pumice unit, Açığındağısırtı ridge (U:32), eastern slope of the Büyükdere gorge, NW of Pasinler. Wign: White ignimbrite, Gign: Grey ignimbrite, Gignb: blocky grey ignimbrite, Rpl: reworked pumice unit. Some of the cavities in the White ignimbrite were carved and used as houses by people who lived in the area in prehistoric times to protect themselves from wild animals and their enemies.

Photo: 2.20. Field photograph showing the sharp contact between the Grey (Gign) and Black ignimbrite (Bign), N of Malikom village (P:33), NW of Pasinler.

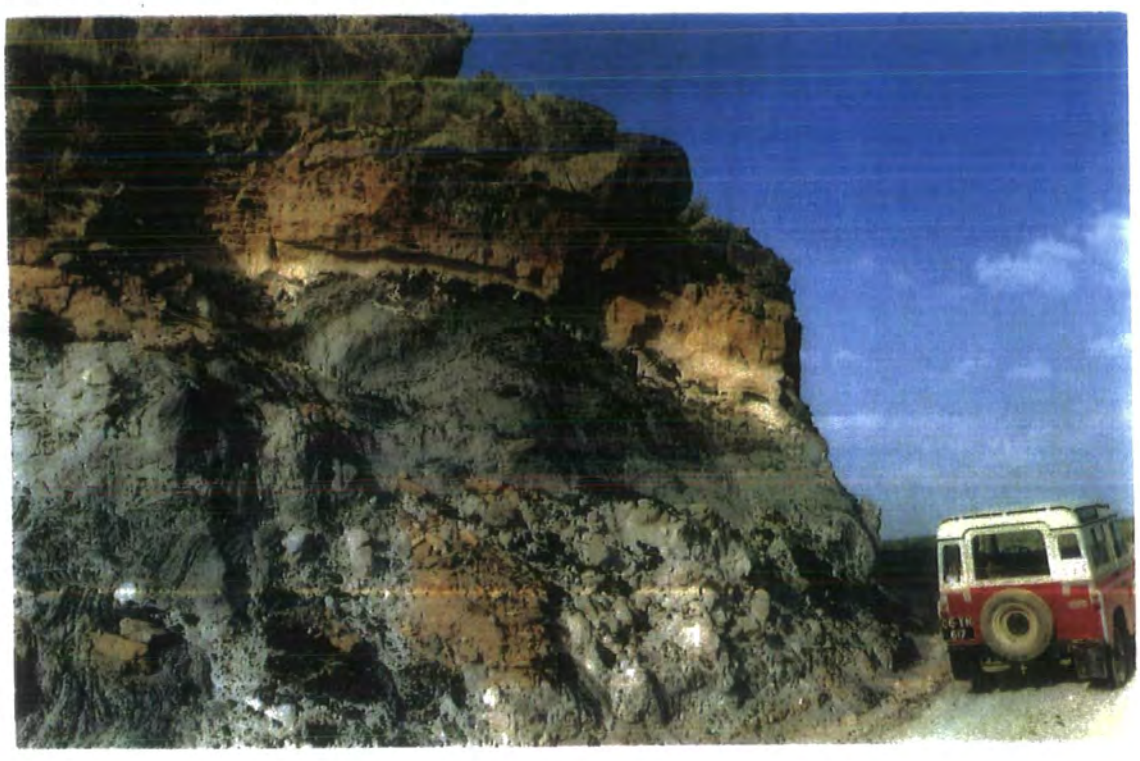

Photo: 2.21. Flow folds in the densely welded parts of the White ignimbrite, S of Tmaryaylası village (Q:43), NE of Pasinler.

Photo: 2.22. Micro-scale flow folds which resemble crenulation cleavage. Açıgmdağısırtı ridge (U:32), eastern slope of the Büyükdere gorge, NW of Pasinler. The coin used as scale is 22 mm in diameter.

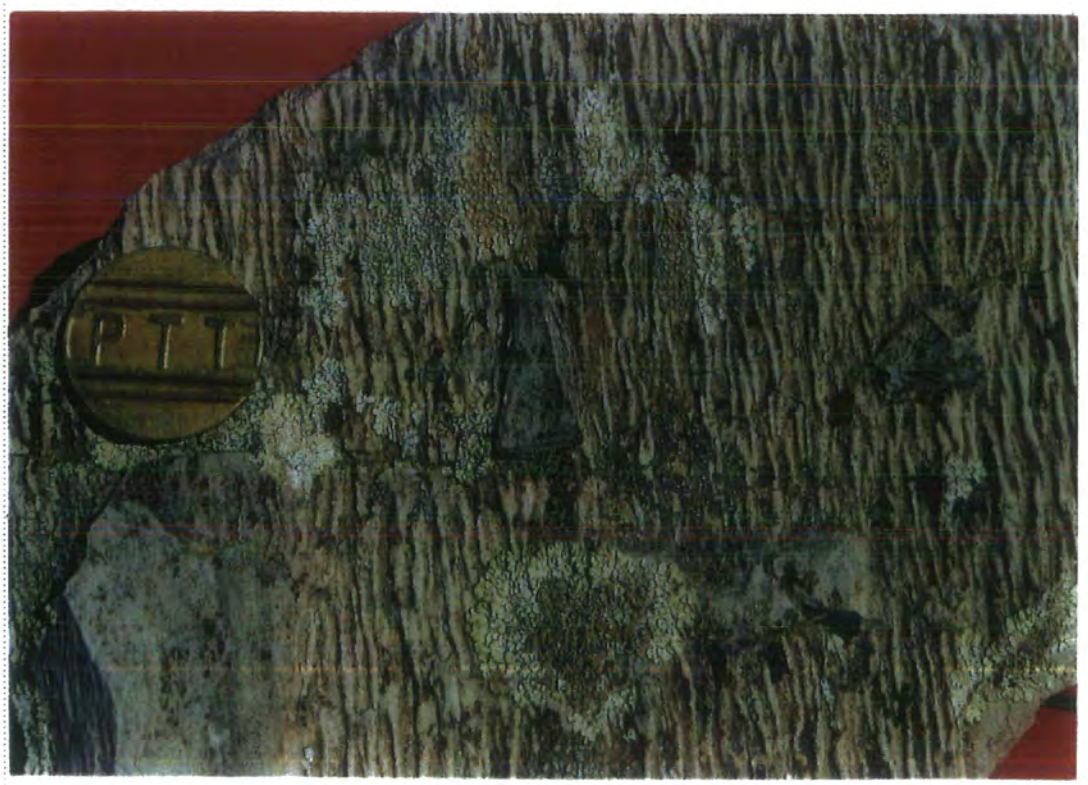

The White ignimbrite gradually changes upward into the Grey ignimbrite. The gradual nature of the contact between the White ignimbrite and the Grey ignimbrite cannot be clearly seen in this particular location because of the scree covering most parts of the outcrop. A 10-15 m thick reworked pumice unit unconformably overlies both the White and the Grey ignimbrite. This unit is very similar to that described above. It is white to cream in colour and made up of lapilli-sized, rounded white pumice fragments with minute angular lithic clasts of aphyric lava, both of which are enclosed in an ash sized matrix of the same composition. This unit also has a lens-shaped geometry with a lateral continuation of approximately 70-100 m. It is almost planar at the upper contact, but its lower contact is wavy and resembles a channel-fill. The geometry and depositional characteristics of these lens-shaped beds of reworked pumice indicate that they were possibly transported (reworked) products of plinian air-fall deposits of white pumice. These would have been deposited as a channel fill in depressions such as the small ravines of temporary streams carved into the soft Grey ignimbrite. There they would have mixed with the fragments of different lavas and pyroclastics.

Photo: 2.23. Close-up photograph of accretionary lapilli in the Grey ignimbrite, Büyükdere gorge (R:32), NE of Pasinler.

The reworked pumice is overlain by another White ignimbrite, similar to that described earlier, which changes gradually to the Grey ignimbrite. The average thickness of the White ignimbrite is 15 to 40 m and that of the Grey ignimbrite is 55-60 m. This White/Grey ignimbrite couple is in turn overlain by yet another succession of White/Grey ignimbrite whose total thickness is 30-40 m. In this part of the section, the gradual change from the White ignimbrite into the Grey ignimbrite is well exposed.

The White/Grey-ignimbrite sequence is overlain by a few m of white-pumice. At its base this contains big angular blocks of grey and white pumice, and obsidian, up to 40-50 cm in diameter and enclosed in a laminar, wavy, grey coloured matrix which shows dune features. This basal layer seems to be a base-surge deposit. If the size of the blocks are taken into account, this layer appears to have formed close to the vent, most probably at the base of a phreatomagmatic eruption column as an outward moving, turbulent cloud of ash and fluid. A typical pumice fall deposit, which is made up of rounded white-pumice clasts in an ash-supported matrix, conformably overlies the base-surge deposit. This layer also shows reverse grading in places.

Photo: 2.24. Pumice fall deposit which contain several blocks of grey and white pumice, and obsidian, Açığındağısırtı ridge (U:32), NW of Pasinler.

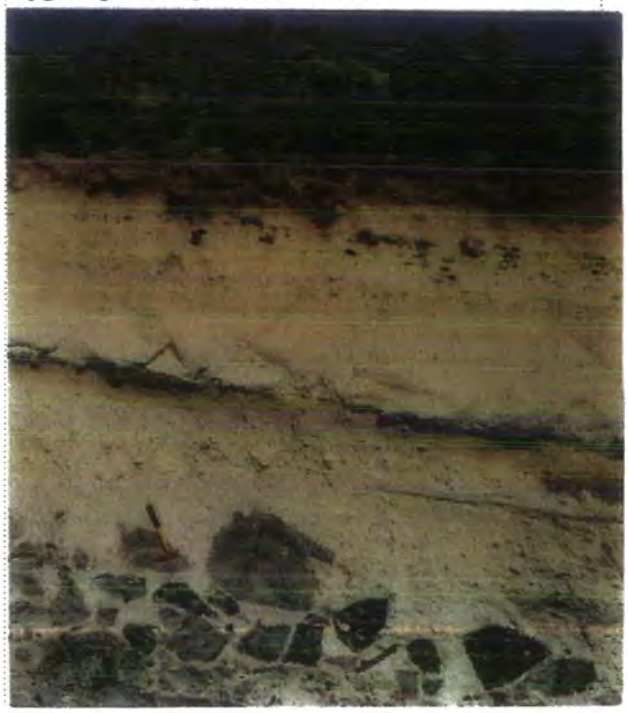

The pyroclastic fall unit is overlain by an olivine-bearing lava with similar geochemical and petrographic characteristics to the Kargapazarı volcanics. It is generally andesitic, trachy-andesitic and sometimes basaltic-andesitic in composition. It is usually

Photo: 2.25. Basal part of the pumice fall deposit seen in Photo 2.24, Açığındağısırtı ridge (U:32), NW of Pasinler.

greenish-dark grey in colour on the fresh surface and aphyric to microporphyritic in texture. It also occasionally shows vesicularity. Its thickness varies from a few metres to 50 m. In general, it has a lensoid geometry extending in a N-S direction for about 4-4.5 km between the Açığındağsırtı ridge and the village of Malikom. Stratigraphically, this unit is the eastward lateral equivalent of the basal part of the Kargapazarı volcanics which become widespread and very thick in the west, around Mt. Kargapazarı. It also forms a lateral continuation to the intermediate to basic lavas overlying the Black-ignimbrite in the Harabedere, Tımar and Sansordere gorges, close to the top of the succession. Both the Kargapazarı volcanics and the underlying Black-ignimbrite are used as marker-horizons for making stratigraphic correlations on the Pasinler Plateau.

The Kargapazarı volcanics are overlain by another succession of pyroclastic flow and fall deposits reaching up to 200 m in thickness in the vicinity of Karagüney hill. This succession is mainly composed of alternations of Grey and White-ignimbrite flows with minute fall deposits. This sequence is very similar to the pyroclastic units at the base of the succession. It has an eroded cone shape and covers around 40 km^2 on the plateau. Stratigraphically, it is the lateral equivalent of the Upper tuff seen in the Timar and the Sansordere gorges, though in these areas the proportion of the pyroclastic-flows to fall deposits is relatively low. The likely reason for this difference is that the Büyükdere gorge contains the proximal part of the pyroclastic deposits. At the time of eruption this area probably was very close to the vent which produced the extensive pyroclastic blanket on the western part of the Pasinler plateau. None of these vents are visible in the field because they are probably all buried by their own pyroclastic products from later eruptions. On the basis of their aerial distribution, and variations in thickness, it can be argued that the main eruptive vent for the Grey/White ignimbrite flows was possibly situated in the area between the Büyükdere and the Timar valleys. This eruption created a pyroclastic edifice which was later partly truncated by erosion.

In the vicinity of Kocagüney hill, about 1 km east of Açığındağsırtı ridge, an almost vertical (85-90°) andesitic dyke with the same texture and composition to the dykes at the base, cuts the pyroclastic units of the basal part of the Upper tuff. It has a strike of N70°E, an outcrop length of about half a km and a thickness of 2-2.5m. It contains flow-oriented plagioclase microlites in a grey, glassy groundmass and exhibits a trachitoid texture. It displays platy-joints aligned parallel to the walls of the dyke. The presence of this dyke proves that the volcanism which produced the Kargapazarı volcanics still remained partly active during the formation of the basal levels of the Upper tuff.

2.3.1.3. The Pasinler Town - Hasandağ Section

To the south of the E-W striking hinge of the monoclinal fold, the volcanics of the Pasinler Plateau are unconformably overlain by the Upper Pliocene Aras formation which is, in turn, overlain by the Quaternary alluvium of the Pasinler plain. Further south on the plain, the volcanic unit is only exposed in the vicinity of Mt. Hasandağ.

On the south slope of Mt. Hasandağ, between the town of Pasinler and the summit of Mt. Hasandağ, a well-exposed volcanic section is present (Fig 2.17). At the base of this section, especially around the small hill on which the Hasankale Castle is founded, a phenocryst-rich, densely-welded, dark coloured ignimbrite unit crops out (Photo 2.26). It is composed of abundant euhedral and subhedral plagioclase laths surrounded by a black or grey, very silica-rich, obsidian-like, glassy groundmass and shows a resinous lustre and an irregular fracture surface. It shows a well-developed vitrophyric and eutaxitic texture with large, 3-5 cm thick and a few tens of cm long fiammé. In some flows, with the increase of tension cracks, presumably resulting from tension during cooling, perlitic texture becomes dominant in this volcanic unit. Its colour changes from black to greyish-beige in places. This unit resembles the Black ignimbrite that widely crops out in the northern areas (Photo 2.26).

Photo: 2.26. Densely welded black ignimbrite, Hasankale castle, S slope of Mt. Büyükdağ, the town of Pasinler.

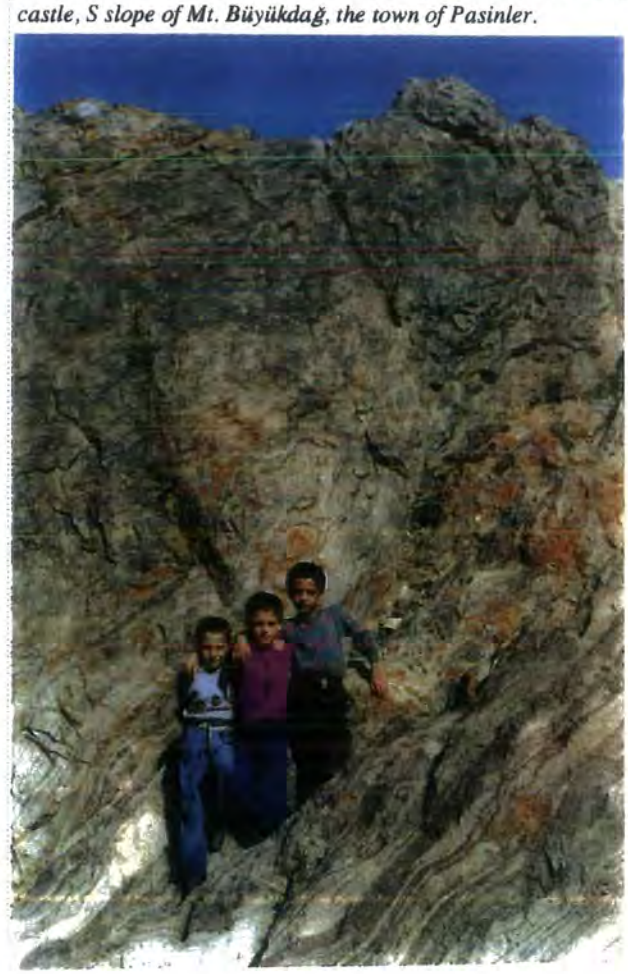

The Black ignimbrite is overlain by an andesite/dacite lava unit. It is pale-grey in colour with plagioclase microlites and minute, fine amphibole microlites. Its texture spans a range from pilotaxitic to micro-porphyritic. It has a thickness of over 100m. Further north, in the vicinity of Büyükdağ hill, the thickness of the unit reaches over 150-200m. In this work, it is named the Büyükdağ andesite after Büyükdağ hill where it is best

exposed. The unit is similar to the Kızılveren amphibole dacite / andesite, except for its finer grained texture. In the upper levels, it is intercalated with the products of reworked pyroclastics and pyroclastic fall deposits. A similar amphibole-bearing, microporphyritic lithology is exposed beneath the Aras formation further north in the vicinity of Sürbehan where the Demirezen dam is under construction.

An aphyric andesitic lava unit, which resembles and is the stratigraphic equivalent of the Kargapazarı volcanics overlies the Büyükdağ andesite (Fig 2.17). This unit has widespread outcrops in the north around the Manastır and Ağıllı hills but disappears on the southwest slope of Mt. Hasandağ. The area situated between the Manastır and Ağıllı hills appears to have been the site of one or more of the vents that produced a discrete edifice of Kargapazarı volcanics. The thickness of the unit reaches a massive 300-350m in this area in contrast to the 10-50 m thickness of the same unit with a few km in the north. The scoria cone at Kızılgüney hill, about 2.5 km west of the Tımar Village, may be part of the same eruptive system (Figure 2.18).

To the northwest of Pasinler, in the vicinity of Tizgi and Serçeboğazı villages and Büyükserçeboğazı hill, a dacitic-rhyolitic lava unit with the same field appearance as the Ardıçlıdağ rhyolite occurs. In the area between Serçeboğazı and Tizgi villages, it is predominantly a creamy-white rhyolite, containing sanidine and displaying a porphyritic texture. Further north, around the Büyükserçeboğazı hill, its texture changes to perlitic. This part of the volcanic unit corresponds to the perlitic-ignimbritic upper levels of the Ardıçlıdağ rhyolite that crops out on Cimcime hill near the Sansordere section.

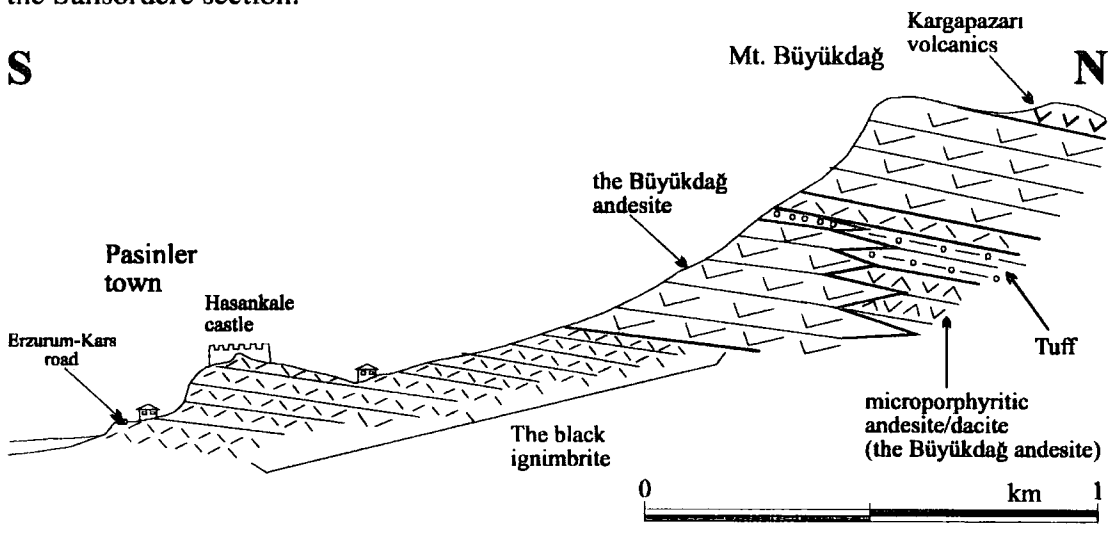

Figure: 2.17. Cross-section passing through the town of Pasinler and Mt. Büyükdağ in the direction of N-E.

2.3.1.4. The Tımar Gorge Section

The Tımar gorge is located between the Büyükdere and Sansordere gorges to the north of Tımar village. Like the Büyükdere gorge, the Tımar gorge contains, on its 300

m deep slopes, spectacular outcrops of the Lower tuff, overlain by the Black ignimbrite and the Kargapazarı volcanics. The volcano-stratigraphy of this area is in general the same as that of the adjacent Büyükdere gorge section. The only difference is that, compared to more western areas, the proportion and thickness of pyroclastic-flow units (the White and Grey ignimbrites) is less than that of the pyroclastic-fall

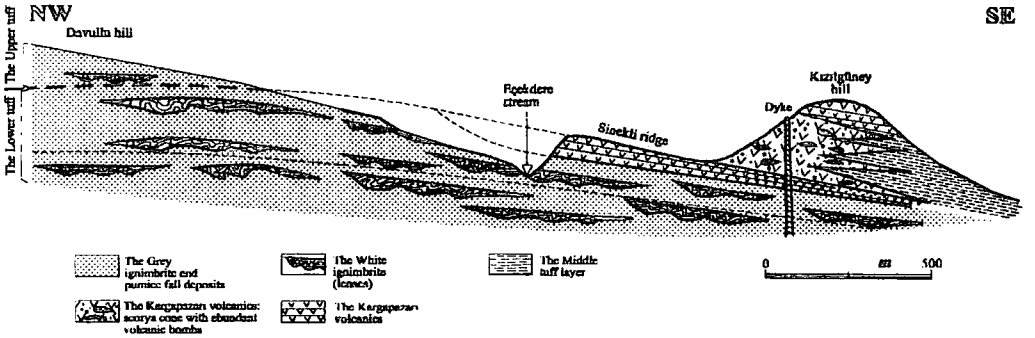

Figure: 2.18. Cross section between the Davullu hill (S:38) and Kızılgüney hill (V:40) showing the relationship between the scoria cone at Kızılgüney hill and underlying pyroclastic units of the lower tuff, N of Pasinler.

deposits in the Tımar gorge section, especially in the Kilisedere side-stream to the NE. This part of the Lower tuff may thus represent a rather distal part of the pyroclastic-flow units, deposited away from the main vent system located near the Büyükdere gorge. Further east, in Sansordere gorge, pyroclastic-flow units become even less abundant and thinner confirming the validity of this assumption. The Black-ignimbrite attains its maximum thickness of 250-300m in the Kilisedere stream between the ruins of Kamışlı and Kuruköy villages (Photo 2.11).

2.3.2. SOUTH OF PASINLER

In the south of the Pasinler Plain, including Ağaçalar, Ortuzu, Bulkasım, Hertev and Ketvan villages and the Mt. Hündül, Alibaba and Gravludağ hills, the basement formations to the Erzurum-Kars Plateau Volcanics are exposed over a large area. The basement is represented by the East Anatolian Accretionary Complex (EAAC). The stratigraphy of this area can be summarised as follows: unconformably overlying the basement is the Eocene Bulkasım formation, made up essentially of ophiolitic clastics and olistostromes. The Bulkasım formation is overlain by the Upper Eocene Narman group. The Güllüce formation, which consists of continental deposits with evaporitic intercalations, and spans the period from Early to Middle Miocene, overlies these formations with an angular unconformity. This unit is in turn overlain by the Hündül limestone which is mainly reefal in character. In this area, the youngest unit, which unconformably overlies all the formations, is the Pliocene Aras formation. Apart from the Narman Group, none of these basement formations outcrop in the northern areas as they are extensively covered by the plateau volcanics.

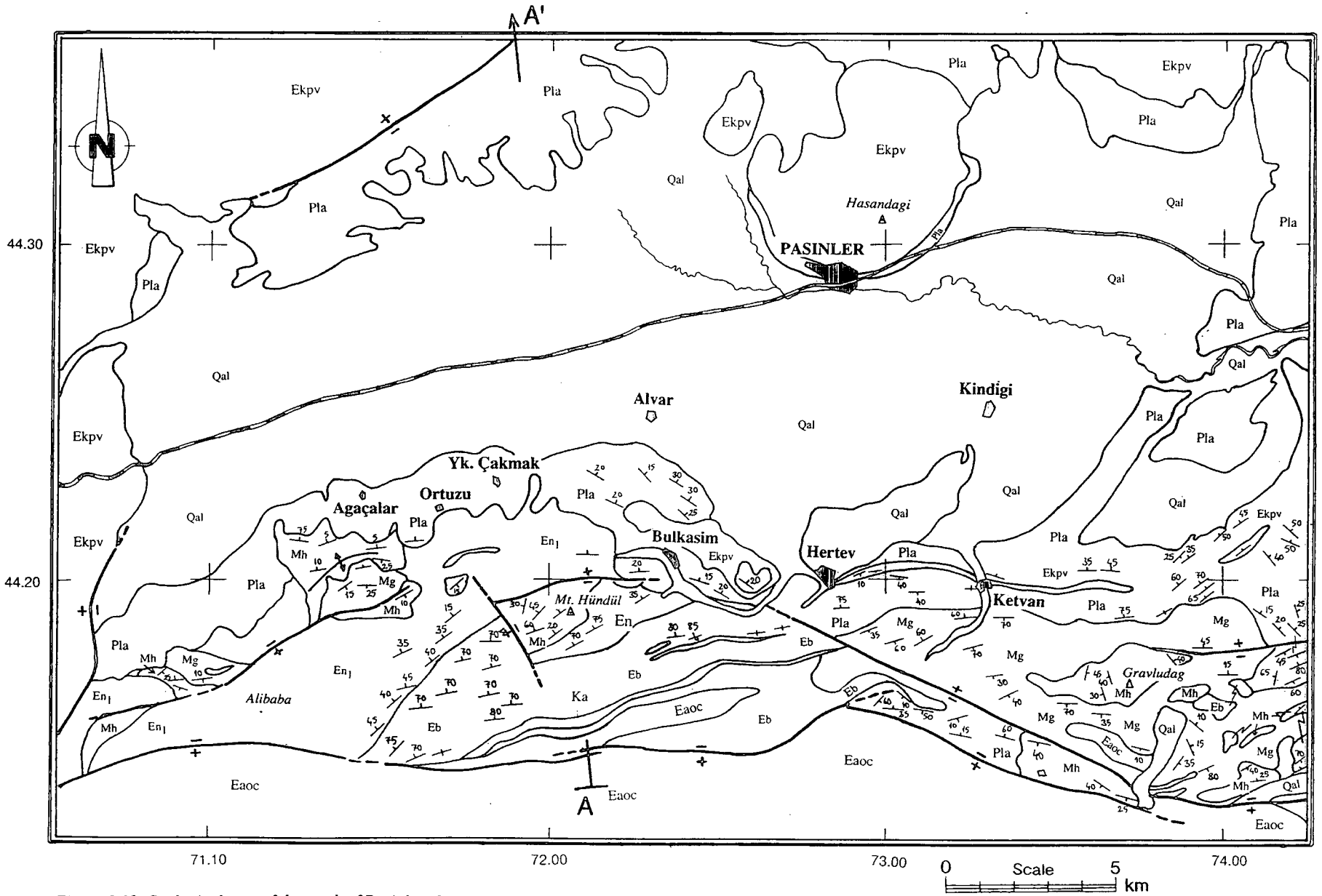

Figure:2.19. Geological map of the south of Pasinler plain, E of Erzurum.

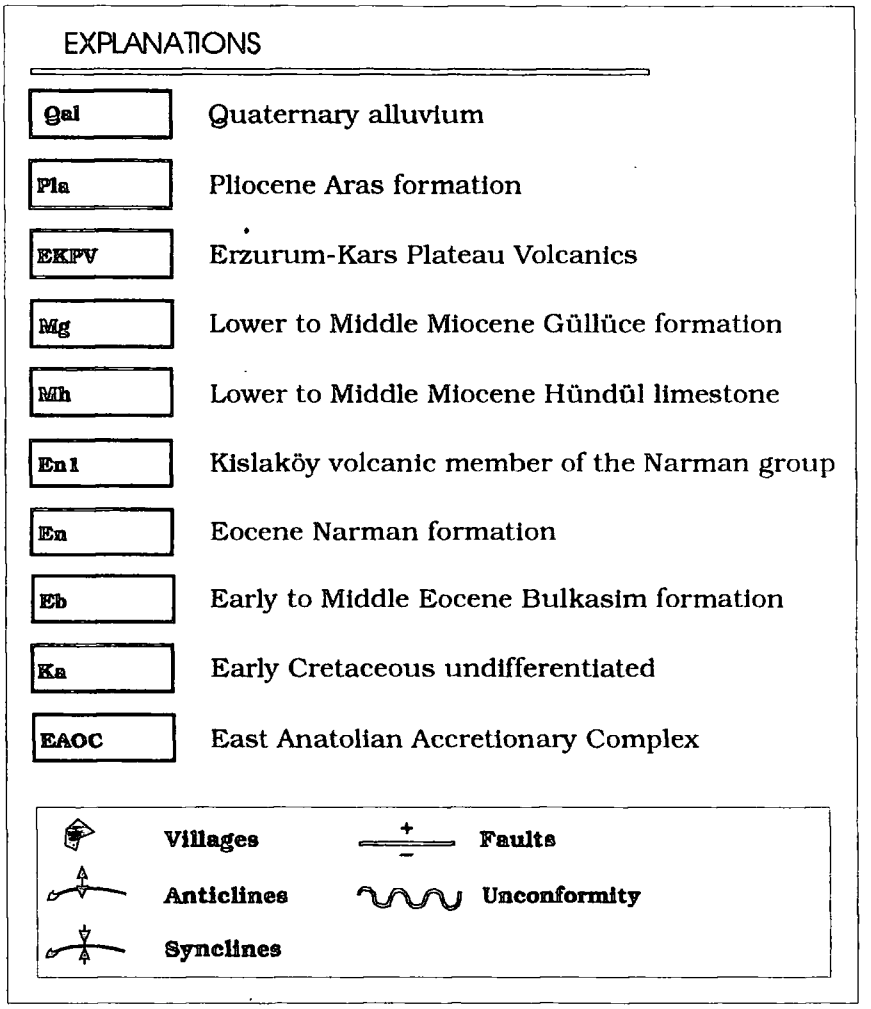
EXPLANATIONS
Qal
Quaternary alluvium
Pla
Pliocene Aras formation
EKPV
Erzurum-Kars Plateau Volcanics
Mg
Lower to Middle Miocene Güllüce formation
Mh
Lower to Middle Miocene Hündül limestone
En1
Kislaköy volcanic member of the Narman group
En
Eocene Narman formation
Eb
Early to Middle Eocene Bulkasim formation
Ka
Early Cretaceous undifferentiated
EAOC
East Anatolian Accretionary Complex
Villages
Faults
Anticlines
Unconformity
Synclines

Figure:2.20. N-S cross section through Pasinler area Between Mt. Dikilitaş and Mt. Kargapazarı ridge.

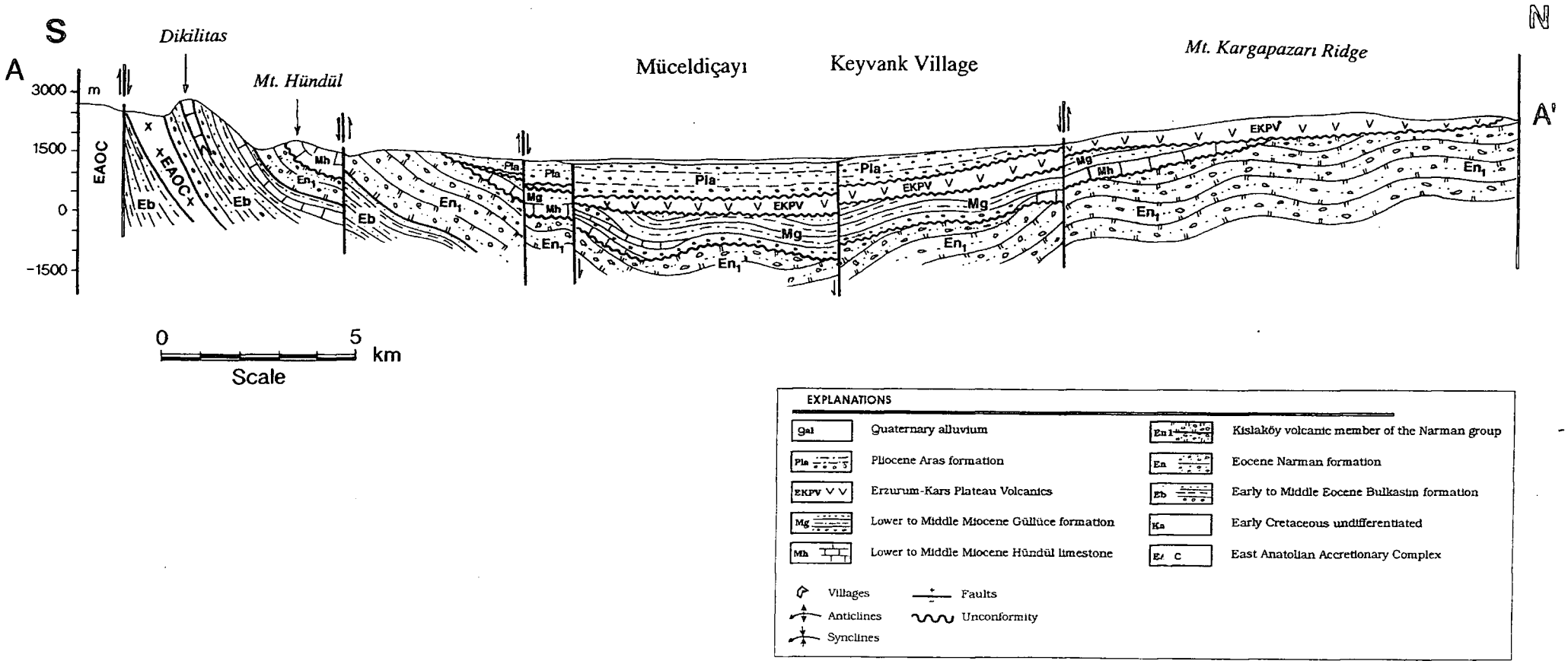

This area is bounded in the north by the Pasinler Plain and in the south by the E-W trending ridge of the EAAC (the Palandöken-Sakaltutan ridge). The border between this ridge and the other formations is marked by a series of E-W striking vertical faults upthrown to the south. In the following paragraphs, the stratigraphy of this area will be introduced briefly from the base to top.

2.3.2.1. The East Anatolian Accretionary Complex (EAAC)

To the south of the town of Pasinler, the basement is represented by an ophiolitic mélange which has been given various names by researchers, including the Eastern Anatolia ophiolitic complex (Koçyiğit, 1985), the East Anatolian Accretionary Complex (Şengör and Yılmaz, 1981), the Sakaltutan Ophiolite (Yılmaz et. al., 1988) and the Yüksekova complex (Turkish Petroleum's geologists: Şahintürk and Kasar, 1980; Erdoğan and Soytürk, 1974; Erakman and Şahintürk, 1980). In this study, this unit will be called the East Anatolian Accretionary Complex (EAAC) in accordance with Şengör and Yılmaz's 1981 description because it is more appropriate to use such a regional name with a genetic significance. The name 'Yüksekova complex', which is widely used by TPAO (Turkish Petroleum Company) for the ophiolitic rocks in the region, may be misleading for this particular area since it was originally used for a group of ophiolitic rocks from the Neotethys' suture zone in the Eastern Taurus Mountain range, far away from the Pasinler area. The term 'East Anatolian Accretionary Complex' of Şengör and Yılmaz (1981) is more appropriate than the 'Eastern Anatolia ophiolitic complex of Koçyiğit' (1985), as this mélange contains not only ophiolitic lithologies but also sedimentary, metamorphic and volcanic rock blocks of different environments and ages.

The EAAC is mainly composed of basic to ultrabasic ophiolitic blocks associated with pelagic, and sometimes neritic, carbonate blocks in a serpentinitic matrix. Serpentinite is the most abundant lithology. In some places it contains lisphenite. It exhibits all the characteristics of an ophiolitic mélange.

In the south of Pasinler area, the EAAC comprises an E-W trending ridge, like a palaeotopographic high. This ridge is located between Mt. Palandöken to the south of Erzurum city and Mt. Sakaltutan, in the south of the Pasinler plain. It is named the Palandöken-Sakaltutan ridge. To the east, this ridge extends through the south of the Horasan Area to the Kağızman area.

2.3.2.2. The Middle Eocene Bulkasım Formation (Eb)

The oldest formation unconformably overlying the EAAC to the south of Pasinler is the Middle Eocene Bulkasım formation. It was named by Turkish

Petroleum's (TPAO) geologists after the nearby Bulkasım village where its best outcrops are exposed. It crops out widely to the south of Bulkasım village and Mt. Hündül. According to TPAO's geologists, the Bulkasım formation is the first sedimentary unit deposited immediately after the emplacement of the EAAC towards the end of the Middle Eocene (Erakman and Şahintürk, 1980). Therefore, close to its base, it contains olistoliths and olistostromes of ophiolitic lithologies which are gathered from the ophiolitic basement. The unit is made up of sandstone associated with the alternations of shale, occasional conglomerate and some intercalations of reefal limestone. It also contains marl and bioclastic limestone interbeds. TPAO geologists argue that it shows the characteristics of a molasse deposit. Palaeontological descriptions of this formation carried out by TPAO have dated this unit as Middle to Upper Eocene (Erakman and Şahintürk, 1980).

2.3.2.3. The Eocene Narman Group (En)

The Narman group shows similar characteristics to those described earlier from the Harabedere gorge section although in the south, it mainly consists of the Kışlaköy volcanics. The Kışlaköy volcanics are made up of the following lithologies: a porphyritic basaltic-andesite unit which contains plagioclase megacrysts and an olivine-bearing basaltic-andesite or basalt, which includes plagioclase, clinopyroxene and olivine microphenocrysts and phenocrysts and exhibits a texture from aphyric to microporphyritic. The Kışlaköy volcanics crop out generally either on the ophiolitic basement or on the Bulkasım formation with angular unconformity. Its outcrops are located mainly between the north slopes of Mt. Hündül and Alibaba hill.

The only area where the flysch-like beds of the Narman formation are exposed is located to the southeast and east of Mt. Hündül.

2.3.2.4. The Güllüce Formation (Mg)

The Bulkasım and Narman formations are unconformably overlain by the Early to Middle Miocene Güllüce formation. To the south of Pasinler, the Güllüce formation crops out widely south of Hertev and Ketvan villages. It is named by Sungurlu et. al. (1972) after the Güllüce village close to the town of Tuzluca, Kars. It is characteristically composed of colourful detrital lithologies. At its base, it starts with a thick conglomerate in red, brown and claret-red colours. The conglomerate often contains very coarse detrital material such as big blocks and boulders. Where the Güllüce formation unconformably sits on the ophiolitic basement, it is entirely composed of ophiolitic clasts. Upward in the succession, it changes into yellow, brown, greenish-grey-coloured shale beds. These shale beds are interfingered with thin- to medium-bedded sandstone and conglomerate beds both of which show poor

sorting. Towards the upper levels, it contains thick halite and gypsum intercalations. The Güllüce formation is unfossiliferous but from its stratigraphic position, it is assumed to be Miocene in age. Its thickness changes considerably from one area to another. The stratigraphic sections measured by TPAO's geologists have revealed a thickness of about 1100-1500m (Erakman and Şahintürk, 1980). If the abundance and size of the detrital material is taken into account, along with the presence of evaporites, the Güllüce formation appears to have formed in a continental environment.

2.3.2.5. The Hündül Limestone (Mlh)

The Hündül limestone's best outcrops are on Mt. Hündül to the southwest of Bulkasım village. It is mainly composed of bioclastic reef limestone. It displays a thick or medium bedding. To the south of Pasinler, the Hündül limestone forms relatively small, sporadic outcrops: 3.5 km south of the Ağaçalar village, on Mt. Hündül and the southeast of the Ketvan village near the Gravludağ hill.

2.3.2.6. The Tuzluyolları Dacite (Mtd)

To the south of Ortuzu village, in a small area close to Tuzluyolları, a brownish-beige coloured, porphyritic textured dacite unconformably overlies the olistostromal beds of the Narman group. It is quite different from the Erzurum-Kars Plateau Volcanics (EKPV) in its general appearence. Compared to the EKPV, it shows more alteration and an unusual brownish colour not usually seen in the EKPV. It consists of plagioclase and altered amphibole phenocrysts in a glassy matrix containing plagioclase microlites. In this volcanic unit, there are some reefal limestone interbeds and lenses containing characteristic fossils of the Burdigalian (A. Üngör, personal communication, 1991). A sample taken from this has been dated at 23.0±0.5 Ma by the K-Ar method which is in agreement with biostratigraphic ages. In this study, this unit is named as the Tuzluyolları dacite. The Tuzluyolları dacite outcrops as very small, discrete and rare exposures on the Erzurum-Kars Plateau. A similar volcanic unit is located north of Horasan, west of Akveren village. It is named the Akveren dacite in that area and will be described in the Horasan area.

2.4. THE HORASAN AREA

The town of Horasan is situated between Pasinler and Karakurt, about 40 km east of Pasinler. Like Pasinler, Horasan is located on a plain called the Horasan plain where the main roads coming from four directions meet. This plain is widely covered

by the loose detrital sediments of the Pliocene Aras formation which were deposited in an inter-mountain basin called the Horasan basin. According to Şaroğlu and Yılmaz (1987), there is strong evidence that this basin was connected to the western Erzurum and Pasinler basins at the beginning of the neotectonic episode about 15 Ma ago. As a result of intensive neotectonic deformation and neovolcanism, these basins became separated. In this study, all the areas around the town of Karaurgan in the north, the town of Sarıkamış in the northeast, the town of Karakurt in the east and Aras and Tahir villages in the south will all be covered in this Section on the Horasan area because the town of Horasan is centrally-located and one of the biggest. As in the Pasinler area, the collision-related volcanics of the Erzurum-Kars Plateau widely outcrop in the northern parts of the Horasan area. However, in the south they form scattered, isolated outcrops. Moreover, the basement formations are widely exposed in the south. Thus, the stratigraphy of this area will be introduced in two main sections, as first the North and then the South of Horasan.

2.4.1. NORTH OF HORASAN TOWN

In the north of Horasan, the area including Çermik, Hızırilyas, Söğütlü, Aşağı and Yukarı Micirgit, Aşağı and Yukarı Horum, Zivin (Süngütaşı), Akveren Altınbulak, Abulbart (Kurbançayırı), Zerkköyü (Sırataşlar), Sırbasan, Yeniköy, Köroğlu villages and Karaurgan town, the Erzurum-Kars Plateau volcanics have been studied at a reconnaissance scale. The area studied is bisected by the old Horasan-Sarıkamış road passes and covers approximately over 400 km^2. In the following paragraphs, the stratigraphy of this northern area will be introduced in order from the basement to top.

2.4.1.1. Basement Units

North of Horasan, the basement is almost entirely composed of an ophiolitic mélange which is called the East Anatolian Accretionary Complex (EAAC). The basement metamorphic rocks are not exposed in this area. They are exposed further east around Karakurt and Kagızman.

2.4.1.1.1. Metamorphic basement rocks

Between Karakurt and Kagızman, the basement is exposed as a pelagic volcano-sedimentary sequence partly of Triassic age (Yılmaz et. al., 1988), metamorphosed in greenschist facies. It is exposed as small, discrete outcrops. The contact between the ophiolitic melange and the metamorphic rocks is generally tectonic in character, although in most places it cannot clearly be observed. Some of these outcrops can be observed along the road-cuts of the Karakurt-Kağızman road.

In the west, the only place where metamorphic basement is present in a 2-3 km^2 area in the vicinity of Kurunlar hill, to the north-east of the town of Çobandere. In this area, its relationship with the ophiolitic rocks cannot be observed, as it is completely covered with younger formations. It is cut in the southeast by a NE-SW trending strike-slip fault which juxtaposes it against the Pliocene Aras formation.

2.4.1.1.2. The East Anatolian Accretionary Complex (EAAC)

In the Horasan area the basement is generally represented by the ophiolitic mélange, known as the East Anatolian Accretionary Complex (Şengör and Yılmaz, 1981). The unit is composed of limestone olistoliths, ranging in age from Triassic to Cenomanian, associated with the blocks of basic and ultrabasic igneous rocks including peridotite, harzburgite, gabbro, diabase, basalt and spilitic pillow lavas, blocks of pelagic limestone with radiolarite, marble, chlorite-sericite schist and limestone containing chert, all of which are mainly enclosed in an intensively deformed serpentinised and sometimes slightly metamorphosed volcano-sedimentary matrix. This matrix changes into sheared greywacke which, in places, entirely consists of ophiolitic clasts, shale and tuff (Koçyiğit, 1985). In some places lisphenite is also present as blocks in this unit.

In the north of Horasan, the East Anatolian Accretionary Complex is mainly exposed in two areas as:

(1) The area east of the town of Karaurgan includes Mt. Kızılcadağ (north of Gerek village), Gökdağ hill, Mt. Karataşdağ and Partnakdere village. This area which covers about 100 km^2 has an elliptical outcrop pattern, the long axis of which extends NE-SW, parallel to a strike-slip fault zone named the Çobandede fault (Koçyiğit, 1985). This fault zone forms the contact between younger formations of the Erzurum-Kars Plateau volcanics and (in the southeast) the Aras formation. According to Koçyiğit (1985), the Çobandede strike-slip fault is mainly left lateral (sinstral) and extends between the town of Tekman in the southwest and Çıldır in the northeast. Even though the left-lateral movement is predominant, there are also some right lateral strike-slip conjugate fault-sets present. In addition to the strike-slip movement they sometimes display dip-slip movement. In general the western or northwestern blocks of these faults are the upthrown-blocks. The fault planes are generally sub-vertical but, in some places, as in the vicinity of Akveren village, they change into reverse faults with the fault plane dipping to the northwest, probably because of the N-S oriented compressive stress which played an important role in the neotectonic evolution of the region.

(2) The second area includes Oluktaş Kiliseköy, Bereketli, Çatalelma, Çardaklı, Döşkaya and Dağgır villages and is the lateral continuation of the same ophiolitic unit cropping out in the south. Between Mt. Karataşdağı and the villages of Oluktaş and Kiliseköy, the EAAC is unconformably overlain by the Erzurum-Kars Plateau volcanics. Between Gözebaşı and Çatalelma the lateral continuation of the Çobandede strike-slip fault marks the contact between the ophiolitic unit and the Kışlaköy volcanic member of the Eocene Narman group.

The Çobandede strike-slip fault runs parallel to the Erzurum-Tibilisi strike-slip fault system with a NE-SW strike. Thus, both fault systems seem to be the parts of the same tectonic system, even though they are approximately 50 km apart.

2.4.1.1.3. The Eocene Bulkasım Formation (Eb)

The first sedimentary formation lying unconformably over ophiolitic basement of the EAAC is the Middle to Upper Eocene Bulkasım formation. The Bulkasım formation is exposed to the east of Mt. Büyükdağ and Topyolu hill as a narrow, sliver of outcrop with a NE-SW trend and covers the western edge of the ophiolitic ridge formed by Mt. Karataşdağ and Mt. Kızılcadağ. It resembles the Bulkasım formation described earlier in the Pasinler area. Further north and northwest, in the vicinity of Narman, the Bulkasım formation is in turn unconformably overlain by the Upper Eocene Narman formation.

2.4.1.1.4. The Eocene Narman Formation (En)

Around Hızırilyas and Çermik villages, about 8 km south of Zivin village, a flysch-like sedimentary unit is exposed. In these outcrops, which cover a few km^2 area, this unit comprises a sequence which is made up of the alternations of thinly-bedded sandstone and shale. The sandstone is generally fine-grained, well-sorted and ungraded, it occasionally includes fragments of plant fossils. The sandstone is generally yellowish-white in colour, in contrast to the greenish grey colour of the alternating shale and marl. The base of the Narman formation is not exposed in this area because it is unconformably covered by younger volcanic (the Akveren dacite and volcanic units of the Erzurum-Kars plateau) and sedimentary formations (Pliocene Aras formation). This unit is not differentiated on TPAO's geological maps but, the exposure is shown as "Eocene flysch" on 1/250000 scale Kars sheet of the geological map of Turkey (Erentöz and Ketin, 1961). According to geologists at MTA, (The Institute of Mineral Research and Exploration), there is some palaeontological evidence that its age is Eocene (L. Gök, A. Arbas, and M. İmik, personal

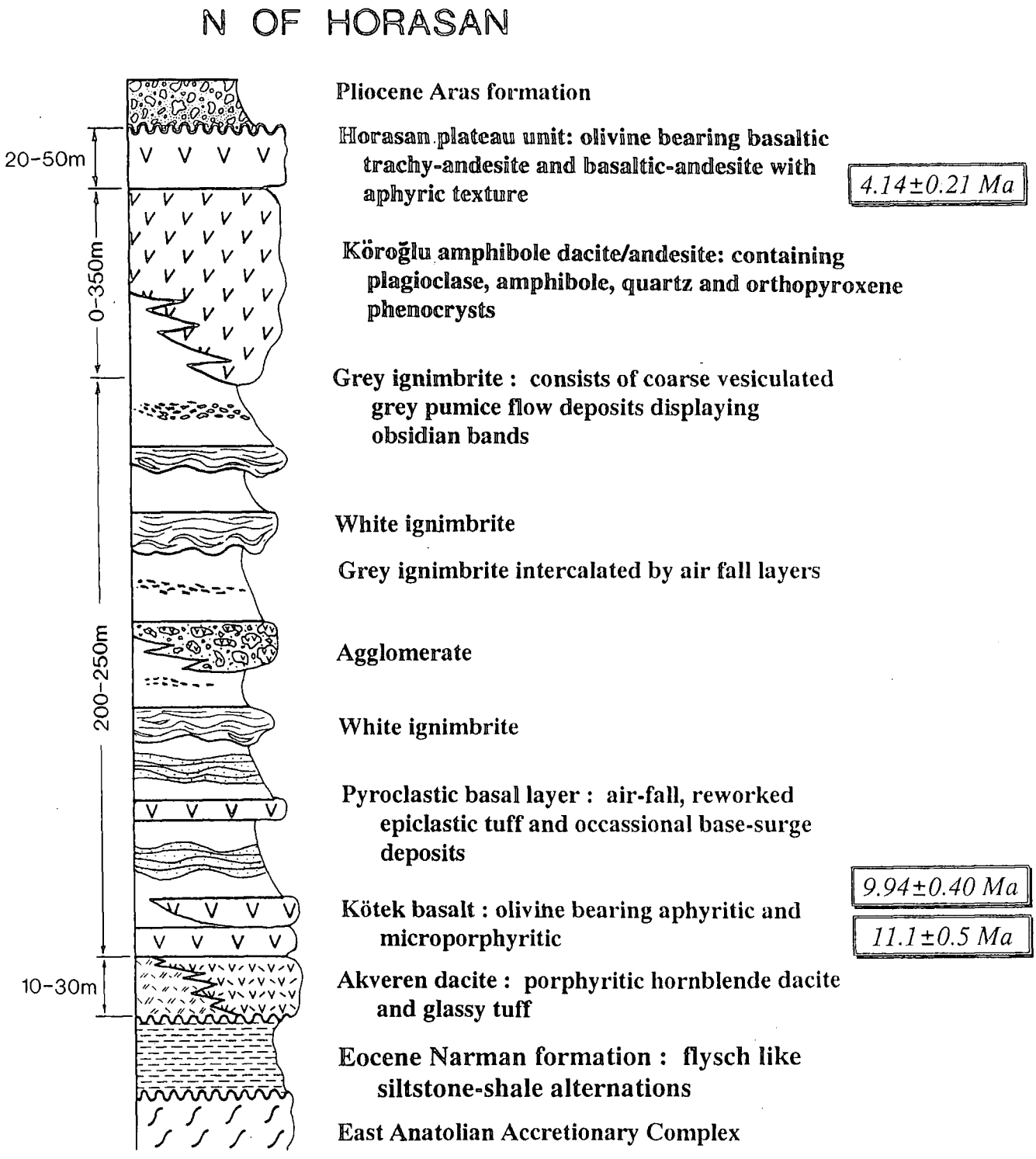

Figure: 2.21. Generalised stratigraphical column of the North of Horasan.

communication, 1990). It bears a close resemblance to the Upper Eocene Narman formation exposed in the Harabedere valley, in the Pasinler area. Unlike the Upper Eocene outcrops in the western areas north of Pasinler and Mt. Kargapazarı, it does not contain any volcanic rock intercalations.

Further north, near town of Bardız, and in the west around Mt. Zozandağ, Mt. Büyükdağ, Mt. Sıçankaledağı and the town of Kışlaköy, the Narman group and its volcanic member (the Kışlaköy volcanics) cover very large areas.

2.4.1.1.5. The Akveren Dacite (Mad)

The Akveren dacite is the lowermost volcanic unit unconformably overlying the ophiolitic basement to the north of the Town of Horasan where it is exposed as small discrete outcrops. In terms of its texture and composition it closely resembles to the Middle Miocene volcanics named in this study as the Tuzluyolları dacite which lies to the south of Pasinler. It is mostly pinkish-beige in colour and porphyritic in texture. It consists of coarse subhedral to euhedral phenocrysts of plagioclase, severely altered phenocrysts and microphenocrysts of brown amphibole and probably biotite all of which are surrounded by an amorphous, glassy groundmass. In general, it is more weathered than the generally fresh lavas located in higher stratigraphic levels. Its texture occasionally changes into intersertal where it contains abundant microlites and microcrystals of plagioclase. One of its best outcrops is located around the Bayırın and Kızıltaş hills to the west of Akveren village, about 6 km northwest of the town of Karaurgan. In these hills, it attains a thickness of over 50 m. In this study, this unit is termed the Akveren dacite after the name of the village where its best outcrops are found. The unit lies unconformably over the Upper Cretaceous EAAC. The unconformity is cut by a NE-SW striking reverse fault displaying a 60-70° dip towards the NE. Along this fault both of these units are thrust together over the upper pyroclastic flow and fall units of the Erzurum-Kars Plateau. This reverse fault is one of the faults that make up the Çobandede strike-slip fault zone.

Another outcrop of the Akveren dacite is situated in a very small area between the town of Karaurgan and Zivin (Süngütaşı) villages in the Büyükçay stream valley, on the southeast slope of Çerkezintaş hill. Ophiolitic basement is not exposed in this area. In contrast to the porphyritic rocks in Akveren village, the Akveren dacite is generally made up here of consolidated and partly vitrified glassy tuff with occasional plagioclase clasts and a small amount of microporphyritic lava, both of which are brick-red in colour. Its apparent thickness never exceeds 10-15m. It is overlain by an aphyric basaltic lava sequence from which a K-Ar age of 11.1±0.5 Ma has been obtained. This proves that the unit should be older than 11 Ma.

Another outcrop of porphyritic dacite is located 1 km north of Hızırilyas village around Hızırilyas-kayalığı hill and Hünkardüzlügü, about 8km south of Zivin (Süngütaşı) village. In this area the unit unconformably lies over the flysch-like,

Figure: 2.22.

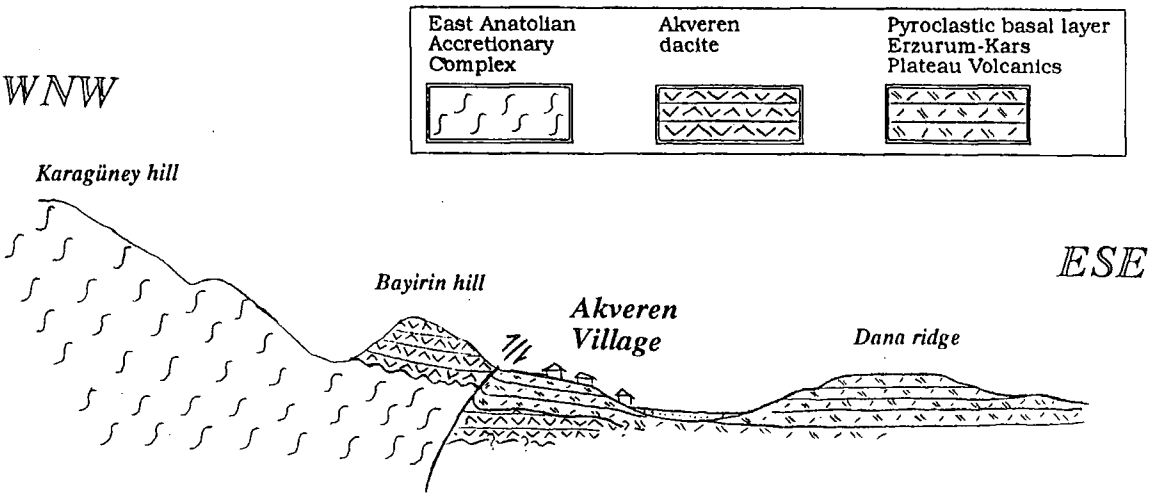

Eocene Narman formation and attains a thickness of 200m. Moreover, it is overlain by the basal pyroclastic layer of the Erzurum-Kars Plateau volcanics.

2.4.1.2. The Erzurum-Kars Plateau Volcanics

2.4.1.2.1. The Kötek Basalt (Köb)

North of Horasan, a basalt layer interbeded with some basaltic agglomerate layers unconformably overlies the basement units at the base of the volcanic succession. Its outcrop forms a rather small area at the base of the Büyükçay stream valley between Zivin (Süngütaşı) and Abulbart villages. In this study it is named the Kötek basalt as its best outcrops are situated around Kötek Village. It is black in colour and displays aphyric to microporphyritic texture. It contains plagioclase and occasional olivine microphenocrysts in a hyalopilitic to intersertal groundmass. It sometimes shows amygdaloidal texture. K-Ar dating ascribes an age of 11.1±0.5 to 9.94±0.40 Ma. To my knowledge, this is the oldest age obtained from the collision-related volcanics in Eastern Anatolia. Thus the Kötek basalt may represent one of the earliest centres of volcanic activity genetically related to the collision event, not only on the Erzurum-Kars Plateau but also all over Eastern Anatolia region.

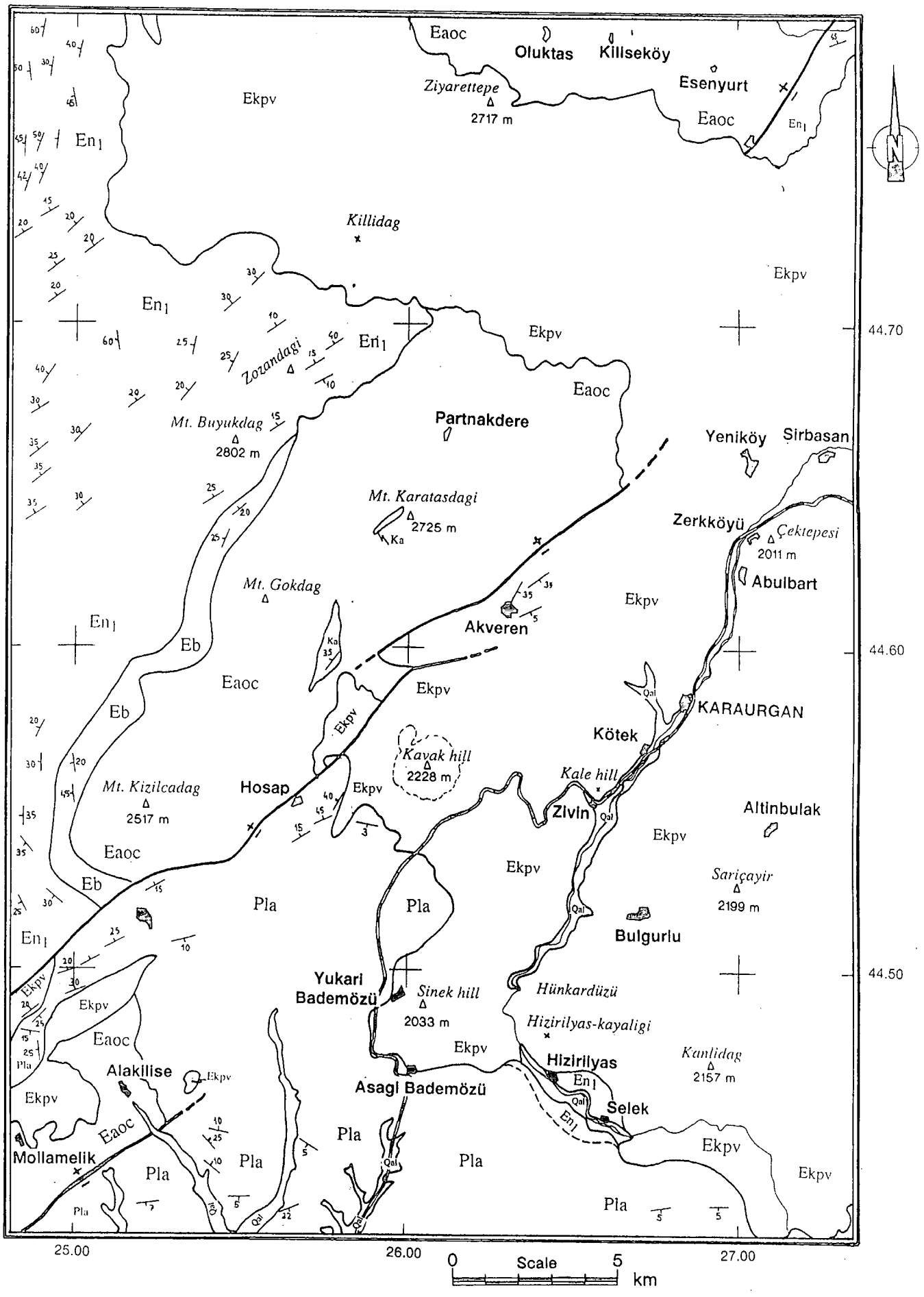

Figure: 2.23. 1/100.000 scaled geological map of the north of Horasan. The map is supplied by TPAO .

2.4.1.2.2. The Pyroclastic Basal Unit (Pblh)

Pyroclastic rocks are the most abundant lithology, accounting for over 60-70% of this part of the volcanic succession. They consist of several pyroclastic flow, fall and rare base-surge units, reworked pyroclastics, some sporadic agglomerates and basic to intermediate lava interbeds. This unit resembles the Lower tuff exposed at the base of the Pasinler area around the Büyükdere and Tımar gorges. One of the main differences between these two areas is that, in the Horasan area, the Pyroclastic basal unit contains several aphyric basaltic to intermediate lava flows and lenses; these are rare in the Pasinler area. These lenses are similar to the Kötek basalt in terms of their composition and texture. Their average thickness is about 2-5 m. At the contact zone of each lava flow with underlying tuff beds, there is a 20-30 cm thick, red to orange-coloured, thermally affected zone.

Pyroclastic fall and reworked tuff beds make up the most abundant material in this part of the volcanic succession. In some parts of the Pyroclastic basal unit, where there is a higher proportion of lithic to juvenile fragments, reworked pyroclastic beds become almost indistinguishable from the volcanoclastic beds of the Pliocene Aras formation. They contain fragments of rounded white pumice, basic and intermediate aphyric lava, hornblende-bearing porphyritic dacite-andesite, white ignimbrite and obsidian in a fine-grained volcanic ash. Even though the proportion of these fragments changes from one place to another, pumice and ash always constitute the main part of the rock.

Pyroclastic-fall deposits are mainly made up of matrix-supported white pumice fragments. The white pumice is mostly rounded and highly vesicular. They are widespread throughout the Pyroclastic basal unit. In some places these deposits make up some small tuff-cones which were possibly the main centres of the explosive eruptions. One of these cones forms Kavak hill, 1 km north of Yukarıhorum village. Its slopes are partly eroded by small radial ravines although its cone shape is still recognisable except for a crater at its top. It covers a 3½-4 km^2 area with a height of about 200-250m above the average plateau level.

Pyroclastic flow units are composed of White and Grey ignimbrite with the same field appearence, texture and composition as described at Pasinler. However, compared to the Pasinler area, these pyroclastic flow units are less abundant in the Horasan area. These ignimbrite flows are well displayed at Kale hill, near Zivin village. In this location, a strongly-welded, compact tuff, which contains very fine flow-oriented, rare biotite microcrystals in a glassy white matrix, is exposed at the base of the unit. This lithology is abundant to the south on both the eastern and

western slopes of the Büyükçay valley between Zivin and Taşkesen villages. At Kale hill, this tuff unit is underlain by a 50-60m thick agglomerate bed which is made up of rounded boulders of aphyric basaltic-andesite and andesite reaching ½ m or more in diameter. This agglomerate bed has a lens-shape and wedges out to the north, its upper and lower contacts are fairly irregular. It is overlain by a succession of White ignimbrite, reworked pyroclastic beds and subordinate base-surge deposits which show characteristic wavy bedding. In this part of the succession, individual White ignimbrite flows sometimes exceed 20 m in thickness.

A similar agglomerate bed to that near Zivin village is exposed at the base of the succession on Sırataşlar ridge close to Zerkköyü village (7-8 km north of Kötek). Its thickness is 25-30m.

Between Zerkköyü and Handere villages, the volcanic succession is composed of intercalations of air-fall, reworked pumice deposits, White/Grey ignimbrite and relatively thin and rare interbedded flows of aphyric basalt and basaltic andesite. In some places, it is also interlayered with the amphibole-bearing porphyritic andesite unit (the Köroğlu amphibole dacite/andesite).

2.4.1.2.3. The Köroğlu Amphibole Dacite / Andesite (Kpad)

Volumetrically, this is the second most abundant unit, in this part of the plateau, after the Pyroclastic basal unit. Characteristically, it displays a porphyritic texture with amphibole phenocrysts, one of its most distinctive features, used to differentiate this unit from the other lava units in the field. It consists of plagioclase (An_{40-57}), brown amphibole (magnesio-ferri-tschermakite, magnesio-ferri-taramite and magnesio-edenite), orthopyroxene (hypersthene) and rare quartz phenocrysts enclosed in a microlithic, glassy groundmass. The porphyritic lavas generally plot in the dacite and andesite fields on the classifications of Peccerillo and Taylor (1976) and also Le Bas et al. (1986) (see Section 3.1). It overlies the Pyroclastic basal unit and is partly interbedded with its upper levels. It shows similarities to the amphibole-bearing porphyritic dacitic and andesitic lavas of the Mt. Dumlu area in terms of its petrography, composition and stratigraphic position. Since its best outcrops are exposed at Mt. Köroğlu, close to Köroğlu village, it is named the Köroğlu amphibole dacite/andesite.

The Köroğlu amphibole dacite/andesite forms numerous domes which have various sizes and geometry on the plateau. Some of these domes reach 500m in thickness and constitute most of the higher peaks on the plateau. They include:

Figure: 2.24. SW-NE cross-section between Hızırilyas village and Mt Köroğlu, N of Horasan.

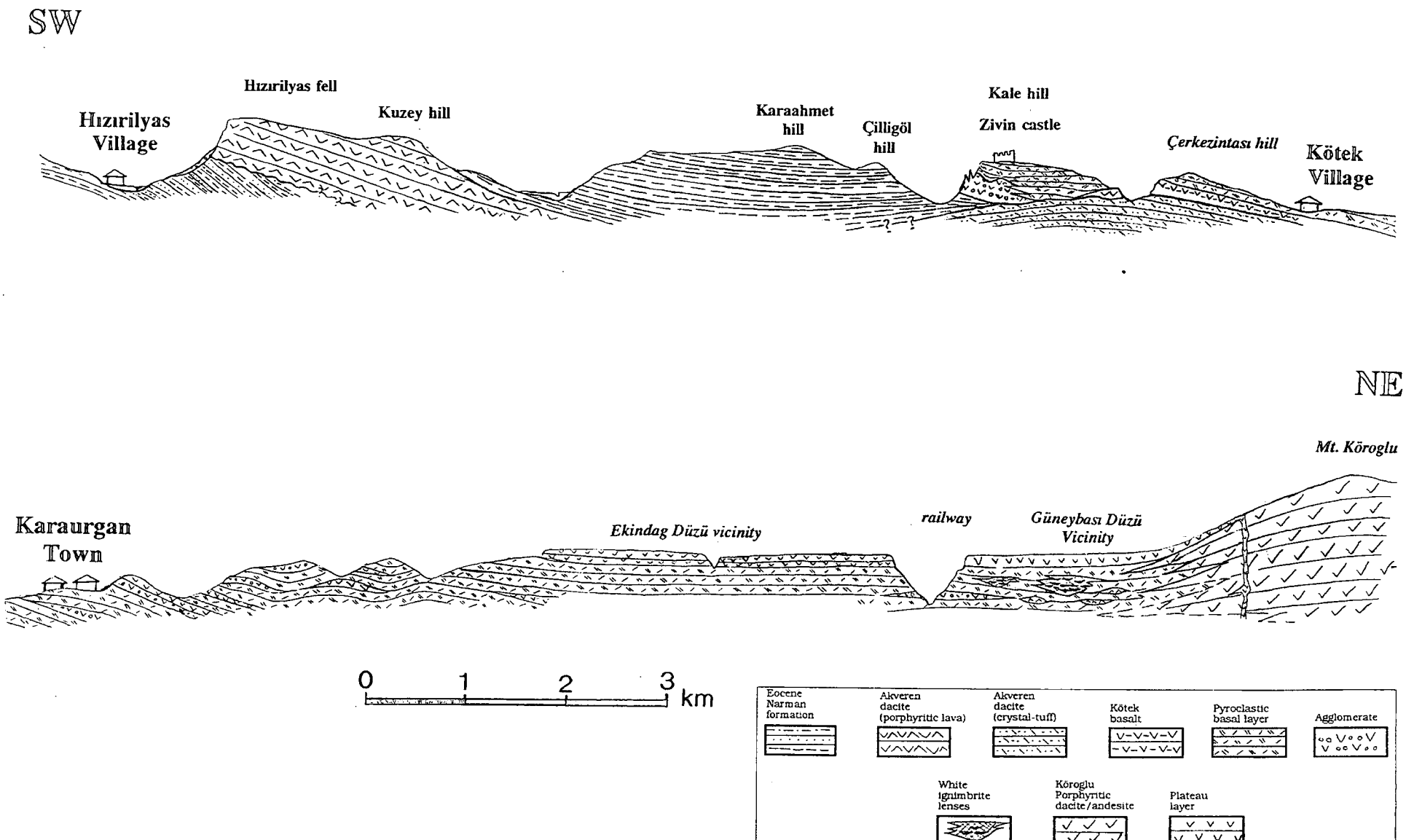

- the Mt. Kanlıdağ, the Çoluyurdu and Kurunlu hills to the northeast of Selek and Çermik villages;
- the Büyükakbaba and Mandırın hills to the north of Aşağımicirgit (İnkaya) village;
- Mt. Süphandağ, one of the biggest eruptive centres in the region, located between Handere village and Karakurt town;
- Mt. Köroğlu, situated to the northeast of Sırbasan village where the unit attains a thickness of over 500 m.

2.4.1.2.4. The Horasan Plateau Unit (Hpl)

This is the uppermost lava unit in the Horasan area which gives the plateau its distinctive morphology in terms of its competent, erosion-resistant nature (Photo 2.27). It surrounds the slopes of the high peaks of the Köroğlu amphibole dacite/andesite domes. In some places, like the Kale ridge and Mağaracık, situated to the north and south of Köroğlu village respectively, it partly overlies the slopes of the Köroğlu amphibole dacite-andesite dome as 10°-20° dipping flows concordant with the slopes. These lava flows appear to be related to fissure eruptions on the side of the porphyritic domes. A similar relationship has been observed further east, north of Uzungazi village, 8 km east of the town of Karakurt, on the south slope of Mt. Süphandağ. The Plateau unit overlies the Köroğlu amphibole dacite/andesite with a dip of 10°-15° to the south in this area.

The unit is made up of black or dark grey-coloured lava flows which are generally horizontal. The Plateau unit spans a relatively narrow compositional range of basalt to basaltic andesite. The lavas forming this unit are predominantly aphyric in texture. They also display vitrophyric, pilotaxitic, intersertal and rare microporphyritic and cumulus textures in places. The thickness of the Plateau unit is variable. At the Terektaşkayaları and Karagölündağ ridges, located to the east of Abulbart (Kurbançayırı) village, the unit is just a few metres thick whereas to the north, around the Köroğludüzü and Ağılkayaları ridges, north of Sırbasan village, it attains a thickness of 70-80m. There it is composed of 7-8 individual lava-flows.

A whole rock K-Ar age of 4.14±0.21 Ma has been obtained from a sample collected from this unit to the northeast of Sırbasan village (Karaderenin ridge).

To the east, around Mt. Süphandağ, to the south and north of the River Aras and further east around Mt. Aladağ and in the Kağızman area, the Plateau unit covers thousands of km^2 in area. Apart from a few volcanic centres, such as the volcanic

Figure: 2.25. Cross section between Selek and Aşşağmicirgirt yaylası villages, NE of Horasan.

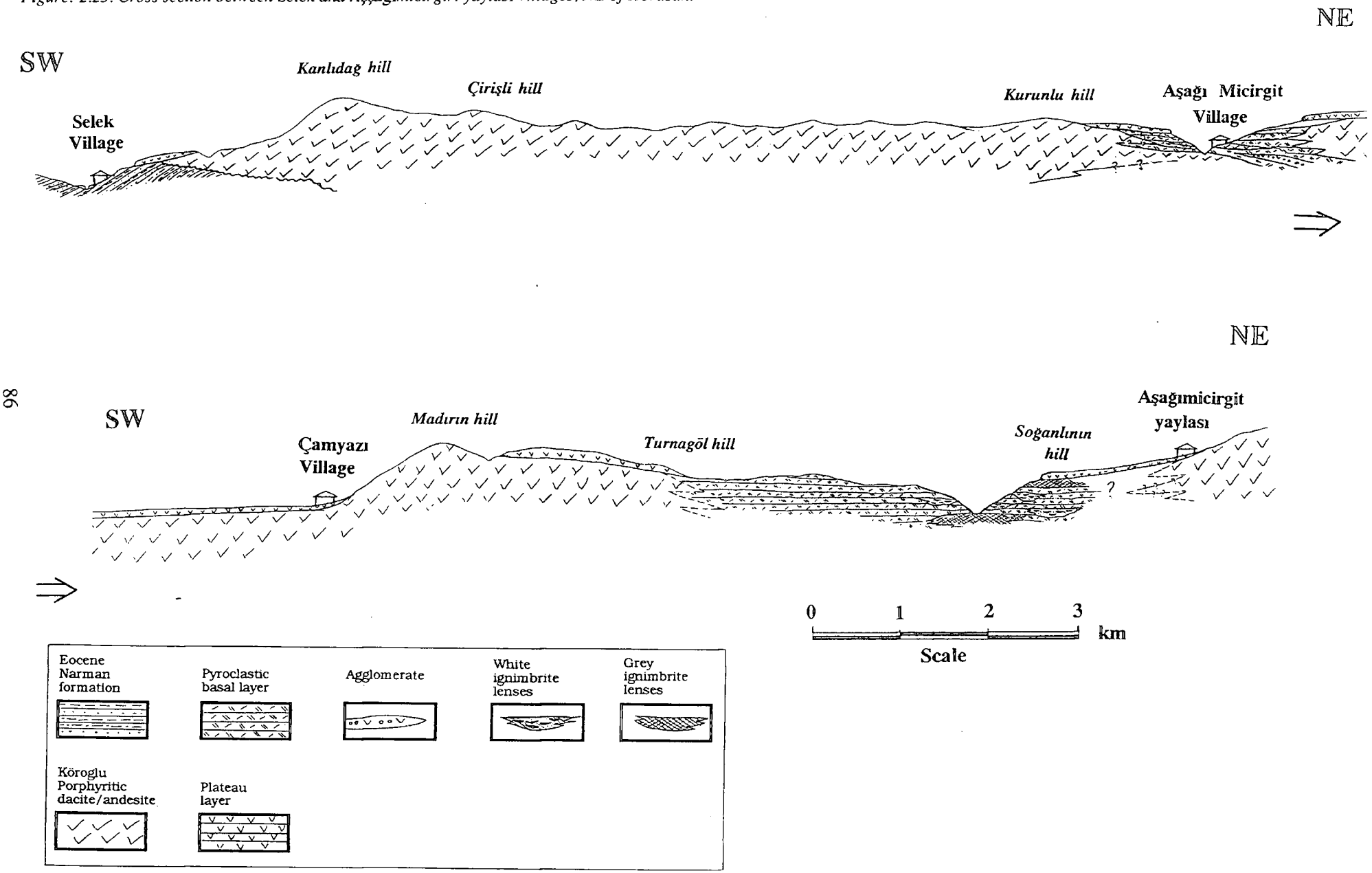

cone of Mt. Aladağ, it is the product of fissure eruptions. In general this unit becomes considerably younger to the east.

Photo: 2.27. A general view of the plateau forming lava flows of the Horasan plateau unit. Güneybaşı Düzü vicinity, N of Sirbasan village, NE of Horasan.

2.4.2. SOUTH OF HORASAN TOWN

In this part of the thesis, the stratigraphy of the area to the south of the town of Horasan including the Aras, Tellalınhanı, Besikom, Haydarkomları, Hotik and Tahir villages and their surrounding areas will be presented.

As in the north, the basement in this area is again made up of the EAAC which is unconformably overlain by the Upper Cretaceous flysch, the Çatköse formation. This is in turn overlain by the Middle to Late Eocene Bulkasım formation. Their outcrops are seen in the vicinity of Ağullu and Tahir villages and Saçtepe hill. The Bulkasım formation is overlain, in turn, by the Upper Eocene Narman formation while the Oligo-Miocene Güllüce formation unconformably overlies the Narman formation. A porphyritic, amphibole and biotite-bearing volcanic unit, the Saçdağ dacite, unconformably overlies the Güllüce formation while the youngest formation, overlying all the former, is the Pliocene Aras formation. In the following paragraphs, these formations will be presented from the base.

2.4.2.1. Basement Units

2.4.2.1.1. The Upper Cretaceous Çatköse Formation (Küç)

The Upper Cretaceous flysch is mainly composed of greenish-grey to khaki-coloured shale/mudstone which has minor interbeds, lenses of sandstone and rarely limestone. This unit is called the Çatköse formation by Turkish Petroleum geologists (Sungurlu et. al., 1972). Shale accounts for about 80% of this unit and is strongly sheared and deformed along some zones. Shale occasionally contains very thin siltstone interbeds and lenses. Sandstone is generally coarse-grained, thin- to medium-bedded with a moderate grading. It rarely contains pebble-sized fragments of ophiolitic rocks and limestone, both of which were gathered from the underlying ophiolitic complex. The limestone is greenish-grey in colour and thin-bedded. It is represented by the clayey-micrite containing Globotruncana sp. The best outcrops of the Çatköse formation are exposed on Toytaş hill, to the north of Tahir village.

2.4.2.1.2. The Middle Eocene Bulkasım Formation (Eb)

In this area, the Middle Eocene Bulkasım formation is composed of a flysch-like sedimentary succession composed of almost the same lithologies as described earlier. In contrast to the northern areas, it also contains fossiliferous sandstone beds which include Nummulites sp. These Nummulite-bearing sandstone beds generally consist of coarse fragments of carbonate. This unit is termed the Ağullu member by Turkish Petroleum geologists (Sungurlu et. al., 1972).

2.4.2.1.3. The Oligo-Miocene Güllüce Formation (Mg)

The Oligo-Miocene formation, named as the Güllüce formation by Sungurlu et. al. (1972), is made up of 'colourful' lithologies as follows: claret-coloured mudstone, poorly sorted polygenetic conglomerate, yellowish-beige-coloured clayey-limestone, and grey or dark green coloured marl-shale. Even from a distance it can easily be differentiated from the other sedimentary formations by these characteristic colours. The thickness of the unit reaches 1100-1500m in the eastern areas (Erakman and Şahintürk, 1980). It does not contain any micro or macro fossils. Mudstone is the most abundant lithology in this unit. Towards the top of the succession it contains gypsum and halite interbeds. This implies that the Güllüce formation was formed in a continental environment.

2.4.2.2. Volcanic Units

To the north of Hacıhalil and Mollaahmet villages, a volcanic succession which is closely similar to those seen in the northern areas, unconformably overlies the Oligo-Miocene Güllüce formation. In the vicinity of Tellalınhanı village and Kızılderbent hill, it is made up of pinkish-beige coloured porphyritic dacite and andesite, probably equivalent to the Köroğlu amphibole dacite/andesite. In this area, it is unconformably overlain by the Pliocene Aras formation.

2.4.2.2.1. The Saçdağ Dacite (Sd)

In the south, a completely different volcanic unit is exposed. This unit differs from the dacites in the northern areas in texture, composition and general field appearance. It occurs around Aşağıaktaş Hotik, Ağullu Çakırkom villages and the Yazılıtaş and Saçdağ hills. This unit unconformably overlies the Bulkasım and

Photo: 2.28. A general view of the Saçdağ dacite, Yazılıtaş village, S of Horasan.

Güllüce formations forms dome-shaped volcanic edifices which are a few kilometres in diameter (Photo 2.28). It therefore appears to be younger than Lower Miocene in age. In this study this unit has been termed the Saçdağ dacite after the best outcrops located at Saçdağ hill. It generally plots in the dacite field in the Peccerillo and Taylor (1976) and Le Bas et al. (1986) classifications. It characteristically displays a coarse porphyritic texture with plagioclase (An_{41-28}), green amphibole (tschermakite-edenite)

and biotite phenocrysts in a white micro- to cryptocrystalline groundmass. It also exhibits pilotaxitic texture.

Photo: 2.29. Dyke of the Saçdağ dacite cutting through detrital beds of the Güllüce formation, Besikom village, S of Horasan.

In the area between Besikom and Haydarkomları, a dyke, very similar to the Saçdağ dacite, cuts the Oligo-Miocene Güllüce formation (Photo 2.29). Its average thickness varies between 10-15 m within a length of 6-7 km. It is almost vertical, with an average strike of N80°E. Compared to the outcrops to the south, it is finer grained, but shows exactly the same mineralogical and geochemical composition. This dyke is the largest seen over the entire region and is subparallel to the other dykes observed further west in the Pasinler area.

2.4.2.3. The Pliocene Aras Formation (Pla)

This comprises the youngest formation, unconformably blanketing the older formations throughout the Northeastern Anatolia region. From its best outcrops in Aras village, it was termed the Aras formation by the geologists of Turkish Petroleum (TPAO) (Sungurlu et al., 1972). It is made up of loose, faintly- to moderately-consolidated detrital sediments such as coarse-grained sandstone, conglomerate, siltstone, and rare clay or marl interbeds. The sandstone is coarse to moderate-grained and poorly sorted. The marl and clay exhibit a greyish-green colour.

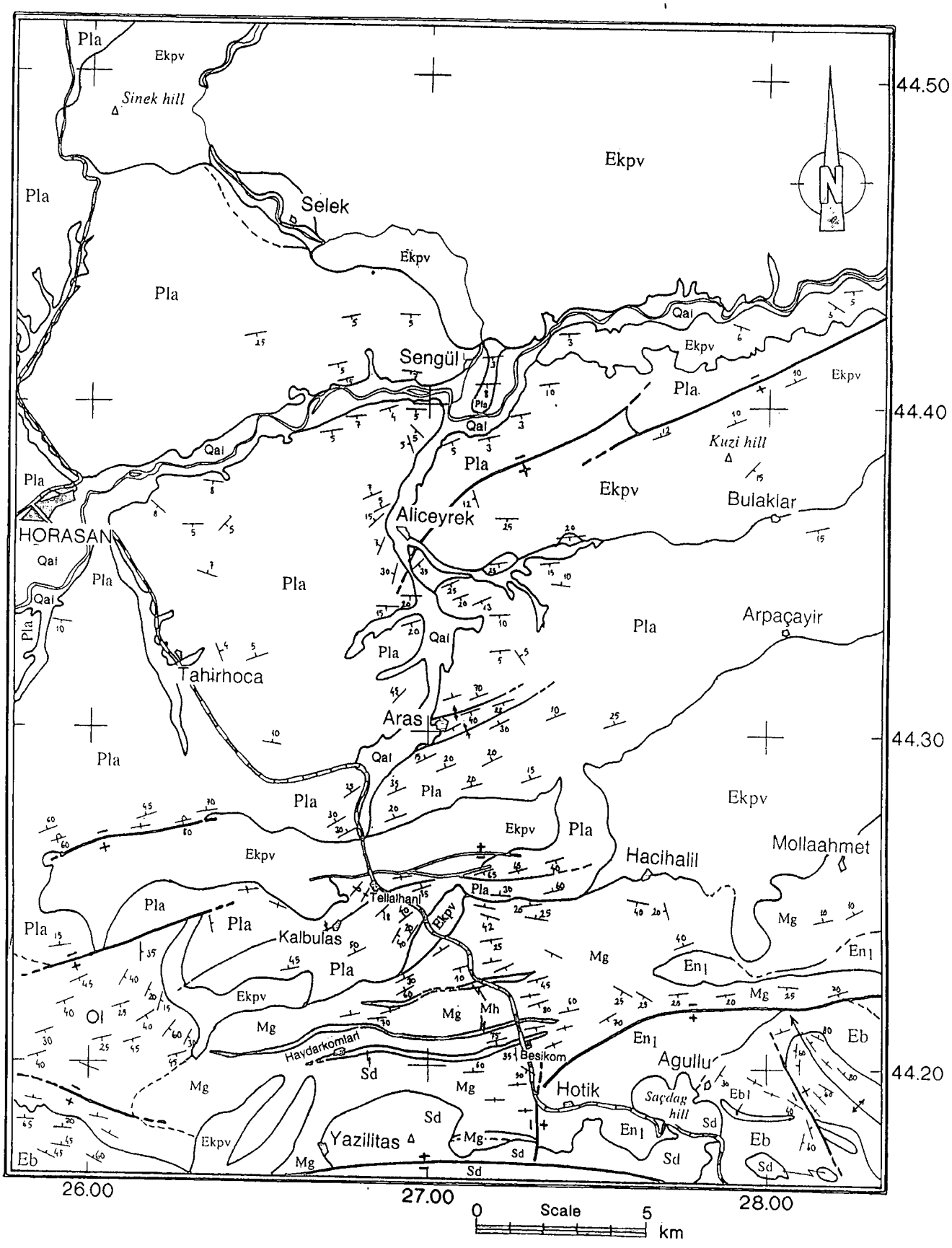

Figure: 2.26. 1/100.000 scaled Geological map of the south of Horasan. The map is taken from TPAO's (Turkish Petroleum Company) archive.

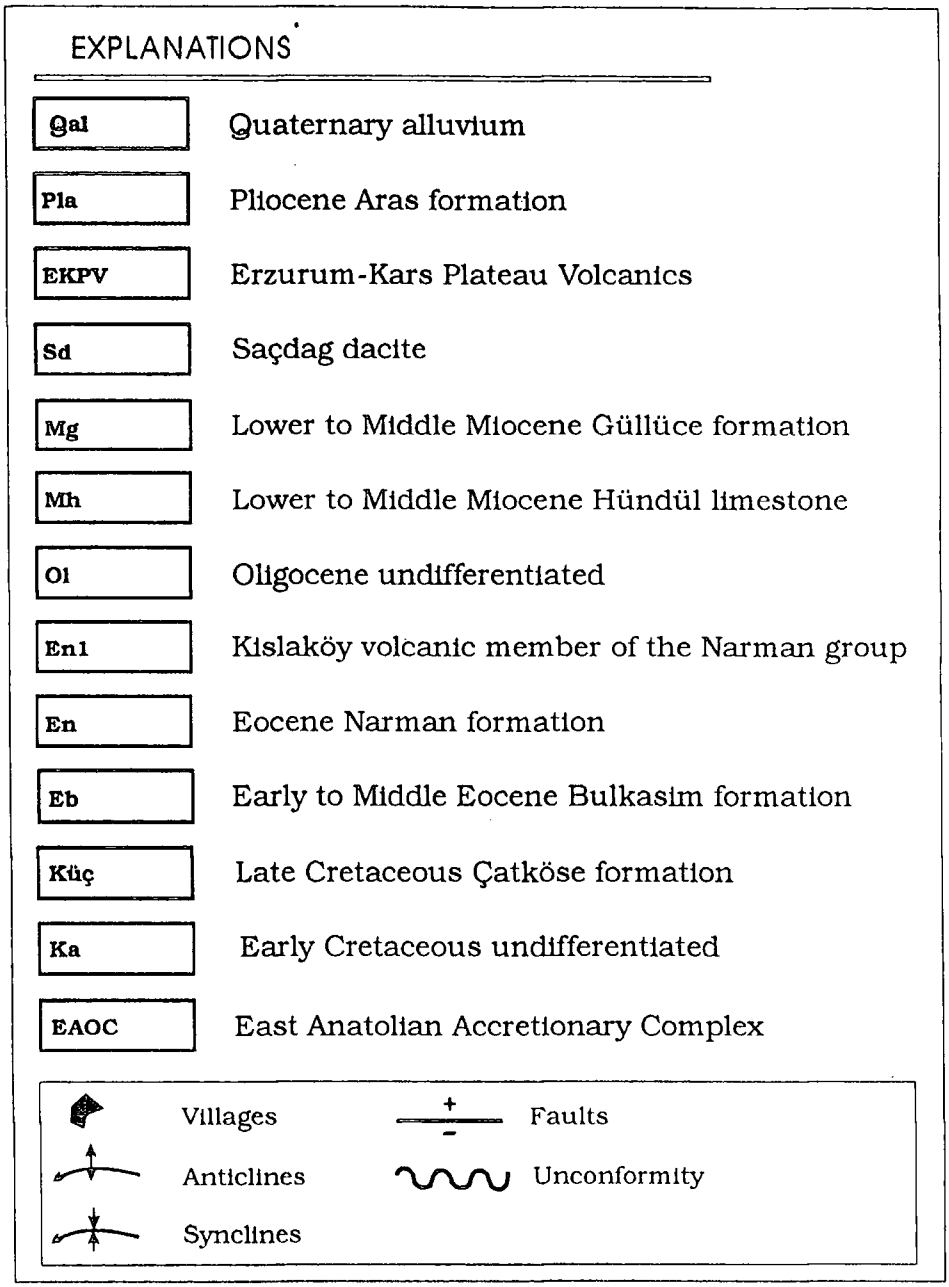
EXPLANATIONS
Qal
Quaternary alluvium
Pla
Pliocene Aras formation
EKPV
Erzurum-Kars Plateau Volcanics
Sd
Saçdag dacite
Mg
Lower to Middle Miocene Güllüce formation
Mh
Lower to Middle Miocene Hündül limestone
Ol
Oligocene undifferentiated
En1
Kislaköy volcanic member of the Narman group
En
Eocene Narman formation
Eb
Early to Middle Eocene Bulkasim formation
Küç
Late Cretaceous Çatköse formation
Ka
Early Cretaceous undifferentiated
EAOC
East Anatolian Accretionary Complex
Villages
Faults
Anticlines
Unconformity
Synclines

The composition of the detrital material within the unit strongly depends on the nature of the underlying formations. Close to the volcanics of the Erzurum-Kars Plateau, it is mainly composed of volcanic clastics such as pumice, ignimbrite and lava fragments which have been gathered from the adjacent volcanic areas. Thus, it becomes almost unrecognisable from reworked interbeds of the pyroclastic basal unit where the volcanic clastics are dominant.

2.5. The Mt. ALADAĞ AREA

Mt. Aladağ (3138 m) is one of the medium-sized strato-volcanoes on the Erzurum-Kars Plateau situated between the towns of Karakurt and Kağızman. It sits on the Horasan plateau unit of the EKPV and rises to a height of 950 m above the average plateau level, with a base area of 75-80 km^2. It has a truncated cone shape, eroded by deep radial ravines on its slopes. The north slope of this cone is especially, deeply eroded or may have collapsed during the eruption, though there is no evidence found in the field supporting the idea of such a major land movement. The lavas erupted from this volcano cover hundreds of km^2 on the plateau and give the plateau its distinctive morphology. This area includes Karapınar, Beşyol, Çardakçatı Akkozyaylası, Belencik, Şehitemin and Gecikmez villages in the west and southwest, Kalebaşı and Odalar villages in the south, Gümüştepe, Çaybük and Ortaköy villages in the north, and finally Çengili and Taşbilek villages in the east. The lavas forming this edifice and the surrounding plateau plot mostly in the andesite and, rarely, dacite fields of Le Bas et al. (1986). They display microporphyritic, hyalopilitic, sometimes seriate textures with phenocrysts of, mainly, plagioclase (An_{37-58}), clinopyroxene (mainly augite with subordinate endiopside) and rarely orthopyroxene (bronzite and hypersthene). The groundmass is entirely composed of volcanic glass. In this study, this unit is named the Aladağ andesite (*Aa*) as its best outcrops lie around Mt. Aladağ. A sample taken from this unit (from the vicinity of Kalebaşı Village) gave a whole-rock K-Ar age of 3.55±0.13 Ma. Thus the central-eruptions which formed the Aladağ andesite are younger than the fissure eruptions which shaped the western part of the plateau (i.e. to the north of Horasan).

South of Mt. Aladağ the Erzurum-Kars Plateau is deeply cut by River Aras which runs approximately from west to east. Between Horasan and Akkoz villages which are situated about 13-15 km east of the town of Karakurt, the Aras river forms a canyon-like 300m deep valley in which a spectacular section of the plateau volcanics is exposed (Photo 2.31). This valley is called the Aras river valley. In this area, the base of the EKPV is not exposed whereas, to the east of Kalebaşı village, the EKPV is

unconformably underlain by the coarse and colourful detrital sediments of the Oligo-Miocene Güllüce formation. The valley gradually deepens eastward cutting through the ophiolitic basement rocks of the East Anatolian Accretionary Complex (EAAC) in the vicinity of Çayarası and Değirmendere villages. From this location eastwards, the EKPV does not outcrop anywhere to the south of the Aras river. The area between Çayarası village and the town of Kağızman entirely consists of the EAAC. The EAAC is not exposed to the north of river Aras, apart from a 7-8 km long narrow band between Değirmendere and Denizgölü villages. In this location, the contact between the Güllüce formation and the EAAC is controlled by the sinistral Kağızman strike-slip fault, which has a strike of ENE-WSW. The Kağızman strike-slip fault, in general, has a vertical fault plane, though in some places, it becomes steeply dipping at ~70° to the north with a dip-slip component. Close to the fault plane, beds of the Güllüce formation become steeper and in some places (e.g. north of Değirmendere village) they dip to the north and northwest at over 50°. Further east, in the vicinity of Kuloğlu village, which is located 15-16 km southeast of Kağızman town, the Aras river valley lies over 1000 m below the plateau level so that the difference in height between the base of the valley and the summit of the Mt. Aladağ reaches 1900m. Between Çayarası village and the town of Kağızman, the orientation of the Aras river valley is predominantly controlled by the Kağızman fault. From Değirmendere village this fault extends laterally to the southwest in the direction of Çayarası, Çolaklı and Güllüceler villages down to the area north of Tahir and Yazılıkaya villages to the south of the town of Horasan.

In the following paragraphs the volcanostratigraphy of Mt. Aladağ will be introduced briefly, starting from the west.

2.5.1. West of Mt. Aladağ

To the west of Mt. Aladağ, in the area between Karakurt town and Şengül village, the volcanostratigraphy of the Erzurum-Kars Plateau lavas closely resembles that of the volcanic succession of north of Horasan. In its lower part, the volcanic succession is made up of alternations of pyroclastic fall, flow and intermediate to basic lava flows (*Apbl*). In this part of the sequence, the pyroclastic units account for over 80-90% of the volcanic pile. They consist of pumice-fall, reworked pyroclastic deposits, white and grey ignimbrite and also obsidian. Obsidian becomes dominant in some parts of the volcanic sequence, e.g. in the vicinity of Mescitli village which is situated between the towns of Sarıkamış and Karakurt. In this area it forms mesa-shaped flows, coulées and lenses which are a few tens of metres thick. It displays a pencil-cleavage in places. It predominantly displays black, grey, brown and red colours. In some places, the

Figure: 2.27. Cross sections cutting through the Erzurum-Kars Plateau volcanics in the Mt. Aladağ area.

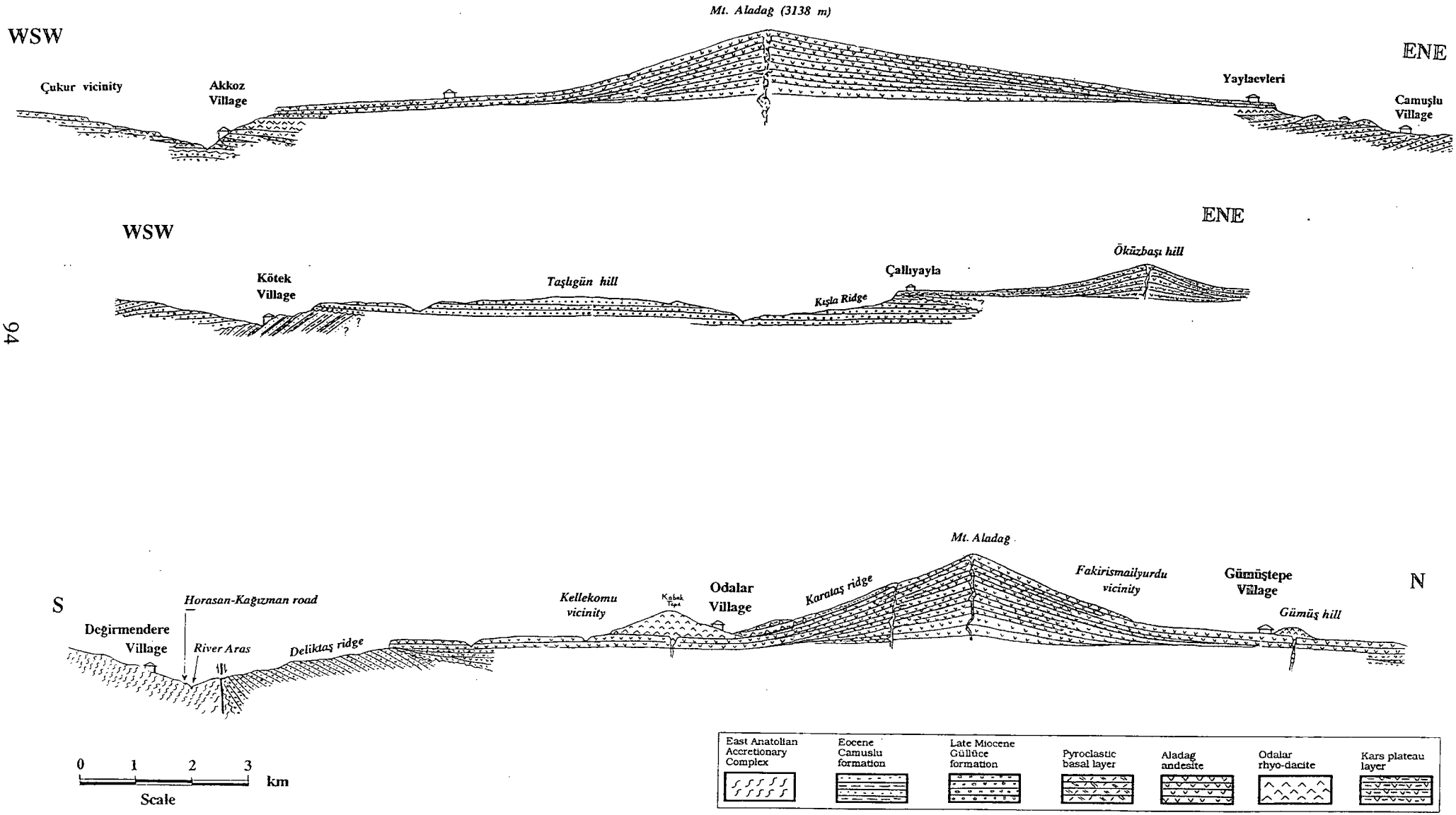

obsidian contains colourless and transparent patches. It is mostly composed of bands of these different colours.

The subordinate lava flows are generally aphyric in texture and andesitic or basaltic-andesitic in composition (*Abil*). At their basal contact with the pyroclastic deposits, they sometimes contain pipe vesicles. A red coloured thermally-affected zone occasionally develops close to the contact in the adjacent pyroclastics in a zone of a few tens of cm. In the vicinity of Beyazkale, where the Ayşah stream joins into the Aras river (7 km east of the Karakurt town), one of these thick andesitic, basaltic-andesitic lava units shows very well-developed columnar jointing with a two-tiered arrangement. At the base of the lava flow, the columns have a horizontal orientation. The colonnade is composed of well-formed, long columns normal to the base of the flow. Towards the top, these columns are slightly curved to the east, presumably because of flow movement, or creep, at the top of the pounded lava lake shortly before it solidified (Photo 2.30).

Photo: 2.31. A general view of the Aras river valley, ~10 km E of the town of Karakurt.

At the top of the succession, the Horasan plateau unit overlies all of these units. In some locations, some small spatter cones overlie the plateau sequence. One of them is located 7 km west of the town of Karakurt, in the vicinity of Uzungazi (Kızıl) village. It has a height of 50-70 m and a basal area of less than ¼ km^2. This cone consists almost entirely of Hawaiian type pyroclastic fall deposits. It is made up of very coarse grained, red (oxidised) scoria and abundant ballistic bombs reaching 50-70 cm in size. It also contains large scoriaceous fragments,

vesicular lava showing spindle and cowpat shapes, bombs with breadcrusted surfaces and some rare lava slabs. Furthermore, it exhibits agglutinated lava spatters in places. A sample taken from one of the ballistic bombs gave a whole-rock K-Ar age of 4.59± 0.19 Ma, which is about 1 Ma older than the Aladağ andesite, about 15-20 km to the east of this locality.

2.5.2. South of Mt. Aladağ

To the east, the basal pyroclastic unit of the Erzurum-Kars Plateau Volcanics (EKPV) gets thinner. The relative percentage of the pyroclastic flow units in the volcanic sequence also decreases. Southwest of Mt. Aladağ, near Akkoz village, the base is a porphyritic rhyolitic lava containing plagioclase phenocrysts, together with some pyroclastic fall deposits. This basal unit is overlain by the aphyric, microporphyritic and sometimes vesicular Aladağ andesite. In this location, individual

Photo: 2.30. Columnar jointing in aphyric basaltic-andesite and andesite lava flow. Ayşah stream (a side-stream of the Aras river), 7 km east of the town of Karakurt.

lava flows occasionally contain a few metres of breccia and debris at their base. This breccia is composed of angular blocks and boulders of the same composition as the lava.

On the south slope of Mt. Aladağ, around Kabak hill and close to Odalar village, a microporphyritic rhyolite-dacite dome overlies the Aladağ andesite (Figure 2.27). It covers slightly over 5 km^2 with a maximum thickness of 200m. It consists of

plagioclase micro-phenocrysts in a light grey, glassy groundmass. It is predominantly porphyritic and vitrophyric in texture. In this study, this unit is named the Odalar rhyodacite (*Orhy*) after the nearby village. A similar, but smaller rhyolitic dome is located north of Mt. Aladağ, on the Gümüştepe hill, close to Gümüştepe village (Figure 2.27). It covers an area less than ¼ km^2 with a thickness of 40-50m. It is made up of rhyolitic lava, obsidian, spherulitic and vitrophyric obsidian and perlite.

2.6. KAĞIZMAN AND EAST OF Mt. ALADAĞ

East of Mt. Aladağ to the state border with Armenia, the Erzurum-Kars Plateau Volcanics (EKPV) have a perfect plateau morphology at a height of 1 km from the base of the Aras river valley and 2 km above the sea level. This study includes only a small part of this plateau, including the eastern slopes of Mt. Aladağ and a 3-5 km wide-band from Paslı village which is situated to the northwest of Örmeli village in the east, and to the northeast of the Kağızman town.

North of Kağızman, the Kötek valley, which runs NW-SE, acts as a border between the Mt. Aladağ and the Kağızman areas. The field studied contains the following areas: Akören, Kozlu, Camuşlu, Çukurayva (Purut), Çilehane and Ortaköy villages located to the east of Mt. Aladağ and to the west of the Kötek stream valley. It also contains Paslı, Yalnızağaç, Böcüklü, Şaban and Örmeli villages in the east. This deeply eroded valley is the only place north of the river Aras where the basement of the Miocene Güllüce formation is exposed. This valley also roughly separates two different lava units of the Kağızman plateau unit. These are the pyroxene-bearing Aladağ andesite unit, which is widespread to the west of valley, and the olivine-bearing basalt and basaltic-andesite lavas that overlie the Aladağ andesite and that become dominant on the plateau to the east. In the following paragraphs, stratigraphy of this area will be introduced from basement formations to the Erzurum-Kars Plateau Volcanics.

2.6.1. THE BASEMENT UNITS

2.6.1.1. The East Anatolian Accretionary Complex (EAAC)

In the Kağızman Area, the basement is represented by the East Anatolian Accretionary Complex (EAAC) which is widely exposed to the south of the Aras river, and around Kağızman, Mt. Üçgözlüklüdağ (2460 m) and Mt. Aşağıdağ (3270 m) in the south. This basement is not exposed to the north of the Aras river except for a few small outcrops. The reason is that the EAAC makes up an approximately E-W striking palaeotopographic ridge, the northern edge of which is cut and modified by the Kağızman fault. In this study, this ridge is called the Kağızman ridge. This ridge can

be followed westward through the area south of Horasan to the Palandöken-Sakaltutan ridge to the south of the towns of Pasinler and Erzurum. According to Şahintürk and Erakman (1978) this ridge has existed in the region since the emplacement of the EAAC in Early to Middle Eocene.

The EAAC is made up of blocks of serpentinised ultrabasics (harzburgite, lherzolite, dunite, pyroxenite) and basic rocks (diabase and spilitic basalt), pelagic limestone and radiolarite, chert, neritic limestone blocks and intensively-deformed turbititic flysch-like deep-sea detrital sediments associated with conglomerate. It also contains sporadic metamorphic rock blocks (marble, schist and quartzite). Its matrix is generally characterised by serpentinite.

2.6.1.2. The Late Cretaceous Kötek Limestone (Ckl)

The EAAC is unconformably overlain by the micritic carbonate beds of the Upper Cretaceous Kötek limestone. The Kötek limestone, named by the Turkish Petroleum (TPAO) geologists (Şahintürk and Erakman, 1978) consists of pinkish to reddish grey coloured, thin-bedded limestone showing abundant small-scale folds. It contains Globotruncana sp. and Globigerinide fossils. It outcrops in the vicinity of Kazıkkıran hill, about 2 km northwest of the town of Kötek, over an area of about 15-20 km^2. The Kötek micrite is only exposed north of the Aras river. Its apparent thickness is about 800m. On the basis of the biostratigraphy it is dated as Late Mastrichtian by TPAO geologists.

2.6.1.3. The Eocene Camuşlu Formation (Ec)

The Kötek limestone is unconformably overlain by a flysch-like sedimentary unit, mainly composed of sandstone and shale alternations. It is named as the Camuşlu formation by TPAO (Erakman and Şahintürk, 1980). Bioclastic-limestone beds, which contain occasional blocks of the underlying Kötek limestone, form the base of the Camuşlu formation. Some beds contain Nummulites sp. This basal limestone gradually changes upwards into medium- to thick-bedded sandstone and shale. Close to the base, the Camuşlu formation contains 5-10 cm thick coal beds. A 70m thick olistostromal bed, which is completely made up of volcanic material, also occurs at this level. Upwards in the succession thick-bedded, greyish-green coloured conglomerate becomes dominant: it is almost entirely composed of coarse ophiolitic material and also contains blocks and boulders and also small-scale sandstone lenses. Close to the apparent top of the Camuşlu formation, these conglomerate beds are overlain by a series of thick-bedded and coarse-grained sandstones. The approximate total thickness of these sandstones is around 400 m. If the grain size distribution, presence of coal bands and lack of turbiditic sedimentary structures are taken into

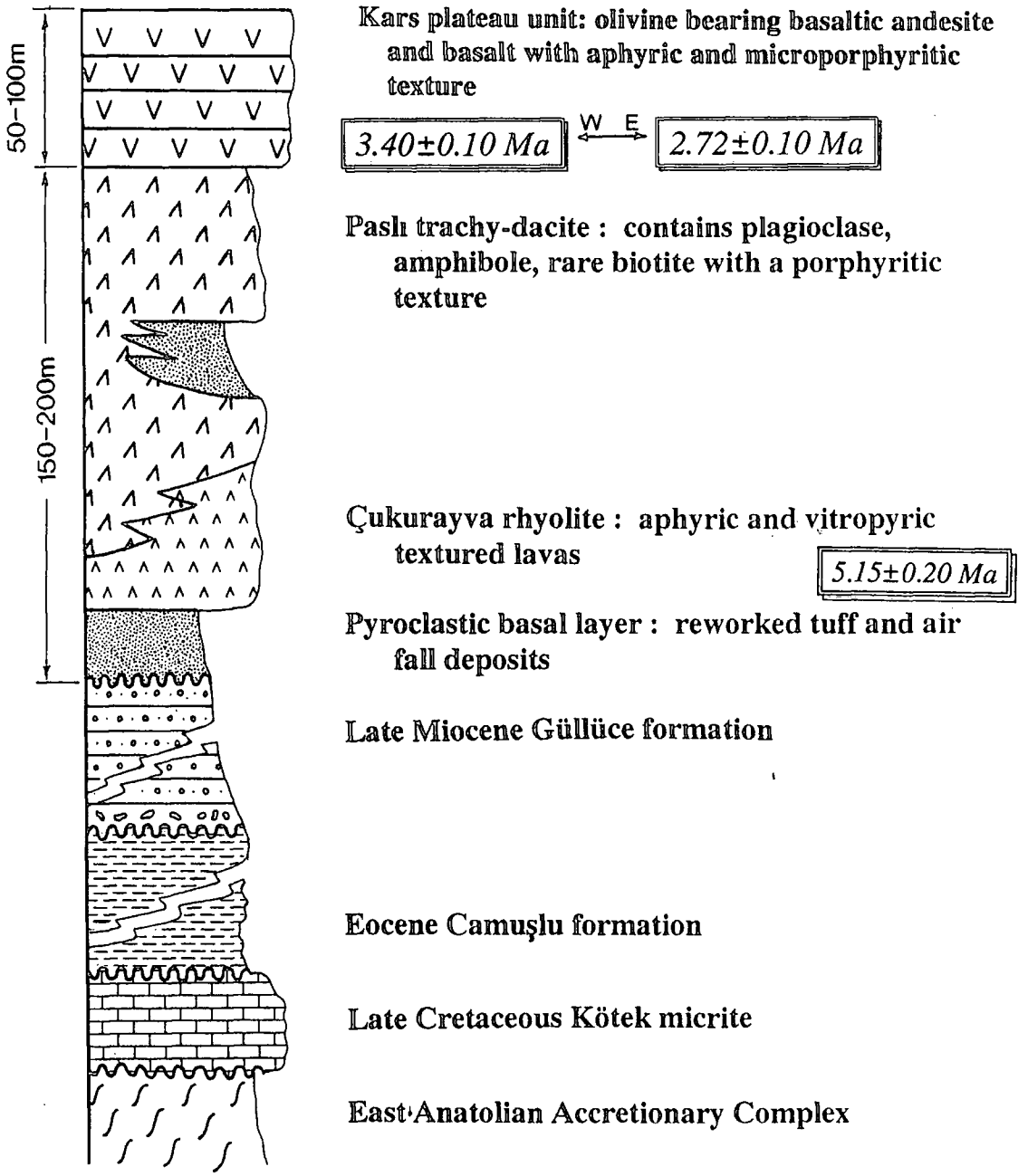

Figure: 2.28. Generalised stratigraphic section of the north of Kağızman.

account, the Camuşlu formation appears to be the product of a shallow water environment, presumably regressive in character.

2.6.1.4. The Late Miocene Güllüce Formation (Mg)

The Late Miocene Güllüce formation overlies both the Kötek micrite and the Camuşlu formation with a spectacular unconformity exposed a few kilometres east of the town of Kötek. As on the western outcrops in the Horasan and Pasinler areas, it is

Photo: 2.32. Field view of the Oligo-Miocene Güllüce formation, S of the town of Kötek, N of Kağızman.

characterised by colourful detrital beds commonly displaying red, scarlet-red, brown, yellow, beige and greenish-grey colours. It starts with a conglomerate showing red, scarlet red and brown colours. Near the top of the sequence, mudstone becomes dominant, displaying scarlet red, yellow, brown and greenish-grey colours. The mudstone includes occasional sandstone and conglomerate beds exhibiting very poor sorting. Towards the uppermost part of the formation, it contains thick halite and gypsum beds interbedded with the coarse detrital sediments. The Güllüce formation does not contain any fossils and considered to be the product of a continental environment. Its average thickness lies between 1100-1500m. North of the river Aras from the town of Kötek to the Soviet border, the formation forms the basement to the EKPV.

2.6.2. THE ERZURUM-KARS PLATEAU VOLCANICS

2.6.2.1. Pyroclastic Basal Unit (Pblk)

East of Mt. Aladağ, the EKPV unconformably overlies coarse detrital beds of the Miocene Güllüce formation. In the vicinity of Kozlu village, about 5 km southwest of Kötek village, the base is chiefly represented by pyroclastic fall deposits of rhyolitic pumice and ash interlayered with relatively thin (a few metres) intermediate to basic lava lenses. Pyroclastic flow units are almost completely absent. The thickness of the pyroclastic basal unit is about 150-200m. This basal unit is overlain by a set of black, aphyric-vitrophyric dacite and andesite flows. This dacite-andesite unit is in turn overlain by microporphyritic-textured Aladağ andesite. At this location, the total thickness of the plateau lava sequence is around 150-200m.

Photo: 2.33. Panoramic view of the Kars plateau looking to the north from Kağızman town. Pinkish to cream coloured unit having a fine dendritic drainage pattern is the continental deposits of the Oligo-Miocene Güllüce formation (Mg). Unconformably overlying the EKPV displays a steep slope forming a widespread plateau.

2.6.2.2. The Çukurayva Rhyolite (Çr)

Further north, to the west of Camuşlu village, a rhyolitic lava unit forms the top of the basal pyroclastic unit. It consists of anorthoclase, andesine-oligoclase and quartz phenocrysts in a pale grey-coloured, glassy groundmass. It shows a penetrative platy jointing on order of 5-6 mm. These joints are generally formed by very tiny vesicles which are laterally connected to make up the planar surfaces. This jointing is widespread in this unit and is one of its characteristic properties. This rhyodacitic unit extends laterally on the east slope of the plateau through Çukurayva (Purut) and Çilehane villages for about 7 km to the vicinity of Boğaz Değirmeni. Its thickness

Figure: 2.29. N-S cross-sections cutting through the eastern part of the Erzurum-Kars Plateau in Kağızman area.

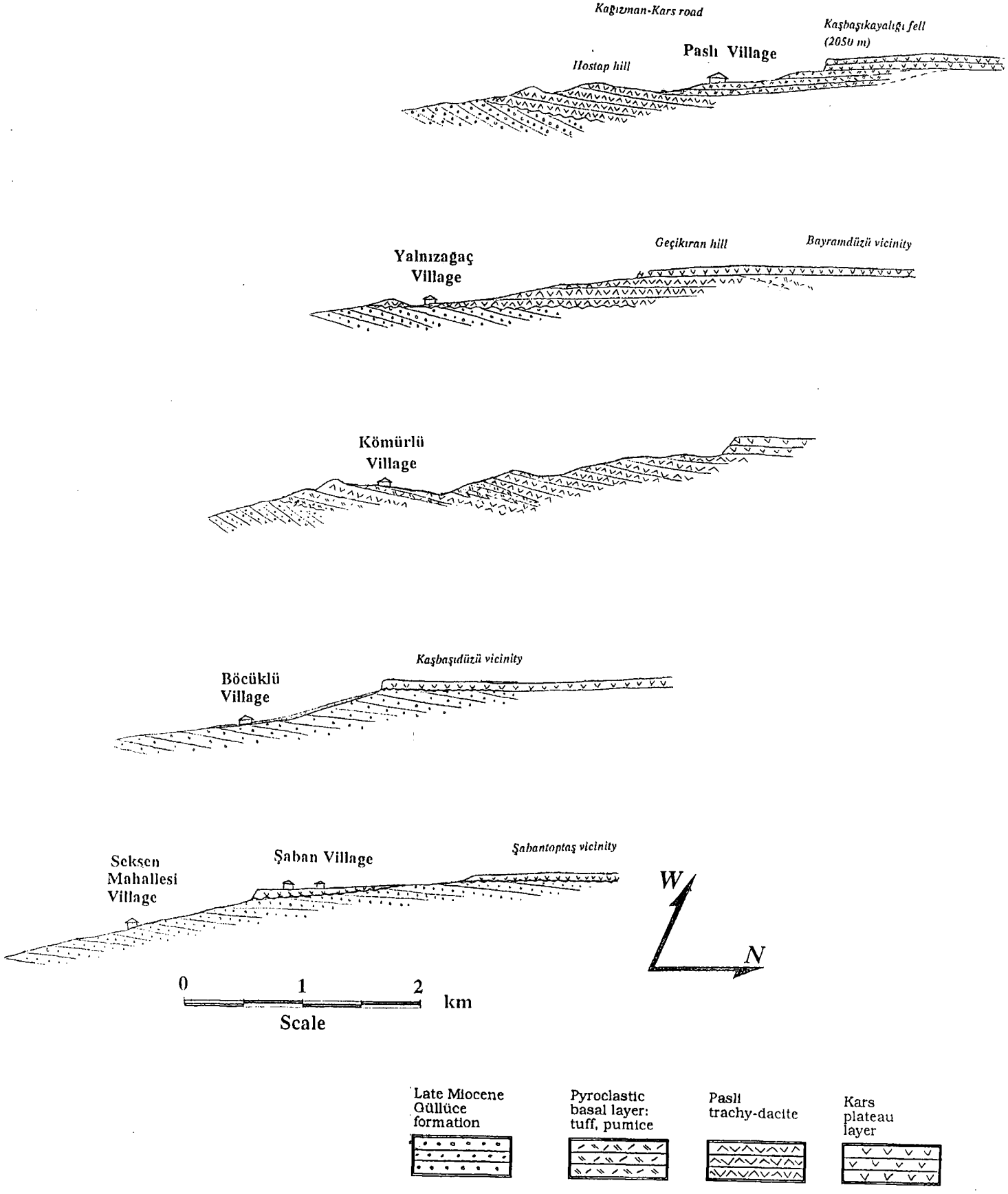

varies between 50 and 150m. In this study, this unit is named as the Çukurayva rhyolite after the nearby village. Northwards the Çukurayva rhyolite gets thinner and becomes interlayered with pyroclastic air-fall deposits. In the vicinity of Boğaz Değirmeni, between Paslı and Ortaköy villages, its thickness decreases considerably down to 50m, where it is overlain by a 100-120m-thick tuff sequence. In this location it shows a well-developed columnar jointing. It wedges out to the east. A sample collected from the base of this unit, close to the base of the volcanic succession, has given a K-Ar whole rock date of 5.15±0.20 Ma.

Photo: 2.34. Field view of the easternmost part of the Kars plateau from the top of the plateau . In this area, total thickness of the EKPV decreases considerably down to ~50-70 m. Looking to the east from Kargakaya castle ruin, N of Örmeli village, NE of Kağızman.

2.6.2.3. The Paslı Trachydacite (Ptd)

Near Paslı village, about 8 km NW of the town of Kötek, a porphyritic trachydacite crops out. It is pale grey in colour and contains coarse euhedral to subhedral phenocrysts of plagioclase (An_{36-45}), quartz, amphibole (magnesio-ferri-tschermakite and magnesio-ferri-taramite) and rare biotite microcrystals. In this study, this unit is named the Paslı trachydacite after the nearby village where its best outcrops are exposed. 1 km northwest of the Paslı village, the unit is intercalated with pyroclastic air-fall and ash deposits. To the east around Kızkalesi, Dana and Kara hills and north of Yalnızağaç village, these tuff intercalations laterally disappear. In this

location the unit directly overlies the Güllüce formation with an angular unconformity. The Paslı trachydacite is overlain by the basic lava flows of the Kars plateau unit at its upper contact.

2.6.2.4. The Kars Plateau Unit (Kpl)

The east slope of Mt. Aladağ is covered by the augite-bearing lava flows of the Aladağ andesite. To the north and east of Paslı village, this unit laterally wedges out to the east and northeast. In this area it is overlain by an olivine-bearing basic to intermediate lava sequence. This unit covers an area of hundreds of km² in the east and north and forms a widespread plateau which is 2 km above sea level (Photos 2.33 and 34). This plateau is called the Kars Plateau after the name of the city of Kars located almost in the centre of this plateau. In this study, this volcanic unit is named as the Kars plateau unit.

The Kars plateau unit comprises the uppermost unit of the succession, covering all the pyroclastic products and acidic lava flows of the EKPV. The contact between the Kars plateau unit and the underlying units is mostly sharp and planar. Compared to the lower levels of the volcanic pile, it consists of relatively more basic lithologies, e.g. basalt, basaltic andesite, basaltic trachyandesite. It generally displays aphyric, microporphyritic and pilotaxitic textures. Its thickness changes from a few tens of

Figure: 2.30. SSW-NNE trending cross-section between Kargakaya castle ruin and Mt. Küçükyağlıca, N of Örmeli village NE of Kağızman.

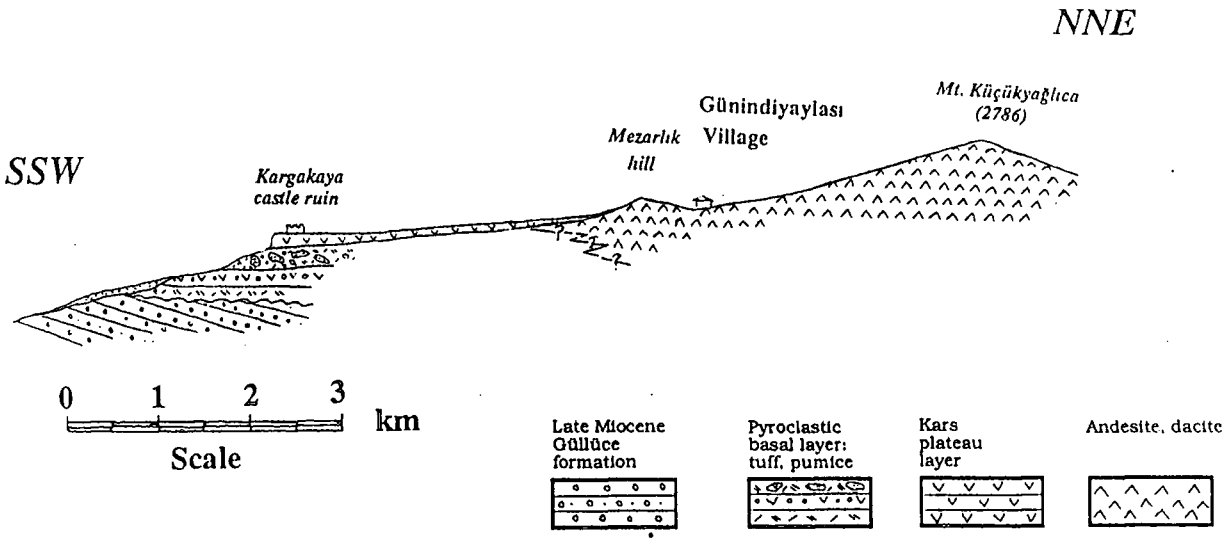

meters to 150-200m. In general it is the product of fissure eruptions. There are also some small volcanic cones on the Kars plateau which typically have a 15 km² base and a height of 600m above the plateau level. These volcanoes indicate that central

eruptions were also important in the formation of the Kars plateau unit. From west to east some of these cones are: Ziyaret hill (2429 m), located 8 km north of the Paslı village close to the Ağadeve village; Öküzbaşı hill (2462 m), located about 12 km north of Kağızman to the east of the Şaban village; Mt. Yağlıca (2961 m) and Küçük Yağlıca (2786 m) hill, situated 19 km northeast of Kağızman; Mt. Tarhan (2586 m), Mt. Kotur (2635 m) and Ciritmeydanı hills (2774 m), located 22 km northeast, 10 km north and 20 km northwest of Mt. Yağlıca respectively. In general the Kars Plateau unit volcanics get younger towards the east. A sample taken from this unit, from 1 km north of Paslı village has given a K-Ar age of 3.40±0.10 Ma. However, southwest of Mt. Yağlıca (further east), a sample has been dated at 2.72±0.10 Ma by the same method.

2.7. SUMMARY

Based on their stratigraphic position in the succession, and also on their petrographic and eruptive properties, the collision related volcanic units on the Erzurum-Kars Plateau can be divided into eight groups as presented in Table 2.1. From base to top these are:

1. Basal basic lava layer: this group includes the oldest (11.1±0.5 Ma) and the most basic rocks from the base of the plateau.

2. Pyroclastic basal layer: consists of pyroclastic fall, flow and occasionally surge deposits of rhyolitic-dacitic composition. Volumetrically, it is the most abundant group on the eastern part of the plateau.

3. Black ignimbrite: comprises the uppermost part of the pyroclastic basal units in the Pasinler area. It is mainly composed of densely welded, phenocryst-rich ignimbrite flows displaying black and red colours and eutaxitic texture with abundant fiammé.

4. Basal intermediate to acidic lava layer: is made up of andesitic and dacitic lava flows which predominantly exhibit aphyric and vitrophyric textures. They are located close to the base of the succession.

5. Amphibole-bearing porphyritic lavas: typically consist of porphyritic dacites and andesites which are made up of phenocrysts of amphibole, plagioclase, ortho- and clinopyroxene and rarely quartz. They make up domes on the plateau and are located almost always in the middle of the stratigraphic column.

6. Plateau layer without olivine: consists of microporphyritic andesitic lavas which are composed of plagioclase and clinopyroxene phenocrysts. This layer outcrops in the Mt. Aladağ area and was produced by central eruptions of Mt. Aladağ volcano.

7. Olivine-bearing plateau layer: represents the uppermost unit on the plateau which is made up of plagioclase, clinopyroxene and olivine.

8. Acidic cones and domes on the plateau: are rare, small, and dome-shaped bodies on the plateau overlying the Olivine-bearing plateau layer. These are composed of rhyolitic and rhyodacitic lavas.

Groups	Y series	Formations
8. Acidic cones and domes on the plateau *(AC)*	High-Y	8.1. Ardıçlıdağ rhyolite (Pasinler) 8.2. Odalar rhyolite (Mt. Aladağ)
7. Olivine-bearing plateau layer *(CA)*	High-Y	7.1. Kargapazarı volcanics (Mt. Kargapazarı, Pasinler)
		7.2. Horasan plateau unit (N of Horasan) 7.3. Kars plateau unit (Kars)
6. Plateau without olivine	High-Y	6.1. Aladağ andesite (Mt. Aladağ)
5. Amphibole-bearing porphyritic lavas *(CA)*	Low-Y	5.1. Dumlu amphibole dacite/andesite (Mt. Dumlu)
		5.2. Arzutu amphibole dacite (Mt. Dumlu)
		5.3. Göllerdüzü amphibole dacite (Mt. Kargapazarı)
		5.4. Kızılveren amphibole dacite/ andesite (Pasinler)
		5.5. Köroğlu amphibole dacite/andesite (N of Horasan)
		5.6. Saçdağ dacite
4. Basal intermediate to acidic lavas *(CA)*	High-Y	4.1. Black andesite/dacite (Pasinler)
	Low-Y	4.2. Güngörmez dacite/andesite (Mt. Dumlu, Mt. Kargapazarı)
		4.3. Girekösek dacite (Mt. Dumlu, Mt. Kargapazarı)
		4.4. Köşk pyroxene dacite (Mt. Kargapazarı)
		4.5. Çobandede dacite (Mt. Kargapazarı)
	High-Y	4.6. Paslı trachy-dacite (Kağızman) 4.7. Çukurayva rhyolite (Kağızman)
3. Black ignimbrite *(AC)*	High-Y	3.1. Black ignimbrite (Pasinler and Mt. Kargapazarı)
2. Pyroclastic basal layer *(AC)*	High-Y	2.1. Grey ignimbrite (Pasinler and Horasan)
		2.2. White ignimbrite (Pasinler and Horasan) 2.3. Pyroclastic fall deposits (Pasinler, Horasan, Mt. Aladağ and Kağızman)
1. Basal basic lava layer *(CA)*	High-Y	1.1. Karapınar basalt (Mt. Kargapazarı) 1.2. Kötek basalt (N of Horasan)

Table: 2.1. Table showing eight stratigraphic levels and corresponding volcanic units used in the classification graphs in Chapter 3. They are arranged according to their stratigraphic position from base to the top. CA: calc-alkaline rocks, AC: alkali-calcic rocks, High-Y: rocks of the high-Y series, Low-Y: the low-Y series (for explanation of these two series see section 3.2).

Chapter 3
MAJOR AND TRACE ELEMENT GEOCHEMISTRY

Introduction

In this chapter, the major and trace element geochemistry of the whole-rock samples from the Erzurum-Kars Plateau is described. Analytical data used in this chapter were obtained from two different techniques: major elements and trace elements including Sc, Cr, V, Ni, Co, Cu, Zn, Ga, Rb, Sr, Y, Zr, Nb, Ba, La, Ce, Nd, Pb and Th were determined by X-Ray Fluorescence (XRF) at the University of Durham while Rb, Sr, Y, Zr, Nb, Cs, Ba, Rare Earth Elements (REEs) from La to Lu and also Hf, Ta, Pb, Th, and U were analysed by Inductively Coupled Plasma Mass Spectrometry (ICP-MS) at the Industrial Research Centre, University of Durham. Techniques employed are detailed in Appendix B. Precision and accuracy of the analytical data is presented in Appendix C, while the full dataset of the XRF and ICP-MS analyses is given in Appendix D and E respectively.

The chapter is subdivided into four main sections:

3.1. In this first section, the Erzurum-Kars Plateau volcanics are classified on the basis of their major element contents using well-known classification and discrimination diagrams such as those of Le Bas et al. (1986) and Peccerillo and Taylor (1976).

3.2. The second section focuses on the classification of volcanic units using their trace element concentrations. After a short introduction to geochemical division of volcanic units based on their Y contents on the plateau, trace element fractionation trends are interpreted by utilising a theoretical Rayleigh fractionation modelling.

3.3. The third section concentrates on interpretation of REE patterns and multi-element patterns with special reference to their petrologic significance.

3.4. In the final section, trace element bivariate diagrams are evaluated.

3.1. Classification of the volcanic units using major element geochemistry

The collision-related volcanics of the Erzurum-Kars Plateau cover a broad compositional range from basalts to rhyolites. Figure 3.1 shows the distribution of main rock types on the plateau in terms of frequency distribution of SiO_2. In fact, this graph shows the distribution of SiO_2 only for the analysed samples. Thus, it does not display the real volumetric relationship of each lithology in the volcanic succession. The relative abundance of pyroclastic compared to lava flows also differs from one place to another on the plateau. Hence, the histogram should be interpreted with caution.

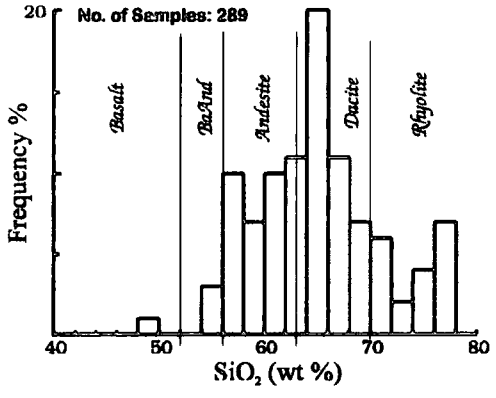

Figure: 3.1. Histogram of SiO_2 values showing the frequency distribution of silica in the Erzurum-Kars Plateau volcanics.

In such interpretations, ideally, the data from each stratigraphic subdivision should be weighted by their estimated volumes. Such a calculation is not possible, especially for the central and eastern part of the Erzurum-Kars Plateau lavas, because of the lack of detailed geological mapping geological mapping which should ideally focus on the division of volcanic units on the plateau. Despite all these problems, the histogram may still give some idea of relative abundance of different rock-types on the plateau, since the samples analysed were systematically collected from different levels of the most representative volcano-stratigraphic sections in the field. This is true especially for the western part of the plateau where intermediate to acidic lavas comprise almost all of the volcanic column. Towards the east of the plateau, pyroclastic deposits become abundant and in some places they can comprise approximately 40-60 volume % of the succession. These pyroclastics, which are generally acidic in composition, have not been sampled as much as the lavas for geochemical purposes. Therefore, to some extent, Figure 3.1 underestimates the relative abundance of acid rocks on the eastern part of the plateau.

As shown by the histogram, basalts are very scarce (especially in the western part of the plateau) and basaltic-andesites comprise only about 2.5 % of the total population of analysed samples. Most of the lavas fall into the intermediate compositional fields of andesite (about 30-35%) and dacite (approximately 45-50%). Rhyolites, which are in general represented by pyroclastic flows, ash falls and lava domes, constitute roughly 15% of the samples.

The volcanics have been classified here on the basis of their alkali and silica contents using the total alkali versus SiO_2 diagram of Le Bas et al. (1986) (Figure 3.2) and the K_2O versus SiO_2 diagram of Peccerillo and Taylor (1976) (Figure 3.4). The data have been plotted on these graphs as eight different groups represented by eight data symbols, each of which basically corresponds to a particular stratigraphic level on the plateau and may include several volcanic units. The division of these groups has been done in the previous chapter (Section 2.7) on the basis of their stratigraphic position on the plateau and petrographic properties as presented in Table 2.1.

Most notably, the data on both the total alkali versus silica and K_2O versus SiO_2 diagrams (Figures 3.2 and 3.4) fall into two distinct areas without any significant overlap. The first area, which includes lavas of groups 1, 4, 5, 6 and 7, (Table 2.1) covers the compositional spectrum from basalts with 49% SiO_2 to dacite and rhyolites with 69.5-70% SiO_2. It forms a coherent linear trend which follows the border between basalt-basaltic andesite-dacite and their high-K equivalents and falls mostly into calc-alkaline and high-K calc alkaline fields. The second area is characterised by its high total alkali and K_2O values and contains mainly intermediate to acidic pyroclastics of groups 2, 3 and 8. It predominantly lies within the alkaline field of Miyashiro (1974) (Figure 3.2) covering the compositional spectrum from trachy-andesite with 65% SiO_2 to rhyolite with a maximum SiO_2 value of 76.5% and forming a sub parallel and slightly concave trend to the former. However, the same

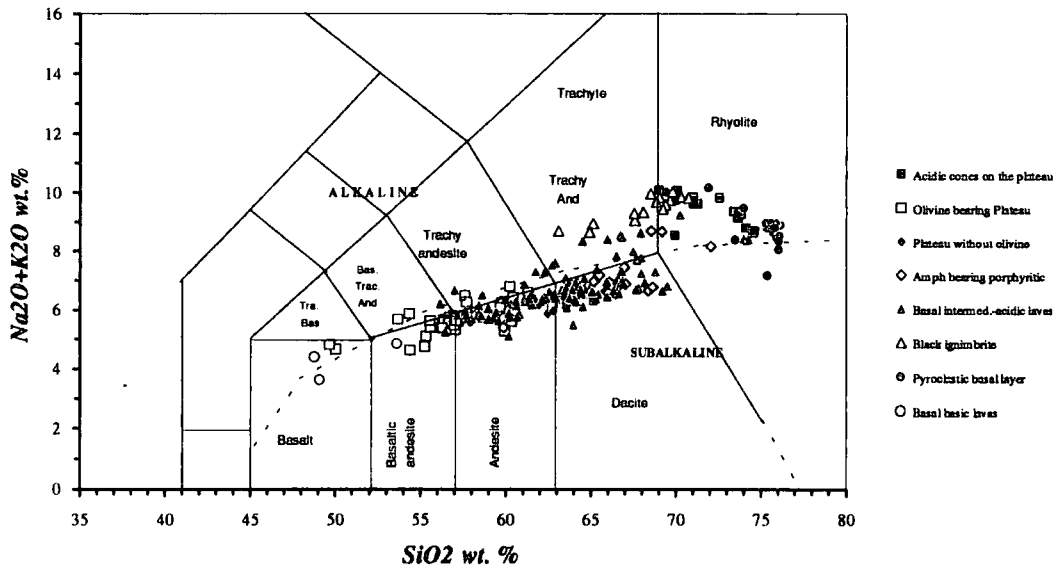

Figure: 3.2. The Erzurum-Kars Plateau volcanics plotted on the total alkali versus SiO_2 diagram of Le Bas et al. (1986). Miyashiro's (1974) border which divides sub-alkaline/alkaline fields is also shown on the diagram by a dashed line.

trend lies entirely in the sub-alkaline field suggested by Irvine and Baraggar (1971).

A more detailed classification of volcanic units based on the nomenclature of Le Bas et al. (1986) reveals the compositional properties of each formation on the plateau. These are shown in Figure 3.5 in ten parts (a-j). The volcanic rocks of both the Ardıçlıdağ rhyolite (Pasinler area) and the Odalar rhyolite, which represent the volcanic domes on the plateau, basically fall within the rhyolite compositional field (Figure 3.5-a). The olivine-bearing plateau lavas plotted in Figure 3.5-b (the Kargapazarı volcanics, the Horasan plateau and the Kars plateau units) form a well-defined trend from basalt to andesite, following the boundary between basaltic andesite-andesite and their trachytic equivalents and occasionally falling in the trachytic basaltic-

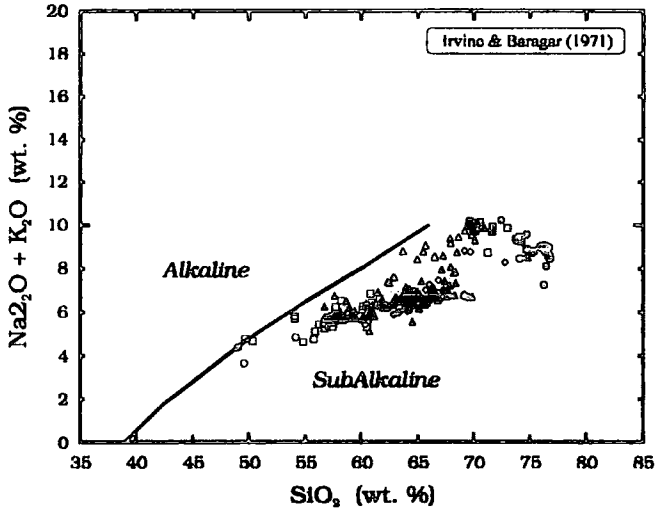

Figure: 3.3. The Erzurum-Kars Plateau volcanics plotted on the classification diagram of Irvine and Baraggar (1971). For key symbols, see Figure 3.4.

trachytic basaltic-andesite and trachytic andesite fields. Therefore, they can be

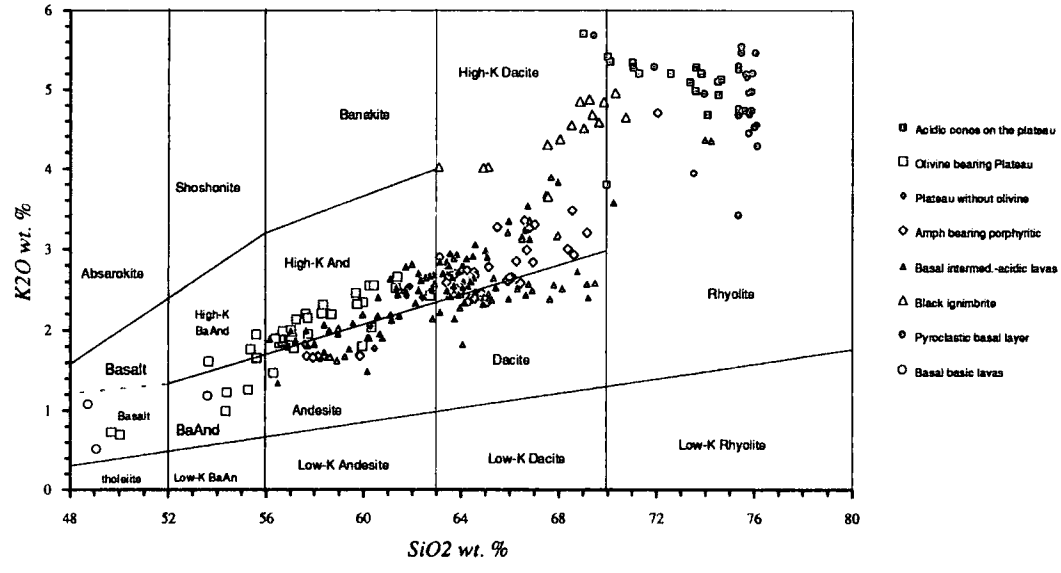

Figure: 3.4. The Erzurum-Kars Plateau volcanics plotted on the K_2O versus SiO_2 classification diagram of Peccerillo and Taylor (1976).

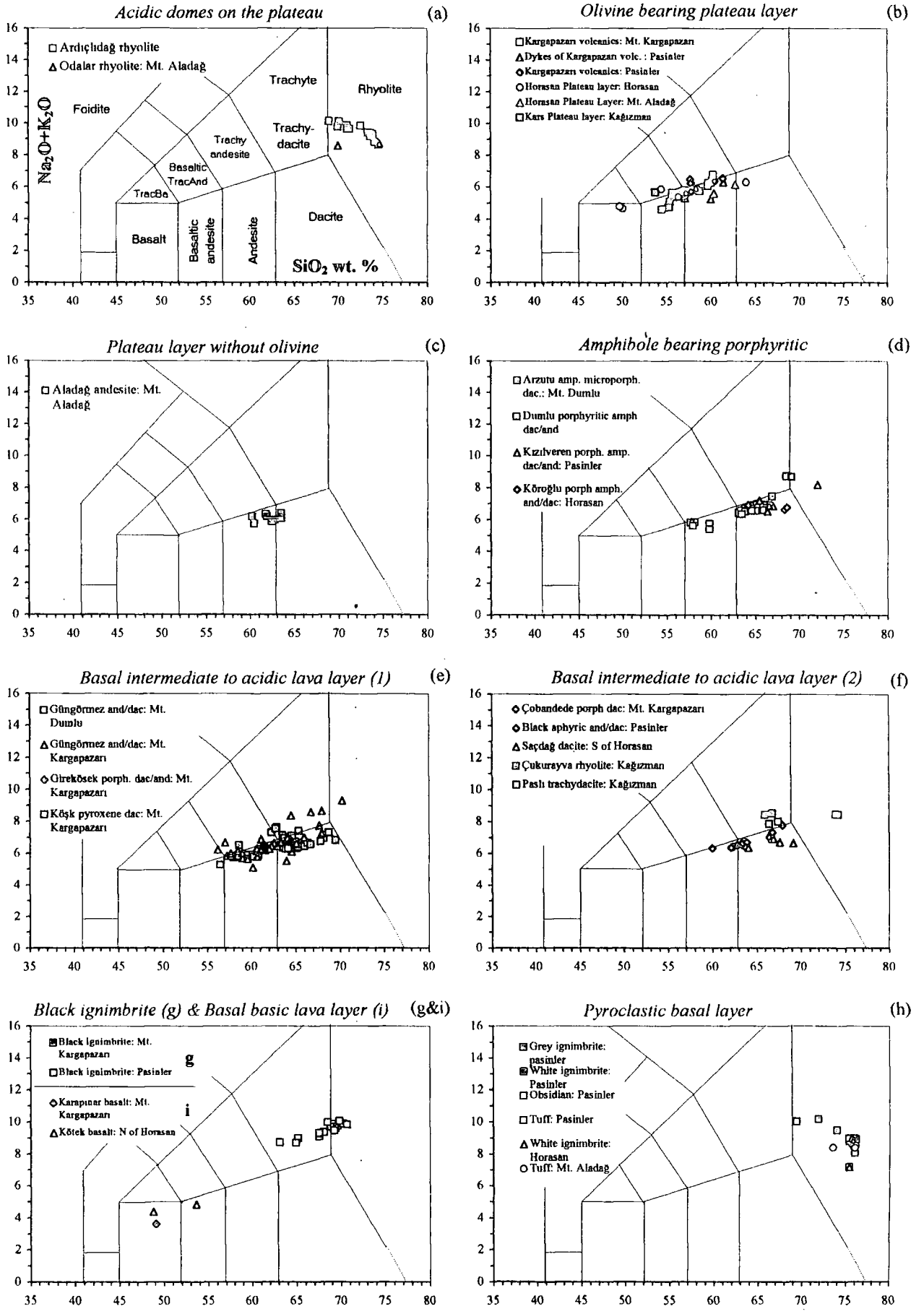

Figure: 3.5. Classification of formations of the Erzurum-Kars Plateau volcanics using the clasification diagrams of Le Bas et al. (1986).

considered to be sub-alkaline (calc-alkaline) in character. The most basic members of this unit are basalts which come from the North of Horasan. Lavas of the plateau unit without olivine (group-6), which is entirely made up of the Aladağ andesite, plot predominantly into the sub-alkaline andesite and partly dacite field (Figure 3.5-c). The porphyritic amphibole-bearing lavas of Mt. Dumlu, Kızılveren (Pasinler) and Köroğlu (North of Horasan) (group-5) plotted in Figure 3.5-d fall mainly into the dacite and partly into the andesite field, a few samples just falling within the trachydacite (from Mt. Dumlu) and rhyolite field (from Pasinler). Classification diagrams of the basal intermediate to acidic lava layer (group-4), presented in two parts in Figures 3.5-e and 3.5-f, show a trend similar to the one displayed in 5-d though, with some scatter into the trachy-andesite and trachydacite fields. The Black ignimbrite predominantly falls within the trachydacite and the rhyolite fields forming a short trend parallel to the boundary between the sub alkaline and their high-K equivalents and showing a mildly alkaline affinity. All samples of the pyroclastic basal layer plot within the rhyolite field (Figure 3.5-h). Samples from the lowermost group (group-1), the basal basic lava layer, mainly fall into the basalt and basaltic-andesite fields.

The calc-alkaline character of the Erzurum-Kars Plateau lavas is also displayed by the variation trend in the AFM plot (Irvine and Baraggar, 1971), where no iron-

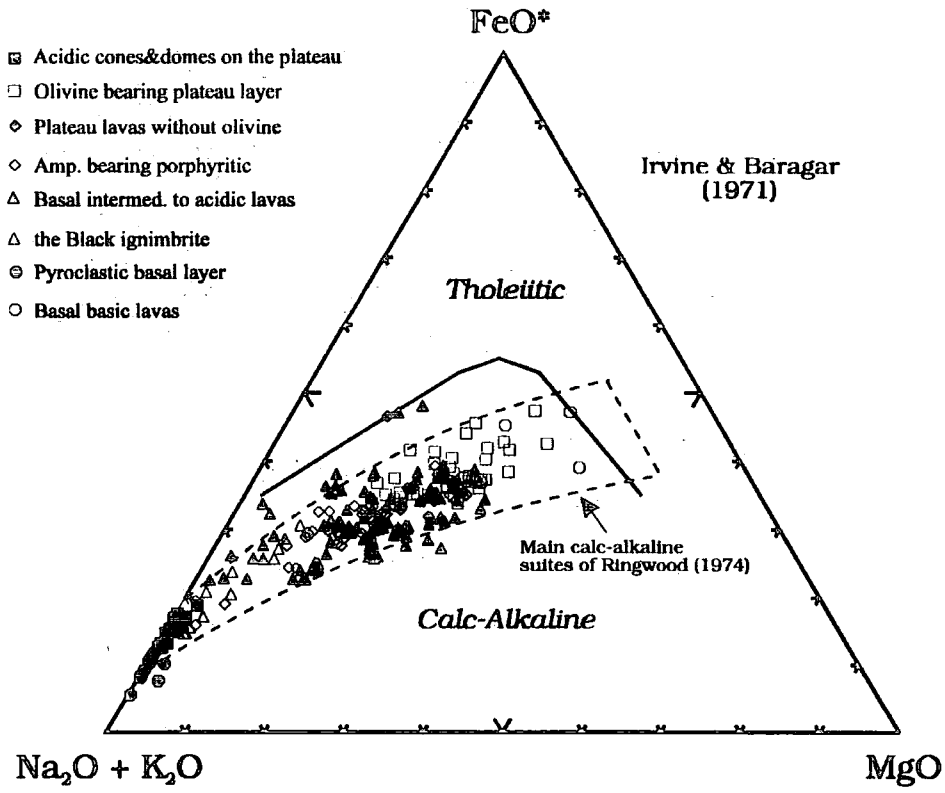

Figure: 3.6. AFM diagram of the volcanics from the Erzurum-Kars Plateau. The dotted area represents the field of the main calc-alkaline suites of Ringwood (1974).

enrichment is visible (Figure 3.6). The trend under consideration fits very well with the field of the main calc-alkaline suites suggested by Ringwood (1974).

Plot of calc-alkali molar ratio against SiO_2 (after Pearce et al., 1990) demonstrates the differences among groups of lavas from the plateau (Figure 3.7). In the lavas of group 1, 4, 5, 6, 7 (the plateau units, basal basic-intermediate and acidic lavas), the molar ratio of Ca to total alkalis is high at intermediate (about 65 % SiO_2) compositions, indicating that they have a calc-alkaline character. In contrast, groups

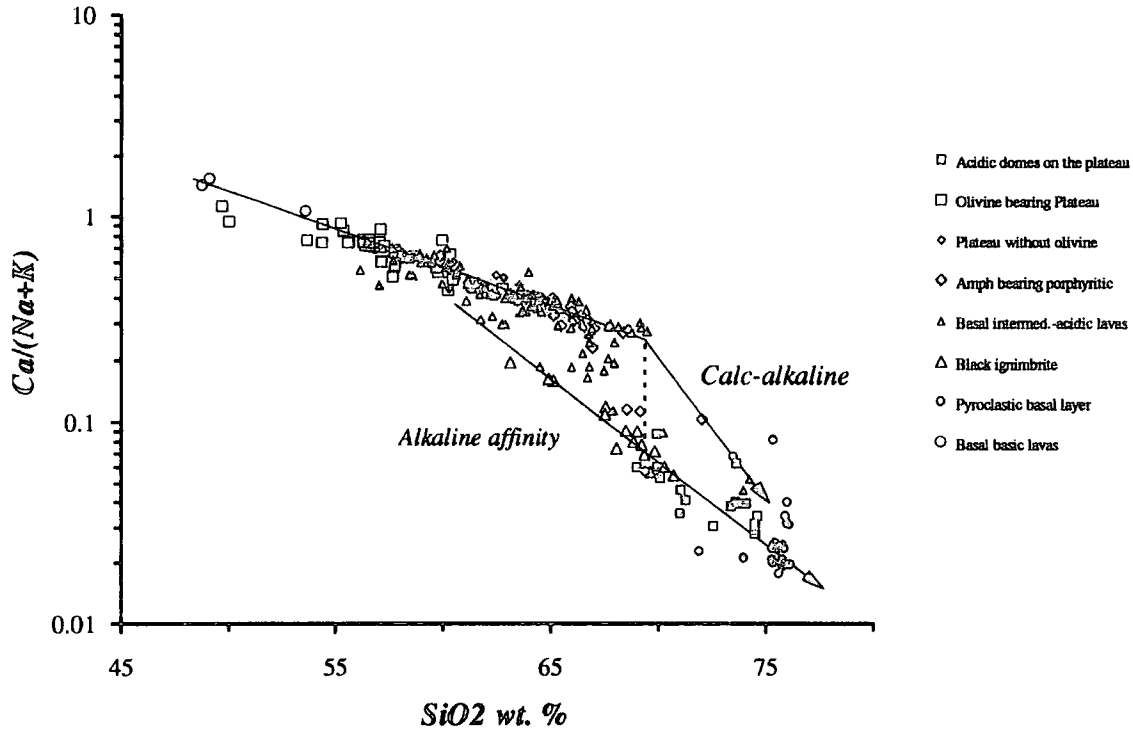

Figure: 3.7. Plot of calc-alkali molar ratio against SiO_2 wt. %.

which are mainly composed of high silica pyroclastic flow and fall deposits (acidic domes on the plateau, the Black ignimbrite and Pyroclastic basal unit) have lower molar ratios supporting their tendency towards a mildly alkaline character. A similar relationship between alkaline rocks of Nemrut, Muş, Tendürek and calc-alkaline rocks of Mt. Ararat and Kars Plateau is shown by Pearce et al. (1990) on the regional scale for the collision volcanism of Eastern Anatolia. According to Pearce et al. (1990), these differences appear to be the result of fractionation since the discrimination is observed only at intermediate compositions. This interpretation is also applicable to the Erzurum-Kars Plateau, not only because the discrimination is apparent only at intermediate compositions but also some of the lavas from both calc-alkaline and alkaline suites are members of the same series (high and low-Y series),

which tend to be genetically related as we shall see in the following sections of this chapter.

Peacock (1931) illustrated the fact that some rock series cannot be properly classified as alkalic or sub-alkalic, as is the case for Erzurum-Kars Plateau lavas. He proposed a twofold classification system which takes the form of a fourfold division into calcic, calc-alkalic, alkali-calcic, and alkalic groups. This classification is widely known as Peacock's alkali-lime index and here is also applied to the Erzurum-Kars plateau lavas to test their character from a different perspective. As is seen in Figure 3.8, total alkalies appear to have two trends, one of which intersects the CaO curve at around 60% SiO_2, falling basically into the calc-alkalic field. The back projection of the second trend seems to intersect the CaO curve at roughly at 57% SiO_2, falling into the alkali-calcic field. Significantly, this second trend, which is represented by the rocks of group-2, 3 and 8, coincides with those samples that plot in the alkaline field in total alkali and K_2O against SiO_2 diagrams. The term alkalic, defined by Peacock, is by no means applicable to the volcanics presented in this work.

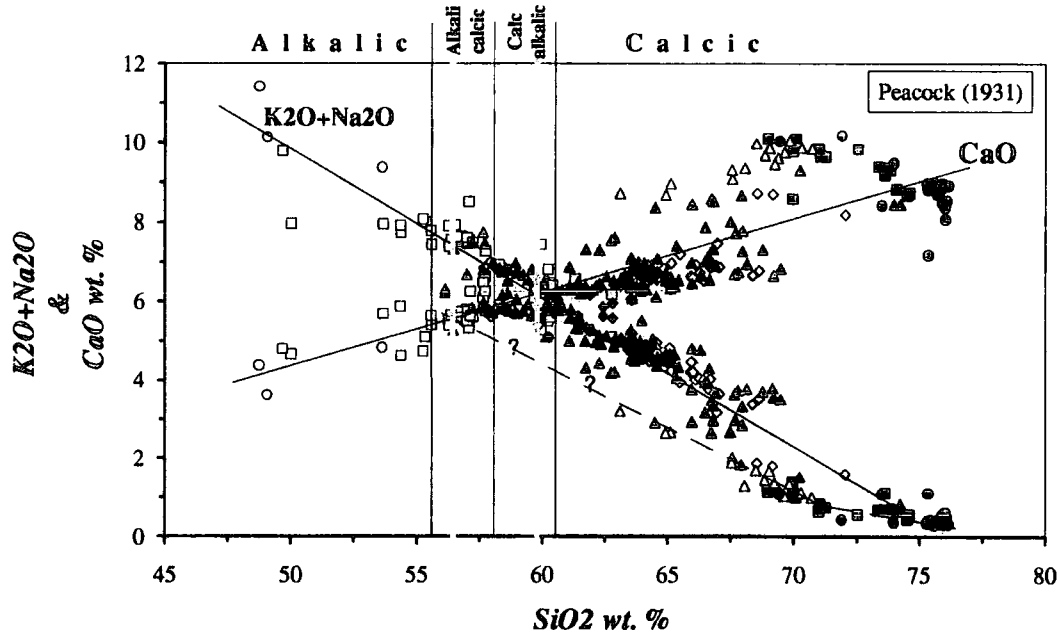

Figure: 3.8. Classification of the Erzurum-Kars Plateau Volcanics according to Peacock's (1931) scheme. Key symbols are as in Figure 3.7.

To sum up, two main series can be differentiated on the Erzurum-Kars Plateau using major element chemistry as follows:

1. Calc-alkaline series: this includes the formations of groups 1, 4, 5, 6 and 7 (Table 2.1), and predominantly consists of lavas spanning the compositional range from basalts to rhyolites. 80-85% of the samples collected from the Erzurum-Kars Plateau belong to this series.

2. Alkali-calcic series: comprises the formations of groups 2, 3, and 8. It includes the most acidic rocks (trachy-dacites and rhyolites) and is generally associated with pyroclastic flow and fall products. Samples from this series display a weak alkalic affinity on all classification diagrams (Figures 3.2, 3.4, 3.7 and 3.8) and constitute about 15-20% of the total number of samples collected from the plateau.

3.1.1. Harker diagrams of major elements

Harker diagrams of major elements plotted against silica are presented in Figure 3.9. The alkali-calcic rocks of the groups 2, 3, and 8 are, in general, depleted slightly in TiO_2 (except for the Black ignimbrite), MgO, CaO, Al_2O_3 P_2O_5 and Na_2O compared to the calc-alkaline lavas of groups 1, 4, 5, 6 and 7. They form a discrete trend which is slightly displaced from, and parallel to, the trend for the main liquid line of descent shown in the diagrams. There are no apparent inter-series differences among the formations of each series.

3.2. Classification of the volcanic units using trace element geochemistry

Trace elements are plotted on log-normal diagrams against SiO_2 in Figure 3.10 to illustrate the compositional differences between different groups on the plateau. In accordance with their major element behaviour, acidic rocks of the alkali-calcic series (groups 2, 3 and 8 in Table 2.1) plot in diverse areas on almost all graphs. They are relatively enriched in Rb, Y, Zr, Nb, La, Ce, Nd, Pb and Th and depleted in Sr, Ba, Cr, V, Ni and Co with respect to the rocks of calc-alkaline series (Figure 3.10-a to s). Within this group Y behaves in a quite different way from the other elements. As is seen on the Y versus SiO_2 diagram, it forms two diverging trends which join at basic compositions of 50-60 % SiO_2 (Figure 3.10-c) Basal, intermediate to acidic lavas and amphibole-bearing porphyritic lavas (groups 4 and 5 respectively) both follow the low-Y trend with a little scatter while group 1, 2, 3, 6, 7, and 8 rocks predominantly align along the high-Y trend.

This diversity of trends at intermediate compositions was first pointed out by Lambert et al. (1974) for Mt. Ararat (Eastern Turkey) and used to suggest an amphibole ± garnet fractionation at depth beneath the Mt. Ararat volcano. The same relationship has also been identified by Pearce et al. (1990) for the eastern part of the Erzurum-Kars Plateau (i.e. the Kars Plateau). According to these authors, strong Y partitioning into amphibole ($K_d^{(amp-liq)}$ =1.1 at basic, 3 at intermediate and 9 at acidic compositions) is responsible for the low-Y trend. Pearce et al. (1990) have argued that within the thickened continental crust of Eastern Anatolia, close to water-saturated conditions, crystallisation should be amphibole-dominated. They maintain

FIG3-09.XLS

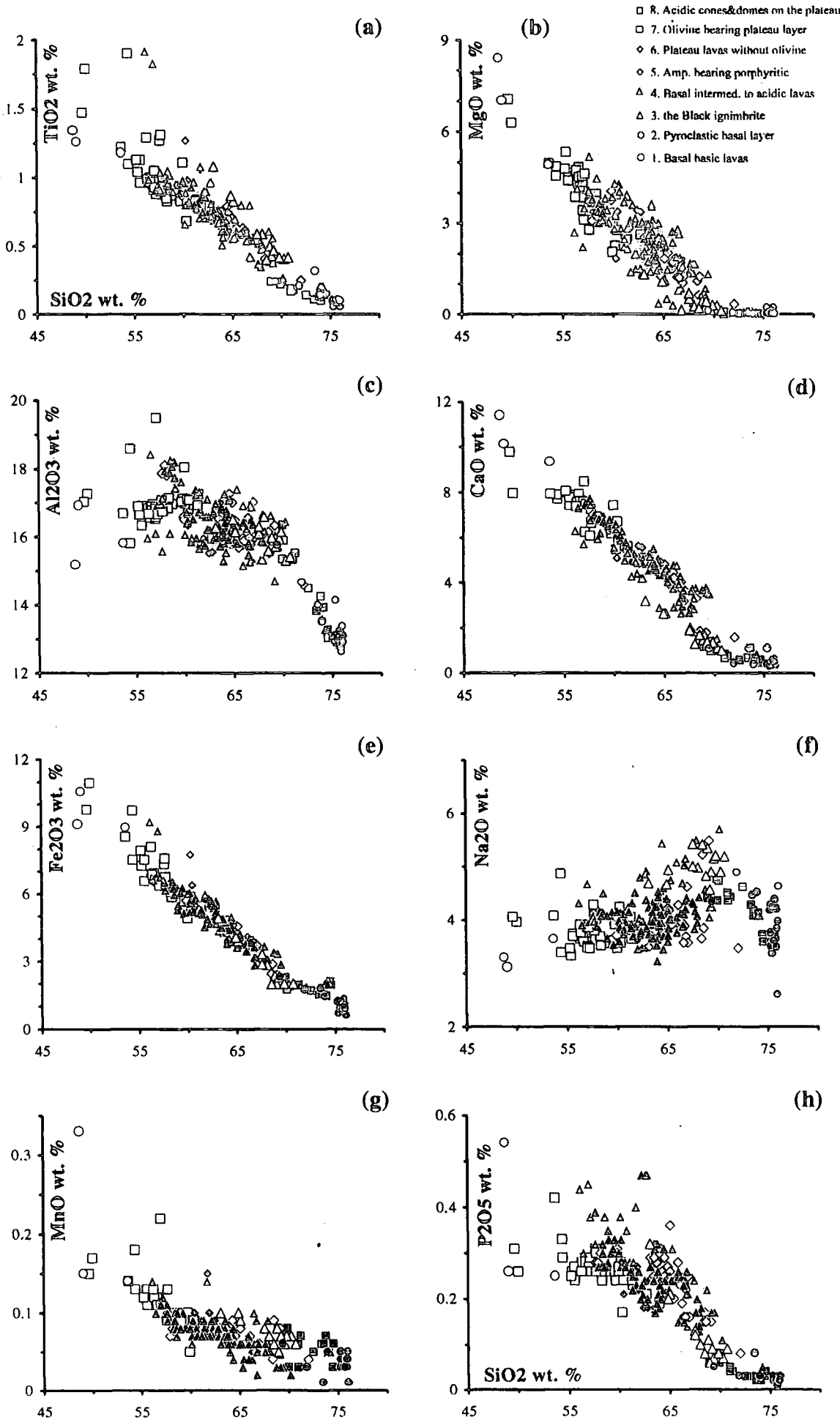

Figure: 3.9. Harker diagrams of the stratigraphical groups from the Erzurum-Kars Plateau.

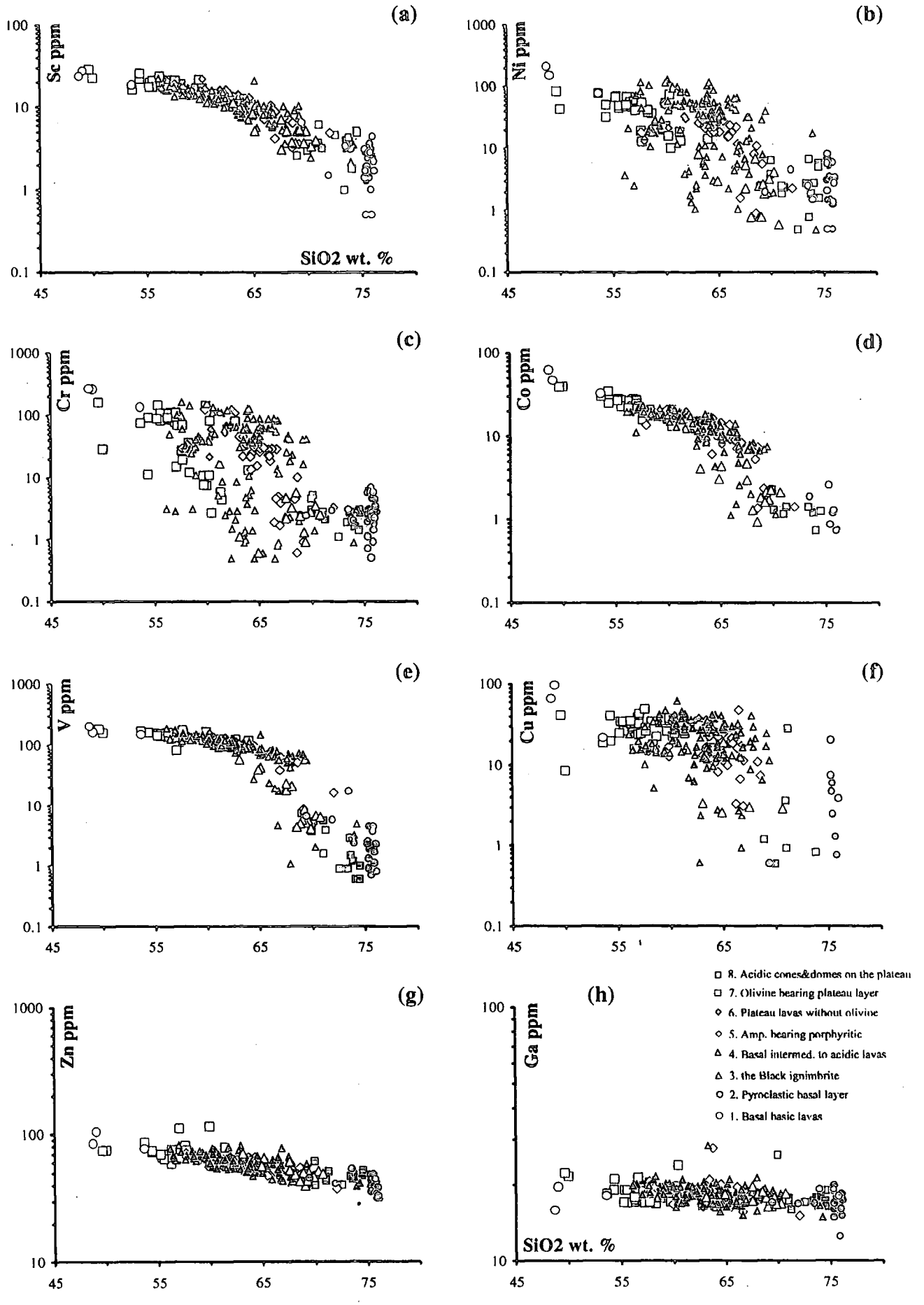

Figure: 3.10. Log-normal plots of Sc, Ni, Cr, Co, V, Cu, Zn, Ga, Rb, Y, Nb, Sr, Zr, Ba, La, Ce, Nd, Th and Pb against SiO2 displaying the differences between volcanic units of the Erzurum-Kars Plateau.

FIG3-10B.XLS

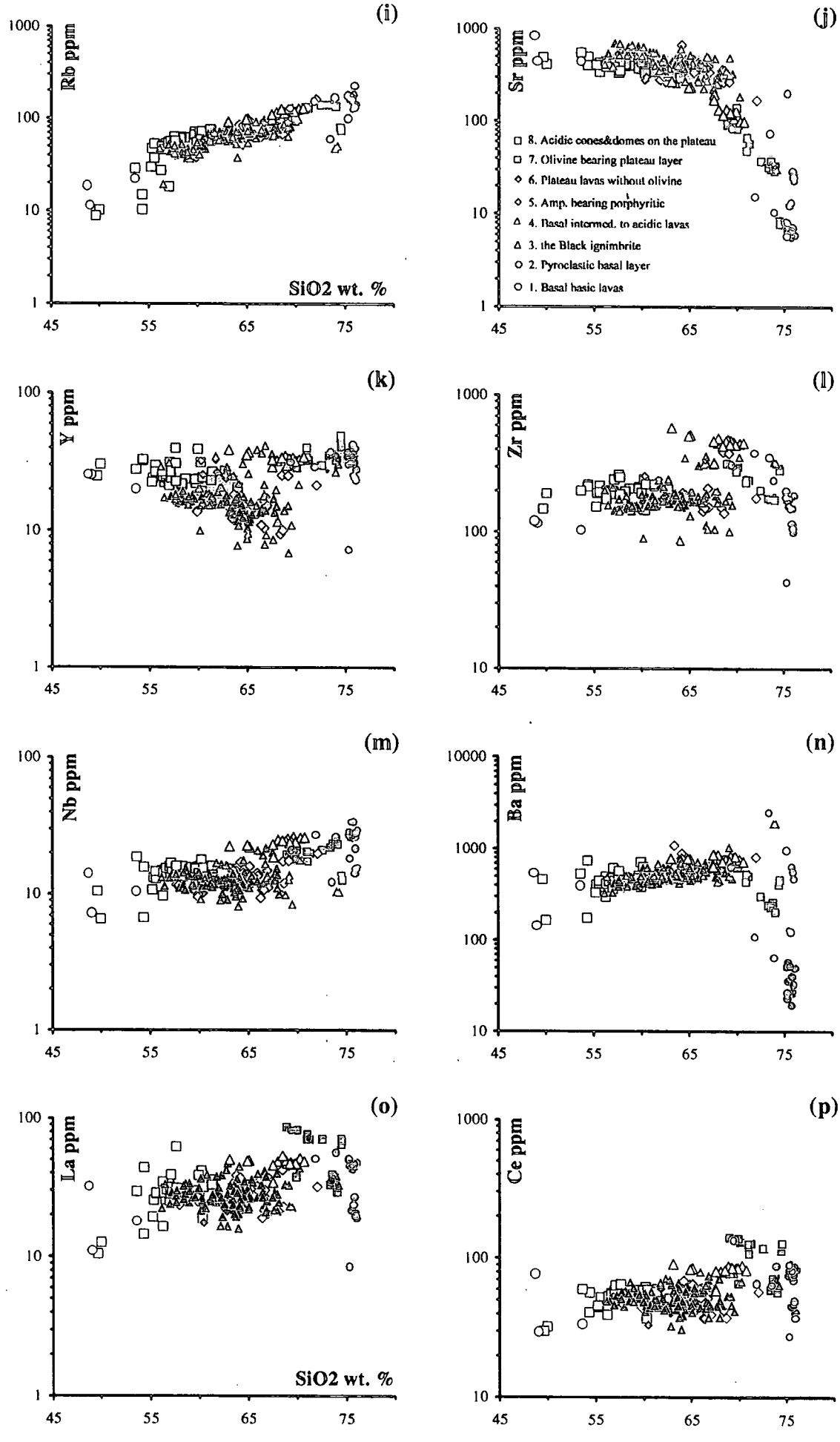

Figure: 3.10. (continued).

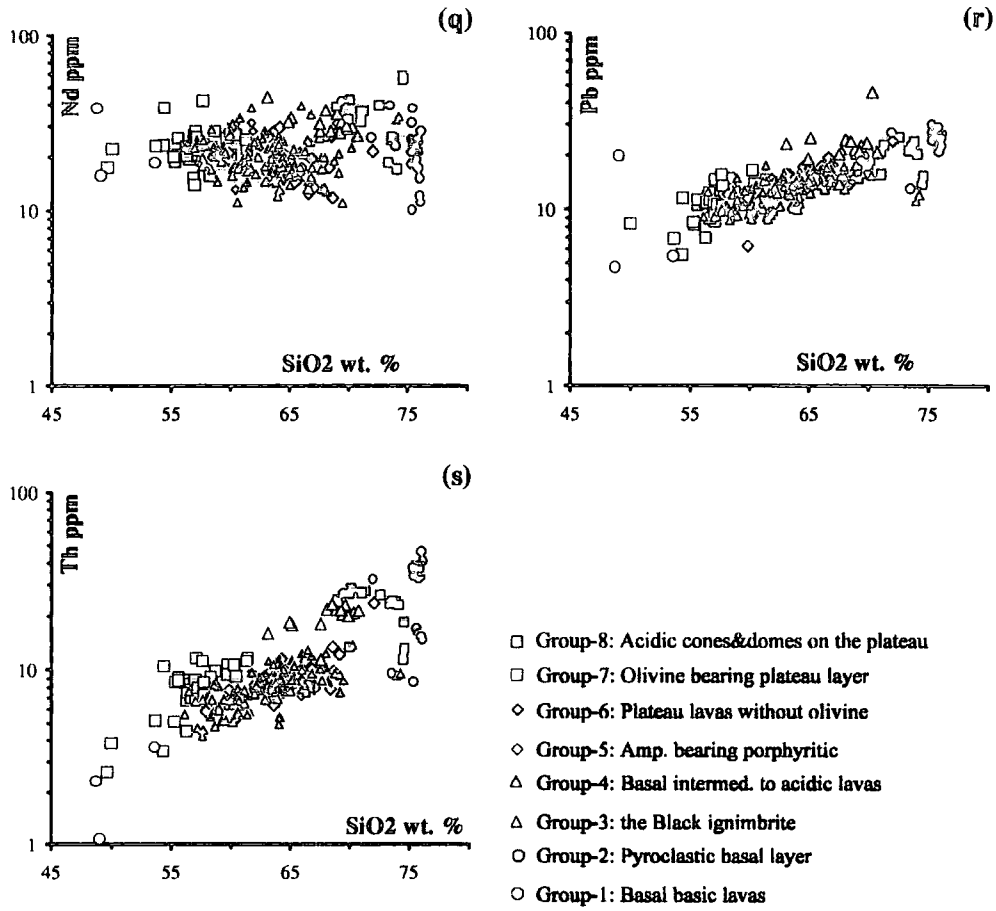

Figure: 3.10. (Continued).

that, if such a magma erupts to the surface in a short period of time, it may contain both amphibole phenocrysts that crystallised at depth as well as ortho- and clinopyroxenes which are on the liquidus under shallower conditions (e.g. group 5: amphibole-bearing porphyritic lavas). When such a magma rises and accumulates in a magma chamber at a relatively shallow depth, the liquidus phases are two pyroxenes and plagioclase. Under these conditions, amphibole is no longer in equilibrium with the magma, hence amphibole phenocrysts are resorbed. This mechanism may also explain the absence of amphibole as a phenocryst phase in basal intermediate to acidic lavas (group 4). Medium rare earth element (MREE) depleted rare earth element patterns of the amphibole-bearing series (Section 3.3.2 Figure 3.27-a and -b) also support amphibole fractionation. Furthermore, some petrographic and textural evidence found in the rocks of the Güngörmez dacite/andesite (group 4) in the Kargapazarı area imply that early amphibole fractionation and subsequent resorption was one of the important processes during the magmatic evolution of these groups. These can be listed as: resorbed brown hornblende phenocrysts which are mantled by ortho- and clinopyroxene respectively; and reaction rims of orthopyroxene surrounding amphibole phenocrysts (Section 6.1.1).

Changes in trace element concentrations during fractionation can be examined and modelled more quantitatively by comparing observed and theoretical fractionation trends on log-log bivariate plots, using vectors to show the amount and change which would take place as a consequence of the crystallisation of a particular mineral or mineral assemblage from the magma. Rb is selected as the fractionation index because it is highly incompatible throughout fractional crystallisation, resulting in a good positive correlation with SiO_2. Theoretical Rayleigh fractionation modelling has been carried out here using the elements Rb and Y to examine the fractionation history of lavas from the high- and low-Y series on the Erzurum-Kars Plateau (Figure 3.11). The Rayleigh fractionation vectors show the effects of removing specified amounts of various minerals from the magma. On this type of diagram, the starting composition is not crucial. Therefore the entire array of vectors may be moved to superimpose on the data points. The Rayleigh equation used for this modelling is

$$C_L / C_0 = F^{(D-1)} \quad \text{where} \qquad \text{Eq. 3.1.}$$

C_L: *weight concentration of a trace element in the liquid*

C_0: *the weight concentration of a trace element in the parental liquid*

F : *the fraction of melt remaining*

D : *bulk distribution coefficient of the fractionating assemblage during crystal fractionation*

This equation is based on the idea that crystals of the minerals crystallising from magma are removed from the site of formation immediately after crystallisation and have no opportunity to re-equilibrate with the magma i.e. at best, surface equilibrium may be attained as can be expected from natural systems.

Mineral/melt distribution coefficients of selected trace elements used here for the modelling have been gathered from a compilation of distribution coefficient (K_d) values suggested by several authors also including my own data for ortho-, clinopyroxenes, amphibole, biotite and plagioclase. These authors are listed in Table 4.11 and details of compilation and calculations are given in Section 4.3.2.

This type of modelling was first applied to the collision-related volcanics of Eastern Anatolia by Pearce et al. (1990), on a regional scale using Y and Rb. They recognised three distinct trends in the region as follows: (1) the Nemrut-Muş-Tendürek trend of increasing Y and Rb which has been interpreted as crystallisation dominated by plagioclase, olivine, pyroxene and magnetite (POAM); (2) a near constant Y trend (Kars-Ararat) which has been explained in terms of plagioclase and

amphibole dominated fractionation; and (3) a low-Y trend (Kars-Ararat) which has been explained by fractionation involving garnet and amphibole.

As is seen on Figure 3.11, positive gradients in general require fractionation of anhydrous mineral assemblages e.g. plagioclase, olivine, pyroxene, magnetite (i.e. POAM) while negative to flat gradients basically necessitate the crystallisation of hydrous minerals like amphibole and also garnet. Flat gradients, which are

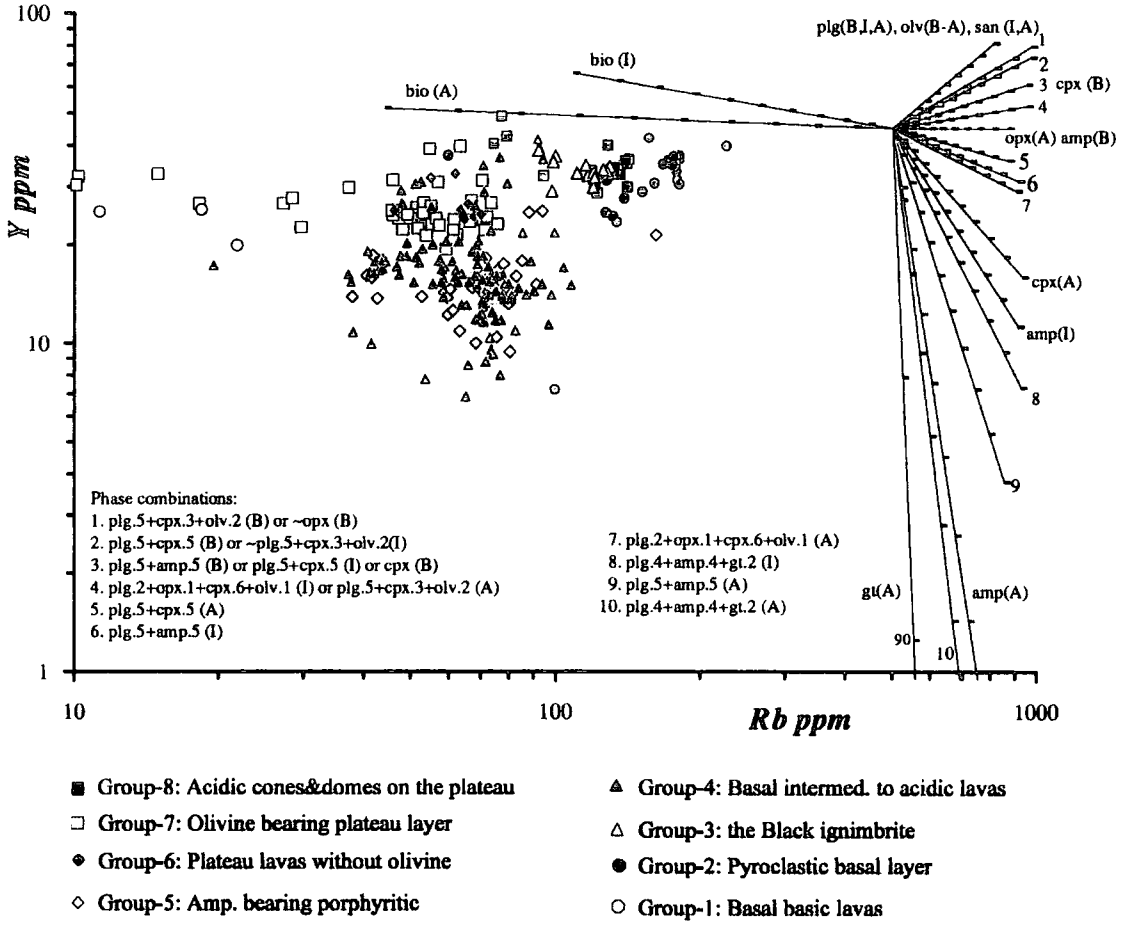

Figure: 3.11. Rb-Y log-log diagram showing theoretical Rayleigh fractionation vectors modelled for crystallisation of individual mineral phases and also phase assemblages. Theoretical vectors are designed for 50% crystallisation. Phase combinations are presented in inset. The number beside each vector is the quantity (in percent) of that mineral or phase combination removed from the melt in order to generate the vector.

Key to abbreviations: amp: amphibole, plg: plagioclase, olv: olivine, bio: biotite, cpx: clinopyroxene, opx: orthopyroxene, gt: garnet. B: basic, I: intermediate, A: acid.

represented here by the high-Y trend, should be interpreted with caution because, as seen on the diagram, they may also result from fractionation of the following assemblages:

vector 3 : plg (50%) + amp (50%) in basic (B) or plg (50%) + cpx (50%) in intermediate to acidic magmas (I, A) or

vector 4: plg (20%) + opx (10%) + cpx (60%) + olv (10%) (in intermediate magmas (I) or plg (50%) + cpx (30%) + olv (20%) (A)

vector 5: plg (50%) + cpx (50%) in acidic magmas

The existence of a flat trend at the basic end (left) of the diagram necessitates the dominance of amphibole in the fractionating assemblage at basic compositions. This is because even domination of clinopyroxene, a mineral with the highest partition coefficient for Y after amphibole at basic compositions ($K_d^{(cpx-liq)} = 0.55$) could not sufficiently create this effect. Alternatively, minor garnet fractionation could produce the same effect, though there is no petrographic evidence for early garnet fractionation anywhere on the plateau nor is garnet likely to crystallise at basic composition. While there is no doubt that amphibole was one of the most important early fractionating minerals in the basic members of the high-Y series, when the magma evolved towards the intermediate to acid compositions, the amphibole-dominated assemblage should have been gradually superseded by anhydrous phases since the flat vectors on the intermediate to acid side of the diagram predominantly result from the fractionation of a mainly anhydrous assemblage with or without a minor amount of amphibole. Therefore, it can be argued that the high-Y series is controlled by the fractionation of POAM at intermediate to acid compositions. In contrast to the high-Y series, the low-Y series display a gradual depletion in Y with increasing Rb which is represented by a distinct negative gradient while the magma evolves to more acid compositions. The lavas following this trend appear to have undergone fractionation of amphibole as the dominant mafic phase during the evolution of this series. Crustal assimilation may create a similar trend to the low-Y trend with enrichment in Rb and depletion in Y only if the crust has unusually low Y concentration, because concentration of Y in average crust is generally high, between 22 and 25 ppm (Taylor and McClennan, 1985; Condie, 1993 and Taylor, 1977).

Medium to heavy rare earth elements that have high partition coefficients for amphibole at intermediate to acid compositions also show two trends coinciding with the high- and low-Y series. In Figure 3.12 (a-d), a similar FC modelling has been carried out for Gd, Tb, Er and Yb. The data used in these diagrams are obtained from ICP-MS analysis of a subset of representative samples that characterise both Y series. Vector rosettes on these diagrams have been plotted for 50% removal of the same minerals and assemblages by fractionation as given in Figure 3.11. The low-Y trend on these diagrams also requires the fractionation of amphibole at intermediate to acidic compositions.

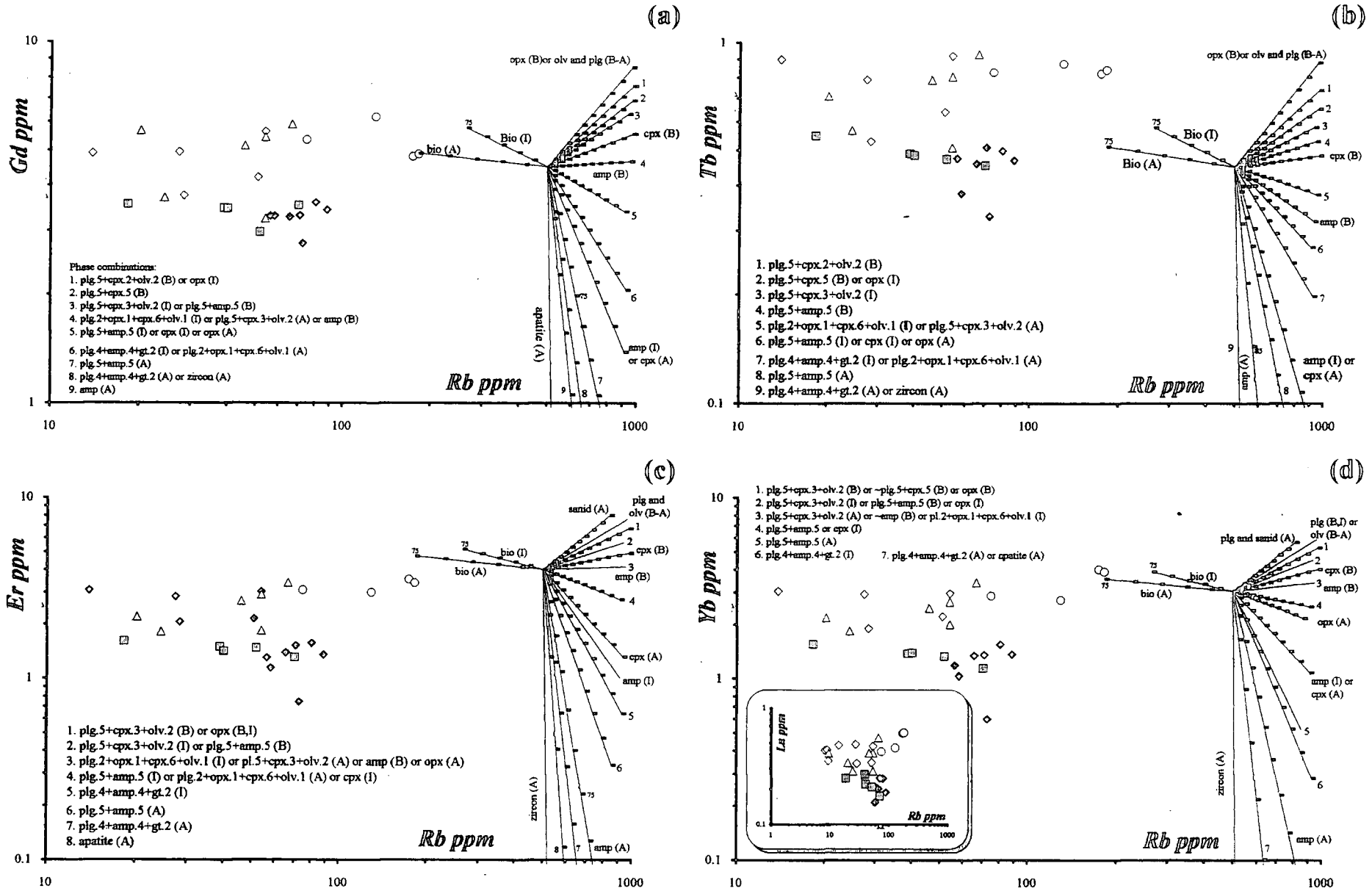

Figure: 3.12. Log-log plots of Gd, Tb, Er and Yb against Rb showing the contrast in REE behaviour between the volcanic units of the high- and low-Y series.

The data and modelling presented in Figures 3.11 and 3.12 are not completely sufficient to provide a definitive answer for the fractionation history of the low- and high-Y series because the modelling cannot take into account the variations in the relative abundance of each mineral in the fractionating assemblage, and variations in bulk partition coefficient during the course of time. There is no doubt about the dominance of amphibole fractionation in the low-Y series at intermediate to acid compositions. On the other hand, the persistent absence of amphibole as a phenocryst phase in the intermediate to acidic volcanic suits that follow the high-Y trend appears to be supporting the idea of an amphibole-free fractionation evolution for these units. This argument may be particularly true for the volcanic rocks of groups 8,7, 6, 3 and 2 since these rocks are dominated by a phenocryst assemblage which is mainly composed of plagioclase, ortho- and clinopyroxene. However this still does not significantly rule out early amphibole fractionation in the formation of these units since amphibole phenocrysts might have been completely resorbed. For these reasons, each of the two Y-trends may correspond to one of two distinctly different magma series which have experienced two different fractionation stories i.e. POAM and hydrous.

Another possibility which should be taken into account is that the initial difference in Y content between the high- and low-Y series may be primary. Even though the low-Y trend converges with the high-Y trend at the basic-end, it is not clear if they were initiated from the same parental magma because of the lack of basic rocks of the low-Y series. Distribution of other trace elements (i.e. Rb, Sr and Zr) indicates that some of these differences might be related to the pre-fractionation processes and may even have resulted from primary differences in the source regions of these two different type of magmas that were later variably modified by the combined effects of fractional crystallisation and/or assimilation. For example, if garnet was a residual phase during the partial melting event, Y and the heavy rare earth elements would be significantly depleted. In any case, irrespective of the starting Y concentration, gradual depletion of Y with increasing acidity of the melt requires fractionation of amphibole in the low-Y series. Consequently, Y concentrations may be used as a primary discriminant in differentiating volcanic rocks of the Erzurum-Kars Plateau into two series which have undergone fractionation of two different mineral assemblages, i.e. hydrous and anhydrous.

As noted earlier, the data from the plateau have been divided into two main series using their Y content as high- and low-Y. A third series (11 samples) which creates a separate trend falling consistently between the low- and high-Y series on several trace element diagrams is also distinguished and termed the transitional series

(11 samples). The new classification of the Plateau lavas based on their Y contents is presented in Table 3.1 and Figure 3.13.

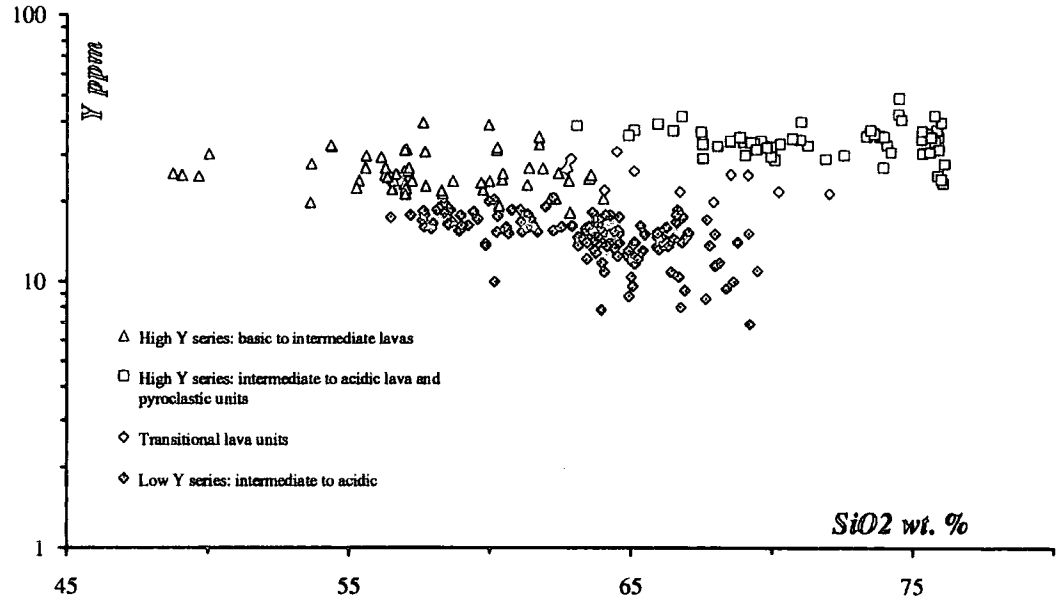

Figure: 3.13. Log-normal plot of Y versus SiO_2 showing the main Y-series after classification of volcanic rocks of the Erzurum-Kars Plateau using their Y concentrations as a primary discriminant.

The high-Y series can be further subdivided into two groups on the basis of their silica contents, namely (1) basic to intermediate and (2) intermediate to acidic lava and pyroclastic units. These two groups fall into two distinct areas on the classification diagrams of both Peccerillo and Taylor (1976) and Le Bas (1986) (Figure 3.14) with a compositional gap. The first group namely basic to intermediate lava units span a compositional range from basalts with 51% SiO_2 and 0.5% K_2O to dacites with a maximum SiO_2 value of 64% and 2.8% K_2O. It makes up a well-defined trend parallel to the border between andesites-dacites and their high-K equivalents.

The second group, namely the intermediate to acidic lava group of the high-Y series, forms another trend covering the compositional range from trachydacite, with 63% SiO_2 and 4% K_2O, to rhyolites with 77% SiO_2 and a maximum of 5.8% K_2O. This group with its distinct high-K and total alkali contents completely coincides with the alkali-calcic group defined earlier. Rocks of the low-Y series form a rather narrow compositional spectrum from andesites (57 % SiO_2) to dacites (69.5% SiO_2).

The transitional series form a sub parallel trend to the intermediate to acidic lava group of the high-Y series predominantly falling in trachydacite and rhyolite fields. Basic to intermediate rocks of the high-Y series and rocks of the entire low-Y

A. HIGH Y SERIES (Y >20 ppm)

Groups	Character	Formations
I. BASIC TO INTERMEDIATE LAVAS		
1. Olivine bearing plateau layer	*CA*	1.1. Kargapazarı volcanics (Mt. Kargapazarı, Pasinler) 1.2. Horasan Plateau unit (N of Horasan) 1.3. Kars Plateau unit (Kars)
2. Plateau lavas without olivine	*CA*	2.1. Aladağ andesite (Mt. Aladağ)
3. Basal intermediate lava layer	*CA*	3.1. Black andesite/dacite (Pasinler)
4. Basal basic lava layer	*CA*	4.1. Karapınar basalt (Mt. Kargapazarı) 4.2. Kötek basalt (North of Horasan)
II. ACIDIC LAVA AND PYROCLASTICS		
1. Acidic lavas	*AC*	1.1. Acidic lava cones on the plateau 1.1.1. Ardıçlıdağ rhyolite (Pasinler) 1.1.2. Odalar rhyolite (Mt. Aladağ) 1.2. Basal acidic lava layer 1.2.1. Çukurayva rhyolite 1.2.2. Paslı trachy-dacite
2. Pyroclastics	*AC*	2.1. Black ignimbrite (Pasinler and Mt. Kargapazarı) 2.2. Basal pyroclastic units 2.2.1. Grey ignimbrite (Pasinler and Horasan) 2.2.2. White ignimbrite (Pasinler and Horasan) 2.2.3. Obsidian (Pasinler, Horasan, Mt. Aladağ and Kagızman 2.2.4. Pyroclastic fall deposits

B. LOW-Y SERIES (Y<20 ppm)

I. AMPHIBOLE BEARING PORPHYRITIC LAVAS	*CA*	1. Dumlu amphibole dacite/andesite (Mt. Dumlu) 2. Arzutu amphibole dacite (Mt. Dumlu) 3. Göllerdüzü amphibole dacite (Mt. Kargapazarı) 4. Kızılveren amphibole dacite /andesite (Pasinler) 5. Köroğlu amphibole dacite /andesite (North of Horasan) 6. Saçdağ dacite (South of Horasan)
II. BASAL INTERMEDIATE TO ACIDIC LAVAS	*CA*	1. Güngörmez dacite/andesite (Mt. Dumlu, Mt. Kargapazarı) 2. Gireköse dacite (Mt. Dumlu, Mt. Kargapazarı) 3. Köşk pyroxene dacite (Mt. Kargapazarı) 4. Çobandede dacite (Mt. Kargapazarı)

C. TRANSITIONAL GROUP

	CA	**Samples:** MK46 and MK47 : Dumlu amphibole dacite /andesite (Mt. Dumlu) MK229, MK240 and MK241: Güngörmez dacite/andesite (Middle lens, Mt. Dumlu) MK4, MK86, MK87, MK88 and MK273: Güngörmez dacite/andesite (Mt. Kargapazarı)

Table: 3.1. Table showing the classification of volcanic formations of the Erzurum-Kars Plateau in terms of their Y content. CA: calc-alkaline rocks; AC: alkali-calcic rocks.

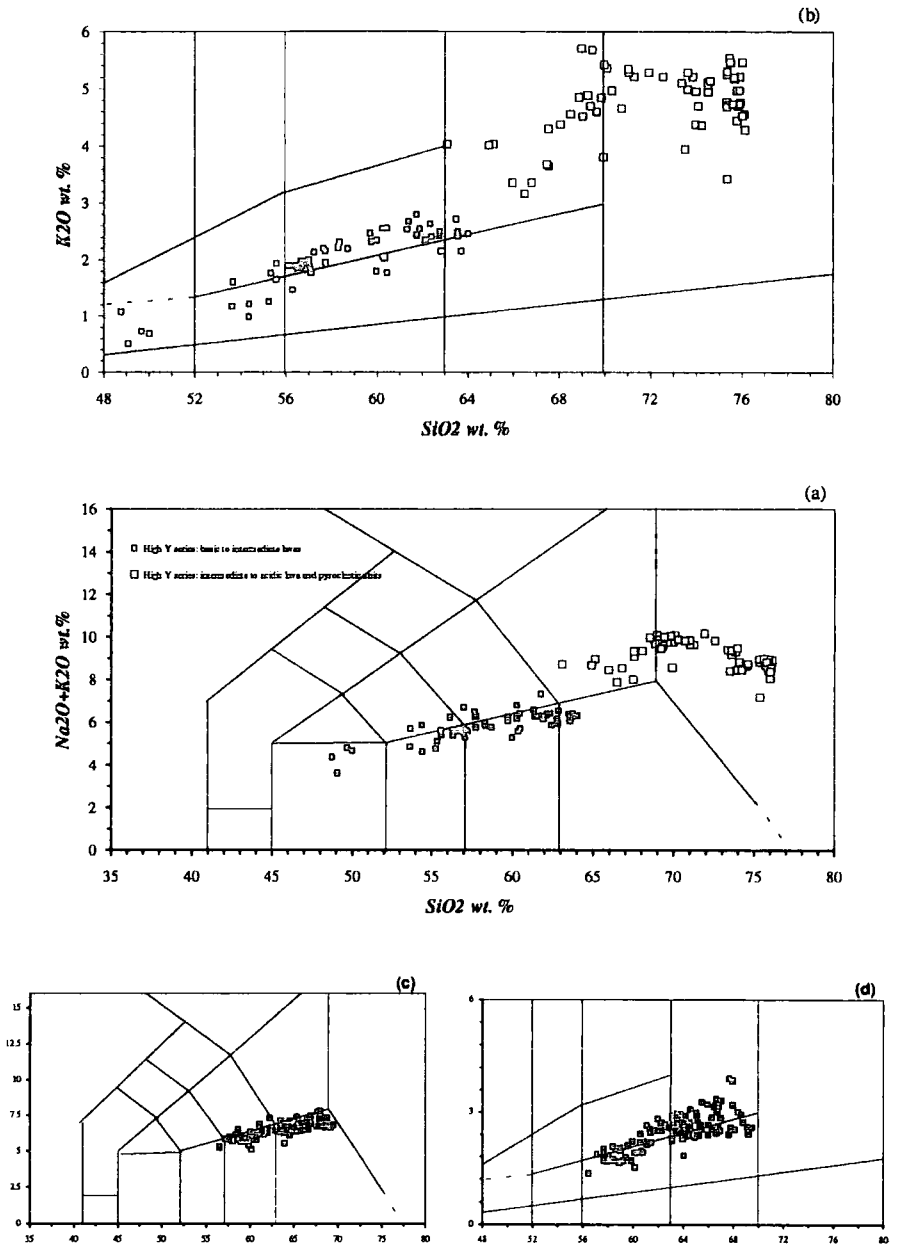

Figure: 3.14. Classification of the Erzurum-Kars Plateau volcanics based on their Y content by using diagrams of Le Bas et al. (1986) and Peccerillo and Taylor (1976). (a) and (b) classification of basic to intermediate and intermediate to acidic lava units of the High-Y series; (c) and (d) classification of the Low-Y series.

series are all calc-alkaline in character.

The compositional differences between the high- and low-Y series can be seen more clearly when the data are presented in the form of histograms. Figure 3.15 illustrates the distribution of SiO_2 in the high- and low-Y series. Most notably, the high-Y series comprises a bimodal character indicated by two peaks located at 56-62% SiO_2 (with frequency % of 25) and at 72-76 % SiO_2 (with an frequency % of about 23) respectively. In contrast, the low-Y series is characterised by unimodal volcanism which covers a narrower SiO_2 range from 56 to 72% having a peak

between 64-68 % SiO_2 with a maximum frequency % of about 45. When these two diagrams are superimposed, the peak of the low-Y series overlaps the depression located between two peaks of the high-Y series so that overall distribution gives the histogram with a single peak as presented in Figure 3.1.

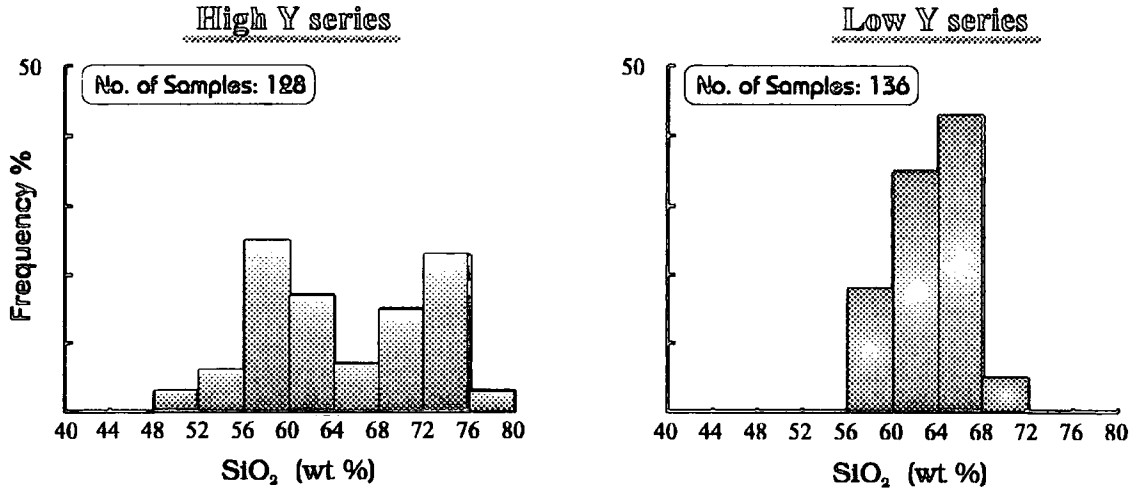

Figure: 3.15. Frequency distribution graphs of SiO_2 for high and low-Y series.

In order to show the compositional differences and distributions of compositions between high- and low-Y series, major and trace element data from both series have been separately plotted onto histograms. Major and trace element histograms are presented in Figures 3.16 and 3.17 respectively. Almost all major elements, especially SiO_2, TiO_2, Fe_2O_3*, CaO and K_2O (Figure 3.16), show two peaks for the high-Y series supporting the idea of bimodal volcanism. Not only major but also trace elements e.g. Ni, Co, Sc, V, Cu, Pb, Zn, Rb, Sr, Y, La and Ce exhibit a distinctive bimodality. The high-Y series almost always covers a broader compositional range on both major and trace element diagrams compared to the low-Y series.

In the following sections, major and trace element geochemistry of the volcanic units will be re-examined from a different perspective in the framework of the new classification namely the low- and high-Y series.

* Tortal iron as Fe_2O_3

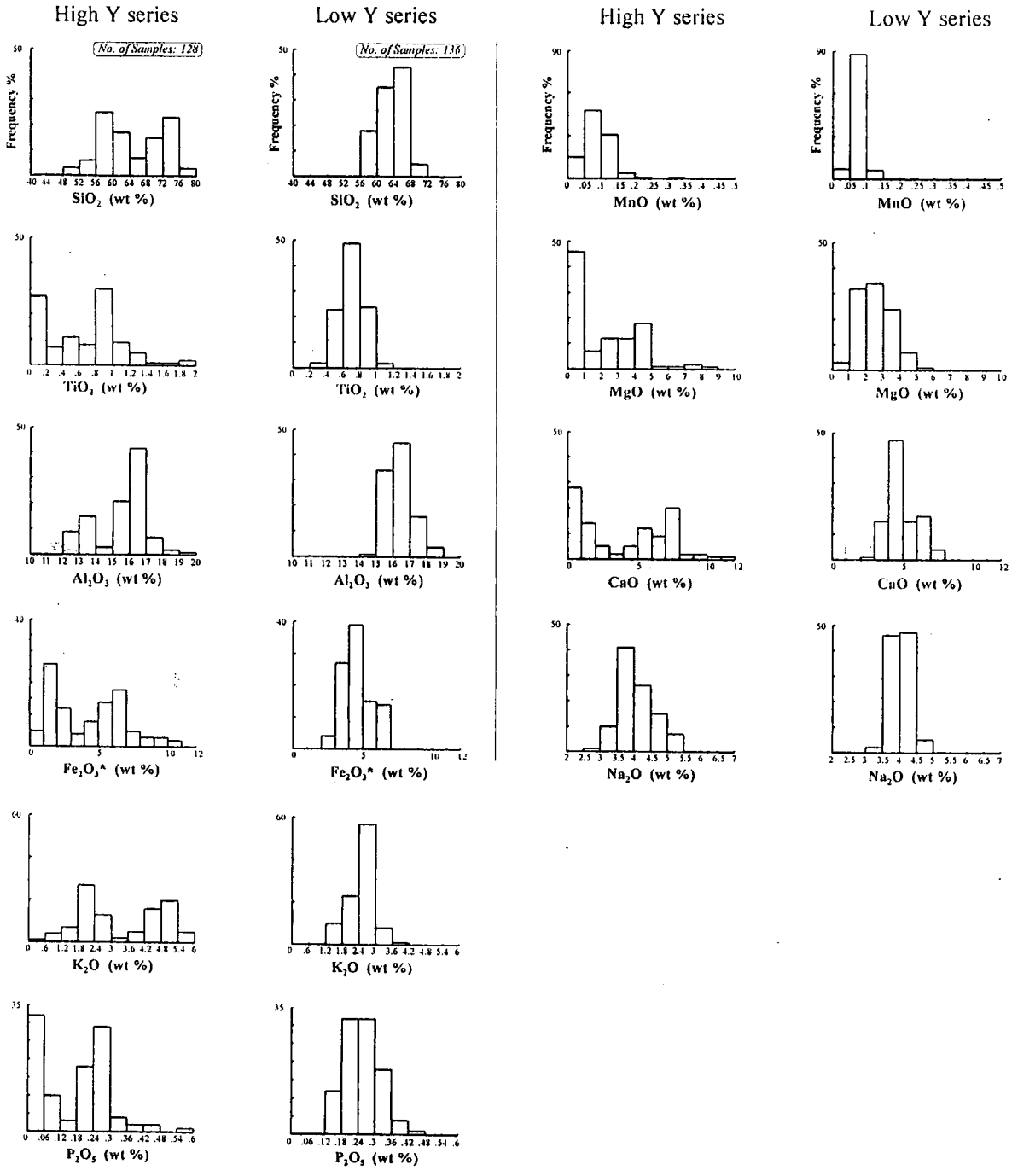

Figure: 3.16. *Major element histograms of high- and low-Y series showing the bimodality of the rocks of the high-Y series.*

Figure: 3.17. Histograms of trace elements showing the differences between the volcanic rocks of the high- and low-Y series.

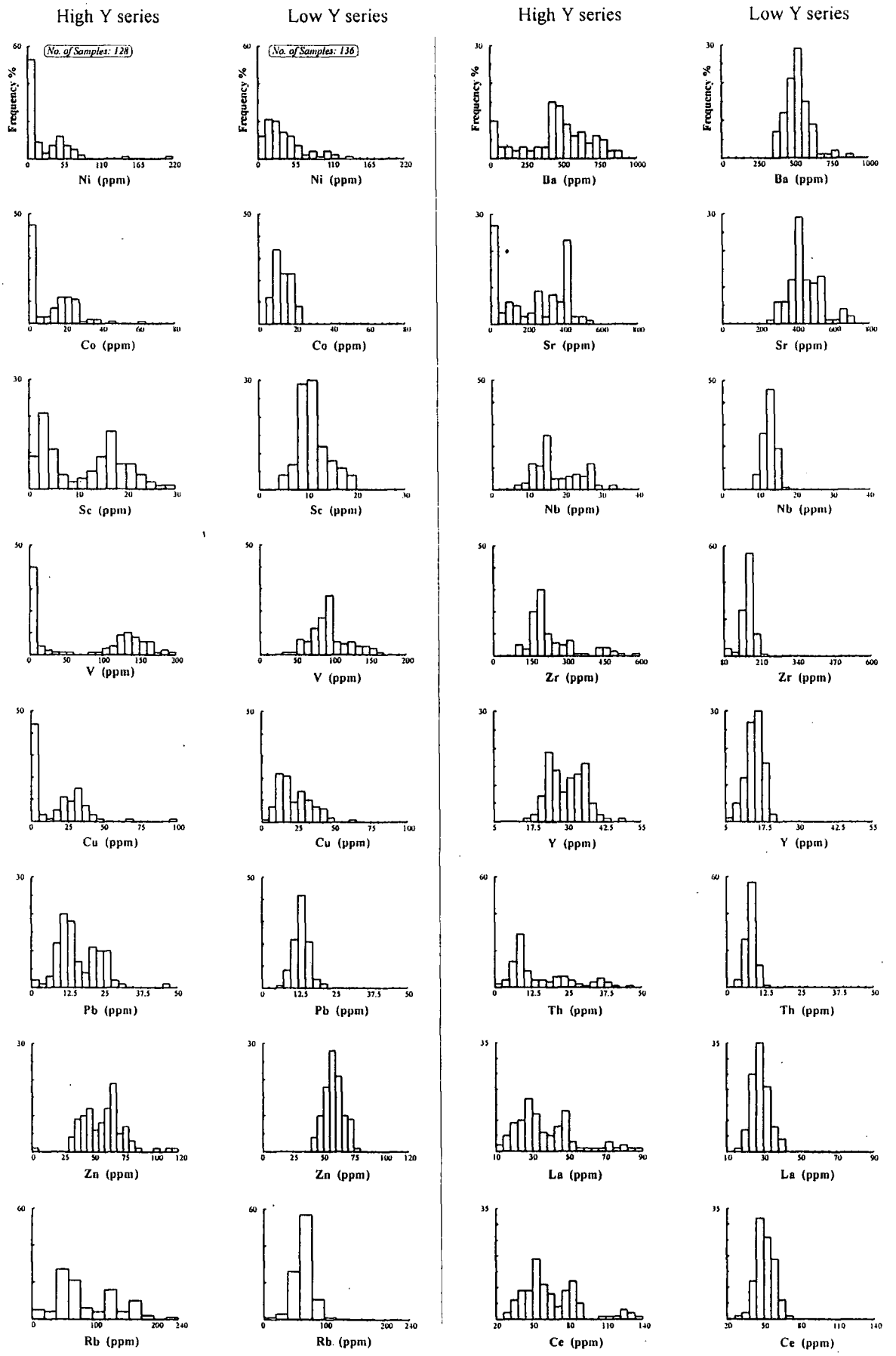

3.2.1. Interpretation of trace element fractionation trends

Trace element data from the Erzurum-Kars Plateau have been divided into four series as presented previously in Figure 3.13 (i.e. 1. basic to intermediate and 2. intermediate to acidic lavas of the high-Y series, 3. transitional lava units and 4. intermediate to acidic lavas of the low-Y series) and plotted on log-normal graphs against SiO_2 to illustrate compositional differences between high- and low-Y series (Figures 3.18-19). The high and low-Y series form two close, but distinctive, differentiation trends on most of the diagrams. Lavas of the high-Y series are in general enriched in Zr (Figure 3.18-d) and Th (Figure 3.19-g), and partly in Nb (Figure 3.18-e) , La, Ce (Figure 3.18-g and h) and Nd (Figure 3.19-f) and slightly depleted in Sr (Figure 3.18-b), Cr, V, Ni and Co (Figure 3.19-b, c, d and e) relative to the rocks of low-Y series for equivalent silica contents. Most of these differences which are seen throughout basic to acidic compositions especially for the highly incompatible elements; namely Zr and Th may be interpreted as due to the high- and low-Y series being related to two different fractionation histories.

Rb and Th show a positive correlation with increasing SiO_2 throughout fractionation for both high- and low-Y series, a feature that enables the use of these elements as fractionation indices. Some samples from the acidic lavas and pyroclastics of the high-Y series form a discrete trend on the Rb versus silica diagram (Figure 3.18-a) between 73 and 76 wt. % SiO_2 that joins the main trend at around 76 wt. % SiO_2. This trend, which is made up of rhyolites and pyroclastics in the Mt. Aladağ and Kağızman areas, appears to have formed by minor biotite fractionation ($K_d^{(bio-liq)}$ =3.2 at intermediate, 4.5 at acid compositions).

On the Th against silica diagram (Figure 3.19-g), acidic units of the high-Y series (in the north of Horasan, Mt. Aladağ and Kağızman areas) form an almost vertical trend diverging from the main trend towards lower Th concentrations. This may be due to minor zircon fractionation at 72 wt. % SiO_2.

Nb (Figure 3.18-e), Nd (Figure 3.19-f) and partly Ce and La (Figure 3.18-h and g) display two diverging trends coinciding with those of the high- and low-Y series seen on the Y against SiO_2 diagram (Figure 3.18-c). Formation of the lower trends is again consistent with the amphibole fractionation during the magmatic evolution of the low-Y series, because these elements are partitioned moderately into amphibole at intermediate to acid compositions (see Table 3.2). On the other hand, Nb can also be partitioned into biotite while Ce and La can be accommodated in clino- and orthopyroxene at acid compositions although concentrations of these elements are less strongly affected by these minerals than by fractionation of amphibole. Although

amphibole fractionation was the major controlling factor in the formation of these lower trends, some of the decrease at the acid end can be attributed to fractionation of pyroxenes.

	Basic	*Intermediate*				*Acid*			
	Amp	Amp	Bio	cpx	opx	Amp	Bio	cpx	opx
Nb	0.3	1	1.4	0.2	0.2	3.5	3.5	0.8	0.7
Nd	0.65	1.7	0.2	1	0.3	4	0.9	2.5	2.5
Ce	0.35	0.7	0.16	0.4	0.1	1.7	0.75	1	1.5
La	0.2	0.5	0.15	0.4	0.2	1.5	0.5	1.2	1.5

Table: 3.2. Table showing partition coefficients of amphibole (amp), biotite (bio), clinopyroxene (cpx) and orthopyroxene (opx) for basic, intermediate and acidic magmas. Partition coefficient values are from a compilation presented in Section 4.3.2.

At the more acid compositions Nb forms a small trend and behaves similar to Rb. It is, again, presumably controlled by a minor biotite fractionation in the acid lava and pyroclastic units in the north of Horasan, Mt. Aladağ and Kağızman areas if magma mixing between the low-Y series and acidic units of the high-Y series was not the major factor in the formation of this trend. This relationship is consistent with the fact that some ignimbrite and pyroclastic flow and fall units contain subordinate biotite in the eastern part of the plateau, from the north of Horasan towards the east.

The Pasinler area is of special importance because it contains one of the most complete volcanic sections which is made up of several lava and pyroclastic flow and fall deposits with a variety of textures and chemical compositions. It is also the best sampled area on the Erzurum-Kars Plateau. This area can be considered to be a model area on the plateau for observing the detailed variations and relationships between the volcanic units of the high- and low-Y series. Therefore, in the following paragraphs, the details of the magmatic evolution of each volcanic series namely the high- and low-Y series, will be presented with special reference to the units in this area. In Figure 3.21, detailed volcano-stratigraphic profiles of major and trace elements are presented to show variations of these elements in different lava and pyroclastic deposits of the stratigraphic column. As is seen on these diagrams, the Kargapazarı volcanics, Black ignimbrite, Ardıçlıdağ rhyolite and the Kızılveren amphibole dacite/andesite have the most profound affect on the patterns shown in these diagrams.

On La and Ce versus SiO_2 diagrams (Figure 3.18-g and h), acid lava and pyroclastic units of the high-Y series exhibit two slightly curved trends one of which appears to be the lateral continuation of the main trend that is formed by basic to intermediate lavas of the high-Y series and the other shows an abrupt displacement from the main trend towards much higher concentrations of these elements and lies

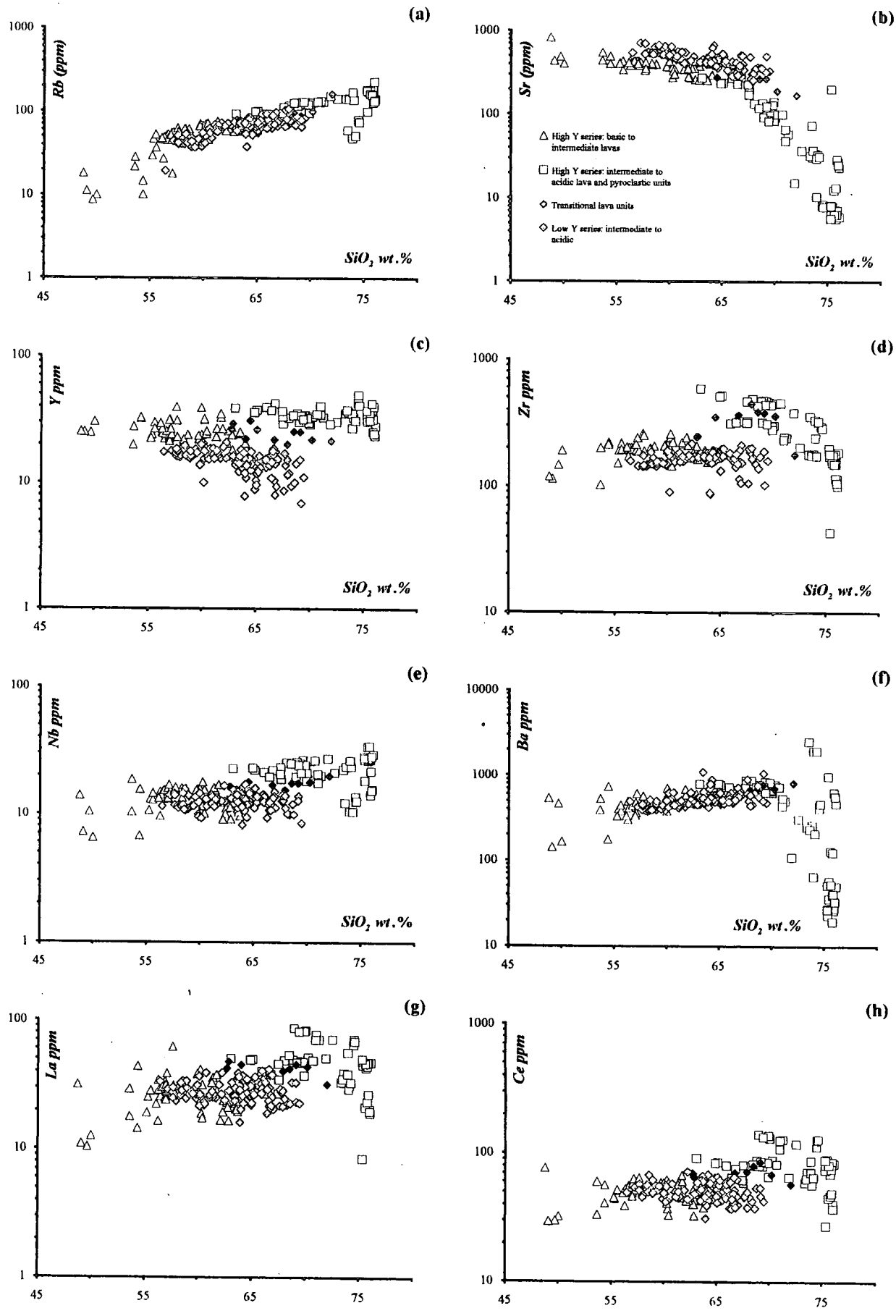

Figure: 3.18. Harker diagrams of Rb, Sr, Y, Zr, Nb, Ba, La and Ce.

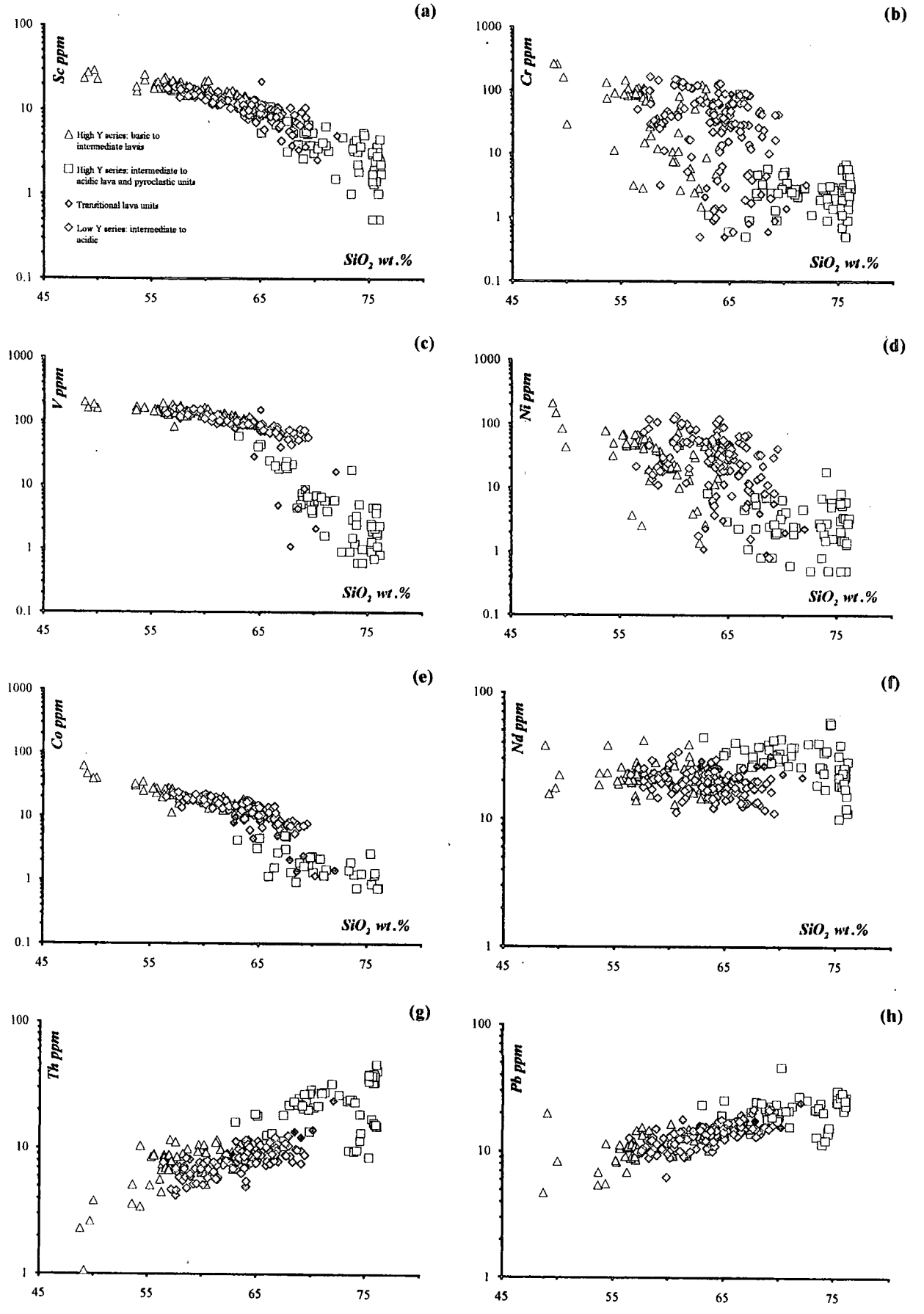

Figure: 3.19. Harker diagrams of Sc, Cr, V, Ni, Co, Nd, Th and Pb.

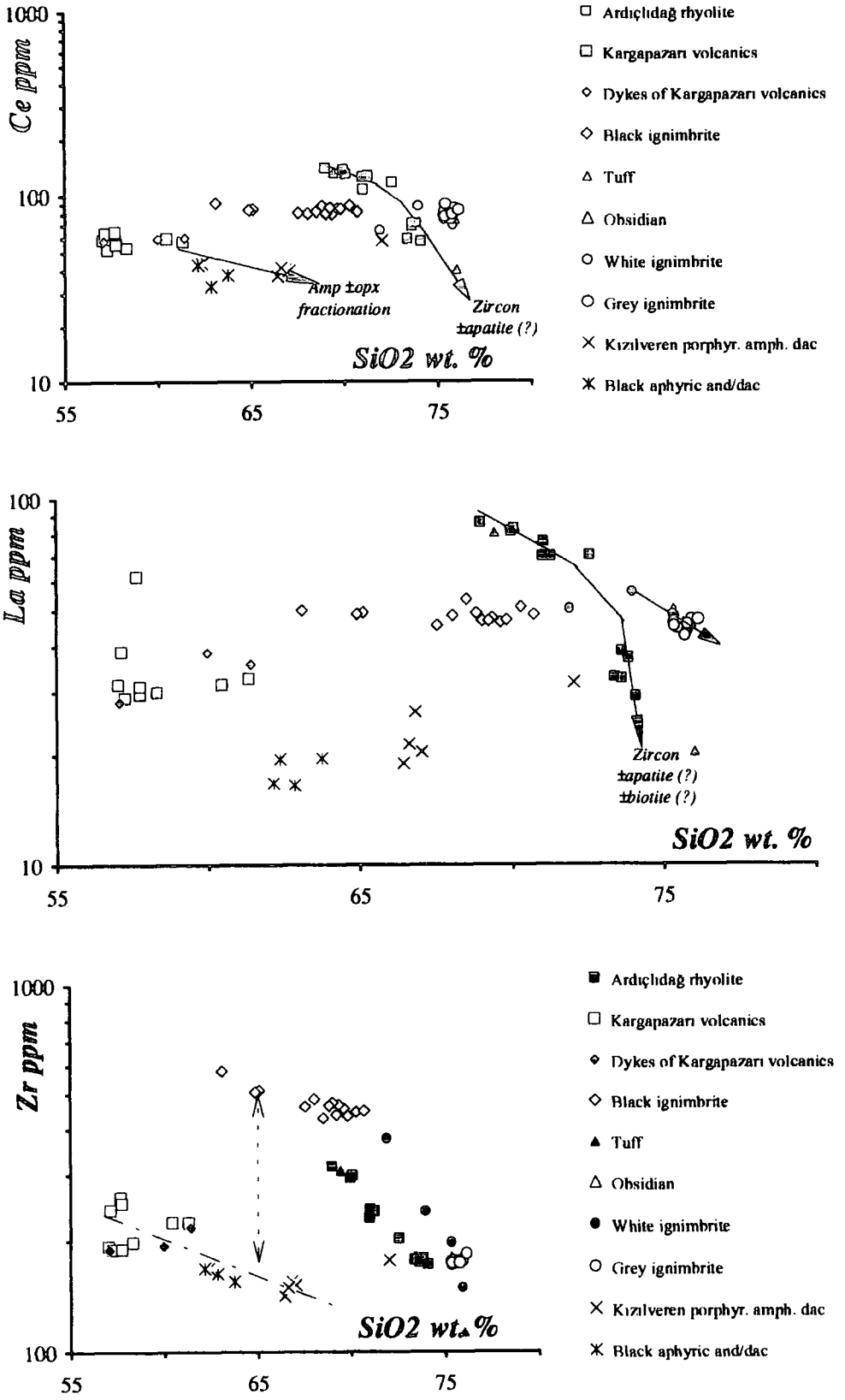

Figure 3.20. SiO_2 versus Ce, La and Zr of samples from the Pasinler area.

sub parallel to the former. Both of them decrease rapidly with increasing acidity of the melt, presumably in response to a minor amount of apatite ± zircon fractionation though there is no evidence in the behaviour of Y for crystallisation of zircon. Zr exhibits exactly the same behaviour as these elements forming two trends that decrease with silica confirming the existence of minor apatite ± zircon crystallisation. The upper trend, which shows higher concentrations of La and Ce is mainly represented by the Ardıçlıdağ rhyolite which is the uppermost volcanic unit in the volcano-stratigraphic column in the Pasinler area (Figure 3.20). This unit appears to have undergone a different chemical evolution compared to other high-Y units on the plateau. The light rare earth enrichment (LREE) in this unit may be explained by the dominance of fractionating phases that lack both pyroxenes and amphibole, in an isolated, relatively shallow (around 13-15 km; see Section 4.2.2.1) magma chamber. Alternatively, it is possible that there may be a difference in source chemistry. Nd shows a similar, but less pronounced pattern to those of La and Ce.

Zr shows a flat trend with increasing Rb in the formations of the low-Y series and in the basic to intermediate formations of the high-Y series (Figure 3.18-d). However, in some of the acid units of the high-Y series, it forms a separate concave trend that starts at much higher concentrations of Zr and then steeply decreases with increasing SiO_2. This trend is mainly made up of three units: the Black ignimbrite, the Ardıçlıdağ rhyolite and the Grey/White ignimbrites on the Pasinler plateau (Figure 3.20-c).

The Black ignimbrite contains quite different concentrations of trace elements from the other units on the plateau. It is composed of abundant plagioclase phenocrysts some of which are corroded, subordinate pyroxene and some accessory zircon. Most remarkably, it is strongly enriched in Zr up to 4 times greater than the value for average liquid line of descent, with the concentrations of up to 580 ppm (A point in Figure 3.22). In Figure 3.22, in Rb versus Zr diagram, data points of the Ardıçlıdağ rhyolite and the White/Grey ignimbrite form two close but coherent hyperbolic curves without overlapping. They approach the data point of the most primitive and Zr-rich Black ignimbrite (component A=> MK78: 92 ppm Rb, 580 ppm Zr and 63.1 SiO_2 wt.%) and join to each other at that point. Two binary mixing curves have been computed for the simple mixing between the component-A and the most Zr depleted points of rhyolitic units (component-B: the Ardıçlıdağ rhyolite and C: the White/Grey ignimbrites). These are plotted in Figure 3.22. The mixing curves fit the data points very neatly as an indication of two separate magma mixing events between a trachytic magma that gave rise to the Black ignimbrite (component-A) and two other rhyolitic magmas which produced the White/Grey ignimbrites (aphyric

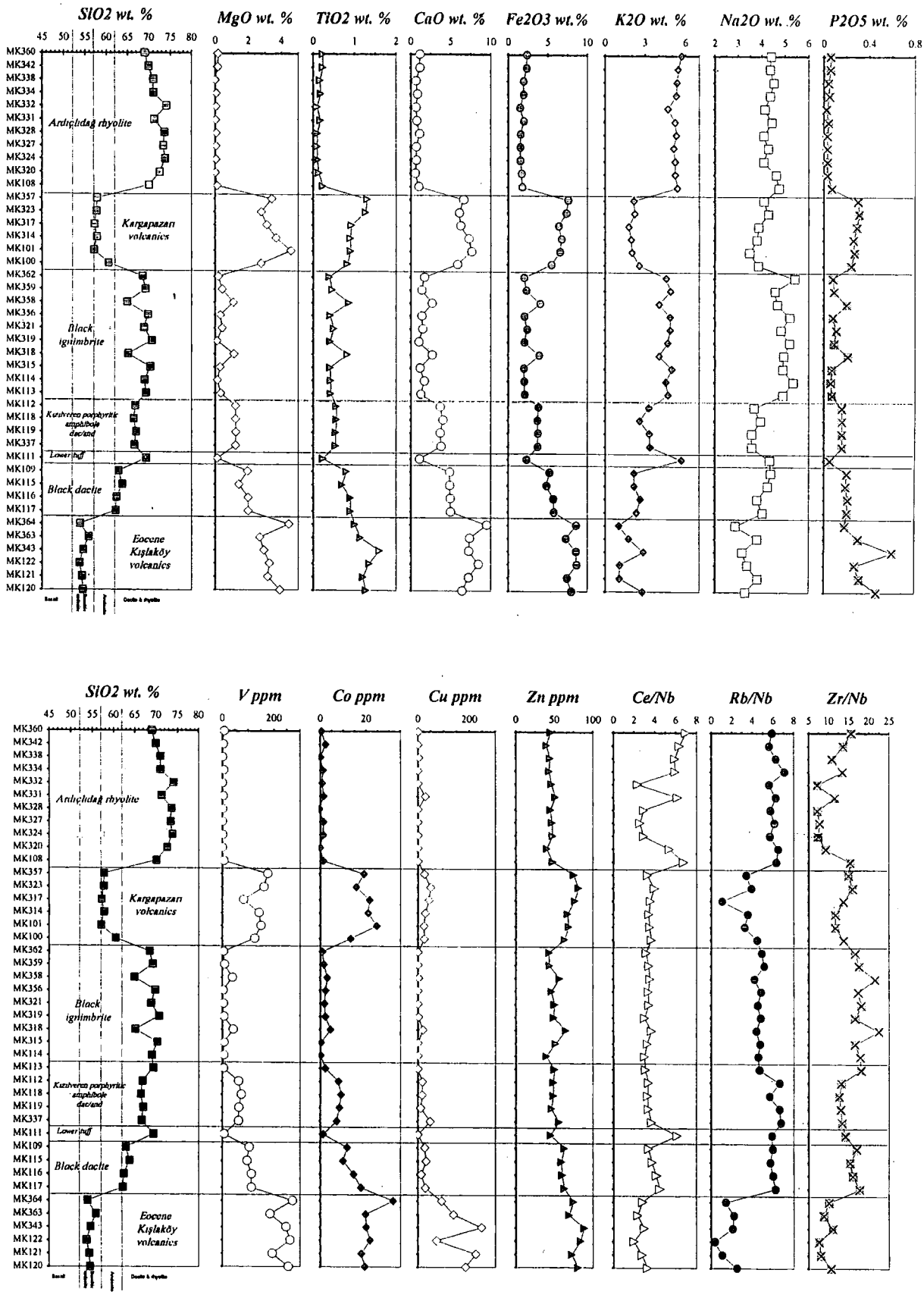

Figure: 3.21. Volcano-stratigraphic profiles of major and trace element chemistry throughout the volcanic sequence of the Pasinler area.

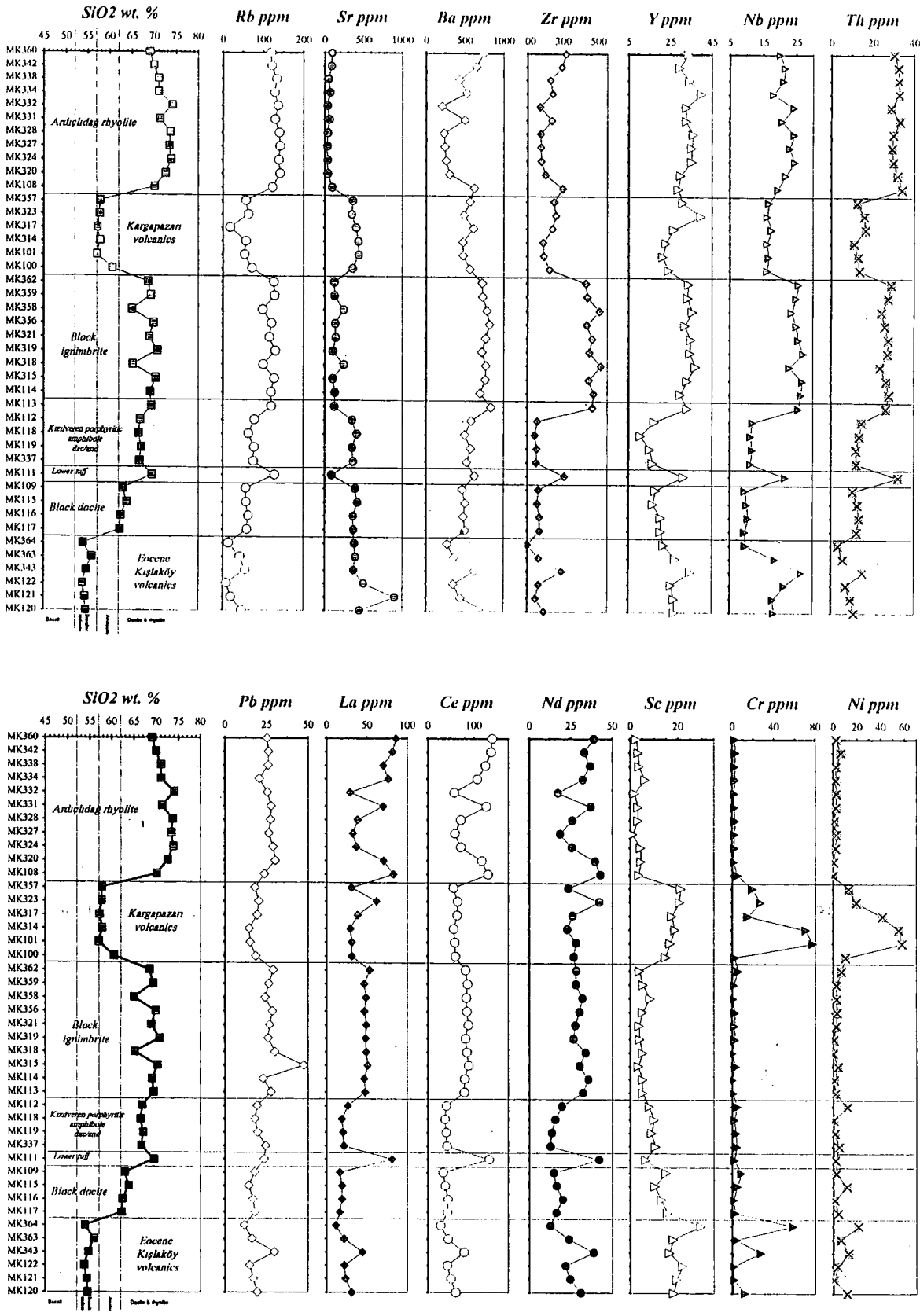

Figure: 3.21 (continued).

rhyolite: component-C) and Ardıçlıdağ rhyolite (crystal-rich rhyolite: component-B) respectively. Most notably, half of the mixing curve between the Black ignimbrite and the Ardıçlıdağ rhyolite is made up of the data points of the Ardıçlıdağ rhyolite which include no black ignimbrite inclusions anywhere in the field. This may

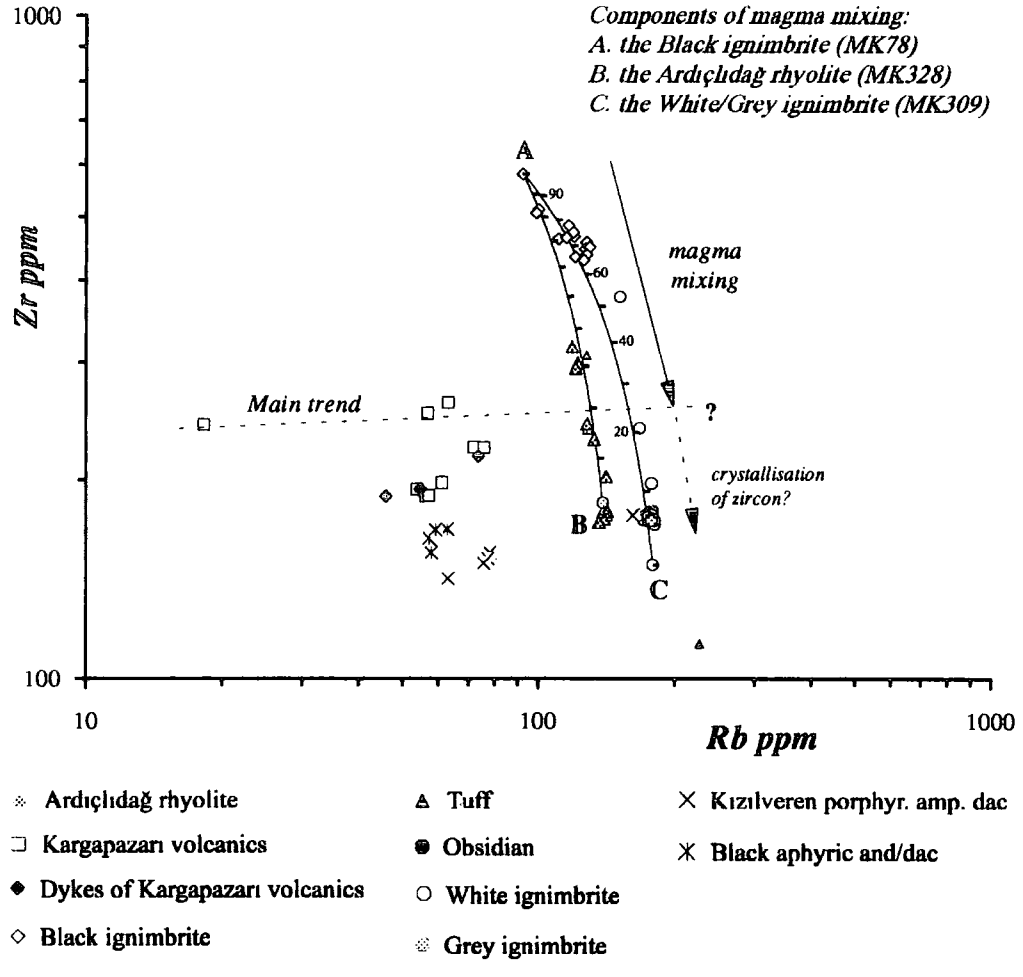

Figure: 3.22. Diagram showing the binary mixing lines between the Black ignimbrite and Ardıçlıdağ rhyolite and between the same unit and the White/Grey ignimbrite.

indicate that the accessory minerals i.e. zircon and apatite. Fractional crystallisation of zircon would produce a similar decreasing trend to these mixing lines, but it would be linear and steeper. On the other hand, the accumulation of zircon in the magma could create a Zr enrichment as may be in the case of some of the data points which belong to the Ardıçlıdağ rhyolite. Therefore, mixing curves on Figure 3.22 should be interpreted with caution for the possible effects of zircon. Fractionation of biotite may also cause the Rb concentration to decrease. This should not be an important factor since biotite is not a major crystallising phase in the Pasinler area.

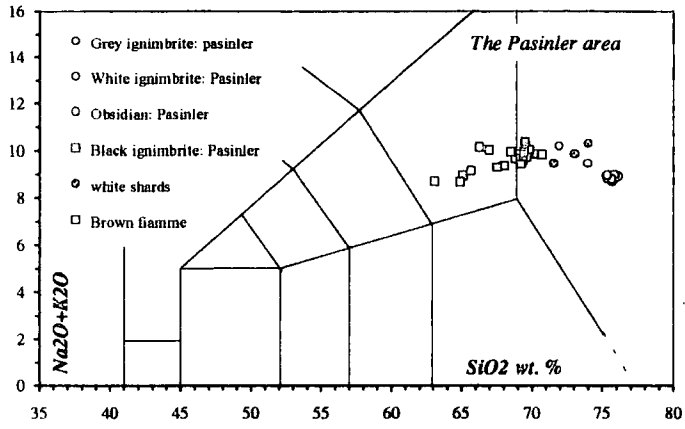

Figure: 3. 23. Composition of the transparent and brownish coloured fiammé from the Black ignimbrite unit, plotted onto the total alkalis versus SiO_2 diagram.

The Black ignimbrite contains abundant black fiammé which display quite different colour, texture and phenocryst content relative to surrounding matrix which is mostly made up of scarlet to black coloured glassy groundmass (Photos 2.10 and 12). This groundmass is made up of of abundant fiammé which are characterised by their brownish colour under the microscope. These reddish fiammé span a compositional range between 66 and 69.5 SiO_2 wt. %, plotting in the same area (e.g. trachyte and trachydacite) with the Black ignimbrite in Figure 3.23. On the other hand, the black fiammé which basically consist of transparent glass under the microscope and which display black, obsidian like lustre on the hand specimen with a typical eutaxitic texture (Photo 2.10) vary between 73% and 74 in SiO_2 and plot close to the field of the White and Grey ignimbrites (rhyolite field). Existence of these patches of rhyolitic glassy material in a trachydacitic matrix may indicate that the trachytic magma was also contaminated by the rhyolitic magma. Since it is apparent that both magmas contaminated each other, they must have been in contact with each other in a magma chamber where the magma mixing between these two magmas was taking place.

Zircon enrichment in the Black ignimbrite and concurrent Zr depletion in underlying White and Grey ignimbrites can be attributed to the accumulation of zircon at the basal (hence more basic) part of a shallow level silicic magma chamber that fed the pyroclastic deposits on the Pasinler plateau. This magma chamber is more likely to have been compositionally and thermally zoned. Alternatively, Zr enrichment in the Black ignimbrite might have been achieved effectively by small degrees of partial melting of a garnet-bearing (relatively deep) source where garnet was involved in partial melting. However, there is no trace element and isotopic evidence for a deeper source on the plateau.

The Black ignimbrite contains accessory zircon microcrystals. This may suggest that Zr enrichment in the Black ignimbrite was not related to the source, in fact, it appears to have been created by the fractional crystallisation process. In the

following paragraphs, the evidence for the presence of a compositionally zoned magma chamber beneath the Pasinler plateau and its temporal evolution will be presented together with the proposed magma chamber model.

The high-Y lavas on the Pasinler plateau are basically composed of four volcanic units (Figures 2.11, 13 and 16 and also 3.21). From base to the top these are:

- the Ardıçlıdağ rhyolite (crystal rich lavas: plagioclase, anorthoclase) (top)
- the Kargapazarı basalt
- the Black ignimbrite
- Aphyric rhyolitic pyroclastic fall and flow (ignimbrite) deposits (base)

Lavas of the low-Y series are excluded from the volcano-stratigraphic column presented above, because they evolved in deeper magma chambers located close to the lower crust (Section 4.2.2.1). Since the contacts of the Black ignimbrite with underlying aphyric rhyolitic products and overlying basaltic andesite are planar without any sign of erosion and weathering all over the Pasinler plateau, these four units seem to have erupted one after another without considerable time interval. Hence this may represent different zones of a compositionally zoned shallow-level silicic magma chamber.

The magma chamber model proposed for the formation of these units on the Pasinler plateau is presented in Figure 3.24 in five parts (a to e) each of which corresponds to a particular stage. In the following paragraphs, these stages will be described.

Figure 3.24-a shows the initial stage of the shallow level magma chamber. In this stage, fractional crystallisation (FC) of basaltic magma should have produced relatively silica-rich derivative liquids (e.g. basaltic andesite and andesite) giving rise to strombolian type of eruptions on the plateau. These eruptions formed small scoria and spatter cones which were later buried by the rhyolitic pyroclastic fall and flow deposits. Some of them were observed and mapped in this study (e.g. scoria cone in the Harabedere gorge). According to Al-in amphibole geobarometry of Schmidt (1992), the depth of the chamber was around 13-15±2 km (see Figure 4.26, p.209).

Figure 3.24-b illustrates the stage in which a lateral compositional and thermal zonation was established in the magma chamber. From base to the top these zones are:

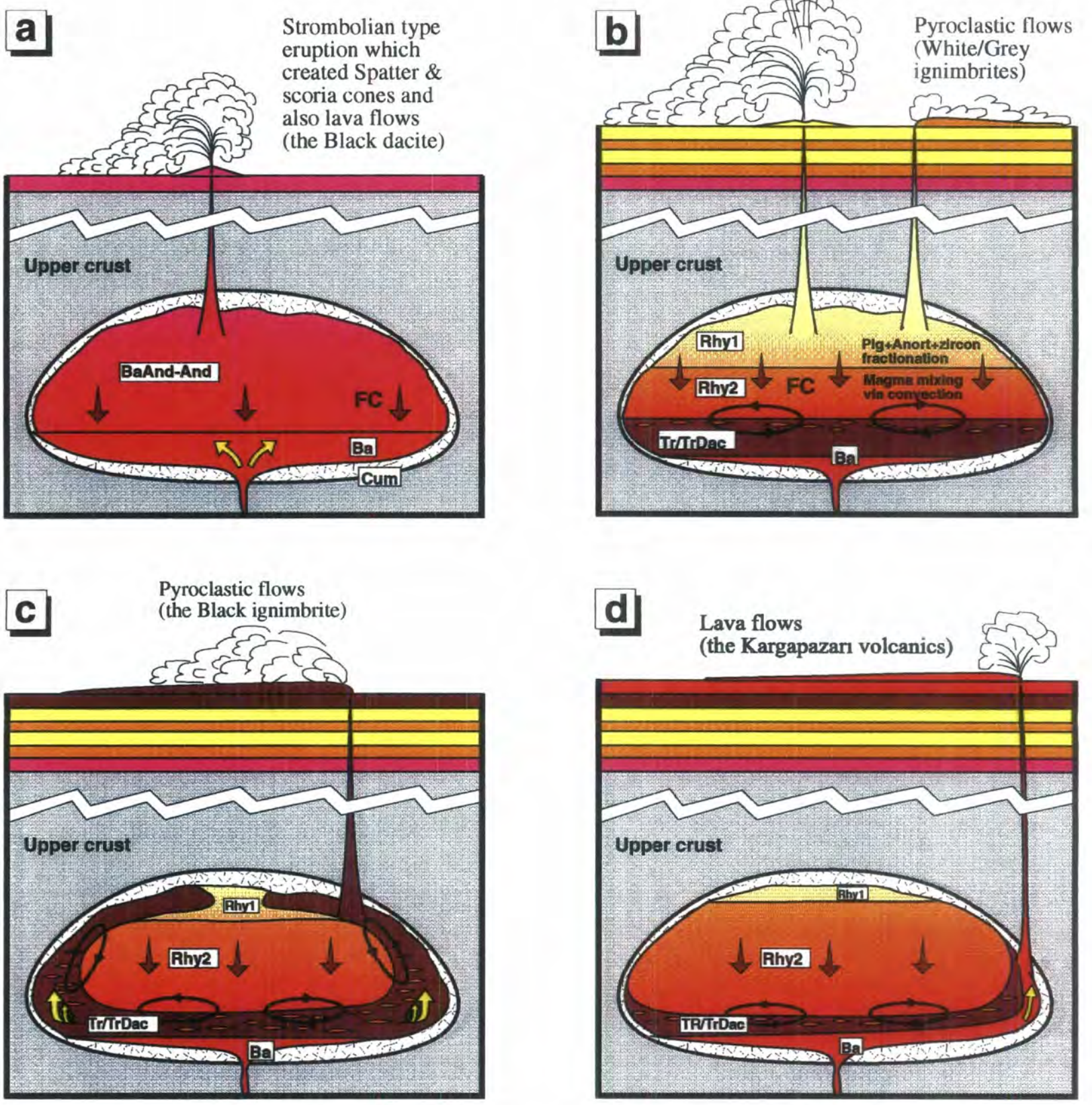

Figure: 3.24. Proposed compositionally and thermally zoned magma chamber model for the Pasinler Plateau, the Erzurum-Kars Plateau, NE Turkey.

a) parental basalt to basaltic-andesite at the base (the Kargapazarı volcanics)

b) trachyte to trachy-dacite with abundant feldspar crystals (the Black ignimbrite)

c) crystal-rich rhyolite (the Ardıçlıdağ rhyolite)

d) aphyric rhyolite at the top (the Grey and White ignimbrites)

In the silica-rich upper parts of the chamber, fractional crystallisation of anorthoclase, sanidine and sodic plagioclase (as indicated by the behaviour of Ba and Sr in Figure 3.25) together with accessory zircon (Figure 3.22) took place. According to Seck's (1971) graphical two-feldspar thermometer, the crystallisation temperature of sanidine in the chamber was around 550-600ºC while that of anorthoclase was around 650-750ºC (Figure 4.30, p. 218). Feldspars and zircon, crystallised from the acidic roof zone of the chamber, accumulated at the basal trachytic zone. Sanidine should have been corroded and completely dissolved in the hotter basal trachytic layer while sodic plagioclase was completely or partly corroded producing embayments and sieve texture in the phenocrysts. Zircon precipitation and accumulation seem to have created Zr enrichment in the trachytic basal zone and relative Zr depletion in the rhyolitic upper zone seen in Figure 3.22. In this stage, a magma mixing event, induced possibly by convection, took place between the trachytic layer and crystal-rich rhyolite producing obsidian-like crystal-rich fiammé which have the same composition with the overlying rhyolitic layer. Fractional crystallisation caused excessive volatile enrichment towards the roof zone of the magma chamber, giving rise to explosive eruptions on the plateau which produced aphyric pyroclastic falls and ignimbrites reaching up to 300-400 m in thickness.

Figure 3.24-c shows the stage in which the rate of precipitation and accumulation became higher in the crystal-rich part of the rhyolitic magma than in the trachytic magma. Eventually, rhyolite became more crystal-rich, viscose and denser than the underlying trachyte. As a result of this, magma chamber stratification was possibly partly or completely destroyed by convective overturn. This destruction was also enhanced by degassing of more basic layers at the base due to cooling of silica-poor magma against overlying rhyolite. Trachytic layer appears to have moved upwards following the walls of magma chamber and erupted on the plateau producing the Black ignimbrite. Geometry of the magma chamber zonation presumably turned into concentric with a central crystal-rich rhyolite core mantled by trachyte. Denser basalt resided at the bottom of the chamber. Trachydacitic magma erupted until its extractable volume was exhausted abruptly.

Figure 3.24-d illustrates the stage when Basaltic to basaltic-andesitic magma which represents probably the lowermost part of the chamber (the Kargapazarı volcanics) erupted perhaps due to excessive degassing of basalt which considerably decreased its density. On the other hand, there is no strong evidence if this basic to intermediate lava sequence was derived from the same or another magma chamber resided deeper in the crust.

In the final stage (Figure 3.24-e), magma chamber zonation was probably reorganised. Rhyolite continued to precipitate feldspar. In the west around Büyükdere gorge, aphyric products were erupted forming the Upper tuff unit while in the east around Harabedere valley, crystal-rich parts of the rhyolite namely the Ardıçlıdağ rhyolite) erupted forming domes on the plateau.

In order to evaluate the extent to which fractional crystallisation of feldspars controls trace element distribution, trace elements, including Sr and Ba, have been plotted against Rb on log-log variation diagrams on which theoretical Rayleigh fractionation vectors have been modelled for the removal of individual minerals or likely mineral assemblages for basic (B), intermediate (I) and acid (A) compositions (Figure 3.25). Rb is chosen as the fractionation index since it has a good positive correlation with increasing SiO_2 for both high- and low-Y series and also it does not substitute in any of the major crystallising phases except biotite. The compiled distribution coefficients given in Table 4.12 have been used for constructing vectors. Theoretical vectors have been calculated using the equation given in Eq. 3.1 for 50% crystallisation, except for biotite calculated for 25% crystallisation. On these diagrams, these clusters of vectors can be moved to any presumed parental compositions.

Sr forms two distinctly parallel trends coinciding with the low- and the high-Y series. Lavas of the low-Y series have consistently higher concentrations of Sr (Figure 3.18-b and 3.25). This may be interpreted as a reflection of differences in the fractional crystallisation histories of these two magmas. Sr decreases steadily with increasing SiO_2 content in both the high- and the low-Y series, however falls rapidly in the acidic lava and pyroclastics of the high-Y series after 67% SiO_2 as a result of plagioclase and alkali feldspar crystallisation. As can be seen in Figure 3.25-a, the trend formed by the data points of acid members of the high-Y series fits well to the vector modelled for plagioclase at acid compositions.

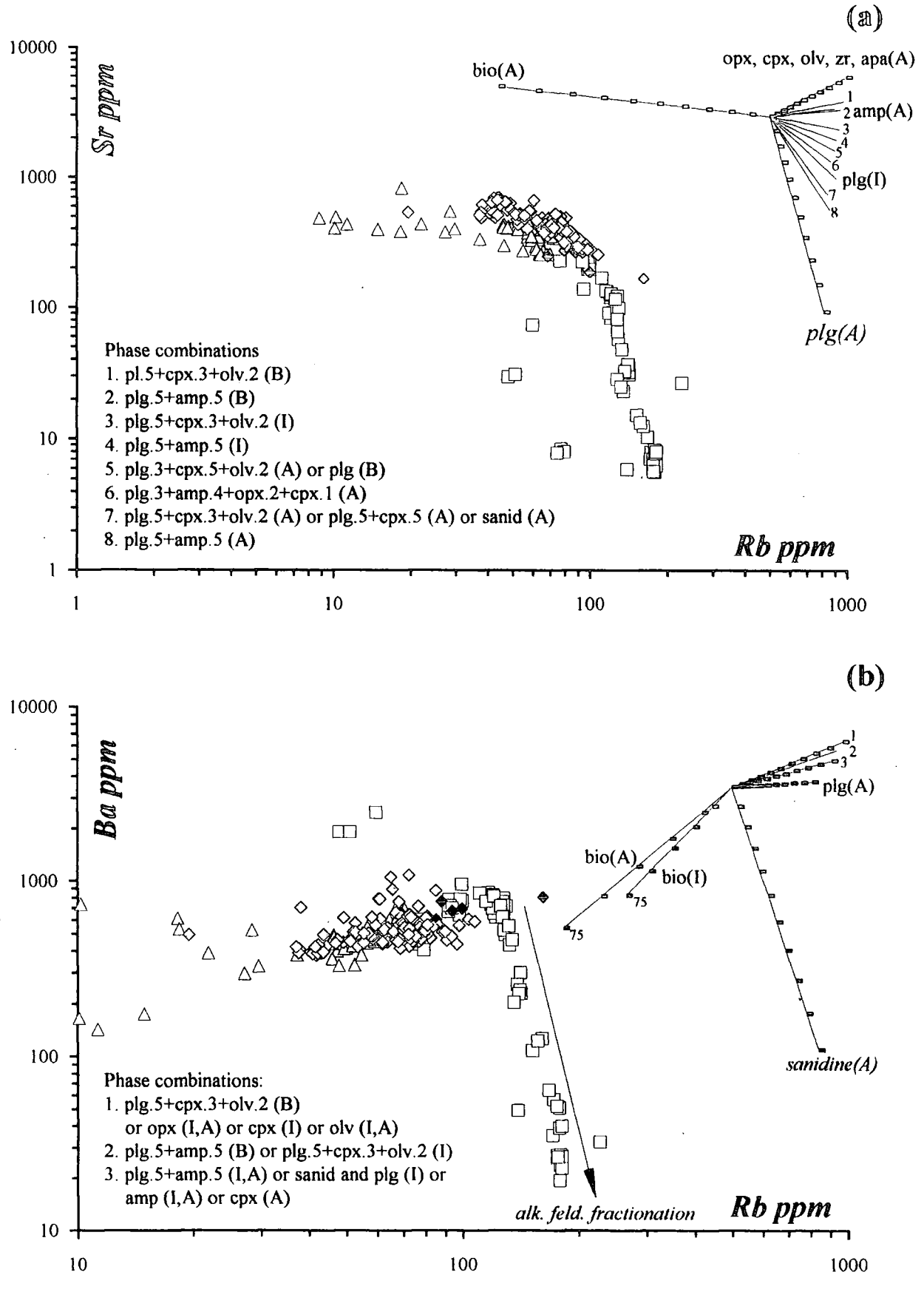

Figure: 3.25. Log-log plots of Y, Sr, Zr and Nb against Rb showing the contrast in trace element behaviour of the volcanic units of the high- and low-Y series.

Ba increases steadily with increasing acidity of the melt in both Y series, but decreases sharply at 65% SiO_2 in the acid members of the high-Y series in response to incoming alkali-feldspar fractionation (Figures 3.18-f and 3.25-b). Ba is also partitioned strongly into biotite ($K_d^{(bio-liq)}$ = 6 at intermediate and 7.5 at acid compositions). However, if the behaviour of Nb is taken into account, it can be argued that biotite fractionation is not a major factor in causing this strong depletion.

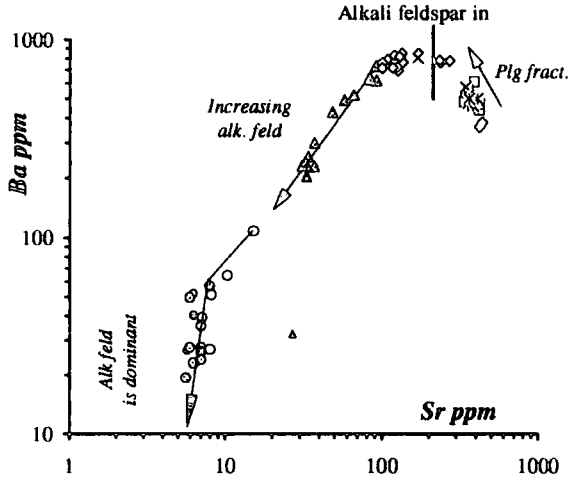

Figure: 3.26. Ba against Sr log-log graph displaying the relative importance of plagioclase and alkali-feldspar fractionation in the volcanic units of Pasinler area. Key symbols are the same as Fig. 3.22.

Figure 3.26 illustrates the relative importance of plagioclase and alkali feldspar fractionation in the volcanics of the Pasinler area. In the Kargapazarı volcanics, the Black andesite/dacite and the Kızılveren amphibole dacite/andesite, Sr decreases moderately with increasing Ba concentration implying that plagioclase is the only fractionating only fractionating feldspar. This trend becomes flat around the Black ignimbrite, an indication of incoming alkali feldspar, and decreases rapidly in the Ardıçlıdağ rhyolite which responds to increasing alkali feldspar fractionation. It forms a sub vertical trend in the Grey and White ignimbrites indicating that alkali feldspar is the dominant phase in the fractionation history of these units.

Ni and Cr fall rapidly in the basic to intermediate lavas of the high-Y series indicating that olivine was one of the most important fractionating mafic phase during the early stages of the fractionation of these series (Figure 3.19-b and d). In contrast, data points of the low-Y series are widely scattered and are not depleted in these elements as much as in the high-Y series. The scatter (between 1 to 10 ppm) in the data points of the acid members of the high-Y series arises from the analytical error in the detection of these elements by XRF.

V values decrease slightly with fractionation in the low-Y series and also in the basic to intermediate members of the high-Y series (Figure 3.19-c). In contrast, they fall rapidly after around 63% SiO_2 in the intermediate to acidic lavas of the high-Y and also in the transitional series. This may indicate the greater importance of magnetite fractionation in these series. V may also be strongly partitioned into amphibole ($K_d^{(amp-liq)}$ =32 and magnetite $K_d^{(mag-liq)}$ =30 at intermediate compositions).

However, the behaviour of Y and other REE invalidates amphibole fractionation in these series.

Co behaves in a similar way to V, forming a relatively flat trend in the low-Y and basic units of the high-Y series and decreasing in the acid units of the high-Y series after 63% SiO_2 in response to magnetite and perhaps orthopyroxene crystallisation (Figure 3.19-e).

3.3. Rare earth element patterns

Among trace elements the rare earth elements (REE) which are represented by 14 elements with atomic numbers 57 to 71, from lanthanum (La) to lutetium (Lu), have a special significance because they form a group whose members have similar physico-chemical properties. The REEs exhibit small regular differences in their mass and ionic radius as a result of a phenomenon called 'the lanthanide contraction' which is controlled by the increasing positive nuclear charge with increasing atomic number. This results in a regular decrease in ionic radii from La to Lu controlling the progressively change in chemical behaviour of REEs. The REE pattern of an igneous rock is controlled by the REE chemistry of its source and crystal-melt equilibria which have taken place during its evolution (Rollinson, 1993). Therefore, REEs can be used as a powerful tool to solve specific problems of petrology.

The relative abundance of the REEs changes regularly under the influence of a number of petrologic processes, e.g. partial melting and fractional crystallisation, depending upon their K_d values. Rock-forming minerals preferentially substitute or exclude some of these elements in a regular fashion, due to the fact that the REEs have progressively changing chemical properties created by the progressive change in their ionic radius. Among these minerals, garnet, amphibole and pyroxenes take more of the HREEs which have low ionic radii. Garnet has quite low K_d values for the LREEs and increasingly higher K_ds for the HREEs. Therefore, if garnet is a crystallising phase, it creates a strong depletion of heavy REEs and enrichment in LREEs in the magma. Feldspars have a minor effect on the REE pattern of the melt since they have low K_ds for all REEs except for Eu. In general, feldspars and apatite take the LREEs, which have high ionic radii. Ortho- and clinopyroxene in general have K_ds that are lower than 1 for REEs. For pyroxenes, the K_ds of the LREEs are slightly lower than those of the M- and HREEs. Therefore fractional crystallisation of pyroxenes causes a LREE enrichment in the melt in most cases. Partition coefficients of REEs for amphibole are highest in the MREEs. They are strongly dependent upon the composition of the melt, coefficients reaching 10 for acidic compositions (see Table 4.12). Therefore, fractional crystallisation of amphibole results in relative depletion in MREEs (especially Ho, Er, Tm and Y) and, to an extend, in HREEs with

respect to LREEs at intermediate to acidic compositions. Because, K_d values of REE for biotite are generally lower than 1, its presence has a little effect on REE patterns. K_d values for olivine are all less than 0.1. Consequently, fractionation of olivine causes all REEs to enrich in the successive melts. Another point which should be taken into account is that the effect of the crystallisation of one of these minerals on REE patterns increases with increasing SiO_2 since K_d values of elements are strongly dependent upon the SiO_2 content of the melt (Section 4.3.1). To sum up, the observed REE distributions can be used to deduce which minerals have been involved in partial melting or fractional crystallisation processes as long as we know the degree to which REEs are held by a particular mineral (i.e. the partition coefficients for these minerals).

In this study, the REE data obtained from the ICP-MS (Inductively Coupled Plasma-Mass Spectrometry) analysis of 34 samples (Table 3.3) have first been normalised to the chondrite composition proposed by Sun and McDonough (1989) to eliminate the Oddo-Harkins effect[1]. The data are then plotted in Figure 3.27 (a-i) in eight parts, each of which coincides with one of the stratigraphic levels of the high- and low-Y series. Samples are plotted in accordance with the increasing SiO_2 content of the rock samples as presented on the legend of each spidergram. LREE/MREE and MREE/HREE ratios have been calculated using the normalised ratios of $(La/Eu^*)_N$ and $(Eu^*/Yb)_N$ respectively and plotted in Figure 3.27-j and -k. Eu* represents the extrapolated Eu value calculated using the normalised values of Sm, Gd and Eu as presented in Equation 3.2. Remarkably, lavas of the high-Y series are in general

$$\frac{r_{Eu}-r_{Gd}}{C^N_{Eu}-C^N_{Gd}}=\frac{r_{Sm}-r_{Gd}}{C^N_{Sm}-C^N_{Gd}}$$

$$C^N_{Eu}=\frac{(r_{Eu}-r_{Gd})(C^N_{Sm}-C^N_{Gd})}{r_{Sm}-r_{Gd}}+C^N_{Gd}$$

$$r_{Eu^{3+}}=0.947 \quad r_{Eu^{2+}}=1.17 \quad r_{Sm^{3+}}=0.958 \quad r_{Gd^{3+}}=0.938$$

Eq. 3.2

r_{Eu}, r_{Gd}, r_{Sm}: ionic radii of Eu, Gd and Sm in Å as given above,

$C^N_{Eu}, C^N_{Gd}, C^N_{Sm}$: the chondrite normalised values of Eu, Gd and Sm.

[1] Oddo-Harkins effect: elements with even atomic numbers always have higher concentrations compared to those with odd atomic numbers. This phenomenon causes zig-zag form on the REE pattern if the REEs are not normalised to their abundances in carbonaceous chondritic meteorites that are believed to be representative of primitive solar system material which may have been parental to the Earth (Coryell, et al., 1963 and Nakamura, 1974). On the other hand, it has recently been apparent that chondritic meteorites are quite variable in composition and chondrites with the standard chondritic REE abundances are quite rare (Boynton, 1984).

enriched variably in LREE while the low-Y series exhibit a distinctive MREE and HREE depletion relative to the high-Y series. In the following paragraphs, differences in REE patterns of main stratigraphic units of the high- and low-Y series will be presented with special reference to their petrologic significance.

3.3.1. REE patterns of the high-Y series

The high-Y basic lavas of the olivine-bearing plateau lavas in the Horasan area (i.e. the Horasan plateau unit), which comprises one of the most basic rock suites on the plateau, has an almost flat REE pattern with slight LREE enrichment (Figure 3.27-c). They have a LREE/MREE $((La/Eu^*)_N)$ ratio of around 2-3 and MREE/HREE $((Eu^*/Yb)_N)$ ratio of about 1.5-1.7. In this unit, MREE and HREEs increase slightly with increasing SiO_2 without any change in pattern shape. This is to be expected in volcanic units which are dominated by the crystallisation of anhydrous phenocryst phases (i.e. olivine, pyroxenes and plagioclase) as the REEs are in general incompatible with these phases and thus become increasingly concentrated in the more evolved liquids. A line representing the REE pattern of the Horasan plateau unit has been plotted on all graphs as a reference to facilitate a comparison between different lava units. The only other sample to show exactly the same pattern to the Horasan plateau reference line is MK289 (49.1 SiO_2%) which was collected from one of the most basic volcanic units, the Karapınar basalt, at the base of the plateau in the Kargapazarı area (Figure 3.27-f).

Other members of andesitic to basaltic-andesitic (53.7-60.3% SiO_2) lavas of the olivine-bearing plateau lavas (i.e. the Kargapazarı volcanics: MK63 and MK101, the Aladağ andesite: MK159 and the Kars Plateau unit: MK175 and MK162; see Table 3.3) all follow roughly similar patterns to that of the Horasan Plateau unit, but with a distinctly greater LREE enrichment (Figure 3.27-d and e). For these samples, the LREE/MREE ratio ranges between 3 and 5.5, reflecting the LREE enrichment, whereas the MREE/HREE ratio is very close to that of the Horasan plateau unit with ratios of 1.5-2. Samples MK175, MK63 and MK159 have exactly the same MREE and HREE profiles as the Horasan Plateau unit, while MK162 and MK101 display a slight depletion in MREE and HREE (Figure 3.27-e) reflected by a slight increase in $(Eu^*/Yb)_N$ ratio relative to Horasan Plateau unit in Figure 3.27-k. In these units, REEs slightly increase with increasing SiO_2 without any substantial change in the pattern. However, LREEs seem to behave in a more complex way showing an inverse correlation with SiO_2 (MK159 and MK63). The LREE enrichment together with the slight depletion in M- and HREEs may be caused by variable degrees of ortho- and clinopyroxene and/or subordinate amphibole fractionation.

The basal basic to intermediate lavas (Figure 3.27-f and g) also have broadly similar patterns to that of the olivine-bearing plateau lavas showing a slight enrichment in LREEs (Figure 3.27-j and k). This also appears to be caused by pyroxene crystallisation in these volcanic units. Except for MK138 and MK117, their LREE/MREE and MREE/HREE ratios are around 3-5 and 1-2 respectively. The LREE/HREE and MREE/HREE profiles of MK117 (the Black andesite, Pasinler) and MK138 (the Kötek basalt, Horasan) resemble those of MK101 (the Kargapazarı volcanics, Pasinler), and MK162 (the Aladağ andesite) with a slight depletion in M- and HREEs compared to the Horasan plateau reference line.

Alkali-calcic suites of the basal acidic lavas which are represented by two obsidians (MK70 and MK345), a porphyritic rhyolite (MK338) and a dacite (MK174), show much steeper LREE/MREE profiles (almost as high as the amphibole bearing porphyritic lavas of the low-Y series, except for MK174) with respect to the reference line of the Horasan plateau lavas, with $(La/Eu^*)_N$ values varying between 4 and 8 (Figure 3.27-j). This may be interpreted as an indication of pyroxene crystallisation in these volcanic units. These units have the highest total REE content (138-258 ppm) of all the volcanic units on the plateau (Table 3.3). The trend to evolved compositions is the same as that seen in the olivine-bearing plateau lavas (increasing REEs with increasing SiO_2 content of the melt) with the exception of MK338 (the Ardıçlıdağ rhyolite, Pasinler). Except MK174 (66.5 wt.% SiO_2), all samples of this unit show a distinctive negative Eu anomaly, increasing with the acidity of the melt, in response to plagioclase and/or alkali feldspar crystallisation under conditions of low oxygen fugacity (see Sections 4.2.3.1 and also 4.3.1.2). Despite their LREE enrichment and strong negative Eu anomaly, basal acidic lavas of the high-Y series exhibit broadly similar MREE and HREE patterns to the Horasan plateau unit reference line with Eu*/Yb values varying between 1 and 2. When we take all these findings into account, it can be argued that alkali-calcic suits of the basal acidic lavas and pyroclastics are dominated by the crystallisation of anhydrous phenocryst phases i.e. plagioclase, alkali feldspar and pyroxenes, like the other units of the high-Y series.

3.3.2. REE patterns of the low-Y series

Amphibole-bearing porphyritic and aphyric lavas of the low-Y series have similar LREE/MREE profiles to the volcanics of the high-Y series but they show

Sample	Formation	Graph	SiO_2	Y (ppm)	Total LREE	Total MREE	Total HREE	Total REE
A. The low-Y series								
1. AMPHIBOLE-BEARING PORPHYRITIC LAVAS								
MK93	Dumlu amph. dac/and, Mt. Dumlu		63.49	17.3	130.5	12.1	3.1	145.8
MK132	Köroğlu amph. and/dac, Horasan		64.18	15.6	147.1	12.2	2.9	162.2
MK251	Dumlu amph. dac/and, Mt. Dumlu		65.08	13.6	116.6	10.7	2.5	129.8
MK268	Göllersüzü amph. dac/and, Kargapaz	*3.27-a*	65.47	15.7	99.0	11.3	3.1	113.4
MK49	Dumlu amph. dac/and, Mt.Dumlu		66.26	17.8	111.7	12.0	3.4	127.0
MK112	Kızılveren amph. dac/and, Pasinler		66.81	18.3	98.4	12.3	3.6	114.4
MK154	Saçdağ dacite, South of Horasan		66.91	9.0	105.6	8.9	1.5	116.0
2. APHYRIC LAVAS WITHOUT AMPHIBOLE								
MK237	Güngörmez and/dac, Mt. dumlu		56.47	16.8	107.8	12.9	3.7	124.3
MK243	Güngörmez and/dac, Mt. dumlu		57.99	17.5	102.6	12.3	3.3	118.2
MK215	Güngörmez and/dac, Mt. dumlu	*3.27-b*	58.53	16.4	100.0	12.0	3.4	115.3
MK277	Güngörmez and/dac, Kargapazarı		60.58	15.9	101.3	10.9	3.3	115.5
MK265	Köşk pyroxene andesite, Kargapazarı		63.90	16.1	101.9	11.5	2.8	116.2
B. The high-Y series								
1. OLIVINE-BEARING PLATEAU LAYER								
MK139	Horasan plateau unit, N of Horasan		49.67	25.5	62.6	14.7	5.5	82.9
MK135	Horasan plateau unit, N of Horasan	*3.27-c*	50.02	29.5	58.6	17.4	6.3	82.3
MK130	Horasan plateau unit, N of Horasan		54.36	31.8	65.9	18.0	7.1	91.0
MK175	Kars plateau unit, Kağızman		53.66	29.6	126.8	18.2	6.7	151.6
MK63	Kargapazarı volcanics, Kargapazarı	*3.27-d*	54.39	26.8	127.3	19.5	6.6	153.4
MK159	Aladağ andesite, Mt. Aladağ		60.26	32.5	97.4	19.7	7.0	124.1
MK162	Kars plateau unit, Kağızman	*3.27-e*	55.25	23.4	81.3	13.6	4.6	99.5
MK101	Kargapazarı volcanics, Pasinler		57.01	23.1	112.9	14.8	5.0	132.7
2. BASAL BASIC TO INTERMEDIATE LAVAS								
MK144	Kötek basalt, Horasan		48.76	25.0	141.5	19.1	5.0	165.7
MK289	Karapınar basalt,Kargapazarı	*3.27-f*	49.09	25.8	57.2	14.7	6.0	78.0
MK158	Aladağ andesite, Mt. Aladağ		61.74	36.6	134.0	21.1	7.9	163.0
MK138	Kötek basalt, Horasan		53.63	20.5	76.2	12.6	4.2	93.1
MK280	Güngörmez and/dac, Kargapazarı	*3.27-g*	56.14	30.8	100.4	18.4	6.0	124.9
MK281	Güngörmez and/dac, Kargapazarı		56.99	32.8	103.2	19.1	6.4	128.7
MK117	Black andesite, Pasinler		62.14	20.8	76.5	11.6	4.5	92.6
3. BASAL ACIDIC LAVAS AND PYROCLASTICS								
MK338	Ardıçlıdağ rhyolite, Pasinler		71.00	30.0	232.0	20.0	6.6	258.7
MK70	Obsidian in Lower tuff, Pasinler	*3.27-h*	75.87	35.8	175.9	17.0	8.8	201.7
MK345	Obsidian in Lower tuff, Pasinler		75.33	36.3	170.8	16.5	8.4	195.8
MK174	Paslı trachydacite, Kağızman		66.48	33.5	112.3	18.9	6.9	138.1
C. The Middle Miocene and Eocene Volcanics								
MK375	Pasinler (Miocene Tuzluyolları dacite)		70.13	15.8	98.7	10.3	3.4	112.4
MK364	Pasinler (Upper Eocene)	*3.27-i*	53.81	21.9	57.9	12.5	5.0	75.3
MK122	Pasinler (Upper Eocene)		53.61	25.8	92.3	15.8	5.7	113.8

Table: 3.3. Table showing detailed information about names of formations, SiO_2 wt.% and Y contents and total REE abundance of ICP-MS samples. For full dataset see Appendix E.

a distinctive depletion in MREEs and HREEs (Figure 3.27-a and b) which is indicated by an increase in their $(La/Eu^*)_N$ (5 to 8) and $(Eu^*/Yb)_N$ (2 to 4.5) ratios (Figure 3.27-j and -k). Total REE, in general decrease with increasing SiO_2 content in the aphyric lava units without amphibole whereas, in amphibole-bearing

porphyritic lavas, there is no clear relationship between REE profiles and SiO_2 content. Decrease in MREEs and partly HREEs associated with enrichment of LREEs appears to be caused by the strong partitioning of these elements into amphibole, especially in felsic and intermediate liquids. This is evident from the partition coefficient patterns of amphiboles (Figure 4.38, p.236) showing a slightly convex-upward pattern from the light to the heavy REEs. A part of the LREE enrichment may be related to pyroxene fractionation. The contrast between the amphibole-free high-Y series and the amphibole-bearing low-Y series is reflected by the total M- and HREE and also $(La/Yb)_N$ versus SiO_2 diagrams presented in Figure 3.28 and 3.29 respectively. Figure 3.28-b and -c show two distinctive trends coinciding with the low- and high-Y series. Total MREE and HREE of the low-Y series consistently decrease with increasing SiO_2 in contrast to the high-Y series whose total M- and HREEs increase slightly with increasing SiO_2. All these features, together with the geobarometer calculations based on the Al contents of amphiboles, are consistent with crystallisation of an amphibole-bearing hydrous assemblage at 20-28 km depth (see Section 4.2.2.1). Modelling of Rayleigh fractionation vectors in Figures 3.11 and 12 also supports this idea.

3.3.3. Multi-element patterns

Pearce (1983) proposed a spidergram whose elements are normalised to Mid Ocean Ridge Basalt (MORB) to assess the extent of involvement of different components (i.e. metasomatised sub-continental lithosphere, mantle, subduction and crustal contamination components) in magma genesis. He based his spidergrams on two parameters: ionic potential (ionic charge for the element in its normal oxidation state, divided by ionic radius) and the bulk distribution coefficients of elements between garnet lherzolite and the melt. The first one, ionic potential is used as a measure of the mobility of an element in aqueous fluids. Elements with low (<3) and high (>12) ionic potentials are mobile and those with intermediate values are generally immobile. In order to produce a smooth and comparable pattern, he placed mobile elements e.g. Sr, K, Rb and Ba on the left of the diagram and arranged all elements so that the incompatibilities of both the mobile and immobile elements increase from the outside to the centre of the pattern during lherzolite melting (Figure 3.30-c). Pearce (1983) showed that, except for Sr, which is strongly influenced by the fractionation of plagioclase, variations both in degree of partial melting and fractional crystallisation can change the level of the pattern but have a little effect on its shape if unusual conditions are not operational (e.g. very low degrees of partial melting or unusual crystallisation histories such as those that involve abundant amphibole and garnet).

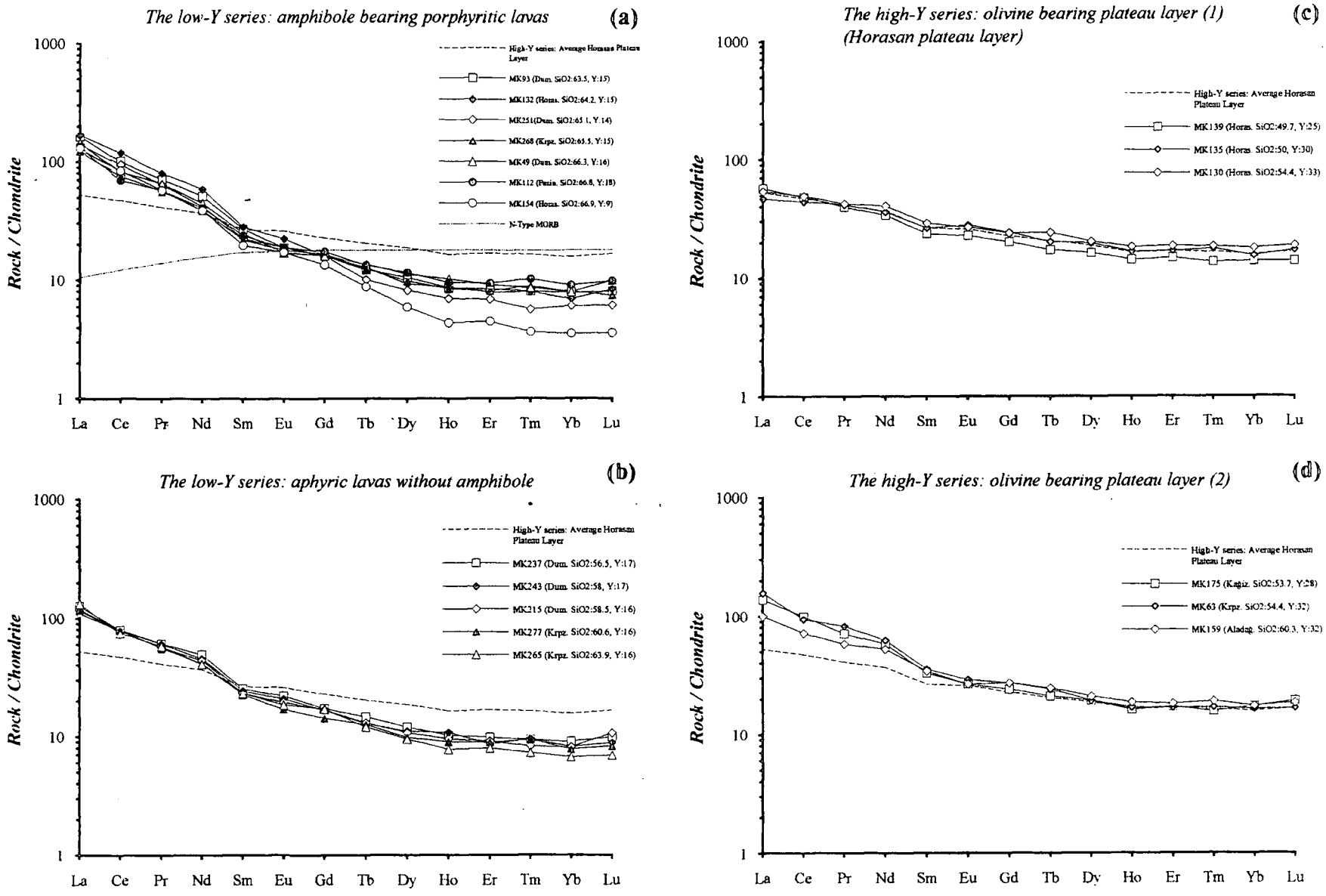

Figure: 3.27. Chondrite normalised REE patterns of the samples from representative units of the high and low-Y series.

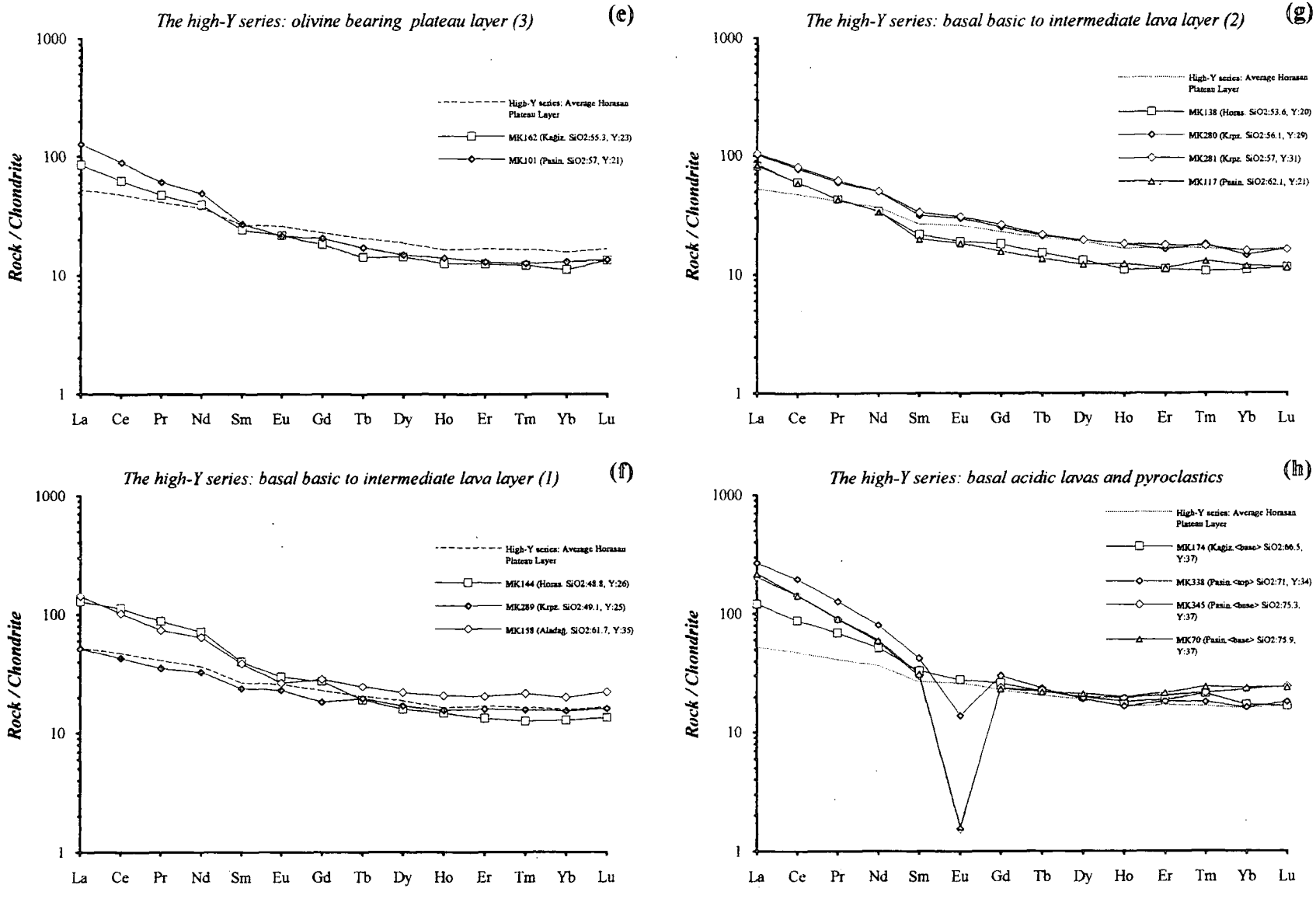

Figure 3.27. (continued).

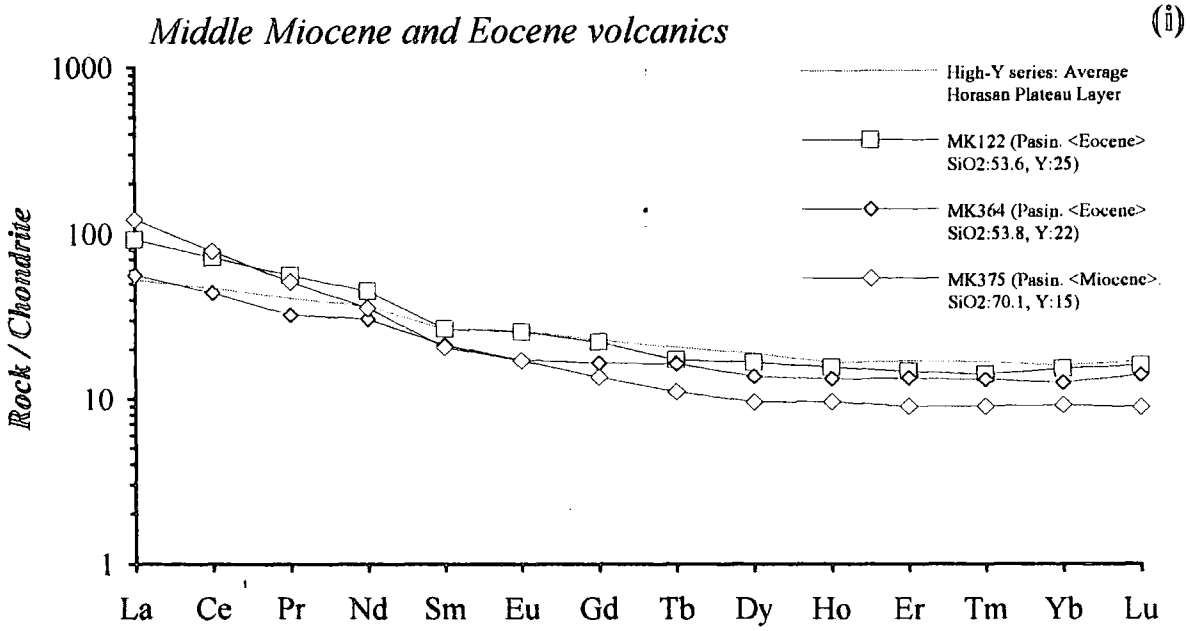

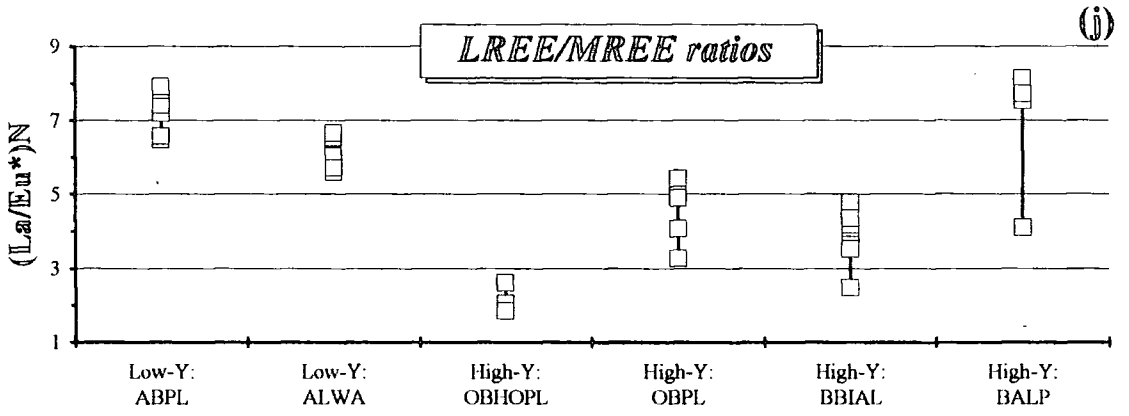

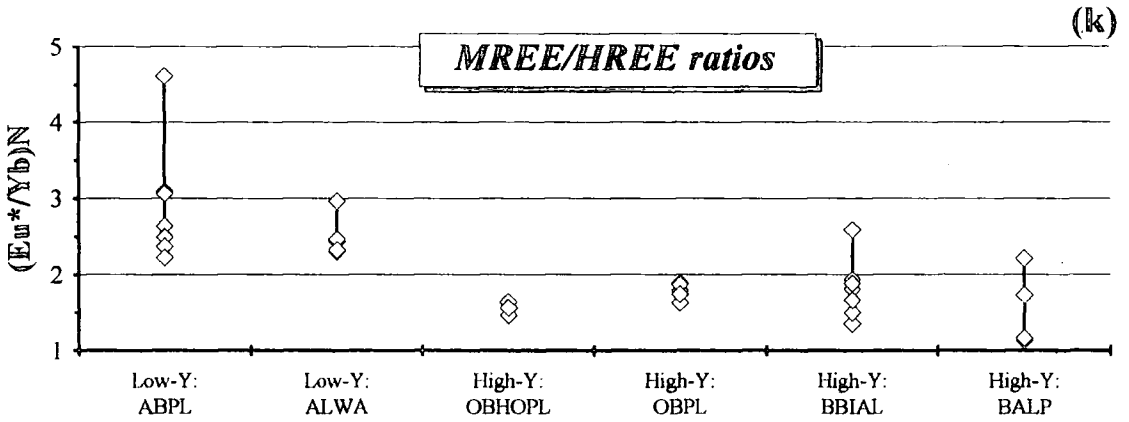

Low-Y: ABPL: amphibole bearing porpyritic lavas

Low-Y: ALWA: aphyric lavas without amphibole

High-Y: OBHOPL: olivine bearing plateau lavas of the Horasan area

High-Y: OBPL: olivine bearing plateau lavas

High-Y: BBIAL: basal intermediate to acidic lava layer

High-Y: BALP: basal acidic lavas and pyroclastics

Figure: 3.27. (Continued).

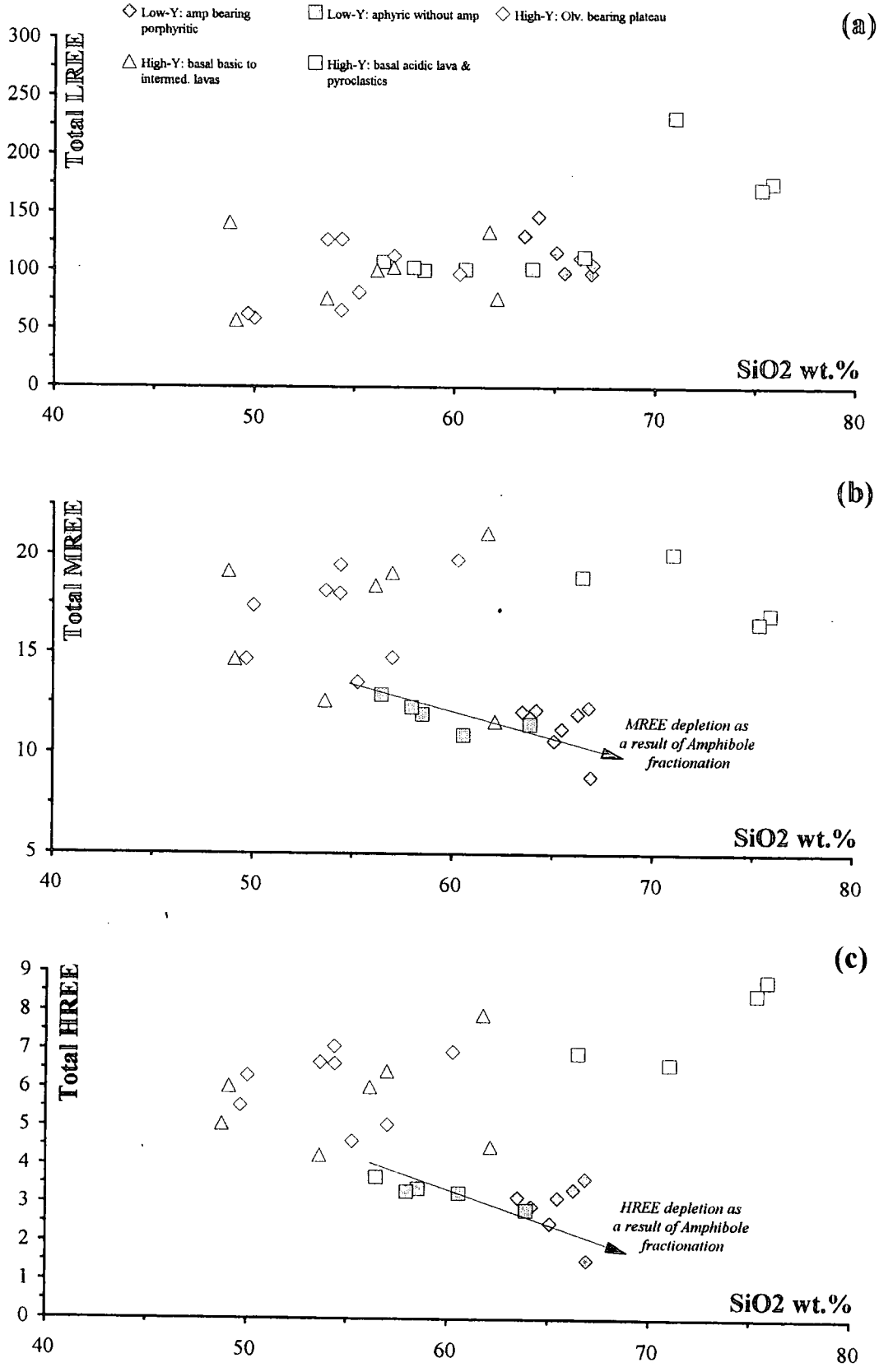

Figure: 3.28. Total LREE (from La to Nd), MREE (from Sm to Ho) and HREE (from Er to Lu) contents plotted against SiO2 wt.% of the samples.

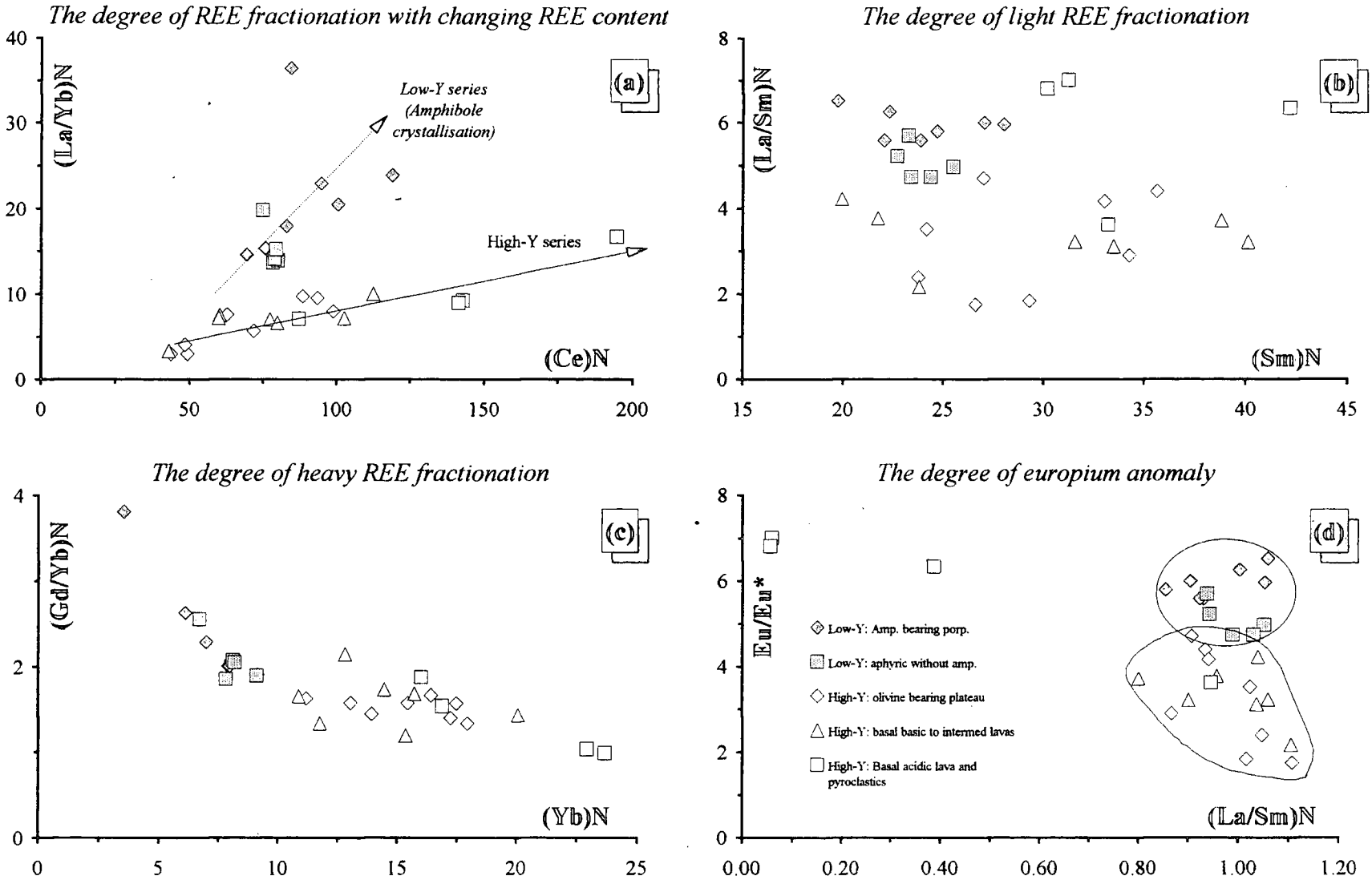

Figure: 3.29. The degree of fractionation of REE patterns for different levels of the Erzurum-Kars Plateau lavas

Therefore, this type of diagram can be conveniently used to contrast source composition and relative involvement of different components across a volcanic province.

Each component that is enriched in a set of different elements from the other components has a unique enrichment pattern on the MORB normalised spidergrams. Basalts derived from mantle enriched by a subduction component (i.e. trace element enriched metasomatised sub-continental lithosphere) display selective enrichment in the large ion lithophile (LIL) elements Sr, K, Rb, Ba, Th and LREEs and to a lesser extend in Sm (Pearce, 1983), because these elements are very mobile (i.e. their ionic potential is either lower than 3 or greater than 12). They are thought to be transported by aqueous fluids from the subduction zone to the overlying zone of mantle melting (Pearce, 1983) and hence enriched in the mantle. On the other hand, plume asthenosphere, or lithosphere enriched by small volume melts from the asthenosphere creates humped patterns with Ba, Th, Ta and Nb the most enriched elements (Pearce et al., 1990). These are the most incompatible elements for small degrees of partial melting of lherzolite. Crustal assimilation shows a similar effect to the subduction component resulting in an enrichment in LIL elements (i.e. the elements which are enriched in the crust), especially in Ba and Th. However, it is far from being diagnostic since the crust has a very heterogeneous composition for those elements from one place to another.

Partial melting or crystallisation of some minerals that have high bulk partition coefficients for the elements that comprise the diagram may significantly effect the shape of the patterns. For example, if amphibole is a crystallising phase, K, Y and the MREEs are significantly depleted while Sm, Ta and Nb are slightly depleted (Pearce et al, 1990). The degree of depletion increases as the magma fractionating amphibole evolves to acidic compositions because partition coefficients (K_d) of MREEs and Y, for amphibole are as much as seven to ten times greater in acidic compositions than they are in basic compositions (see Table 4.12). If garnet is a residual phase in the source, M- to HREEs and also Y are depleted (Pearce et al, 1990) since garnet significantly retains these elements during partial melting. A useful precaution is to consider multi-element patterns only for basalts since K_ds for amphibole are the smallest at basic compositions and also the relative amount of amphibole in the crystallising assemblage increases towards intermediate and acidic compositions. These patterns are most reliable when pyroxene, plagioclase and oxides, those minerals that have considerably lower partition coefficients of the elements under consideration (excluding Sr), are the only residual and crystallising phases (Pearce et al, 1990).

In Figures 3.30, representative volcanic rock samples from different stratigraphic levels of the Erzurum-Kars plateau are normalised to the average mid-ocean basalt (MORB) of Sun and Donough (1989). The plots are presented in nine multi-element diagrams (from 3.35-a to -i), each coinciding with one of the distinct units on the plateau. Among these samples only MK135, MK139, MK144 and MK289 fall into the basalt field of Le Bas et al. (1986) (Table 3.3) while MK63, MK101, MK130, MK175, MK162 and MK237 classify as basaltic andesites. Apart from only one basaltic-andesite sample from the low-Y series (MK237), all of these basic samples belong to the high-Y series. The more evolved samples (i.e. andesites, dacites and rhyolites) that have been plotted onto the diagrams in Figure 3.30 should be interpreted carefully because of the possible effects of fractionation of some minerals such as amphibole.

Notably, all samples show a selective enrichment in LIL elements (Sr, K, Rb, Ba, Th) (25-100×MORB) and the LREEs (La and Ce) (4-10×MORB) and also a slight enrichment in the incompatible high field strength elements (HFS: Ta, Nb, Hf, Zr and Y) (1-3×MORB) relative to MORB. The patterns closely resemble to active continental margin patterns of Pearce (1983) involving a characteristic subduction component. Therefore these patterns suggest that the lavas forming the Erzurum-Kars Plateau were derived from mobile trace element enriched, metasomatised, sub-continental lithosphere although assimilation of crust could also contribute significantly to the formation of this pattern. According to Pearce et al. (1990), this subduction component was inherited from pre-collision subduction events which were operational during Cretaceous and Eocene times as a result of the subduction of the oceanic plate of the Neo-Tethys ocean beneath the region.

Basalts from the Horasan plateau unit (MK130, MK135 and MK139), which exhibit the flattest REE patterns (Figure 3.27-c) with the highest radiogenic isotope ratios, comprise the least LILE and MREE enriched samples (see Figure 3.30-d). The most mobile elements, K, Rb, Ba and Th, are enriched in these samples between 10 to 25 times the abundance of MORB. In contrast, other basalts (MK144 and MK289) from the basal basic lava layer of the high-Y series are enriched in these elements 20 to 100 times (Figure 3.30-d and f). Therefore, the basaltic lavas of the Horasan plateau lavas may be considered to be the most primitive lavas on the plateau, having relatively little contamination from the continental crust. They represent the closest composition to that of the sub-continental lithosphere component with a distinctive subduction signature. They also appear to be free of the effects of fractional crystallisation of amphibole.

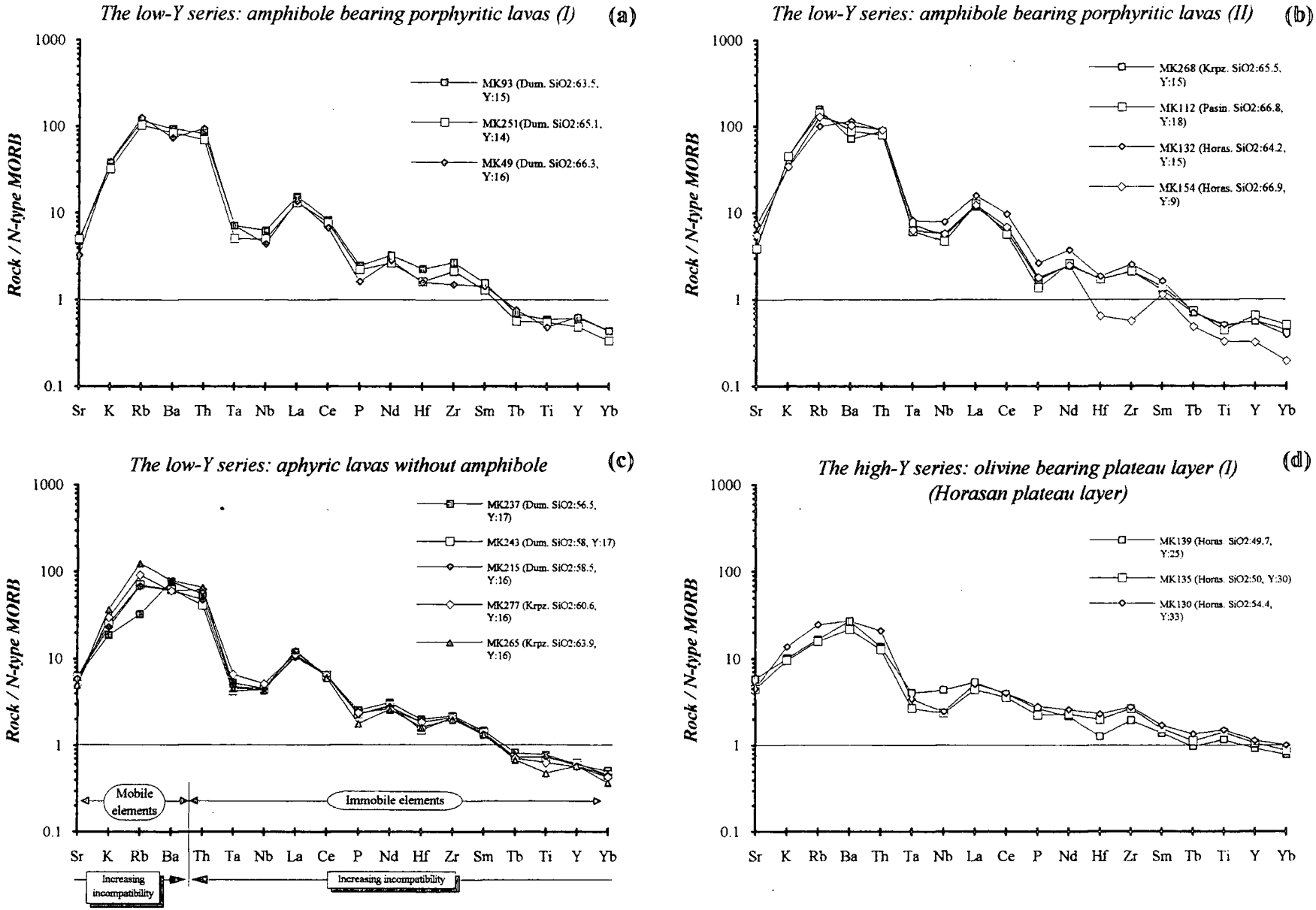

Figure: 3.30. N-type MORB-normalised patterns for the samples from the Erzurum-Kars Plateau showing a consistent subduction signature. MORB normalisation values are taken from Sun and McDonough (1989).

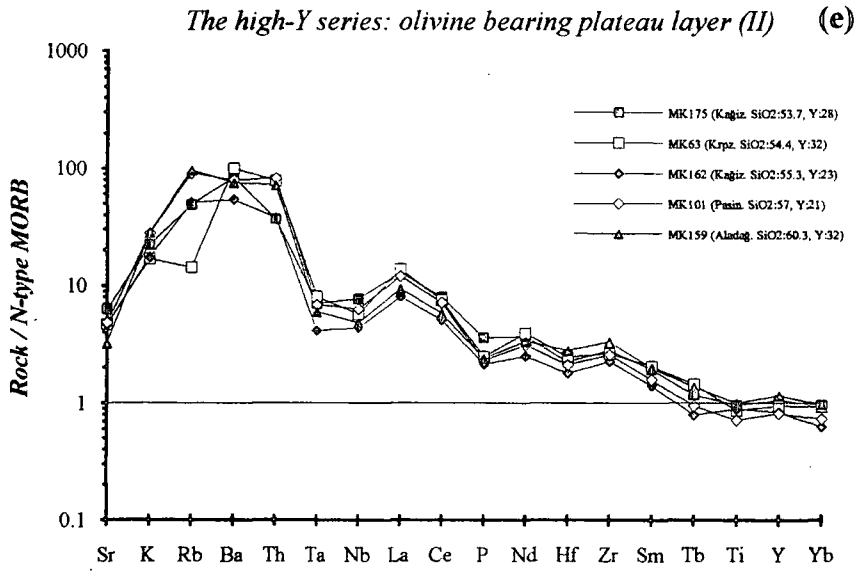

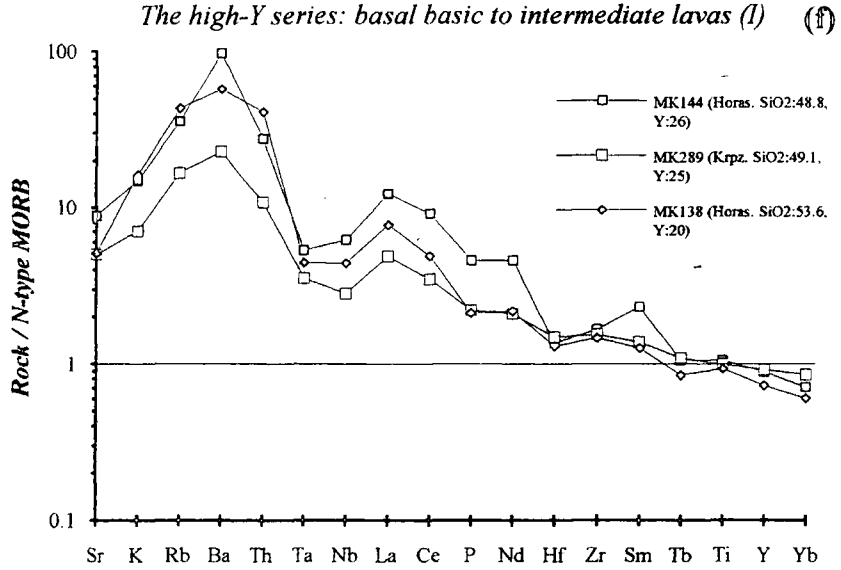

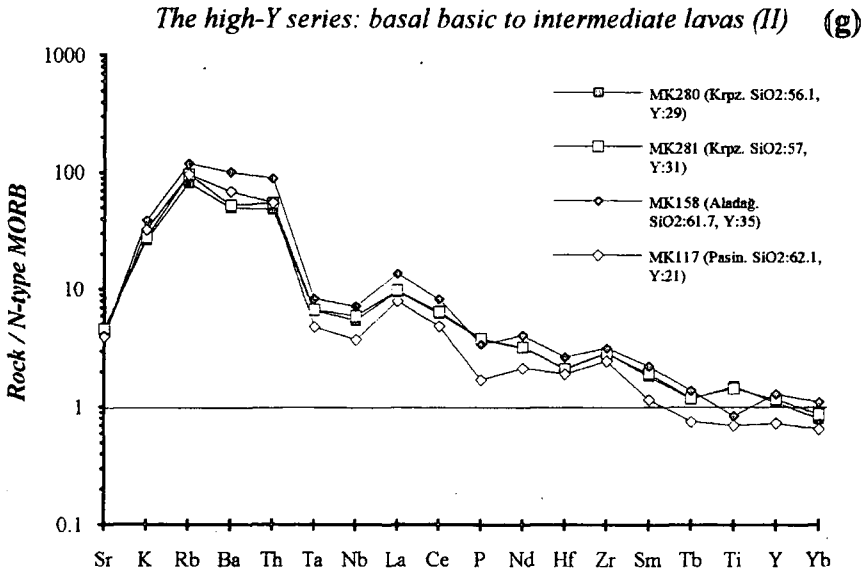

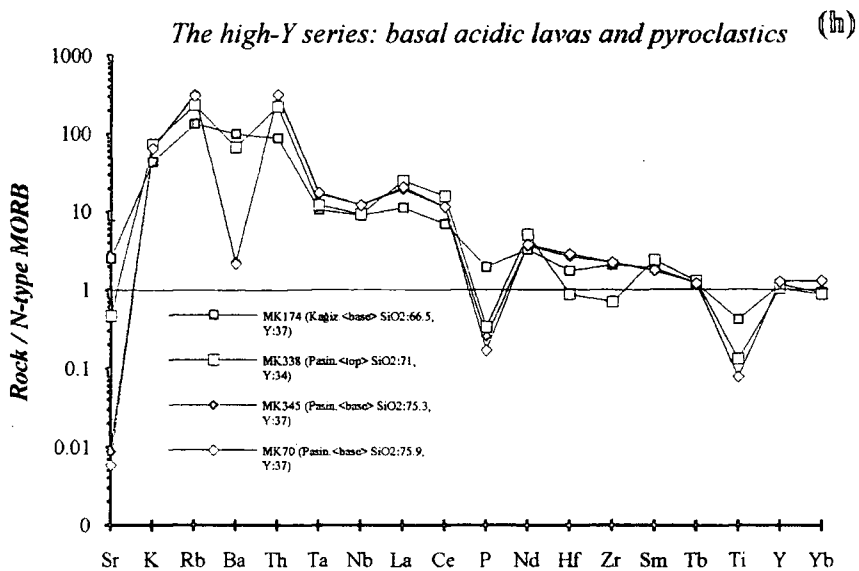

Figure: 3.30. (continued)

The Middle Miocene and Eocene volcanics (i)

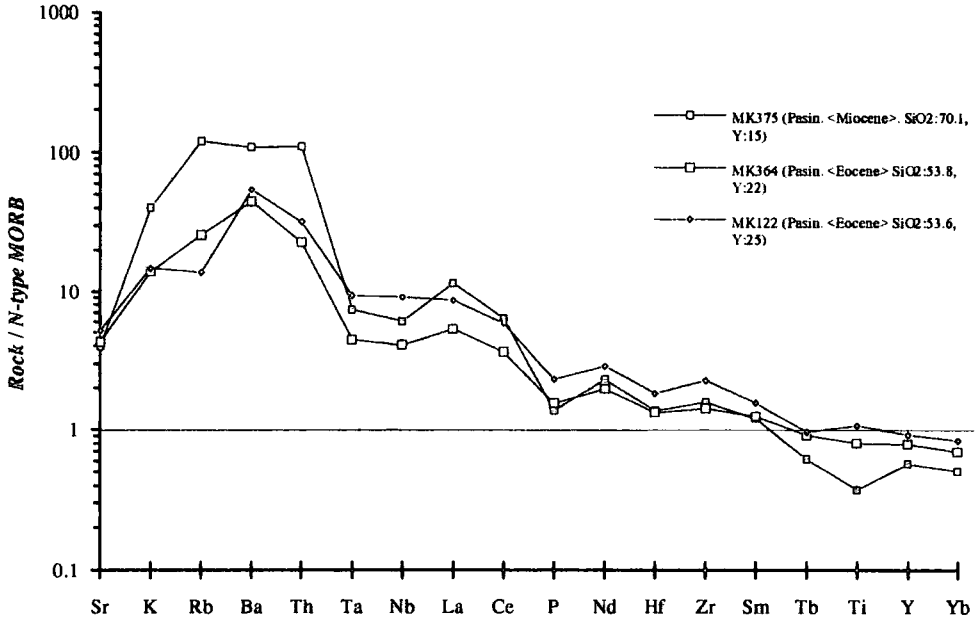

Sample	Area	Formation	Graph	SiO_2	Y (ppm)
BASALTS					
The high-Y series					
1. OLIVINE BEARING PLATEAU LAYER					
MK139	North of Horasan	Horasan plateau unit	*3.24-d*	49.67	25.5
MK135		Horasan plateau unit		50.02	29.5
2. BASAL BASIC TO INTERMEDIATE LAVAS					
MK144	North of Horasan	Kötek basalt, Horasan	*3.24-f*	48.76	25.0
MK289	Mt. Kargapazarı area	Karapınar basalt		49.09	25.8
BASALTIC ANDESITES					
The high-Y series					
1. OLIVINE BEARING PLATEAU LAYER					
MK63	Kargapzarı area	Kargapazarı volcanics	*3.24-e*	54.39	26.8
MK101	North of Pasinler	Kargapazarı volcanics	*3.24-e*	57.01	23.1
MK130	North of Horasan	Horasan plateau unit	*3.24-d*	54.36	31.8
MK175	North of Kağızman	Kars plateau unit	*3.24-e*	53.66	29.6
MK162		Kars plateau unit		55.25	23.4
The low-Y series					
2. APHYRIC LAVAS WITHOUT AMPHIBOLE					
MK237	Mt. Dumlu area	Güngörmez andesite/dacite	*3.24-c*	56.47	16.8

Table: 3.4. Table showing detailed information about names of formations, SiO_2 wt.% and Y contents and total REE abundance of the most basic samples analysed by ICP-MS. For full dataset see Appendix E.

In Figure 3.30-i, multi-element patterns of two basaltic-andesitic samples from the Upper Eocene Kışlaköy volcanics (MK364 and MK122) from the north of Pasinler and a sample from the Early to Middle Miocene Tuzluyolları dacite (MK375) from the south of Pasinler are presented. The Eocene volcanics are representative of the active continental margin volcanism that is responsible for the metasomatism of the sub-continental lithosphere by supplying LIL and LREEs during the Cretaceous-Eocene period. As can be expected, their multi-element patterns are very similar to those of the Erzurum-Kars Plateau volcanics with a distinctive subduction signature.

3.4. Trace element bivariate diagrams

In Figure 3.31, the Th/Yb ratio of the basic to intermediate volcanic rock samples selected from representative levels of the Erzurum-Kars Plateau has been plotted against their Ta/Yb ratio in order to investigate the contribution from subduction, mantle and assimilation components. This diagram, which was proposed by Pearce (1982), is based upon the difference in behaviour between Th and Ta. Yb, which is the least incompatible and mobile REE, is used here as the normalising factor in order to minimise variations created by partial melting and fractional crystallisation provided that olivine, pyroxenes and plagioclases are the dominant crystallising or residual phases. Ta and Th are selected since they are highly incompatible with the possible fractionating minerals in basaltic liquids, a feature that significantly eliminates the effects of fractionation in the distribution of these elements. Unlike Th, other mobile elements i.e. Sr, K, Rb and Ba that characterise the subduction component, are compatible with some of the crystallising phases. Therefore, these elements cannot be conveniently used for this type of diagrams. The Th/Ta ratio is almost constant in MORB source. Therefore, basalts derived from the convecting upper mantle, plume asthenosphere or lithosphere enriched by low-degree melts from the convecting upper mantle lie on the diagonal trend named the mantle metasomatism trend (Pearce et al., 1990). The reason is that both Th and Ta behave in a similar fashion under these conditions since both are incompatible elements with similar low K_ds. Source heterogeneity in the mantle affects both Th and Ta equally resulting in an alignment along the diagonal trend. In contrast to the MORB source, the greater mobility of Th in aqueous fluids created by the subduction component results in an increase in Th relative to Ta. This results in a parallel trend to that for mantle metasomatism but shifted towards the Th/Yb axis on the diagram. Assimilation of crust in general creates almost the same effect, although assimilation of granulite facies crust, which has low Th concentrations, can cause a shift in the opposite direction (Pearce et al., 1990). Crystallisation of amphibole decreases Ta/Yb

slightly more than Th/Yb because the K_d value of Ta for amphibole in basic compositions is 0.25 which is five times higher than that of Th (0.05) (see Table 4.12).

Figure 3.31 shows that all lavas of the Erzurum-Kars Plateau display a consistent displacement from the mantle metasomatism trend towards higher Th/Yb values forming a sub-parallel trend to the mantle array. This can be explained if these

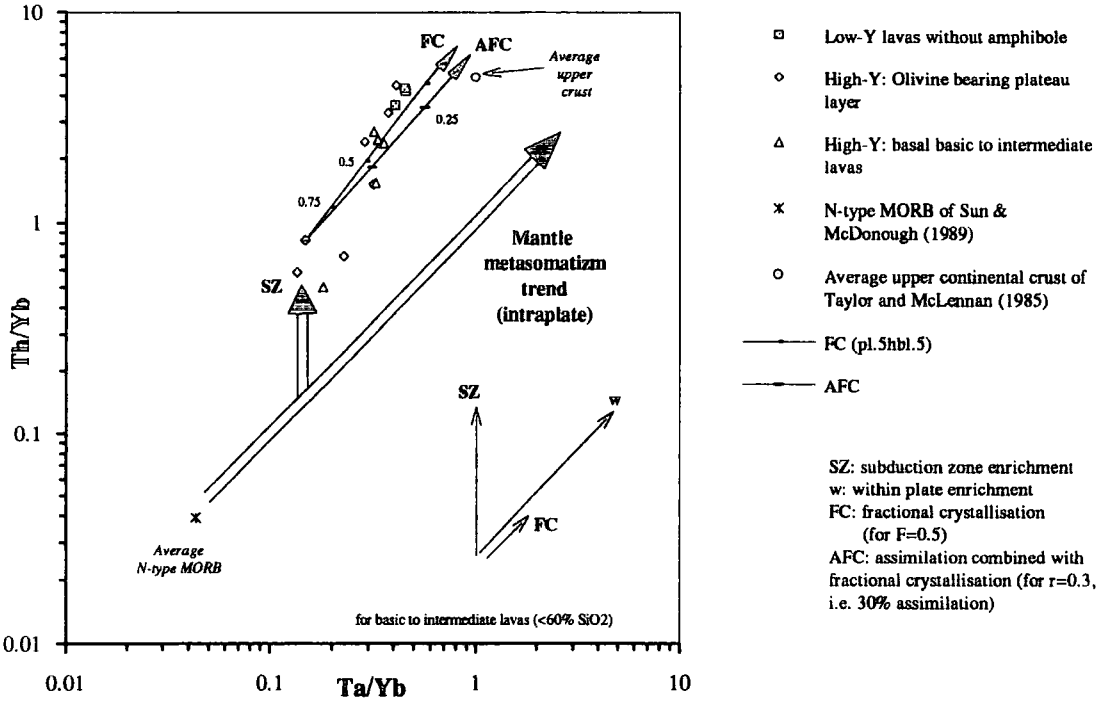

Figure: 3.31. Th/Yb versus Ta/Yb diagram (after Pearce, 1983) for basaltic to intermediate lavas (< 60% SiO_2) from the Erzurum-Kars Plateau.

lavas were derived from lithospheric-mantle that had been previously enriched by a subduction component. The model is in good agreement with Pearce et al.'s (1990) interpretation for the eastern part of the plateau. This enrichment is represented on the diagram by the vertical arrow labelled SZ located between the mantle array and the subduction component enriched trend. Notably, the basic rocks of the Horasan Plateau unit and basal basic to intermediate lavas of the high-Y series have the lowest ratios of Th/Yb and Ta/Yb. These ratios increase with increasing acidity of the melt. In order to show the relative affects of different components and processes, both AFC and FC vectors have been modelled and plotted on Figure 3.31. Both vectors are modelled for the fractionation of an amphibole (50%) plagioclase (50%) assemblage in an intermediate magma because fractional crystallisation of amphibole is not only the dominant process in the whole evolution of the low-Y series but also in the early stages of the high-Y series on the Erzurum-Kars Plateau as shown in the earlier

sections. The AFC vector is calculated for 30% assimilation of the continental upper crust (r=0.3). This ratio agrees well with the results of oxygen isotope modelling which suggest an assimilation rate of around 30-35% (see Section 5.2.3, Figures 5.11 to 5.17, pp.291-299). The upper crustal composition is taken from Taylor and McClennan (1985). One or both of these two processes (FC and AFC) may be responsible for the formation of this trend.

Chapter 4
MINERAL GEOCHEMISTRY

Introduction

In this chapter geochemical analyses of plagioclase, ortho- and clinopyroxenes, olivine and amphibole in samples from the different stratigraphic levels of the Erzurum-Kars Plateau will be presented in order to assess variations in their compositions in terms of conditions of crystallisation. Analytical data have been obtained using three different techniques: electron micro-probe (Durham), ICP-MS (Inductively Coupled Plasma Mass Spectrometry) (Durham) and multicollector mass spectrometer (NERC, Nottingham). Details of each analytical technique, sample preparation, accuracy and precision of the data together with the full geochemical dataset are presented in Appendix F.

The chapter is subdivided into three main sections:

4.1. Classification of minerals: this part utilises the calculation of mole fractions of end-member minerals for each rock forming mineral using results of electron probe analyses and subsequent classification according to the conventions established by the International Mineralogical Association (IMA)

4.2. Geothermo-barometer calculations: in this section, crystallisation temperature and pressure calculations of different minerals and also mineral assemblages are presented based on their major and trace element compositions and isotopic ratios. These calculations can provide important information about the physio-chemical conditions (P/T) of magma processes.

4.3. Calculation of distribution (or partition) coefficients of the elements: this section focuses on the calculation of the distribution of trace, rare earth, and some major elements between different minerals and magma liquid using electron probe and ICP-MS data. It also involves the results of an extensive compilation of partition coefficients proposed by several researchers.

4.1. Classification of Minerals

4.1.1. Distribution of the composition of plagioclases

A total of 355 point analyses were performed on a sum of 73 representative samples selected from the key levels of five sub-areas (i.e. Mt. Dumlu, Mt. Kargapazarı, Pasinler, Horasan and Kağızman) using a Geoscan electron microprobe at the University of Durham. In each sample, mega- and phenocrysts, microphenocrysts, and microlites were analysed to reveal the compositional differences between different crystallising phases. Phenocrysts which show particular crystal textures such as zoning, resorption or magmatic corrosion were emphasised in selecting samples for analyses. Analyses of at least two points, one near the rim the other in the centre, were conducted on zoned phenocrysts. The mole fractions of the three feldspar end-members i.e. albite, anorthite and orthoclase were calculated using the Na, Ca and K contents of plagioclases (in atoms per formula unit). Then the data were plotted on albite-anorthite-orthoclase ternary classification diagrams and presented in five figures each of which coincides with one of the five sub-areas mentioned above (Figure 4.1-4.5). Each figure is made up of several diagrams which are arranged to reflect the volcano-stratigraphic position of formations they contain. These are presented from base to top. At the top of each diagram, a frequency distribution graph of the data is also presented.

Mt. Dumlu area (Figure 4.1): in this area, there are basically two units: the Güngörmez andesite/dacite and the Dumlu amphibole dacite/andesite. The Güngörmez andesite/dacite is displayed in three diagrams coinciding with the different stratigraphic levels of this unit (i.e. lowermost, basal part and upper lens). There are only four analyses available from the base of the unit; these fall into the labradorite and andesine fields. Plagioclases of the basal part of the volcanic sequence are characterised by almost the same composition as the lowermost part, with only one exception plotting in the oligoclase field. The distribution of plagioclase compositions at this level is continuous as shown by the frequency distribution plot which displays a smooth shape between An_{30} and An_{60}. The upper lens shows almost the same compositional range as the lowermost and basal lenses however, the data tend to plot into two separate compositional areas i.e. andesine and labradorite. Compared to the Güngörmez andesite/dacite, the amphibole-bearing lavas of the Dumlu dacite/andesite cover a narrower compositional range between andesine and labradorite (An_{35-65}). They too plot into two discrete areas which are roughly separated by the border between the andesite and labradorite fields. In fact, over 60% of plagioclases in this unit have An_{50-60}. Two analyses fall into the andesine field and are shown by cross shaped symbols belong to Arzutu amphibole dacite/andesite.

Mt. Kargapazarı (Figure 4.2): apart from one sample falling into the oligoclase and another into the bytownite fields, the plagioclases of the Güngörmez andesite/dacite vary in composition between labradorite and andesine. Most of the plagioclases lie in the range An_{50-60}. Both the Çobandede dacite and the Black ignimbrite contain only andesine with one exceptionally calcic analysis from the Çobandede dacite plotting in the bytownite field. Anorthite varies between 30-40 % in the plagioclases of these two units. The composition of plagioclases from the Kargapazarı volcanics at the top of the volcanic pile is basically characterised by bytownite and labradorite with only one relatively sodic analysis plotting into the andesine field. The most abundant compositional range for this unit is An_{60-70} with a peak of about 35-40% An, as is seen in the inset frequency-distribution graph. The data appear to plot into two separate areas with a break at around An_{60}.

Pasinler area (Figure 4.3): The Eocene Kışlaköy volcanics which make up the apparent basement of the Pasinler area have a narrow range of plagioclase compositions (An_{55-60}). The Black andesite also displays a relatively narrow range in its plagioclase composition, mainly in the labradorite field. Plagioclases of the Kızılveren amphibole dacite/andesite unit mainly fall in the andesine and labradorite fields displaying a similar distribution to the compositional distribution of plagioclases in the Mt. Dumlu amphibole dacite/andesite. The composition of plagioclases in the Black ignimbrite spans a very wide range from labradorite to oligoclase with one sample falling into anorthoclase field. The data on this diagram seem to plot into three separate areas as follows: An_{24-33}, An_{38-44}, An_{60-65}. The Kargapazarı volcanics contain the most calcic plagioclases of the volcanic units in this area, classifying as bytownite and labradorite (An_{52-78}). As can be expected, the distribution of plagioclase compositions in this unit closely resembles that of the Kargapazarı volcanics in Mt. Kargapazarı area. The Ardıçlıdağ rhyolite contains the most sodic and potassic feldspars on the plateau. Except for one sample falling into the andesine field, the feldspar compositions concentrate in two main areas: the first covers the oligoclase field and the border between anorthoclase and oligoclase; and the second falls mainly into the sanidine field (Or_{53-60}).

Horasan area (Figure 4.4): Plagioclases from the Saçdağ dacite in the south of Horasan are mainly composed of andesine and oligoclase (An_{27-44}). The Köroğlu amphibole dacite/andesite has plagioclases varying in composition between An_{40} and An_{57} which is a similar but narrower compositional range to those of the Dumlu (Mt. Dumlu) and the Kızılveren dacite/andesite units. The uppermost formation, the Horasan plateau unit, contains plagioclases whose compositional range is mainly between An_{55} and An_{73}. Only two samples from this unit fall into the andesine field.

Kağızman area (Figure 4.5): plagioclases from the Aladağ andesite, which covers a large area around the volcanic cone of Mt. Aladağ, are mainly represented by labradorite and andesine (An_{38-48}). Over 60% of plagioclases in this unit lie in the range An_{50-60}. The Çukurayva rhyolite and the Paslı trachy-dacite contain much more sodic plagioclase plotting into the andesine, oligoclase and anorthoclase fields. The uppermost unit, the Kars plateau unit contains only labradorite-type plagioclases.

Figure 4.6 displays the plagioclase compositions of the cores and rims of zoned individual plagioclase phenocrysts in the formations of the Erzurum-Kars Plateau. An additional point analysis, called the 'mid-point', was sometimes performed between the rim and core of some coarse phenocrysts. It is apparent from the figure that oscillatory and/or reverse zoning is quite common in the plagioclase phenocrysts of the volcanics on the plateau. Petrographic studies also support that plagioclase phenocrysts have complex zoning patterns. Some phenocrysts, such as those numbered MK36-7 and MK112-1, have less calcic mid-points compared to their cores and rims. In Figures 4.7 and 4.8, the anorthite (An) compositions of plagioclase crystals ranging from mega-crystals to microlites in grain size are plotted against the SiO_2 (Figure 4.8) and Mg-number of their host rocks (Figure 4.7). Figure 4.8 is presented in six parts, each of which corresponds to one of the main stratigraphic levels on the Erzurum-Kars Plateau. In Figure 4.7, the same data are divided into ten series with respect to different crystal textures and sizes of plagioclases and plotted against SiO_2 and Mg number of the melt. Even though a trend between anorthite content of plagioclases and acidity of the melt exists (Figure 4.7-a and b) there is a widespread scatter on all these diagrams. For comparison a linear regression line has been plotted through about 350 data points. In theory, if they had been crystallised in equilibrium with the magma, their anorthite value would have decreased progressively with increasing SiO_2 of the host rock, forming a linear or sublinear trend with negative gradient and without substantial scatter. This relationship thus indicates that most of the plagioclase megacrysts and phenocrysts were not in equilibrium with the magma as represented by the surrounding groundmass. In other words, they are xenocrysts in their groundmasses. It can thus be argued that a considerable amount of the plagioclase phenocrysts from different units of the plateau crystallised at depth in equilibrium with magma(s) of different composition(s) from their groundmass.

4.1.1.1. Composition of Plagioclases and their inclusions as evidence of magma mixing

Kuno (1936 and 1950) was the first researcher to provide petrographic evidence of magma mixing such as reverse zoning of pyroxenes and dusty cores of

Ca-rich plagioclase phenocrysts in intermediate lavas. Recent studies show that magma mixing is a widespread igneous phenomenon and seems to be operational particularly in systems where magma is vapour-saturated. In one of these studies, Eichelberger (1975) showed petrographic evidence of desegregation and dispersal of fragments of basic rocks in acidic melts. Anderson (1976) presented evidence of magma mixing of two or more compositionally distinct magmas by using inclusions of glass in large phenocrysts. He describes these inclusions of glass as tiny windows looking into the magma reservoir. More recently, Gourgaud and Villament (1992) emphasised the magma mixing process from the simultaneous eruption of two contrasting magmas (basalt and trachyte) to the genesis of trachyandesite, the product of magma mixing in the Grande Cascade sequence in Massif Central, France.

Halsor (1989) argues that andesites may be produced by magma mixing by means of repeated or episodic injection of fresh hydrous basaltic magma into an existing rhyolitic magma chamber. He believes that, during the injection, density instabilities are created when volatiles are released during crystallisation. The resultant mixing causes rapid skeletal growth of plagioclase in the rhyolite, trapping pockets of the magma which solidifies eventually as 'rhyolitic glass inclusions'. According to the author, these glass inclusions are not in equilibrium, either with the whole rock or with the groundmass.

Plagioclase mega- and phenocrysts containing brownish coloured clear rhyolitic glass inclusions are common in the amphibole-bearing porphyritic lavas of the Erzurum-Kars Plateau especially in the Mt. Dumlu area. Unfortunately only two of these inclusions were analysed by electron microprobe, as presented in Table 4.1 together with the analysis of their host plagioclase phenocryst and the whole rock XRF analysis. The compositions of these inclusions are quite different from those of both host plagioclase and the whole rock. They are strongly enriched in SiO_2 (72.5-74 %) and K_2O and depleted in all other major elements. They probably represent the composition of the rhyolitic magma before mixing. These textures, together with the complex compositional zonal patterns and reaction textures (i.e. reaction rims, and textures of resorption and corrosion) indicate that 'magma mixing' between a rhyolitic to andesitic magma and injecting basaltic magma might be operational in the evolution of the low-Y series of Erzurum-Kars Plateau volcanics. Results of the Al-in-hornblende barometer of Schmidt (1992) shows that most of these magma chambers that fractionated amphibole-bearing mineral assemblages located at a depth of around 20-30 km (see section 4.2.2.1). The absence of equilibrium between plagioclase phenocrysts and the matrix (Figures 4.7 and 4.8) indicated by widespread scatter of data points also appears to support the idea of magma mixing. Vertical

thermal and compositional zonation and the lowering of pressure as magma rises to the shallower depths might also be partly responsible for these complexities.

The rapid injection of basaltic magma not only changes the entire composition of magma in the chamber but also results in an increase in temperature of the reservoir. This may give rise to resorption of existing crystals and subsequent crystallisation of more calcic plagioclase at the outer zones of phenocrysts. The experiments of Tsuchiama (1985) suggest that, if basic and acid magmas mix, sodic feldspar in the acid magma dissolves because of the heat effect developing sieve textures. When crystallisation eventually resumes, the sieve texture is coated by euhedral growths of more calcic plagioclase. Repetitive or sporadic injection of hotter

	MK93 w.r.	MK93-3c Plg	MK93-11g1 Glass inc.	MK93-11g2 Glass inc.
SiO_2	63.49	53.13	72.51	74.07
TiO_2	0.75	0.16	0.56	0.41
Al_2O_3	16.1	28.33	11.68	11.76
FeO	4.71	0.64	1.32	1.74
MnO	0.07	0.00	0.00	0.09
MgO	2.43	0.31	0.16	0.13
CaO	4.94	12.20	0.91	0.91
Na_2O	3.58	4.75	2.89	2.52
K_2O	2.76	0.24	5.74	5.90
Total	98.83	100.05	95.76	97.56
Ab		40.82		
An		57.82		
Or		1.36		

Table: 4.1. Table displaying the composition of whole-rock (w.r.), plagioclase megacryst (Plg) and glass inclusions (Glass inc.) it contains.

basic magma into an acidic magma chamber, which is associated with turbulent mixing in a semi-open system, creates complex oscillatory zoning which is marked by several resorption cycles producing rounded crystal shapes and reaction rims e.g. sieve texture. These kinds of textures are also present in the zoned plagioclase phenocrysts of the Erzurum-Kars plateau volcanics. Furthermore, the results obtained from Sun et al.'s (1971) plagioclase thermometer, which are in good agreement with Lindsley and Andersen's (1983) two pyroxene scheme, give temperatures varying between 1000 and 1050°C (see section 4.2.1 and 4.2.3.1). These are higher than that which can be expected from dacitic/andesitic magmas and may also be attributed to the addition of hotter basic magma into the intermediate to acidic magma chambers that fed the volcanic eruptions of the amphibole-bearing porphyritic lavas on the Erzurum-Kars Plateau. As can be seen in Figure 4.7-a and c, corroded plagioclase mega- and phenocrysts are generally characterised by a wider scatter in their An

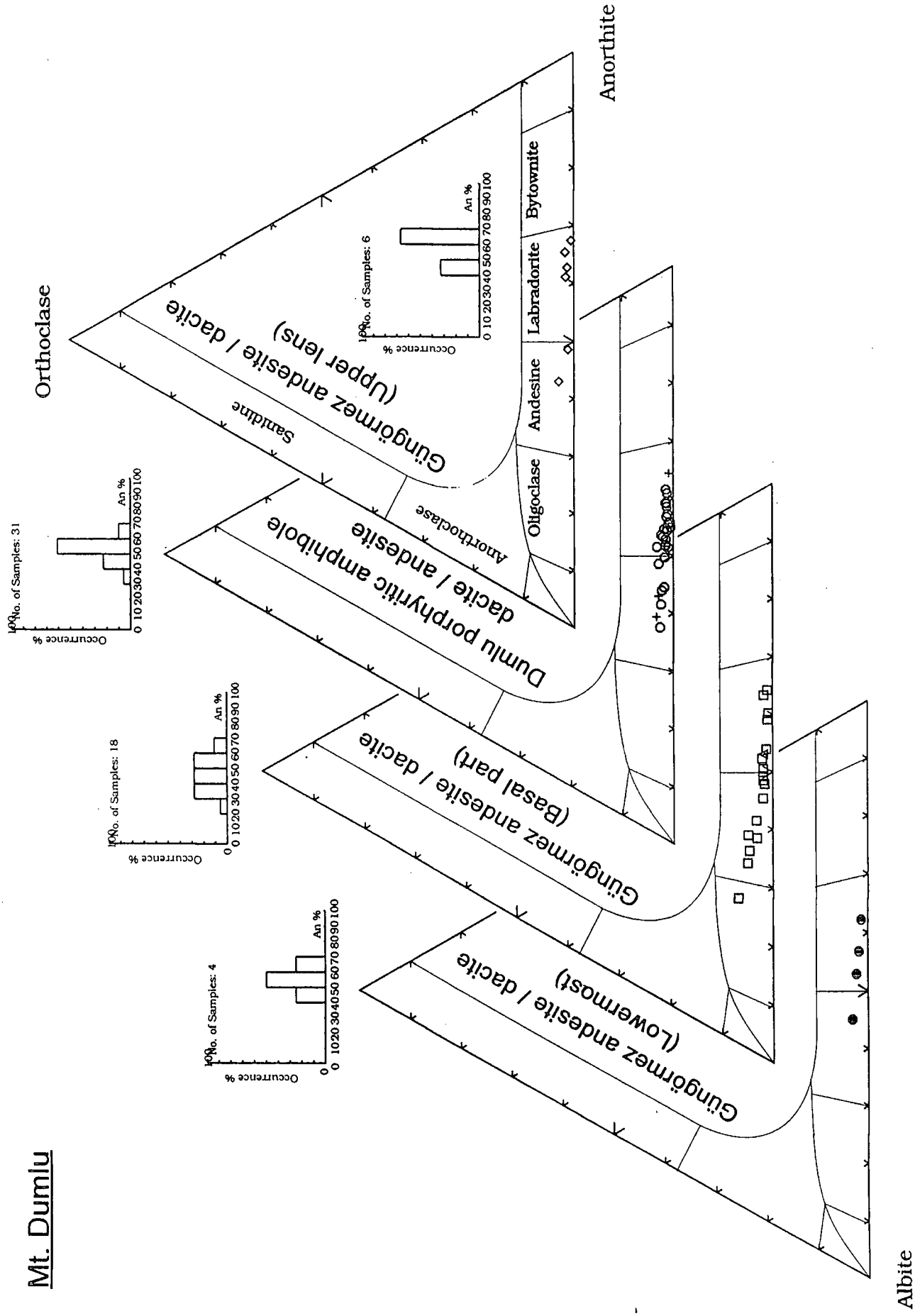
Mt. Dumlu
Orthoclase
Anorthite
Albite
Sanidine
Anorthoclase
Oligoclase
Andesine
Labradorite
Bytownite
Güngörmez andesite / dacite (Upper lens)
Dumlu porphyritic amphibole dacite / andesite
Güngörmez andesite / dacite (Basal part)
Güngörmez andesite / dacite (Lowermost)
No. of Samples: 31
No. of Samples: 6
No. of Samples: 18
No. of Samples: 4
Occurrence %
An %
0 10 20 30 40 50 60 70 80 90 100

Figure: 4.1

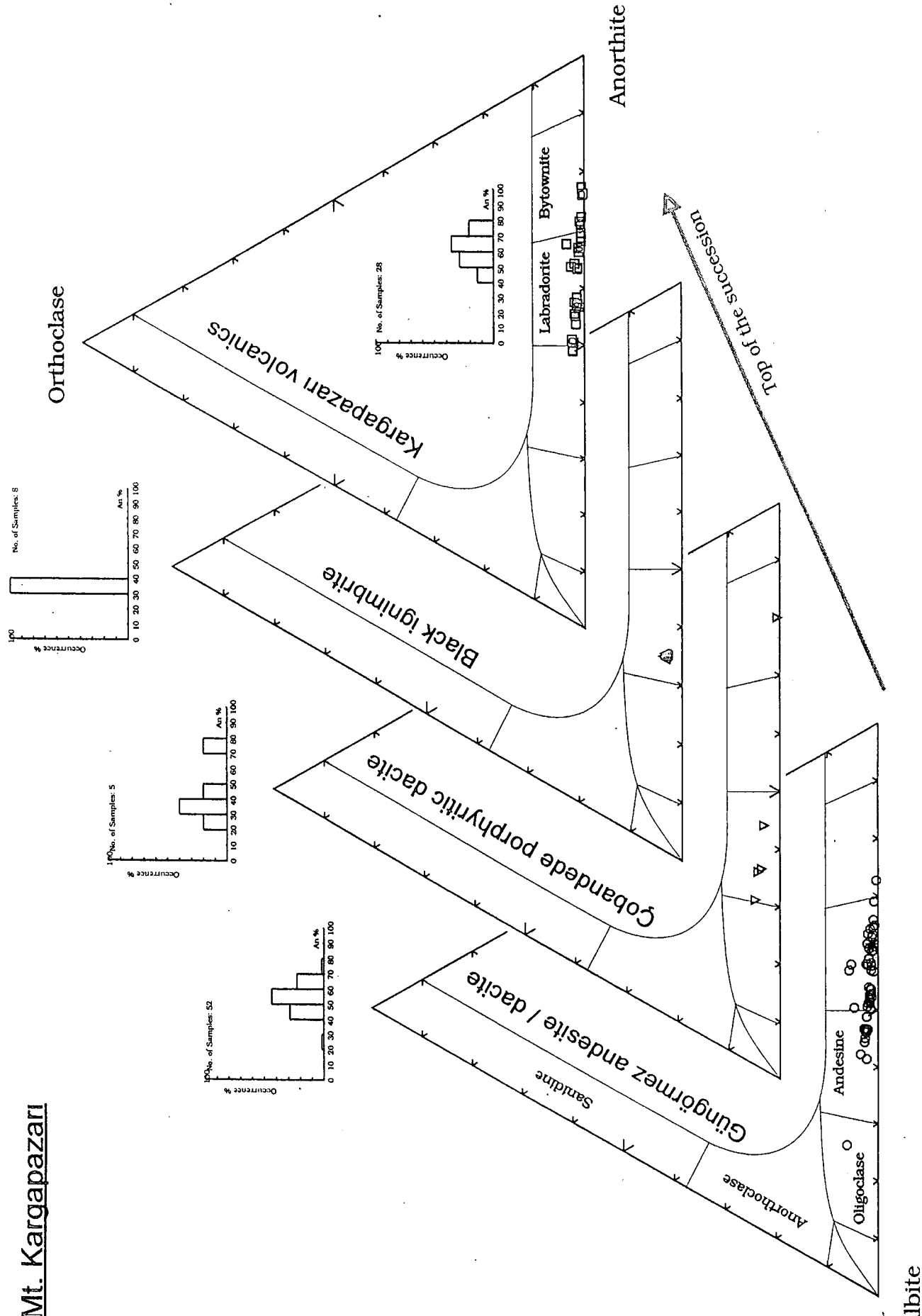
Mt. Kargapazarı
Orthoclase
Anorthite
Albite
Karagapazarı volcanics
Black ignimbrite
Çobandede porphyritic dacite
Güngörmez andesite / dacite
Top of the succession
Labradorite
Bytownite
Andesine
Oligoclase
Anorthoclase
Sanidine
No. of Samples: 28
No. of Samples: 8
No. of Samples: 5
No. of Samples: 52
An %
Occurrence %

Figure: 4.2

Figure: 4.3

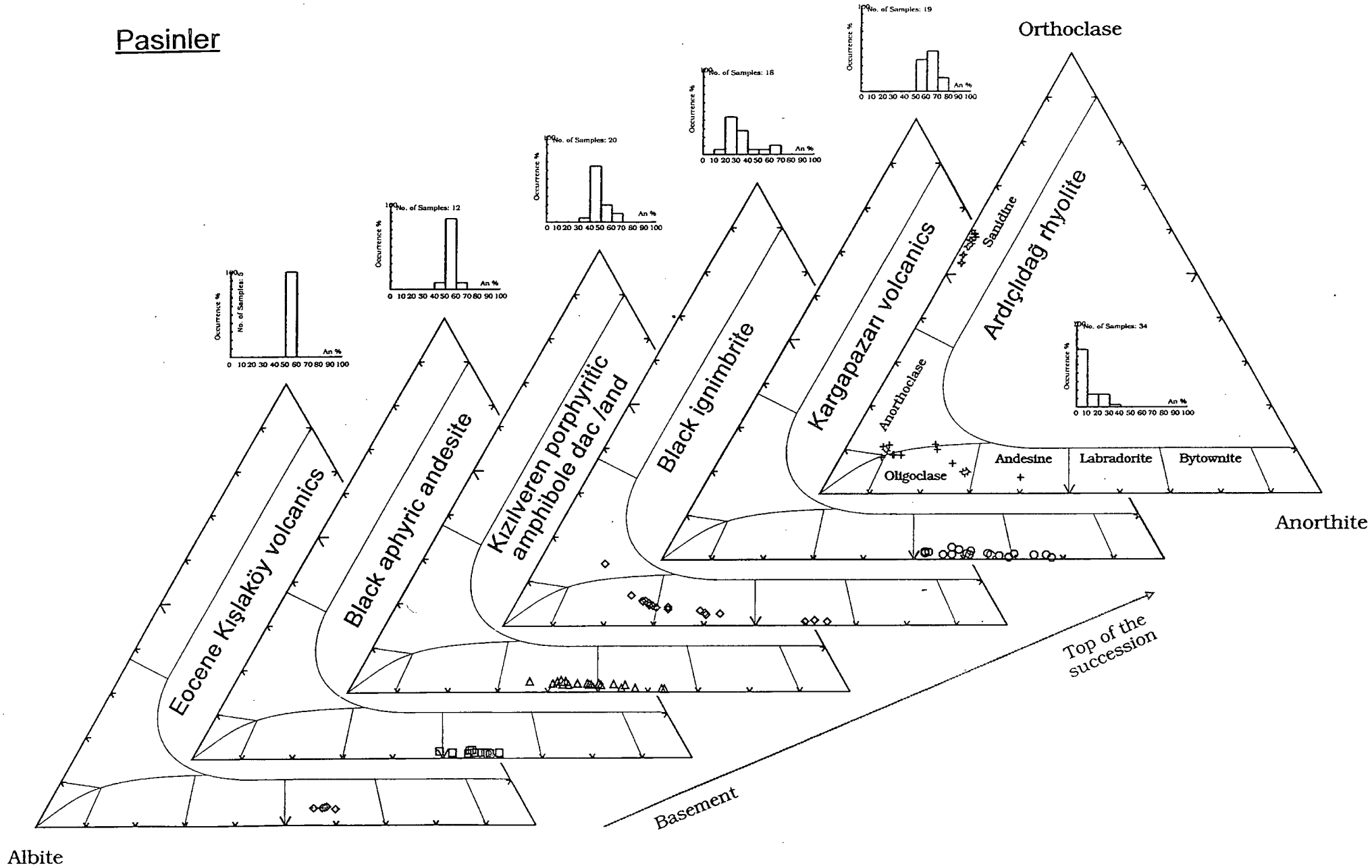
Pasinler
Orthoclase
Albite
Anorthite
Eocene Kışlaköy volcanics
Black aphyric andesite
Kızılveren porphyritic amphibole dac /and
Black ignimbrite
Kargapazarı volcanics
Ardıçlıdağ rhyolite
Sanidine
Anorthoclase
Oligoclase
Andesine
Labradorite
Bytownite
Top of the succession
Basement
No. of Samples: 12
No. of Samples: 20
No. of Samples: 18
No. of Samples: 19
No. of Samples: 34
Occurrence %
An %
0 10 20 30 40 50 60 70 80 90 100

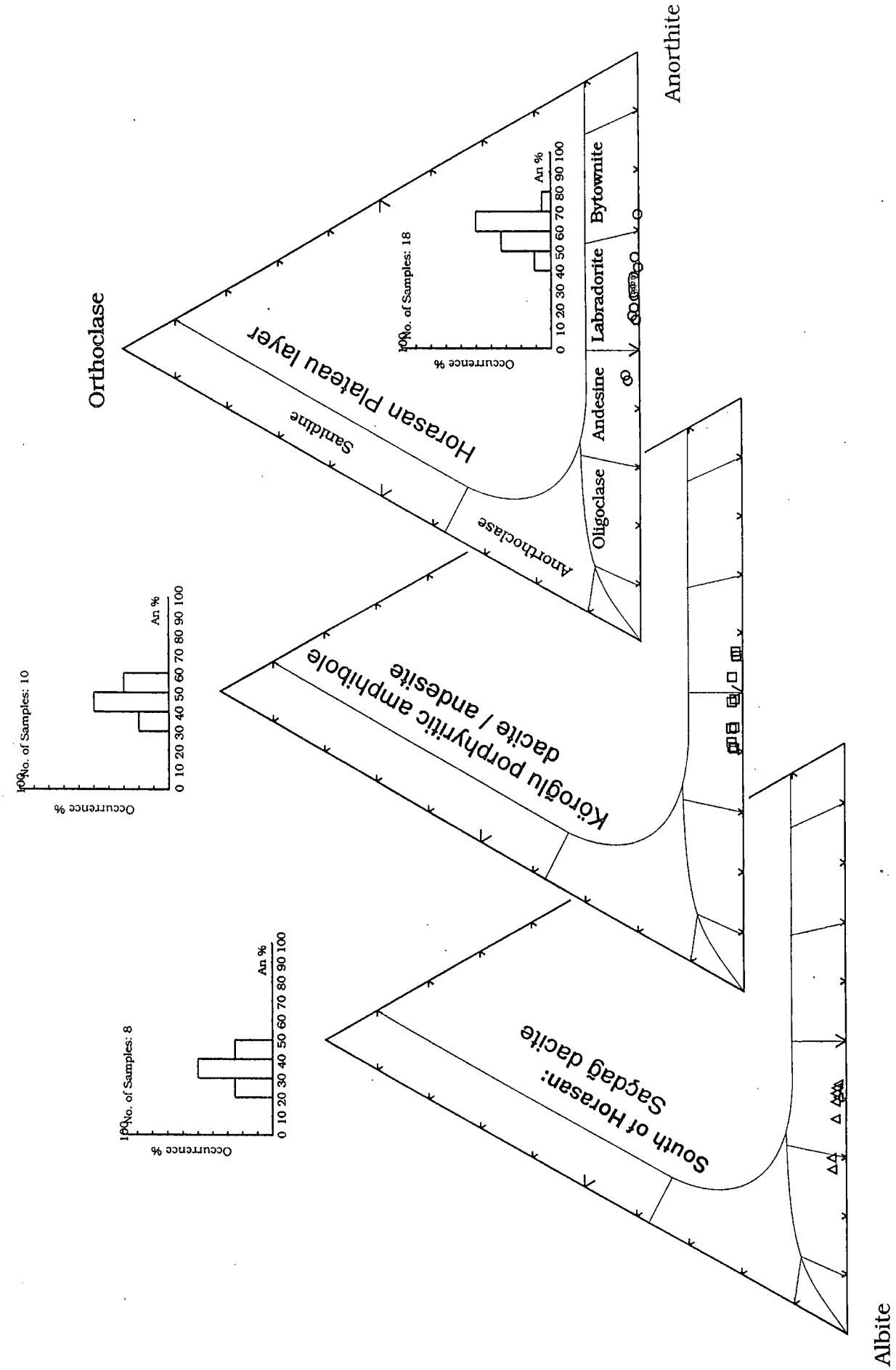
Horasan
Orthoclase
Anorthite
Albite
Horasan plateau layer
Sanidine
Anorthoclase
Oligoclase
Andesine
Labradorite
Bytownite
An %
No. of Samples: 18
Occurrence %
Kiroglu porphyritic amphibole
dacite / andesite
An %
No. of Samples: 10
Occurrence %
South of Horasan:
Saçdağ dacite
An %
No. of Samples: 8
Occurrence %

Figure: 4.4

Figure: 4.5

Kagizman

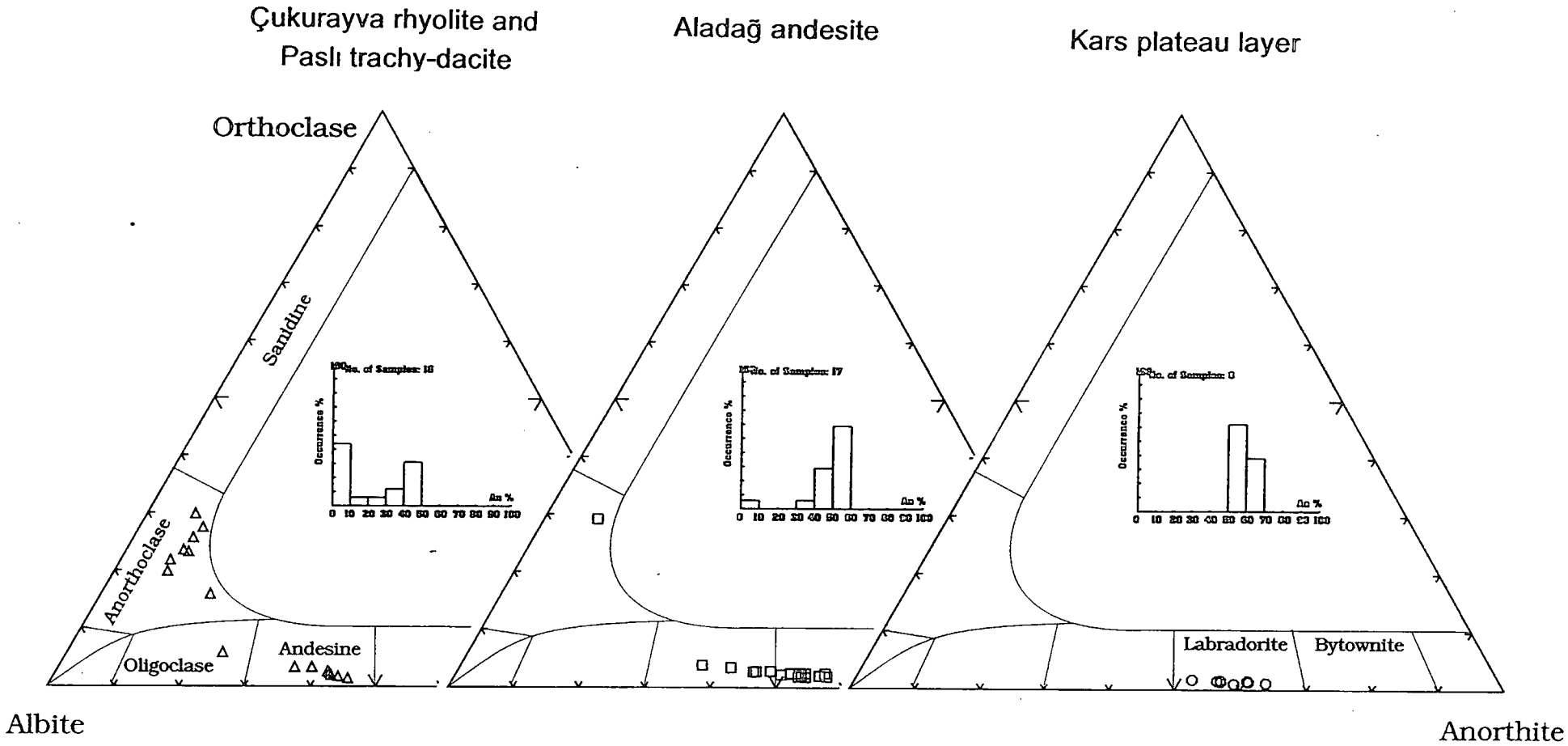

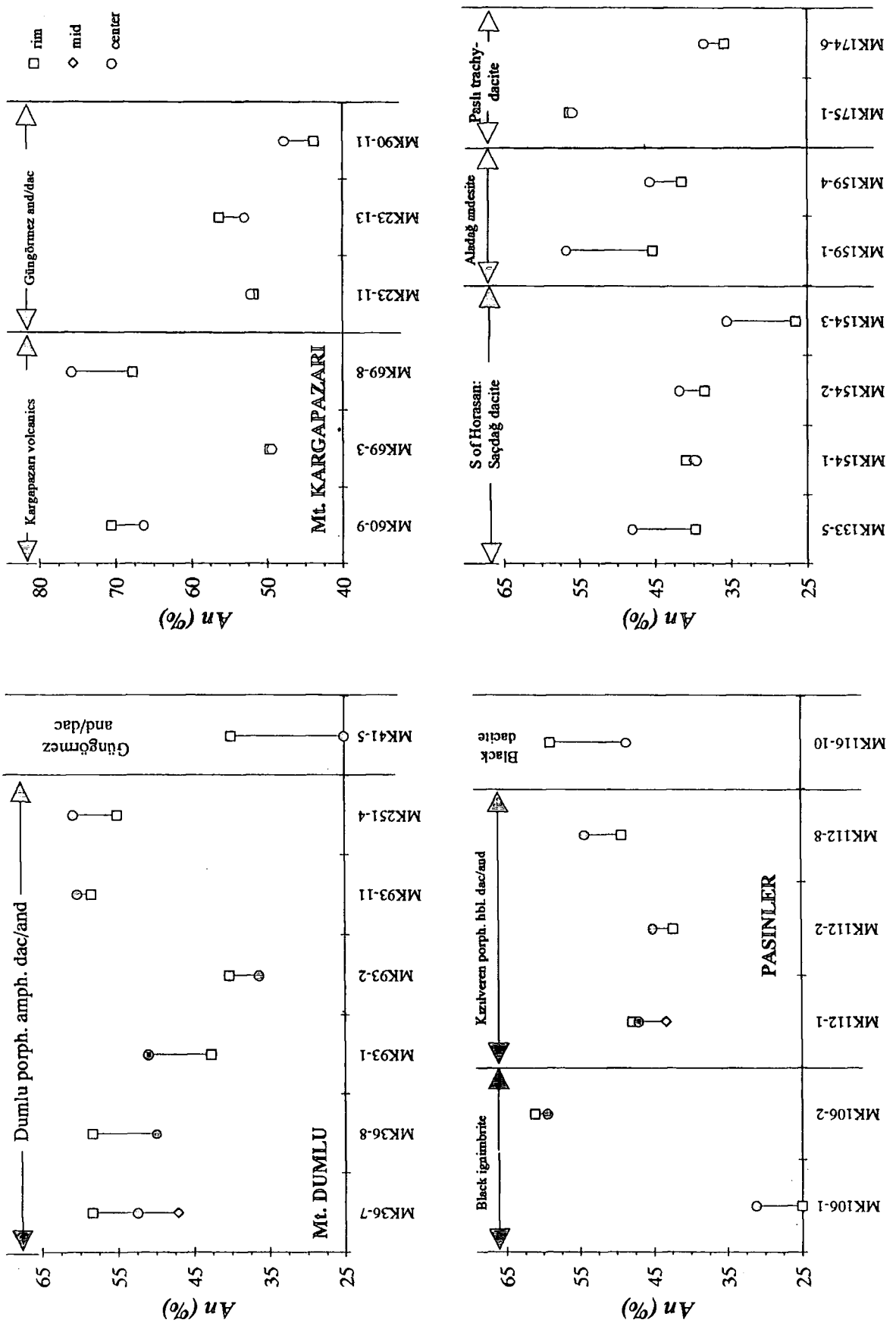
rim
mid
center
Güngörmez and/dac
Kargapazarı volcanics
Mt. KARGAPAZARI
MK90-11
MK23-13
MK23-11
MK69-8
MK69-3
MK60-9
An (%)
Pasli trachy-dacite
Aladağ andesite
S of Horasan: Saçdağ dacite
MK174-6
MK175-1
MK159-4
MK159-1
MK154-3
MK154-2
MK154-1
MK133-5
Dumlu porph. amph. dac/and
Güngörmez and/dac
Mt. DUMLU
MK41-5
MK25I-4
MK93-11
MK93-2
MK93-1
MK36-8
MK36-7
Black dacite
Kızılveren porph. hbl. dac/and
Black ignimbrite
PASINLER
MK116-10
MK112-8
MK112-2
MK112-1
MK106-2
MK106-1

Figure: 4.6

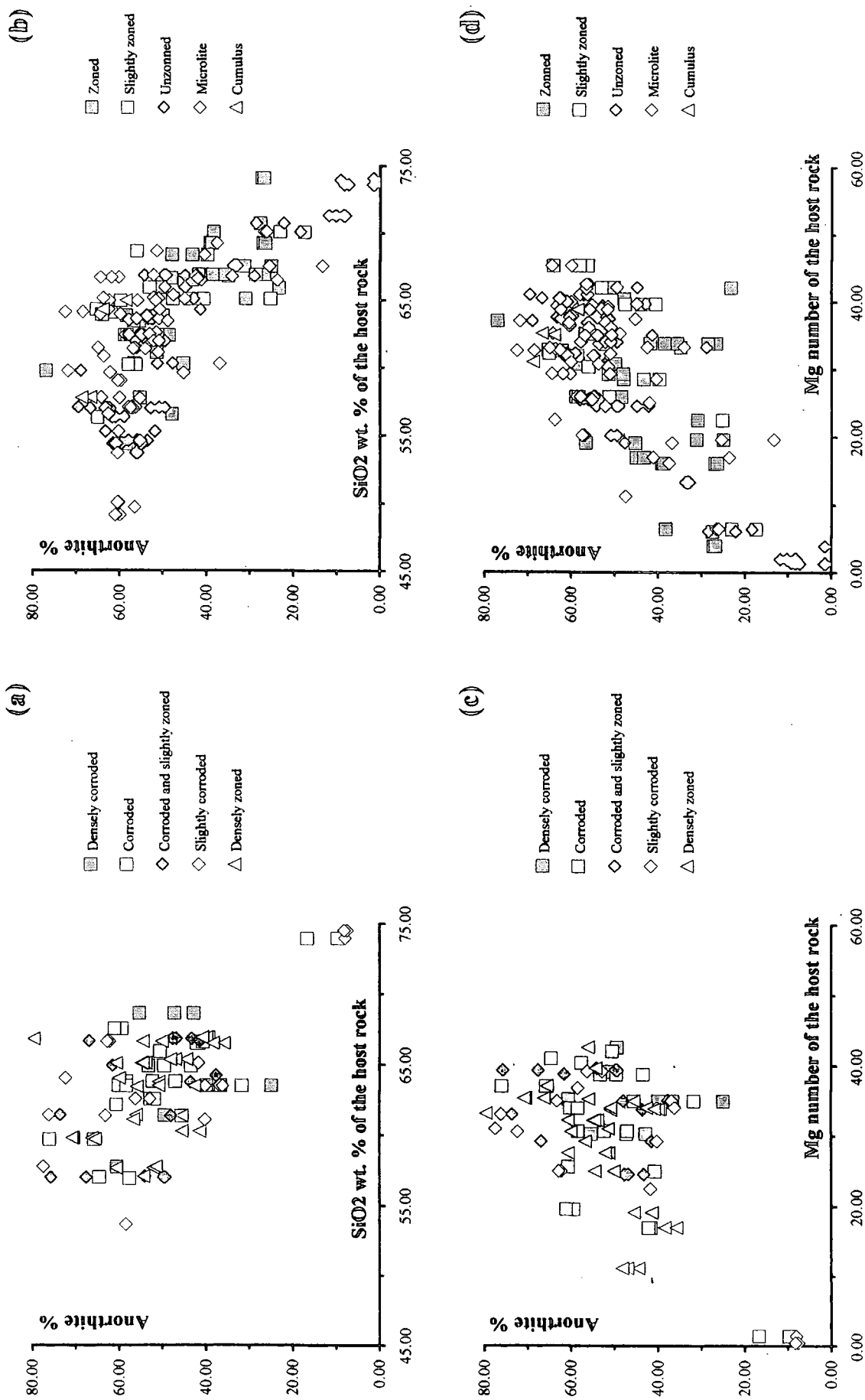

Figure: 4.7. Anorthite contents of the plagioclase crystals plotted against SiO2 and Mg-number of their host rock. They are divided into series according to their textures and crystal sizes.

FIG4-07.XLS

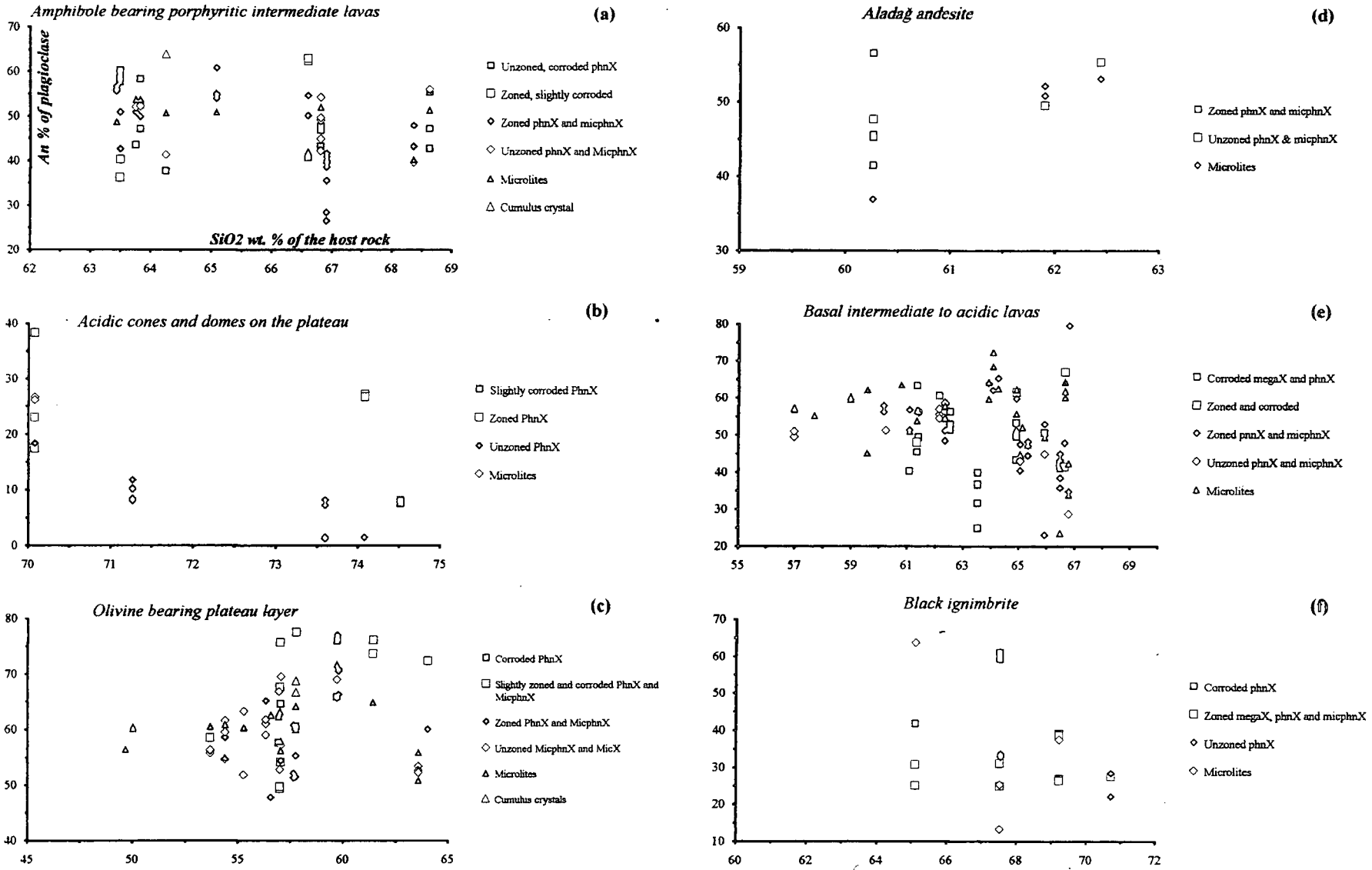

Figure: 4.8. Anorthite contents of the plagioclase crystals plotted against SiO2 content of their host rock. The data are presented in six parts, each of which corresponds to one of the main stratigraphic levels on the Plateau.

content compared to uncoroded and zoned plagioclases that contain An_{10-75}. Surprisingly, plagioclase microlites display almost the same anorthite range as mega- and phenocrysts (Figures 4.7-b and d).

4.1.2. Distribution of the composition of pyroxenes and their classification

4.1.2.1. Calculations of pyroxene end-members

Some of the earlier calculation schemes for pyroxene end-members have been suggested by Banno (1959), Kushiro (1962), Yoder and Tilley (1962), White (1964) and Essene and Fyfe (1967). Since most of these methods in general are sequential schemes that usually differ in the order of the sequence, they may lead to an overestimation of the component calculated first. Although Dietrich and Petrakakis (1986) have developed an algebraic method which involves the calculation of 11 linearly independent pyroxene components to overcome this problem, Lindsley (1986) showed the invalidity of this calculation for some special cases by comparing the results with crystal-chemistry experiments. Except for Essene and Fyfe (1967), all of the methods mentioned above have a major disadvantage in that acmite $NaFe^{3+}Si_2O_6$ is the first end-member to be calculated. However, there is no way of estimating acmite content, since the Fe_2O_3 content cannot be determined by electron-microprobe. Therefore the possible error from this unknown Fe_2O_3 may be propagated throughout the calculation of all subsequent end-members. Mysen and Heier (1972) have suggested a recalculation scheme for ferrous and ferric iron contents of pyroxenes to produce a sum of cations equal to 4.00. Despite its superiority to other calculation schemes, the method of Essene and Fyfe (1967) has an important weakness since it ignores TiO_2 and K_2O content in the calculation of pyroxene end-members. This cannot be justified since some titanaugites may contain over 4% TiO_2. Cawthorn and Collerson (1974) have suggested an alternative scheme which minimises the significance of Fe_2O_3 contents and allows for a more rigorous determination of end-member concentrations. The method they have put forward is somewhat similar to that of Kushiro (1962), except that jadeite is calculated before acmite. In their method, all 12 major element oxides may be recalculated into pyroxene end-members such that the effect of unknown Fe_2O_3 content is minimal. Their technique thus allows the important end-members of pyroxenes to be calculated in a way which is independent of oxidation ratio. Several other calculation methods have been developed to calculate the structural formulae of the pyroxenes (e.g.

Dollase and Newman, 1984) however, the well known scheme of Yoder and Tilley (1962) has remained the most used. When this method is followed, the pyroxene formula unit is normalised to 6 oxygen atoms.

More recently, the Subcommittee on Pyroxenes of the Commission on New Minerals and Mineral Names of the International Mineralogical Association (IMA) approved a new classification for pyroxene minerals which compiles the widely accepted methods of classifying pyroxenes and simplifies the nomenclature (Morimoto, 1989). As the IMA proposes, if Fe_2O_3 is not available, the formula is calculated to four cations (Fe, Mg, Ca and Na) to estimate the Fe^{3+} by charge balance. Cations are then allocated to their structural sites. According to the IMA proposal, Si^{4+} and particular amounts of Al^{3+} and Fe^{3+} are situated in tetrahedral sites. The remaining cations are considered as belonging to M1 and M2 sites. Each pyroxene is then assigned to one of the four chemical groups defined by Morimoto and Kitamura (1983) as follows: (1) Ca-Mg-Fe pyroxenes (Quad), (2) Na-Ca pyroxenes (Na-Ca), (3) Na pyroxenes (Na) and (4) other pyroxenes (Other). The quad pyroxenes are classified in the enstatite-ferrosilite-diopside-hedenbergite quadrilateral whereas the Na-Ca and Na pyroxenes are plotted in the Quad-Jd-Ae triangle. Despite the use of this new classification system, the calculation of pyroxene end-members remains necessary for many studies. For this, some authors (e.g. McHone, 1987 and Gómez, 1990) have developed computer programs. Among them, the PX program developed by Gómez (1990) (written with the TurboBasic compiler) operates on IBM-PC computers and can simultaneously calculate the two normalisation schemes of Kushiro (1964) and Cawthorn and Collerson (1974) and classifies the pyroxenes according to IMA suggestions. In addition to that, the program also calculates the wollastonite (Wo) -enstatite (En) and ferrosilite (Fs) parameters, following the scheme devised by Lindsley and Anderson (1983), so that these components can be directly plotted on the graphical thermometer calibrated by Lindsley (1983) (see section: 4.2.1).

4.1.2.2. Distribution of the compositions of pyroxenes on the Erzurum-Kars Plateau

A total of 61 representative volcanic rocks samples from the 6 sub areas and 12 volcanic units on the Erzurum-Kars Plateau were selected for analyses (table: 4.2). Polished thin sections of these samples were studied microscopically, then analysis of a total of 308 pyroxene crystals was carried out using the Geoscan electron microprobe at the University of Durham. Up to 10 points were analysed in each rock for pheno-, micro-phenocrysts and microcrysts in order to study within-grain

compositional differences. The data obtained were used to calculate end-member compositions of the analyses using the PX program of Gómez (1990). Then they were plotted on the enstatite (En: $Mg_2Si_2O_6$) - ferrosilite (Fs: $Fe_2Si_2O_6$) - diopside (Di: $CaMg_2Si_2O_6$) - hedenbergite (Hd: $CaMg_2Si_2O_6$) classification quadrilateral in terms of the molecular end-members of these minerals. They are presented in Figure 4.10 in twelve parts (a-l) each represents one of the 12 representative units on the plateau.

Area	Formation
1. Mt. Dumlu Area	Dumlu amphibole dacite/andesite
	Güngörmez andesite/dacite
2. Mt. Kargapazarı	Güngörmez andesite/dacite
	Kargapazarı volcanics
	Çobandede dacite
3. Pasinler	Kargapazarı volcanics
	Black ignimbrite
	Kızılveren amphibole dacite/andesite
	Black andesite/dacite

Area & formation
4. Horasan plateau unit
5. Aladağ andesite
6. Kars plateau unit

Table 4.2. showing areas and volcanic units from which representative samples selected for electron microprobe analyses.

Mt. Dumlu area: Clinopyroxene pheno- and micro-phenocrysts of the Güngörmez andesite/dacite in Mt. Dumlu area form a relatively tight group plotting onto the border between the endiopside and augite fields (Figure 4.10-a). On the other hand, orthopyroxenes mainly fall into the bronzite field. The Dumlu amphibole dacite/andesite contains slightly more calcic and Fe-rich clinopyroxenes compared to the Güngörmez andesite/dacite. Clinopyroxenes of this unit mainly classify as augite with a few samples falling into the salite and only one sample plotting into the endiopside field. Orthopyroxenes of the unit classify mainly as bronzite and partly hypersthene (Figure 4.10-b).

Mt. Kargapazarı: clinopyroxenes of the Güngörmez andesite/dacite in Mt. Kargapazarı fall into the diopside, salite, endiopside and augite fields. However, they predominantly concentrate on the intersection of the four borders dividing these four fields (Figure 4.10-c). Orthopyroxenes of this unit cover the entire length of the bronzite field with only two samples plotting into the hypersthene field. There are only three analyses available from the Çobandede dacite. The only clinopyroxene analysis plots in the augite field close to the border between augite and salite and two orthopyroxenes fall in the middle of the bronzite field (Figure 4.10-d). Clinopyroxenes of the Kargapazarı volcanics form a similar compositional pattern to that shown by the Güngörmez andesite/dacite though they are slightly less calcic.

Except for one sample, they all classify as augite and endiopside (Figure 4.10-e). Orthopyroxene is rather rare in this unit. It plots in the less magnesian part of bronzite field.

Pasinler area: except for one sample falling into the ferroaugite field, clinopyroxenes of the Kargapazarı volcanics in the Pasinler area plot into both the endiopside and augite fields, similar to those in Kargapazarı area (Figure 4.10-f). Orthopyroxenes of this unit plot as bronzite. Clinopyroxenes of the Black ignimbrite all classify as augite while orthopyroxenes are confined into a restricted area of the bronzite field (Figure 4.10-g). Similar to the Black ignimbrite, clinopyroxenes of both the Kızılveren amphibole andesite and the Black andesite/dacite plot in the augite field whereas orthopyroxenes span a wider compositional range from bronzite to hypersthene (Figures 4.10-h and i).

Clinopyroxenes of the Horasan plateau unit, Aladağ andesite and Kars plateau unit all predominantly plot in the augite field on the classification quadrilateral with the exception of a few which scatter into the endiopside field from the Horasan plateau unit and Aladağ andesite (Figures 4.10-j to l). In addition, four samples from the Horasan plateau unit plot into the salite field. Orthopyroxenes from both the Horasan plateau unit and the Aladağ andesite vary in composition between bronzite and hypersthene.

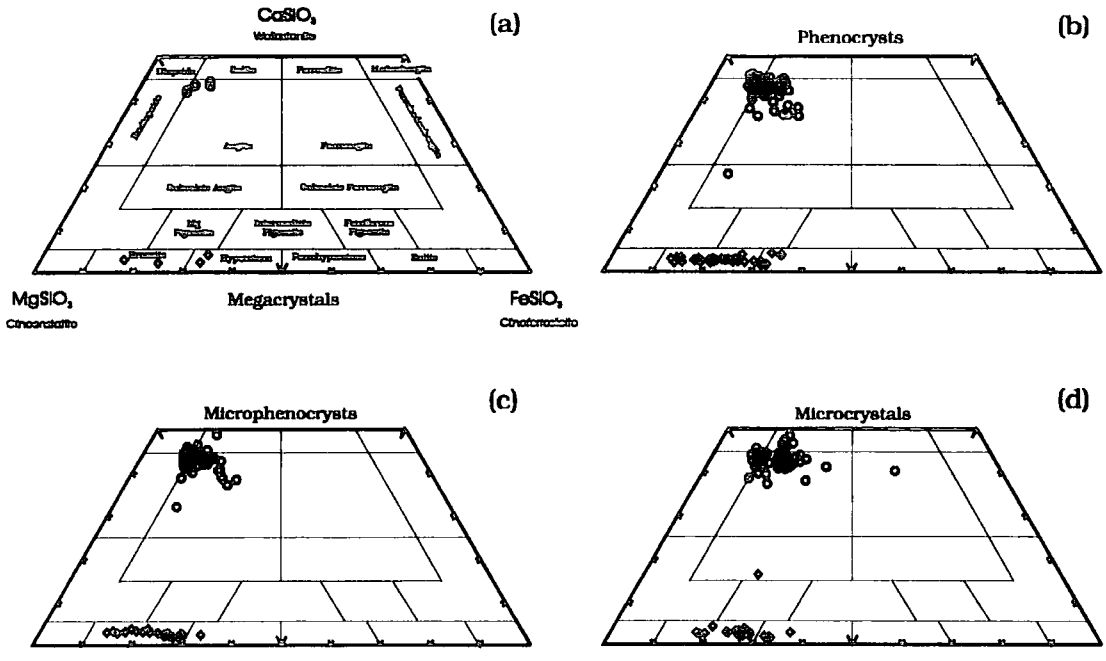

Figure: 4.9. Distribution of the composition of pyroxene mega- (a), pheno- (b), microphenocrysts (c) and microcrysts (d: groundmass crystals) from the Erzurum-Kars Plateau.

Distribution of the compositions of pyroxenes with respect to crystal grain size is assessed above in Figure 4.9. The composition of orthopyroxenes for all grain sizes does not show any clear variations. It covers a compositional range between bronzite

Figure: 4.10

Mt. DUMLU

Güngörmez andesite / dacite

Dumlu porphyritic amphibole dacite / andesite

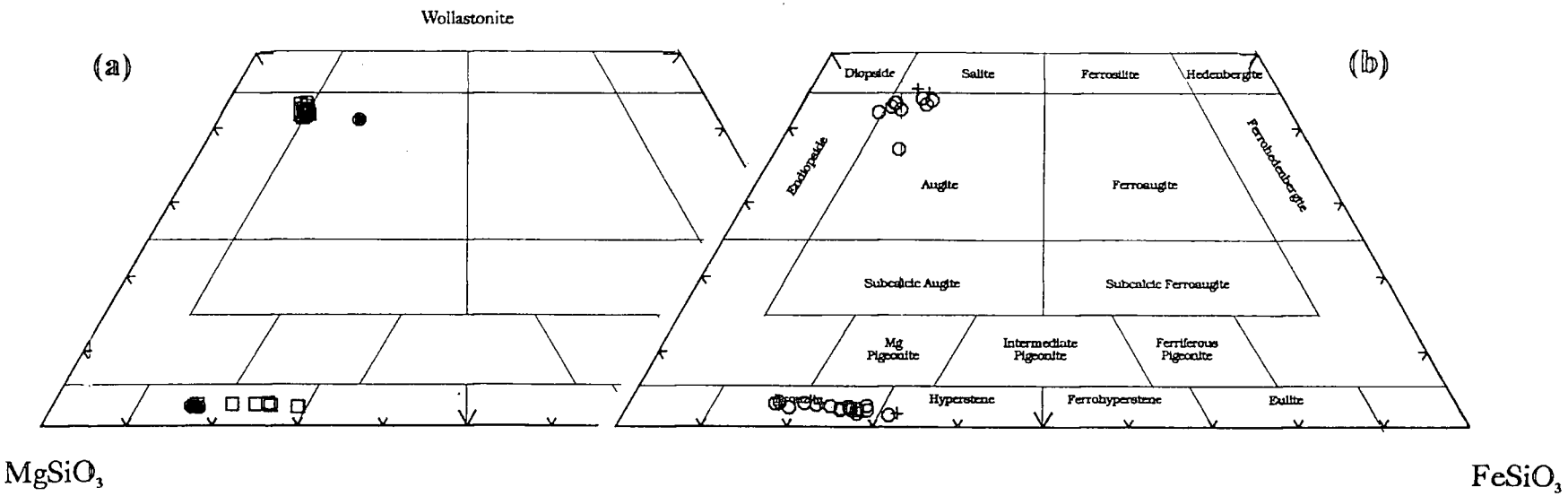

Mt. KARGAPAZARI

Güngörmez andesite / dacite

Çobandede porphyritic dacite

Kargapazarı volcanics

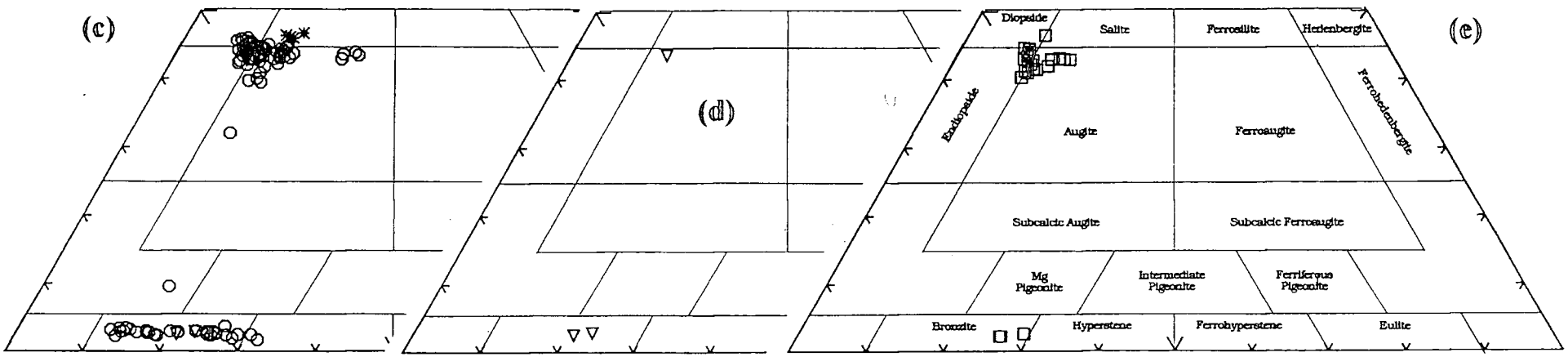

Kargapazarı volcanics

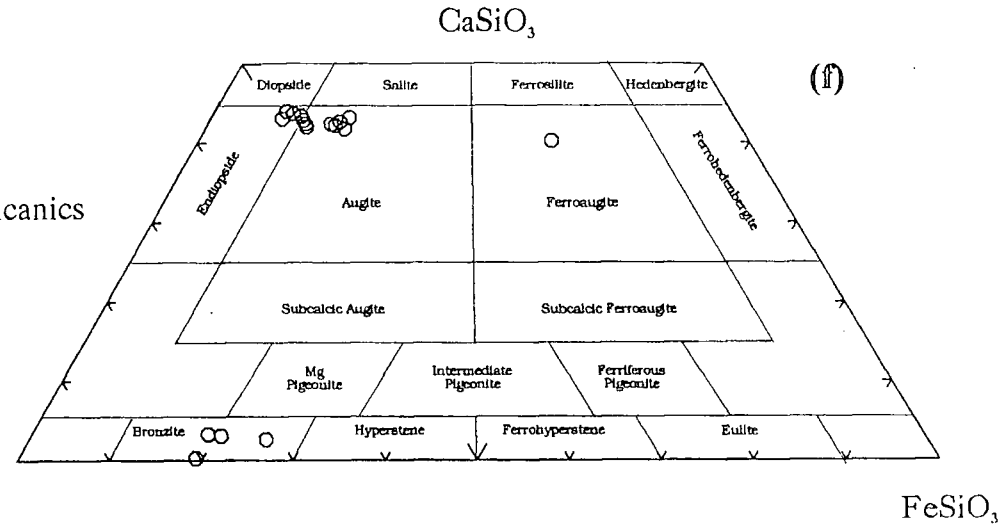

Black ignimbrite

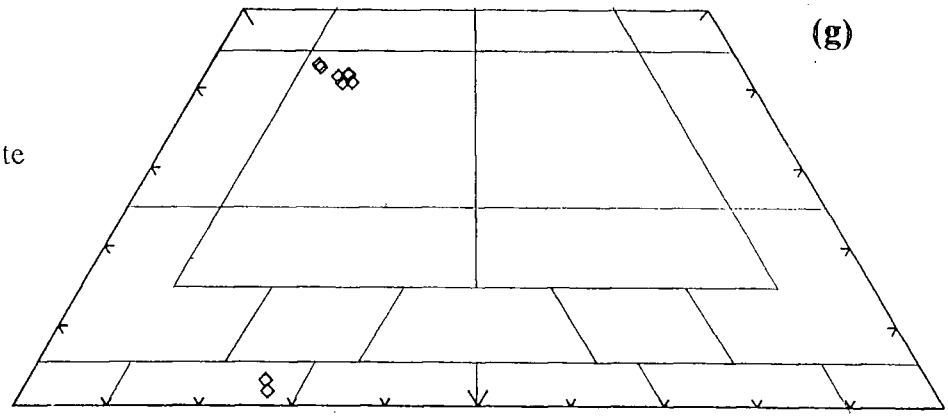

Kızılveren porphyritic amphibole dac /and

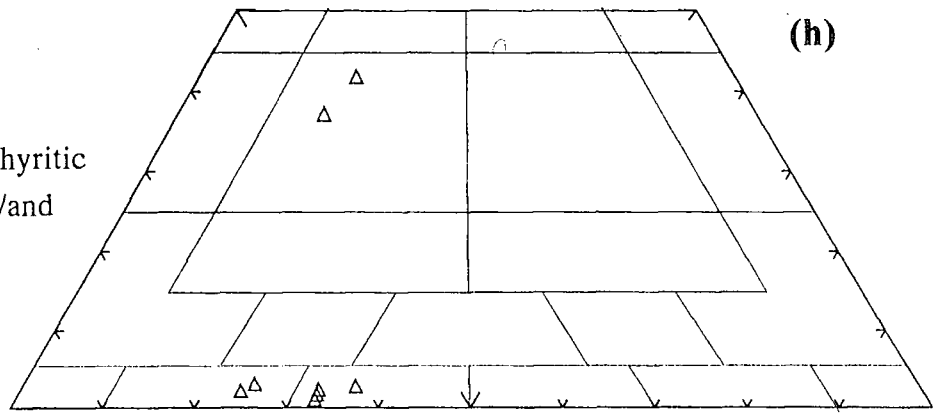

Black aphyric andesite

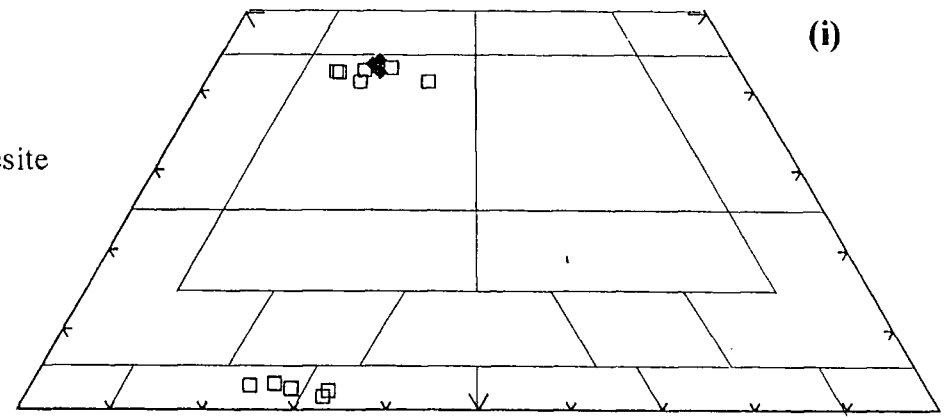

$CaSiO_3$

Horasan Plateau layer

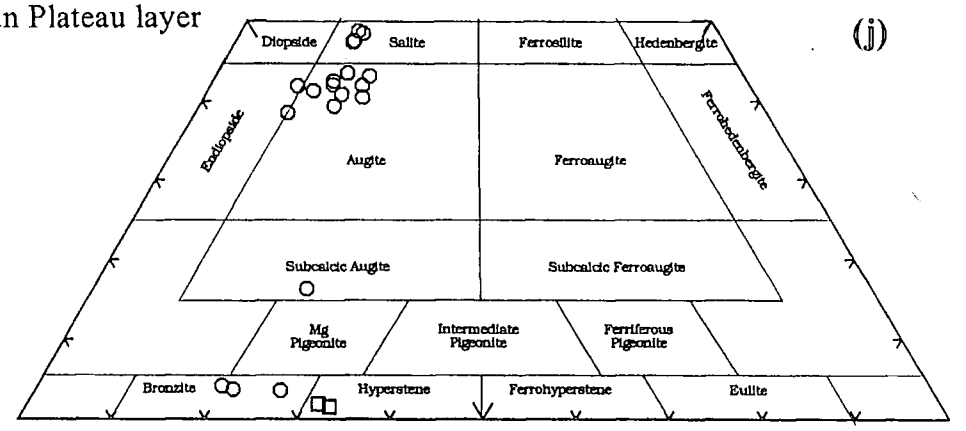

(j)

Aladağ andesite

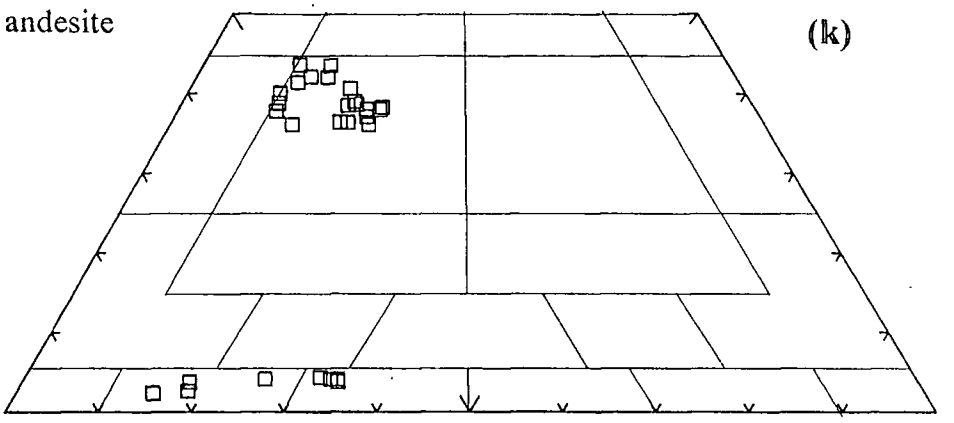

(k)

Kars plateau layer

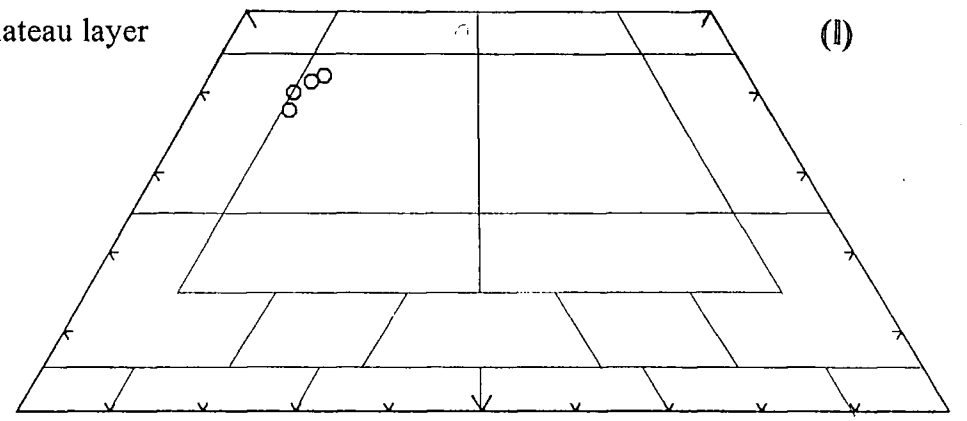

(l)

$MgSiO_3$ $FeSiO_3$

and hypersthene. However, clinopyroxenes tend to be more calcic and also iron-rich when grain size gets smaller.

4.1.3. Classification and distribution of the composition of amphiboles

Amphiboles form an enormously diverse mineral family whose compositional space is defined by A, B, C and T site occupancies. These sites are subdivided mainly into 13 tetrahedral domains which basically constitute their main end-members (Currie, 1991). The conventions for naming amphiboles have been established by the International Mineralogical Association (IMA) (Leake, 1978; Leake and Winchell, 1978; Rock and Leake, 1984). According to the IMA, an amphibole has the ideal formula:

$$A_{0\text{-}1}B_2C_5T_8O_{22}(OH,F,Cl)_2$$

where the *A* site is generally occupied by Na and K, the *B* site by Na, Li, Ca, Mn, Mg and Fe^{2+}, the *C* position by Mg, Fe^{2+}, Mn, Al, Fe^{3+} and Ti, and finally the T position is occupied by Si and Al. These 13 end-members and their site occupancies are presented in table 4.3 together with a more detailed subdivision of each end-member.

tremolite *(A) (B) (C) (T)* ( ) (Ca_2) (Mg_5) (Si_8)	ferro-actinolite ferro-anthophyllite magnesio-anthophyllite tirodite dannemorite
winchite ( ) (CaNa) (Mg_4Al) (Si_8)	ferro-alumino ferro-ferri magnesio-ferri
riebeckite ( ) (Na_2) ($Fe^{3+}{}_2Fe^{2+}{}_3$) (Si_8)	magnesio-riebeckite ferro-glaucophane glaucophane holmquistite
hornblende ( ) (Ca_2) (Mg_4Al) (Si_7Al)	ferro-alumino ferro-ferri magnesio-ferri
barroisite ( ) (CaNa) (Mg_3Al_2) (Si_7Al)	magnesio-alumino ferro-alumino ferro-ferri magnesio-ferri
tschermakite ( ) (Ca_2) (Mg_3Al_2) (Si_6Al_2)	magnesio-alumino ferro-alumino ferro-ferri magnesio-ferri
richterite (Na) (CaNa) (Mg_5) (Si_8)	ferro-richterite

arfvedsonite *(A) (B) (C) (T)* (Na) (Na_2) ($Fe^{3+}Fe^{2+}{}_4$) (Si_8)	magnesio-arfvedsonite eckermannite ferro-eckermannite kozulite
edenite (Na) (Ca_2) (Mg_5) (Si_8)	magnesio-edenite ferro-edenite
kataphorite (Na) (CaNa) (Mg_4Al) (Si_7Al)	magnesio-alumino ferro-alumino ferro-ferri magnesio-ferri
nyboite (Na) (Na_2) (Mg_3Al_2) (Si_7Al)	magnesio-alumino ferro-alumino ferro-ferri magnesio-ferri
pargasite (Na) (Ca_2) (Mg_4Al) (Si_6Al_2)	ferro-pargasite hastingsite magnesio-hastingsite
taramite (Na) (Na_2) (Mg_3Al_2) (Si_6Al_2)	magnesio-alumino ferro-alumino ferro-ferri magnesio-ferri

Table: 4.3. Table showing amphibole end-members which are used in the calculation scheme suggested by Currie (1991).

In theory, it is possible to calculate mole fractions of the end-member minerals by using analyses of amphiboles as source data and by assigning elements to A, B, C and T sites. However, this is an overwhelmingly difficult task since it requires complex and time-consuming calculations involving site occupancies and valances of elements. Another problem in this determination is to reduce results of microprobe analyses lacking H_2O and Fe^{3+}. To perform the recalculation of chemical analyses of

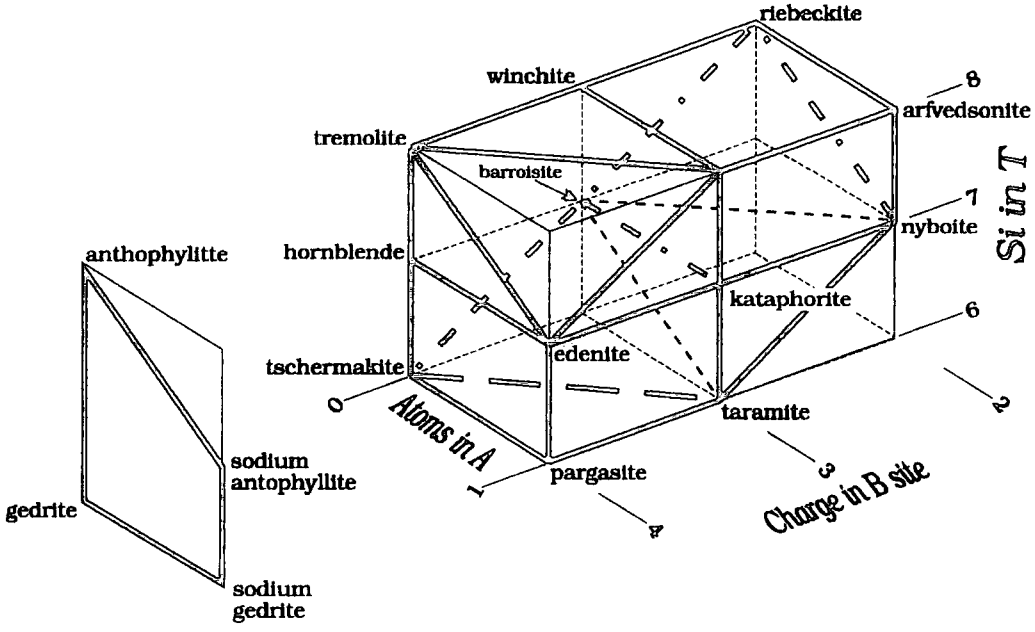

Figure: 4.11. Illustration of the compositional space of amphiboles based on their site occupancies in the amphibole formulae (Currie, 1991). In fact, each space may contain more than one end-member. Amphibole composition space is located between two plains as follows: edenite-tremolite-richterite and riebeckite-barroisite-tschermakite-taramite-nyboite.

amphiboles into their structural formulae and eventually to classify them according to the IMA scheme, Richard and Clarke (1990) and Currie (1991) developed computer programs. Currie's (1991) AMPHIBOLE program, which is written in BASIC and runs on IBM computers, starts from the composition of an individual amphibole and carries out site assignments of end-members followed by calculation of mole fractions based on these assignments. He argues that this assignment cannot be made in totally unambiguous fashion especially when it comes to reducing the results of electron microprobe analyses which lack H_2O and Fe^{3+}.

In this work, amphibole end-member mole fractions of a total of 57 electron microprobe analyses gathered from a subset of 21 representative samples have been calculated using Currie's (1991) software. The results together with electron microprobe analyses are presented in Appendix F.1. The mole fractions of main end-members of individual samples from a total of 8 volcanic units on the plateau are plotted in Figure 4.15 while average values for each unit are presented in Figure 4.12.

As is seen in Figures 4.12 and 4.15, amphibole phenocrysts of the Erzurum-Kars Plateau volcanics are made up mainly of five end-members as follows: barroisite, tschermakite, edenite, kaersutite and taramite. Variation between the phenocrysts of individual samples is minor and is mostly between different phenocrysts, except for samples MK36, MK90, MK261, MK337, MK318, MK133 and MK154. The relative abundance of barroisite changes between 0 and 25% among the volcanic units of the plateau with an average of 10% (Figure 4.15). It is at a maximum in the Ardıçlıdağ rhyolite (Pasinler) and absent in Paslı trachy-dacite (Kağızman). The most abundant end-member is represented by tschermakite whose abundance spans a range of 25-45% with an average of about 32%. Edenite is also an abundant end-member ranging from 8-10% to 30% with an average of slightly less than 20%. Kaersutite is a relatively less abundant end-member in amphiboles of the plateau. On average it is around 10% with a maximum percentage of 15. Interestingly, amphiboles from the Ardıçlıdağ rhyolite (Pasinler area) and Horasan plateau unit do not contain any kaersutite at all. The final end-member, taramite, constitutes 16-17% of the end-member compositions of average amphiboles and varies between 15-30% among different units on the plateau.

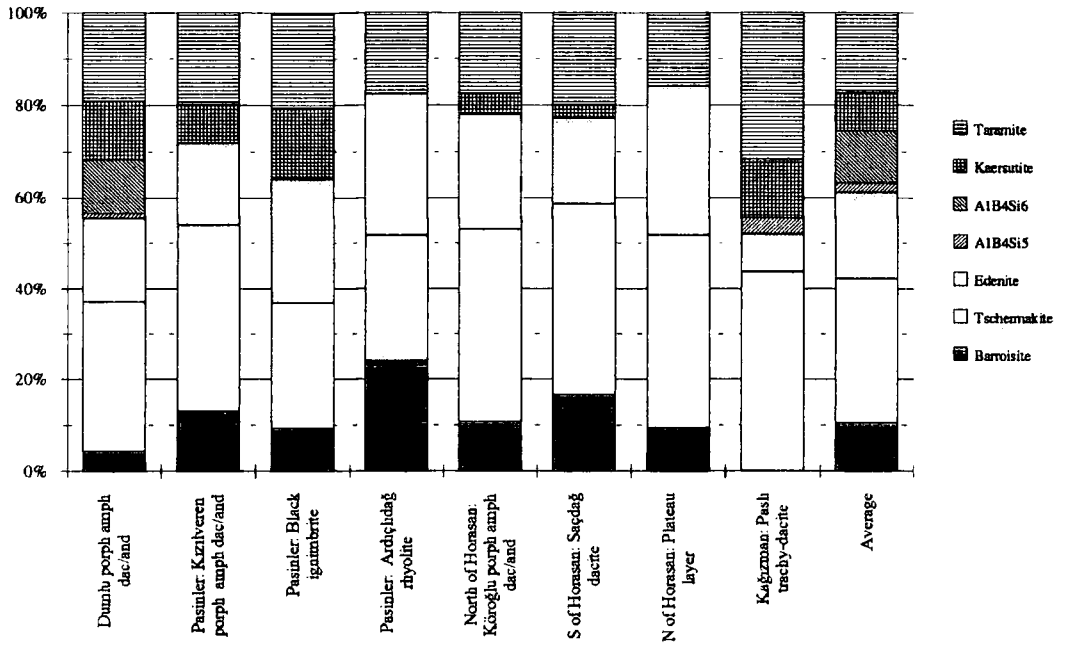

Figure: 4.12. Distribution of the average composition of amphibole phenocrysts in different units of the Erzurum-Kars Plateau.

Figure 4.16 illustrates the distribution of the relative abundance of more detailed end-members in different volcanic units on the plateau. Most notably, magnesio-types

of the end-members are very abundant compared to ferro-types with the exception of the Ardıçlıdağ rhyolite.

To make a comparison between the different classification schemes, the same data have been plotted on the classification diagram of Hawthorne (1981) (Figures

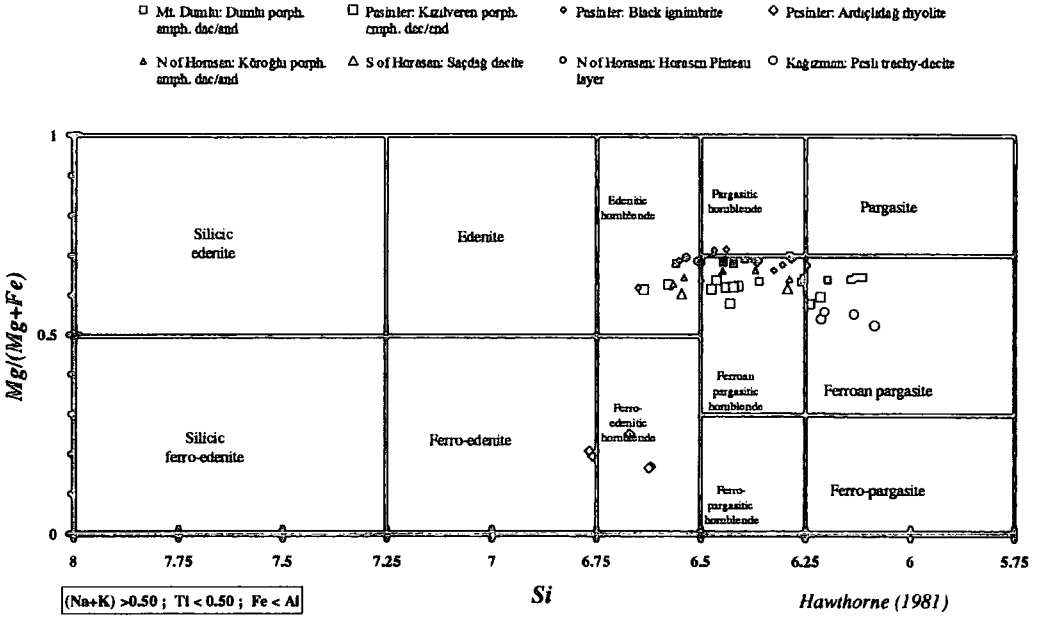

Figure: 4.13. Amphibole phenocrysts plotted on the classification diagram of Hawthorne (1981)

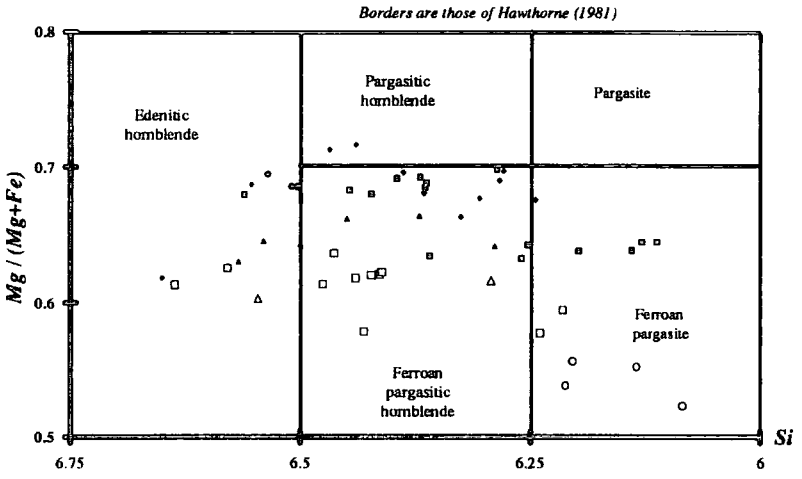

Figure: 4.14. Diagram displaying a zoomed view of Figure 4.13. Symbols are same as those of Figure 4.13.

4.13 and 4.14). According to Hawthorne's (1981) scheme, amphiboles predominantly classify as ferroan pargasitic hornblende, ferroan pargasite, partly edenitic hornblende and rarely pargasitic hornblende. In contrast, the composition of amphiboles from the Ardıçlıdağ rhyolite fall into a discrete area which in general

coincides with ferro edenitic hornblende and partly with ferro edenite. Strikingly, the main data appear to follow two closely located trends one having relatively high, the other low Mg/(Mg+Fe). These trends span a compositional area that includes edenitic hornblende, ferroan-pargasitic hornblende and ferroan pargasite. The high Mg/(Mg+Fe) trend is composed of the Dumlu amphibole dacite/andesite, the Black ignimbrite (Pasinler) and the Horasan plateau unit, whereas the low Mg/(Mg+Fe) trend includes the Kızılveren amphibole dacite/andesite, the Saçdağ dacite (S of Horasan) and the Paslı trachy-dacite (Kağızman) units. The Köroğlu amphibole dacite/andesite is transitional between these two trends. Figure 4.14 is a close-up diagram of Figure 4.13 which illustrates these trends in more detail.

Amphibole formula units of Ti, Al and Mg, normalised to 23 oxygen atoms, are plotted against the SiO_2 content of their host rocks in order to examine low and high Mg/(Mg+Fe) trends more closely (Figure 4.17). Amphiboles of the low Mg/(Mg+Fe) trend, in general, contain lower abundance of Ti and Mg than those of the high Mg/(Mg+Fe) trend. This might be interpreted as an indication of replacement of some of the pyroxene phenocrysts by amphiboles (as pseudomorphs) since pyroxenes contain lower concentrations of Ti, and Mg than amphiboles, resulting in lower concentration of these elements in transformed amphiboles.

In Figure 4.18, the distribution of the end-member compositions of each amphibole phenocryst is plotted against the SiO_2 content of its host-rock. As can be seen from the figure, mole fractions of amphibole end-members whose A, B and C sites are generally occupied by Na, Ca, Mg and Al (i.e. barroisite and edenite except for taramite) increase with increasing SiO_2 in accordance with the increase of these elements including Na in the melt with differentiation. Barroisite, edenite and kaersutite display a widespread scatter along the silica range of the melt from 63% to 69% showing a positive correlation with increasing SiO_2 (Figure 4.18-a and b). In contrast, mole fractions of tschermakite and taramite remain almost constant, at about 45-50% and 20-30% respectively, along the compositional range of SiO_2 from 63% to 69%. They decrease with differentiation between 69% and 70% SiO_2.

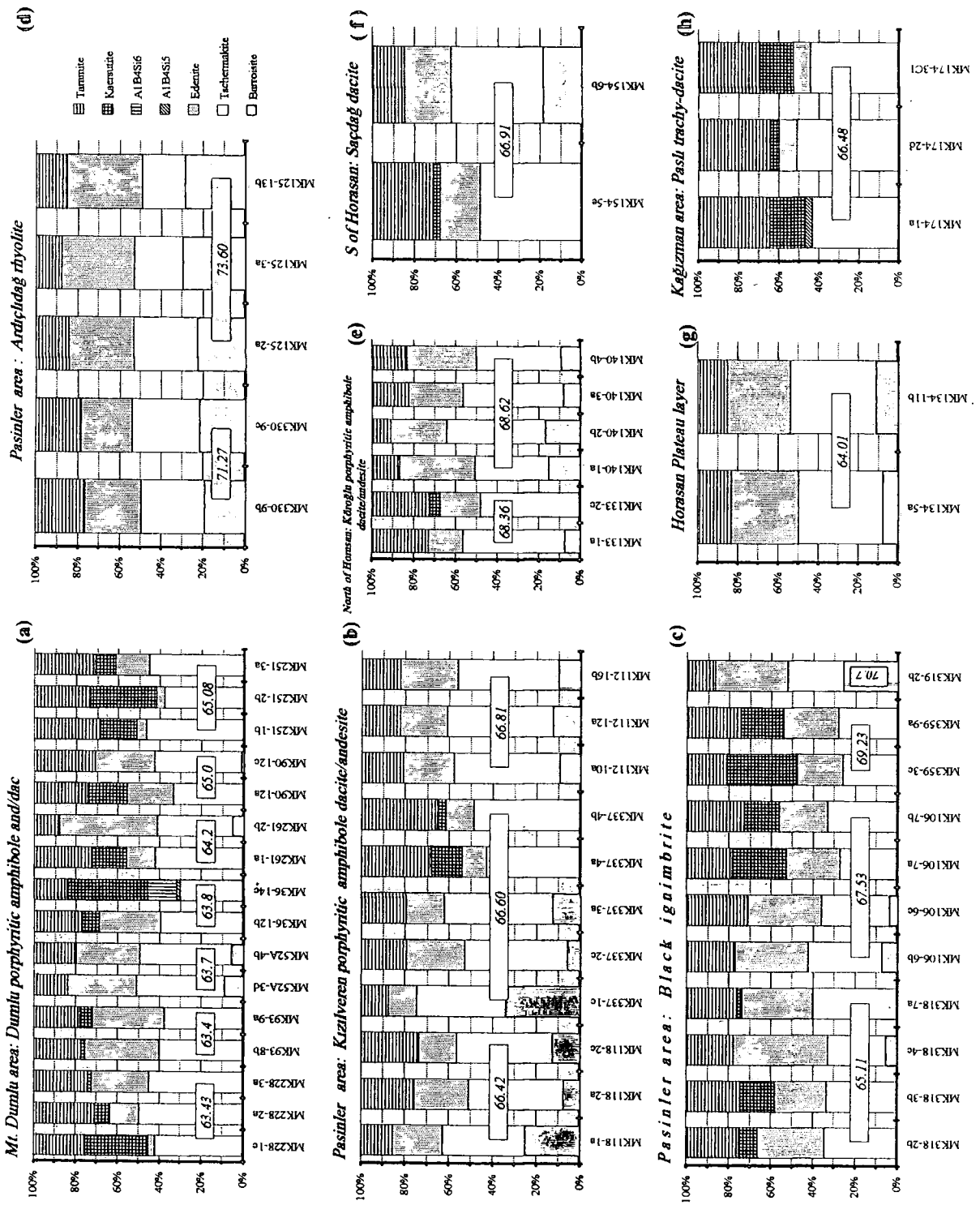

Figure: 4.15. End-member compositions of amphiboles of individual samples from differentand formations of the Erzurum-Kars Plateau Labels represent SiO2 wt.% content of whole rock samples.

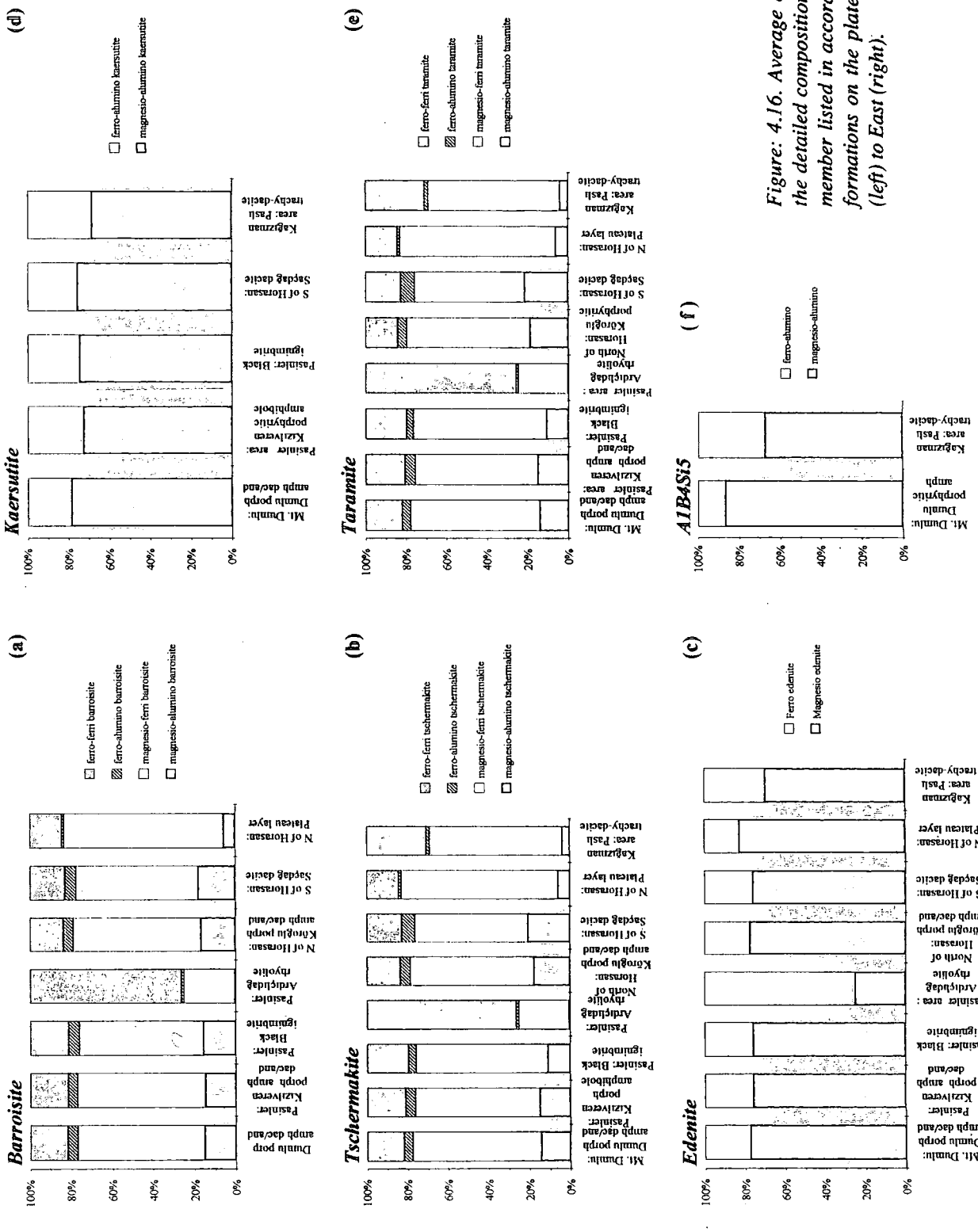

Figure: 4.16. Average distribution of the detailed composition of each end-member listed in accordance with the formations on the plateau from West (left) to East (right).

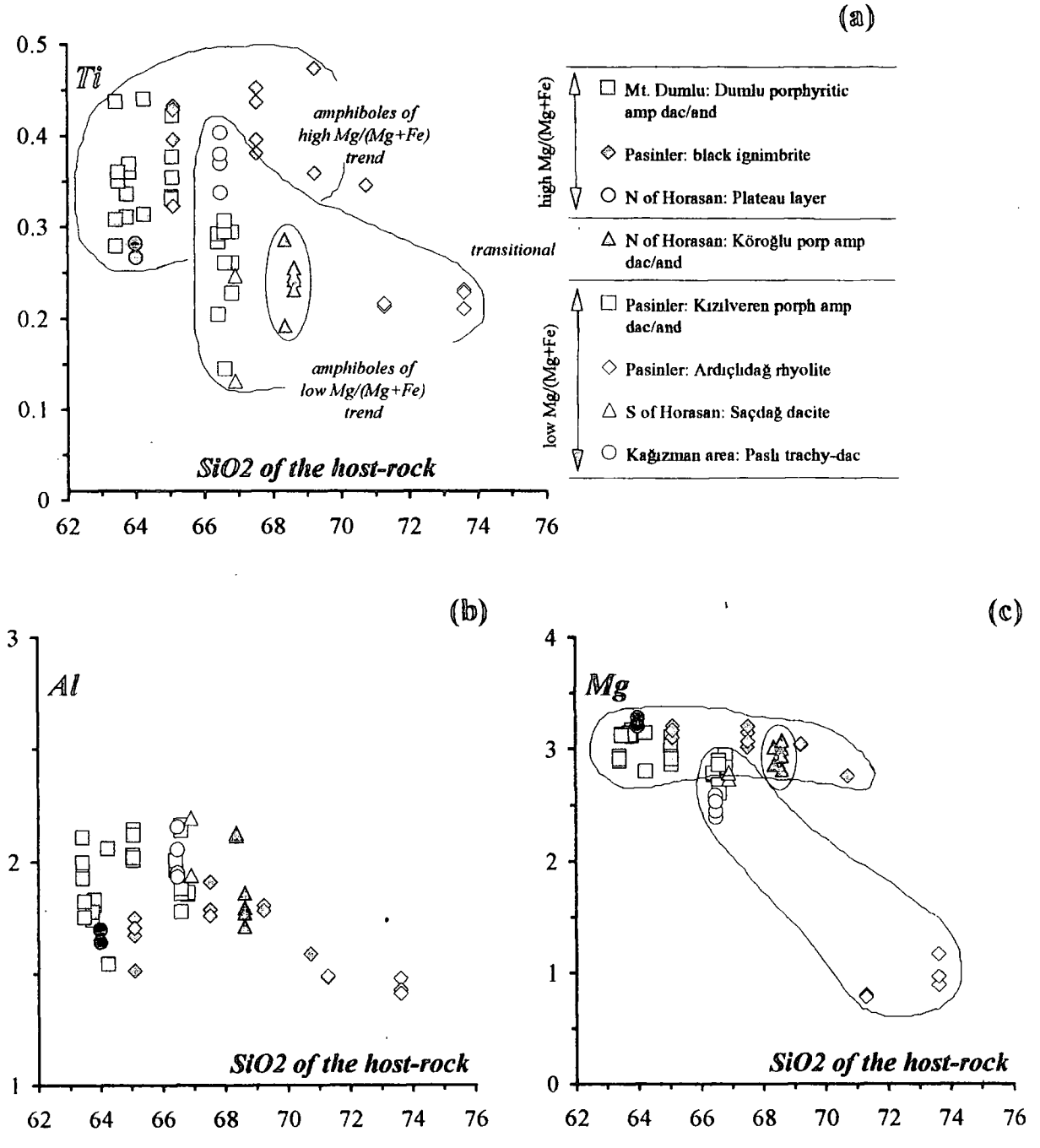

Figure: 4.17. Ti (a), Al (b) and Mg (c) molar ratios of amphiboles plotted against the SiO2 content of their host-rocks. Notably, volcanic units belonging to high and low Mg/(Mg+Fe) trends (figure 4.13 and 14) tend to plot close areas on the diagrams.

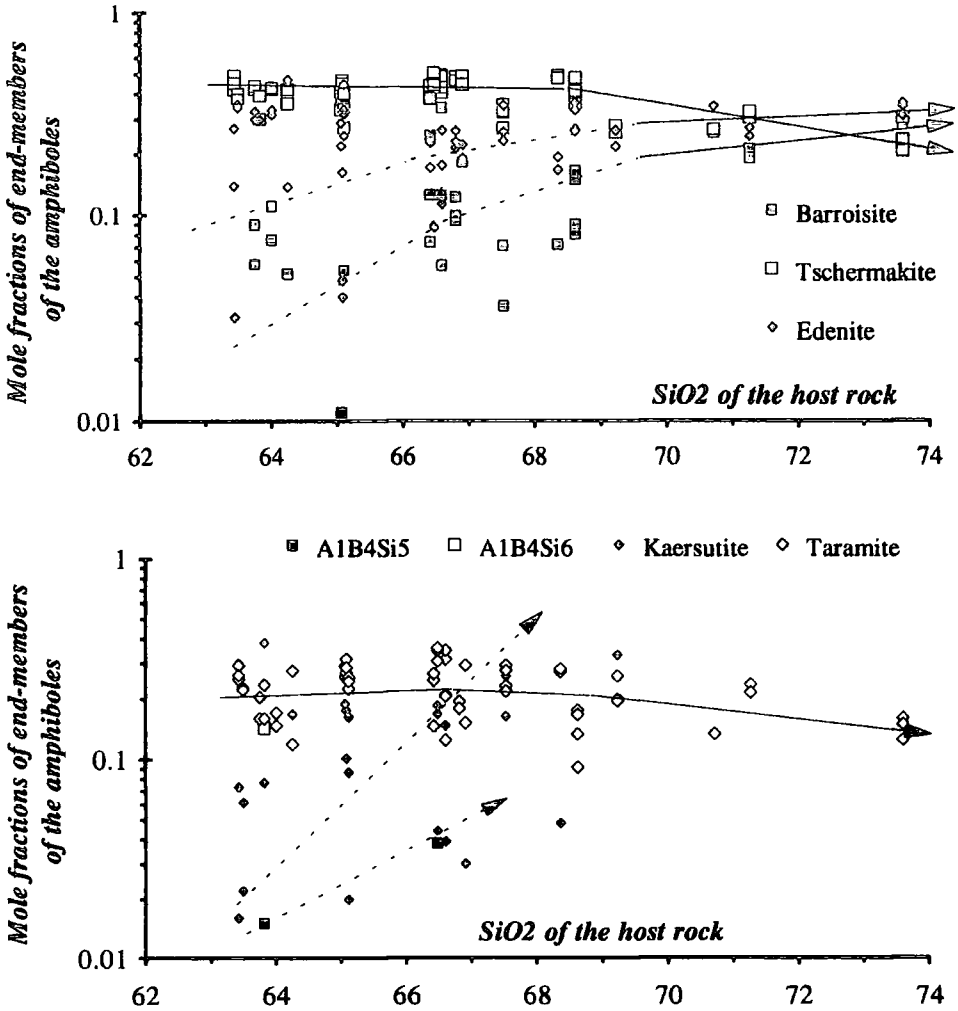

Figure: 4.18. Distribution of the end-member compositions of amphibole phenocrysts plotted against the SiO_2 content of their host-rocks.

4.1.4. Olivine

Olivine is a scarce phenocryst phase on the Erzurum-Kars Plateau. Generally, it occurs as micro-phenocrysts and micro-crystals in the groundmass of basaltic and basaltic-andesitic rocks. Apart from a few samples from the Güngörmez andesite/dacite in the Mt. Kargapazarı area, the only formations on the plateau which contain olivine are the Karapınar basalt(Mt. Kargapazarı), the Kargapazarı volcanics (Mt. Kargapazarı and Pasinler), the Horasan Plateau unit (north of Horasan), and the Kars plateau unit (north of Kağızman). These formations basically constitute the olivine-bearing plateau lavas differentiated earlier in the Stratigraphy Chapter (Table 2.1). Figure 4.19 illustrates that the distribution of the average composition of olivine from different formations occupies a relatively narrow range between chrysolite

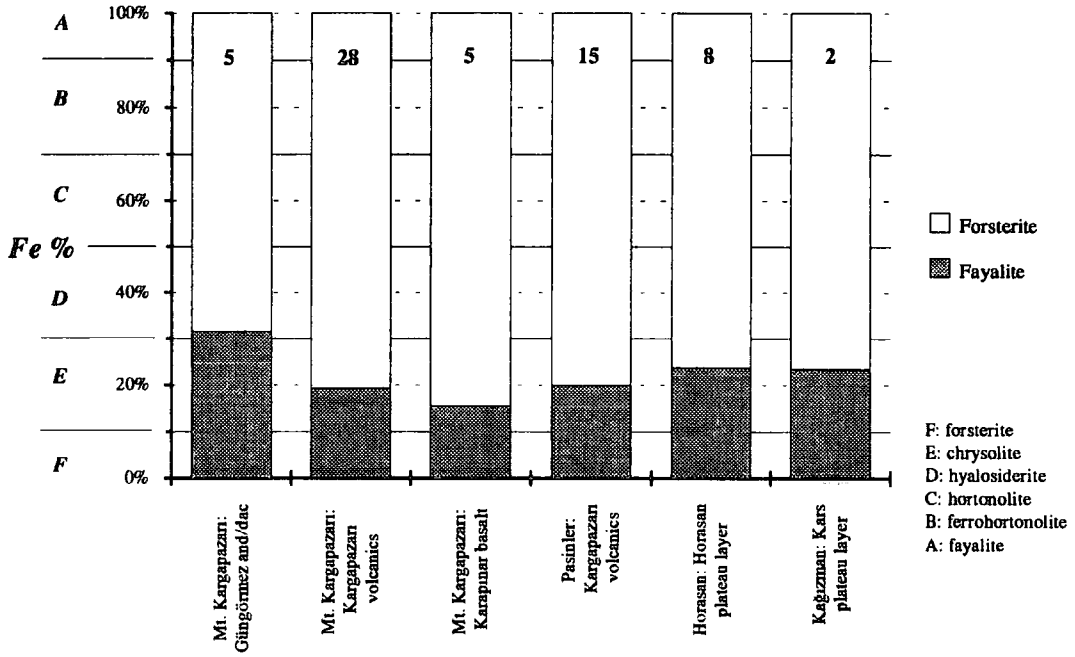

Figure: 4.19. Distribution of average composition of olivine phenocrysts, microphenocrysts and microcrysts from the different formations of the Erzurum-Kars Plateau.
(Forsterite (Fo): Mg_2SiO_4 ; Fayalite (Fa): Fe_2SiO_4). Numbers on the bars represent the number of point analyses from each unit.

(Fo_{85}) and hyalosiderite (Fo_{68}). The most forsterite-rich olivines come from Karapınar basalt in Mt. Kargapazarı area while the most fayalite-rich ones are from Güngörmez andesite/dacite. Figure 4.20 shows the composition of individual point analyses of olivines from different formations on the plateau in five parts. They are arranged according to the increasing SiO_2 content of the melt from left to right. The numbers on the labels presented on each bar represent the SiO_2 weight % of host-rocks.

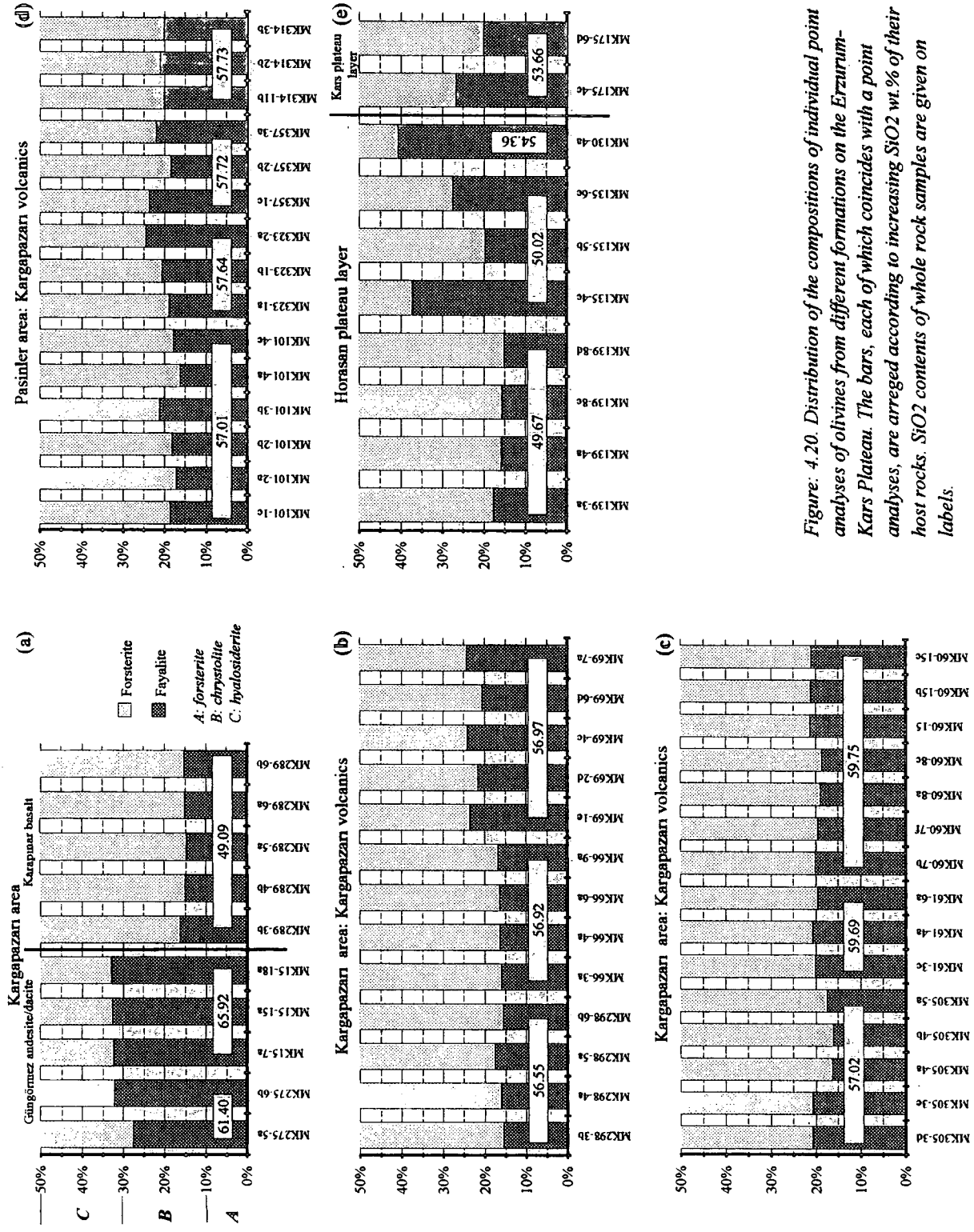

Figure: 4.20. Distribution of the compositions of individual point analyses of olivines from different formations on the Erzurum-Kars Plateau. The bars, each of which coincides with a point analyses, are arreged according to increasing SiO2 wt.% of their host rocks. SiO2 contents of whole rock samples are given on labels.

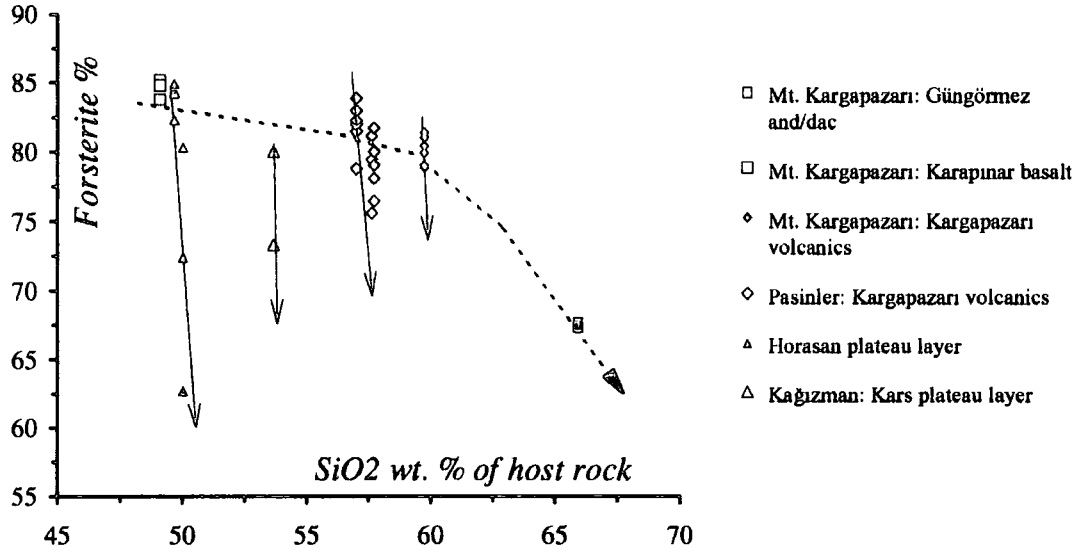

Figure: 4.21. Distribution of the composition of olivines plotted against SiO_2 content of their host-rocks.

Figure 4.21 shows the distribution of forsterite against silica content of the melt. Even though there is a wide scatter especially in data points of the Horasan plateau unit, Forsterite (Mg_2SiO_4) appears to decrease slightly in the SiO_2 between 48 and 60%. After 60% SiO_2 it decreases rapidly with fractionation.

4.2. Calculation of solidus pressures and temperatures using the chemical composition of minerals

In recent years, as a result of developments in experimental techniques, which enable researchers to simulate natural systems in the laboratory, several methods for calculating solidus pressures and temperatures of different minerals have been proposed. Some of these methods are accurate to approximately 20° to 30°C for geothermometry calculations and ± 0.5 kbar for geobarometry calculations. Four different geothermo-barometers have been applied to the samples from the Erzurum-Kars Plateau. These are:

4.2.1. The two-pyroxene geothermometer of Lindsley and Andersen (1983).

4.2.2. Amphibole-plagioclase geothermometers and geobarometers:
- 4.2.2.1. Al-in-hornblende barometer of Schmidt (1992)
- 4.2.2.2. Amphibole-plagioclase geothermometer of Blundy and Holland (1990).

4.2.3. Feldspar geothermometers
- 4.2.3.1. Calculations based on temperature dependence of Eu and Sr distribution coefficients of plagioclases (Sun et al., 1974)
- 4.2.3.2. Plagioclase thermometer of Kudo and Weill (1970)
- 4.2.3.3. Two feldspar thermometer of Seck (1971) and Brown and Parson (1981)

4.2.4. The oxygen-isotope thermometers: using $\delta^{18}O$ of cogenetic plagioclase, amphibole and biotite.

In the following paragraphs calculations carried out with respect to these methods will be presented followed by a comparison between these different methods using the same samples.

4.2.1. The two-pyroxene thermometry

The Ca content of high-Ca pyroxene (augite) decreases with increasing temperature, while that of the low-Ca phase (orthopyroxene or pigeonite) increases. This property has been used by some petrologists to determine temperatures of the formation of many igneous rocks. Calculation of the pyroxene end-members has critical importance because pyroxene-thermometer calculations rely on the precision of the end-member calculations.

Most of the two-pyroxene thermometers have been designed for pyroxene pairs whose compositions plot in the diopside-enstatite-hedenbergite-ferrosilite quadrilateral that is, wollastonite+enstatite+ferrosilite usually total 90% or more. These methods involve at least two steps, as follows: (1) projection onto the quadrilateral which is followed by (2) using the quadrilateral to determine crystallisation temperatures of the pyroxenes. The first attempts were made by Boyd (1969 and 1973), Wood and Banno (1973), Wells (1977), Saxena (1976), Mercier (1976) and Kretz (1982). Ishii (1975) developed a three pyroxene thermometer using augite + pigeonite + orthopyroxene. Lindsley (1983) showed that only the two-pyroxene thermometers of Kretz (1982), Lindsley and Andersen (1983) and Ross and Huebner (1979) were successful over a wide range of temperatures and pyroxene compositions. The most frequently used thermometers project the quadrilateral compositions to the diopside (Di) - enstatite (En) join and employ either a phase diagram or solution model for that join to yield temperatures (Lindsley, 1983). The most successful of all these thermometers is that of Lindsley and Andersen (1983). This uses an empirical projection scheme that approximates the activities of wollastonite (Wo), enstatite (En), and ferrosilite (Fs) in natural pyroxenes, thereby permitting the use of quadrilateral phase relations for thermometry.

Lindsley and Andersen (1983) estimated that the placement of the isotherms on the diagrams is accurate to approximately 20° to 30°C within the experimentally calibrated range. Lindsley (1983) indicates that, when possible errors in composition are taken into account, the thermometer is probably accurate to ±50°C for pyroxenes having low contents of non-quadrilateral components.

In this study a sub-group of 33 volcanic rock samples, which contain coexisting clino- and orthopyroxene phenocrysts and are representative of the different levels of the volcanic succession on the Erzurum-Kars Plateau, were selected for the pyroxene-thermometer calculations. A total of 200 points of pyroxene crystals (93 ortho- and 107 clinopyroxene) from these samples were analysed by a Geoscan Electron Microprobe, using the energy dispersive system at the University of Durham. Details of analytical procedures and conditions of analyses are presented in Appendix B. The data gathered were used to calculate the Wo-En-Fs parameters according to the projection scheme suggested by Lindsley and Andersen (1983). Calculations were performed on an IBM-PC computer using the PX program developed by Gómez (1990). Having completed the calculations, the data were plotted on the Di-En-Hd-Fs quadrilateral of Lindsley (1983) which is calibrated for 1 atmosphere pressure and contoured at 100°C intervals using these

Wo-En-Fs parameters. In fact, the use of low-pressure diagram for pyroxene phenocrysts is appropriate only if the host magmas resided and fractionated in relatively shallow magma chambers. However, pressures gathered from amphibole phenocrysts, following the scheme proposed by Schmidt (1992) (see section 4.2.2.1) varies between 3.5 and 7.5 kbar, with an average of 5.8 kbar, indicating a rather deep crystallisation story for that particular phase. In any case estimated pyroxene temperatures would be negligibly different at 5 kb, since there is only a slight difference between the contours of the diagrams calibrated for 1 and 5 kb. These diagrams are presented in Figure 4.23 and distribution of the pyroxene solidus temperatures for different levels of the volcanic succession is illustrated in Table 4.4. On these diagrams, both clino- and orthopyroxene compositions indicate similar temperatures; however, the much wider variation in Ca composition in clinopyroxene allows for more precise temperature estimates.

Figure 4.22 shows the distribution of two-pyroxene temperatures plotted against SiO_2 % of their host rocks. As can be seen on the diagram, there is a negative linear correlation between the pyroxene temperatures and SiO_2 content of the host rock indicating that acidity of the melt has a strong influence on the pyroxene temperatures. There seem to be two parallel trends on the diagram as low and relatively high temperature trends. The two-pyroxene temperatures for the low-

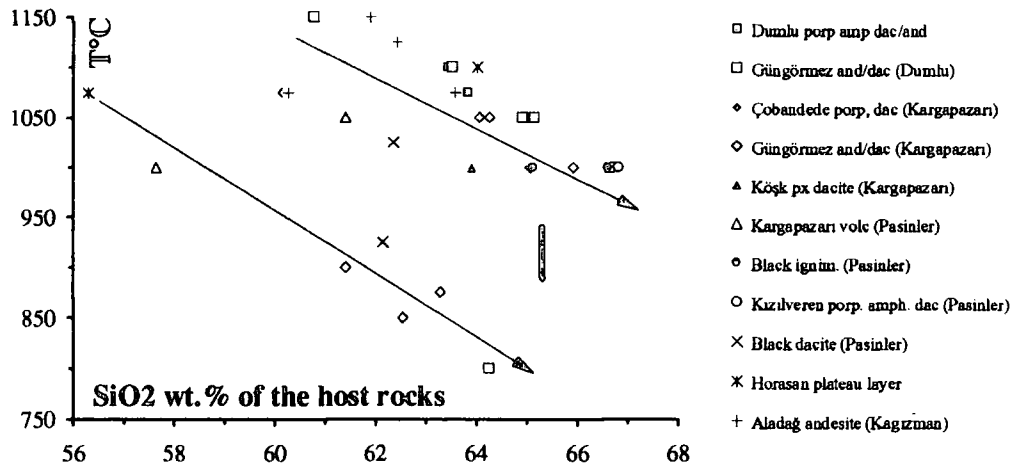

Figure: 4.22. Figure showing the distribution of two-pyroxene temperature of the volcanic units for different sub-areas and levels of the Erzurum-Kars Plateau. The accuracy of the thermometer (±50°C) is presented by a vertical line located between two trends.

temperature trend decrease from about 1075°C at 58% SiO_2 to 800°C at 65% SiO_2 while the temperatures for the high-temperature trend decrease from 1150°C to 975-1000°C in a silica range between 60-61 and 66-67 wt. % SiO_2. The low-temperature

trend, in general, belongs to the more calcic clinopyroxene microcrysts and micro-phenocrysts that generally make up groundmass, whereas the high-temperature trend predominantly consists of less-calcic clinopyroxene phenocrysts. Therefore, the lower temperatures may constrain the eruption temperature while the higher ones may indicate minimum liquidus temperatures. The temperatures listed in Table 4.4 are probably reasonable estimates for the crystallisation range. Given the probable ±50°C accuracy, a substantial amount of these estimates appear to be the same temperatures.

Table 4.4: Two pyroxene thermometer results of the samples from different levels of the volcanic succession on the Erzurum-Kars plateau.

Area	Y series	Formation	Sample no	Pyroxene thermometer
Mt. Dumlu	*low*	Dumlu amphibole dacite/andesite	MK251	1050°C
			MK228	1100°C
			MK36	1050-1100°C
			MK93	1100°C
	low	Güngörmez and./dac. (Upper lens)	MK217	1000°C
	low	Black dacite	MK50	1000-1100°C
	low	Arzutu amphibole dacite	MK261	800°C
	low	Güngörmez and./dac. (Lower part)	MK38	1150°C
			MK41	1100°C
	low	Güngörmez and./dac. (Lowermost part)	MK259	1050°C
Mt. Kargapazarı	*low*	Çobandede dacite	MK17a	950-1050°C
	low	Güngörmez andesite/dacite	MK15	950-1050°C
			MK21	800-950°C
			MK23	750-950°C
			MK83	1000-1100°C
			MK84	1000-1100°C
			MK90	900-1100°C
			MK98	1000-1150°C
			MK275	900°C
	low	Köşk pyroxene dacite	MK265	1000°C
Pasinler	*high*	Kargapazarı volcanics	MK323	1000°C
			MK310	1050°C
	high	Black ignimbrite	MK318	950-1050°C
			MK337	950-1050°C
	low	Kızılveren amphibole dacite/andesite.	MK112	1000°C
	high	Black dacite	MK116	1000-1050°C
			MK117	900-950°C
Horasan	*high*	Horasan plateau unit	MK131	1050-1100°C
			MK134	1000-1200°C
Mt. Aladağ	*high*	Aladağ andesite	MK147	1050-1200°C
			MK148	1150°C
			MK159	1050-1100°C
			MK166	1000-1150°C

Figure: 4.23. Diagrams showing the liquidus temperatures of pyroxenes which are plotted on the Di-En-Hd-Fs quadrilateral of Lindsley (1983) that is calibrated for 1 atmosphere pressure and contoured at 100°C intervals.

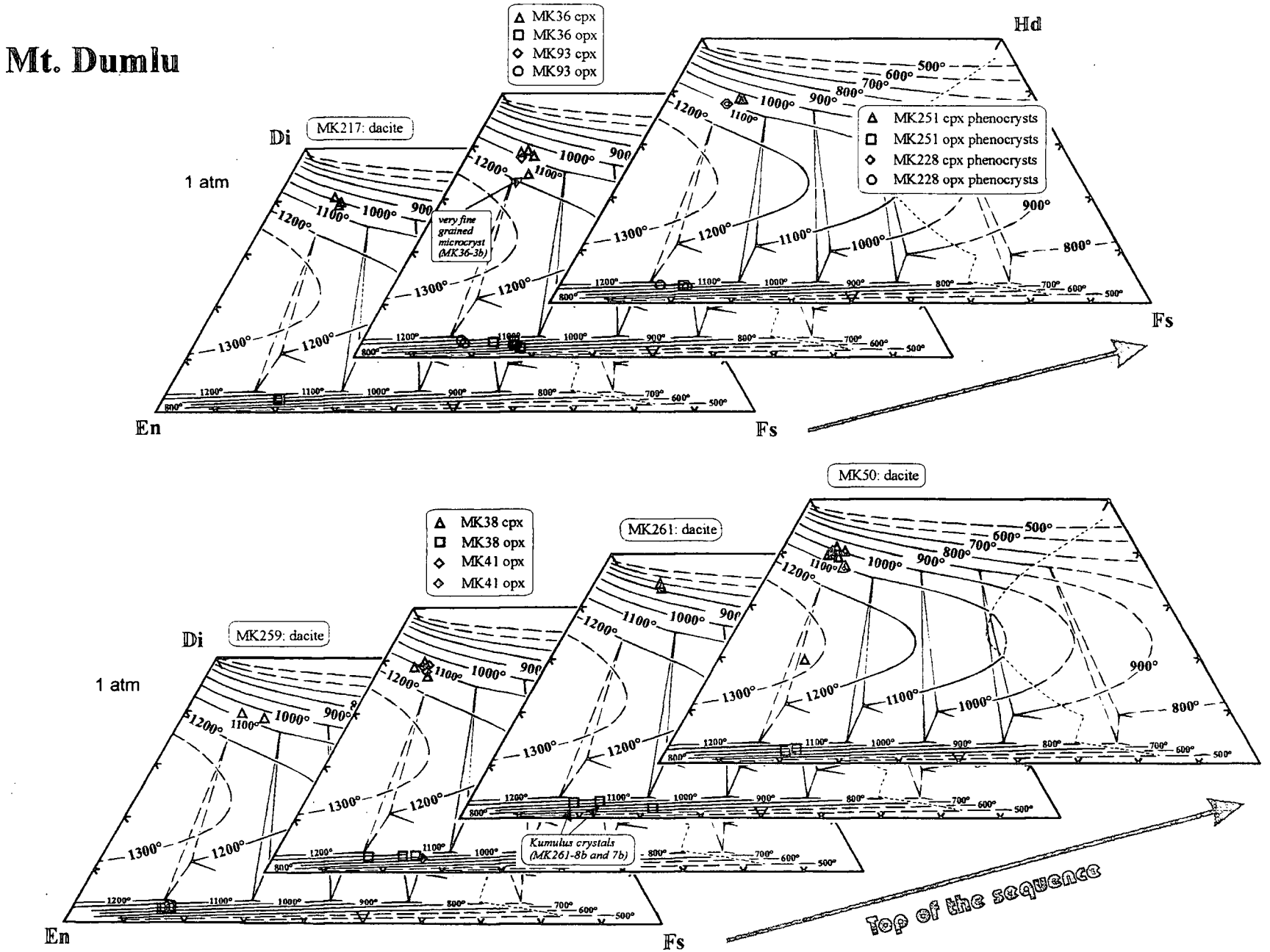

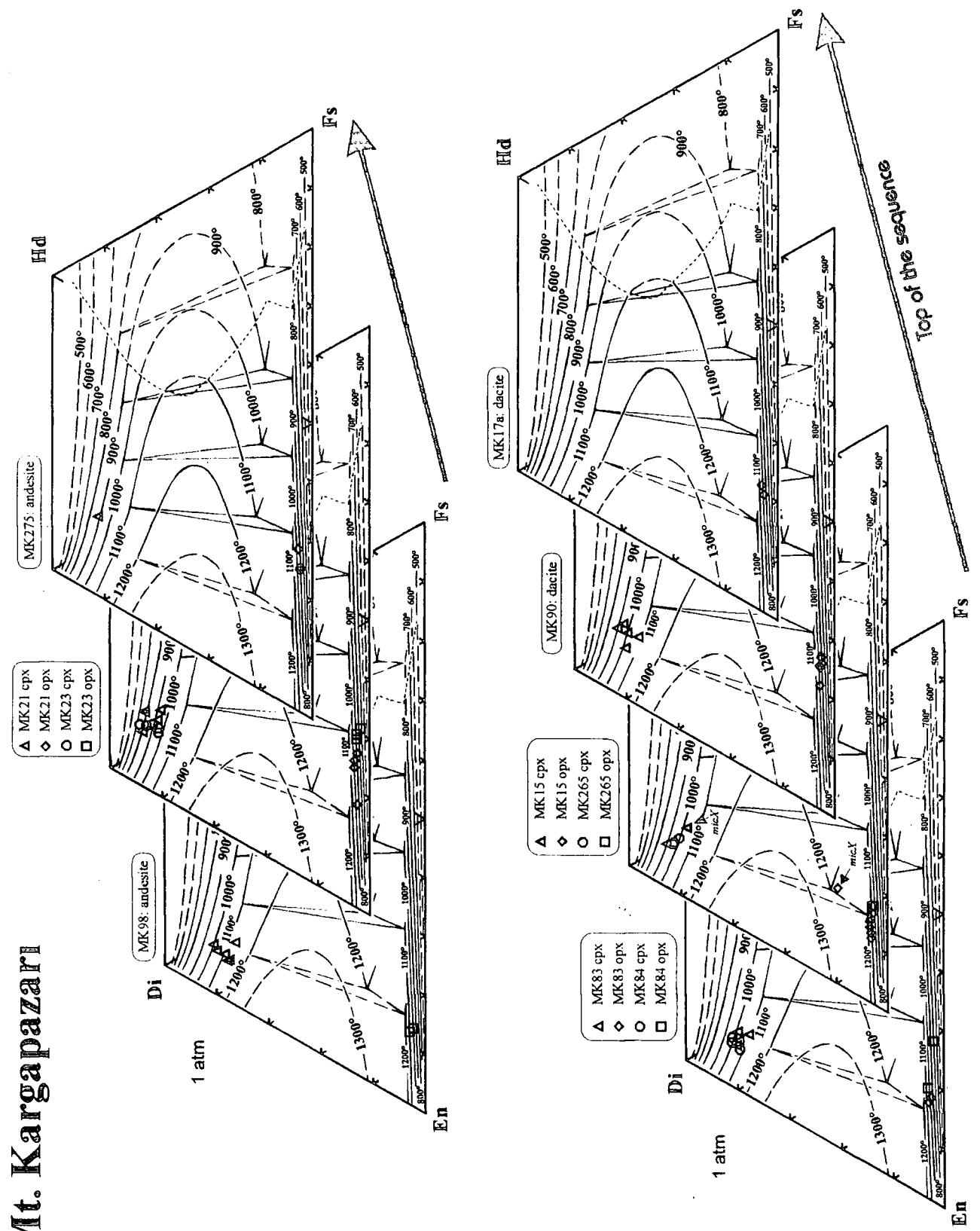

Figure: 4.23. (continued)

Figure: 4.23. (continued)

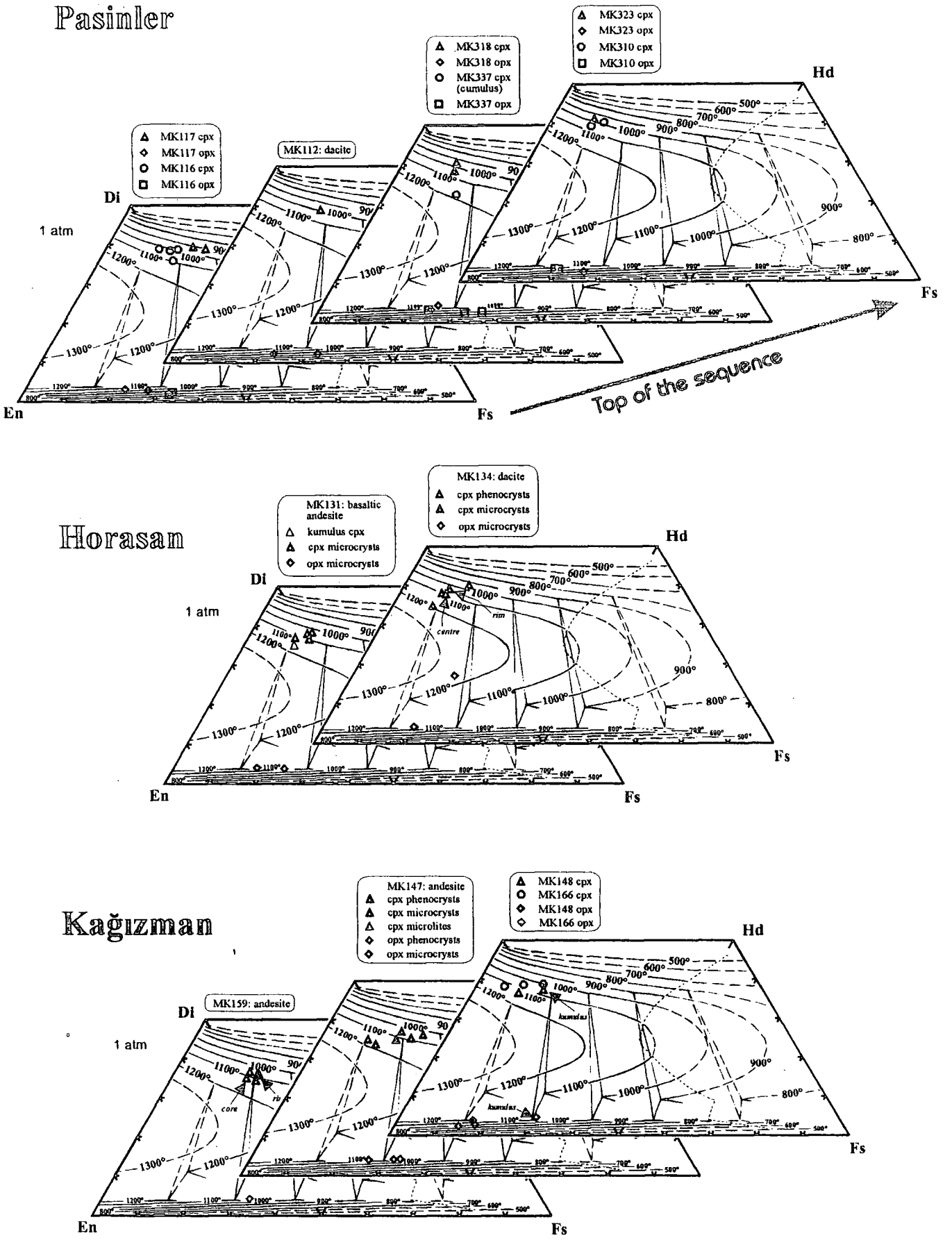

4.2.2. Amphibole-plagioclase geothermometer and geobarometer

4.2.2.1. Al-in-hornblende barometer

The linear increase in Al^{tot} content of magmatic hornblende with pressure and its usability as a geobarometer were first discussed by Hammarstrom and Zen (1986). These authors proposed the empirical calculation, presented in equation 1. By using a bigger data set, Hollister et al. (1987) produced a better calibration with a reduced error (equation 2). Johnson and Rutherford (1989) also performed an experimental calibration at high temperatures (equation 3). More recently, Schmidt (1992) experimentally calibrated Al^{tot} of magmatic hornblende under water-saturated conditions at pressures of 2.5-13 kbar and temperatures of 700-655°C (equation 4).

$$P(\pm 3\ \text{kbar}) = -3.92 + 5.03\ Al^{tot} \qquad r^2 = 0.80 \qquad \text{(Eq. 1)}$$

$$P(\pm 1\ \text{kbar}) = -4.76 + 5.64\ Al^{tot} \qquad r^2 = 0.97 \qquad \text{(Eq. 2)}$$

$$P(\pm 0.5\ \text{kbar}) = -3.46 + 4.23\ Al^{tot} \qquad r^2 = 0.99 \qquad \text{(Eq. 3)}$$

$$P(\pm 0.6\ \text{kbar}) = -3.01 + 4.76\ Al^{tot}_{hbl} \qquad r^2 = 0.99 \qquad \text{(Eq. 4)}$$

In the formulae above, Al^{tot} is the total Al content of hornblende in atoms per formula unit. According to Schmidt (1992), one point which should be taken into account is that as the pressure calculated from hornblende composition is indirectly also a function of fluid composition, any indications of fluid should be carefully considered. Furthermore, Blundy and Holland (1990) argue that the existence of sub-solidus re-equilibration and patchy amphibole zoning (especially in plutonic rocks) may cast doubt upon the assumption on which these barometers are based.

In this study, 57 point analyses by electron microprobe at Durham University were carried out on a subset of 21 representative amphibole-bearing samples. These were selected from a total of 8 volcanic units on the plateau (Table 4.5). Solidus pressures for these minerals were then calculated by applying Schmidt's (1992) equation to the data set. The calibration line between Al^{tot} and pressure, and the distribution of solidus pressures between different units on the Erzurum-Kars Plateau, are illustrated in Figures 4.24 and 4.25 respectively. Most notably, porphyritic amphibole-bearing units i.e. the Dumlu (Mt. Dumlu), the Kızılveren (Pasinler area), the Köroğlu amphibole-andesite/dacite (North of Horasan) and also the Paslı trachy-dacite (Kağızman area) all have considerably higher solidus pressures. These are in the range of 5.5-7.5 kbar, compared to the other units on the plateau i.e. the Ardıçlıdağ rhyolite (3.5-4 kbar) and the Horasan plateau unit (4.5-5 kbar). The solidus pressures of amphibole crystals vary in each volcanic formation as presented in Table 4.5. Some rock samples contain both high and low pressure

crystals (e.g. MK228, MK251 and MK337). This may be ascribed to at least two phases of amphibole crystallisation at different depths since it is believed that these differences are not related to analytical errors.

Area	Pressure (kb)	Sample no
Mt. Dumlu area	⇓	⇓
Dumlu amphibole dac/and (low-Y; *CA*)	6.8 - 7.2	MK261 MK251* MK228*
	6.5 - 6.7	MK90 (MK228*) (MK251*)
	5.3 - 5.7	MK36 MK52A MK93
Pasinler area	⇓	⇓
Kızılveren amphibole dac/and (low-Y; *CA*)	7.1 - 7.3	MK337*
	6.3 - 6.5	MK118
	5.5 - 5.9	MK112 MK337*
Black ignimbrite (high-Y; *AC*)	5.6 - 5.5	MK359 MK106
	4.1 - 5.3	MK318 MK319
Ardıçlıdağ rhyolite (high-Y; *AC*)	3.7 - 4.1	MK125 MK330
Horasan area	⇓	⇓
Köroğlu amphibole dac/and (low-Y; *CA*)	7.1	MK133
	5.1 - 5.9	MK140
Horasan plateau unit (high-Y; *CA*)	4.8 - 5.1	MK134
Saçdağ dacite (low-Y; *CA*)	6.2 - 7.3	MK154
Kağızman area	⇓	⇓
Paslı trachy-dacite (high-Y; *AC*)	6.2 - 7.3	MK174

Table: 4.5. Table displaying the crystallisation pressures of amphibole phenocrysts collected from a total of 8 volcanic units on the Erzurum-Kars Plateau. '' sign indicates the samples those contain both high and low pressure amphibole phenocrysts.*

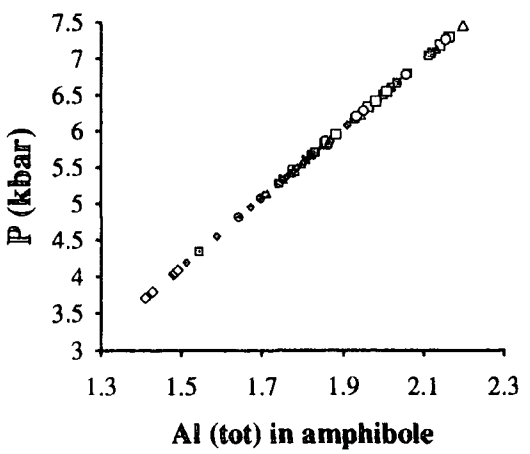

Figure: 4.24. Total Al contents of amphibole pheno-crysts plotted versus calculated solidus pressures (kbar). Key symbols are the same as presented in Figure 4.27.

Using these pressure results, it is possible to calculate the depth of the magma chamber in which the amphibole fractionation took place, based on the assumption that the hydrostatic pressure in the chamber was equal to the lithostatic pressure. The density of the overlying column is of special importance for this calculation, because the pressure is directly related to the density as

related to the density as can be seen in the following equation:

$$P = h\rho g \qquad \text{(Eq. 4)}$$

where

P: is the pressure in Pa, *ρ: is the density of the overlying column (kg.m^{-3})*

h: is the depth in m *g: the acceleration due to gravity (9.80665 m.s^{-2})*

The overlying column should be represented predominantly by the continental crust which is theoretically supposed to be made up of granitic-type material (ρ=2600-2700 kg.m^{-3}) if the assumed thickness of the continental crust in Eastern Anatolia of about 50 km is taken into account. On the other hand, it is apparent that the crust in the region cannot be considered completely homogeneous since it is known to contain considerable volumes of ophiolitic rock and ophiolitic mélange material. However, it is almost impossible to add this variable to the calculation since we do not have any

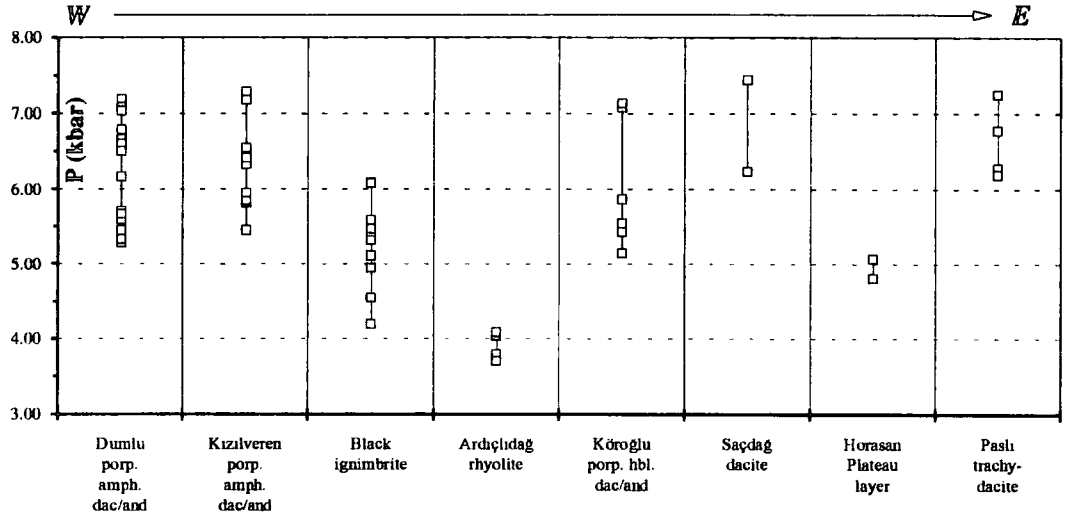

Figure: 4.25. Distribution of solidus pressures of amphibole phenocrysts from the different levels of plateau from the west (left) to the east (right).

reliable information about the relative volume of denser ophiolitic material in the crust. Therefore, the density of the overlying column is presumed to be around 2700 kgm^{-3} which is close to that of continental crust (2600-2700 kgm^{-3}). Equation 4 can be converted into

$$h\ (\text{km}) = \frac{P\ (\text{pascal})}{\rho\ (\text{kg.m}^{-3}) \times g\ (\text{m.s}^{-2}) \times 10^3} = \frac{P \times 10^8\ (\text{kbar})}{2700 \times 9.80665 \times 10^3} \qquad \text{(Eq. 5)}$$

$$h = \frac{P}{0.2648} \qquad h \text{ is in km} \qquad \text{(Eq. 6)}$$

The depth of amphibole fractionation of different units from different areas on the plateau has been calculated based on the above equation and the results are presented in Figure 4.26. On this diagram the amphibole bearing porphyritic lava

units which coincide with the low-Y series dominantly plot into a depth range approximately between 19-28 km. In contrast, volcanic units of the high-Y series display relatively shallow depths except for the Paslı trachy-andesite (Kağızman area). The Ardıçlıdağ rhyolite and the Horasan plateau unit span much narrower ranges, between 14-15.5 and 18-19 km respectively while the Black ignimbrite covers a range between 16 and 23 km. The Paslı trachy-dacite (Kağızman area) plots in a much deeper range between 23.5-27.5 km compared to the other units of high-Y series. It should be emphasised again that these calculations rely on the estimate of

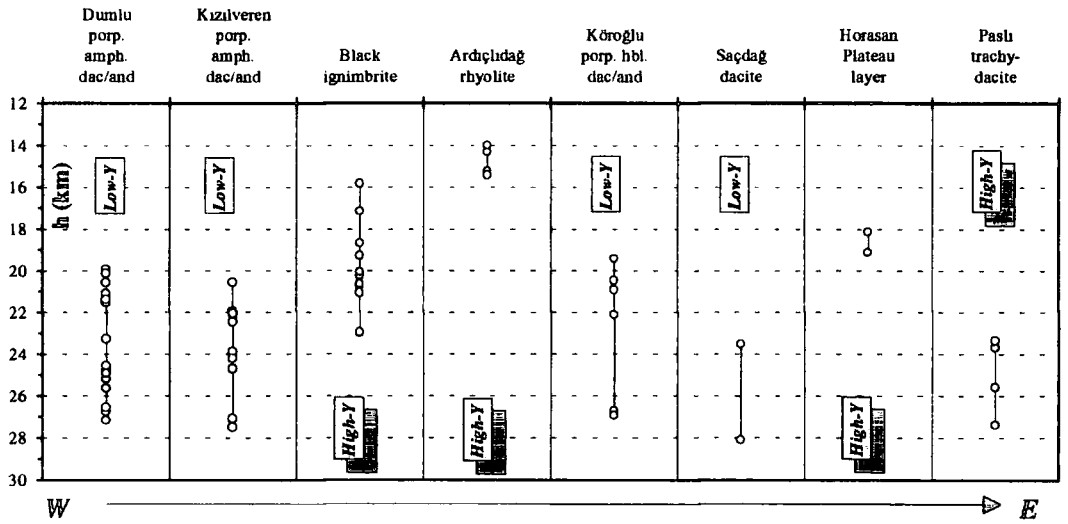

Figure: 4.26. The diagram showing the depth of crystallisation of amphibole crystals from different parts and units of the plateau. They are arranged from west (left) to east (right).

the density of the lithosphere and also on the accuracy of the chemical analyses. For instance, a slight increase in the density dramatically decreases the depth. Therefore, they should be considered as internally-consistent, broad approximations to the reality and probably maximum estimations of the depth of amphibole fractionation.

4.2.2.2. Amphibole-plagioclase geothermometer

Experimental studies carried out using a wide range of starting materials and a wide range of pressures and temperatures have proven that amphibole has the important potential for indicating crystallisation conditions. However, their compositional complexity has restrained their use as geothermometers and barometers. As Hammarstrom and Zen (1992) discussed, formulations of thermobarometers involving amphiboles are inherently problematic because of the theoretical handicap of using a single equation to relate two intensive variables, P and T, to measured compositions. Therefore, to date, there are few publications on thermometric applications of amphibole compositions. Most of these papers concentrate on the use of amphibole stability in the calculation of crystallisation

temperature of metamorphic amphiboles (e.g. Holland and Richardson, 1979; Graham and Powell, 1984). Nabelek and Lindsley (1985) are the first researchers to propose a preliminary empirical calibration of a hornblende-plagioclase thermometer. More recently, Blundy and Holland (1990) have suggested a new amphibole-plagioclase geothermometer by using their experimental data on amphiboles together with the data gathered from several previously published articles. Their semi-empirical thermodynamic model uses the Al^{iv} content of amphibole coexisting with plagioclase in silica-saturated rocks as the main parameter, since they believe that the aluminium content of hornblende is a strong function of temperature. Blundy and Holland (1990) have analysed the data using three different amphibole activity models to calibrate the thermometer reactions and obtained equations 7 and 8. These model reactions are:

edenite + 4 quartz = tremolite + albite
pargasite + 4 quartz = hornblende + albite

According to the authors, the thermometer is tolerant of ferric iron recalculation procedures from electron-probe data and should yield temperatures of equilibration for hornblende-plagioclase assemblages with uncertainties of about ±75°C (2σ) over a equilibration temperature range of 500°-1100°C. The thermometer should only be used in this temperature range for assemblages with plagioclase less calcic than An_{92} and with amphiboles containing less than 7.8 Si atoms. The equations are:

$$T = \frac{0.677P - 48.98 + Y}{-0.0429 - 0.008314 \ln K} \qquad \text{(Eq. 7)}$$

and

$$K = \left(\frac{Si - 4}{8 - Si}\right) X_{Ab}^{Plag} \qquad \text{(Eq. 8)}$$

where:

Si: is the number of Si atoms per formula unit in amphiboles,
P: is the pressure in kbar,
T: is the temperature in K (Kelvin),
Y: represents plagioclase non-ideality
Y=0 for $X_{Ab} > 0.5$ and $Y=-8.06+25.5(1-X_{Ab})^2$ for $X_{Ab} < 0.5$

As seen from the formulation, the required input variables are pressure, Ab content of coexisting plagioclase and the atomic Si content of the amphibole.

Blundy and Holland (1990) have deduced that the Al-in-hornblende geobarometers of Hammarstrom and Zen (1986), Hollister et al. (1987), Johnson and Rutherford (1989) and Schmidt (1992) are subject to considerable uncertainty unless the equilibration temperature is well known. They also added that Al^{iv} in these

amphiboles is strongly temperature-dependent and that this dependency masks any pressure effect, although a weak pressure correlation is evident.

Blundy and Holland's (1990) paper has become the focus of a series of theoretical discussions by researchers who work in this field. Recently, a number of comment and reply papers evaluating Blundy and Holland's (1990) paper have been published. In one of these papers, Hammarstrom and Zen (1992) have tested Blundy and Holland's geothermometry on representative samples of tonalites and granodiorites and concluded that the hornblende geobarometer is temperature-independent. They also criticised the Blundy and Holland's proposed equilibria (edenite + 4 quartz = tremolite + albite; pargasite + 4 quartz = hornblende + albite) claiming that it may not account for all the pressure-sensitive compositional variations in calcic amphiboles. They chose not to use Al^{iv} content alone, which was the main component in Blundy and Holland's (1990) paper, in formulating their barometer because, its computation is so dependent on the mineral formula calculation scheme chosen. Rutherford and Johnson (1992) suggested that the strong "temperature effect" is also the result of increased SiO_2 activity. They based this suggestion on experiments at successively greater degrees of crystallisation than those on which Blundy and Holland (1990) have based their formulation. Hornblende tetrahedral sites are occupied only by Si and Al cations, and the Al^{iv} abundance is clearly a function of both Al_2O_3 and SiO_2 activities. They have cited Spear's (1981) paper as an example in which this effect is well demonstrated. Spear (1981) found that the Si occupancy in amphibole crystallised from basalt increased by 20 % (0.8-1.0 per formula unit) when SiO_2 saturation was forced on the system. Rutherford and Johnson (1992) argue that, even though Blundy and Holland (1990) recognised the importance of SiO_2 activity, they did not hold it constant or quantified in their experimental calibration. According to Rutherford and Johnson (1992), if variations in silica activity are not considered, the geothermometer is really an expression of the combined effects of T and SiO_2 activity. In addition to these comments, Poli and Schmidt (1992) have also criticised Blundy and Holland's (1990) theoretical approach in interpreting of amphibole crystal chemistry.

In this study, Blundy and Holland's (1990) equation has been applied to 57 electron micro probe analyses, from a subset of 21 samples, whose coexisting plagioclase phenocrysts had also been analysed for which solidus pressures had previously been calculated using Schmidt's (1992) equation (Table 4.5). Non of these amphibole phenocrysts have more than 7.8 Si atoms per formula unit nor are the coexisting plagioclase phenocrysts more calcic than An_{92}, satisfying all prerequisites for the calculation. Since geothermometer calculations of some of these samples are

also conducted using three other different methods, this presents a good opportunity to correlate the results of these methods with Blundy and Holland's (1990) method.

Figure 4.27 demonstrates the relationship between the distribution of solidus temperatures of amphibole phenocrysts and the SiO_2 content of their host rocks. Notably, solidus temperatures decrease with increasing SiO_2 content of magma from 925°C at 63% SiO_2 to 700°C at 74% SiO_2 emphasising the importance of composition of magma on crystallisation temperatures. Figure 4.28 shows a positive linear correlation between the solidus temperatures and pressures. These results should be interpreted with caution because some plagioclases are not in equilibrium with melt and hence they may not be in equilibrium with amphiboles.

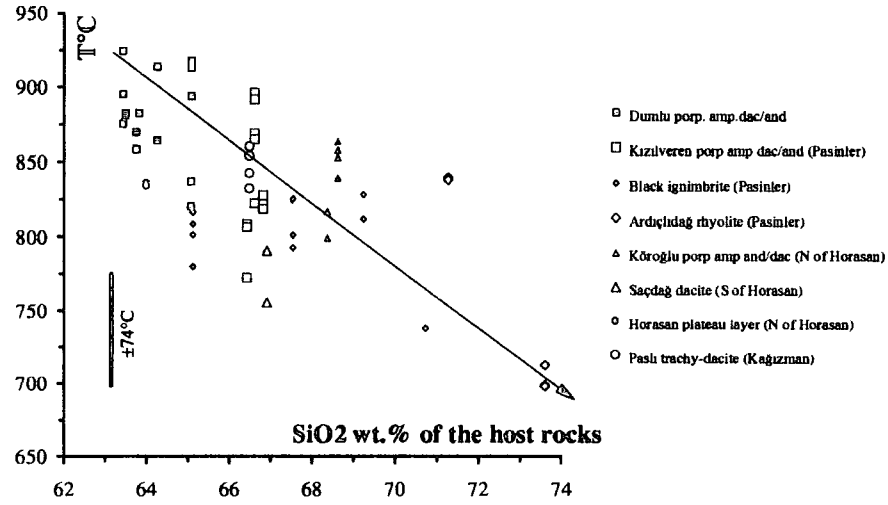

Figure: 4.27. Distribution of geothermometer calculations of amphiboles from different units and areas of the plateau plotted against SiO_2 contents of their host rocks.

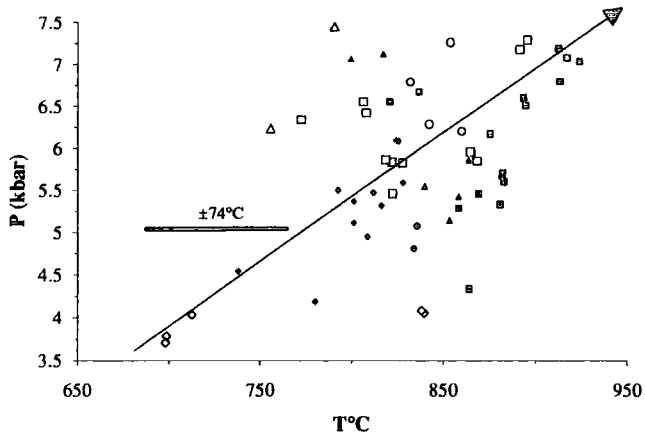

Figure: 4.28. Diagram illustrating a positive correlation between liquidus pressures and temperatures of amphibole phenocrysts calculated by using Schmidt's (1992) and Blundy and Holland's (1990) formulations respectively. Key symbols are the same as presented above in Figure 4.27.

4.2.3. Feldspar geothermometers

4.2.3.1. Calculations based on the temperature dependence of Eu and Sr distribution coefficients in plagioclases

Distribution coefficients are not only a function of bulk composition but also functions of temperature, pressure and oxygen fugacity of a melt system. In order to understand the effects of these controlling factors some researchers carry out experimental studies in which synthetic or natural starting materials are doped with the element of interest. The advantage of this approach is that variations in the physical conditions of the system (i.e. temperature, pressure and oxygen fugacity) can be more adequately monitored. In such a study Sun et al. (1974) experimentally investigated the distribution coefficients of Eu and Sr for plagioclase-liquid and clinopyroxene-liquid pairs, as a function of temperature and oxygen fugacity, using an oceanic ridge basalt enriched with Eu and Sr as the starting material. They conducted their laboratory experiments between 1190° and 1140°C over a range of oxygen fugacities between 10^{-8} and 10^{-14} atm. One of the most interesting findings from their study was that distribution coefficients for Sr were strongly dependent upon temperature but independent of oxygen fugacity, a feature that enabled researchers to use these values in their calibrations for geothermometer calculations. They used linear regression to derive the following equations:

$$\log D_{Sr}^{PL} = \frac{(6570 \pm 300)}{T} - (4.30 \pm 0.21) \qquad \text{(Eq. 9)}$$

$$\log D_{Sr}^{CPX} = \frac{(18430 \pm 2140)}{T} - (13.62 \pm 1.49) \qquad \text{(Eq. 10)}$$

According to the authors, the standard deviations about the mean of ΔT ($\Delta T = T_{calculated} - T_{measured}$) are around ±10°C at the 2σ level. Therefore, they claim that these equations can define geothermometers of very high precision. Sun et al. (1974) also proposed the following equation related to the distribution coefficient of Eu:

$$\log D_{Eu}^{PL} = \frac{(2460 \pm 930)}{T} - (0.15 \pm 0.01)\log f_{O_2} - (3.86 \pm 0.65) \qquad \text{(Eq. 11)}$$

This equation may give important information on the oxidation conditions of the magma in which plagioclase fractionation takes place.

In this study, the crystallisation temperature of plagioclase phenocrysts and the oxygen fugacity of magma from which these crystals grew are calculated using Sun et al.'s (1974) equations and previously defined Sr and Eu mineral/melt (matrix) partition coefficients of eight plagioclase mineral separates. The results are presented

in Table 4.6 (see section 4.3.1 for the calculation of K_d values). The temperatures display a rather narrow range between 1040°-1120°C while oxygen fugacities span a range between 10^{-12} and $10^{-14.7}$ atm. Table 4.6 also illustrates two-pyroxene temperatures for three samples which have been calculated using the composition of coexisting ortho- and clinopyroxene crystals following the Lindsley and Andersen (1983) method. Except for sample MK277, both methods produce consistent results with just a maximum of 44°C difference.

Some of the plagioclase phenocrysts of the low-Y series (all samples except MK277 and MK174) appear to be not in equilibrium with matrix perhaps due to magma mixing between dacitic and basic magmas at depth (Section 4.1.1). Therefore, calculations based on the temperature dependence of Eu and Sr distribution coefficients of plagioclases should be interpreted with caution (Section 4.3.1). On the other hand, close agreement between the two pyroxene geothermometer of Lindsley and Andersen (1983) and the method of Sun et al. (1974) (within ±40°C difference) may indicate that these results are reliable (see Figure 4.34).

Sample no	MK277	MK132	MK251	MK268	MK49	MK174	MK112	MK154
Rock type	*Andesite*	*Dacite*	*Dacite*	*Dacite*	*Dacite*	*Dacite*	*Dacite*	*Dacite*
SiO2 wt % of host rock	60.58	64.18	65.08	65.47	66.26	66.48	66.81	66.91
Kudo and Weill (1970) thermom	1189	1177	1212	1212	1210	1209	1205	1180
Two pyroxene thermometer (°C)	900		1050				1000	
D_{Sr}	2.70	3.34	3.22	3.65	2.85	2.64	4.87	3.45
D_{Eu}	1.20	0.69	0.56	1.47	2.96	1.24	0.63	0.78
T°K (Kelvin)	1388.4	1362.1	1366.5	1351.1	1382.1	1391.3	1317.4	1358.0
T°C	1115.3	1089.0	1093.3	1077.9	1108.9	1118.1	1044.2	1084.9
Oxygen fugacity (10^{-x}) atm	$10^{-14.5}$	$10^{-12.6}$	$10^{-12.1}$	$10^{-14.7}$	$10^{-17.0}$	$10^{-14.6}$	$10^{-12.0}$	$10^{-12.9}$

Table: 4.6. Table demonstrating the results of geothermometer and oxygen fugacity calculations based on Sun et al.'s (1974) equations.

4.2.3.2. Plagioclase thermometer of Kudo and Weill

Albite ($NaAlSi_3O_8$) and anorthite ($CaAl_2Si_2O_8$) form a continuous solid solution series at high temperatures. In such an ideal solution, melting temperatures are related to mole fractions of the main constituents of these two minerals in the coexisting phases, namely plagioclase and magma. Therefore, in theory, it is possible to calculate crystallisation temperatures using these mole fractions. However, this is not an easy task because it involves complex multicomponent magmatic systems necessitating a good understanding of the activities of plagioclase constituents in the magmatic liquid. In their empirical approach, Kudo and Weill (1970) derived an expression for the activity coefficients of the plagioclase constituents, Na, Ca, Al and Si and subsequently suggested a plagioclase thermometer described by a set of linear

regression trends for different conditions of crystallisation (equations 15-18). The data they used were gathered from the electron microprobe analyses of coexisting plagioclase and liquid (glass) of quenched samples from equilibrium melting experiments of natural granitic rocks at water pressures from 0.5 to 5 kbar. In this study Kudo and Weill's (1970) equations (Eq. 15: 5 kbar water pressure) have been used to calculate the crystallisation temperatures of the plagioclase phenocrysts whose temperatures had been previously calculated using Sun et al.'s (1974) scheme. The results are presented in Figure 4.29 and also in Table 4.6 for comparison.

$\ln \lambda/\sigma + 1.29 \times 10^{-4}\phi'/T = 10.34 \times 10^{-3}T - 17.24$ (dry) (Eq. 12)

$\ln \lambda/\sigma + 1.29 \times 10^{-4}\phi'/T = 11.05 \times 10^{-3}T - 17.86$ (P_{H_2O}=0.5 kb) (Eq. 13)

$\ln \lambda/\sigma + 1.29 \times 10^{-4}\phi'/T = 11.14 \times 10^{-3}T - 17.67$ (P_{H_2O}=1.0 kb) (Eq. 14)

$\ln \lambda/\sigma + 1.29 \times 10^{-4}\phi'/T = 12.18 \times 10^{-3}T - 16.63$ (P_{H_2O}=5.0 kb) (Eq. 15)

and

$$\lambda = \frac{X_{Na}X_{Si}}{X_{Ca}X_{Al}} \quad \text{(Eq. 16)} \qquad \sigma = \frac{X_{Ab}}{X_{An}} \quad \text{(Eq. 17)}$$

$$\phi' = X_{Ca} + X_{Al} - X_{Ca} - X_{Si} \quad \text{(Eq. 18)}$$

where

$X_{Na}, X_{Si}, X_{Ca}, X_{Al}$: mole fractions of the oxides of element, Na, Si, Ca and Al, in the magma. Their sum equals to 1.

X_{Ab}, X_{An} : mole fractions of Albite and Anorthite in the plagioclase phenocrysts.
T : is the temperature in Kelvin.

Equations can be solved following the method presented below (for Eq. 12):

$$\frac{\ln \lambda}{\sigma} + \frac{1.29 \times 10^{-4}\phi'}{T} = 10.34 \times 10^{-3}T - 17.24$$

$$\left(10.34 \times 10^{-3}\right)T^2 - \left(\frac{\ln \lambda}{\sigma} + 17.24\right)T - 1.29 \times 10^{-4}\phi' = 0$$

(Eq. 19)

$$a = +10.34 \times 10^{-3}$$

$$b = -\left(\frac{\ln \lambda}{\sigma} + 17.24\right)$$

$$c = 1.29 \times 10^{-4}\phi'$$

$$\Delta = b^2 - 4ac$$

$$T_{1,2} = \frac{-b + \sqrt{\Delta}}{2a}$$

Kudo and Weill (1970) suggested that their equations yield reasonable plagioclase crystallisation temperatures when applied to magmatic systems. However, subsequent work (Stormer and Carmichael, 1970; Brown and

Carmichael, 1971; Mathez, 1973) showed that temperatures calculated following Kudo-Weill's scheme were always higher than the expected values. In this study, the results calculated using Kudo and Weill's (1970) method are consistently 100-150°C higher than those obtained by Sun et al.'s (1974) scheme (Figure 4.26, Table 4.6) supporting the conclusion of Stormer and Carmichael (1970), and Brown and Carmichael (1971).

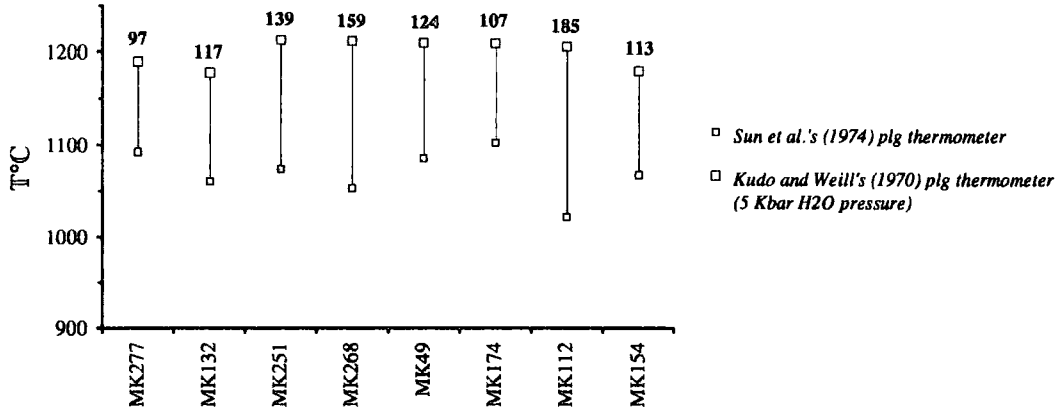

Figure: 4.29. Comparison of plagioclase thermometers of Sun et al. (1974) and Kudo and Weill (1970). Numbers that are presented at the top of each sample represent the difference between the results of two methods.

4.2.3.3. Two feldspar thermometers

There are several methods in the literature that use the compositions of coexisting high-Na plagioclase and high-K feldspar in the calculation of the crystallisation temperatures of these minerals. The temperature calculations are based on the assumption that, if complete stable equilibrium between feldspars was attained, the composition of coexisting feldspar pairs would depend only on pressure and temperature, for a given total feldspar composition. If equilibrium is attained only with respect to alkali exchange, the compositions also will depend on Al-Si order in both frameworks. However, many rocks may contain feldspar pairs which were not in equilibrium (Brown and Parsons, 1981).

Barth (1951, 1968) is the first researcher to propose a two-feldspar geothermometer. His empirical calibration is based on the supposition that the distribution coefficient $K_D = N_{Ab,AF}/N_{Ab,\ PL}$ (where $N_{Ab,AF}$ and $N_{Ab,\ PL}$ are the albite contents of the alkali feldspar and plagioclase respectively) depends to a negligible extend on pressure (P), Al-Si order and bulk composition of the feldspar, but is mainly a function of temperature (T). He later recognised that K_D is not independent of composition and eventually modified his method. Perchuk and Ryabchikov (1968) also constructed a geothermometry method using ternary experimental data. More recently, Seck (1971) developed a two-feldspar thermometer using his experimental

data and proposed his model as a ternary diagram on which he drew isotherms terminating at the line $K_D = 1$. There are also several authors who tried to improve earlier graphical thermometer methods by putting them on a theoretical, thermodynamic, basis, Stormer (1975) and Powell and Powell (1977). Finally, Brown and Parsons (1981) presented an extensive review of literature on this topic and discussed the thermodynamic basis of earlier two-feldspar thermometers. They made several modifications to Seck's (1971) thermometer and proposed a more practical and reliable thermometer. Their thermometer is calibrated for $P = 1$ Kbar, but may be used at higher pressures by adding 18°C/kbar to the temperature obtained. They argue that, to apply their thermometer it is necessary to be sure that feldspar pairs are in equilibrium, though accept that it is difficult to be sure about this in most cases.

A total of 42 coexisting sanidine, sodic-plagioclase and anorthoclase phenocrysts (22 sanidine/anorthoclase and 24 plagioclase), from 6 samples, gathered from three rhyolitic formations on the plateau, were analysed by electron microprobe. Mole fractions of these minerals were calculated from their constituent elements. The data were plotted onto Seck's (1971) graphical thermometer and presented in five parts in Figure 4.30. The same data were also plotted in Brown and Parson's (1981) diagram (Figure 4.31). The results from these two methods are presented in Table 4.7 for comparison. Crystallisation temperatures of plagioclase and anorthoclase phenocrysts calculated using the method of Seck (1971) are consistently higher than solidus temperatures for sanidine with a difference of around 100-200°C. Geothermometer results obtained using Brown and Pearson's (1981) graphical method give similar temperatures to those gathered from plagioclase compositions using Seck's diagram. Both methods give exactly the same temperatures for the samples MK125 and MK330 however, there is about 100°C difference for the samples MK108 and MK332.

Area	Formation	Sample no	Graphical thermometers (°C)		
			Seck (1971)		Brown&Pearson (1981)
			Sanidine	Plagioclase anorthoclase	
Pasinler area	Ardıçlıdağ rhyolite	**MK108**	~550	750	825
		MK125	~550	650	650
		MK330	~550	650	650
		MK332	~550	~700	825
Mt. Aladağ area	Odalar rhyolite	**MK171**	750-800		
Kağızman area	Paslı trachy-dacite	**MK167**	825		

Table: 4.7. The results and comparison of two-feldspar geothermometers of Brown and Parsons (1981) and Seck (1971).

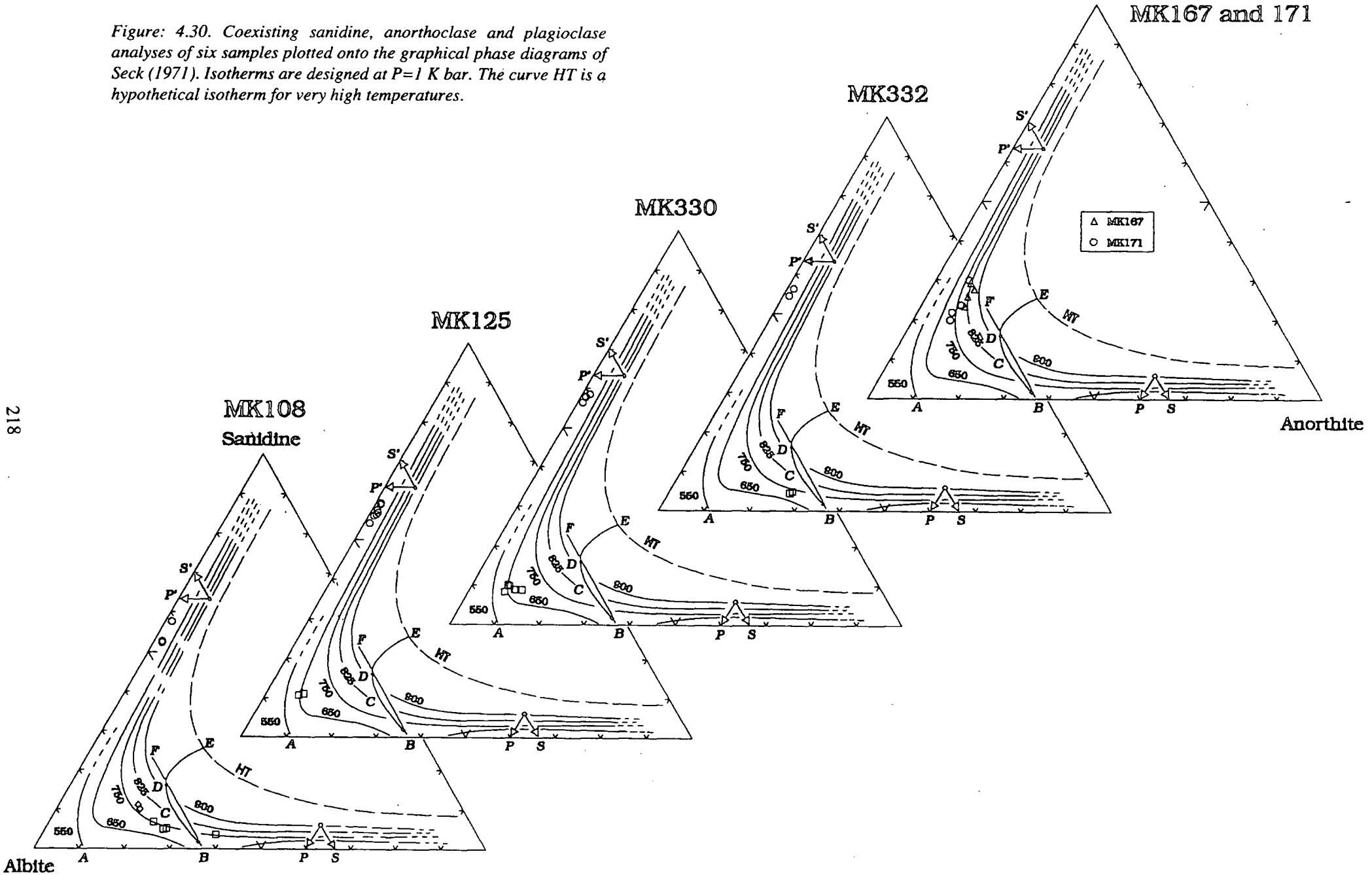

Figure: 4.30. Coexisting sanidine, anorthoclase and plagioclase analyses of six samples plotted onto the graphical phase diagrams of Seck (1971). Isotherms are designed at P=1 K bar. The curve HT is a hypothetical isotherm for very high temperatures.

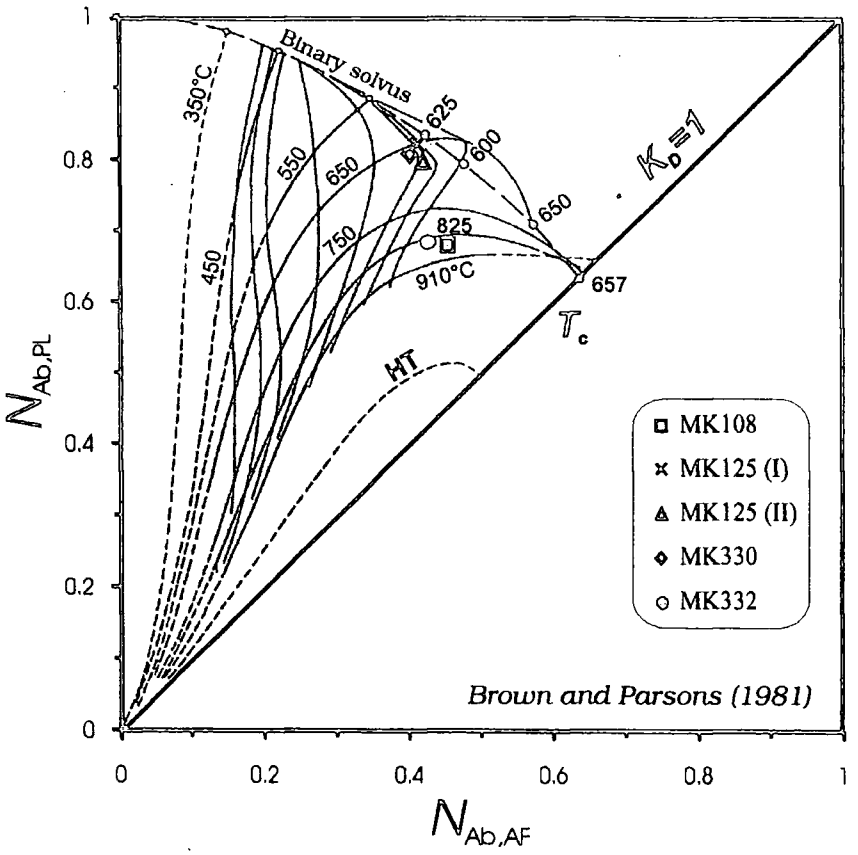

Figure: 4.31. Electron microprobe data of five samples plotted in the graphical two-feldspar thermometer of Brown and Parsons (1981) which is adjusted to 1 k bar. Lines with temperatures are the isotherms contoured in $N_{An,PL}$. Lines without numbers intersecting the isotherms are contoured in $N_{Or,PL}$.

4.2.4. $\delta^{18}O$ isotope geothermometer

The temperature control on isotopic fractionation of elements with low atomic numbers has long been recognised and applied in isotopic thermometry for low temperature systems, such as in the study of sedimentary rocks i.e. determination of the temperature of ancient ocean waters. Subsequently, this method has been adopted for higher temperature systems based on the distribution of stable isotopes between cogenetic mineral pairs. Isotopic fractionation occurs due to slight variations in the physical and chemical properties of isotopes and is proportional to differences in their masses (Faure, 1986). It is greatest where there is a large relative difference in mass between the isotopes of two atoms. These kind of elements are the ones which have low atomic numbers, like O and H. The isotopic fractionation is highest at low temperatures and gets smaller when the temperature is increased. Therefore, they become less sensitive at high temperatures. The isotopic fractionation is indicated by the "fractionation factor α " which is defined as:

$$\alpha = \frac{R_A}{R_B} \qquad \text{(Eq. 20)}$$

where

R_A: is the ratio of the heavy to the light isotope in phase A,
R_B: is the same in phase B

The equilibration of oxygen isotopes ($^{18}O/^{16}O$) between individual minerals has been measured experimentally by several researchers over a wide range of temperatures (e.g. Chiba et al., 1989; Matthews et al., 1983 and Matsuhisa et al. 1979). Subsequently, the data have been used to calibrate geothermometers. The relationship between temperature and fractionation factor is defined by the equation

$$\ln \alpha \approx \frac{1}{T^2} \qquad \text{(Eq. 21)}$$

where

α: fractionation of ^{18}O isotope between two minerals
T: is the absolute temperature (Kelvin).

This equation is valid only at high temperatures over 1000 Kelvin and minerals without hydrogen in the form of hydroxyl ions or water. Values for α are close to unity and vary in the third decimal place. Therefore, the natural logarithm of such numbers enables the following mathematical approximation (Faure, 1986):

$$1000 \ln \alpha_{\min A - \min B} = A\left(10^6 / T^2\right) + B \qquad \text{(Eq. 22)}$$

where

T: absolute temperature in Kelvin
A and B: are constants determined by experiments

A further useful approximation enables us to use $\delta^{18}O$ values in the formulation to calculate solidus temperatures of mineral pairs (Faure, 1986):

$$\Delta_{\min A - \min B} = \delta_{\min A} - \delta_{\min B} \approx 1000 \ln \alpha_{\min A - \min B} = A\left(10^6 T^{-2}\right) + B \qquad \text{(Eq. 23)}$$

The basic assumptions of oxygen isotope geothermometry are that the coexisting minerals reached isotopic equilibrium with one another and with the source of oxygen, namely magma, and that isotopic compositions have subsequently not altered (Hall, 1987). Therefore, the reliability of this method is not only limited by the accuracy and precision of the analytical data but also by the existence of an isotopic equilibrium when minerals exchanged oxygen isotopes with water and each other at high temperatures.

In this study, equilibration temperatures of 7 mineral pairs, which were separated from a total of 6 samples and were supposed to be crystallised in

equilibrium with each other, have been calculated using the equation presented above and $\delta^{18}O$ analyses of 13 mineral separates (one plagioclase-orthopyroxene, five plagioclase-amphibole and one plagioclase-biotite). The results are presented in Table 4.8. A and B are the coefficients from the equation 15. These values are taken from the compilation of Friedman and O'Neil (1977) who recalculated Bottinga & Javoy's (1975) data to a fractionation factor of 1.0412 for CO_2-H_2O in the light of recent experimental work by Matsuhisa et al. (1979) and Matthews et al. (1983). The coefficient, A, is calculated according to the equation $A=1.70-1.04\beta$, as suggested by Faure (1986), where β is the mole fraction of anorthite in the coexisting plagioclase.

Mineral pair	**Plg-Px**	**Plg - Amph**					**Plg-Bio**
Sample no	MK251	MK112	*MK154*	MK49	MK93	MK268	*MK154*
Two-Px therm.	1050°C	1000°C			1100°C		
β	0.551	0.48	0.36	0.50	0.50	0.50	0.36
A	1.12696	1.68	1.80	1.66	1.66	1.66	1.80
B	0	-0.3	-0.3	-0.3	-0.3	-0.3	-0.6
T **range**	*>500*			*>500*			*>500*
$\delta^{18}O_{plg}$	7.4	7.9	7.7	8.4	7.9	8.3	7.7
$\delta^{18}O_{opx}$	6.3						
$\delta^{18}O_{hbl}$		6.9	6.8	7.7	6.7	7.2	
$\delta^{18}O_{bio}$							6.2
Δ	1.1	1	0.9	0.7	1.2	1.1	1.5
T (Kelvin)	1012.2	1137.0	1224.5	1289.5	1052.9	1088.2	925.6
T°C	739.0	863.8	951.3	1016.4	779.7	815.1	652.5

Table: 4.8. Table showing the $\delta^{18}O$ geothermometer results of 7 mineral pairs. Plg: plagioclase, Px: pyroxene, Amph: amphibole and Bio: biotite. Lindsley's (1983) available two pyroxene thermometer results are also presented in the table for comparison.

As can be seen in the table, $\delta^{18}O$ temperatures are consistently lower (between 136 and 320°C) than those determined by the two-pyroxene thermometer of Lindsley (1983). One of the samples, MK154, contains $\delta^{18}O$ analyses of three mineral separates; plagioclase, amphibole and biotite. There is a 298°C difference between the thermometry results of plagioclase-amphibole and plagioclase-biotite pairs. If these minerals were equilibrated isotopically at the same temperature, then pairs of these minerals would yield the same temperature. Therefore, this may be a sign of disequilibration among these minerals, assuming that alteration was not effective after the solidification of this rock. In fact, this result appears to be quite normal since biotite, in general, would be expected to crystallise after plagioclase at relatively lower temperatures. Denies (1977) draws attention to the fact that less than 50% of

mineral triplets published until now yielded similar temperatures using oxygen isotope geothermometry.

4.2.5. Comparison of geothermometer results gathered using different methods

Figures 4.32 and 4.33 illustrate the comparison of geothermometer results for individual samples taken from the different volcanic units of the Erzurum-Kars Plateau. Except for MK277, temperature estimates from the two pyroxene geothermometer of Lindsley and Andersen (1983) and those using the method of Sun et al. (1974) agree to within ±10°C difference (Figure 4.29). In contrast, the

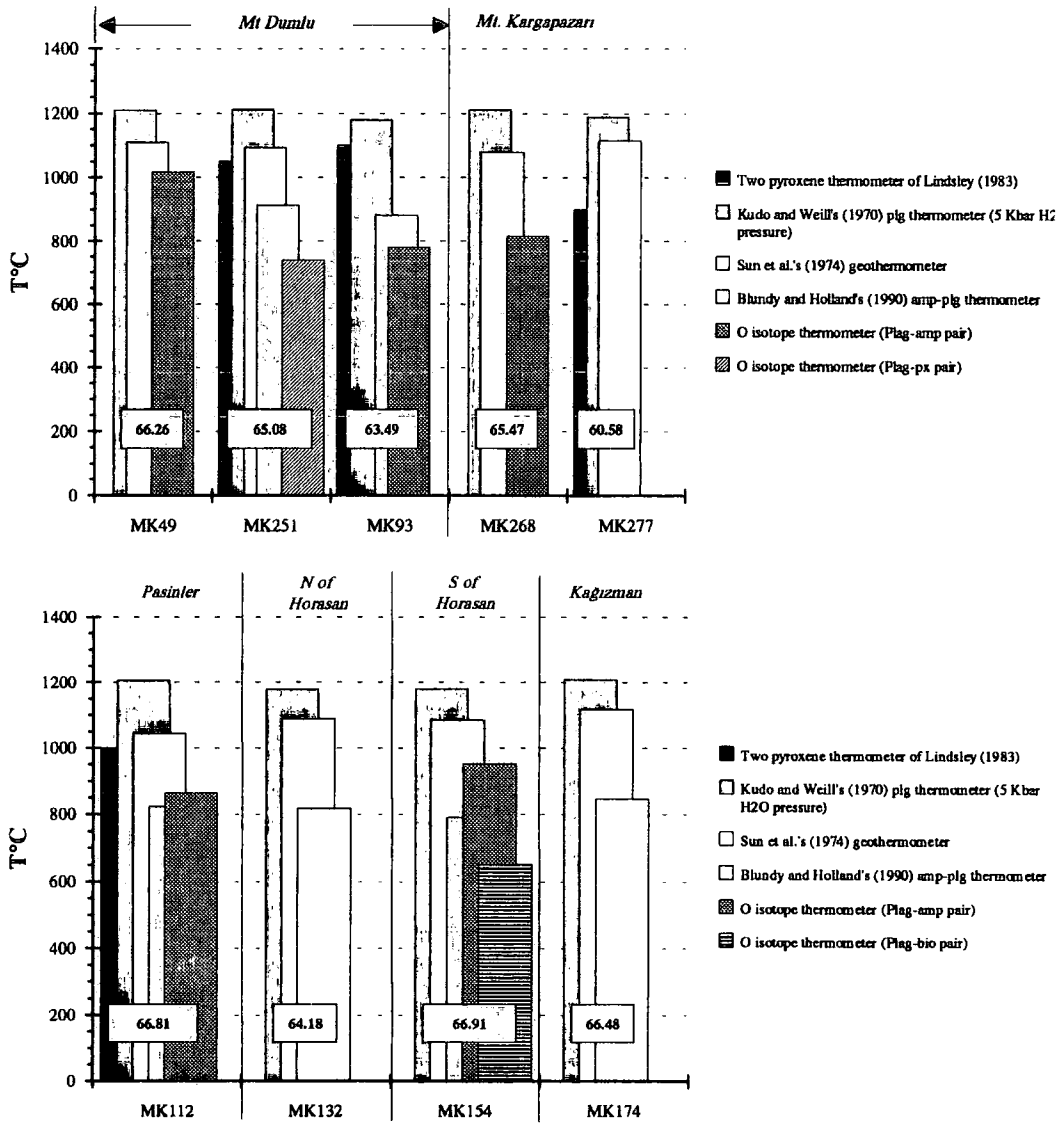

Figure: 4.32. Comparison of techniques used for calculation of liquidus temperatures of different minerals in individual samples. SiO_2 content of each host rock sample is presented on the labels on each bar.

amphibole-plagioclase geothermometer of Blundy and Holland (1990) gives temperatures which are consistently about 220°C lower (in a range between -160 and -276°C) than those obtained by these two methods (Figures 4.29, 30 and 31), while the plagioclase thermometer of Kudo and Weill (1970) yields consistently the highest temperatures among all the methods. $\delta^{18}O$ isotope geothermometers using plagioclase-pyroxene, plagioclase-amphibole and plagioclase-biotite pairs also give

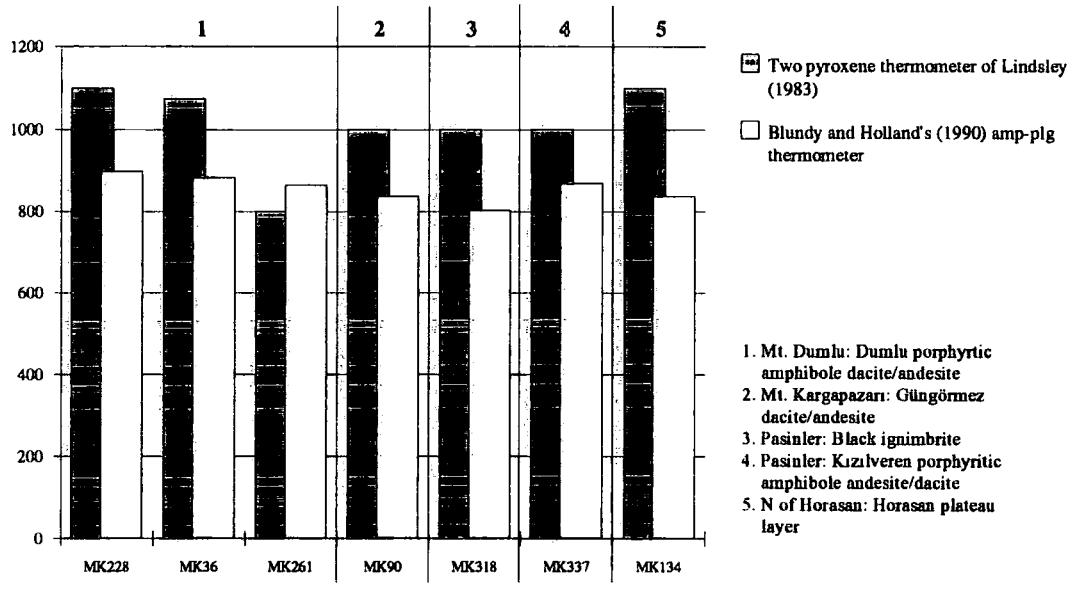

Figure: 4.33. Comparison between the geothermometer methods of Lindsley (1983) and Blundy & Holland (1990).

consistently lower temperatures than Lindsley and Andersen's (1983) and Blundy and Holland's (1990) temperatures, the difference varying from 70 to 300°C. Notably, the $\delta^{18}O$ values of the plagioclase-amphibole pairs tend to give higher temperatures than plagioclase-pyroxene and plagioclase-biotite.

Figure 4.34 illustrates the relationship between temperatures obtained from different geothermometry methods and the SiO_2 content of the melt. All the temperatures obtained using different methods steadily decrease with increasing SiO_2 content of the melt except for Kudo and Weill's (1970) geothermometer. Therefore, Kudo and Weill's (1970) calculation scheme which gives consistently the highest liquidus temperatures appears to be in error. With the exception of two plagioclase-amphibole pair, all oxygen isotope thermometer results yield consistently lower temperatures than those of Lindsley and Andersen (1983) and Sun et al. (1974). Among all of these geothermometer calculation schemes, the methods proposed by Lindsley and Andersen (1983) and Sun et al. (1974) appear to be the best estimates for liquidus temperatures of the volcanic units on the Erzurum-Kars Plateau because

they closely agree to each other within ±10°C difference and are reasonable estimates for the crystallisation range.

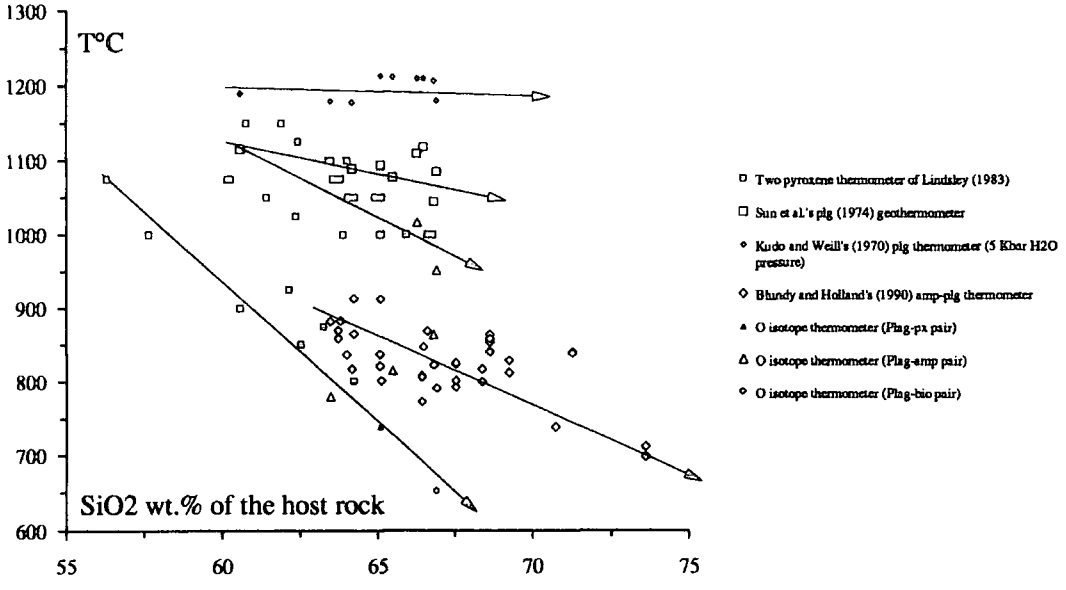

Figure: 4.34. Comparison of geothermometer results which were obtained using seven different calculation methods plotted against SiO_2 content of the host magma.

4.3. Partition Coefficients

When a mineral is in chemical equilibrium with a liquid, trace elements are partitioned between the two phases according to their chemical activity in each (Cox et al., 1989). The extent to which an element is incorporated into a mineral crystallising from a magma can be expressed conveniently by means of a *partition coefficient* which is defined by the following equation:

$$K_d = \frac{C^{mineral}_{element_i}}{C^{melt}_{element_i}} \qquad \text{(Eq. 24)}$$

where

K_d : *partition coefficient of an element,*

$C^{mineral}_{element_i}$: *concentration of an element in a particular mineral (in ppm),*

$C^{melt}_{element_i}$: *concentration of an element in magma (in ppm).*

This equation is valid only for the elements whose concentrations are lower than 1%. The validity of measured partition coefficients is also dependent upon the existence of an equilibrium between the phenocryst phases and the melt. Mineral phenocrysts can be examined for the existence of equilibrium or disequilibrium following two main ways; petrographic studies and stable isotopic analyses of minerals.

In petrographic studies, phenocryst reaction rims or corrosion, the coexistence of phenocrysts of incompatible mineralogical or chemical compositions are all considered to be the evidence for disequilibrium. In addition to these, in the case of zoned phenocrysts e.g. plagioclases the partition coefficients theoretically apply only to the outermost zone since it is the only part which was in contact and hence in equilibrium with the magmatic liquid presently represented by the groundmass. However, in most cases, separating the outer zones from the phenocrysts is almost impossible. Therefore, the calculated partition coefficients of zoned minerals such as plagioclases should be considered as approximate values.

Isotopes of the elements having low atomic numbers especially those of hydrogen and oxygen ($^{18}O/^{16}O$) are fractionated between different minerals and the melt as a function of temperature of the system if they crystallise in equilibrium with each other and with the melt. This provides a good opportunity to examine whether or not equilibration was maintained during the crystallisation. The equilibration of these isotopes between minerals and melt has been measured by several researchers for different temperatures and calibrated for geothermometer calculations (see section 4.2.4). Consequently, it is theoretically possible to calculate crystallisation

temperatures of minerals by using the distribution of stable isotopes between cogenetic mineral pairs. When there is more than one mineral pair available in a sample, temperatures calculated from these coexisting mineral pairs should be similar to each other if they crystallised in equilibration with each other and the magmatic liquid. However, it should be emphasised that the results are also sensitive to errors in analytical data and to the alteration after solidification.

Mineral/melt partition coefficients of an element are direct indicators of its compatibility or incompatibility in a mineral-magmatic liquid system. A value of greater than 1 indicates that this particular trace element is preferentially enriched in a particular mineral phase and is therefore a compatible element. If it is lower than 1 it is called incompatible element. Almost all REE and Large Ion Lithophile (LIL) elements are incompatible with most of the rock forming minerals except for some ferro-magnesian minerals e.g. amphibole and pyroxenes.

The value of K_d depends on several variables such as composition, pressure, temperature and oxygen fugacity of the mineral-liquid system, and also on crystal chemistry. Therefore, a single K_d value for a mineral alone is usually meaningless. Partition coefficients ideally should be evaluated as functions of one or a set of these physical and chemical variables, many of which are co-variant in natural systems. In most cases, isolating one of these effects from others is a difficult problem.

Another point which should be taken into account is that K_d values may vary from one volcanic suite to another as can be well exemplified by high-silica rhyolites of Mahood and Hildreth (1983). Therefore, more care should be paid to selecting the most appropriate values for a particular magmatic suite for use in petrologic modelling. The best attempt could be the determination of K_d values by using samples collected from that particular magmatic suite under consideration.

In order to obtain the most appropriate K_d values for this study, a subset of representative rock samples were selected to calculate partition coefficients of rock forming minerals in the volcanics of the Erzurum-Kars Plateau. Details of sample preparation and calculations are presented in the following paragraphs.

4.3.1. Calculation of Partition Coefficients

Porphyritic rock samples collected from different levels and formations of the Erzurum-Kars plateau were studied microscopically in order to select the phenocrysts that are freshest and have no accessory mineral inclusions and zoning. Twelve representative samples which conform to these prerequisites and cover a SiO_2 range from 63.5 to 71.0 wt.% were selected for mineral separation. These fresh rock

samples were broken into small pieces by a jaw-crusher. To avoid contamination of the next sample, the jaw-crusher was cleaned by wire brush and alcohol prior to each session of crushing. Then the samples were sized by sieving with a mesh to get rid of very fine and coarse particles. Phenocryst fragments were separated from the sieved rock samples by hand-picking under the binocular microscope. Not all mineral phases could be obtained from each sample. Mineral fragments, especially transparent minerals (e.g. feldspars) were carefully examined for accessory mineral inclusions. When found, the inclusions were removed from the phenocryst fragments, by breaking the crystals and discarding the piece containing the inclusion. If that proved impossible, the grains were completely rejected. This procedure could not be carried out on mafic and non-transparent minerals such as amphiboles and pyroxenes. Therefore, darker minerals provided greater possibilities for unobserved inclusions. The purity of mineral separates in general is better than 95% as judged from microscope inspection. Microscopic work and microprobe analyses indicate that phenocrysts with the exception of plagioclase from dacites display little or no zoning.

A total of 23 mineral separates were obtained from a total of 12 rock samples as presented in Table 4.10. These separates were cleaned in reagent grade acetone followed by de-ionised water. Then they were prepared for the ICP-MS analyses together with the whole-rock samples following a series of acid digestion and evaporation stages as described in Appendix B.

Major elements of these minerals were analysed on polished thin sections of the samples by using a Geoscan electron micro-probe while the analyses of major elements of the whole-rock samples were done on their fusion disks by a Phillips PW-1400 X-Ray Fluoresance Spectrometer (XRF) at the University of Durham. Trace elements of whole-rock samples were analysed on pressed-powder pellets using the same XRF. Rare Earth Elements (REEs) and a subset of trace elements (Rb, Sr, Y, Zr, Nb, Cs and Ba) in both whole rock and mineral separates were analysed on a VG-Plasmaquad Inductively Coupled Plasma Mass Spectrometer (ICP-MS) at the Industrial Research Centre, University of Durham. Mineral and whole rock datasets are presented in Tables 4.13 to 4.17 and also in Appendix E and F.

Figure 4.35 illustrates the distribution of end-member compositions of plagioclase, clino- and orthopyroxene and amphibole mineral separates. Composition of plagioclase phenocrysts spans a range between An_{35} and An_{60} (andesine and labradorite) with a few scatter falling into the oligoclase field (MK154 and MK174). All orthopyroxene separates fall into the bronzite field while clinopyroxene phenocrysts (MK265) classify as endiopside and only one of them as augite. The most abundant end-member of amphibole is represented by tschermakite whose

percentage changes roughly between 40-50. Edenite and taramite are also abundant ranging from 8-10% to 33%. Barroisite and kaersutite constitute relatively less abundant end-members in the amphibole separates.

Some of the mineral separates have been analysed for $\delta^{18}O$. One of them, MK154, contains $\delta^{18}O$ analyses of three mineral separates (plagioclase, amphibole and biotite) enabling the inspection of the existence of equilibration between these minerals. Oxygen isotope thermometry calculations have been conducted on plagioclase-amphibole and plagioclase-biotite pairs on this sample and a 298°C difference has been found between these two pairs (section 4.2.4). This can be interpreted as an indication of disequilibration among these minerals. Therefore, the calculated partition coefficients of these three minerals in MK154 should be interpreted with caution. Most probably, among them, the only mineral that crystallised in equilibrium with the magmatic liquid may be biotite since it would be expected to crystallise after all these minerals. The widespread scatter in the distribution of composition of plagioclase phenocrysts (see section 4.1.1, Figures 4.7 and 4.8) against SiO_2 and magnesium number of their host-rocks suggest that most of the plagioclase phenocrysts in the volcanics of the Erzurum-Kars Plateau are

Area	formation	sample no	SiO_2 % of whole-rocks	mineral separates
Mt. Dumlu area	Dumlu amphibole dacite/andesite	MK49	66.26	amphibole (amph) plagioclase (plg) (An_{45-55})
		MK93	63.49	amph
		MK251	65.08	orthopyroxene (opx) (Bronzite) amph plg (An_{52-62})
Mt. Kargapazarı	Göllerdüzü amphibole dacite/andesite	MK268	65.47	amph plg
	Köşk pyroxene andesite/dacite	MK265	63.90	clinopyroxene (cpx) (endiopside and augite)
	Güngörmez andesite/dacite	MK277	60.58	opx (Bronzite) plg (An_{50-58})
Pasinler	Ardıçlıdağ rhyolite	MK338	71.00	anorthoclase
	Kızılveren amphibole dacite/andesite	MK112	66.81	amph plg (An_{44-55})
Horasan	Köroğlu amphibole dacite/andesite	MK132	64.18	opx amph plg (An_{40-49})
	Saçdağ dacite	MK154	66.91	biotite (bio) amph plg (An_{27-43})
	Kötek basalt	MK144	48.76	olivine (olv)
Kağızman	Paslı trachy-dacite	MK174	66.48	amph plg (An_{37-46})

Table: 4.10. Table presenting detailed information about mineral separates. For the classification of amphiboles see Figure 4.35.

Figure: 4.35. The distribution of end-member compositions of plagioclase, clino- and orthopyroxene and amphibole mineral separates.

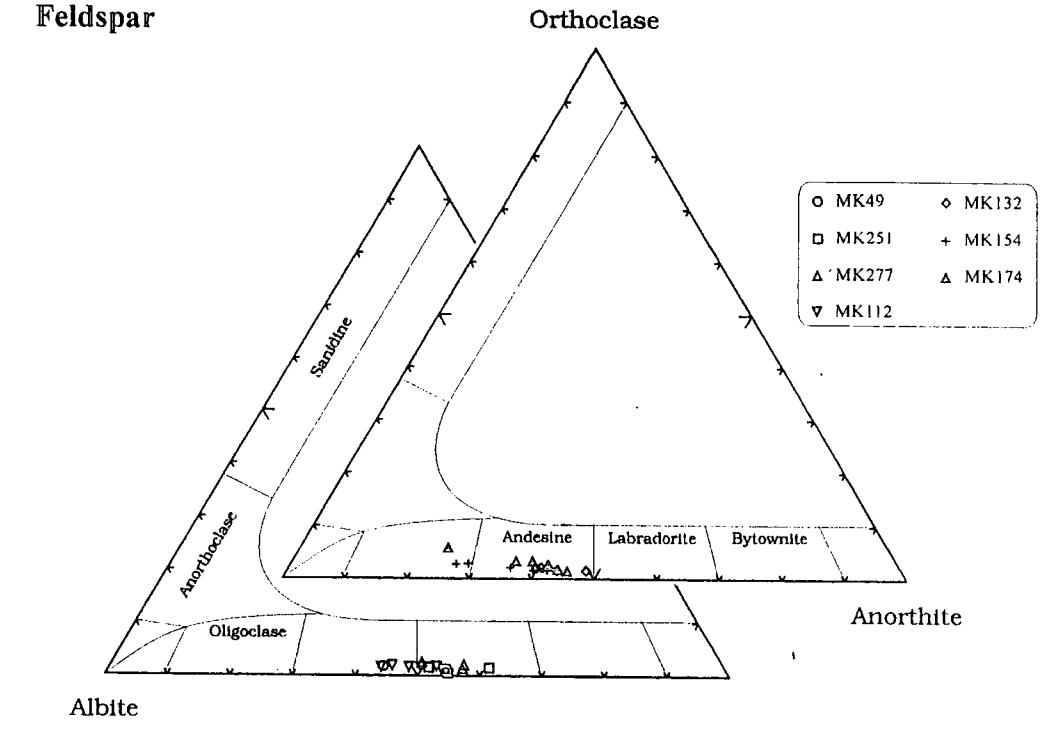

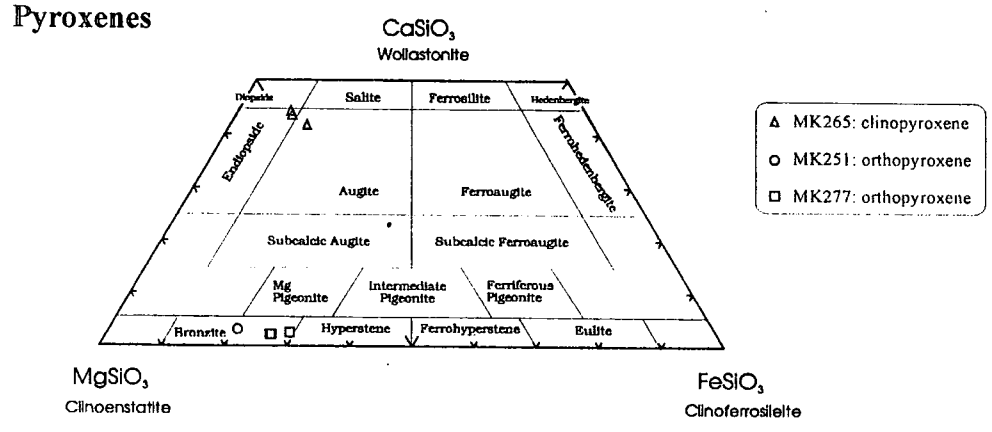

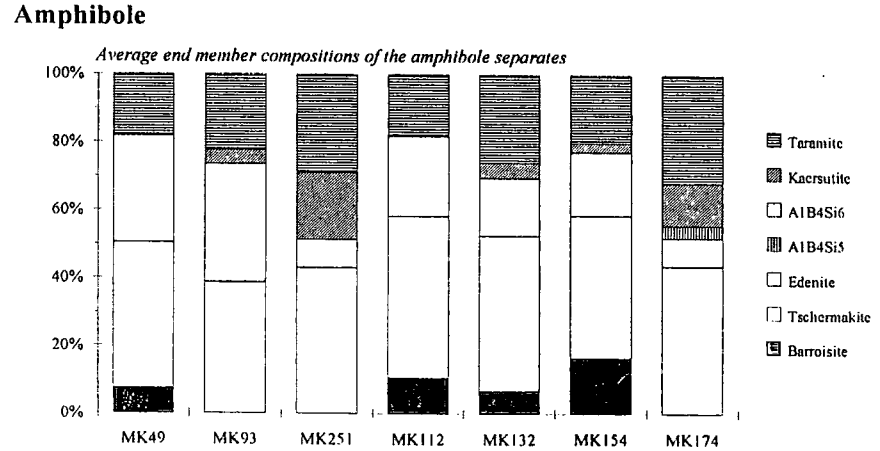

xenocrysts. Geobarometry calculations based on the Schmidt's (1992) equations (see section 4.2.2.1) indicate a 25-30 km deep crystallisation history for some of the amphibole phenocrysts implying that some amphiboles may also be in disequilibrium with their matrix.

Almost all whole-rock samples contain various amounts of phenocrysts of different minerals. Therefore, analysed whole-rock concentrations, in theory, do not represent those in liquid magma. In order to determine the percentage of each phase and correct this effect, modal analyses of minerals were performed using the photographs of thin sections of the samples. Liquid magma or in other words, matrix compositions of the samples were calculated from these modal analyses by subtracting the total mineral effect from each whole-rock analyses. The total mineral effect for each element in each sample was calculated by using equation 25. The results of these calculations, together with the whole-rock and mineral analyses are presented in Table 4.13.

$$C_{liq-magma} = \frac{C_{whole-rock} - \left(\%min_A \times C_{min_A} + \%min_B \times C_{min_B} + ... + \%min_i \times C_{min_i}\right)}{1 - \sum_{min=A}^{i} min_i} \qquad \text{(Eq. 25)}$$

where

$C_{liq-magma}$: *concentration of a particular element in magma liquid,*

$\%min_A$: *volumetric percentage of mineral A in the rock obtained from modal analyses,*

C_{min_A} : *concentration of the same element in mineral A,*

$C_{whole-rock}$: *concentration of the element in whole-rock sample.*

As mentioned earlier, in the case of zoned crystals and some xenocrysts that crystallised earlier in equilibrium with a magma whose composition is different from surrounding matrix, the only part that can be used to calculate partition coefficients is the outermost zone. This zone, in general, cannot be practically separated from crushed rock samples and can only be analysed using one of the microbeam techniques e.g. ion-probe when available. Consequently, under these conditions, calculated matrix compositions (using Eq. 25) are not representative of the magmatic liquid hence, resultant partition coefficients may be in error. In order to overwhelm this effect, both mineral/whole-rock and mineral/calculated matrix partition coefficients have been computed in this study. Theoretically, the real K_d value should locate between these two partition coefficient values.

Mineral/melt (calculated matrix) and mineral/whole rock partition coefficients for 8 amphibole, 8 plagioclase, 3 ortho- and 1 clino-pyroxene, 1 olivine, 1 anorthoclase and 1 biotite mineral separates were calculated and presented in tables 4.14, 4.15, 4.16 and 4.17 in four parts. It should be noted again that the mineral-matrix K_d values presented in these tables are all true partition coefficients that are valid only for equilibrium crystallisation conditions.

Among the variables controlling K_ds the melt composition, especially the SiO_2 content of the melt, is the most important single factor controlling mineral/melt partition coefficients (Rollinson, 1993). Other factors, temperature, pressure and oxygen fugacity of the melt also result in variations in K_d values. However, in most cases SiO_2 correlates with all these factors as well (Pearce and Norry, 1979). Therefore, at this stage, assessing the partition coefficients as a function of SiO_2 content of the melt seems to be the best approach to exhibit the relationship between different K_d values.

Since some of the plagioclases are not in equilibrium with matrix probably due to magma mixing between dacitic and basic magmas at depth (Section 4.1.1), the SiO_2 content of the melt with which they theoretically equilibrated should be

	SiO_2 of host-rock (a)	Average predicted SiO_2 (b)
MK49	63.49	63.03
MK251	65.08	61.43
MK277	60.58	61.77
MK112	66.81	63.15
MK132	64.18	64.37
MK154	66.91	65.74
MK174	66.48	64.72

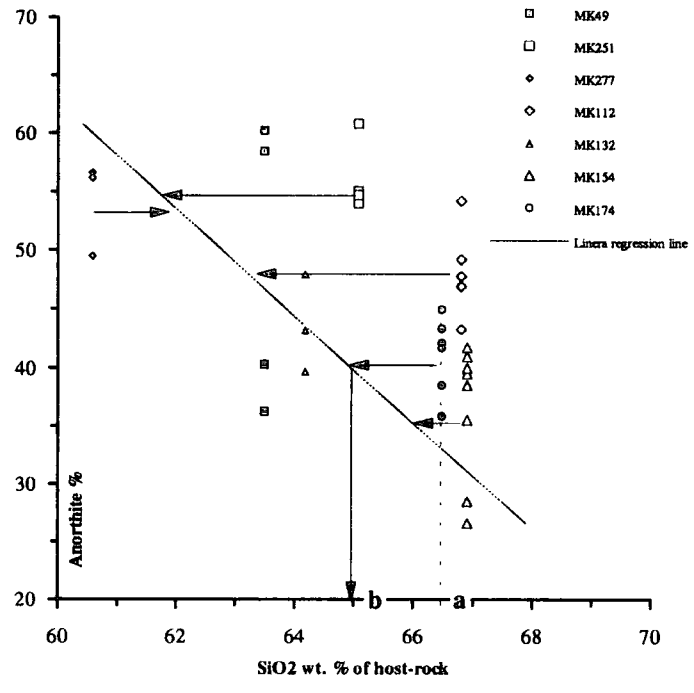

Figure: 4.36.

estimated before plotting the plagioclase K_ds against silica. This can be done by means of a regression line or a best-fit line calculation taking SiO_2 as the dependent

and anorthite content as the independent variable. The linear regression calculation has been carried out on a sum of 330 plagioclase analysis to draw the best-fit line presented in Figure 4.36 and to obtain predicted SiO_2 values shown in the inset table. Each sample contains at least three point analysis that differ in An content. Therefore, predicted SiO_2 values for each sample have been averaged to determine a single value that can be used for mineral separates since the each separate is supposed to be a mixture of these minerals.

In Figure 4.37 the mineral/melt (matrix) partition coefficients of six minerals: ortho- and clinopyroxene, amphibole, plagioclase, anorthoclase and biotite have been plotted against the SiO_2 content of the melt to examine the relationship between these two variables. Predicted SiO_2 values (Figure 4.36) have been used for the partition coefficients of plagioclases. A line has been drawn through data points of each mineral to show the general trend between K_d values and acidity of the melt. Strikingly, most of the K_d values, especially for the elements Sr, Y, Zr, Nb, Ce, Nd, Sm, Gd, Tb, Dy, Ho, Er, Tm, Yb, Lu and Hf, exhibit a reasonable positive linear correlation with increasing SiO_2 content of the melt even though SiO_2 varies in a relatively narrow range from 60 to 71 SiO_2 wt.%. The difference in K_d between the most acidic and basic ends of the diagrams sometimes reaches as much as three to four times the value of the most basic one supporting the idea that silica content of the melt is the most significant factor controlling K_d values of the collision-related volcanics of the Erzurum-Kars Plateau. The scatter in the data points of each mineral is probably caused by other factors such as temperature, pressure and oxygen activity of the melt reflecting the difference in the conditions under which these minerals formed.

Figure 4.38 shows chondrite-normalised REE diagrams of mineral separates and their partition coefficients. REE partition patterns gathered from a compilation of partition coefficients (see section 4.3.2) are also presented in inset diagrams for basic (50% SiO_2), intermediate (60% SiO_2) and acidic (70% SiO_2) rocks (arranged from base to top respectively) for comparison. It is apparent from the partition coefficient patterns that plagioclase separates MK49 and MK268 and amphibole separate MK49 have much higher K_d values, probably due to accessory mineral inclusions such as zircon and also due to disequilibration between minerals and melt. The difference in crystallisation temperatures calculated for plagioclase-amphibole and plagioclase-biotite pairs for MK154 indicates a disequilibrium between these minerals as mentioned earlier. Therefore, these separates are excluded from the calculations and compilation and are not presented in Figure 4.39. All analysed phenocrysts display the LREE enriched (chondrite-normalised) pattern of their host rocks. Phenocrysts of amphibole, ortho and clinopyroxenes also show a slightly Eu-depleted pattern.

FIG4-37A.XLS

Figure: 4.37. Calculated mineral-magmatic liquid partition coefficients of six minerals; amphibole, plagioclase, ortho- and clinopyroxenes, anorthoclase and biotite, plotted against SiO_2 contents of their host melt. The lines have been drawn through data points of the partition coefficients of each mineral to exhibit the relationship between K_d values and SiO_2 of the magma liquid.

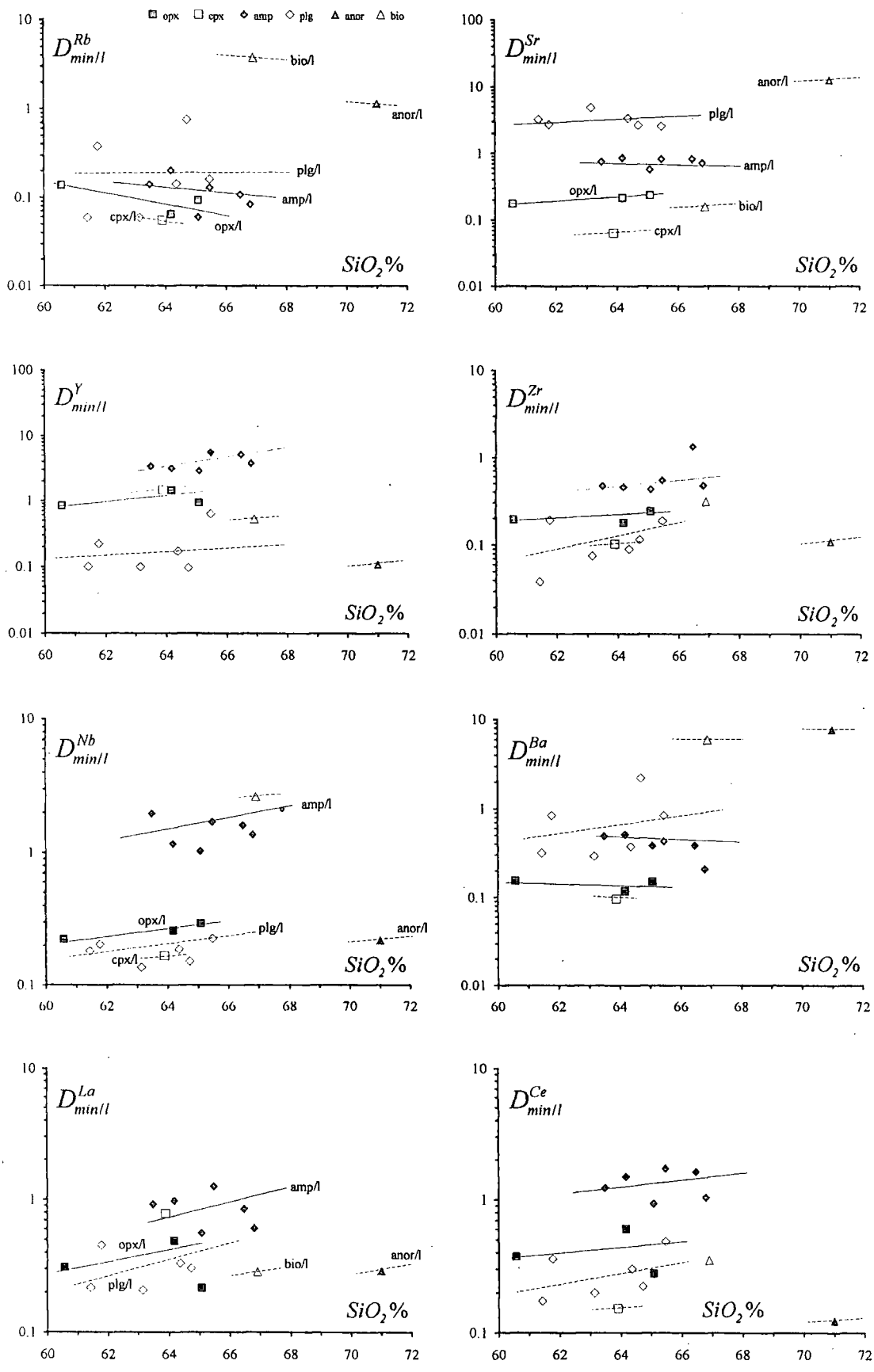

Figure: 4.37. (continued)

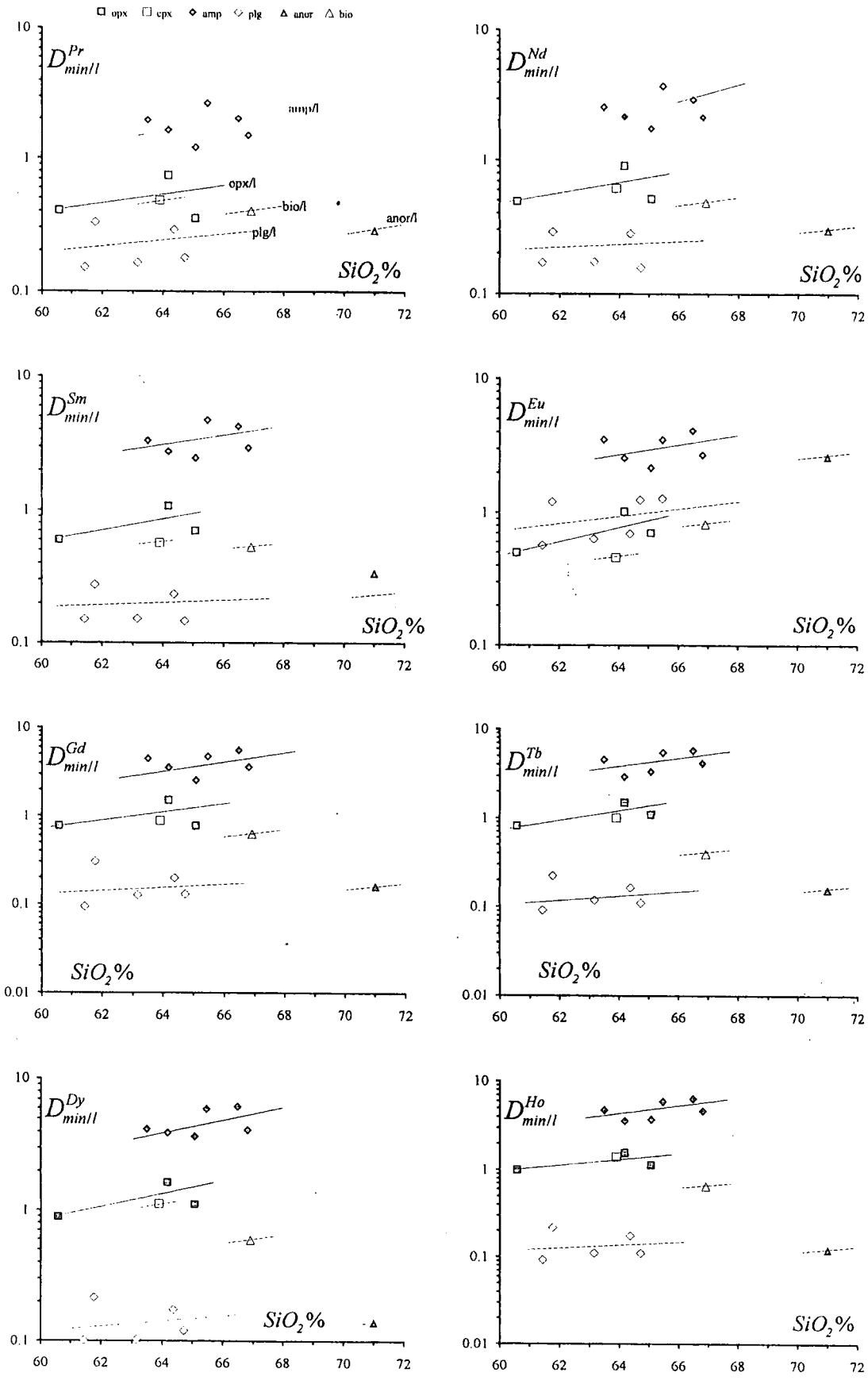

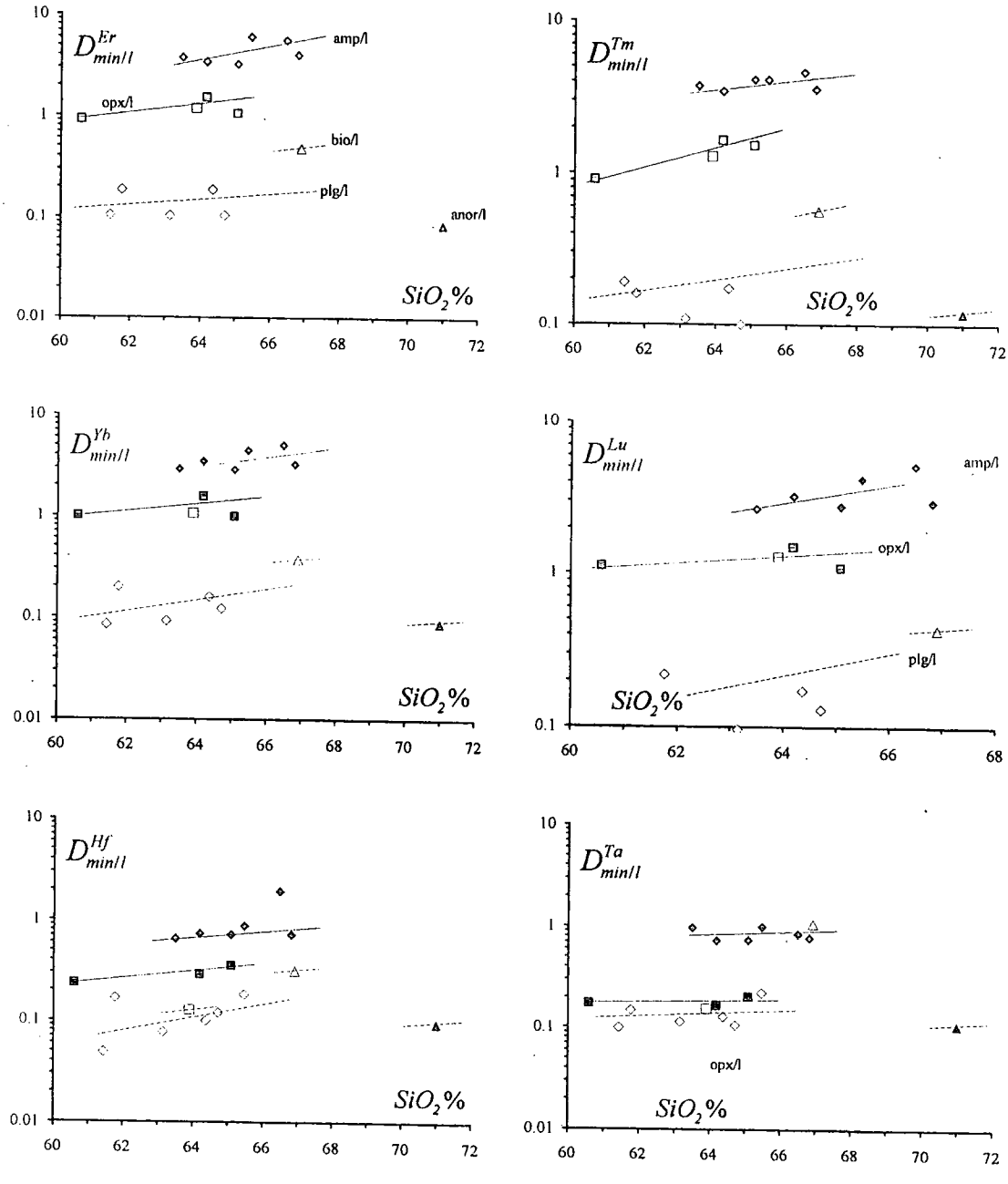

Figure: 4.37. (continued)

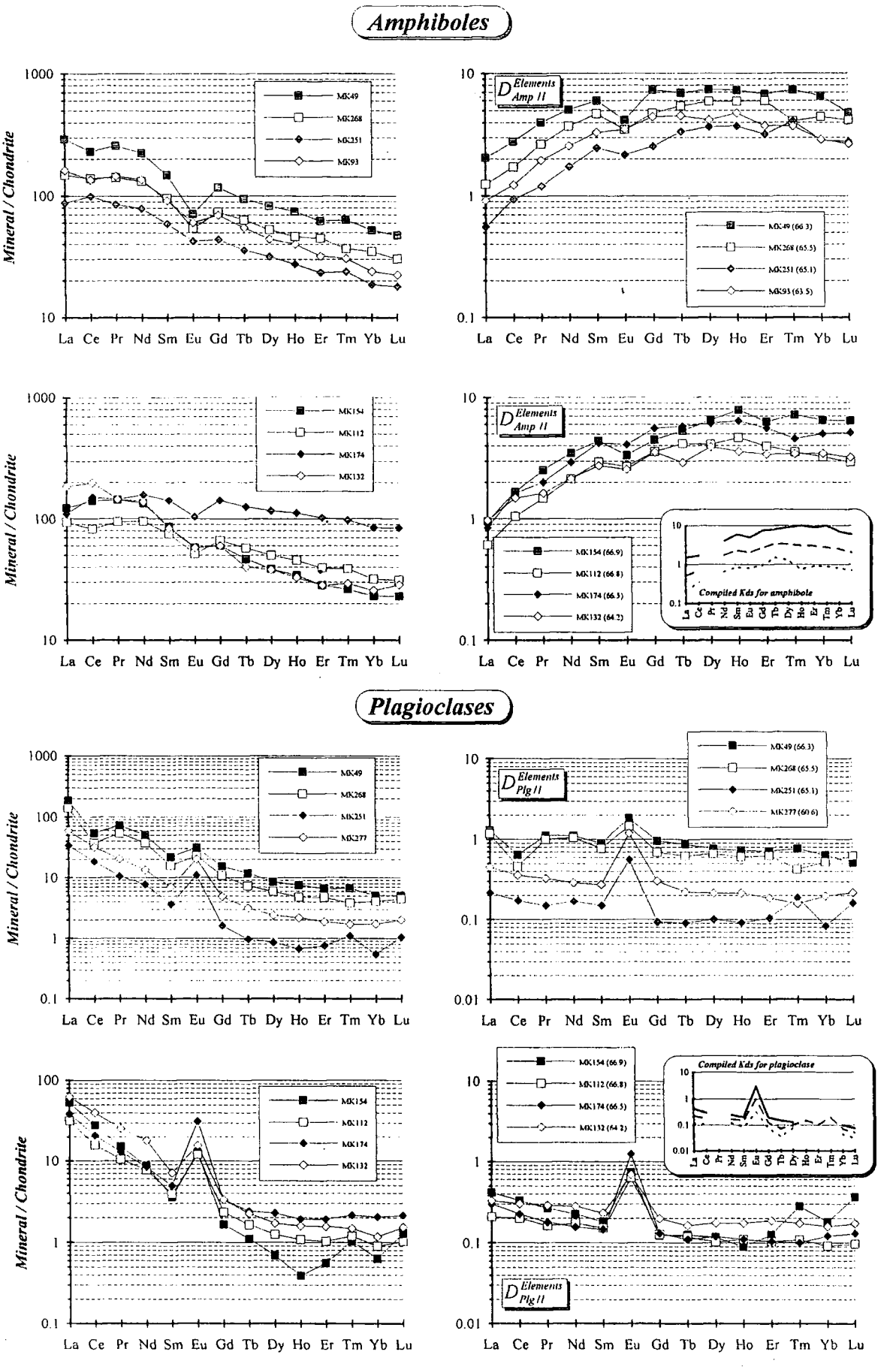

Figure: 4.38. Chondrite normalised REE diagrams and partition coefficient patterns of minerals separates. Compiled K_d values are displayed in inset graphs for comparison.

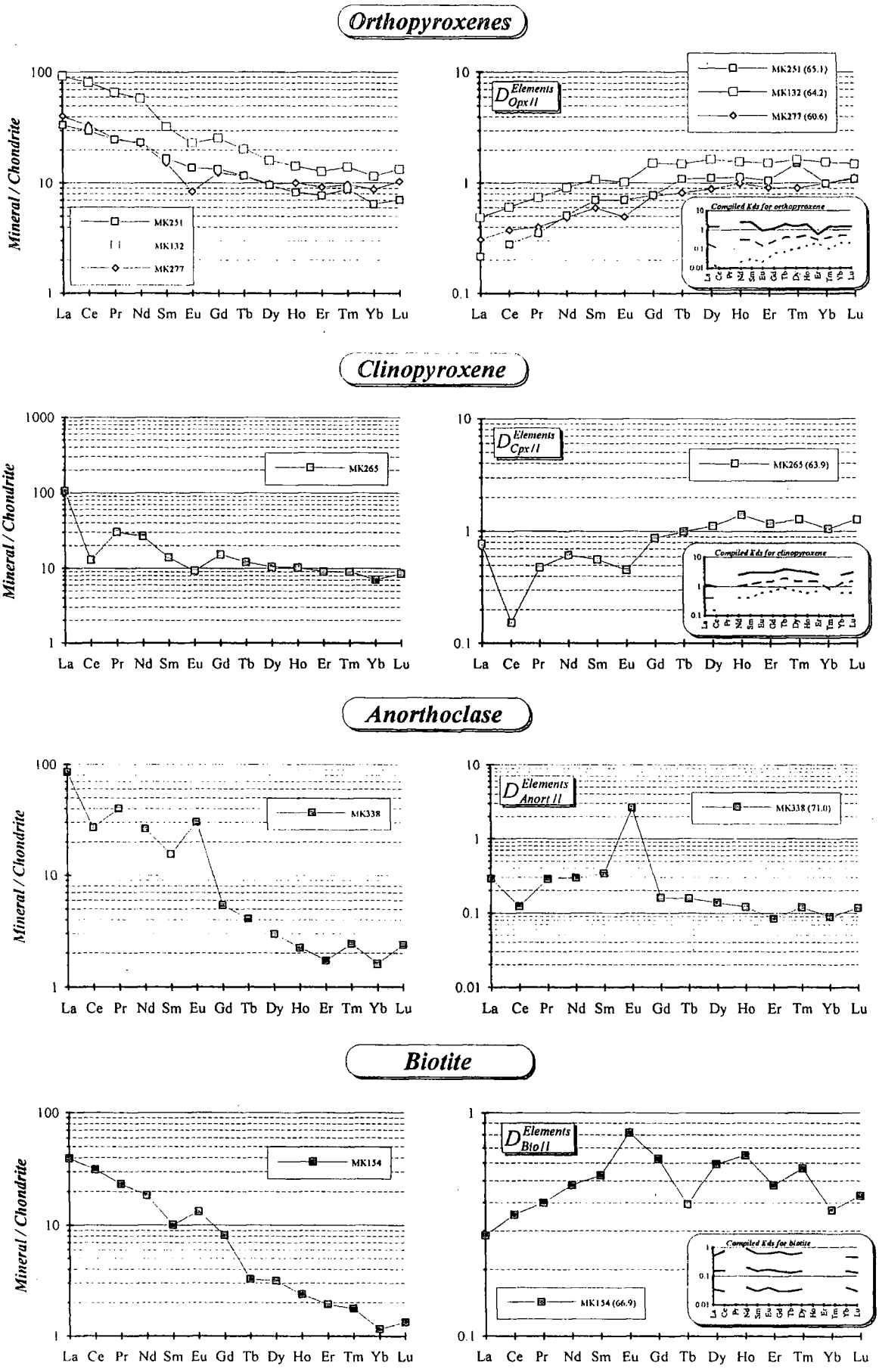

Figure: 4.38. (continued)

Figure 4.39 displays the partition coefficient patterns of 26 elements arranged according to the order of their incompatibility which decreases from Cs to Lu and Fe. In order to make a comparison between the values obtained in this study and the published values, compiled K_d values for basic, intermediate and acidic rocks are also plotted onto the diagrams.

4.3.1.1. Amphibole

The amphibole partition coefficients display a slightly convex-upward pattern from the light (LREEs) to the heavy rare earth elements (HREEs) with a slight negative Eu anomaly (Figure 4.38). This negative Eu anomaly is also present in clino- and orthopyroxenes. The reason is that Eu is in divalent state at low oxygen fugacity conditions resulting in its preferential incorporation into plagioclase (Drake, 1975) and rejection from the ferromagnesian minerals like pyroxenes and amphibole. The partitioning of REE increases from 0.6-1.5 for La to 3-8 for the elements between Gd and Er. Two of the amphibole separates, MK154 and MK49, show an abnormal enrichment in HREEs compared to others. This may be caused by the contamination effects of some accessory mineral inclusions such as zircon which are preferentially enriched in HREEs and/or disequilibration between the mineral and magma liquid. Amphibole partition patterns in Figure 4.39 are in a very good agreement with published values except for two samples: MK174 which is about four times enriched in Zr and Hf and MK132 which displays a minute enrichment in Rb and Th with respect to compiled values.

Romick et al. (1992) argue that amphibole partition coefficients for the REEs are highly dependent upon melt composition, temperature and pressure. According to these authors, distribution coefficients for amphibole increase at constant pressure with decreasing temperature and increasing silica content of the melt. This is evident from the positive correlation between amphibole partition coefficients and SiO_2 content of the melt (Figure 4.37). As the magma evolves to high dacitic compositions, amphibole REE K_ds increase to high values and amphibole fractionation becomes the dominant influence on the REE concentrations. The preferential extraction of the MREE and HREEs by hornblende (Figure 4.38) creates a downward concave REE pattern and high La/Yb ratios, an important feature which is well seen in the volcanic formations of low-Y series on the Erzurum-Kars Plateau (see Section 3.3.2).

4.3.1.2. Plagioclase

Plagioclase is depleted relative to the host magma in all trace and rare earth elements except Sr, Eu and, to some extent, also in Ba (Figure 4.37). The chondrite normalised and partition coefficient patterns of plagioclases which are presented in

Figure 4.38 indicate that plagioclase shows a preference for light rare earth elements (LREEs) over medium rare earth elements (MREEs) and HREEs. Except for one anomalous plagioclase separate (MK154), the chondrite-normalised REE concentrations of plagioclases exhibit a steep but smooth decrease from around 30-60 times chondrite for La to 1-2 for Lu with a positive anomaly at Eu. The partition of REEs decreases steadily from 0.15-0.4 for La to 0.1-0.2 for Lu. Eu, Sr and Ba are significantly enriched in all plagioclase separates almost 3 to 6 times for Sr, 0.7 to 1.5 times for Eu and 0.4 to 2 times for Ba over the magma liquid (Figures 4.36 and 37).

Similarities between partition behaviour of Eu and Sr can be explained by their similar ionic radii (Eu^{2+} and Sr^{2+}). The anomalous enrichment of Eu in plagioclase is attributed to its partial existence in the divalent state (Eu^{2+}) in contrast to the other REEs which are always trivalent. The valance state of Eu is controlled predominantly by oxygen activity of the melt however, it is independent of temperature (Drake, 1975). Europium forms Eu^{2+} at low oxygen activities under relatively reducing conditions and Eu^{3+} at high oxygen activities i.e. atmospheric conditions. Eu^{2+} is much more compatible than Eu^{3+} in plagioclase. Therefore, plagioclases that formed under low oxygen fugacities display higher partition coefficients for Eu which are generally greater than 1. This property has been used by some researchers (e.g. Sun et al., 1974) to construct equations constraining oxygen fugacity of the melt in which plagioclase phenocrysts were formed. In contrast to Eu, distribution coefficients for Sr are strongly depended upon temperature but independent of oxygen fugacity of the melt; a feature that was used by Sun et al. (1974) to construct their experimental plagioclase geothermometer (see Section 4.2.3.1).

Partition coefficients of plagioclases presented in this study (Figure 4.38) are almost completely within the range of published values. However, they tend to be slightly higher than the compiled values of acidic rocks especially for Cs, Th, U, Ta, Nb, Zr, Hf, Yb and Lu. Because of the presence of disequilibrium between plagioclase phenocrysts and magma liquid, the K_d values for plagioclase should be considered as approximate values and used with caution.

4.3.1.3. Anorthoclase

Anorthoclase exhibits a preference for LREE over HREE showing similar REE and K_d patterns to the plagioclase with a characteristic positive Eu anomalies (Figure 4.37). The partition coefficients of REE decrease from 0.3 for La to 0.15-0.10 for Lu. Anorthoclase concentrates Eu, Sr and Ba three times for Eu, ten times for Sr and nine times for Ba over the liquid (Figure 4.37). These values are almost two times greater

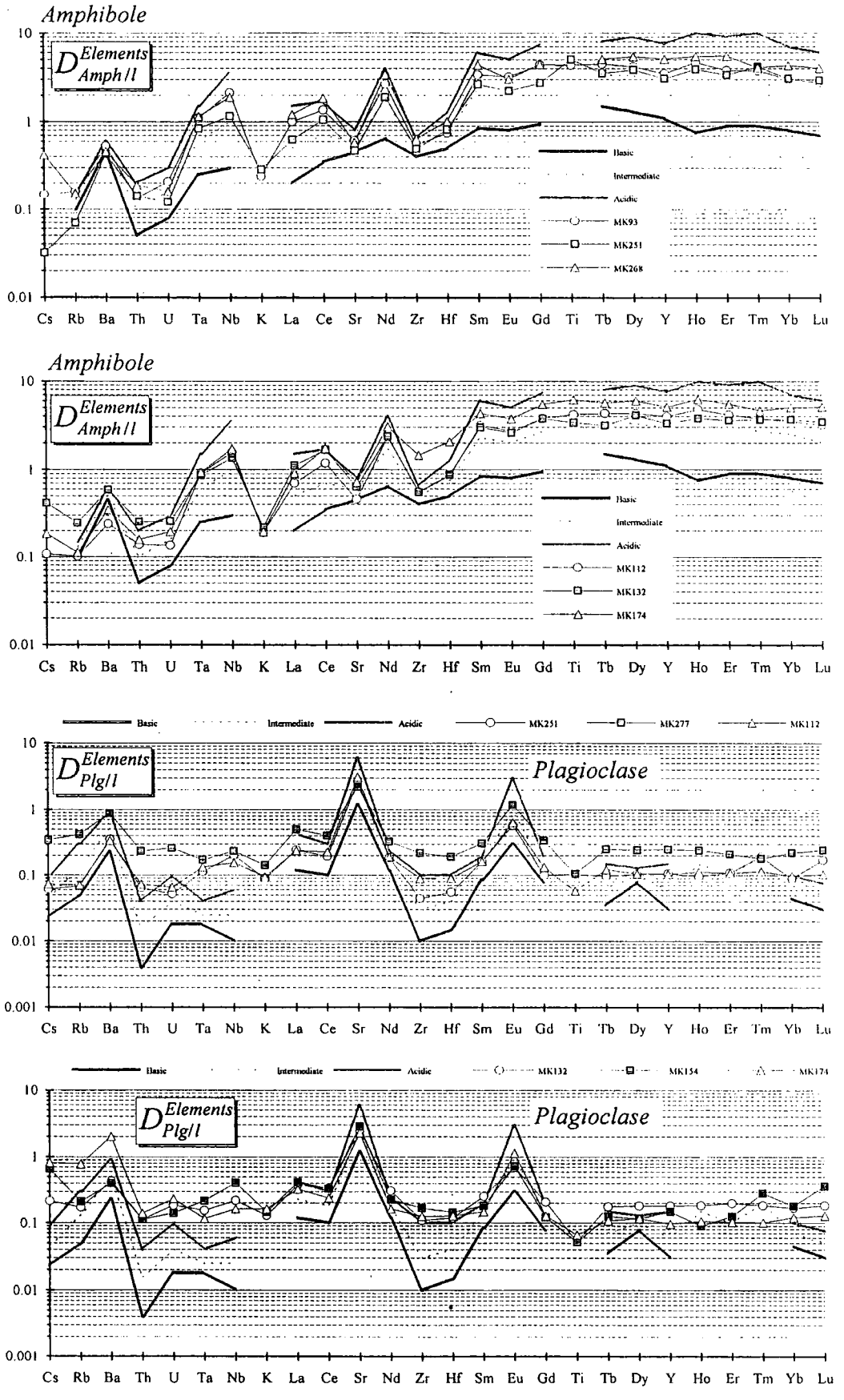

Figure: 4.39. Partition coefficient patterns of mineral separates arranged according to their decreasing incompatibility from left (Cs) to right (Fe). For comparison, compiled K_d values for basic, intermediate and acidic rocks are illustrated on each diagram by solid, dotted and grey lines respectively.

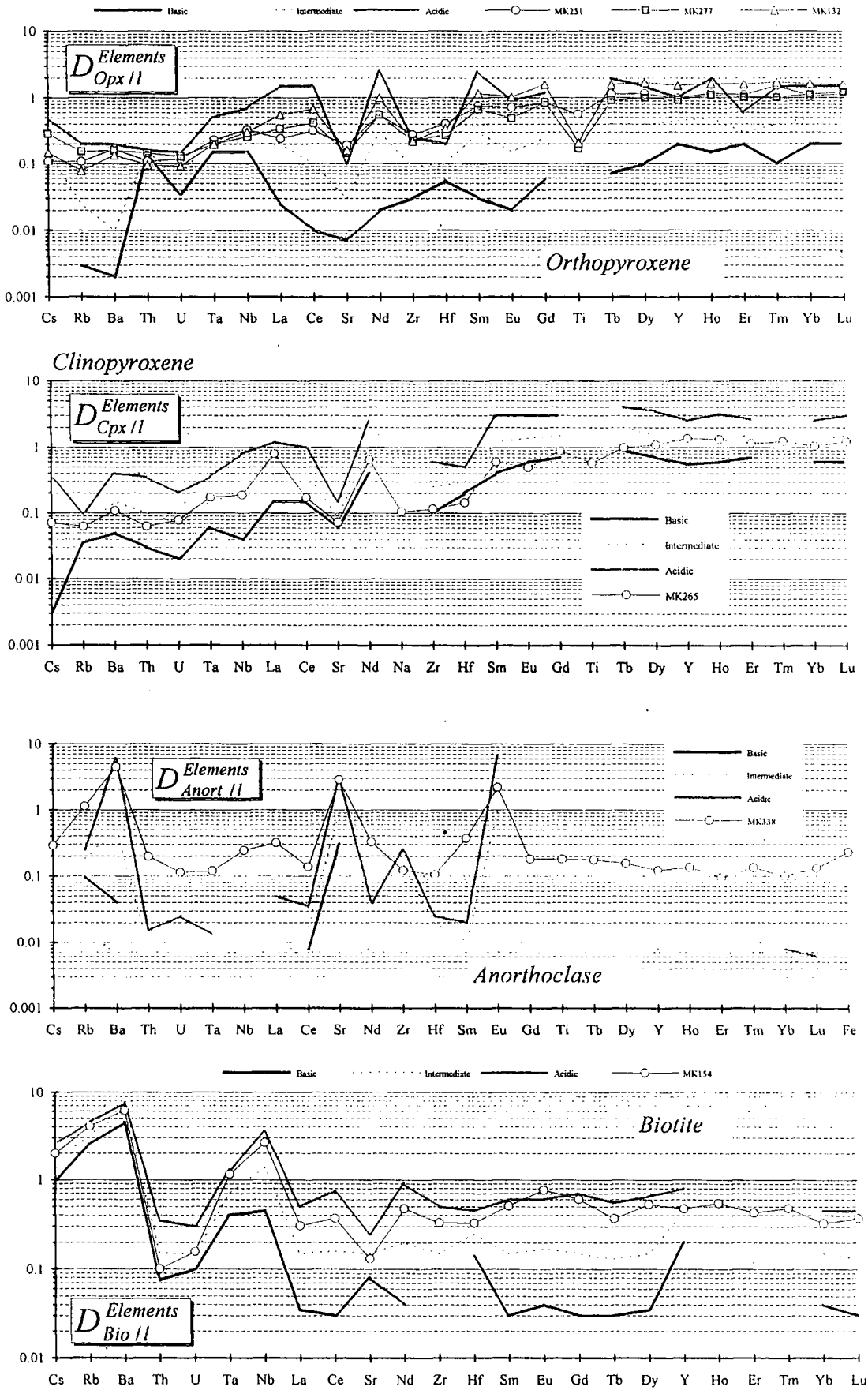

Figure: 4.39. (continued)

than those of plagioclase. Another difference between the REE K_d patterns of anorthoclase and plagioclase is that anorthoclase partition coefficients for LREE and some MREE (Pr, Nd and Sm) are almost twice the values of those of plagioclase, except for one anomalously low Ce value.

4.3.1.4. Orthopyroxene

The partition coefficient patterns of orthopyroxene illustrate a relative enrichment of HREE over LREE. One of the separates, MK132, show unusually higher REE values presumably caused by some sub-microscopic accessory mineral inclusions. In addition, MK251 exhibits a Tm anomaly. Except for MK132, the partition of REE increases fairly steadily from 0.3 for La to 1.0 to 1.5 for Yb. MK277 and MK132 display slight negative Eu anomalies. The partition coefficients of orthopyroxene plots about in the limits of the published range except for MK132.

4.3.1.5. Clinopyroxene

Clinopyroxene exhibits a higher partition coefficients for the MREEs and HREEs compared to the LREEs. La and Ce behave in a fashion antithetic to other LREEs. Partition coefficients of all elements between Gd and Lu including Y exceed 1. This is presumably related to preferential substitution of HREE ions at the Mg-site in the clinopyroxene as previously discussed by Nagasawa (1973). Partition coefficients of clinopyroxene are completely consistent with the compiled values as can be seen in Figure 4.39.

4.3.1.6. Biotite

Biotite shows a slight preference for HREE over LREE with respect to the concentrations of these elements in magma. Notably, it displays a positive Eu anomaly. This positive Eu anomaly could be due to slight contamination of the separate by plagioclase. Except for Eu, partition coefficients for biotite are in good agreement with the published values reported by several authors as evidenced by Figure 4.39. Elements that are strongly enriched in biotite over the host magma liquid are Cs (2 times), Rb (4.5 times), Ba (7 times), Ta (~1.5 times) and Nb (3 times). It is less strongly enriched in MREE and HREE. Biotite is depleted relative to matrix in Th, U and Sr (Figure 4.37).

4.3.2. Compilation of partition coefficient values

Partition coefficient data for trace and rare earth elements for the minerals; amphibole, plagioclase, sanidine, anorthoclase, clino- and orthopyroxene and biotite have been compiled from a total of about 70 articles and added to the data obtained in

this study to construct a table of recommended mineral-melt partition coefficients for acidic, intermediate and basic volcanic rocks. Only those papers which have specifically aimed establishing appropriate partition coefficients have been used for the compilation. Host-rock and, when available, matrix compositions presented in these papers completely cover the SiO_2 compositional range from basalt to high-silica rhyolites. The source of partitioning data is summarised in Table 4.11.

The mineral-melt partition data come from two basically different sources: (1) analyses of phenocryst-matrix pairs of natural rock samples; and (2) synthesis of equilibrium crystalline and melt phases using experimental techniques that are carried out under controlled melt composition, temperature, pressure and oxygen activity conditions followed by their analysis.

Among the papers published to date, most of the data have been obtained by analyses of separated mineral phenocrysts and the matrix which theoretically represents the magmatic liquid in which these phenocrysts crystallised. Different analytical techniques having different sensitivities including X-Ray, Electron Probe, Instrumental Neutron Activation (INAA) and recently Inductively Coupled Plasma Mass Spectrometer (ICP-MS) analysis have been used by the researchers to determine the major and trace element concentrations of these two phases for several rock-forming minerals. In this method, analytical error is only one of the factors affecting the reliability of partition coefficient (K_d) determinations. Variations in K_d values arise from several factors predominantly as a result of the complexity of natural systems including change in distribution coefficients during crystal growth (Pearce and Norry, 1979), disequilibration between the minerals and magmatic liquid, and presence of sub microscopic accessory mineral inclusions which are generally strongly enriched in some trace and REE elements. Inefficiency of phase separation also causes errors. One of the weakest aspects of this method is that, in most cases, it is difficult to determine the crystallisation conditions i.e. temperature, pressure and oxygen activity of the mineral-melt system upon which K_d values are strongly dependent. Therefore, values obtained using this technique by different authors may vary within large ranges, especially when measured element ratios between matrix and phenocrysts in natural rocks are compared with the partition coefficients that have been determined by experimental techniques in equilibrium conditions. In recent years, experimental methods have increasingly been used in determination of partition coefficient values of different elements for rock-forming minerals under controlled conditions. Some of the experiments use natural starting materials while the others facilitate the use of synthetic materials. In some of these experiments starting materials are doped with the elements of interest up to percent levels so that they can be detectable by the electron microprobe. Some researchers

have developed new and more sophisticated doping techniques by using α-, β- or γ-active or fissionable isotopes followed by auto-radiography.

Having completed synthesis of crystal-melt phases, element concentrations of these phases are determined either in-situ by using a microbeam technique e.g. electron microprobe or separating these phases using conventional heavy liquids and hand-picking followed by analysis by precise techniques e.g. Instrumental Neutron Activation Analysis (INAA). The advantage of the experimental techniques over the natural phenocryst-matrix method is that the dependence of partition coefficients on physico-chemical conditions and the behaviour of various trace elements as a function of the atomic structures of crystals and melts can be examined quantitatively (Irving, 1978). However, this method also has some significant limitations because, an experimental system created in a laboratory environment cannot exactly simulate complex natural systems. In his review Irving (1978) has presented an extensive discussion on potentials and weaknesses of experimental determination techniques of partition coefficients published until 1978.

In recent years, developments of sophisticated and high precision analytical techniques have stimulated the research on more accurate and in-situ K_d determination. One of these techniques developed is the ion microprobe, an analytical device which is capable of detecting several elements simultaneously and in general more accurately than electron probe at natural low concentration levels even without need for doping. However, this method suffers from molecular ion interferences with analytical peaks of element ions and also poorly defined roles of structural and chemical matrix effects on ion yields (Kuehner et al., 1989). It also involves complex correction and calibration procedures. Ray et al. (1983), Kuehner et al. (1989) and Hart and Dunn (1993) are some of the researchers who used this technique in their K_d determinations.

Another technique which has recently been developed for determination of in-situ K_d is the proton microprobe which is basically another microbeam technique. It has many advantages compared to other techniques for analysing natural and experimentally produced mineral-glass pairs. Its precision and accuracy are very high, it can even determine concentrations of only a few ppm and, unlike the ion-probe technique, it does not require calibration procedures since it is a standardless technique. Determinations of this sort are employed by few researchers such as Green et al. (1989) and Adam et al. (1993).

As can be expected, the evaluation of a vast amount of trace and rare earth element partition coefficient data for different minerals compiled from several

Table: 4.11. Source of compilation of partition coefficient data.

AMPHIBOLE

1 M. Keskin (this study)
2 Schnetzler and Philpotts (1968)
3 Higuchi & Nagasawa (1969)
4 Schnetzler & Philpotts (1970)
5 Philpotts & Schnetzler (1970)
6 Nagasawa and Schnetzler (1971)
7 Nagasawa (1973)
8 Sun&Hanson (1976)
9 Arth & Barker (1976)
10 Schock (1977)
11 Compilation of Pearce & Norry (1979)
12 Compilation of Cox et al. (1979)
13 Compilation of Gill (1981)
14 Villemant et al. (1981)
15 Compilation of Henderson (1982)
16 Dupuy et al (1983)
17 Dostal et al (1983)
18 Wörner et al. (1983)
19 Fujimaki et al. (1984)
20 Irving & Frey (1984)
21 Lemarchand et al. (1987)
22 Bacon and Druitt (1988)
23 Romick et al. (1992)
Experimental
24 Drake & Holloway (1977)
25 Mysen (1978)
26 Nicholls & Harris (1980)
27 Green & Pearson (1985b)
28 Adam et al. (1993)

PLAGIOCLASE

1 M. Keskin (this study)
2 Schnetzler & Philpotts (1968)
3 Higuchi & Nagasawa (1969)
4 Schnetzler & Philpotts (1970)
5 Philpotts & Schnetzler (1970)
6 Dudas et al. (1971)
7 Nagasawa (1971)
8 Nagasawa and Schnetzler (1971)
9 Nagasawa (1973)
10 Hart & Brooks (1974)
11 Arth (1976)
12 Arth & Barker (1976)
13 Sun and Hanson (1976)
14 Compilation of Cox et al. (1979)
15 Compilation of Pearce & Norry (1979)
16 Compilation of Gill (1981)
17 Compilation of Henderson (1982)
18 Dostal et al (1983)
19 Wörner et al. (1983)
20 Nash & Crecraft (1985)
21 Lemarchand et al. (1987)
22 Bacon and Druitt (1988)
23 Stix and Gorton (1990)
24 Romick et al. (1992)
Experimental
25 Sun et al. (1974)
26 Drake & Weill (1975)

CLINOPYROXENE

1 M. Keskin (this study)
2 Onuma et al.(1968)
3 Schnetzler and Philpotts (1968)
4 Schnetzler & Philpotts (1970)
5 Nagasawa&Schnetzler (1971)
6 Nagasawa (1973)
7 Hart & Brooks (1974)
8 Sun and Hanson (1976)
9 Schock (1977)
10 McCallum and Charette (1978)
11 Compilation of Pearce & Norry (1979)
12 Compilation of Cox et al. (1979)
13 Larsen (1979)
14 Compilation of Gill (1981)
15 Compilation of Henderson (1982)
16 Mahood&Hildreth (1983)
17 Dostal et al (1983)
18 Dupuy et al. (1983)
19 Wörner et al. (1983)
20 Irving & Frey (1984)
21 Fujimaki et al. (1984)
22 Nash&Crecraft (1985)
23 Lemarchand et al. (1987)
24 Michael (1988)
25 Bacon and Druitt (1988)
26 Mahood and Stimac (1990)
27 Sisson (1991)
Experimental
28 Sun et al. (1974)
29 Mysen (1978)
30 Nicholls & Harris (1980)
31 Ray et al. (1983)
32 Green & Pearson (1985a)
33 Green et al. (1989)
34 Kuehner et al. (1989)
35 Adam et al. (1993)
36 Hart & Dunn (1993)

ORTHOPYROXENE

1 M. Keskin (this study)
2 Onuma et al. (1968)
3 Schnetzler & Philpotts (1970)
4 Philpotts & Schnetzler (1970)
5 Nagasawa&Schnetzler (1971)
6 Schock (1977)
7 Compilation of Pearce & Norry (1979
8 Compilation of Coxet al. (1979)
9 Compilation of Gill (1981)
10 Compilation of Henderson (1982)
11 Mahood&Hildreth (1983)
12 Fujimaki et al. (1984)
13 Irving & Frey (1984)
14 Nash&Crecraft (1985)
15 Bacon and Druitt (1988)
16 Sisson (1991)
Experimental
17 Mysen (1978)
18 Colson et al. (1988)
19 Colson & Gust (1989)
20 Green et al. (1989)
21 Nielsen et al. (1992)

OLIVINE

1 M. Keskin (this study)
2 Schnetzler and Philpotts (1968)
3 Schnetzler & Philpotts (1970)
4 Philpotts & Schnetzler (1970)
5 Hart & Brooks (1974)
6 Compilation of Pearce & Norry (1979)
7 Compilation of Cox et al. (1979)
8 Compilation of Gill (1981)
9 Compilation of Henderson (1982)
10 Mahood&Hildreth (1983)
11 Lemarchand et al (1987)
12 Michael (1988)
13 Mahood and Stimac (1990)
Experimental
14 Mysen (1978)

SANIDINE

1 Philpotts & Schnetzler (1970)
2 Nagasawa (1971)
3 Nagasawa (1973)
4 Arth (1976)
5 Hildreth (1977)
6 Compilation of Cox et al. (1979)
7 Leeman & Phelps (1981)
8 Villemant et al. (1981)
9 Mahood & Hildreth (1983)
10 Wörner et al. (1983)
11 Nash & Crecraft (1985)
12 Lemarchand et al. (1987)
13 Mahood and Stimac (1990)
14 Stix and Gorton (1990)
Experimental
15 Guo & Green (1989)

ANORTHOCLASE

16 M. Keskin (this study)
17 Sun and Hanson (1976)
18 Mahood and Stimac (1990)

BIOTITE

1 M. Keskin (this study)
2 Higuchi & Nagasawa (1969)
3 Schnetzler & Philpotts (1970)
4 Philpotts & Schnetzler (1970)
5 Compilation of Cox et al. (1979)
6 Villemant et al. (1981)
7 Compilation of Henderson (1982)
8 Mahood&Hildreth (1983)
9 Irving & Frey (1984)
10 Nash&Crecraft (1985)
11 Adam et al. (1993)

GARNET

1 Schnetzler & Philpotts (1970)
2 Philpotts & Schnetzler (1970)
3 Irving & Frey (1978)
4 Compilation of Pearce & Norry (1979)
5 Compilation of Cox et al. (1979)
6 Compilation of Gill (1981)
7 Compilation of Henderson (1982)
Experimental
8 Mysen (1978)
9 Nicholls & Harris (1980)
10 Green et al. (1989)

APATITE

1 Nagasawa&Schnetzler (1971)
2 Nagasawa (1970)
3 Fujimaki (1986)
4 Mahood and Stimac (1990)
5 Bacon and Druitt (1988)
6 Irving & Frey (1984)

MAGNETITE

1 Schock (1977)
2 Schock (1979)
3 Compilation of Pearce & Norry (1979)
4 Compilation of Gill (1981)
5 Compilation of Henderson (1982)
6 Wörner et al. (1983)
7 Mahood & Hildreth (1983)
8 Dostal et al (1983)
9 Nash & Crecraft (1985)
10 Smith and Leeman (1987)
11 Lemarchand et al. (1987)
12 Bacon and Druitt (1988)

ALLANITE

1 Brooks et al (1981)
2 Mahood & Hildreth (1983)

published papers and obtained by a wide range of different methods under different conditions has imposed a great problem. One of the most important decisions to be taken in such an extensive compilation before starting to calculate recommended values is the selection of a most effective single factor against which most mineral-melt partition coefficients are correlated. This factor should also be widely available in most of the papers. As mentioned earlier, there are a number of factors i.e. temperature, pressure, composition of magma liquid that control the partition coefficients. Although the relative importance of these factors changes from one mineral to another, and with respect to the physico-chemical conditions of the system, the SiO_2 content of the melt is considered to be the most significant single factor that controls partition coefficients. It also, in general, correlates with other factors, as well proven in studies by Watson (1976) and Ryerson and Hess (1978). In their compilation, Pearce and Norry (1979) used SiO_2 content of the melt as the main parameter to estimate their recommended partition coefficients for Ti, Zr, Y and Nb. Mahood and Hildreth (1983) also consider compositional effects to be of first importance while temperature effects to be of secondary importance in silicic magmas. The SiO_2 content of the melt is readily available in most of the papers unlike temperature, pressure and oxygen fugacity which have been presented only in a few papers most of which are based on experimental determinations. Therefore, SiO_2 content of the melt has been selected and used as the main parameter in this study.

Each mineral/melt partition coefficients obtained from the papers listed in Table 4.11 have been plotted against the SiO_2 content of the matrix of that particular sample. When there are no data available for the matrix, whole rock analyses of the host rocks have been used. These 174 diagrams are not presented here because they occupy very large space and also it is beyond the scope of this thesis to discuss them in detail. Partition coefficients for most of the elements display a positive correlation with the acidity of their melt and can be as much as tens of times higher in acid than in basic melts. There is sometimes a wide scatter of results for the partition of an element in a particular mineral-matrix pair while for others the values are more consistent. Some of the scatter may be a result of analytical error but probably a large part arises from the dependence of coefficients on temperature, pressure and oxygen activity. Some distinct lithologies having distinct major element compositions (e.g. pantellerites) sometimes tend to scatter away from the general trend. A best fit line indicating the general trend between the partition coefficients and the SiO_2 contents of the melts has been drawn through data points. Then, mineral-melt partitioning values for basic, intermediate and acidic rocks have been determined on these lines

Table: 4.12. Table illustrating the compilation of mineral-melt partition coefficients for plagioclase, sanidine, amphibole, biotite, clino- and orthopyroxene, olivine and garnet Italics are the approximate values.

PLAGIOCLASE	Cs	Rb	Ba	Th	U	Ta	Nb	La	Ce	Sr	Nd	Zr	Hf	Sm	Eu	Gd	Tb	Dy	Y	Ho	Er	Tm	Yb	Lu
Basic (50% SiO2)	0.023	0.05	0.23	0.004	0.018	0.018	0.01	0.12	0.1	1.2	0.12	0.01	0.015	0.085	0.3	0.08	0.035	0.08	0.03		0.07		0.045	0.03
Intermediate (60% SiO2)	0.045	0.13	0.5	0.015	0.04	0.025	0.025	0.23	0.18	2.6	0.17	0.03	0.04	0.15	0.95	0.13	0.07	0.1	0.06	*0.15*	0.1	*0.2*	0.07	0.05
Acidic (70% SiO2)	0.095	0.3	0.9	0.04	0.1	0.04	0.06	0.43	0.3	6	0.25	0.1	0.1	0.2	3	0.2	0.15	0.13	0.15		0.18		0.1	0.075
SANIDINE																								
Basic		0.1	0.04			*0.007*			0.008	0.3		0.1			*0.3*								*0.001*	
Intermediate		0.18	0.5	*0.008*		0.009			0.017	0.9		0.15	*0.02*	*0.01*	1								*0.003*	*0.002*
Acidic		0.25	6	*0.015*	*0.025*	0.013		*0.05*	0.035	3	*0.04*	0.25	0.025	*0.02*	6.5		*0.015*						*0.008*	0.006
AMPHIBOLE																								
Basic		0.1	0.45	0.05	0.08	0.25	0.3	0.2	0.35	0.45	0.65	0.4	0.5	0.85	0.8	0.95	1.2	1.3	1.1	1	0.9	0.9	0.8	0.7
Intermediate		0.13	0.5	0.1	0.16	0.6	1	0.5	0.7	0.6	1.7	0.5	0.75	2.3	2	2.7	3.4	3.3	3	3	3	2.8	2.5	2
Acidic		0.15	0.6	0.2	0.3	1.5	3.5	1.5	1.7	0.8	4	0.65	1.3	6	5	7.5	8	9	9	10	8.5	8.5	7	6
BIOTITE																								
Basic	*1*	2.5	*4.5*	0.075	*0.1*	0.4	*0.45*	*0.035*	0.03	0.08	0.04		*0.14*	0.03	0.04	*0.03*	0.03	*0.035*	*0.2*		*0.03*		0.04	*0.03*
Intermediate	*1.6*	3.2	*6*	0.15	*0.15*	0.7	*1.4*	*0.15*	0.16	0.15	0.2	*0.15*	0.25	0.15	0.17	*0.15*	0.13	*0.15*	*0.45*		*0.1*		0.15	*0.13*
Acidic	*2.5*	4.5	*7.5*	0.35	*0.3*	1.3	3.5	0.5	0.75	0.25	0.9	*0.5*	0.45	0.6	0.6	*0.7*	0.55	*0.65*	0.8		*0.4*		0.45	0.45
CLINOPYROXENE																								
Basic	0.003	0.035	0.05	0.03	0.02	0.06	0.04	0.15	0.15	0.06	0.4	0.1	*0.2*	0.4	0.6	0.7	0.9	0.7	0.55	0.6	0.7		0.6	0.6
Intermediate	*0.03*	0.06	0.15	0.1	0.07	0.15	0.2	0.4	0.4	0.09	1	0.25	*0.3*	1.2	1.4	1.5	2	1.5	1.2	1.5	1.5	*0.8*	1.3	1.5
Acidic	*0.35*	0.1	0.4	0.35	0.2	0.35	0.8	1.2	1	0.15	2.5	0.6	*0.5*	3	3	3	4	3.5	2.5	3.2	2.6		2.5	3
ORTHOPYROXENE																								
Basic		0.003	0.002	0.13	*0.035*	0.15	*0.15*	0.025	0.01	0.007	0.02	0.03	0.055	0.03	0.02	0.06	0.07	0.1	0.2	*0.15*	0.2	0.1	0.2	0.2
Intermediate	*0.15*	0.025	0.01	0.15	*0.07*	0.25	*0.2*	0.2	0.1	0.03	0.3	0.09	0.1	0.3	0.15	0.25	0.4	0.4	0.45	*0.5*	0.3	*0.4*	0.5	0.5
Acidic	*0.5*	0.2	0.2	0.16	*0.15*	0.5	*0.7*	1.5	1.5	0.1	2.5	0.25	0.2	2.5	0.9	1.2	2	1.5	1	*2*	0.6	*1.5*	1.5	1.5
OLIVINE																								
Basic	0.0004	0.002	0.002	0.04	0.045	0.04	0.01	0.04	0.01	0.002	0.01	0.01	0.03	0.01	0.01		0.04	0.015	0.01				0.025	0.15
Intermediate	0.0004	0.035	0.01	0.1	0.1	0.1	0.01	0.15	0.06	0.02	0.06	0.01	0.06	0.05	0.06		0.1	0.07	0.01				0.15	0.35
Acidic				0.3	0.2	0.25	0.01	0.6	0.4		0.4	0.01	0.15	0.2	0.3		0.25	0.35	0.01				0.7	0.8
GARNET																								
Basic		0.001	0.001				0.1	0.03	0.03	0.002		0.3	0.3	0.5	0.35	2.4	1.3		2	3		*1*	5.5	10
Intermediate		0.005	0.006				*0.1*	0.1	0.15	0.008		0.6	*1*	1.2	0.9	5	4	*15*	12	10		*3.5*	17	25
Acidic		0.02	0.02				*0.1*	0.4	0.7	0.05	*0.7*	1.3	*4*	3	2	12	15	*30*	35	35		*10*	50	60

Copyright © by Mehmet Keskin

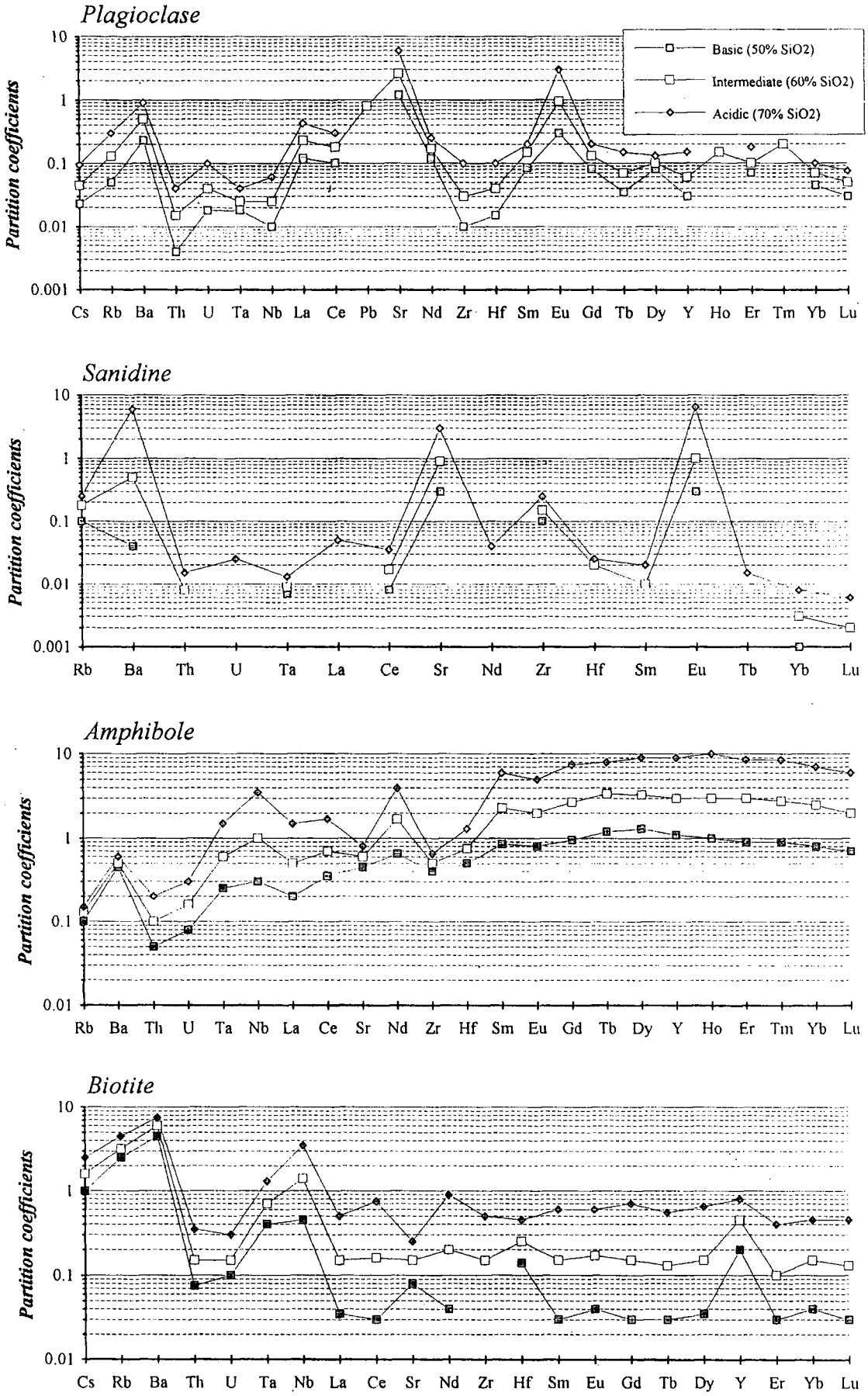

Figure: 4.40. Graphs illustrating compiled partition coefficients for plagioclase, sanidine,amphibole, biotite, clino- and orthopyroxene, olivine and garnet.

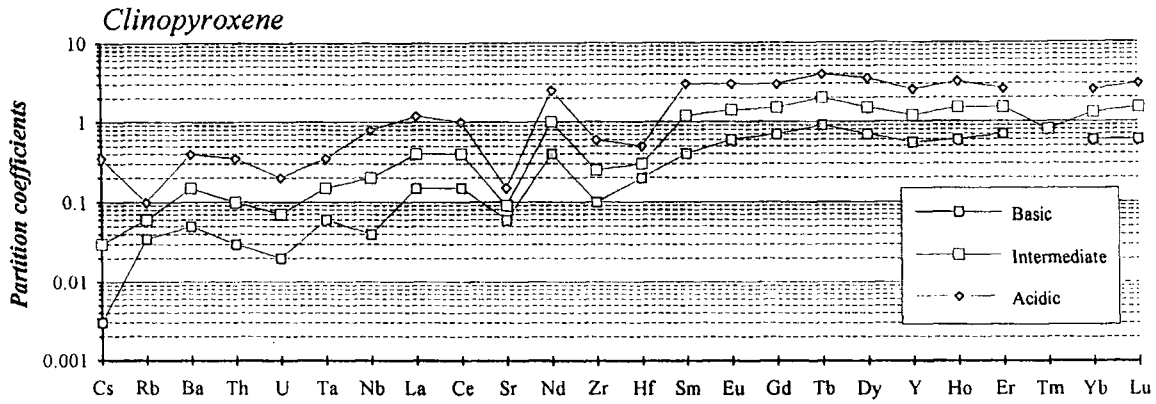

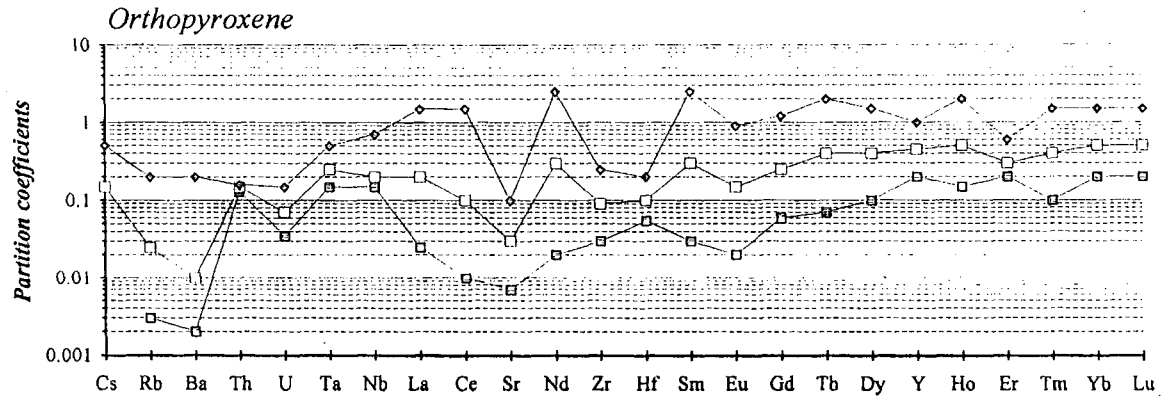

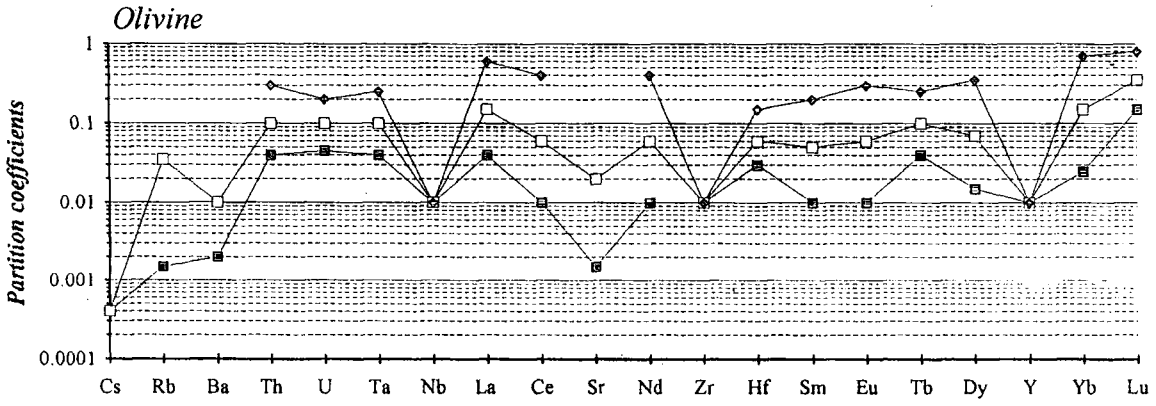

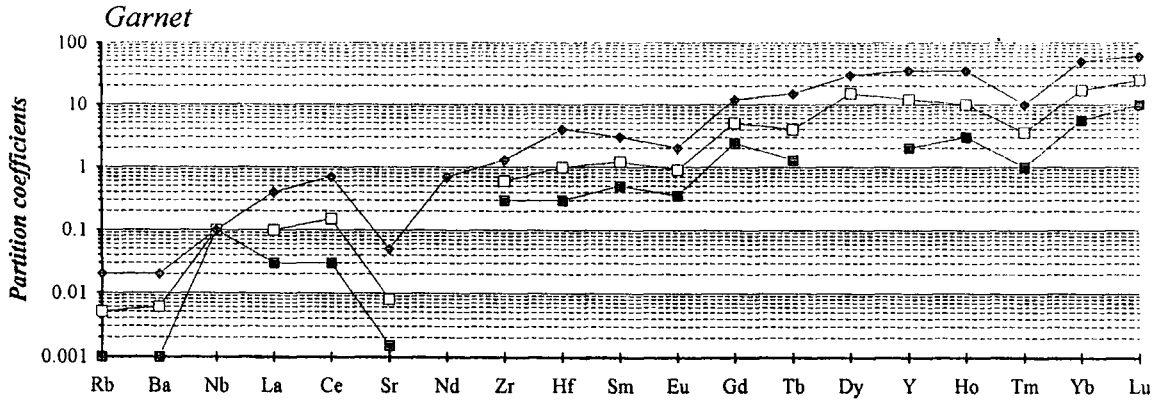

Figure: 4.40. (Continued)

for each element at 50, 60 and 70% SiO_2 respectively. The results are presented in Table 4.12 and Figure 4.40.

4.3.3. Onuma diagrams

Based on the partition coefficients of two kinds of pyroxene (augite and bronzite), Onuma et al. (1968) pointed out that, when trace element partition coefficients are plotted against these element's ionic radii, the partition coefficients of elements of the same charge tend to fit a smooth curve and each curve tends to parallel others. They concluded that trace elements occupy lattice sites of these crystals, rather than occurring as heterogeneous grains. In other words, trace element partition coefficients is determined primarily by crystal structure. The second significant conclusion of their study is that, for trace ions of the same charge, the difference between ionic radius of the trace element's ion and that of host ion is the most important factor determining the partition coefficients. In the literature, these diagrams were named as Onuma diagrams after that paper.

Higuchi and Nagasawa (1969) applied same sort of diagram to four more mineral (plagioclase, hornblende, biotite and olivine). Their diagrams also displayed similar type of patterns. Jensen (1973) extensively revised the previous work in the light of better estimates of effective ionic radii of Whittaker and Muntus (1970) by using about 50 analyses taken from the literature. She showed that, when plotted against the new radii, multi element plots of mineral/matrix K_ds curves display high degree of regularity.

In fact the relationship between ionic radius and charge in determining element distribution in crystals had been discovered long ago by Goldschmidt (in 1937) and named Goldschmidt's Rules. These are: (1) ions of similar radii and the same charge will enter into a crystal in amounts proportional to their concentration in the liquid, (2) an ion of a smaller radius but with the same charge as another, will be incorporated preferentially into a growing crystal, (3) an ion of the same radius but with a higher charge than other will be incorporated preferentially into a growing crystal (Henderson, 1990). On the other hand, the problem is not a simple one and certain elements, especially transition elements, do not obey these rules. The reason for that these elements are non-spherical because spatial distribution of electron density around the nucleus (namely orbitals) is variable and each is defined by its quantum number. In addition to this, bond type and strength, and type of the bonding polyhedron are the other factors controlling the element distribution between melt and a particular mineral.

Once the Onuma diagram, in other words the partition coefficient/radius curves, for a given mineral is properly established, it is possible to determine the sites of this particular mineral, and the elements that preferentially occupy these sites. It is also possible to predict partition coefficients of unanalysed elements from these curves as long as we now their valency states and ionic radii. Conversely, if the K_d of an element is known, its valency state can be found from curves of other elements on the diagram. On Onuma diagrams, the apex of the peaks indicates the optimum ionic radius for a cation in a given structural position, while the width of the peak is an expression of the ability of the lattice to adapt to non-ideal cations in that position (Jensen, 1973).

There are some difficulties in drawing the curves on the diagrams. If an element has two cation positions of different co-ordination number, then there will be two effective radii which should be taken into account. These two radii cannot be plotted into the same diagram because the relative distribution of an element between such positions is rarely known (Jensen, 1973). Ideally, all lines on a diagram are expected to be parallel or sub-parallel and peak at the same points with approximately the same slope. On the other hand, as Jensen (1973) showed, this is not necessarily the case and the individual curves may have different slopes. In addition, the positions on the vertical scale and the relative position of curves of different valency may be different and a slight shift may occur if two peaks overlap strongly.

In this study, the mineral/matrix partition coefficients of 8 amphibole and 8 plagioclase and 3 orthopyroxene have been plotted on Onuma diagrams, in order to analyse the trace and major element distribution between the crystals of these minerals and melt and also to determine the sites in these minerals. Before plotting the data, K_d values of each element were plotted against the SiO_2 content of their host rock. Then, a regression line was fitted to the data points of each element taking SiO_2 as the independent and K_d value as the dependent variable. Extrapolated Eu^{3+} values (Eq. 3.1) were used for the partition coefficient of Eu. Since 65% SiO_2 is located in the middle of silica range, it is probably the most reliable point at which best estimates of K_d values can be predicted. Partition coefficients of each element for these three minerals were estimated on their best fit lines at 65% SiO_2. Then they were plotted on Onuma graphs against ionic radii values which were recommended by Shannon (1976) as presented in Figures 4.41-a to c. Finally, standard error bars for each K_d value and curves connecting the elements of the same valency state have been drawn out on these diagrams. Transition elements (e.g. Sc, Co, Cr) were not analysed in this study, therefore there are some gaps between the data points especially on the left hand side of the diagrams. This does not seem to be a major

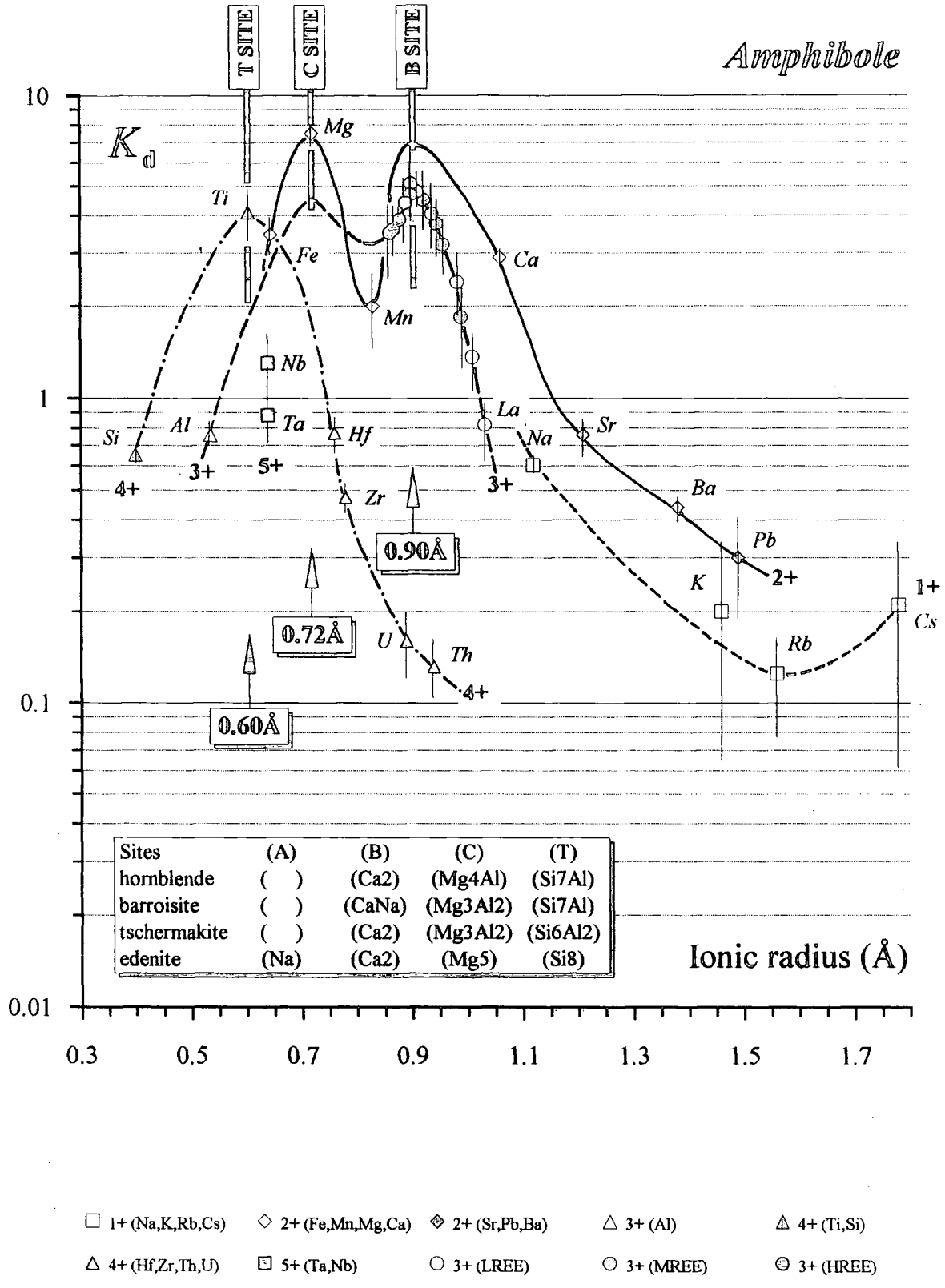

Figure: 4.41-a. Mineral/matrix partition coefficients of amphiboles plotted against ionic radius of each element. Ionic radii values are taken from Shannon (1976).

problem, since data points can be successfully connected to each other to produce smooth curves. Figure 4.41-a is of amphibole and shows three peaks at approximately 0.60, 0.72 and 0.90 Å corresponding to T, C and B sites respectively. As can be seen on the diagram, B site is mainly occupied by Ca and Mn and to an extent by M- to HREEs while C site is mainly filled by Mg and to a lesser extent Fe and also Al. Ti appears to be dominant in T site with relatively subordinate Al, Si and Hf.

In bronzite ($M_2Si_2O_6$) there are two co-ordination sides (M_I and M_{II}) both of which are almost equivalent and occupied by Mg^{2+} and Fe^{2+} in sixfold coordination (Figure 4.41-b). Larger ions Sr^{2+}, Ba^{2+}, REE^{3+}, U^{4+} and Th^{4+} can not easily substitute in the small sites available for Mg^{2+} and Fe^{2+}. Therefore, partition coefficients of larger ions such as those of REEs and Ca^{2+} and Na^{+} are quite smaller than those of K_ds of clinopyroxenes as seen in Figure 4.41-c. Plagioclase shows a well formed peak at about 1.16 Å formed by Ca, Sr and Na (Figure 4.41-c).

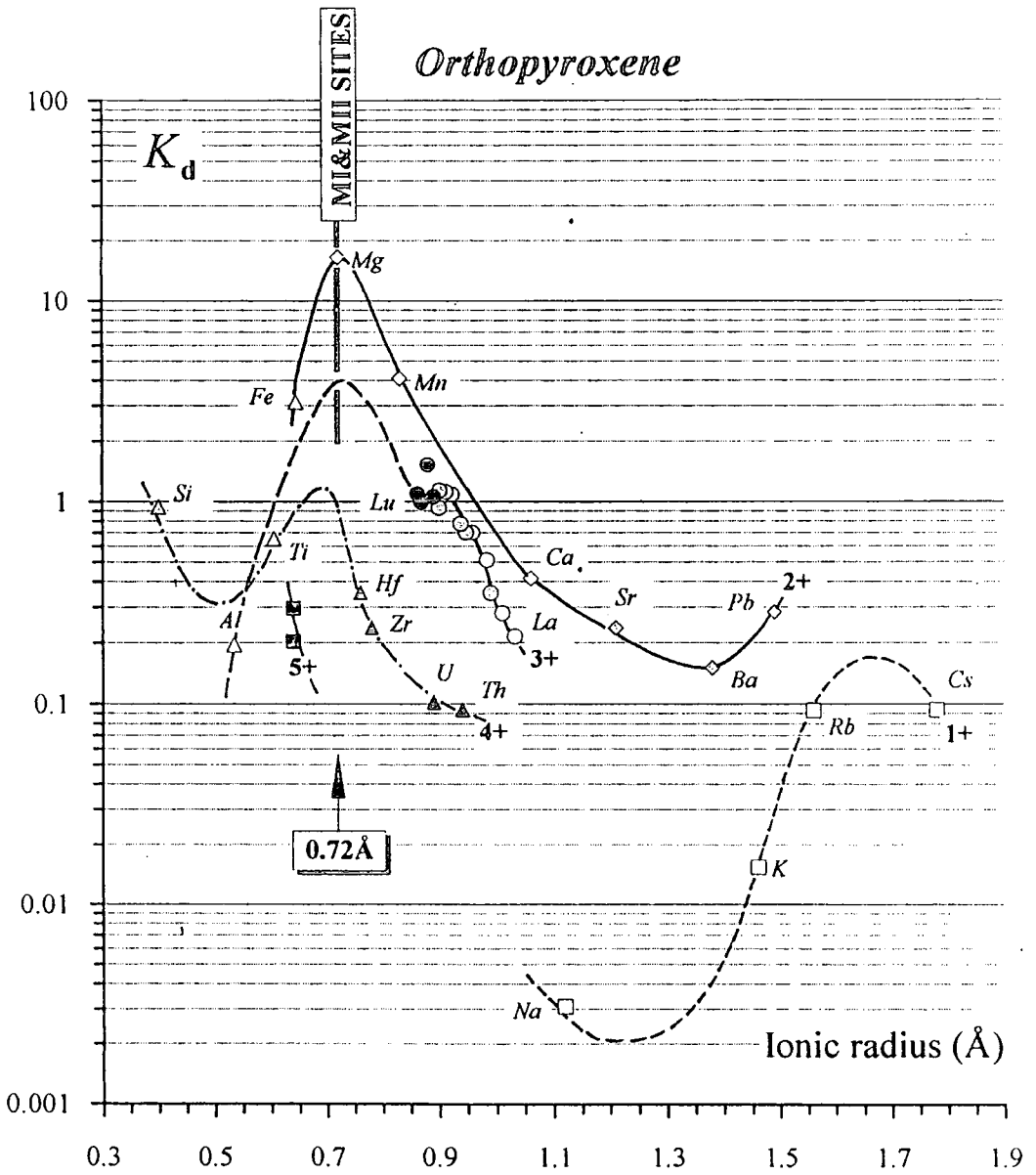

Figure: 4.41-b. Onuma diagram of orthopyroxenes

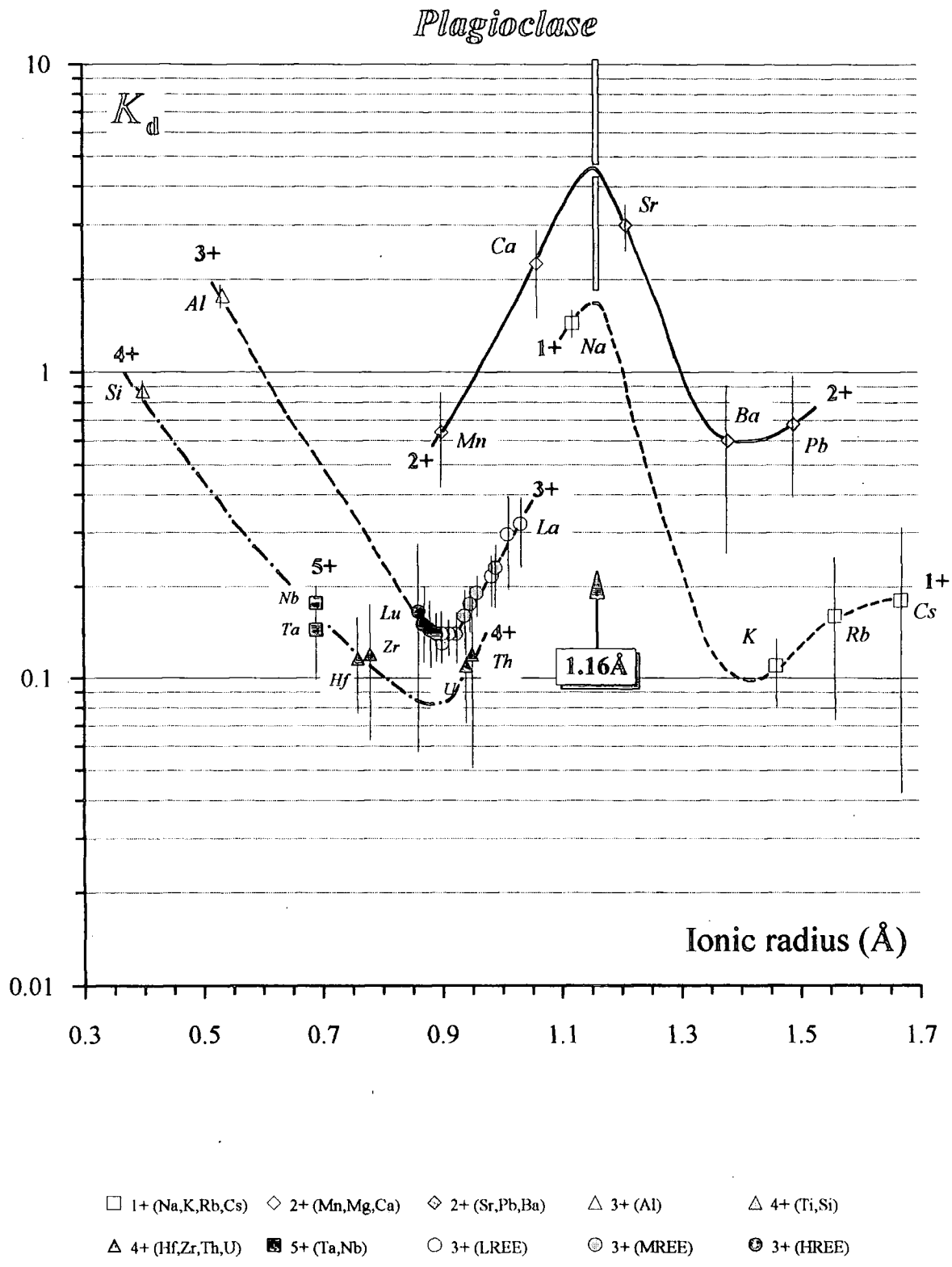

Figure: 4.41-c. Onuma diagram of plagioclase.

Table: 4.13. Table displaying the calculation of the concentration of elements in the matrix.

Sample	MK93					MK49				MK251					MK268				MK277				MK112				
Area	Mt. Dumlu					Mt. Dumlu				Mt. Dumlu					Mt. Kargapazarı				Mt. Kargapazarı				Pasinler area				
SiO_2 % of mineral		2.83	12.67	0.83			7.17	10.00			2.17	11.33	1.67			3.00	16.00			13.83	2.83			3.00	15.00	0.50	
Type	wr	amp	aver. plg	aver. opx	matrix	wr	amp	plg	matrix	wr	amp	plg	opx	matrix	wr	amp	plg	matrix	wr	plg	opx	matrix	wr	amp	plg	aver. opx	matrix
Analysed	♁	♁	♀	♀		♁	♁	♁		♁	♁	♁	♁		♁	♁	♁		♁	♁	♁		♁	♁	♁	♀	
Si	296774	207560	264488	250052	**305145**	309722	210879	261189	**324138**	304207	199681	252470	252678	**314805**					283172	253983	251591	**289088**	312293	207597	265023	250052	**325229**
Ti	4496	19601	294	1341	**4653**	3657	17958	364	**2817**	4197	21181	438	2392	**4300**					4796	506	813	**5643**	3417	14334	199	1341	**3621**
Al	85209	55635	140914	10668	**78514**	83463	55058	143439	**78681**	87273	65062	149627	15847	**80920**					83886	148757	6654	**75744**	84151	57385	141167	10668	**75093**
Fe	32943	92380	2815	132741	**34505**	26928	93615	3370	**24000**	31894	104115	3288	101745	**32492**					36510	4356	136360	**38456**	26718	111495	2828	132741	**27344**
Mn	542	271	335	4420	**544**	465	1510	312	**393**	620	844	245	2563	**626**					620	476	4451	**513**	465	1789	367	4420	**410**
Mg	4913	29395	247	50926	**4336**	3822	29611	320	**2012**	4388	27246	289	55448	**3345**					8250	196	51632	**8113**	2507	26844	278	50926	**1725**
Ca	35306	82912	69031	8438	**28856**	28874	82198	74206	**18785**	34449	80120	82043	11362	**27378**					43597	81350	8395	**38527**	26301	79996	70419	8438	**16314**
Na	26558	19133	43995	1276	**24420**	28784	17500	41151	**28268**	31232	19789	37325	96	**31324**					30490	36806	2062	**30408**	27300	15900	42592	1276	**25065**
K	22910	5508	2723	594	**26777**	23657	4781	2218	**27880**	19507	5583	1725	349	**22615**					18096	2580	365	**21273**	27061	5127	2565	594	**32539**
Rb	65.5	10.4	19.9	6.2	**74.84**	70.9	28.7	29.7	**79.55**	58.2	4.0	4.0	6.3	**67.81**	88.3	13.5	14.1	**105.73**	51.8	21.8	8.0	**58.31**	80.5	8.2	5.7	6.2	**97.39**
Sr	431	261	1056	85	**345.78**	299	77	749	**263.62**	452	212	1183	87	**367.43**	342	199	880	**240.76**	443	987	64	**365.04**	349	160	1082	85	**222.31**
Y	17.3	60.2	4.8	17.5	**17.70**	17.8	117.1	13.8	**9.72**	13.6	41.9	1.5	13.5	**14.55**	15.7	79.9	9.9	**14.51**	15.9	3.9	14.8	**17.92**	18.3	72.8	1.9	17.5	**19.31**
Zr	200	109	21	40	**232.07**	111	76	34	**123.70**	157	77	7	43	**181.71**	155	100	29	**181.75**	156	34	35	**180.42**	156	88	14	40	**185.20**
Nb	14.6	31.1	3.4	4.2	**15.86**	10.4	25.6	4.1	**9.79**	11.8	13.6	2.4	3.9	**13.13**	12.9	24.5	2.9	**14.42**	12.0	2.8	3.1	**13.87**	10.9	17.1	1.7	4.2	**12.46**
Cs	2.4	0.4	0.7	0.3	**2.76**	3.6	1.3	1.4	**4.12**	1.7	0.1	0.1	0.2	**1.98**	4.5	1.9	0.8	**5.30**	1.4	0.5	0.4	**1.61**	3.5	0.4	0.3	0.3	**4.22**
Ba	596	314	433	84	**635.09**	462	194	526	**477.90**	535	230	189	90	**598.23**	450	206	379	**472.80**	385	339	62	**403.16**	556	134	188	84	**642.19**
La	38.46	38.31	17.99	13.16	**41.81**	33.95	69.36	44.17	**29.65**	33.10	20.75	8.07	8.01	**37.26**	29.23	35.16	33.26	**28.22**	28.13	14.04	9.56	**31.10**	31.64	22.13	7.57	13.16	**36.54**
Ce	61.49	83.15	18.83	29.32	**67.53**	50.80	141.42	32.86	**45.12**	57.96	60.79	11.23	18.16	**64.92**	46.31	85.58	22.77	**49.51**	48.57	19.56	20.35	**54.34**	42.40	50.39	9.65	29.32	**48.21**
Pr	6.72	13.87	2.63	3.68	**7.12**	6.12	24.56	6.87	**4.44**	6.03	8.08	1.01	2.36	**6.72**	5.32	13.46	5.10	**5.06**	5.31	1.95	2.40	**5.97**	5.41	9.03	0.99	3.68	**6.10**
Nd	23.89	63.93	8.82	16.25	**24.89**	20.79	105.35	23.22	**13.18**	19.50	37.01	3.63	10.88	**21.35**	18.11	61.93	17.46	**16.62**	19.31	6.29	10.62	**21.77**	18.95	44.52	3.61	16.25	**20.85**
Sm	4.13	14.07	1.30	3.30	**4.24**	3.78	22.72	3.38	**2.18**	3.41	9.04	0.55	2.57	**3.67**	3.37	14.76	2.44	**3.14**	3.48	1.07	2.33	**3.91**	3.65	11.53	0.60	3.30	**3.92**
Eu	1.09	3.52	1.14	0.87	**1.00**	0.99	4.13	1.82	**0.61**	1.10	2.47	0.64	0.80	**1.13**	1.03	3.15	1.32	**0.90**	0.99	1.18	0.49	**0.98**	1.09	2.97	0.70	0.87	**1.10**
Gd	3.26	14.31	1.11	3.52	**3.21**	3.30	24.18	3.14	**1.51**	3.29	9.03	0.33	2.76	**3.55**	3.41	15.17	2.23	**3.21**	2.97	1.01	2.55	**3.31**	3.58	13.58	0.48	3.52	**3.78**
Tb	0.46	2.06	0.14	0.55	**0.45**	0.51	3.54	0.45	**0.26**	0.38	1.34	0.04	0.44	**0.40**	0.47	2.38	0.27	**0.44**	0.47	0.12	0.43	**0.53**	0.50	2.15	0.06	0.55	**0.52**
Dy	2.69	11.23	0.76	3.00	**2.69**	2.85	21.13	2.19	**1.35**	2.09	8.03	0.22	2.43	**2.18**	2.49	13.47	1.52	**2.28**	2.50	0.61	2.50	**2.81**	2.96	12.72	0.32	3.00	**3.09**
Ho	0.49	2.27	0.14	0.61	**0.48**	0.58	4.24	0.43	**0.28**	0.40	1.55	0.04	0.47	**0.41**	0.48	2.62	0.27	**0.44**	0.51	0.12	0.57	**0.57**	0.54	2.58	0.06	0.61	**0.56**
Er	1.39	5.28	0.39	1.63	**1.41**	1.52	10.33	1.10	**0.81**	1.14	3.86	0.13	1.27	**1.21**	1.35	7.43	0.78	**1.24**	1.48	0.31	1.52	**1.67**	1.57	6.54	0.17	1.63	**1.65**
Tm	0.21	0.78	0.06	0.28	**0.21**	0.22	1.63	0.17	**0.11**	0.15	0.61	0.03	0.23	**0.15**	0.23	0.94	0.10	**0.23**	0.24	0.04	0.25	**0.27**	0.26	0.99	0.03	0.28	**0.28**
Yb	1.35	4.06	0.34	1.52	**1.40**	1.36	8.90	0.87	**0.76**	1.04	3.17	0.09	1.10	**1.11**	1.37	5.90	0.70	**1.33**	1.33	0.29	1.49	**1.49**	1.55	5.41	0.15	1.52	**1.67**
Lu	0.20	0.57	0.06	0.26	**0.21**	0.25	1.20	0.13	**0.19**	0.16	0.45	0.03	0.18	**0.16**	0.19	0.77	0.11	**0.18**	0.21	0.05	0.26	**0.23**	0.25	0.79	0.03	0.26	**0.27**
Hf	4.69	3.51	0.47	1.24	**5.40**	3.26	3.36	0.78	**3.55**	3.33	2.72	0.19	1.35	**3.81**	3.54	3.59	0.64	**4.10**	3.83	0.74	1.04	**4.44**	3.50	2.96	0.32	1.24	**4.12**
Ta	0.95	1.03	0.16	0.18	**1.07**	0.95	0.99	0.25	**1.03**	0.67	0.56	0.08	0.15	**0.77**	0.96	1.10	0.21	**1.11**	0.88	0.15	0.18	**1.02**	0.81	0.74	0.11	0.18	**0.94**
Pb	12.97	17.89	10.83	4.09	**13.22**	13.23	6.34	14.22	**13.71**	12.35	2.78	7.23	3.82	**13.45**	14.65	4.28	10.64	**15.82**	11.46	9.47	4.13	**12.04**	15.57	6.01	6.49	4.09	**17.66**
Th	9.94	1.33	1.55	1.01	**11.59**	11.47	2.76	3.37	**13.20**	8.35	1.19	0.53	0.91	**9.72**	10.59	2.01	2.06	**12.60**	7.50	1.76	1.09	**8.67**	9.51	1.32	0.69	1.01	**11.48**
U	2.24	0.47	0.56	0.29	**2.58**	2.70	1.00	1.07	**3.04**	2.01	0.24	0.10	0.24	**2.35**	3.28	0.53	0.76	**3.88**	2.06	0.54	0.27	**2.38**	3.06	0.41	0.20	0.29	**3.70**
$\delta^{18}O$	8.2	6.7	7.4	6.0		9.0	7.7	8.4		7.3		7.4	6.3		10.0	7.2	8.3		7.2	6.7	6.7		9.4	6.9	7.9	6.0	

Copyright © by Mehmet Keskin

Table: 4.13. (Continued)

Sample	MK132					MK154					MK174				MK265			MK338			
Area	*N of Horasan*					*S of Horasan*					*Kağızman area*				*Mt. Kargapazarı*			*Pasinler area*			
SiO_2 % of mineral		2.33	15.83	3.00			3.33	9.67	0.83			2.17	9.83			13.83			10.67	2.00	
Type	*wr*	*amp*	*plg*	*opx*	*matrix*	*wr*	*amp*	*plg*	*biotite*	*matrix*	*wr*	*amp*	*plg*	*matrix*	*wr*	*cpx*	*matrix*	*wr*	*sanid*	*aver. plg*	*matrix*
Analysed	♁	♁	♁	♁		♁	♁	♁	♁		♁	♁	♁		♁	♁		♁	♁	♈	
Si	300000	204073	268802	245886	**311158**	312761	207373	277001	184393	**322083**	310751	193833	272949	**317856**	298691	247858	**306849**	331879	307944	264488	**336347**
Ti	3897	13156	205	818	**4482**	2518	10423	130	30047	**2215**	3237	20031	216	**3161**	3657	2118	**3904**	1019	186	294	**1138**
Al	86532	65796	136156	9503	**80113**	86691	64222	132959	72172	**82507**	83780	61237	134292	**78694**	81028	9454	**92516**	81134	98512	140914	**77642**
Fe	31684	99912	2091	160118	**30723**	22172	113670	1325	142269	**19819**	27698	131593	2447	**27956**	30775	48145	**27987**	13429	851	2815	**15209**
Mn	465	1495	431	6246	**221**	465	2083	200	3529	**402**	774	3491	316	**759**	542	568	**538**	465	108	335	**511**
Mg	2993	27520	257	45698	**1192**	3276	25883	280	25546	**2524**	1638	22744	112	**1288**	7380	33546	**3181**	20	175	247	**-4**
Ca	33662	79139	62651	5556	**27567**	26301	79235	53983	8079	**21324**	22727	80266	58566	**17305**	35521	152032	**16821**	4717	2113	69031	**3562**
Na	33235	18643	47626	1669	**31978**	32716	17634	52263	8683	**31337**	34867	19576	50203	**33531**	26188	2772	**29946**	33458	36935	43995	**32792**
K	20254	4433	2630	1067	**24991**	20752	4731	3061	66307	**22918**	26231	5107	4285	**29203**	22661	318	**26247**	44327	80499	2723	**40860**
Rb	56.3	13.8	9.7	4.4	**68.91**	72.8	26.7	15.4	294.8	**78.91**	74.9	8.4	58.5	**78.37**	70.3	4.4	**80.83**	129.5	148.7	19.9	**129.63**
Sr	652	416	1621	104	**485.72**	500	162	1425	66	**413.00**	230	166	524	**198.37**	454	33	**521.25**	42	121	1056	**9.50**
Y	15.6	51.7	2.8	24.2	**16.77**	9.0	54.4	1.3	4.3	**8.13**	33.5	170.8	3.2	**33.45**	16.1	22.0	**15.20**	30.0	3.7	4.8	**33.81**
Zr	189	104	21	41	**230.81**	42	74	7	14	**44.81**	156	227	20	**169.45**	148	17	**168.80**	52	6	21	**58.71**
Nb	18.3	24.8	4.0	5.5	**21.45**	13.4	30.3	5.4	35.5	**13.43**	21.0	36.4	3.4	**22.63**	10.1	1.9	**11.47**	22.0	5.4	3.4	**24.43**
Cs	1.2	0.5	0.3	0.2	**1.41**	2.2	1.3	1.5	4.5	**2.34**	1.5	0.3	1.2	**1.57**	2.8	0.2	**3.22**	3.0	0.9	0.7	**3.29**
Ba	725	429	314	99	**840.51**	648	322	259	4024	**671.88**	631	219	1268	**570.33**	499	55	**570.60**	425	1907	433	**244.27**
La	39.57	43.80	14.87	21.92	**45.08**	30.53	29.10	12.68	9.35	**32.79**	28.45	25.97	9.23	**30.65**	31.44	25.22	**32.44**	63.34	20.24	17.99	**69.65**
Ce	72.67	121.51	24.73	49.47	**81.73**	51.63	86.27	17.10	19.27	**54.48**	53.28	92.31	12.76	**56.85**	45.75	7.89	**51.83**	119.19	16.56	18.83	**134.03**
Pr	7.59	13.79	2.45	6.29	**8.50**	5.39	13.65	1.43	2.22	**5.55**	6.48	13.82	1.23	**6.89**	5.52	2.86	**5.95**	12.05	3.81	2.63	**13.28**
Nd	27.24	64.59	8.40	27.24	**29.92**	18.09	63.04	4.06	8.63	**18.02**	24.14	73.88	3.94	**25.17**	19.20	12.49	**20.27**	37.46	12.28	8.82	**41.19**
Sm	4.28	12.80	1.08	4.99	**4.65**	3.02	13.24	0.55	1.54	**2.91**	5.08	21.81	0.75	**5.15**	3.56	2.14	**3.79**	6.45	2.39	1.30	**7.06**
Eu	1.29	3.35	0.91	1.33	**1.31**	1.00	3.35	0.73	0.77	**0.94**	1.61	6.06	1.84	**1.48**	1.09	0.54	**1.18**	0.80	1.77	1.14	**0.67**
Gd	3.29	12.33	0.68	5.25	**3.47**	2.77	12.41	0.34	1.68	**2.68**	5.34	29.27	0.69	**5.27**	3.53	3.14	**3.59**	6.16	1.12	1.11	**6.89**
Tb	0.48	1.50	0.08	0.77	**0.51**	0.33	1.74	0.04	0.12	**0.31**	0.83	4.71	0.09	**0.81**	0.45	0.45	**0.45**	0.87	0.15	0.14	**0.98**
Dy	2.37	9.70	0.43	4.08	**2.48**	1.51	9.81	0.18	0.80	**1.34**	4.98	29.78	0.58	**4.85**	2.42	2.66	**2.38**	4.82	0.76	0.76	**5.41**
Ho	0.49	1.86	0.09	0.81	**0.52**	0.25	1.94	0.02	0.13	**0.21**	1.02	6.34	0.11	**0.99**	0.44	0.58	**0.42**	0.93	0.13	0.14	**1.05**
Er	1.30	4.69	0.26	2.10	**1.38**	0.74	4.68	0.09	0.32	**0.67**	3.08	16.96	0.32	**3.04**	1.31	1.51	**1.28**	2.99	0.29	0.39	**3.38**
Tm	0.21	0.75	0.04	0.36	**0.22**	0.09	0.67	0.03	0.04	**0.08**	0.54	2.51	0.05	**0.55**	0.19	0.23	**0.18**	0.46	0.06	0.06	**0.52**
Yb	1.19	4.36	0.20	1.96	**1.26**	0.60	3.91	0.11	0.20	**0.53**	2.87	14.39	0.35	**2.87**	1.14	1.20	**1.13**	2.72	0.27	0.34	**3.07**
Lu	0.21	0.73	0.04	0.34	**0.23**	0.09	0.58	0.03	0.03	**0.08**	0.42	2.14	0.05	**0.42**	0.18	0.22	**0.17**	0.46	0.06	0.06	**0.51**
Hf	3.80	3.34	0.46	1.33	**4.58**	1.32	3.02	0.19	0.43	**1.38**	3.59	7.42	0.46	**3.85**	3.34	0.48	**3.80**	1.82	0.19	0.47	**2.05**
Ta	1.07	0.93	0.17	0.21	**1.29**	0.83	0.97	0.18	0.97	**0.90**	1.40	1.31	0.16	**1.55**	0.61	0.11	**0.69**	1.62	0.20	0.16	**1.82**
Pb	13.62	12.47	5.58	4.32	**15.63**	14.74	12.11	14.12	6.56	**14.99**	15.70	4.58	18.86	**15.63**	12.53	3.03	**14.06**	21.49	25.60	10.83	**21.23**
Th	10.92	2.76	1.23	1.04	**13.48**	10.97	1.97	1.24	1.10	**12.50**	10.57	1.68	1.48	**11.80**	8.04	0.51	**9.25**	26.50	5.27	1.55	**29.66**
U	3.74	0.96	0.70	0.35	**4.57**	3.05	1.06	0.43	0.48	**3.44**	3.09	0.60	0.72	**3.42**	2.19	0.17	**2.51**	4.02	0.46	0.56	**4.53**
$\delta^{18}O$	6.5	6.0	5.6	5.1		9.3	6.8	7.7	6.2		7.3	6.9	6.8							7.4	

EXPLANATION

♁ : *analysed mineral samples*
♈ : *not analysed, averaged*
wr: whole-rock
aver: average

plg: plagioclase
amp: amphibole
cpx: clinopyroxene
opx: orthopyroxene
anorth: anorthoclase

Copyright © by Mehmet Keskin

AMPHIBOLE

Sample	MK112			MK132			MK154			MK174			MK112		MK132		MK154		MK174	
Area	Pasinler area			N of Horasan			S of Horasan			Kağızman area			←		K_ds					→
SiO_2													66.81		64.18		66.91		66.48	
T°C (px)													1000							
T°C (plg)													1020		1060		1067		1100	
P (kbar)													~5.7		~7		~6.5		~6.6	
O fugacity													$10^{-12.3}$		$10^{-13.1}$		$10^{-13.2}$		$10^{-14.8}$	
Type	*wr*	*matrix*	*amp*	*wr*	*matrix*	*amp*	*wr*	*matrix*	*amp*	*wr*	*matrix*	*amp*	*amp/mtrx*	*amp/wr*	*amp/mtrx*	*amp/wr*	*amp/mtrx*	*amp/wr*	*amp/mtrx*	*amp/wr*
Si	312293	325229	207597	300000	311158	204073	312761	322083	207373	310751	317856	193833	0.64	0.66	0.66	0.68	0.64	0.66	0.61	0.62
Ti	3417	3621	14334	3897	4482	13156	2518	2215	10423	3237	3161	20031	3.96	4.19	2.94	3.38	4.70	4.14	6.34	6.19
Al	84151	75093	57385	86532	80113	65796	86691	82507	64222	83780	78694	61237	0.76	0.68	0.82	0.76	0.78	0.74	0.78	0.73
Fe	26718	27344	111495	31684	30723	99912	22172	19819	113670	27698	27956	131593	4.08	4.17	3.25	3.15	5.74	5.13	4.71	4.75
Mn	465	410	1789	465	221	1495	465	402	2083	774	759	3491	4.37	3.85	6.76	3.22	5.18	4.48	4.60	4.51
Mg	2507	1725	26844	2993	1192	27520	3276	2524	25883	1638	1288	22744	15.56	10.71	23.09	9.20	10.26	7.90	17.66	13.89
Ca	26301	16314	79996	33662	27567	79139	26301	21324	79235	22727	17305	80266	4.90	3.04	2.87	2.35	3.72	3.01	4.64	3.53
Na	27300	25065	15900	33235	31978	18643	32716	31337	17634	34867	33531	19576	0.63	0.58	0.58	0.56	0.56	0.54	0.58	0.56
K	27061	32539	5127	20254	24991	4433	20752	22918	4731	26231	29203	5107	0.16	0.19	0.18	0.22	0.21	0.23	0.17	0.19
Rb	80.5	97.4	8.2	56.3	68.9	13.8	72.8	78.9	26.7	74.9	78.4	8.4	0.08	0.10	0.20	0.25	0.34	0.37	0.11	0.11
Sr	349	222	160	652	486	416	500	413	162	230	198	166	0.72	0.46	0.86	0.64	0.39	0.32	0.84	0.72
Y	18.3	19.3	72.8	15.6	16.8	51.7	9.0	8.1	54.4	33.5	33.5	170.8	3.77	3.98	3.09	3.32	6.69	6.06	5.11	5.10
Zr	156	185	88	189	231	104	42	45	74	156	169	227	0.47	0.56	0.45	0.55	1.65	1.77	1.34	1.46
Nb	10.9	12.5	17.1	18.3	21.5	24.8	13.4	13.4	30.3	21.0	22.6	36.4	1.38	1.57	1.16	1.36	2.26	2.26	1.61	1.73
Cs	3.5	4.2	0.4	1.2	1.4	0.5	2.2	2.3	1.3	1.5	1.6	0.3	0.09	0.11	0.34	0.42	0.56	0.59	0.18	0.18
Ba	556	642	134	725	841	429	648	672	322	631	570	219	0.21	0.24	0.51	0.59	0.48	0.50	0.38	0.35
La	31.64	36.54	22.13	39.57	45.08	43.80	30.53	32.79	29.10	28.45	30.65	25.97	0.61	0.70	0.97	1.11	0.89	0.95	0.85	0.91
Ce	42.40	48.21	50.39	72.67	81.73	121.51	51.63	54.48	86.27	53.28	56.85	92.31	1.05	1.19	1.49	1.67	1.58	1.67	1.62	1.73
Pr	5.41	6.10	9.03	7.59	8.50	13.79	5.39	5.55	13.65	6.48	6.89	13.82	1.48	1.67	1.62	1.82	2.46	2.53	2.01	2.13
Nd	18.95	20.85	44.52	27.24	29.92	64.59	18.09	18.02	63.04	24.14	25.17	73.88	2.14	2.35	2.16	2.37	3.50	3.48	2.94	3.06
Sm	3.65	3.92	11.53	4.28	4.65	12.80	3.02	2.91	13.24	5.08	5.15	21.81	2.94	3.16	2.75	2.99	4.54	4.39	4.24	4.29
Eu	1.09	1.10	2.97	1.29	1.31	3.35	1.00	0.94	3.35	1.61	1.48	6.06	2.71	2.72	2.56	2.59	3.56	3.35	4.10	3.75
Gd	3.58	3.78	13.58	3.29	3.47	12.33	2.77	2.68	12.41	5.34	5.27	29.27	3.59	3.79	3.55	3.75	4.64	4.49	5.56	5.48
Tb	0.50	0.52	2.15	0.48	0.51	1.50	0.33	0.31	1.74	0.83	0.81	4.71	4.15	4.31	2.92	3.15	5.65	5.30	5.78	5.69
Dy	2.96	3.09	12.72	2.37	2.48	9.70	1.51	1.34	9.81	4.98	4.85	29.78	4.12	4.30	3.92	4.09	7.30	6.50	6.13	5.99
Ho	0.54	0.56	2.58	0.49	0.52	1.86	0.25	0.21	1.94	1.02	0.99	6.34	4.64	4.75	3.58	3.79	9.38	7.88	6.39	6.21
Er	1.57	1.65	6.54	1.30	1.38	4.69	0.74	0.67	4.68	3.08	3.04	16.96	3.97	4.16	3.39	3.60	7.00	6.29	5.57	5.51
Tm	0.26	0.28	0.99	0.21	0.22	0.75	0.09	0.08	0.67	0.54	0.55	2.51	3.54	3.76	3.43	3.63	8.40	7.13	4.58	4.63
Yb	1.55	1.67	5.41	1.19	1.26	4.36	0.60	0.53	3.91	2.87	2.87	14.39	3.24	3.48	3.45	3.67	7.35	6.51	5.01	5.01
Lu	0.25	0.27	0.79	0.21	0.23	0.73	0.09	0.08	0.58	0.42	0.42	2.14	2.92	3.17	3.20	3.42	7.36	6.39	5.10	5.09
Hf	3.50	4.12	2.96	3.80	4.58	3.34	1.32	1.38	3.02	3.59	3.85	7.42	0.72	0.85	0.73	0.88	2.18	2.30	1.93	2.06
Ta	0.81	0.94	0.74	1.07	1.29	0.93	0.83	0.90	0.97	1.40	1.55	1.31	0.78	0.91	0.72	0.87	1.08	1.17	0.85	0.93
Pb	15.57	17.66	6.01	13.62	15.63	12.47	14.74	14.99	12.11	15.70	15.63	4.58	0.34	0.39	0.80	0.92	0.81	0.82	0.29	0.29
Th	9.51	11.48	1.32	10.92	13.48	2.76	10.97	12.50	1.97	10.57	11.80	1.68	0.12	0.14	0.20	0.25	0.16	0.18	0.14	0.16
U	3.06	3.70	0.41	3.74	4.57	0.96	3.05	3.44	1.06	3.09	3.42	0.60	0.11	0.14	0.21	0.26	0.31	0.35	0.18	0.19
$\delta^{18}O$	9.4		6.9	6.5		6	9.3		6.8	7.3		6.9								

Table: 4.14. Mineral/matrix and mineral/whole-rock distribution coefficients for amphiboles.

Copyright © by Mehmet Keskin

Copyright © by Mehmet Keskin

AMPHIBOLE

Sample	MK49			MK93			MK251			MK268			MK49		MK93		MK251		MK268	
Area	Mt. Dumlu			Mt. Dumlu			Mt. Dumlu			Mt. Kargapazarı			← K_ds →							
SiO_2													66.26		63.49		65.08		65.47	
T°C (px)															1100		1050			
T°C (plg)																	1073			
P (kbar)															~5.5		~6.7-7			
O fugacity																	$10^{-12.4}$			
Type	*wr*	*matrix*	*amp*	*wr*	*matrix*	*amp*	*wr*	*matrix*	*amp*	*wr*	*matrix*	*amp*	*amp/mtrx*	*amp/wr*	*amp/mtrx*	*amp/wr*	*amp/mtrx*	*amp/wr*	*amp/mtrx*	*amp/wr*
Si	309722	324138	210879	296774	305145	207560	304207	314805	199681				0.65	0.68	0.68	0.70	0.63	0.66		
Ti	3657	2817	17958	4496	4653	19601	4197	4300	21181				6.38	4.91	4.21	4.36	4.93	5.05		
Al	83463	78681	55058	85209	78514	55635	87273	80920	65062				0.70	0.66	0.71	0.65	0.80	0.75		
Fe	26928	24000	93615	32943	34505	92380	31894	32492	104115				3.90	3.48	2.68	2.80	3.20	3.26		
Mn	465	393	1510	542	544	271	620	626	844				3.85	3.25	0.50	0.50	1.35	1.36		
Mg	3822	2012	29611	4913	4336	29395	4388	3345	27246				14.72	7.75	6.78	5.98	8.14	6.21		
Ca	28874	18785	82198	35306	28856	82912	34449	27378	80120				4.38	2.85	2.87	2.35	2.93	2.33		
Na	28784	28268	17500	26558	24420	19133	31232	31324	19789				0.62	0.61	0.78	0.72	0.63	0.63		
K	23657	27880	4781	22910	26777	5508	19507	22615	5583				0.17	0.20	0.21	0.24	0.25	0.29		
Rb	70.9	79.5	28.7	65.5	74.8	10.4	58.2	67.8	4.0	88.3	105.7	13.5	0.36	0.40	0.14	0.16	0.06	0.07	0.13	0.15
Sr	299	264	77	431	346	261	452	367	212	342	241	199	0.29	0.26	0.75	0.61	0.58	0.47	0.82	0.58
Y	17.8	9.7	117.1	17.3	17.7	60.2	13.6	14.5	41.9	15.7	14.5	79.9	12.04	6.57	3.40	3.49	2.88	3.07	5.51	5.08
Zr	111	124	76	200	232	109	157	182	77	155	182	100	0.62	0.68	0.47	0.54	0.43	0.49	0.55	0.64
Nb	10.4	9.8	25.6	14.6	15.9	31.1	11.8	13.1	13.6	12.9	14.4	24.5	2.61	2.47	1.96	2.13	1.03	1.15	1.70	1.90
Cs	3.6	4.1	1.3	2.4	2.8	0.4	1.7	2.0	0.1	4.5	5.3	1.9	0.30	0.34	0.13	0.15	0.03	0.03	0.36	0.42
Ba	462	478	194	596	635	314	535	598	230	450	473	206	0.40	0.42	0.49	0.53	0.38	0.43	0.43	0.46
La	33.95	29.65	69.36	38.46	41.81	38.31	33.10	37.26	20.75	29.23	28.22	35.16	2.34	2.04	0.92	1.00	0.56	0.63	1.25	1.20
Ce	50.80	45.12	141.42	61.49	67.53	83.15	57.96	64.92	60.79	46.31	49.51	85.58	3.13	2.78	1.23	1.35	0.94	1.05	1.73	1.85
Pr	6.12	4.44	24.56	6.72	7.12	13.87	6.03	6.72	8.08	5.32	5.06	13.46	5.53	4.01	1.95	2.06	1.20	1.34	2.66	2.53
Nd	20.79	13.18	105.35	23.89	24.89	63.93	19.50	21.35	37.01	18.11	16.62	61.93	8.00	5.07	2.57	2.68	1.73	1.90	3.73	3.42
Sm	3.78	2.18	22.72	4.13	4.24	14.07	3.41	3.67	9.04	3.37	3.14	14.76	10.41	6.02	3.32	3.40	2.46	2.65	4.71	4.38
Eu	0.99	0.61	4.13	1.09	1.00	3.52	1.10	1.13	2.47	1.03	0.90	3.15	6.73	4.19	3.52	3.23	2.18	2.24	3.50	3.04
Gd	3.30	1.51	24.18	3.26	3.21	14.31	3.29	3.55	9.03	3.41	3.21	15.17	16.04	7.33	4.45	4.38	2.54	2.74	4.72	4.44
Tb	0.51	0.26	3.54	0.46	0.45	2.06	0.38	0.40	1.34	0.47	0.44	2.38	13.87	6.94	4.54	4.47	3.35	3.52	5.43	5.06
Dy	2.85	1.35	21.13	2.69	2.69	11.23	2.09	2.18	8.03	2.49	2.28	13.47	15.64	7.41	4.18	4.18	3.68	3.84	5.91	5.40
Ho	0.58	0.28	4.24	0.49	0.48	2.27	0.40	0.41	1.55	0.48	0.44	2.62	14.90	7.28	4.76	4.66	3.74	3.90	5.93	5.46
Er	1.52	0.81	10.33	1.39	1.41	5.28	1.14	1.21	3.86	1.35	1.24	7.43	12.69	6.78	3.75	3.80	3.20	3.38	5.98	5.48
Tm	0.22	0.11	1.63	0.21	0.21	0.78	0.15	0.15	0.61	0.23	0.23	0.94	15.29	7.33	3.73	3.77	4.09	4.16	4.09	4.09
Yb	1.36	0.76	8.90	1.35	1.40	4.06	1.04	1.11	3.17	1.37	1.33	5.90	11.66	6.56	2.90	3.02	2.86	3.06	4.44	4.32
Lu	0.25	0.19	1.20	0.20	0.21	0.57	0.16	0.16	0.45	0.19	0.18	0.77	6.51	4.77	2.65	2.77	2.76	2.93	4.17	4.03
Hf	3.26	3.55	3.36	4.69	5.40	3.51	3.33	3.81	2.72	3.54	4.10	3.59	0.95	1.03	0.65	0.75	0.71	0.81	0.87	1.01
Ta	0.95	1.03	0.99	0.95	1.07	1.03	0.67	0.77	0.56	0.96	1.11	1.10	0.96	1.04	0.97	1.09	0.73	0.84	1.00	1.14
Pb	13.23	13.71	6.34	12.97	13.22	17.89	12.35	13.45	2.78	14.65	15.82	4.28	0.46	0.48	1.35	1.38	0.21	0.22	0.27	0.29
Th	11.47	13.20	2.76	9.94	11.59	1.33	8.35	9.72	1.19	10.59	12.60	2.01	0.21	0.24	0.12	0.13	0.12	0.14	0.16	0.19
U	2.70	3.04	1.00	2.24	2.58	0.47	2.01	2.35	0.24	3.28	3.88	0.53	0.33	0.37	0.18	0.21	0.10	0.12	0.14	0.16
$\delta^{18}O$	9		7.7	8.2		6.7	7.3			10		7.2								

wr: whole rock analyses *amp: amphibole*
matrix: calculated matrix composition according to modal analyses of phenocryst phases
amp/mtrx: mineral matrix pair; amp/wr: mineral whole rock pair partition coefficients

T°C (px): two pyroxene geothermometer of Lindley and Andersen (1983)
T°C (plg): plagioclase thermometer of Sun et al. (1974)
P (kbar): Al in hornblende geobarometer of Schmidt (1992)

Table: 4.14. (Continued)

Copyright © by Mehmet Keskin

PLAGIOCLASE

Sample	MK49			MK251			MK268			MK277			MK49		MK251		MK268		MK277	
Area	Mt. Dumlu			Mt. Dumlu			Mt. Kargapazarı			Mt. Kargapazarı			← K_ds →							
SiO_2													66.26		65.08		65.47		60.58	
Recalc. SiO_2													63.03		61.43				61.77	
T°C (px)															1050				900	
T°C (plg)															1070				1090	
P (kbar)															-6.7-7					
O fugacity															$10^{-12.4}$				$10^{-14.8}$	
Type	*wr*	*matrix*	*plg*	*wr*	*matrix*	*plg*	*wr*	*matrix*	*plg*	*wr*	*matrix*	*plg*	*plg/mtrx*	*plg/wr*	*plg/mtrx*	*plg/wr*	*plg/mtrx*	*plg/wr*	*plg/mtrx*	*plg/wr*
Si	309722	324138	261189	304207	314805	252470				283172	289088	253983	0.81	0.84	0.80	0.83			0.88	0.90
Ti	3657	2817	364	4197	4300	438				4796	5643	506	0.13	0.10	0.10	0.10			0.09	0.11
Al	83463	78680.8	143439	87273	80919.8	149627				83886	75743.7	148757	1.82	1.72	1.85	1.71			1.96	1.77
Fe	26928	24000	3370	31894	32492	3288				36510	38456	4356	0.14	0.13	0.10	0.10			0.11	0.12
Mn	465	393	312	620	626	245				620	513	476	0.79	0.67	0.39	0.40			0.93	0.77
Mg	3822	2011.84	320	4388	3345.26	289				8250	8113.05	196	0.16	0.08	0.09	0.07			0.02	0.02
Ca	28874	18785.2	74206	34449	27378	82043				43597	38527	81350	3.95	2.57	3.00	2.38			2.11	1.87
Na	28784	28267.8	41151	31232	31324.1	37325				30490	30407.6	36806	1.46	1.43	1.19	1.20			1.21	1.21
K	23657	27880	2218	19507	22615	1725				18096	21273	2580	0.08	0.09	0.08	0.09			0.12	0.14
Rb	70.9	79.5	29.7	58.2	67.8	4.0	88.3	105.7	14.1	51.8	58.3	21.8	0.37	0.42	0.06	0.07	0.13	0.16	0.37	0.42
Sr	299	264	749	452	367	1183	342	241	880	443	365	987	2.84	2.51	3.22	2.62	3.65	2.57	2.70	2.23
Y	17.8	9.7	13.8	13.6	14.5	1.5	15.7	14.5	9.9	15.9	17.9	3.9	1.42	0.78	0.10	0.11	0.68	0.63	0.22	0.25
Zr	111	124	34	157	182	7	155	182	29	156	180	34	0.28	0.31	0.04	0.04	0.16	0.19	0.19	0.22
Nb	10.4	9.8	4.1	11.8	13.1	2.4	12.9	14.4	2.9	12.0	13.9	2.8	0.42	0.40	0.18	0.20	0.20	0.23	0.20	0.23
Cs	3.6	4.1	1.4	1.7	2.0	0.1	4.5	5.3	0.8	1.4	1.6	0.5	0.34	0.38	0.05	0.06	0.14	0.17	0.30	0.34
Ba	462	478	526	535	598	189	450	473	379	385	403	339	1.10	1.14	0.32	0.35	0.80	0.84	0.84	0.88
La	33.95	29.65	44.17	33.10	37.26	8.07	29.23	28.22	33.26	28.13	31.10	14.04	1.49	1.30	0.22	0.24	1.18	1.14	0.45	0.50
Ce	50.80	45.12	32.86	57.96	64.92	11.23	46.31	49.51	22.77	48.57	54.34	19.56	0.73	0.65	0.17	0.19	0.46	0.49	0.36	0.40
Pr	6.12	4.44	6.87	6.03	6.72	1.01	5.32	5.06	5.10	5.31	5.97	1.95	1.55	1.12	0.15	0.17	1.01	0.96	0.33	0.37
Nd	20.79	13.18	23.22	19.50	21.35	3.63	18.11	16.62	17.46	19.31	21.77	6.29	1.76	1.12	0.17	0.19	1.05	0.96	0.29	0.33
Sm	3.78	2.18	3.38	3.41	3.67	0.55	3.37	3.14	2.44	3.48	3.91	1.07	1.55	0.90	0.15	0.16	0.78	0.72	0.27	0.31
Eu	0.99	0.61	1.82	1.10	1.13	0.64	1.03	0.90	1.32	0.99	0.98	1.18	2.96	1.84	0.56	0.58	1.47	1.28	1.20	1.19
Gd	3.30	1.51	3.14	3.29	3.55	0.33	3.41	3.21	2.23	2.97	3.31	1.01	2.08	0.95	0.09	0.10	0.70	0.65	0.30	0.34
Tb	0.51	0.26	0.45	0.38	0.40	0.04	0.47	0.44	0.27	0.47	0.53	0.12	1.75	0.88	0.09	0.10	0.63	0.58	0.22	0.25
Dy	2.85	1.35	2.19	2.09	2.18	0.22	2.49	2.28	1.52	2.50	2.81	0.61	1.62	0.77	0.10	0.11	0.67	0.61	0.22	0.24
Ho	0.58	0.28	0.43	0.40	0.41	0.04	0.48	0.44	0.27	0.51	0.57	0.12	1.50	0.73	0.09	0.10	0.61	0.56	0.22	0.24
Er	1.52	0.81	1.10	1.14	1.21	0.13	1.35	1.24	0.78	1.48	1.67	0.31	1.35	0.72	0.10	0.11	0.63	0.58	0.19	0.21
Tm	0.22	0.11	0.17	0.15	0.15	0.03	0.23	0.23	0.10	0.24	0.27	0.04	1.61	0.77	0.19	0.19	0.43	0.43	0.16	0.18
Yb	1.36	0.76	0.87	1.04	1.11	0.09	1.37	1.33	0.70	1.33	1.49	0.29	1.14	0.64	0.08	0.09	0.52	0.51	0.20	0.22
Lu	0.25	0.19	0.13	0.16	0.16	0.03	0.19	0.18	0.11	0.21	0.23	0.05	0.70	0.51	0.16	0.17	0.62	0.60	0.22	0.24
Hf	3.26	3.55	0.78	3.33	3.81	0.19	3.54	4.10	0.64	3.83	4.44	0.74	0.22	0.24	0.05	0.06	0.16	0.18	0.17	0.19
Ta	0.95	1.03	0.25	0.67	0.77	0.08	0.96	1.11	0.21	0.88	1.02	0.15	0.25	0.27	0.10	0.11	0.19	0.22	0.15	0.17
Pb	13.23	13.71	14.22	12.35	13.45	7.23	14.65	15.82	10.64	11.46	12.04	9.47	1.04	1.07	0.54	0.59	0.67	0.73	0.79	0.83
Th	11.47	13.20	3.37	8.35	9.72	0.53	10.59	12.60	2.06	7.50	8.67	1.76	0.26	0.29	0.05	0.06	0.16	0.19	0.20	0.24
U	2.70	3.04	1.07	2.01	2.35	0.10	3.28	3.88	0.76	2.06	2.38	0.54	0.35	0.40	0.04	0.05	0.20	0.23	0.23	0.26
$\delta^{18}O$	9.0		8.4	7.3		7.4	10.0		8.3	7.2		6.7								

wr: whole rock analyses *plg: plagioclase*
matrix: calculated matrix composition according to modal analyses of phenocryst phases
plg/mtrx: mineral matrix pair; plg/wr: mineral whole rock pair partition coefficients

T°C (px): two pyroxene geothermometer of Lindley and Andersen (1983)
T°C (plg): plagioclase thermometer of Sun et al. (1974)
P (kbar): Al in hornblende geobarometer of Schmidt (1992)

Table: 4.15. Mineral/matrix and mineral/whole-rock distribution coefficients of plagioclases.

PLAGIOCLASE

Sample	MK112			MK132			MK154			MK174			MK112		MK132		MK154		MK174	
Area	*Pasinler area*			*N of Horasan*			*S of Horasan*			*Kağızman area*			←		$K_d s$					→
SiO_2													**66.81**		**64.18**		**66.91**		**66.48**	
Recalc SiO_2													63.15		64.37		65.74		64.72	
T°C (px)													1000							
T°C (plg)													1020		1060		1060		1100	
P (kbar)													~5.7		~7		~6.5		~6.6	
O fugacity													$10^{-12.3}$		$10^{-13.1}$		$10^{-13.2}$		$10^{-14.8}$	
Type	*wr*	*matrix*	*plg*	*wr*	*matrix*	*plg*	*wr*	*matrix*	*plg*	*wr*	*matrix*	*plg*	*plg/mtrx*	*plg/wr*	*plg/mtrx*	*plg/wr*	*plg/mtrx*	*plg/wr*	*plg/mtrx*	*plg/wr*
Si	312293	325229	265023	300000	311158	268802	312761	322083	277001	310751	317856	310751	0.81	0.85	0.86	0.90	0.86	0.89	0.98	1.00
Ti	3417	3621	199	3897	4482	205	2518	2215	130	3237	3161	216	0.05	0.06	0.05	0.05	0.06	0.05	0.07	0.07
Al	84151	75093	141167	86532	80113	136156	86691	82507	132959	83780	78694	134292	1.88	1.68	1.70	1.57	1.61	1.53	1.71	1.60
Fe	26718	27344	2828	31684	30723	2091	22172	19819	1325	27698	27956	2447	0.10	0.11	0.07	0.07	0.07	0.06	0.09	0.09
Mn	465	410	367	465	221	431	465	402	200	774	759	316	0.89	0.79	1.95	0.93	0.50	0.43	0.42	0.41
Mg	2507	1725	278	2993	1192	257	3276	2524	280	1638	1288	112	0.16	0.11	0.22	0.09	0.11	0.09	0.09	0.07
Ca	26301	16314	70419	33662	27567	62651	26301	21324	53983	22727	17305	58566	4.32	2.68	2.27	1.86	2.53	2.05	3.38	2.58
Na	27300	25065	42592	33235	31978	47626	32716	31337	52263	34867	33531	50203	1.70	1.56	1.49	1.43	1.67	1.60	1.50	1.44
K	27061	32539	2565	20254	24991	2630	20752	22918	3061	26231	29203	4285	0.08	0.09	0.11	0.13	0.13	0.15	0.15	0.16
Rb	80.5	97.4	5.7	56.3	68.9	9.7	72.8	78.9	15.4	74.9	78.4	58.5	0.06	0.07	0.14	0.17	0.19	0.21	0.75	0.78
Sr	349	222	1082	652	486	1621	500	413	1425	230	198	524	4.87	3.10	3.34	2.48	3.45	2.85	2.64	2.28
Y	18.3	19.3	1.9	15.6	16.8	2.8	9.0	8.1	1.3	33.5	33.5	3.2	0.10	0.10	0.17	0.18	0.16	0.15	0.10	0.10
Zr	156	185	14	189	231	21	42	45	7	156	169	20	0.08	0.09	0.09	0.11	0.16	0.17	0.12	0.13
Nb	10.9	12.5	1.7	18.3	21.5	4.0	13.4	13.4	5.4	21.0	22.6	3.4	0.14	0.16	0.19	0.22	0.41	0.41	0.15	0.16
Cs	3.5	4.2	0.3	1.2	1.4	0.3	2.2	2.3	1.5	1.5	1.6	1.2	0.06	0.07	0.18	0.22	0.63	0.66	0.79	0.82
Ba	556	642	188	725	841	314	648	672	259	631	570	1268	0.29	0.34	0.37	0.43	0.39	0.40	2.22	2.01
La	31.64	36.54	7.57	39.57	45.08	14.87	30.53	32.79	12.68	28.45	30.65	9.23	0.21	0.24	0.33	0.38	0.39	0.42	0.30	0.32
Ce	42.40	48.21	9.65	72.67	81.73	24.73	51.63	54.48	17.10	53.28	56.85	12.76	0.20	0.23	0.30	0.34	0.31	0.33	0.22	0.24
Pr	5.41	6.10	0.99	7.59	8.50	2.45	5.39	5.55	1.43	6.48	6.89	1.23	0.16	0.18	0.29	0.32	0.26	0.27	0.18	0.19
Nd	18.95	20.85	3.61	27.24	29.92	8.40	18.09	18.02	4.06	24.14	25.17	3.94	0.17	0.19	0.28	0.31	0.23	0.22	0.16	0.16
Sm	3.65	3.92	0.60	4.28	4.65	1.08	3.02	2.91	0.55	5.08	5.15	0.75	0.15	0.16	0.23	0.25	0.19	0.18	0.15	0.15
Eu	1.09	1.10	0.70	1.29	1.31	0.91	1.00	0.94	0.73	1.61	1.48	1.84	0.63	0.64	0.69	0.70	0.78	0.73	1.24	1.14
Gd	3.58	3.78	0.48	3.29	3.47	0.68	2.77	2.68	0.34	5.34	5.27	0.69	0.13	0.13	0.20	0.21	0.13	0.12	0.13	0.13
Tb	0.50	0.52	0.06	0.48	0.51	0.08	0.33	0.31	0.04	0.83	0.81	0.09	0.12	0.12	0.16	0.18	0.13	0.13	0.11	0.11
Dy	2.96	3.09	0.32	2.37	2.48	0.43	1.51	1.34	0.18	4.98	4.85	0.58	0.10	0.11	0.17	0.18	0.13	0.12	0.12	0.12
Ho	0.54	0.56	0.06	0.49	0.52	0.09	0.25	0.21	0.02	1.02	0.99	0.11	0.11	0.11	0.17	0.18	0.11	0.09	0.11	0.11
Er	1.57	1.65	0.17	1.30	1.38	0.26	0.74	0.67	0.09	3.08	3.04	0.32	0.10	0.11	0.19	0.20	0.14	0.13	0.10	0.10
Tm	0.26	0.28	0.03	0.21	0.22	0.04	0.09	0.08	0.03	0.54	0.55	0.05	0.11	0.12	0.17	0.18	0.33	0.28	0.10	0.10
Yb	1.55	1.67	0.15	1.19	1.26	0.20	0.60	0.53	0.11	2.87	2.87	0.35	0.09	0.10	0.16	0.17	0.20	0.18	0.12	0.12
Lu	0.25	0.27	0.03	0.21	0.23	0.04	0.09	0.08	0.03	0.42	0.42	0.05	0.10	0.10	0.17	0.18	0.42	0.36	0.13	0.13
Hf	3.50	4.12	0.32	3.80	4.58	0.46	1.32	1.38	0.19	3.59	3.85	0.46	0.08	0.09	0.10	0.12	0.14	0.15	0.12	0.13
Ta	0.81	0.94	0.11	1.07	1.29	0.17	0.83	0.90	0.18	1.40	1.55	0.16	0.11	0.13	0.13	0.15	0.20	0.22	0.11	0.12
Pb	15.57	17.66	6.49	13.62	15.63	5.58	14.74	14.99	14.12	15.70	15.63	18.86	0.37	0.42	0.36	0.41	0.94	0.96	1.21	1.20
Th	9.51	11.48	0.69	10.92	13.48	1.23	10.97	12.50	1.24	10.57	11.80	1.48	0.06	0.07	0.09	0.11	0.10	0.11	0.13	0.14
U	3.06	3.70	0.20	3.74	4.57	0.70	3.05	3.44	0.43	3.09	3.42	0.72	0.05	0.07	0.15	0.19	0.13	0.14	0.21	0.23
$\delta^{18}O$	9.4		7.9	6.5			9.3		7.7	7.3		6.8								

Table: 4.15. (Continued)

Copyright © by Mehmet Keskin

OLIVINE

ORTHOPYROXENE

CLINOPYROXENE

Sample	MK144			MK251			MK277			MK132			MK251		MK277		MK132		MK265			MK265	
Area	N. of Horasan			Mt. Dumlu			Mt. Kargapazarı			N. of Horasan			←		$K_d s$			→					
SiO_2	48.76												65.08		60.58		64.18					63.90	
T°C (px)													1050		900							1000	
T°C (plg)													1070		1090		1060						
P (kbar)													~6.7-7				~7						
O fugacity													$10^{-12.4}$		$10^{-14.8}$		$10^{-13.1}$						
Type	*wr*	*olv*	*olv/wr*	*wr*	*matrix*	*opx*	*wr*	*matrix*	*opx*	*wr*	*matrix*	*opx*	*opx/mtrx*	*opx/wr*	*opx/mtrx*	*opx/wr*	*opx/mtrx*	*opx/wr*	*wr*	*matrix*	*cpx*	*cpx/mtrx*	*cpx/wr*
Si				304207	314805	252678	283172	289088	251591	300000	311158	245886	0.80	0.83	0.87	0.89	0.79	0.82	298691	306849	247858	0.81	0.83
Ti				4197	4300	2392	4796	5643	813	3897	4482	818	0.56	0.57	0.14	0.17	0.18	0.21	3657	3904	2118	0.54	0.58
Al				87273	80920	15847	83886	75744	6654	86532	80113	9503	0.20	0.18	0.09	0.08	0.12	0.11	81028	92516	9454	0.10	0.12
Fe				31894	32492	101745	36510	38456	136360	31684	30723	160118	3.13	3.19	3.55	3.73	5.21	5.05	30775	27987	48145	1.72	1.56
Mn				620	626	2563	620	513	4451	465	221	6246	4.10	4.14	8.67	7.18	28.25	13.44	542	538	568	1.06	1.05
Mg				4388	3345	55448	8250	8113	51632	2993	1192	45698	16.58	12.64	6.36	6.26	38.34	15.27	7380	3181	33546	10.55	4.55
Ca				34449	27378	11362	43597	38527	8395	33662	27567	5556	0.42	0.33	0.22	0.19	0.20	0.17	35521	16821	152032	9.04	4.28
Na				31232	31324	96	30490	30408	2062	33235	31978	1669	0.00	0.00	0.07	0.07	0.05	0.05	26188	29946	2772	0.09	0.11
K				19507	22615	349	18096	21273	365	20254	24991	1067	0.02	0.02	0.02	0.02	0.04	0.05	22661	26247	318	0.01	0.01
Rb	20.3	1.5	0.07	58.2	67.8	6.3	51.8	58.3	8.0	56.3	68.9	4.4	0.09	0.11	0.14	0.15	0.06	0.08	70.3	80.8	4.4	0.05	0.06
Sr	801	67	0.08	452	367	87	443	365	64	652	486	104	0.24	0.19	0.17	0.14	0.21	0.16	454	521	33	0.06	0.07
Y	25.0	2.2	0.09	13.6	14.5	13.5	15.9	17.9	14.8	15.6	16.8	24.2	0.93	0.99	0.83	0.93	1.44	1.55	16.1	15.2	22.0	1.45	1.37
Zr	124	9	0.07	157	182	43	156	180	35	189	231	41	0.24	0.28	0.19	0.22	0.18	0.22	148	169	17	0.10	0.12
Nb	14.5	6.9	0.47	11.8	13.1	3.9	12.0	13.9	3.1	18.3	21.5	5.5	0.29	0.33	0.22	0.26	0.26	0.30	10.1	11.5	1.9	0.17	0.19
Cs	0.6	0.2	0.29	1.7	2.0	0.2	1.4	1.6	0.4	1.2	1.4	0.2	0.09	0.11	0.25	0.28	0.12	0.15	2.8	3.2	0.2	0.06	0.07
Ba	616	198	0.32	535	598	90	385	403	62	725	841	99	0.15	0.17	0.15	0.16	0.12	0.14	499	571	55	0.10	0.11
La	30.61	1.90	0.06	33.10	37.26	8.01	28.13	31.10	9.56	39.57	45.08	21.92	0.21	0.24	0.31	0.34	0.49	0.55	31.44	32.44	25.22	0.78	0.80
Ce	68.85	4.35	0.06	57.96	64.92	18.16	48.57	54.34	20.35	72.67	81.73	49.47	0.28	0.31	0.37	0.42	0.61	0.68	45.75	51.83	7.89	0.15	0.17
Pr	8.33	0.42	0.05	6.03	6.72	2.36	5.31	5.97	2.40	7.59	8.50	6.29	0.35	0.39	0.40	0.45	0.74	0.83	5.52	5.95	2.86	0.48	0.52
Nd	33.69	2.01	0.06	19.50	21.35	10.88	19.31	21.77	10.62	27.24	29.92	27.24	0.51	0.56	0.49	0.55	0.91	1.00	19.20	20.27	12.49	0.62	0.65
Sm	6.14	0.42	0.07	3.41	3.67	2.57	3.48	3.91	2.33	4.28	4.65	4.99	0.70	0.75	0.60	0.67	1.07	1.17	3.56	3.79	2.14	0.57	0.60
Eu	1.74	0.12	0.07	1.10	1.13	0.80	0.99	0.98	0.49	1.29	1.31	1.33	0.70	0.72	0.50	0.49	1.02	1.03	1.09	1.18	0.54	0.46	0.49
Gd	5.67	0.38	0.07	3.29	3.55	2.76	2.97	3.31	2.55	3.29	3.47	5.25	0.78	0.84	0.77	0.86	1.52	1.60	3.53	3.59	3.14	0.88	0.89
Tb	0.71	0.05	0.07	0.38	0.40	0.44	0.47	0.53	0.43	0.48	0.51	0.77	1.09	1.15	0.81	0.92	1.49	1.61	0.45	0.45	0.45	1.00	1.00
Dy	4.05	0.35	0.09	2.09	2.18	2.43	2.50	2.81	2.50	2.37	2.48	4.08	1.11	1.16	0.89	1.00	1.64	1.72	2.42	2.38	2.66	1.12	1.10
Ho	0.83	0.07	0.08	0.40	0.41	0.47	0.51	0.57	0.57	0.49	0.52	0.81	1.13	1.18	0.99	1.11	1.56	1.65	0.44	0.42	0.58	1.40	1.33
Er	2.20	0.22	0.10	1.14	1.21	1.27	1.48	1.67	1.52	1.30	1.38	2.10	1.06	1.11	0.91	1.03	1.52	1.61	1.31	1.28	1.51	1.18	1.15
Tm	0.32	0.05	0.15	0.15	0.15	0.23	0.24	0.27	0.25	0.21	0.22	0.36	1.52	1.54	0.90	1.03	1.64	1.73	0.19	0.18	0.23	1.28	1.23
Yb	2.18	0.22	0.10	1.04	1.11	1.10	1.33	1.49	1.49	1.19	1.26	1.96	0.99	1.06	1.00	1.12	1.55	1.65	1.14	1.13	1.20	1.06	1.05
Lu	0.34	0.04	0.13	0.16	0.16	0.18	0.21	0.23	0.26	0.21	0.23	0.34	1.09	1.16	1.11	1.24	1.49	1.60	0.18	0.17	0.22	1.28	1.24
Hf	2.79	0.23	0.08	3.33	3.81	1.35	3.83	4.44	1.04	3.80	4.58	1.33	0.36	0.41	0.23	0.27	0.29	0.35	3.34	3.80	0.48	0.13	0.14
Ta	0.71	0.20	0.28	0.67	0.77	0.15	0.88	1.02	0.18	1.07	1.29	0.21	0.20	0.23	0.17	0.20	0.16	0.20	0.61	0.69	0.11	0.15	0.17
Pb	5.55	9.66	1.74	12.35	13.45	3.82	11.46	12.04	4.13	13.62	15.63	4.32	0.28	0.31	0.34	0.36	0.28	0.32	12.53	14.06	3.03	0.22	0.24
Th	3.34	0.18	0.05	8.35	9.72	0.91	7.50	8.67	1.09	10.92	13.48	1.04	0.09	0.11	0.13	0.15	0.08	0.10	8.04	9.25	0.51	0.06	0.06
U	1.03	0.06	0.06	2.01	2.35	0.24	2.06	2.38	0.27	3.74	4.57	0.35	0.10	0.12	0.11	0.13	0.08	0.09	2.19	2.51	0.17	0.07	0.08
$\delta^{18}O$				7.3		6.3	7.2		6.7	6.5		5.1											

wr: whole rock analyses *olv: olivine, opx: orthopyroxene, cpx: clinopyroxene*
matrix: calculated matrix composition according to modal analyses of phenocryst phases
opx or cpx/mtrx: mineral matrix pair: opx or cpx/wr: mineral whole rock pair partition coefficients

T°C (px): two pyroxene geothermometer of Lindley and Andersen (1983)
T°C (plg): plagioclase thermometer of Sun et al. (1974)
P (kbar): Al in hornblende geobarometer of Schmidt (1992)

Copyright © by Mehmet Keskin

Table: 4.16. Mineral/matrix and mineral/whole-rock distribution coefficients of olivine, ortho- and clinopyroxenes.

Table: 4.17. Mineral/matrix and mineral/whole-rock distribution coefficients of anorthoclase and biotite.

	ANORTHOCLASE					BIOTITE				
Sample	**MK338**			**MK338**		**MK154**			**MK154**	
Area	***Pasinler area***					***S of Horasan***				
SiO_2				71.00					66.91	
T°C (plg)				650-750					1067	
T°C (anor-1)				~550						
T°C (anor-2)				650-800						
P (kbar)									~6.5	
O fugacity									$10^{-13.2}$	
Type	*wr*	*matrix*	*anort*	*anort/mtrx*	*anort/wr*	*wr*	*matrix*	*biotite*	*bio/mtrx*	*bio/wr*
Si	331879	336347	307944	0.92	0.93					
Ti	1019	1138	186	0.16	0.18					
Al	81134	77642	98512	1.27	1.21					
Fe	13429	15209	851	0.06	0.06					
Mn	465	511	108	0.21	0.23					
Mg	20	0	175		8.65					
Ca	4717	3562	2113	0.59	0.45					
Na	33458	32792	36935	1.13	1.10					
K	44327	40860	80499	1.97	1.82					
Rb	129.5	129.6	148.68	1.15	1.15	72.8	78.9	294.76	3.74	4.05
Sr	42	9	121	12.75	2.86	500	413	66	0.16	0.13
Y	30.0	33.8	3.70	0.11	0.12	9.0	8.1	4.27	0.52	0.47
Zr	52	59	6	0.11	0.12	42	45	14	0.31	0.33
Nb	22.0	24.4	5.36	0.22	0.24	13.4	13.4	35.48	2.64	2.65
Cs	3.0	3.3	0.86	0.26	0.29	2.2	2.3	4.45	1.91	1.99
Ba	425	244	1907	7.81	4.48	648	672	4024	5.99	6.21
La	63.34	69.65	20.24	0.29	0.32	30.53	32.79	9.35	0.29	0.31
Ce	119.19	134.03	16.56	0.12	0.14	51.63	54.48	19.27	0.35	0.37
Pr	12.05	13.28	3.81	0.29	0.32	5.39	5.55	2.22	0.40	0.41
Nd	37.46	41.19	12.28	0.30	0.33	18.09	18.02	8.63	0.48	0.48
Sm	6.45	7.06	2.39	0.34	0.37	3.02	2.91	1.54	0.53	0.51
Eu	0.80	0.67	1.77	2.63	2.22	1.00	0.94	0.77	0.82	0.77
Gd	6.16	6.89	1.12	0.16	0.18	2.77	2.68	1.68	0.63	0.61
Tb	0.87	0.98	0.15	0.16	0.18	0.33	0.31	0.12	0.39	0.37
Dy	4.82	5.41	0.76	0.14	0.16	1.51	1.34	0.80	0.59	0.53
Ho	0.93	1.05	0.13	0.12	0.14	0.25	0.21	0.13	0.65	0.55
Er	2.99	3.38	0.29	0.08	0.10	0.74	0.67	0.32	0.48	0.43
Tm	0.46	0.52	0.06	0.12	0.14	0.09	0.08	0.04	0.57	0.48
Yb	2.72	3.07	0.27	0.09	0.10	0.60	0.53	0.20	0.37	0.33
Lu	0.46	0.51	0.06	0.12	0.13	0.09	0.08	0.03	0.43	0.37
Hf	1.82	2.05	0.19	0.09	0.11	1.32	1.38	0.43	0.31	0.33
Ta	1.62	1.82	0.20	0.11	0.12	0.83	0.90	0.97	1.08	1.16
Pb	21.49	21.23	25.60	1.21	1.19	14.74	14.99	6.56	0.44	0.45
Th	26.50	29.66	5.27	0.18	0.20	10.97	12.50	1.10	0.09	0.10
U	4.02	4.53	0.46	0.10	0.12	3.05	3.44	0.48	0.14	0.16
$\delta^{18}O$						9.3		6.2		

wr: whole rock analyses anort: anorthoclase, bio: biotite
matrix: calculated matrix composition according to modal analyses of phenocryst phases
bio or anort/mtrx: mineral matrix pair, bio or anort/wr: mineral whole rock pair partition coefficients
T°C (plg): two feldspar thermometer of Seck (1971) obtained from the composition of plagioclases
T°C (anor-1): Seck's (1971) graphical thermometer based on the composition of anorthoclase
T°C (anor-2): Graphical thermometer of Brown and Parsons (1981)
P (kbar): Al in hornblende geobarometer of Schmidt (1992)

Copyright © by Mehmet Keskin

Chapter 5: ISOTOPE GEOCHEMISTRY AND PETROLOGIC MODELLING

Introduction

This chapter gives detailed descriptions of the isotope systematics of the Erzurum-Kars Plateau volcanics. The chapter consists of two main sections. The first section describes variations in the isotopic ratios of the samples collected from the representative levels of the plateau. The next section presents petrologic modelling based mainly on the framework of assimilation combined with fractional crystallisation (AFC).

In this study, a subset of 23 samples have been chosen for isotope analysis from the representative levels of six sections on the plateau as presented in Figure 5.1. Locations of these sections on the plateau, stratigraphic relationships between volcanic units in each section and their average thickness have been indicated in the figure together with K-Ar dating results. It can be argued that these 23 samples provide an almost complete temporal and spatial record of collision-related volcanism on the Erzurum-Kars Plateau. Sr and Pb isotopic compositions of all these samples were measured on a Finnegan MAT 262 multicollector mass spectrometer while Nd isotopic ratios were obtained from a VG354 multicollector mass spectrometer at the NERC Isotope Geosciences Laboratory (NIGL), Nottingham. In addition to this, a subset of eleven samples and 22 mineral separates also obtained from these samples were analysed for oxygen isotopes ($\delta^{18}O$) using a gas source multicollector mass spectrometer also located at NIGL. All of these whole rock and mineral separate samples have also been analysed by ICP-MS for the REEs at the Industrial Research Centre, University of Durham. Details of the sample preparation and analytical techniques are given in Appendix B and the full isotopic dataset is presented in Table 5.1.

Mt. Dumlu Area

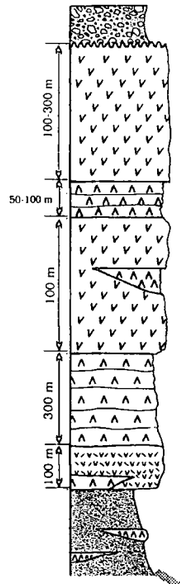

Pliocene Aras formation

Dumlu porphyritic amphibole dacite/ andesite

MK93 (radiogenic and O isotopes, min. sep.)

MK49 (radiogenic and O isotopes, min. sep.)

Güngörmez andesite/dacite (upper lens)

MK251 (radiogenic and O isotopes, min. sep.)

Güngörmez andesite/dacite (middle lens)

Güngörmez andesite/dacite (lower layer)

MK 29 K-Ar dating 5.66±0.10 Ma

MK 50 K-Ar dating 5.87±0.11 Ma

Arzutu microporphyritic amphibole dacite

MK 259 K-Ar dating 6.54±0.14 Ma

The lower tuff layer

Mt. Kargapazari Area

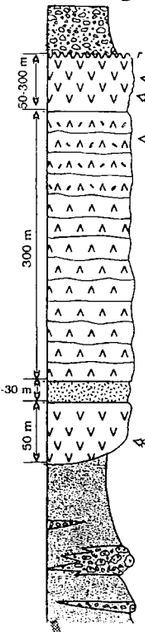

Pliocene Aras formation

Kargapazari volcanics

MK 63 (radiogenic isotopes)

MK 61 K-Ar dating 5.73±0.22 Ma

MK277 (radiogenic and O isotopes, min. sep.)

Güngörmez andesite/dacite

MK268 (Göllerdüzü porp. amph. dacite; radiogenic and O isotopes, min. sep.)

MK 12 K-Ar dating 6.79±0.21 Ma

MK281 (radiogenic isotopes)

MK265 (radiogenic isotopes, min. sep.)

MK 84 K-Ar dating 7.34±0.19 Ma

Black ignimbrite (porphyritic)

Karapinar basalt

MK289 (radiogenic isotopes)

Basal tuff layer

Agglomerate

North of Pasinler (Harabedere Valley)

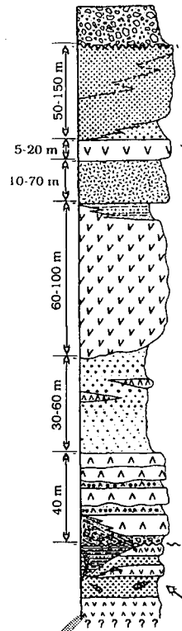

Pliocene Aras formation

Ardiçlidag rhyolite

MK338 (radiogenic isotopes, min. sep.)

Upper tuff layer

Kargapazari volcanics

MK101 (radiogenic isotopes)

Black ignimbrite

Middle tuff layer

Kizilveren porphyritic hornblende dacite/andesite

MK112 (radiogenic and O isotopes, min. sep.)

Lower tuff layer

Black aphyric andesite

MK 117 (radiogenic isotopes)

K-Ar dating: 7.83 ± 0.12 Ma

Eocene Narman group:
1. Narman formation
2. Kislaköy volcanic member

MK377 (S of Pasinler, Tuzluyollari dacite) K-Ar dating 23.0±0.5 Ma

MK343 (radiogenic and O isotopes, min sep.) K-Ar dating 38.5±0.7 Ma

North of Horasan

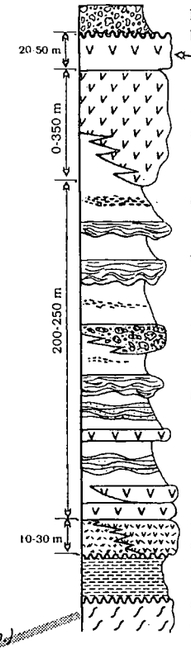

Pliocene Aras formation

Plateau layer

MK 134 K-Ar dating 4.14±0.21 Ma

MK 130 and MK 139 (radiogenic isotopes)

Köroglu porphyritic hornblende dacite/andesite

MK 132 (radiogenic and O isotopes, min. sep.)

Grey ignimbrite

White ignimbrite

Agglomerate

MK 154 (S of Horasan, Saçdag rhyodacite) (radiogenic and O isotopes, min. sep.)

Pyroclastic surge and fall deposits

MK 138 K-Ar dating 9.94 ± 0.40 Ma

MK 144 (radiogenic isotopes, min. sep.) K-Ar dating 11.1 ± 0.5 Ma

Porphyritic andesite and tuff, pink in colour

Eocene Narman formation

Cretaceous East Anatolian Accretionary Complex

NW of Pasinler (Büyükdere valley)

Aras formation (Pliocene)

White ignimbrite

Grey pumice (pyroclastic flow with obsidian bands)

Kargapazari volcanics

White ignimbrite

Reworked pumice with small scaled channels and erosion surfaces.

Dykes of olivine-basaltic-andesite

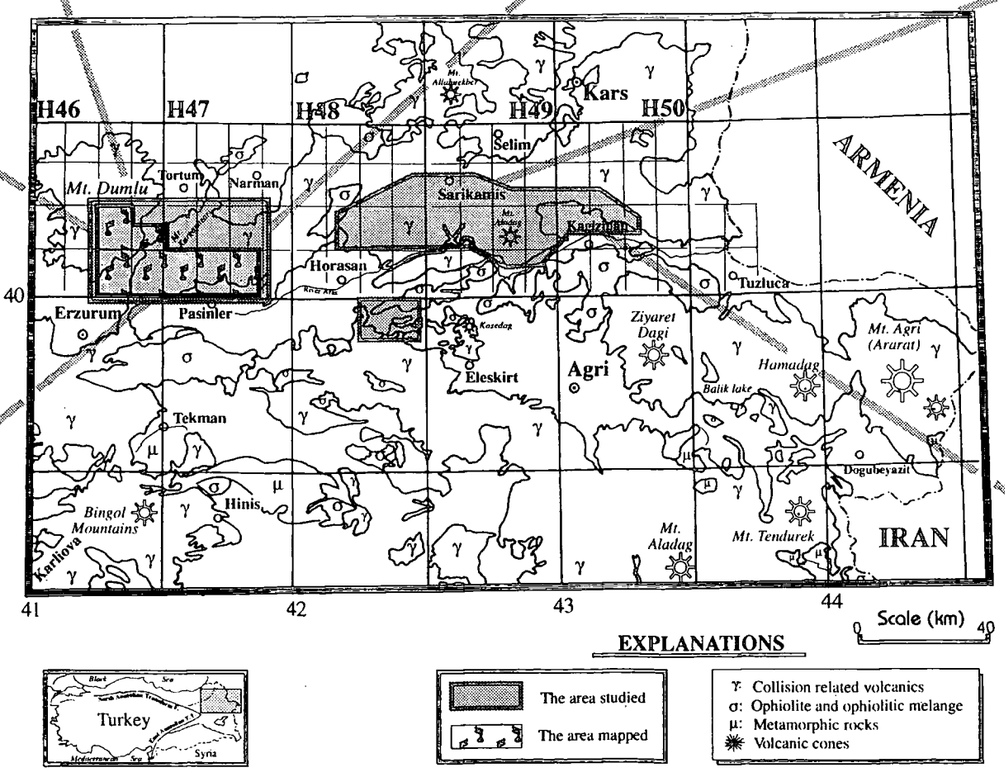

North of Kagizman

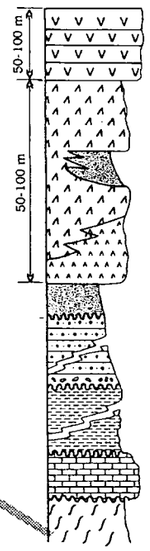

Kars plateau layer

MK175 (radiogenic isotopes) K-Ar dating 2.72 ± 0.10 Ma

MK162 K-Ar dating 3.40 ± 0.10 Ma

Pasli trachy-dacite

Tuff

MK174 (radiogenic and O isotopes, min. sep.)

Çukurayva rhyolite

MK169 K-Ar dating 5.15 ± 0.20 Ma

MK158 (radiogenic isotopes)

Pyroclastic basal layer

Late Miocene Güllüce formation

Eocene Camuslu formation

Late Cretaceous Kötek limestone

East Anatolian Accretionary Complex

Figure: 5.1. Location map showing locations of each stratigraphic section from which samples for isotope analyses were collected.

Table: 5.1. Isotopic analyses of samples from the Erzurum-Kars Plateau, NE Turkey. For the location and stratigraphic position of each sample, see Figure 5.1.

Area	Unit	Str. Position	Sample no	Lithology	SiO_2	Age (Ma)	$^{87}Sr/^{86}Sr$	$^{143}Nd/^{144}Nd$	$^{206}Pb/^{204}Pb$	$^{207}Pb/^{204}Pb$	$^{208}Pb/^{204}Pb$	$\delta^{18}O$
Mt. Dumlu	Dpad	top	**MK251**	dacite	65.08	~5.5	0.704619±7	0.512723±2	18.647	15.604	38.715	7.3
	Dpad	top	**MK93**	dacite	63.49	~5.5	0.704748±7	0.512725±3	18.660	15.610	38.725	8.2
	Dpad	top	**MK49**	dacite	66.26	~5.5	0.704605±7	0.512758±3	18.639	15.597	38.690	9.0
Mt. Kargapazarı	Kv	top	**MK63**	BaAnd	54.39	5.73±0.22	0.704829±7	0.512725±3	18.940	15.644	38.990	
	Gpaa	mid	**MK268**	dacite	65.47	~6	0.704596±7	0.512761±3	18.666	15.593	38.698	10.0±0.3
	Gad	mid	**MK277**	andesite	60.58	~6	0.704355±7	0.512786±3	18.683	15.606	38.736	7.2±0.7
	Gad	base	**MK281**	TrachyAnd	56.99	~6.7	0.703967±7	0.512904±3	18.735	15.604	38.764	
	Çpd	base	**MK265**	dacite	63.90	~7	0.704583±7	0.512738±3	18.696	15.610	38.769	
	Kb	base	**MK289**	basalt	49.09	~7	0.703910±7	0.512853±4	17.663	15.553	37.494	
Pasinler area	Ard	top	**MK338**	rhyolite	71.00	~5	0.705400±8	0.512831±4	18.943	15.621	38.918	
	Kv	top	**MK101**	BaAnd	57.01	~5.5	0.704734±7	0.512754±3	18.937	15.638	38.966	
	Kpd	mid	**MK112**	dacite	66.81	~5.5	0.704496±7	0.512846±5	18.798	15.614	38.834	9.4
	Baad	base	**MK117**	andesite	62.14	7.83±0.12	0.704236±7	0.512831±3	18.817	15.625	38.867	
	Enı	basement	**MK343**	BaTrachyAnd	54.56	38.5±0.7	0.704573±6	0.512814±3	18.625	15.605	38.593	7.5
Horasan area	Hpl	plateau	**MK130**	BaTrachyAnd	54.36	~4.1	0.703396±6	0.512934±5	18.940	15.623	38.902	
	Hpl	plateau	**MK139**	basalt	49.67	~4.1	0.703708±7	0.512935±3	18.934	15.668	39.040	
	Kpad	mid	**MK132**	dacite	64.18	~4.1	0.704730±7	0.512790±4	18.946	15.626	38.926	6.5
	Sd	base	**MK154**	dacite	66.91	~6	0.704822±6	0.512727±3	19.045	15.728	39.185	9.3
	Köb	base	**MK144**	basalt	48.76	11.1±0.5	0.704582±7	0.512799±3	19.024	15.665	39.075	
Mt. Aladağ	Aa	plateau	**MK168**	andesite	60.45	~3.5	0.704053±7	0.512864±2	18.905	15.629	38.909	
	Abil	base	**MK158**	TrachyAnd	61.74	~5	0.704523±7	0.512832±4	18.989	15.619	38.936	
Kağızman area	Kpl	plateau	**MK175**	BaTrachyAnd	53.66	2.72±0.10	0.704303±6	0.512805±3	19.068	15.632	38.993	
	Ptd	base	**MK174**	trachy-dacite	66.48	~5	0.704367±7	0.512878±3	19.030	15.617	38.985	7.3±0.3

Copyright © by Mehmet Keskin

Units:

Mt. Dumlu area: *Dpad*: the Dumlu amphibole dacite/andesite,

Mt. Kargapazarı area: *Kv*: the Kargapazarı volcanics, *Gpaa*: the Göllerdüzü amphibole dacite, *Gad*: the Güngörmez andesite/dacite, *Çpd*: the Çobandede dacite, *Kb*: the Karapınar basalt

Pasinler area: *Ard*: the Ardıçlıdağ rhyolite, *Kv*: the Kargapazarı volcanics, *Kpd*: the Kızılveren amphibole dacite/andesite, *Baad*: the Black andesite/dacite, *Enl*: the Upper Eocene Kışlaköy volcanic member of the Narman Group.

Mt. Aladağ area: *Aa*: the Aladağ andesite, *Abil*: Aladağ basal intermediate lavas

Kağızman area: *Kpl*: the Kars plateau unit, *Ptd*: the Paslı trachydacite

5.1. Isotope systematics

In accordance with the behaviour of trace elements, Isotopic ratios of the low- and high-Y series also support the idea of the presence of two different magma types that appear to have experienced two different fractionation stories. Apart from a few exceptions (e.g. MK281, 154 and 132), samples from the high- and low-Y series consistently plot into two separate and sometimes partly overlapping areas on most of the diagrams (Figure 5.2-a to g). The high-Y series almost always comprises the more radiogenic rocks and spans a wider range in all isotopic ratios.

One of the samples from the low-Y series, MK154 from South of Horasan (Saçdağ dacite), has much higher $^{207}Pb/^{204}Pb$ and $^{208}Pb/^{204}Pb$ ratios, plotting out of the fields of both the high- and low-Y series in all diagrams. This may suggest that the magma that formed this unit evolved in a quite different way from all other units on the plateau. Two high-Y samples, MK117 and MK281, behave like the low-Y series on the isotope ratio diagrams, consistently plotting in the low-Y field (Figure: 5.2). In fact, MK117 (the Black andesite/dacite unit in Pasinler area) is compositionally very similar to the low-Y lavas. The Y concentration of this rock is 20.8 ppm, a value which is almost transitional between the low- and high-Y series. Therefore, this sample may be considered to be a member of the low-Y group. On the other hand, MK281 has a much higher Y content (32.8 ppm), even though the volcanic unit (the Güngörmez andesite/dacite) from which it was collected is in general a low-Y unit in the Mt. Kargapazarı area. Location of this sample is very close to this unit's contact with the overlying high-Y lavas of the Kargapazarı volcanics. The other lava flows in this unit lower in the succession are all low-Y. Formation of this upper layer may be explained as either that the magma forming these Y-rich lavas was contaminated by the high-Y magma by means of magma mixing at depth or that that magma experienced a similar magmatic evolution to that of the high-Y series. As mentioned earlier in Section 4.1.1.1, there is petrographic evidence (e.g. glass inclusions and complex zoning patterns in plagioclase phenocrysts) of magma mixing between the amphibole bearing porphyritic lavas of the low-Y series and olivine bearing high-Y series. One of the amphibole-bearing porphyritic samples of the low-Y series,

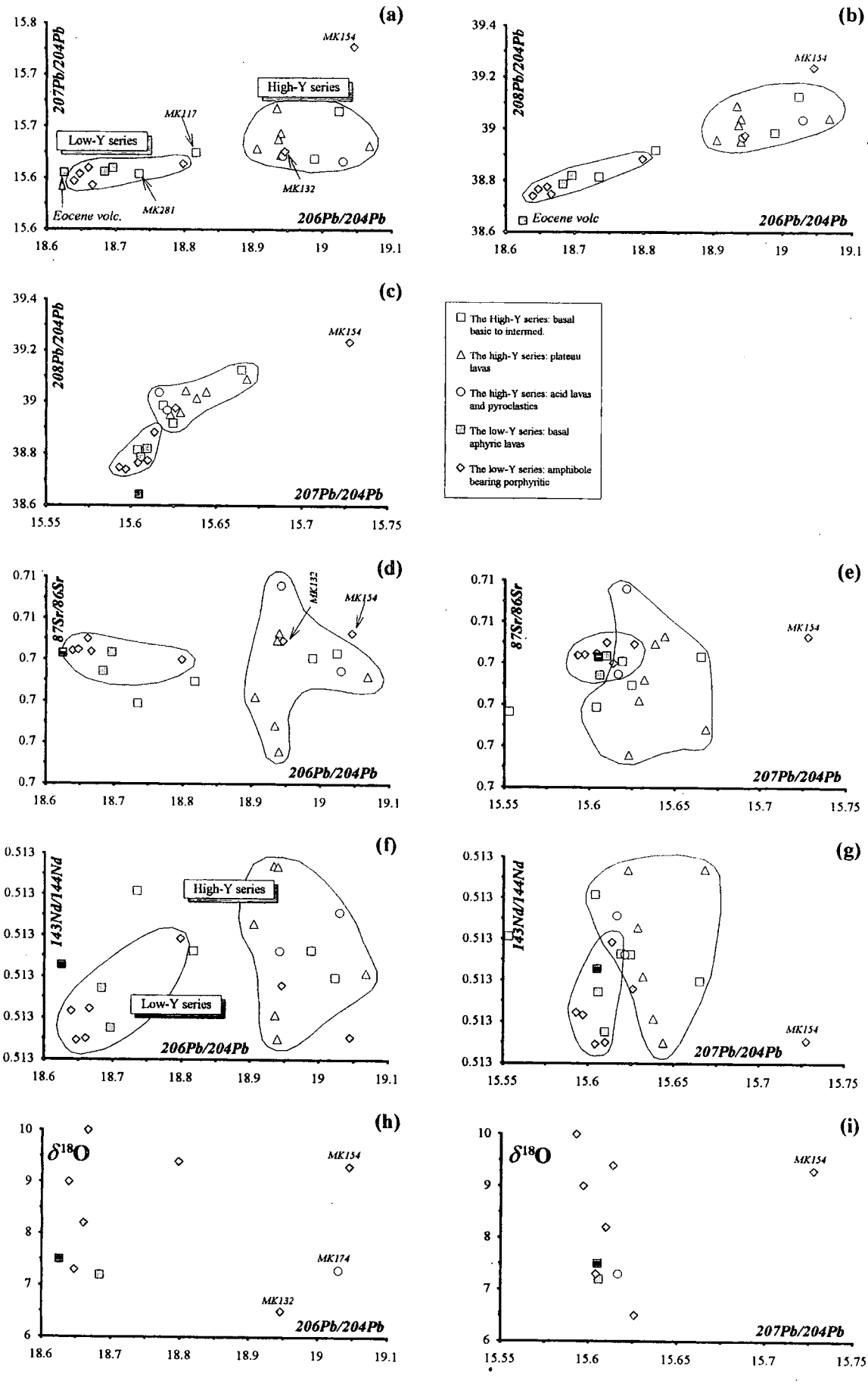

Figure: 5.2. Isotope diagrams showing the differences between the low- and high-Y series.

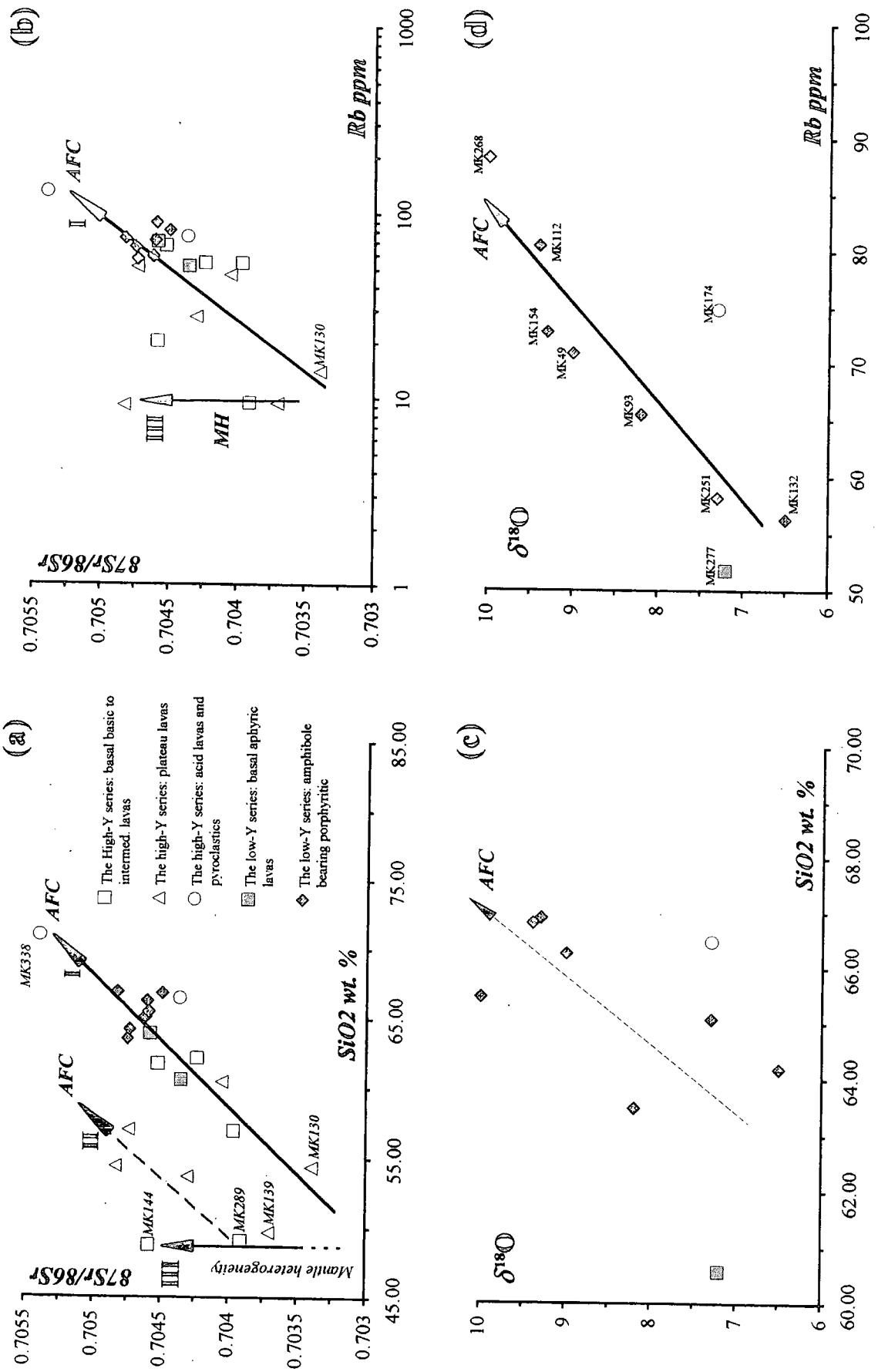

Figure: 5.3. 87Sr/86Sr and 18O/16O versus SiO2 and Rb diagrams of the lavas of the high- and low-Y series.

FIG5-03.XLS

MK132 (the Köroğlu amphibole dacite/andesite), falls into the field of the high-Y series on all diagrams (Figure 5.2). This may indicate that the unit experienced a similar magmatic evolution to that of the high-Y series.

The diagrams of $^{87}Sr/^{86}Sr$ against SiO_2 and $^{87}Sr/^{86}Sr$ against Rb seem to display three separate trends (Fig. 5.3-a and b). The first two trends (trend-I and -II), which are composed of both the low- and high-Y series, show a linear correlation between Sr isotope ratios and silica implying the importance of the combined assimilation and fractionation (AFC) in the origin of these volcanics. The third trend (trend-III), which coincides with the plateau lavas of the high-Y series, follows a near vertical (but slightly scattered) line probably constituting a mantle metasomatism trend. None of the low-Y lavas belong to this trend. $\delta^{18}O$ increases gradually with increasing SiO_2 and Rb (Figure 5.3-c and d), strengthening the idea of an AFC-dominated evolution of these series.

Sr and Nd isotope covariation diagram presented in Figure 5.4 indicates that both the high- and low-Y series follow the mantle array and fall into the second quadrant (similar to Columbia River basalts), with the exception of a few samples plotting in the first quadrant. Sources having these characteristics have higher Sm/Nd ratios than Chondritic Uniform Reservoir (CHUR) and lower Rb/Sr ratios than Uniform Reservoir (UR) and are known to consist of the residual solids after withdrawal of a partial melt from undifferentiated mantle (Faure, 1986). The Horasan Plateau lavas (MK130 and MK139) and the basal basic lavas (MK289: the Karapınar basalt in Mt. Kargapazarı area) of the

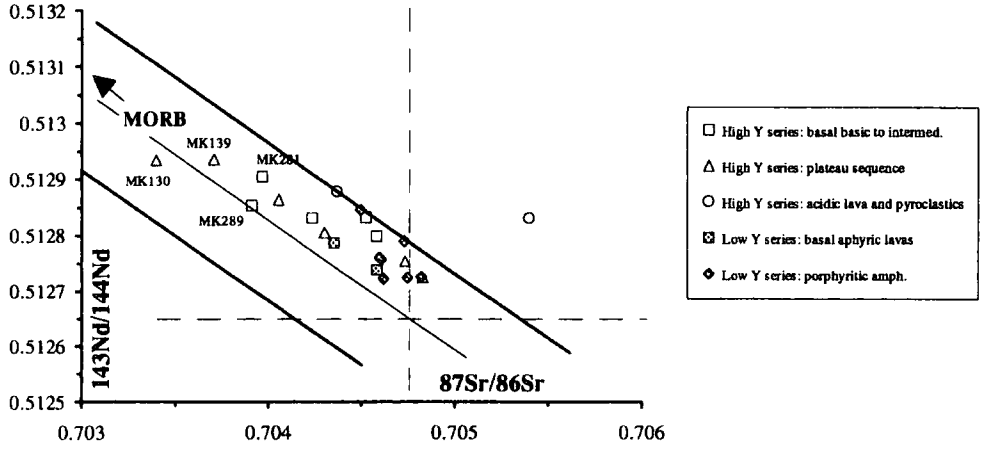

Figure: 5.4. Sr vs. Nd isotope covariation diagram of the samples from the Erzurum-Kars Plateau in relation to mantle array.

high-Y series comprise the most primitive units on the plateau in terms of their SiO_2 content.

5.2. Assimilation combined with fractional crystallisation (AFC) modelling of the isotopic data

As noted earlier, the linear or curvilinear positive correlation between Sr isotopic ratios and SiO_2 (Figure 5.3) shows that the combined assimilation and fractional crystallisation (AFC) was one of the most important processes in the magmatic evolution of the Erzurum-Kars Plateau Volcanics. Therefore, it is more appropriate to examine changes in trace element concentrations and isotopic ratios in the EKPV from the perspective of AFC. This can be effectively done by comparing observed trends formed by the data points and theoretical AFC curves on trace element and isotope graphs to show the amount and change which would take place when end-members of known (or in some cases predicted) chemistry are mixed during fractional crystallisation for different ratios of assimilation to crystallisation. In the following paragraphs, the trace element and isotopic data from the Erzurum-Kars Plateau volcanics will be interpreted in the framework of assimilation combined with fractional crystallisation after a short introduction to the theory.

5.2.1. Theory

Bowen (1956) is one of the first researchers who discussed the effects of assimilation during magmatic evolution. He emphasised that assimilation is not only a simple mixing process between two end-members but also involves combined fractional crystallisation which is required by the heat balance of the system. However, the first attempts to develop petrologic models which account for some of the isotope and trace element relationship in the volcanic suits were focused on describing mathematical equations concerning only the mixing process and ignoring the basic principles indicated by Bowen. Vollmer (1976), Faure et al. (1974), Bell and Powell (1969), Sun et al. (1975) developed and applied such equations to trace elements and Sr, Pb isotope ratios. In most cases, these equations were only applicable to specific problems.

Langmuir et al. (1978) further developed a general mixing equation for three possible plots in a two component system, i.e. ratio-ratio, ratio-element, and element-

element, and examined ways to test for mixing and to place limits on the composition of end-members. Langmuir et al. (1978)'s equations were subsequently adapted by DePaolo and Wasserburg (1979) for use with the epsilon (ε) notation of Nd and Sr isotopes. Allègre and Minster (1978) suggested a large number of models, although these models have not yet been widely applied to the problems of igneous petrogenesis.

Taylor (1980) pointed out that, although wall-rock assimilation and fractional crystallisation are often treated separately, heat-balance considerations suggest that these two processes should be coupled. In accordance with Bowen's argument, he demonstrated that heat required for assimilation can readily be provided by the latent heat of crystallisation of the magma. Taylor showed that assimilation of most common rock types by a magma will not drastically change the liquid line of descent of the later magmatic differentiates, at least as far as major element variations are concerned. However, compared to the major elements, the trace elements and particularly the isotopic compositions are very much affected by the combined assimilation-fractional crystallisation process. The isotopic effects are highly dependent upon the concentrations of the various elements in the magma and in the assimilated wall rock. He calculated the effects of concurrent assimilation and fractional crystallisation on the strontium and oxygen isotopic compositions of a magma and showed that the resulting ratios are significantly different from those predicted by simple two-end-member models. He proved that simple mixing lines or mixing hyperbolae alone have, in general, limited relevance in modelling processes of magmatic assimilation. According to Taylor, this is a 3-end-member problem at a minimum: namely the magma, the country rocks and the cumulates. However, instead of giving the details of his calculations, he only presented them in graphical form.

DePaolo (1981) developed a mathematical model which presents the equations for both isotopic and trace element variations and describes the contamination of magma by assimilation of wall-rock coupled to concurrent fractional crystallisation. He proved that the tenet of the simple mixing model, that the concentration in the magma would change in the direction of that in the wall-rock, was not necessarily true if fractional crystallisation was also operating.

DePaolo concentrated on showing the variety of trends which can originate when end-members of known chemistry are mixed during fractional crystallisation. However, a researcher is usually encountered with the opposite situation. He collects a body of isotope and trace element data which shows various trends. Then, he tries to characterise the chemistry of the end-members of the mixture under consideration. In other words, the primary concern is the characterisation of the chemistry of the end-members of the mixture. Usually the main source component, normally of mantle origin, is reasonably easily identified but the 'contaminant' is often unknown (Powell, 1984). Powell (1984) attempted to resolve this problem by inverting the AFC equations of DePaolo (1981). He derived equations for contours of the ratio of the rate of assimilation to the rate of fractional crystallisation in the isotope or trace element region where the contaminant might be located. According to Powell, it is more than likely that AFC usually operates in the evolution of magmas, but unless there is an isotope and/or trace element contrast between magma and contaminant, AFC will not leave a recognisable imprint on the chemistry of magmas. In other words, assimilation must involve material which is sufficiently different isotopically from the original magma in order to produce identifiable isotopic trends. Usually it is the presence of isotopic variation, correlated with major and trace element chemistry which is diagnostic of AFC (Powell, 1984).

AFC modelling carried out in this study has been constructed using the equations of DePaolo (1981). A program which is capable of simultaneously calculating the AFC curves for eight elements and their isotopic ratios, eight r (assimilation rate) values and bulk partition coefficients (D) has been developed for the modelling. The program, named *AFC-Wizard,* is basically a spreadsheet file that utilises the dynamic links in Microsoft Excel® 4.0 for calculating twenty F values on each AFC curve and up to eight curves in each graph. It can be used for every possible element and isotopic ratio with every possible combination of partition coefficients and r values. The program AFC-Wizard is presented in Appendix G. Details of DePaolo's (1981) formulation used are summarised below:

M_m = *mass of magma*
M_m^o = *initial mass of magma*

M_c = *crystallisation rate (mass/unit time)*
M_a = *assimilation rate (mass/unit time)*
C_a = *elemental concentration in wall-rock*
C_m = *elemental concentration in magma*
C_m^o = *original elemental concentration in magma*
D = *bulk solid/liquid partition coefficient for the element between the fractionating crystalline phases and the magma*
Dc_m = *elemental concentration in crystallising phases*

$$F = \frac{M_m}{M_m^o} \quad \textit{the ratio of magma mass to original magma mass} \qquad \text{(Eq. 5.1)}$$

$$r = \frac{M_a}{M_c} \quad \textit{the ratio of the rate of assimilation to fractional crystallisation} \qquad \text{(Eq. 5.2)}$$

$$z = \frac{r + D - 1}{r - 1} \qquad \text{(Eq. 5.3)}$$

a) General equations applicable to most of the cases:

$$C_m / C_m^o = F^{-z} + \left(\frac{r}{r-1}\right)\frac{C_a}{zC_m^o}(1 - F^{-z}) \quad \text{(this formula is not applicable for } r=1\text{)} \qquad \text{(Eq. 5.4)}$$

$$C_m / C_m^o = 1 + \left(\frac{r}{r-1}\right)\frac{C_a}{C_m^o}\ln F^{-z} \quad \text{(for the special case of } r+D=1 \text{ and } z=0\text{)} \qquad \text{(Eq. 5.5)}$$

For the isotopic ratio ε:

$$\frac{\varepsilon_m - \varepsilon_m^o}{\varepsilon_a - \varepsilon_m^o} = 1 - (C_m^o / C_m)F^{-z} \qquad \text{(Eq. 5.6)}$$

where ε_m =isotope ratio in the magma, ε_m^o = initial isotope ratio in magma and ε_a =isotope ratio in the wall rock. ε could be replaced by any isotope ratio or any normalised parameter describing such ratios.

In this equation C_m is given by Equation 4. ε could be replaced by any isotope ratio such as $^{207}Pb/^{204}Pb$, $^{87}Sr/^{86}Sr$ or any normalised parameter describing such ratios (ε_{Sr} or ε_{Nd}).

For light stable isotopes such as $\delta^{18}O$ there is a possibility of fractionation between the crystallising phases and magma so that the isotope ratio in the fractionating crystals is displaced from that of the magma by a factor 'α'. In that case the equation becomes:

$$\delta_m - \delta_m^o = \left(\frac{r}{r-1}\right)\frac{C_a}{zC_m}\left[\delta_a - \delta_m^o - \frac{D\Delta}{z(r-1)}\right](1 - F^{-z}) - \frac{D\Delta}{r-1}\ln F\left[1 - \left(\frac{r}{r-1}\right)\frac{C_a}{zC_m}\right] \qquad \text{(Eq. 5.7)}$$

where $\Delta = \delta_{crystals} - \delta_{magma}$, δ_a: δ^1 values of the contaminant, δ_m: δ values of the magma and δ^o_m: δ values of initial magma.

5.2.2. Estimation of end-member compositions

Estimation of the compositions of possible crustal contaminants and source component for the collision-related volcanics of the Erzurum-Kars Plateau is a very difficult problem because the compositions of mantle and crust (e.g. from xenoliths) beneath the Eastern Anatolia region are almost completely unknown apart from a phyllite collected far away from the plateau, from Bitlis Metamorphic rocks in the south, by Pearce et al. (1990). Furthermore, only a few EKPV lavas can be regarded as representative of a primary magma. Therefore, determination of the main source component is also problematic, though the most primitive magma can still be regarded as the main component.

On the Erzurum-Kars Plateau, the basement is mainly composed of two units as mentioned before in the Stratigraphy chapter. These are the Upper Eocene volcano-sedimentary units called the Narman group and the Late Cretaceous East Anatolian Accretionary Complex. The Narman group is predominantly made up of calc-alkaline intermediate to basic lavas occasionally intercalated with flysch both of which belong to Pontides whereas the East Anatolian Accretionary Complex (EAAC) consists of a typical ophiolitic mélange which includes blocks of diverse rock types such as ultramafic and basic rocks (serpentine, gabbro, basalt and other ophiolitic units) associated with pelagic and neritic limestone, detrital rocks and also rare metamorphic blocks. According to the geologists of Turkish Petroleum Company (Şahintürk and Erakman, 1978) , the EAAC was emplaced in the area during the Eocene period and sandwiched between the terrain blocks or micro-plates of Eastern Anatolia which are represented at present by the Pontide and Bitlis massifs respectively. If their interpretation was true then we would have a more complex picture that seems to involve a

---

[1] δ notation represents deviations relative to Standard Mean Ocean Water (SMOW) as permil (‰), where $\delta^{18}O(‰)=[\ (^{18}O/^{16}O_{(sample)} / {}^{18}O/^{16}O_{SMOW})-1\ ]x\ 10^3$

heterogeneous crust which may be composed of a wide range of lithologies from andesite/dacite to ophiolite. The composition of crust in the region should definitely be quite different from the granodioritic average upper crustal compositions proposed by some authors including Shaw et al. (1967) (Canadian shield) and Taylor and McClennan (1985). Geological maps and field observations in this study suggest that the composition of crust in the north of the plateau is more likely to be close to calc-alkaline andesitic rocks of the Eocene volcanics of the Pontides, because these units cover large areas in the north comprising the basement of the Erzurum-Kars Plateau volcanics (EKPV) in most places. Furthermore, the arc magmatism that gave rise to these volcanic units between Cretaceous and Late Eocene time might have significantly modified the total composition of bulk crust and also that of sub-continental lithosphere leaving a distinctive imprint of an arc component as shown by multi-element patterns (Section 3.3.3). The basement is mainly represented by the EAAC in the south.

Isotopic ratios of the Erzurum-Kars Plateau Volcanics (EKPV), especially Pb isotopes, resembles closely to those of the Pannonian Basin volcanics in Hungary and also to Neogene alkali basalts from western and Central Europe; Eifel, Massif Central and Poland.

The Pannonian Basin is an inter-arc basin which has been active since the Palaeocene. The volcanics in this basin are alkaline in character and erupted in an extensional basin following Eocene-Miocene subduction and its calc-alkaline volcanism (Isztin et al., 1993). They formed between 11.7 and 1.4 Ma almost in the same time span with the EKPV as a result of lithospheric thinning created by back-arc extension. Salters et al. (1988) suggested that either the source of the alkaline magmas had been modified by the earlier subduction or the magmas had interacted with the lower crust. In a more recent study backed by a larger database, Isztin et al. (1993) argued that the magmas erupting to form the Pannonian Basin volcanics were dominantly derived from asthenospheric partial melting, but they also mentioned, on the basis of their Pb isotopic data, that in most cases these volcanics had been modified by melt components from the enriched lithospheric mantle through which they had ascended. Unlike the EKPV, the $\delta^{18}O$ values of the Pannonian basin lavas indicate that they have not

been significantly contaminated with the crustal material. They display a distinctive subduction signature created by subduction and metasomatism of the lithosphere by slab-derived fluids created presumably by introduction of marine sediments into the mantle. This signature is characterised by enrichment in K, Rb, Ba, Pb and Sr and it is also seen in the EKPV.

Figure: 5.5. $^{207}Pb/^{204}Pb$ versus $^{206}Pb/^{204}Pb$ diagram showing generalised fields of the extensional basic lavas of Pannonian Basin in Hungary (Isztin et al., 1993), collision related volcanics of the Erzurum-Kars Plateau volcanics (this study) and granulitic xenoliths from the Pannonian basin and Central Europe (references are listed below).

A: *Proposed asthenospheric A Component of Wilson and Downes (1991). This component has affinities with the source of HIMU and OIB.*

B: *Proposed mafic-igneous granulite xenolith mixing end-member of Wilson and Downes (1991) in Central Europe*

I. *Lower crustal xenoliths; Eifel granulite xenoliths (T=450 Ma) (Rudnick and Goldstein, 1990)*

II. *Metasedimentary granulites (Downes et al., 1991)*

III. *Acid and intermediate (felsic) meta-igneous granulites (Downes et al., 1991)*

IV. *Mafic and ultramafic cumulates (Downes et al., 1991)*

V. *Pannonian basin lavas (Isztin, 1993)*

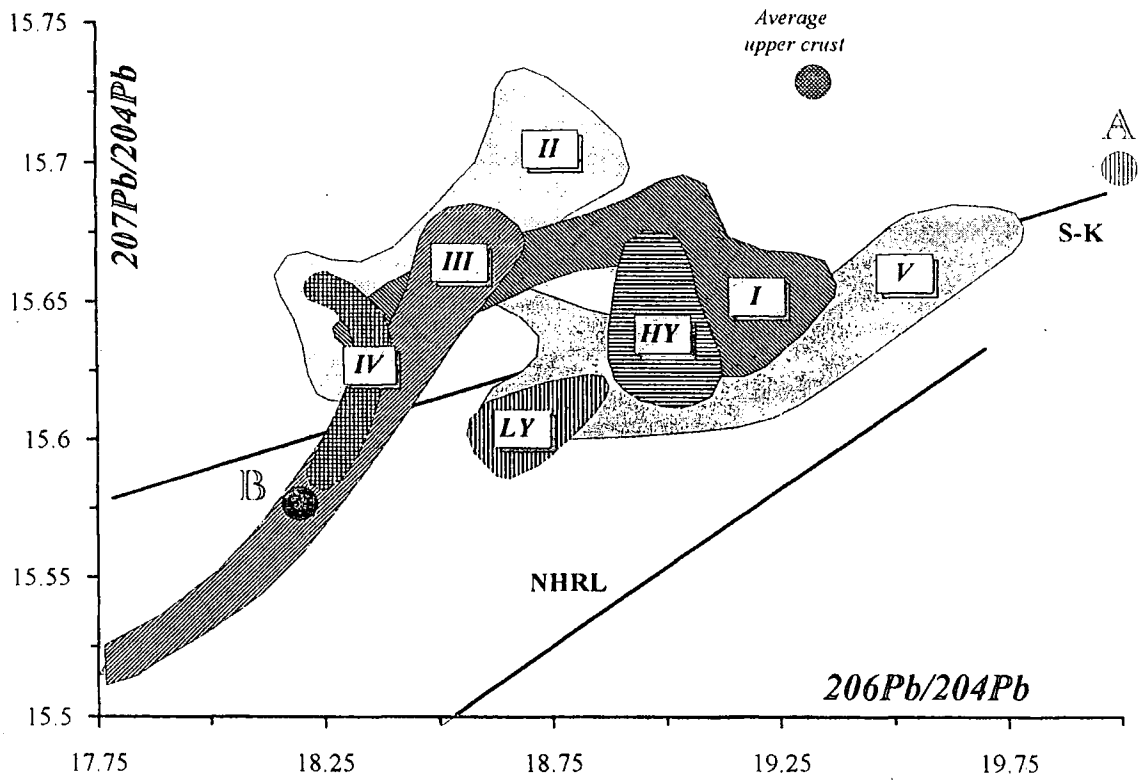

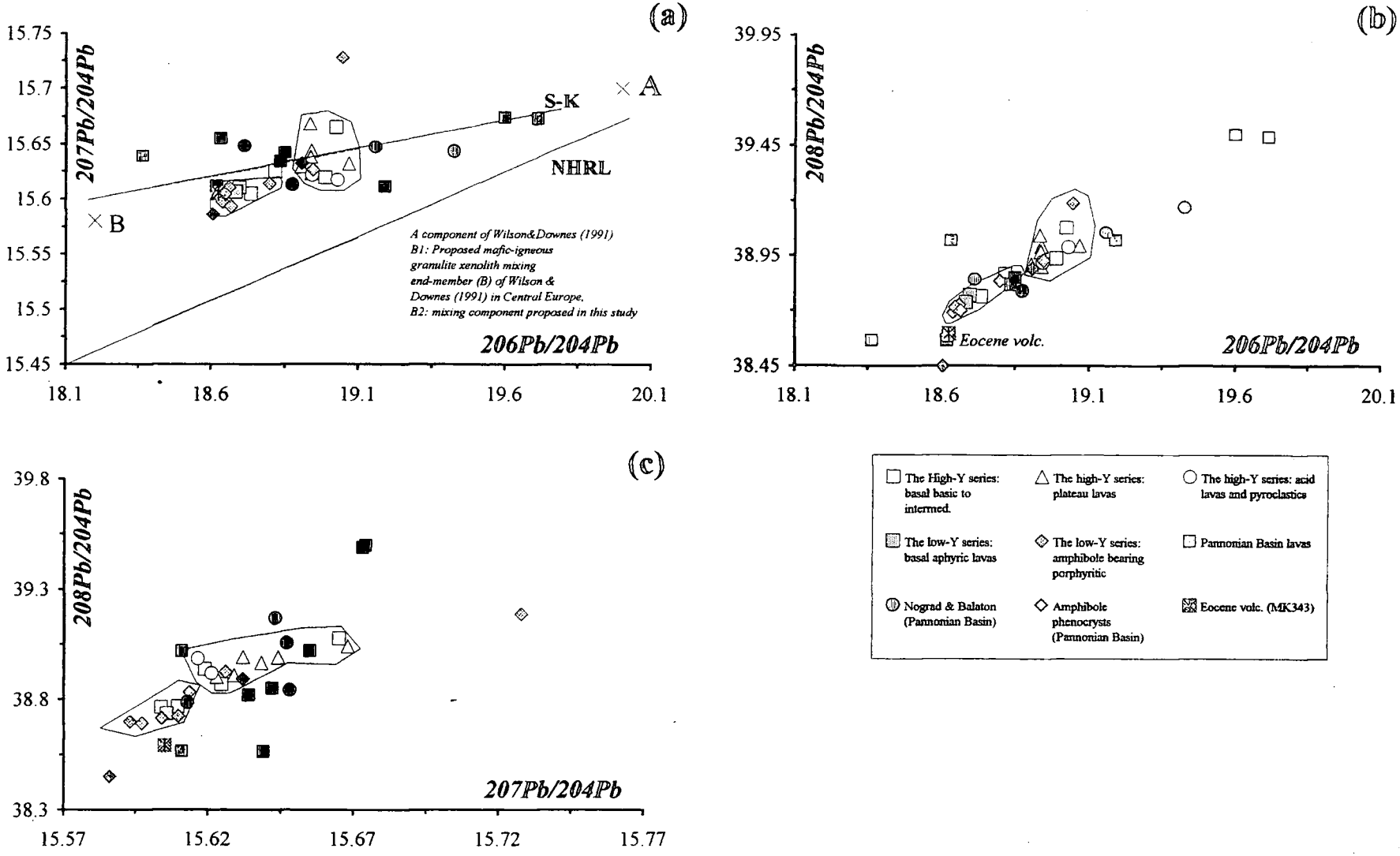

Figure: 5.6. $^{207}Pb/^{204}Pb$ and $^{208}Pb/^{204}Pb$ versus $^{206}Pb/^{204}Pb$ diagrams showing the samples studied. For comparison, northern hemisphere Pb reference line (NHRL) is that of Hart (1984) and S-K is the average crustal Pb evolution curve of Stacey and Kramers (1975).

For comparison, isotopic data from this basin (Isztin et al., 1993) have been plotted onto the $^{207}Pb/^{204}Pb$ versus $^{206}Pb/^{204}Pb$ and $^{208}Pb/^{204}Pb$ diagrams (Figure: 5.6). $^{207}Pb/^{204}Pb$ and $^{208}Pb/^{204}Pb$ ratios of both areas are almost the same whereas the Pannonian Basin lavas span a much wider range in their $^{206}Pb/^{204}Pb$ ratio. The range in $^{87}Sr/^{86}Sr$ in both the EKPV and the Pannonian Basin lavas is very similar to that observed in xenoliths from the basin which were published by Downes et al. (1992) and Downes and Dupuy (1987). These may imply that collision-related volcanics of the Erzurum-Kars Plateau may have a similar lithospheric source, represented by these xenoliths, to those of Central European and Hungarian volcanics. The mantle xenoliths are composed of spinel lherzolites or harzburgites and also pyroxenites. Unfortunately, there are no published Pb isotopic data available for mantle xenoliths apart from those in an abstract by Zindler et al. (1988). They mentioned that fertile spinel lherzolites from the Massif Central have Pb isotopic ratios clustering around the geochron, close to the MORB field. There are also some mafic meta-igneous granulite xenoliths present in the late Tertiary-Quaternary lavas of the Central Europe. These represent the lower crust or crust-mantle transition zone in this region and are thought to have been formed by magmatic (basaltic) underplating of the crust during the Hercynian orogeny (Downes et al., 1990). Among these xenoliths, the older crustal material is represented by granulitic metasediments (Downes et al., 1991). Notably, $^{206}Pb/^{204}Pb$ and $^{207}Pb/^{204}Pb$ ratios of the high-Y series of the EKPV partly overlap with those of mafic granulitic xenoliths from Eifel (Figure 5.5, field-I). Eifel granulites have $\delta^{18}O$ values spanning a range between +6 and +10‰. This was interpreted by Wilson and Downes (1991) as a sign of contamination of the granulitic lower crust by upper crustal material.

Wilson and Downes (1991) explained the isotopic characteristics in alkaline magmas from western Europe in terms of mixtures between two mantle sources -one asthenospheric (component A) and the other an enriched lithospheric mantle (component B). In their view, component A may be a mixture of DM and HIMU mantle components whereas component B has enriched mantle characteristics. They argued that Pb isotopic signature in these volcanics has been mainly controlled by the lithospheric source (i.e. component B). Both the Pannonian Basin volcanics and some of the mafic granulitic xenoliths form linear trends between component A and B on

the diagrams, partly overlapping each other (Figure 5.5). Wilson and Downes (1991) argued that the primitive magmas in the region are extremely unlikely to have been contaminated by the lower crust during their ascent to the surface, as also proven by their low $\delta^{18}O$ content (6-7.2 ‰). They infer that the Pannonian basin volcanics were derived from the subcontinental lithospheric upper mantle of the same age and the same geochemical characteristics as the least contaminated granulite xenoliths, namely the hypothetical mixing end-member B. This source has an isotopic composition of $\delta^{18}O \approx +6.5$ ‰ and $^{206}Pb/^{204}Pb \approx 18.2$. Wilson and Downes (1991) suggest that the isotopic composition of these granulitic xenoliths may constrain the $^{206}Pb/^{204}Pb$ ratio of metasomatised lithospheric upper mantle in the Pannonian Basin.

In Figures 5.7 and 5.8, $^{206}Pb/^{204}Pb$ isotopic ratios of the samples from the EKPV have been plotted against Th/Pb and U/Pb ratios and $^{143}Nd/^{144}Nd$ respectively. These ratios have been chosen because U and Th are the only elements whose abundance cannot be altered significantly by crystallisation of both POAM and hydrous (e.g. amphibole bearing) phases. In addition, assimilation of crust should cause these ratios to increase because these two elements are, in theory, enriched in the upper crust more than Pb compared to their ratio in the lower crust or mantle lithosphere provided that Pb is not significantly affected by fractional crystallisation. In fact, Pb can only be affected by crystallisation of feldspar at intermediate to acid compositions. Th and U concentrations for upper crust were taken from Taylor's (1977) recommended andesitic bulk crust values as 4.8 and 1.25 ppm respectively, because these values are more likely to be close to those of the Eocene volcanics on the plateau.

In Figure 5.7, data points seem to form three trends heading towards three different end-members. One of these trends, which is basically composed of the low-Y series, seems to approach a $^{206}Pb/^{204}Pb$ ratio which is similar to the component-B of Wilson and Downes (1991), while the other two trends, which consist mainly of the high-Y series, appear to head towards two different probable upper crustal compositions (components A1 and A2). The Pb isotopic ratio of A1 resembles closely to average upper crust of Zartman and Doe (1981). $^{206}Pb/^{204}Pb$ isotopic ratio of the third trend, named component-A2, has been approximated from the general alignment of

Figure: 5.7. $^{207}Pb/^{204}Pb$ versus Th/Pb and U/Pb diagrams of the low- and high-Y series from the Erzurum-Kars Plateau.

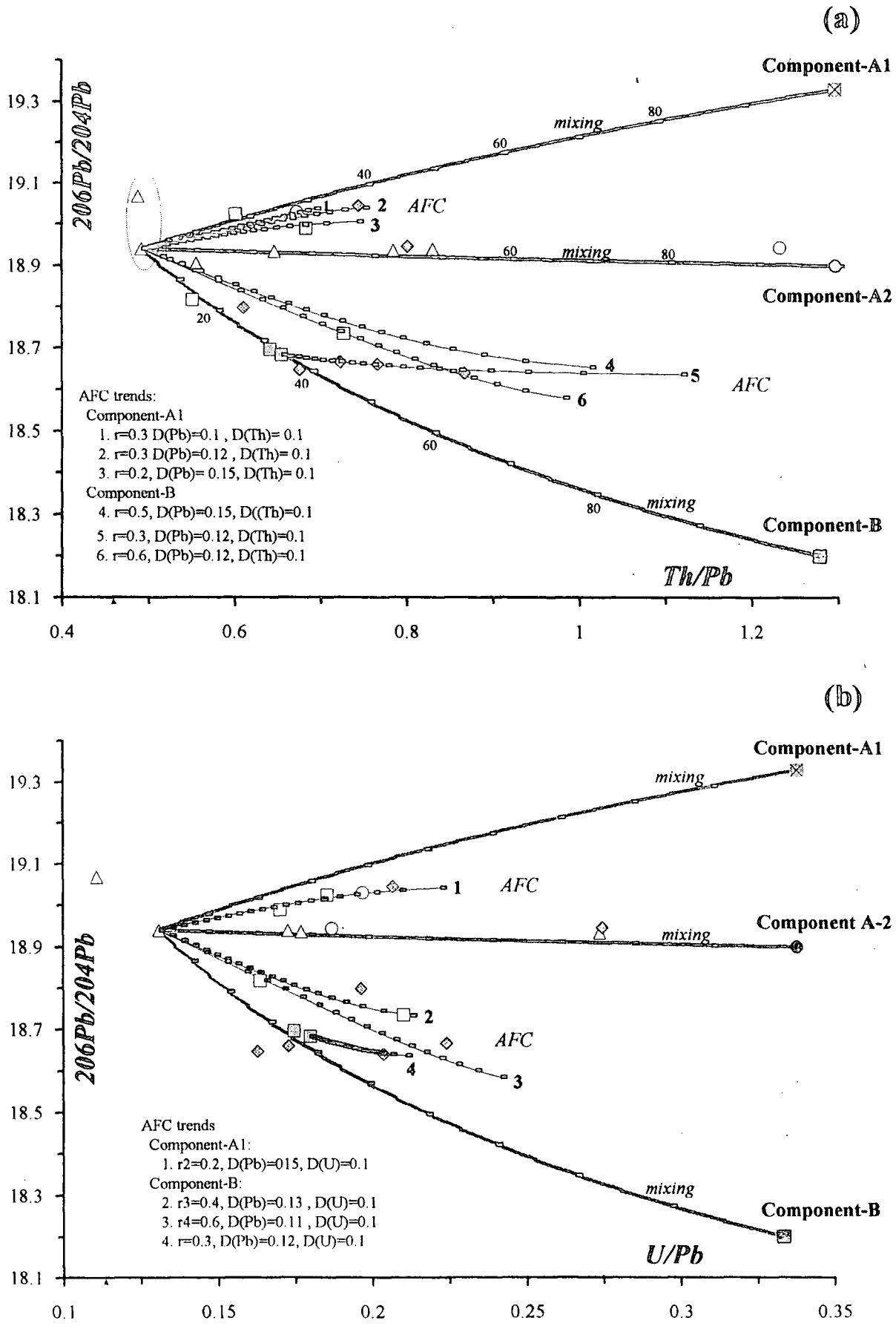

Figure: 5.8. $^{143}Nd/^{144}Nd$ versus $^{206}Pb/^{204}Pb$ diagram displaying the possible lower and upper crust compositions and AFC curves.

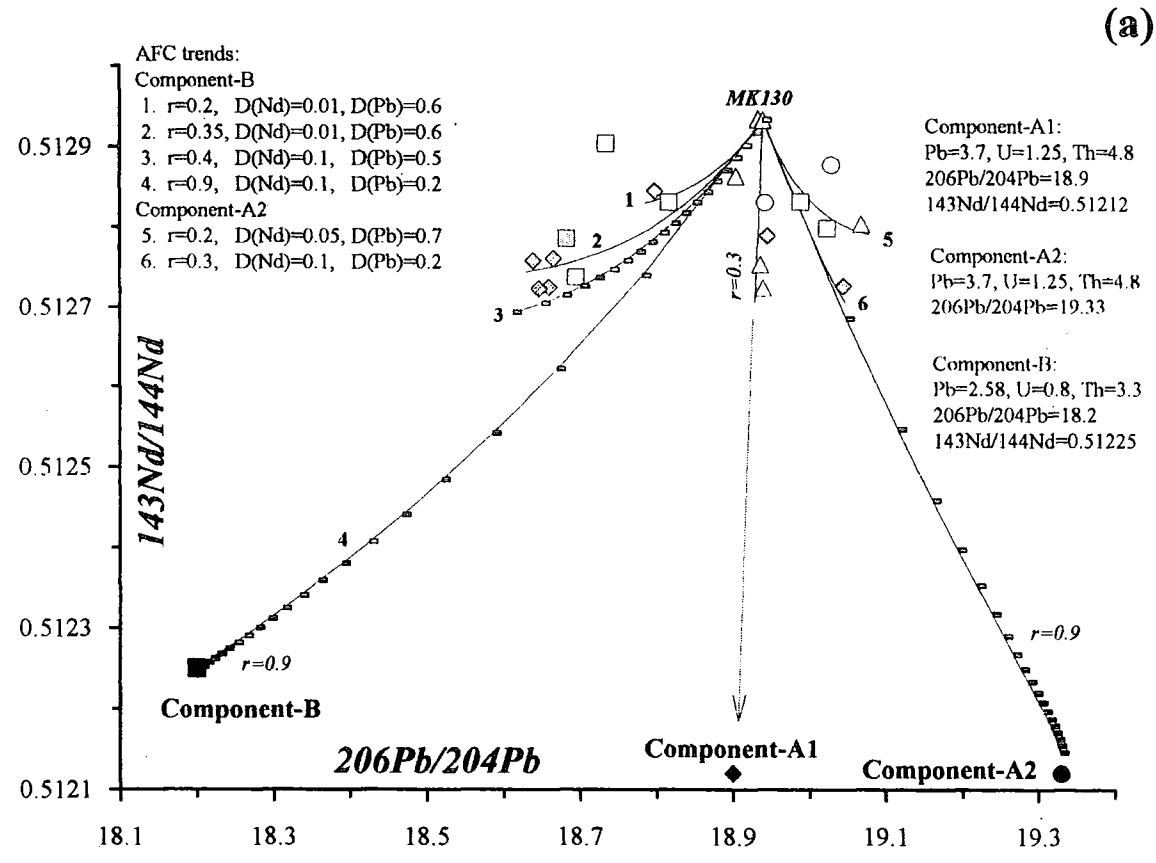

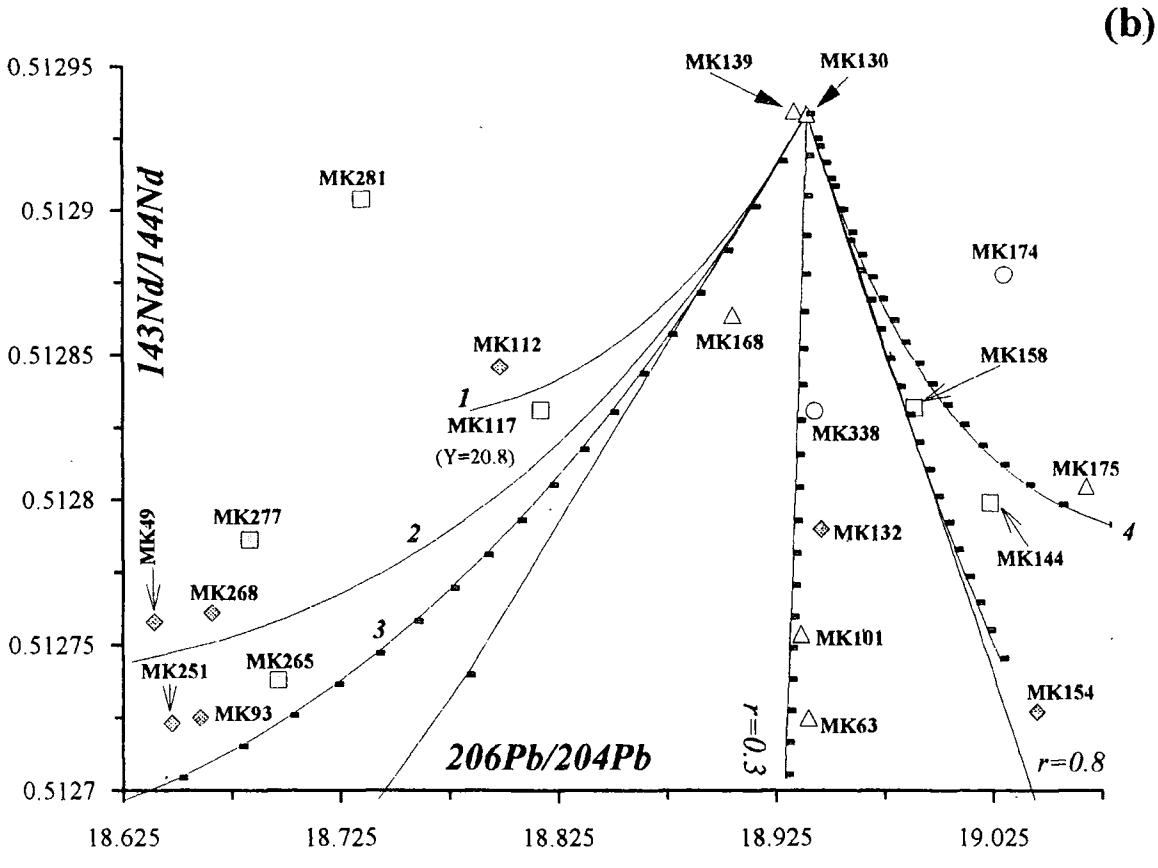

data points forming the second trend as 18.9. These three trends are also seen in $^{143}Nd/^{144}Nd$ versus $^{206}Pb/^{204}Pb$ diagram (Figure: 5.8) with some scatter. In $^{206}Pb/^{204}Pb$ versus Th/Pb diagram, one of the samples from the acidic units of the high-Y series (MK338) appears to constrain the concentration of Pb in the upper crust to about 3.7 ppm, if it is assumed that the Th content of the crust is about 4.8 ppm. This value is significantly lower than the values proposed by Taylor and McClennan (1985) and Condie (1993) (Table 5.1). It should be noted that domination of feldspar as a fractionating phase (especially in intermediate to acidic units) can also contribute to the depletion of Pb and hence this value may actually be higher.

Not having sufficient information to determine precise end-member compositions for these three trends (especially for Pb), simple binary mixing curves between the most primitive lava and these end-members have been constructed and plotted onto the graphs. The geometric relationship of the general alignment of data points to the estimated composition of end-members is also taken into account in the construction of these curves. In Figure 5.7, some of the data points appear to align on the binary mixing curves while the others seem to follow AFC curves (r ranges from 0.2 to 0.5) diverging either from the starting composition or from a particular point on the mixing curves. As a preliminary interpretation, the low-Y series in the EKPV may have interacted predominantly with the lower crust, which is similar in composition to the B component of Wilson and Downes (1991), while the high-Y series dominantly assimilated upper crustal material. Geobarometer calculations based on the composition of amphiboles from the low-Y series indicate crystallisation depths that vary between 20 and 28 km showing agreement with the idea that the low-Y series may have assimilated lower crustal material. In addition to this, the higher Sr and slightly lower Rb contents of the low-Y series with respect to those of high-Y series (Figure 3.18-a and b in Section 3.2.2) also favour contributions from the lower crust, because many lower-crustal mafic granulites are greatly enriched in Sr (as much as 700-1800 ppm) and depleted in Rb as emphasised by Hildreth and Moorbath (1988). The low-Y series that comprises the lower trend in Figure 5.7 has $\delta^{18}O$ values between +6.5 and +10‰ SMOW. This range necessitates assimilation of significant amount of $\delta^{18}O$-rich material which is unusually high for the lower crust. $\delta^{18}O$ content of the lavas from low-Y

series is mostly higher than mean granulitic values of Downes et al. (1991) (Table 5.2). Some metasedimentary granulites from Massif Central xenoliths in France and also some granitoids have $\delta^{18}O$ values as high as +11.8. However, these values still appear to be too small to form the observed enrichment and variation in the low-Y series.

Type of granulites from Massif Central	$\delta^{18}O$	$^{206}Pb/^{204}Pb$	$^{207}Pb/^{204}Pb$	$^{208}Pb/^{204}Pb$
Mafic liquids	+8.6 ± 0.9	18.164	15.609	38.265
Mafic and ultramafic cumulates	+8.0 ± 0.8	18.276	15.637	38.417
Acid and intermediate (felsic) meta-igneous	+9.7 ± 0.4	18.310	15.600	38.586
Metasediments	+9.7 to 11.0	18.597	15.661	38.511

Table: 5.2. Average oxygen and Pb isotopic composition of granulitic mantle xenoliths from French Massif Central (Downes et al., 1991)

As mentioned earlier, $^{206}Pb/^{204}Pb$ versus $^{143}Nd/^{144}Nd$ diagram (Figure 5.8) also shows three trends which seem to approach three different crustal composition. The $^{143}Nd/^{144}Nd$ composition of the upper crust, namely components A1 and A2, is taken from Harmon (1981) (0.51212) while the composition of component B has been estimated as 0.51225, a value which is lower than that of Wilson and Downes (1991), because this value gives results in AFC models that are compatible with the other isotopic ratios and elements (see the following section). The scatter of data points within trend I and III could be caused by variations in $^{143}Nd/^{144}Nd$ in the component B. It can also be related to plagioclase fractionation as implied by the AFC curves *1* (D_{Pb}=0.6), *2* (D_{Pb}=0.6), *3* (D_{Pb}=0.5) and *5* (D_{Pb}=0.7) which have been drawn onto the diagram. A third, and probably more likely, alternative is that both of these factors may have been operational.

Pinarelly et al. (1993) pointed out that crustal contamination of a mantle-derived magma can produce crustal Pb isotopic signatures even for low degrees of contamination due to the strong depletion in Pb of mantle-derived melts with respect to crustal materials. In contrast, Sr isotopes can still maintain a memory of the mantle signature since Sr is far more enriched in the magma than its concentration in the crust. Furthermore, it seems that there is no substantial contrast between Sr isotopic ratio of

primitive magma and the crust on the Erzurum-Kars Plateau. Therefore, Pb isotopic ratios can be more effectively used for modelling of crustal assimilation than those of $^{87}Sr/^{86}Sr$ and $^{143}Nd/^{144}Nd$. In order to examine the extent of crustal assimilation that might have taken place, Pb isotopic ratios of the high- and low-Y series have been plotted against each other in Figure 5.9 together with the A1 A2 and B components. $^{208}Pb/^{204}Pb$ ratios of these components have been estimated from the general trend of data points on these diagrams and presented in Table 5.3. $^{206}Pb/^{204}Pb$ and $^{207}Pb/^{204}Pb$ ratios of component A2 have been assumed to be the same as the proposed upper crust of Zartman and Doe (1981) whereas $^{206}Pb/^{204}Pb$ ratio of component A1 is slightly lower than this value as judged from Figure 5.7 and 5.8. The $^{207}Pb/^{204}Pb$ isotopic ratio of component B has been estimated to be slightly lower than that of Wilson and Downes' (1991) B component. When binary mixing lines are constructed between these components and the most primitive sample (MK130) which is assumed to be representative of primary magma, they fit well to the data points, especially on $^{208}Pb/^{204}Pb$ versus $^{206}Pb/^{204}Pb$ (5.9-b) and $^{207}Pb/^{204}Pb$ (5.9-c) diagrams. The slight scatter of data points especially in $^{207}Pb/^{204}Pb$ ratios may be related to compositional variations in the lower and upper crustal end-members caused by their heterogeneity. These mixing lines give bulk weight fractions (f) of components A1, A2 and B up to 0.4. If estimation of the end member compositions are close to the reality, then it can be argued that the low-Y series has assimilated a lower crustal material or mixed with crustal anatectic melts which are compositionally similar to component B of Wilson and Downes (1991), whereas the high-Y series basically assimilated two different upper crustal compositions up to 40%.

One of the low-Y samples, MK154 from the Saçdağ dacite in south of Horasan, plots in the area of upper crust between components A1 and A2. This may indicate that the magma which produced this unit was a crustal melt.

In Figure 5.10 the $^{206}Pb/^{204}Pb$, $^{207}Pb/^{204}Pb$ isotopic ratios of the components A1, A2 and B are plotted against their Th/Pb ratios and also each other. Also plotted are the average lower crustal composition of Zartman and Doe (1981) and mantle composition of Sun and Donough (1989). Th and U values for the lower crust have been

Figure: 5.9 Pb isotope diagrams showing mixing lines between the most primitive sample on the Erzurum-Kars Plateau and proposed lower (component B) and upper crustal (components A1 and A2) compositions.

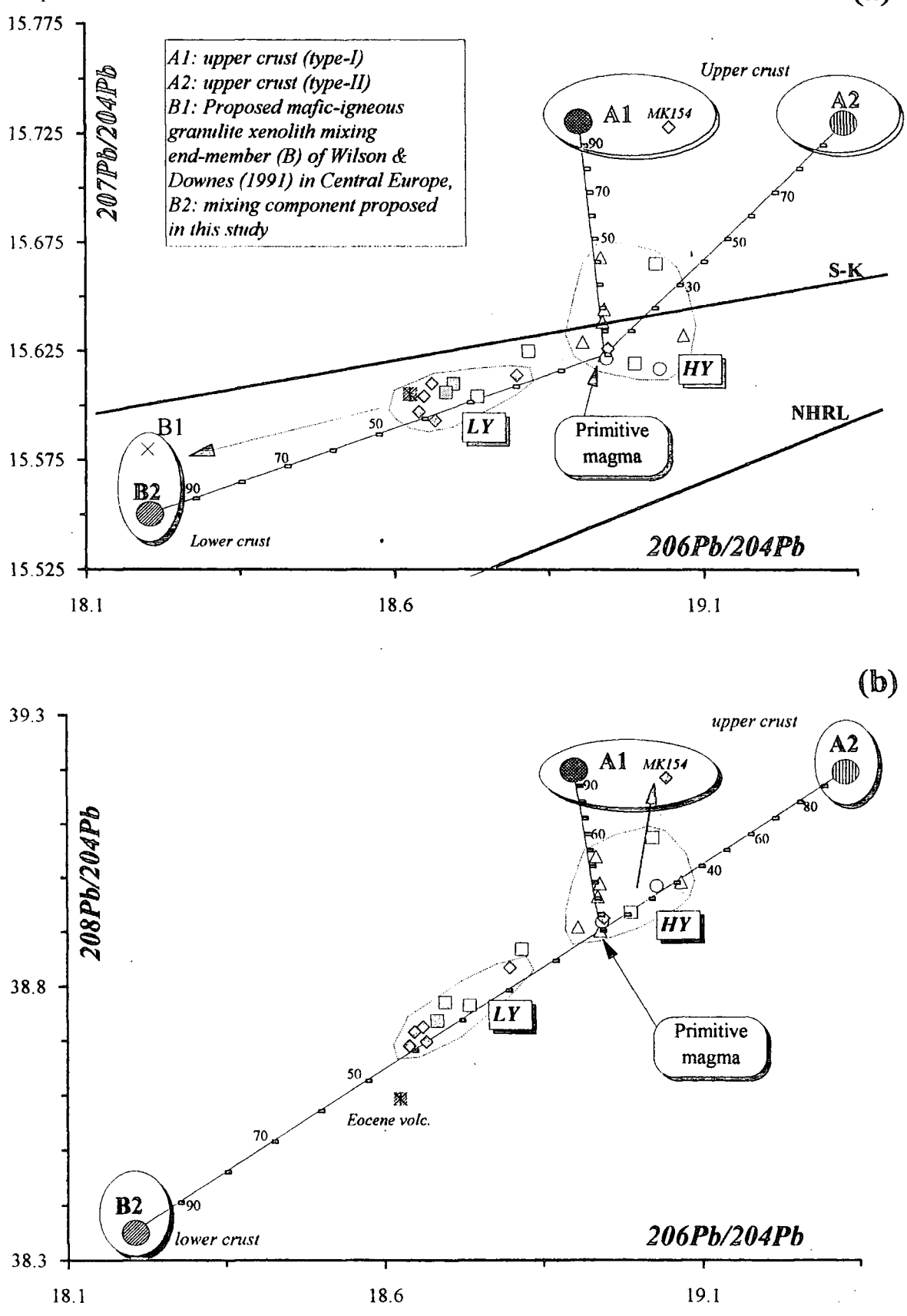

Figure: 5.9 (continued)

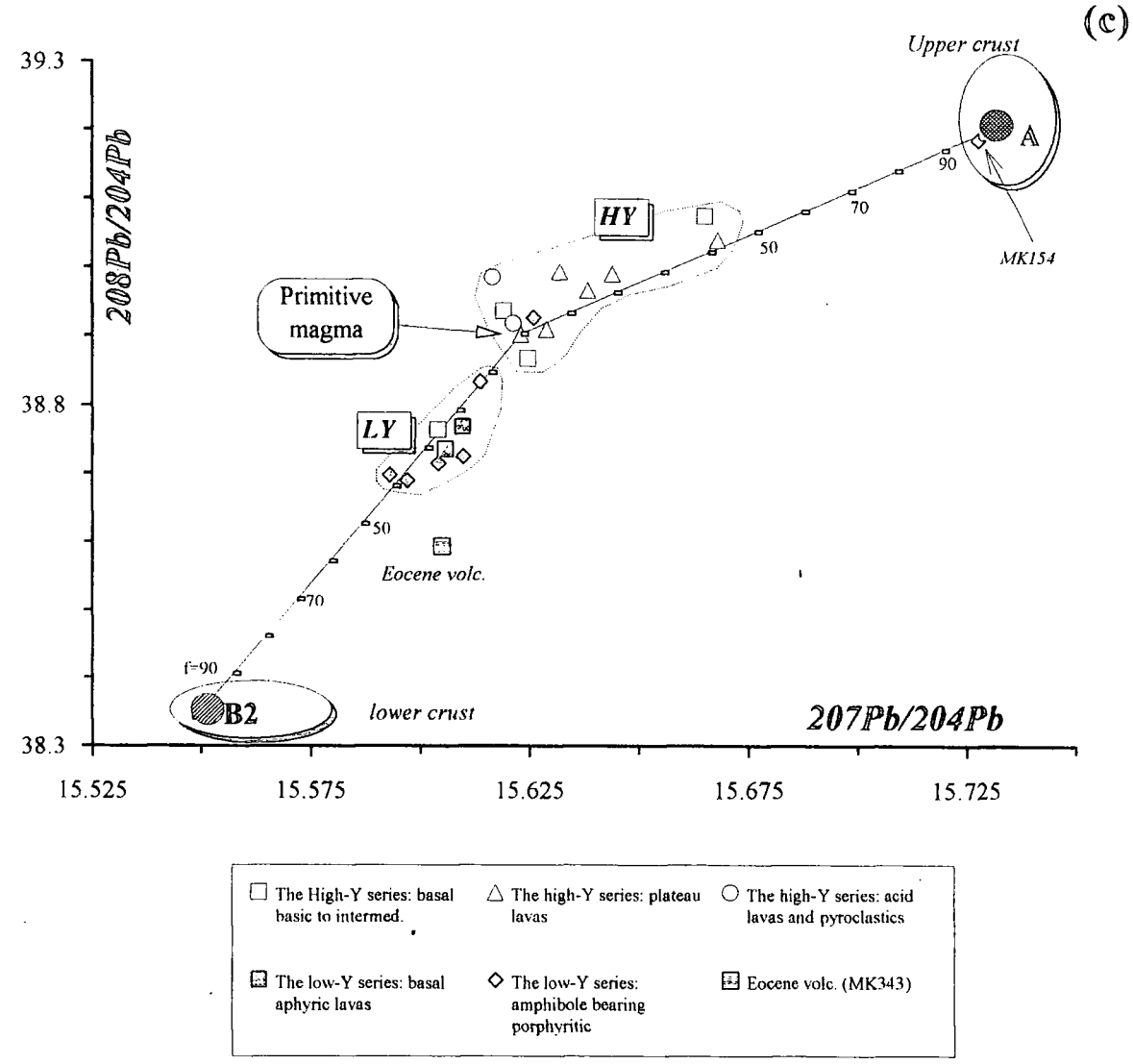

taken from Taylor and McClennan (1985). Note that, when binary mixing lines are constructed between proposed upper crustal composition and the average lower crust of Zartman and Doe (1981) in these diagrams, the granulitic lower crust composition of Wilson and Downes (1991) appears to plot on the mixing lines at a point which is approximately made up of a mixture of 55% upper and 45% lower crustal material. What this may indicate is that the composition of component B that was assimilated in the lavas of low-Y series on the Erzurum-Kars Plateau may be different from that of granulitic lower crust of Wilson and Downes (1991). It may be a transition zone between the lower and upper crust. Alternatively, it may be an enriched granulitic lower

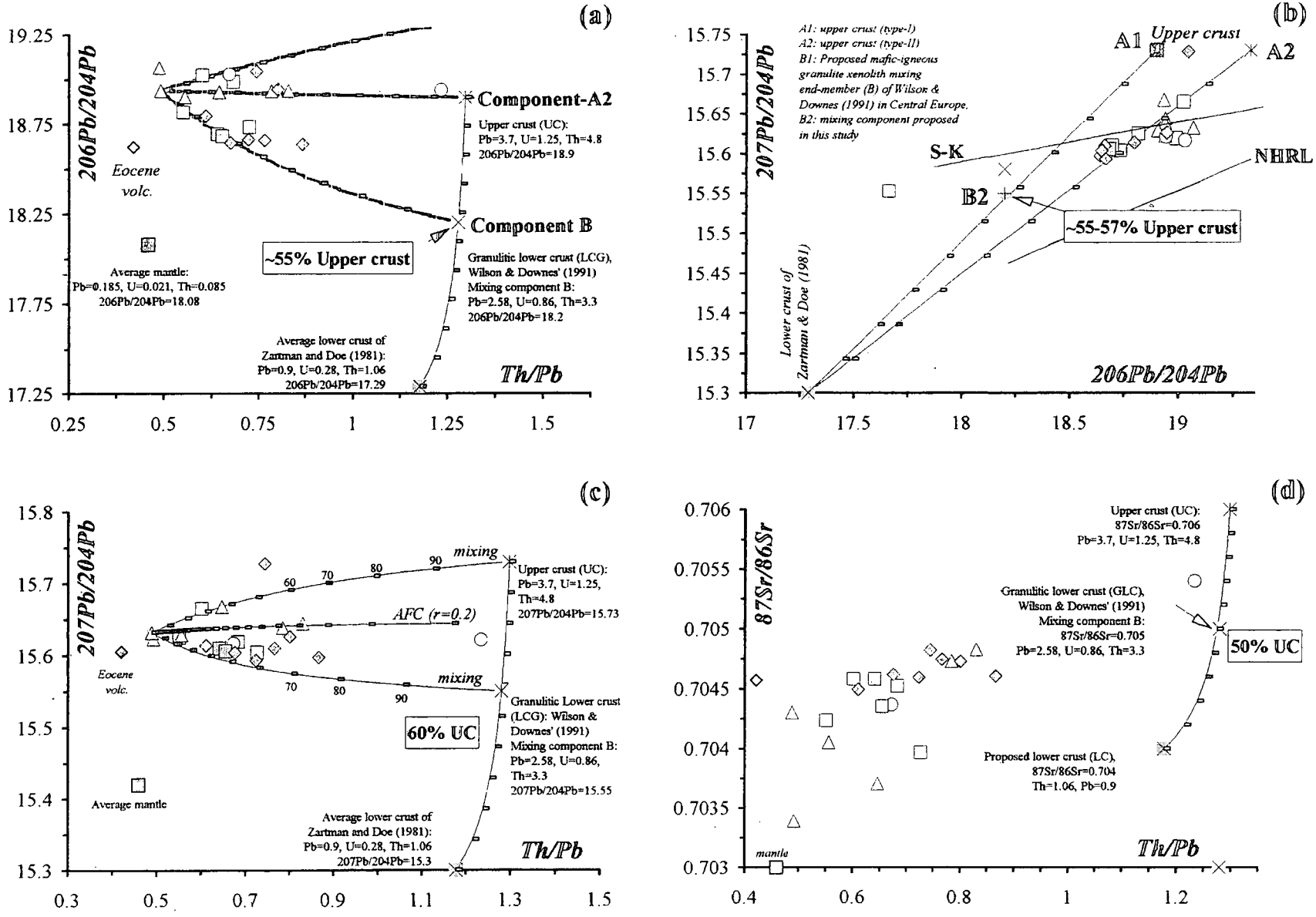
(a)
206Pb/204Pb
Th/Pb
Component-A2
Upper crust (UC):
Pb=3.7, U=1.25, Th=4.8
206Pb/204Pb=18.9
Eocene volc.
Component B
~55% Upper crust
Granulitic lower crust (LCG), Wilson & Downes' (1991) Mixing component B:
Pb=2.58, U=0.86, Th=3.3
206Pb/204Pb=18.2
Average mantle:
Pb=0.185, U=0.021, Th=0.085
206Pb/204Pb=18.08
Average lower crust of Zartman and Doe (1981):
Pb=0.9, U=0.28, Th=1.06
206Pb/204Pb=17.29
(b)
207Pb/204Pb
206Pb/204Pb
A1: upper crust (type-I)
A2: upper crust (type-II)
B1: Proposed mafic-igneous granulite xenolith mixing end-member (B) of Wilson & Downes (1991) in Central Europe.
B2: mixing component proposed in this study
A1
Upper crust
A2
S-K
NHRL
B2
~55-57% Upper crust
Lower crust of Zartman & Doe (1981)
(c)
207Pb/204Pb
Th/Pb
mixing
AFC (r=0.2)
mixing
Upper crust (UC):
Pb=3.7, U=1.25, Th=4.8
207Pb/204Pb=15.73
Eocene volc.
60% UC
Granulitic Lower crust (LCG): Wilson & Downes' (1991) Mixing component B:
Pb=2.58, U=0.86, Th=3.3
207Pb/204Pb=15.55
Average mantle
Average lower crust of Zartman and Doe (1981):
Pb=0.9, U=0.28, Th=1.06
207Pb/204Pb=15.3
(d)
87Sr/86Sr
Th/Pb
Upper crust (UC):
87Sr/86Sr=0.706
Pb=3.7, U=1.25, Th=4.8
Granulitic lower crust (GLC), Wilson & Downes' (1991) Mixing component B:
87Sr/86Sr=0.705
Pb=2.58, U=0.86, Th=3.3
50% UC
Proposed lower crust (LC),
87Sr/86Sr=0.704
Th=1.06, Pb=0.9
mantle

Figure: 5.10.

	Proposed upper crust				Bulk crust	Lower crust							
Author	Taylor & McLennan (1985)	Condie (1993)		Zartman &Doe (1981)	Harmon (1981) isotopically evolved crust	Taylor (1977)	Taylor & Mc Clennan (1985)	Wilson & Downes (1991) B component *	Wilson & Downes (1991) A component **	Zartman &Doe (1981)	Eocene volcanics in Pasinler area (MK343)	Mixing component A on the Erzurum-Kars Plateau (This study)		Mixing component B on the Erzurum-Kars Plateau (This study)
Model		*Restoration model*	*Map model*			*The andesite model*						A1	A2	
Rb	112	87.00	83.00			42	5.3				55	**87**	**87**	**55**
Sr	350	269.00	289.00			400	230				359	**400**	**400**	**350**
Nb	25	10.30	9.80			11	6				26	**11**	**11**	
Nd	26	26.90	25.60			16	12.7				39	**16**	**16**	**14**
Pb	20	18.00	17.00			10	4				25	**3.7**	**3.7**	**2.58**
Th	10.7	9.10	8.60			4.8	1.06				10	**4.8**	**4.8**	**3.3**
U	2.8	2.40	2.20			1.25	0.28				0.8	**1.25**	**1.25**	**0.86**
Radio-isotopic data														
87Sr/86Sr					0.735000		0.711700	0.705000	0.703000		0.704573	**0.706000**	**0.706000**	**0.705000**
143Nd/144Nd					0.512120		0.510710	0.512500	0.513500		0.512814	**0.512120**	**0.512120**	**0.512250**
206Pb/204Pb				19.330				18.200	20.000	17.290	18.625	**18.900**	**19.330**	**18.200**
207Pb/204Pb				15.730				15.580	15.700	15.300	15.605	**15.730**	**15.730**	**15.550**
208Pb/204Pb				39.060						38.560	38.593	**39.060**		**38.693**
d18 O					19			6.5			*7.5*	**19**	**19**	**13.75**

* : Composition of lower crust within Central Europe; B mixing component of Wilson & Downes (1991)
Mafic igneous granulite xenoliths Massif Central and Eifel district of the Rhenish Massif

** : Composition of lower crust within Central Europe; A mixing component of Wilson & Downes (1991)

Table: 5.3. Table showing recommended lower and upper crust compositions of several authors and the values used in this study for comparison.

crustal component that is similar to the Pannonian Basin granulites in its composition but perhaps affected by more upper crustal contamination that gave rise to its higher $\delta^{18}O$ content. If what the low-Y series assimilated was a mixture of 55% upper and 45% lower crust, or a composition which is more or less equivalent to this mixture, then it would be possible to approximate the concentration of some of other trace elements and also isotopic ratios on the basis of this estimation. Along the lines of this interpretation, unknown concentrations of some trace elements (e.g. Rb and Sr) and also isotopic ratios (e.g. $\delta^{18}O$) have been calculated and presented in Table 5.3. In my opinion, this seems to be the only viable approach to the estimation of composition of upper and lower crustal compositions in the region. It should be noted again that these numbers on which I will construct my petrologic modelling are only very broad approximations to reality even if they may be consistent with each other on most diagrams.

5.2.3. AFC modelling of the high- and low-Y series

The AFC equations of DePaolo (1981) presented in Section 5.2.1 have been used for the modelling of trace element and isotopic data from the low- and high-Y series. It should be noted that the precise values of r are not very meaningful due to the possible variations in end-member compositions and also variations in bulk partition coefficient values (D) of elements during the course of fractional crystallisation.

Throughout the modelling, two types of crustal compositions have been used. Composition of component-B, which appears to be representative of deeper parts of the crust, has been used to depict the assimilated crust for the low-Y series, and Component-A, which is basically upper crustal in composition, has been employed for the high-Y series (Table 5.3). Concentrations of Sr=400 and Nd=16 (ppm) for upper crust have been taken from Taylor (1977) while Rb value (87 ppm) has been obtained from the restoration model upper crustal composition of Condie (1993). Composition of lower crustal abundance (component-B) of these elements have been estimated from their upper crustal compositions following the way described in the previous section as Sr=350, Nd=14 and Rb=55. The $^{143}Nd/^{144}Nd$ ratio and $\delta^{18}O$ value of the upper crust is of Harmon's (1981) isotopically evolved crust while its $^{87}Sr/^{86}Sr$ ratio

has been estimated as 0.706, a value which seems to be reasonable for a crust whose Sr isotope composition is close to that of, but higher than, the Eocene volcanics on the plateau. Values of $\delta^{18}O$=13.75, $^{143}Nd/^{144}Nd$=0.512250, $^{87}Sr/^{86}Sr$=0.705 and Th=3.3 have been used to represent Component-B.

Figures 5.11 and 5.12 display the first AFC modelling of the low- and high-Y series respectively. Rb/Th and Rb/U ratios have been chosen for this modelling because they are not affected by both the crystallisation either of POAM or of hydrous (basically amphibole bearing) phases. Even though Rb may be partitioned strongly into biotite ($K_d^{bio/l}$ =3.2 at intermediate 4.5 at acid compositions), this should not pose a problem for the modelling, since it is apparent that biotite is not a major crystallising phase on the Erzurum-Kars Plateau. On the other hand, Nb cannot be used for the AFC modelling, because it is significantly depleted by the crystallisation of amphibole both in the high- and low-Y series. The sample MK139, one of the most basic lavas from the Horasan Plateau unit, has been chosen as the basic end-member for these diagrams, since it plots at the end of the AFC trend. Bulk partition coefficients (D) of 0.1 for Rb and U and 0.01 for Th have been used for the modelling assuming that they were constant throughout the crystallisation. Theoretical AFC curves have been calculated for different values of r (r is the ratio of assimilation rate to crystallisation rate). The ratio of remaining magma mass to original magma mass (F values) have been marked on each curve at 5% intervals.

There is only one sample, MK132 (the Köroğlu amphibole andesite/dacite, north of Horasan), which plots between the r=0 and 0.05 curves on both Rb/Th and Rb/U versus Rb diagrams, implying very little or no crustal assimilation. The same sample plots very close to the most primitive lava end-member in Figure 5.9 indicating that it is quite primitive in its composition. The majority of samples on the Rb/Th vs. Rb diagram are scattered between r=0.1 and 0.3 and clustered around the $r3$=0.1 curve indicating that the low-Y series may have assimilated a crust (as much as 30% of the fractional crystallisation rate) as much as 10-20% whose composition is similar to Component-B (Figure 5.11-a). On the other hand, on the Rb/U versus Rb diagram, the same set of data points scatter within AFC trends with r values between 0.2 and 0.5.

Figure: 5.11. AFC modelling of the low-Y series on Rb/Th and Rb/U versus Rb diagrams.

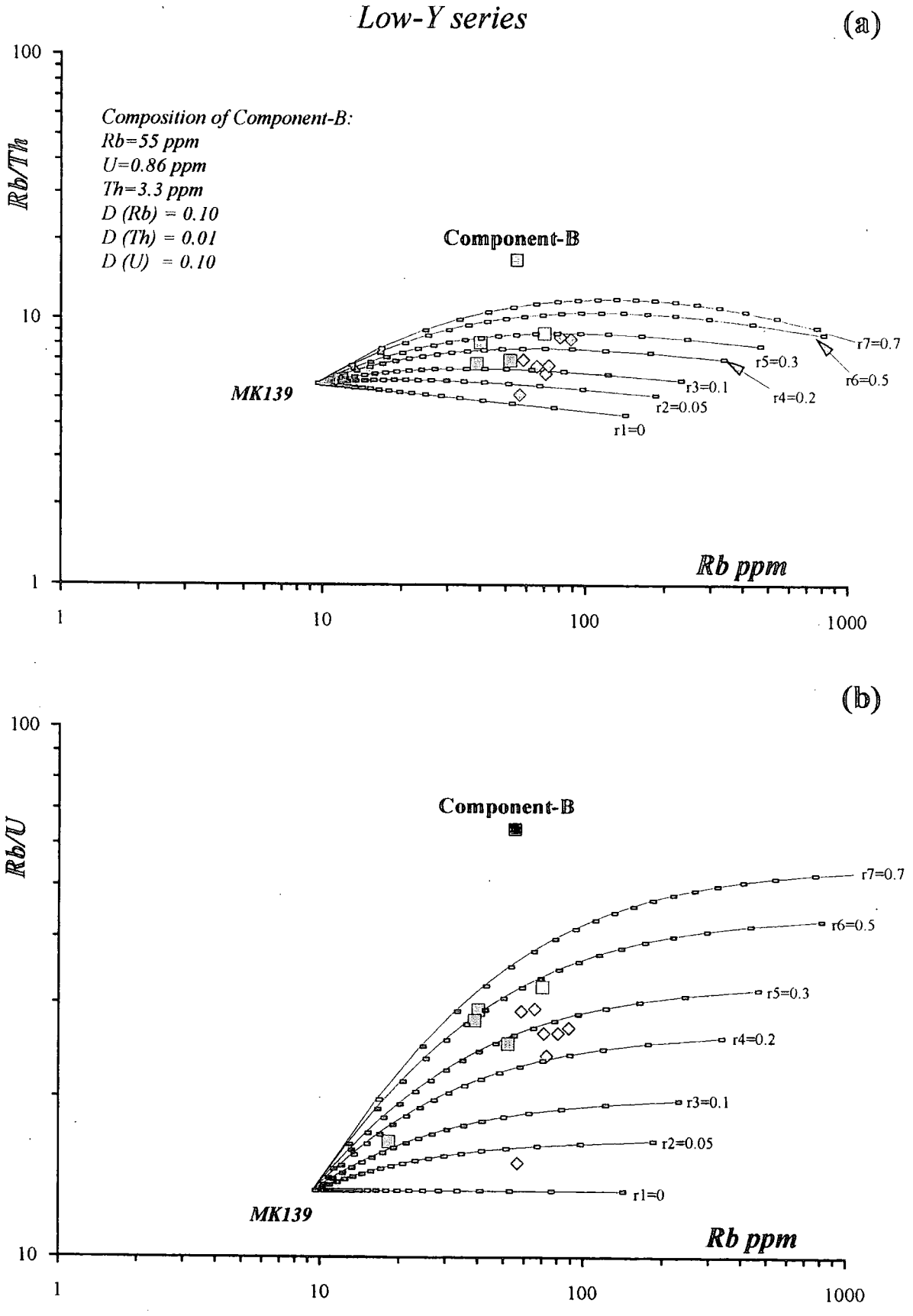

Figure: 5.12. AFC modelling of the high-Y series on Rb/Th and Rb/U versus Rb diagrams.

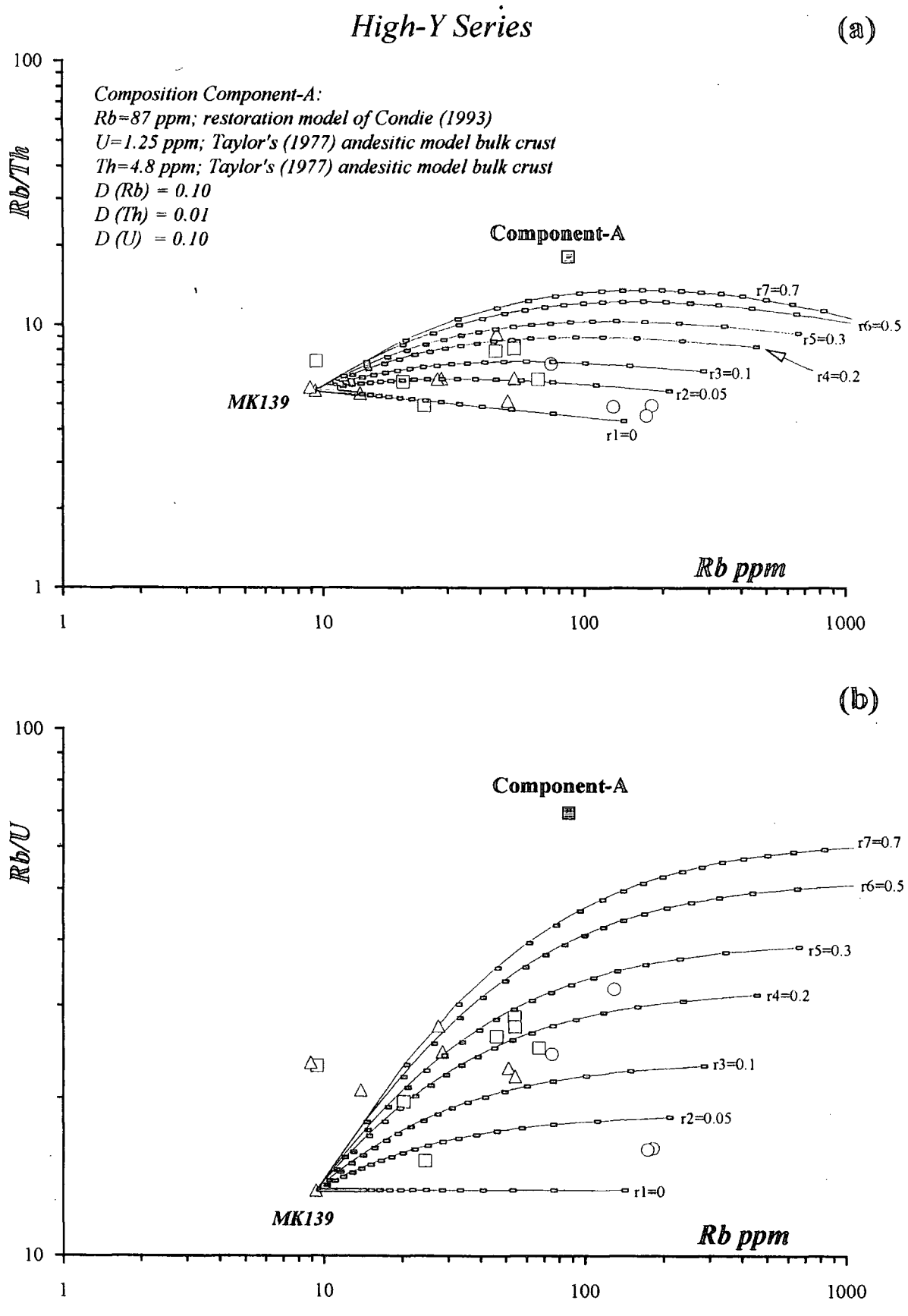

The same types of diagram have been constructed for the high-Y series using the same D values and taking the upper crustal composition of Component-A as the assimilant (Figure 5.12). Notably, four samples from the intermediate to acidic units of the high-Y series and one basic plateau lava follow the r=0 vector while the others plot between the curves of 5% and 20% assimilation. The Rb/U versus Rb diagram again show relatively higher assimilation rates relative to FC rates for the same samples, because U concentration of the assimilant upper crust is probably more variable than that of Th.

Another AFC model has been constructed by plotting the same trace element ratios against the $^{87}Sr/^{86}Sr$ isotopic ratio for both the high- and low-Y series (Figures 5.13 and 5.14 respectively). The AFC curves on these diagrams are drawn according to expected range of r (between 0.05 and 0.6) and bulk partition coefficients of Sr (D_{Sr}=2-3) as presented in inset tables (Figure 5.13-b). Predicted trace element concentrations and Sr isotopic ratios for component-A and B (Table 5.3) have been used for the high- and low-Y series respectively. Most of the data points of the low-Y series plot in range of assimilation rates between 15% and 30% (Figure 5.13) whereas those of high-Y series (Figure 5.14) seem to have relatively lower r values between 0 and 15%. These results are in good agreement with those obtained from the trace element modelling presented in Figures 5.11 and 5.12.

A comparable model has been produced by plotting $\delta^{18}O$, a more assimilation-sensitive isotope, against Th, U and Rb (Figure 5.15-a to c). Since oxygen isotope data are available only for the low-Y series, the Component-B has been chosen as the contaminant. As $\delta^{18}O$ is a light stable isotope, it may fractionate between the crystallising phases and magma resulting in a displacement from that in the magma by a factor named 'α'. This fractionation has been corrected using DePaolo's (1981) equation (Equation 5.7). The assimilation rates obtained from the diagrams in Figure 5.15 span a range between 0.1 and 0.35 and are consistent again with the previous AFC diagrams. Similar to its behaviour in previous diagrams, MK132 (Köroğlu amphibole andesite/dacite, N of Horasan) shows very little or no sign of assimilation.

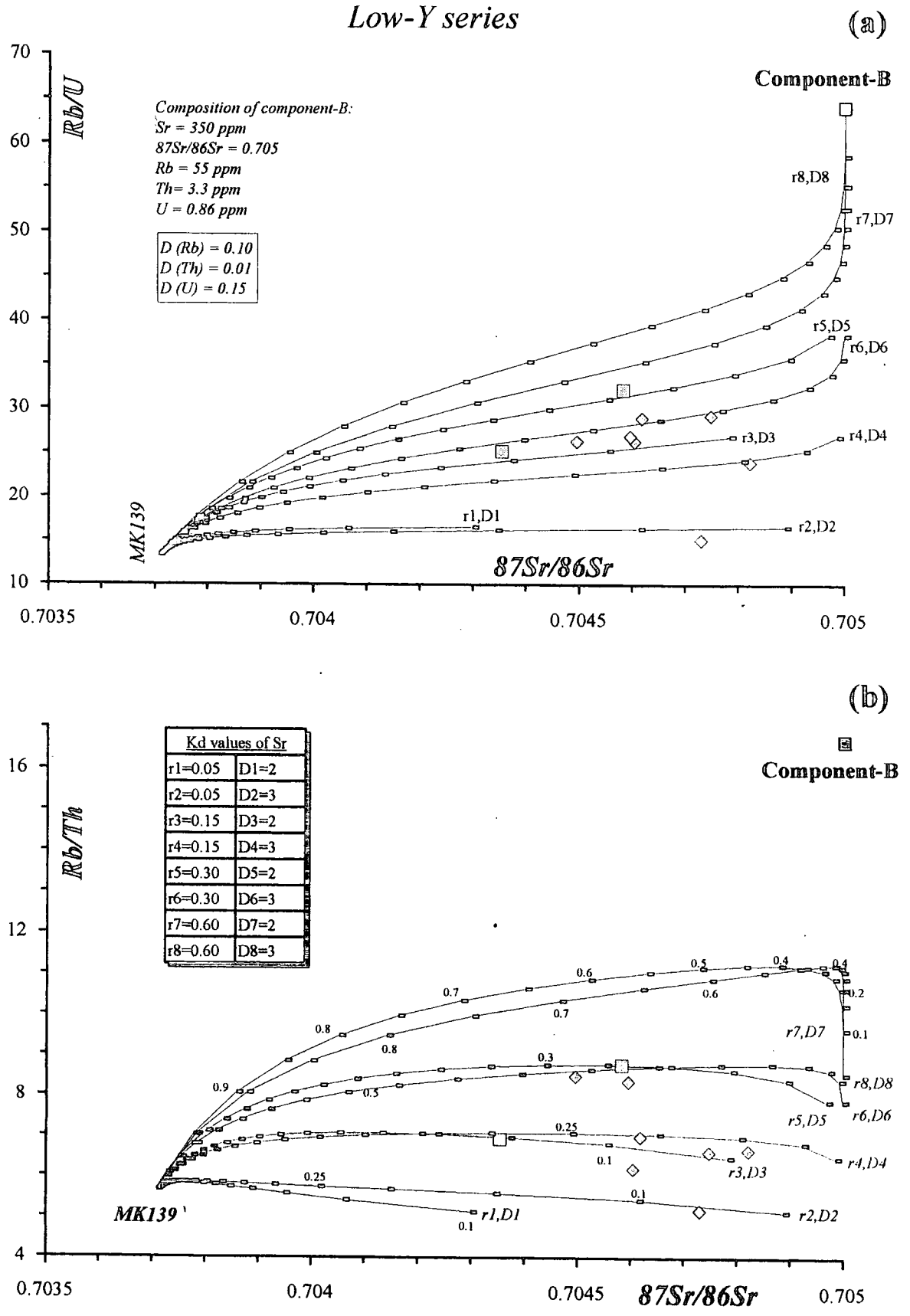
Low-Y series
(a)
Component-B
Composition of component-B:
Sr = 350 ppm
87Sr/86Sr = 0.705
Rb = 55 ppm
Th= 3.3 ppm
U = 0.86 ppm
D (Rb) = 0.10
D (Th) = 0.01
D (U) = 0.15
Rb/U
MK139
87Sr/86Sr
r8,D8
r7,D7
r5,D5
r6,D6
r3,D3
r4,D4
r1,D1
r2,D2
70
60
50
40
30
20
10
0.7035
0.704
0.7045
0.705
(b)
Component-B
Kd values of Sr
r1=0.05 D1=2
r2=0.05 D2=3
r3=0.15 D3=2
r4=0.15 D4=3
r5=0.30 D5=2
r6=0.30 D6=3
r7=0.60 D7=2
r8=0.60 D8=3
Rb/Th
MK139
87Sr/86Sr
16
12
8
4
0.7035
0.704
0.7045
0.705

Figure:5.13.

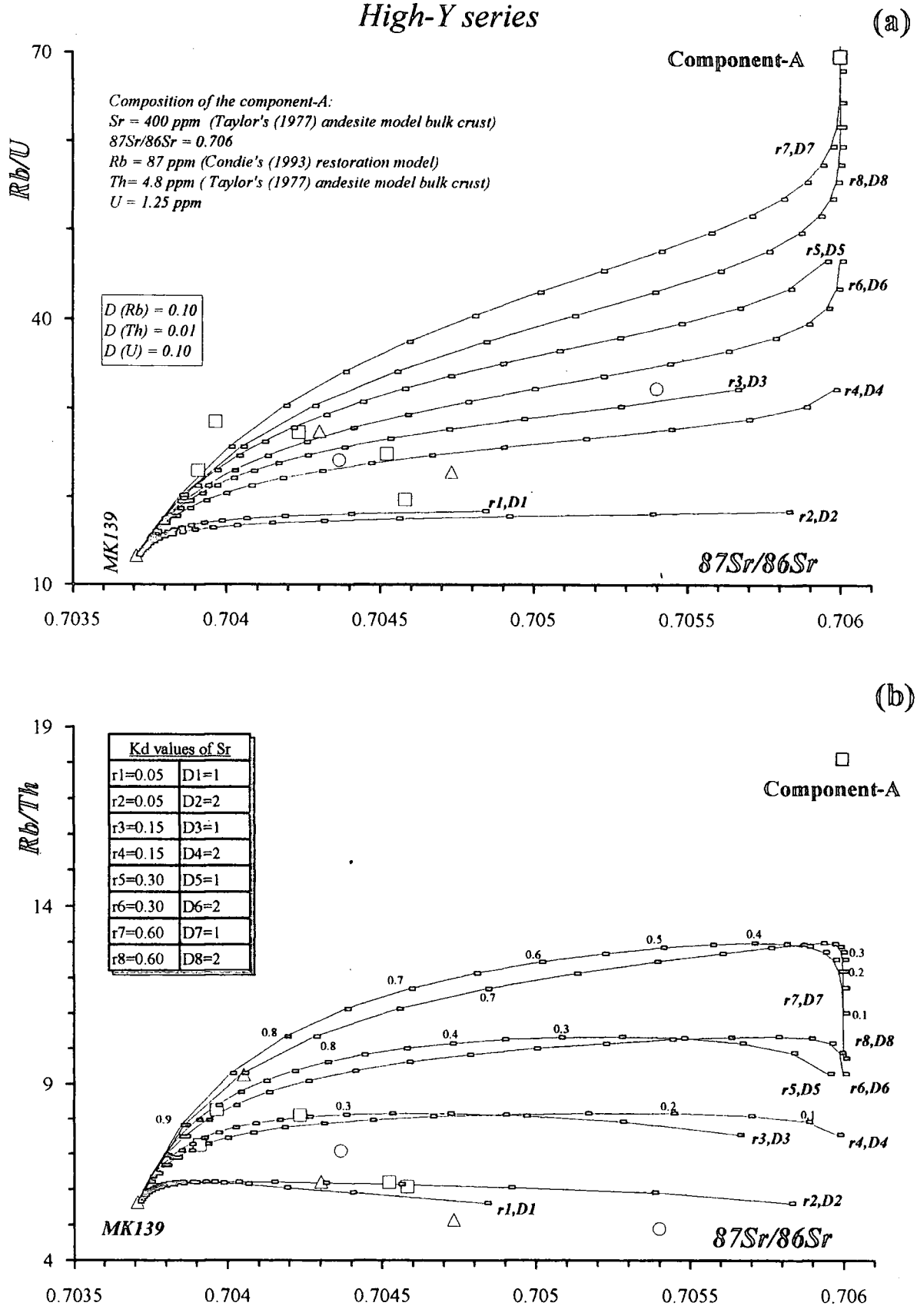
High-Y series
(a)
Component-A
Composition of the component-A:
Sr = 400 ppm (Taylor's (1977) andesite model bulk crust)
87Sr/86Sr = 0.706
Rb = 87 ppm (Condie's (1993) restoration model)
Th= 4.8 ppm (Taylor's (1977) andesite model bulk crust)
U = 1.25 ppm
D (Rb) = 0.10
D (Th) = 0.01
D (U) = 0.10
r7,D7
r8,D8
r5,D5
r6,D6
r3,D3
r4,D4
r1,D1
r2,D2
MK139
87Sr/86Sr
Rb/U
70
40
10
0.7035
0.704
0.7045
0.705
0.7055
0.706
(b)
Kd values of Sr
r1=0.05 D1=1
r2=0.05 D2=2
r3=0.15 D3=1
r4=0.15 D4=2
r5=0.30 D5=1
r6=0.30 D6=2
r7=0.60 D7=1
r8=0.60 D8=2
Component-A
Rb/Th
19
14
9
4
MK139
87Sr/86Sr

Figure:5.14.

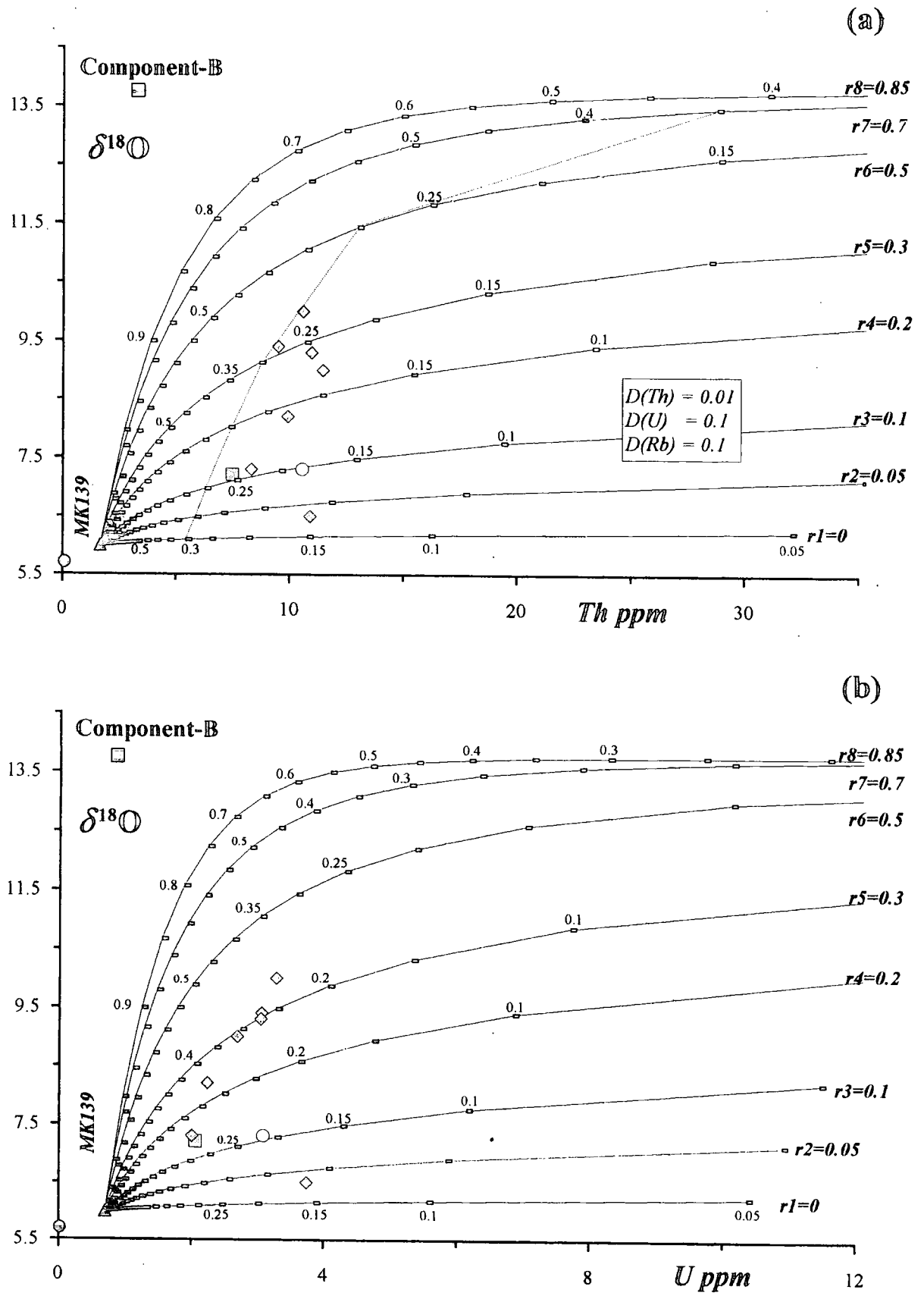
(a)
Component-B
δ18O
MK139
D(Th) = 0.01
D(U) = 0.1
D(Rb) = 0.1
r8=0.85
r7=0.7
r6=0.5
r5=0.3
r4=0.2
r3=0.1
r2=0.05
r1=0
Th ppm
(b)
Component-B
δ18O
MK139
r8=0.85
r7=0.7
r6=0.5
r5=0.3
r4=0.2
r3=0.1
r2=0.05
r1=0
U ppm

Figure: 5.15.

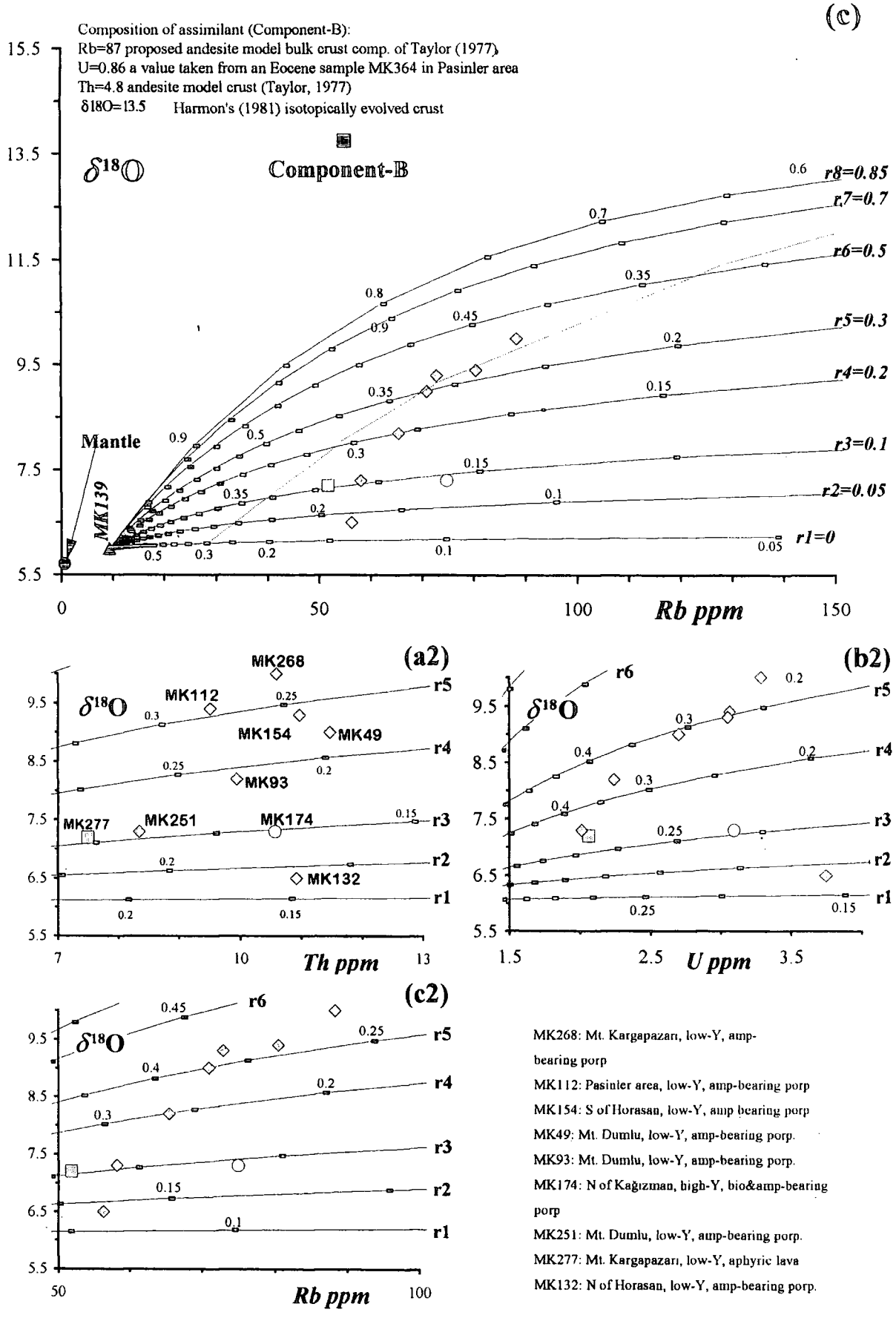

Figure: 5.15. Diagrams showing assimilation combined with fractional crystallisation (AFC) processes in the volcanic units of the low- and high-Y series.

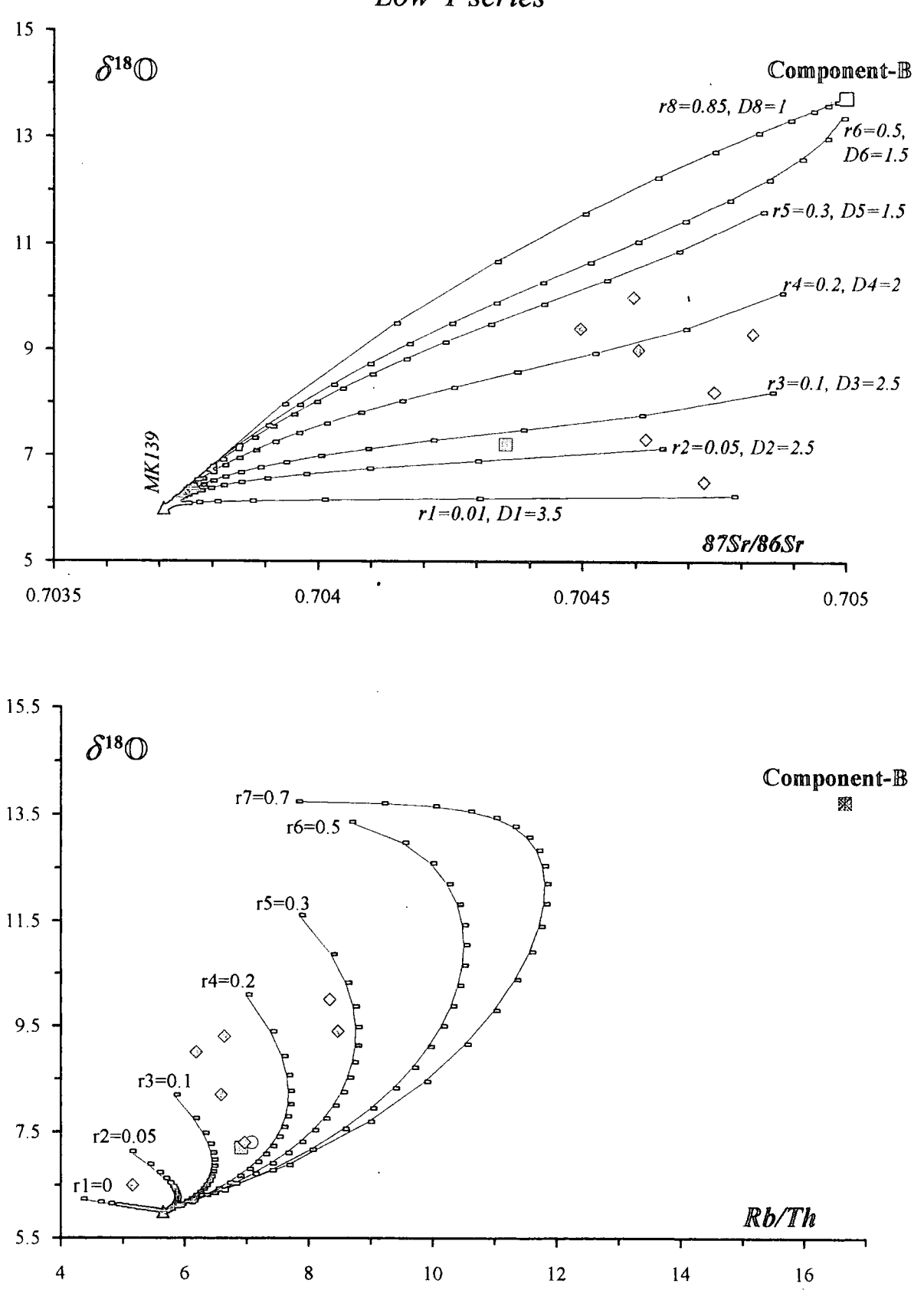
Low-Y series
δ18O
Component-B
r8=0.85, D8=1
r6=0.5, D6=1.5
r5=0.3, D5=1.5
r4=0.2, D4=2
r3=0.1, D3=2.5
r2=0.05, D2=2.5
r1=0.01, D1=3.5
MK139
87Sr/86Sr
15
13
11
9
7
5
0.7035
0.704
0.7045
0.705
δ18O
Component-B
r7=0.7
r6=0.5
r5=0.3
r4=0.2
r3=0.1
r2=0.05
r1=0
Rb/Th
15.5
13.5
11.5
9.5
7.5
5.5
4
6
8
10
12
14
16

Figure: 5.16

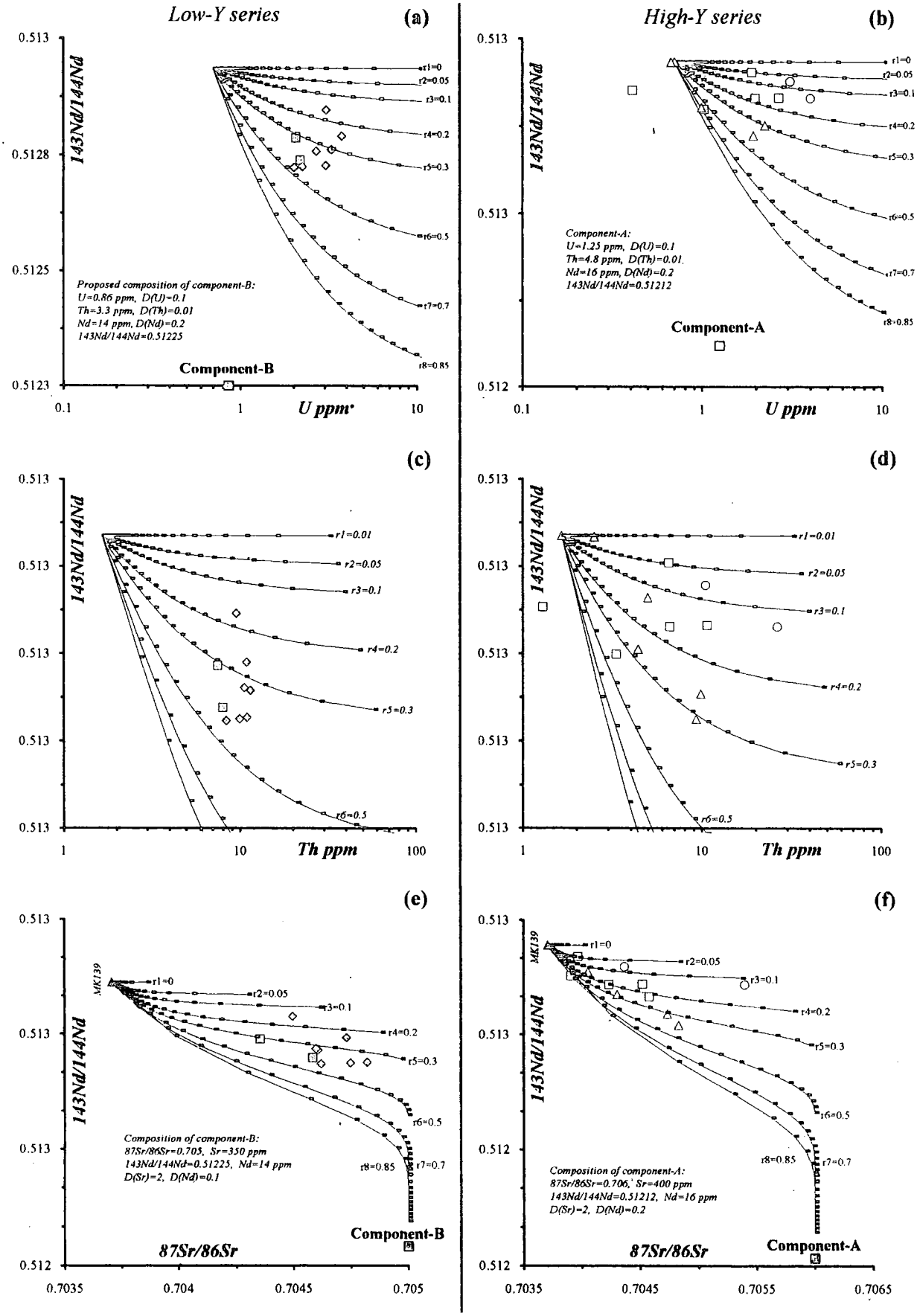
Low-Y series
(a)
143Nd/144Nd
0.513
0.5128
0.5125
0.5123
r1=0
r2=0.05
r3=0.1
r4=0.2
r5=0.3
r6=0.5
r7=0.7
r8=0.85
Proposed composition of component-B:
U=0.86 ppm, D(U)=0.1
Th=3.3 ppm, D(Th)=0.01
Nd=14 ppm, D(Nd)=0.2
143Nd/144Nd=0.51225
Component-B
0.1
1
U ppm
10
High-Y series
(b)
0.513
0.513
0.512
Component-A:
U=1.25 ppm, D(U)=0.1
Th=4.8 ppm, D(Th)=0.01
Nd=16 ppm, D(Nd)=0.2
143Nd/144Nd=0.51212
Component-A
(c)
r1=0.01
r2=0.05
r3=0.1
r4=0.2
r5=0.3
r6=0.5
1
10
Th ppm
100
(d)
(e)
MK139
Composition of component-B:
87Sr/86Sr=0.705, Sr=350 ppm
143Nd/144Nd=0.51225, Nd=14 ppm
D(Sr)=2, D(Nd)=0.1
87Sr/86Sr
0.7035
0.704
0.7045
0.705
(f)
Composition of component-A:
87Sr/86Sr=0.706, Sr=400 ppm
143Nd/144Nd=0.51212, Nd=16 ppm
D(Sr)=2, D(Nd)=0.2
0.7055
0.7065

Figure: 5.17.

The same type of modelling was performed by plotting $\delta^{18}O$ versus $^{87}Sr/^{86}Sr$ and Rb/Th in Figure 5.16 and $^{143}Nd/^{144}Nd$ versus Th, U and $^{87}Sr/^{86}Sr$ in Figure 5.17. Assimilation rate in all of these diagrams is almost the same to those have found in previous diagrams.

5.3. Summary

Isotope systematics of the collision-related volcanics of the Erzurum-Kars Plateau indicate the presence of two distinctively different magma types; the high- and low-Y series. This is consistent with the findings based on trace element behaviour of these two series as presented in Chapter 3. Lavas of the high-Y series are always more radiogenic and span a wider range in their isotopic composition. Isotope-trace element systematics suggest that assimilation combined with fractional crystallisation was an important process for both series as can be expected from the thickened crust of Eastern Anatolia as a whole. Only a small number of lavas from the most basic units of the high-Y series were erupted to the surface without extensive assimilation and hence retain their mantle heterogeneity signature. Results of petrologic modelling suggest that the isotopic and trace element variations between the high- and low-Y series are not significantly dependent upon the variations in the composition of their source material. These differences appear to have been extensively controlled by the composition of crustal material which they have assimilated. The magma that gave rise to the low-Y series appears to have assimilated a lower crustal material which is isotopically similar to the granulitic xenoliths from Central Europe and Pannonian Basin in Hungary, whereas the high-Y series has predominantly been contaminated by the upper crust. Geobarometry calculations based on the composition of amphibole phenocrysts imply a much deeper fractionation history for the low-Y series (20-28 km) compared with the high-Y series (14-18 km), which is consistent with the conclusion based on the isotopic data. What these findings may indicate is that composition of lower crust beneath the Eastern Anatolia region is similar to that of Hungary and Central Europe. On the other hand, the lower crust in Eastern Anatolia seems to be more enriched in $\delta^{18}O$ than that of the Pannonian Basin and Central Europe. Alternatively, this lower crustal assimilant may be a transition zone between lower and upper crust or a zone which is complicated by thrusting and thus a mixture of the two.

Chapter 6: PETROGRAPHY

In this chapter, the petrographic properties of the volcanic units on the Erzurum-Kars Plateau will be described briefly with special reference to the petrographic differences between the low- and high-Y series. The chapter starts by describing the textural and mineralogical differences between the lavas of high- and low-Y series. The following paragraphs focus on the textures that display evidence of magmatic processes such as magma mixing and early history of fractional crystallisation.

6.1. Textural and mineralogical differences between the high- and low-Y series

Lavas of the low-Y series are generally intermediate in composition (andesite to dacite), containing predominantly plagioclase, pyroxene and occasionally amphibole. In contrast, the lavas of the high-Y series display a bimodal character, span a wide compositional range from basaltic andesite to rhyolite, lack intermediate rocks and have no amphibole phenocrysts. Basic members of the high-Y series, especially those from the plateau lava units, frequently contain olivine phenocrysts together with plagioclase and clinopyroxene while the acidic members of the high-Y series are predominantly aphyric and rarely porphyritic containing alkali feldspar and plagioclase phenocrysts.

6.1.1. Lavas of the low-Y series

Lavas of the low-Y series can be subdivided into two units on the basis of their texture and phenocryst assemblage: (1) the aphyric lavas; and (2) the amphibole-bearing porphyritic domes.

6.1.1.1. The aphyric lavas

The aphyric lavas are in general andesitic and dacitic in composition, rarely vesicular, with subordinate microcrystals and microphenocrysts of plagioclase, clino- and occasionally orthopyroxene. They widely outcrop in the Mt. Dumlu and Mt. Kargapazarı areas (the Güngörmez andesite/dacite; Section 2.1.3). Almost 90% of these lavas are composed of glassy and sometimes partly cryptocrystalline groundmass which encloses predominantly plagioclase, and rarely pyroxene microlites and microphenocrysts. They do not contain amphibole. In some lava flows, the texture changes to vitrophyric with increasing phenocryst content. The aphyric lavas also

display microlitic textures from hyaloplitic to pilotaxitic and sometimes a combination of microlitic and porphyritic textures (e.g. the Girekösek dacite, the Köşk pyroxene andesite and the Çobandede dacite). The anorthite content of plagioclase phenocrysts in these lavas varies between 40% and 65% (andesine-labradorite). As mentioned earlier in Section 4.1.1, some of these plagioclase phenocrysts are not in equilibrium with the magma, i.e. they are xenocrysts. Rare phenocrysts of clinopyroxene are represented by augite and endiopside while orthopyroxene is predominantly bronzite (Section 4.1.2.2).

Aphyric to porphyritic lavas of the low-Y series very rarely contain amphibole xenocrysts. They are either individual phenocrysts with reaction rims (Photo 6.1) displaying signs of resorption, or phenocrysts which are surrounded and hence protected by glomeroporphyritic crystal clots of other phenocrysts such as plagioclase and pyroxenes (Photo 6.2 and 6.3). Amphiboles are predominantly pargasitic. All of these amphibole xenocrysts display corona textures (sample MK90, the Güngörmez andesite/dacite in Mt. Kargapazarı) and have corroded shapes (Photo 6.1). They are mantled by clinopyroxene of non-uniform width. Similar textures are also present in amphibole-bearing porphyritic lavas of the low-Y series. This is apparent in Photos 6.4 and 6.5, where an amphibole phenocryst is surrounded by ortho- and clinopyroxene rims respectively. All these textures appear to have been resulted from incomplete

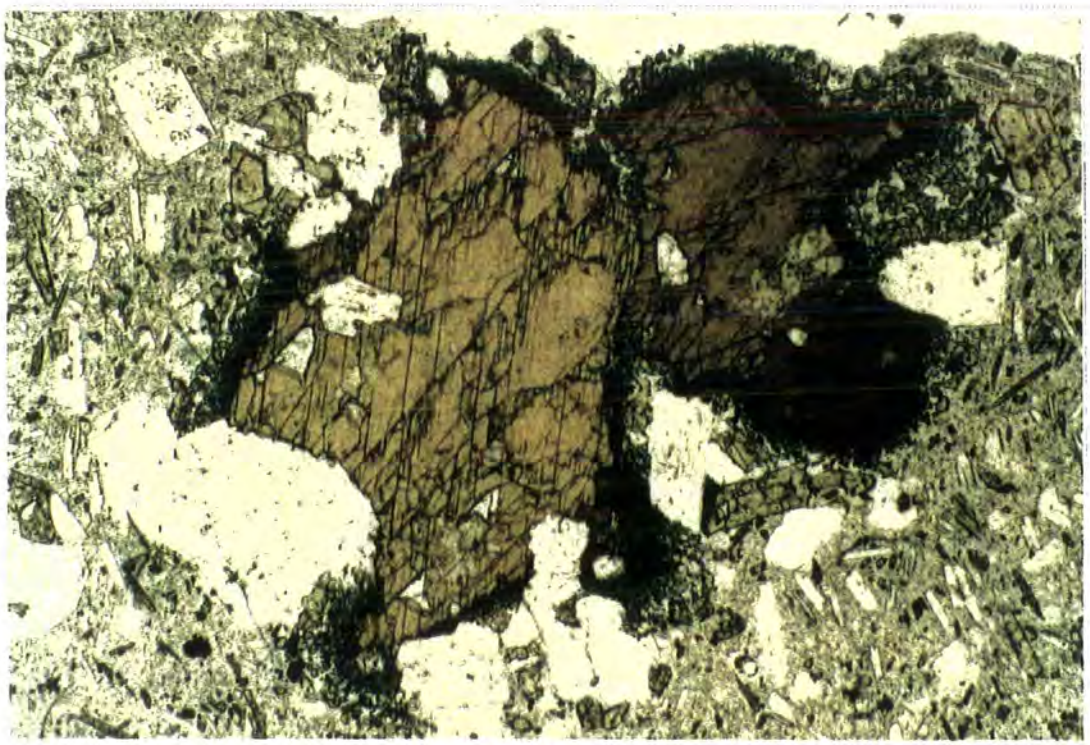

Photo: 6.1. Amphibole phenocryst in dacite with corroded shape and reaction rim composed of clinopyroxene microcrystals. Sample MK90, Mt. Kargapazarı area, Güngörmez andesite/dacite. Magnification x4, plane-polarised light (PPL).

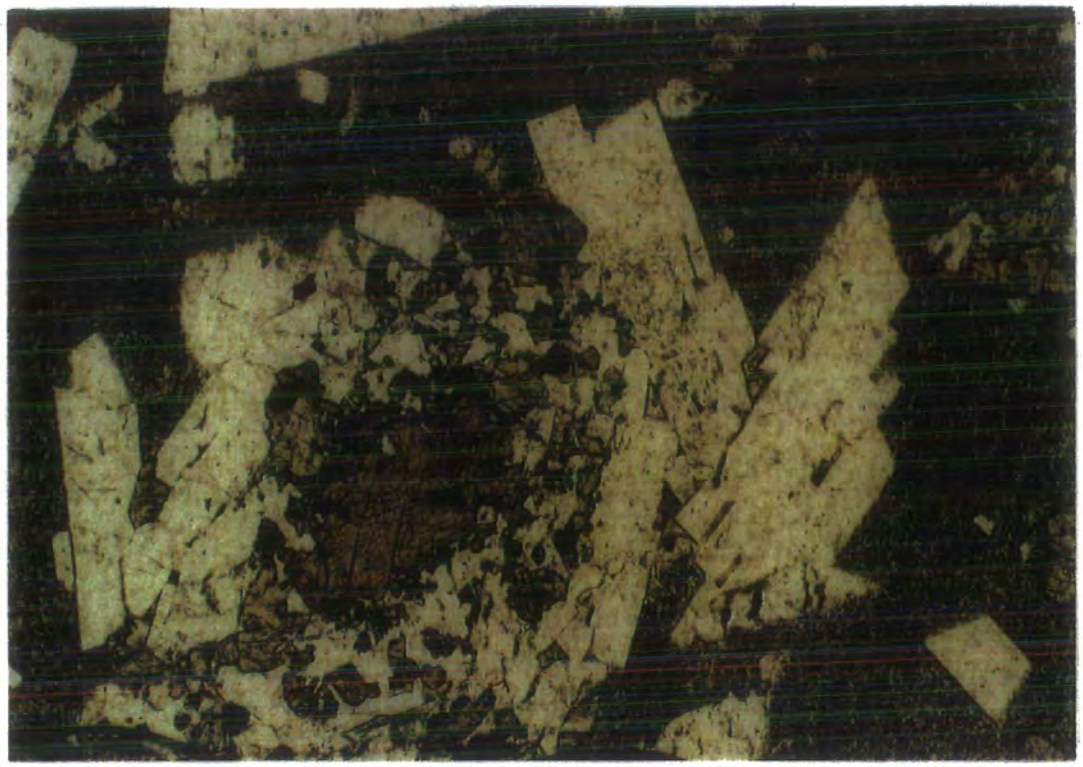

Photo: 6.2. Glomeroporphyritic dacite, sample MK90, Güngörmez andesite/dacite, Mt. Kargapazarı, close to the base of the volcanic succession. The amphibole xenocryst in the middle is surrounded by crystal clots of euhedral plagioclase and anhedral clinopyroxene. This is the only amphibole found in this unit and it is protected from resorption by its plagioclase armour. Magnification: 4x, PPL.

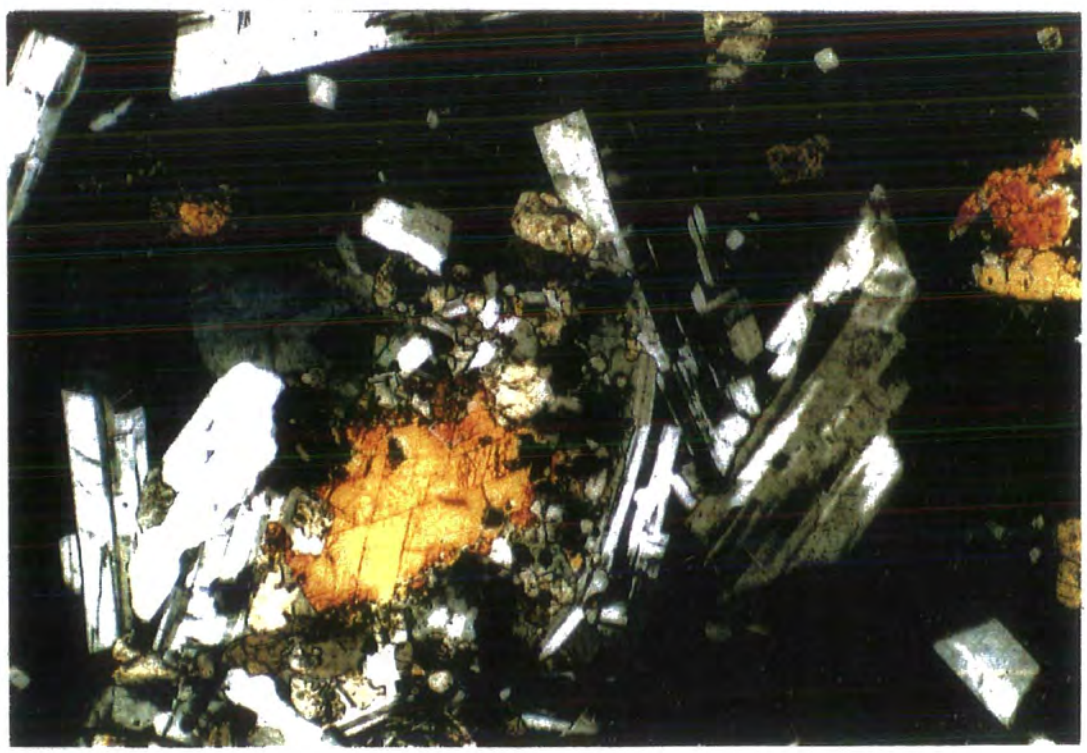

Photo: 6.3. The same view under cross-polarised light (XPL).

reaction of the inner amphibole pheno- or xenocryst with melt as a result of disequilibrium between the crystal phase and surrounding magma. This idea is also supported by geochemistry of these rocks. Trace element systematics, especially those of Y and MREE to HREEs, indicate that amphibole should have been crystallised as an early mafic phase at depth in both low- and high-Y series (Section 3.2). Experimental studies by Gill (1981), Green (1982) and Foden and Green (1992) also suggest that crystallisation at depth, in the thickened crust beneath the Erzurum-Kars plateau, should initially be amphibole-dominated. En route to the surface, almost all of these amphiboles were resorbed via decompressive incongruent melting. As a result of this reaction, they formed pyroxene-rich coronas around amphibole xenocryst if they were not completely resorbed.

6.1.1.2. Amphibole bearing porphyritic domes (andesites/dacites)

Amphibole-bearing porphyritic domes of the low-Y series, which are andesitic to dacitic in composition, are abundant in the western part of the plateau, especially around Mt. Dumlu. They are also present in the Pasinler and Horasan areas, and are almost completely absent around the Kağızman area. These lavas display a well-developed porphyritic texture with plagioclase, amphibole and orthopyroxene phenocrysts, subordinate clinopyroxene microcrystals and microphenocrysts and rare quartz phenocrysts. They sometimes show trachytic texture. All these phenocrysts are enclosed in a microlitic (intersertal or hyaloplitic) groundmass. The amphibole phenocrysts are subhedral to anhedral in shape. They seldom show textures related to resorption such as skeletal crystal shapes and reaction rims. The orthopyroxene phenocrysts, which are predominantly represented by bronzite, are characteristically lath-shaped, fresh and mostly euhedral. Clinopyroxene is in general augite in composition and makes up subordinate microcrystals and microlites in the groundmass. The plagioclase phenocrysts are typically labradorite-andesine in composition (Section 4.1.1) and most of them show oscillatory zoning. They are generally euhedral to subhedral in shape, commonly forming glomeroporphyritic texture.

The plagioclase phenocrysts often display a subparallel arrangement forming a trachytic texture. They display complex oscillatory zoning and sometimes reverse zoning patterns occasionally associated with a zonal arrangement of melt inclusions and a sieve texture. Most of them exhibit albite twinning. Some of the coarse plagioclase phenocrysts contain brownish coloured clear rhyolitic glass inclusions. These textures together with the complex zoning, resorption and corrosion patterns may be indicative of magma mixing between a rhyolitic to andesitic magma and injecting of hot basaltic magma. The presence of this magma mixing event has already been discussed in Section 4.1.1.1, hence it will not be mentioned here again.

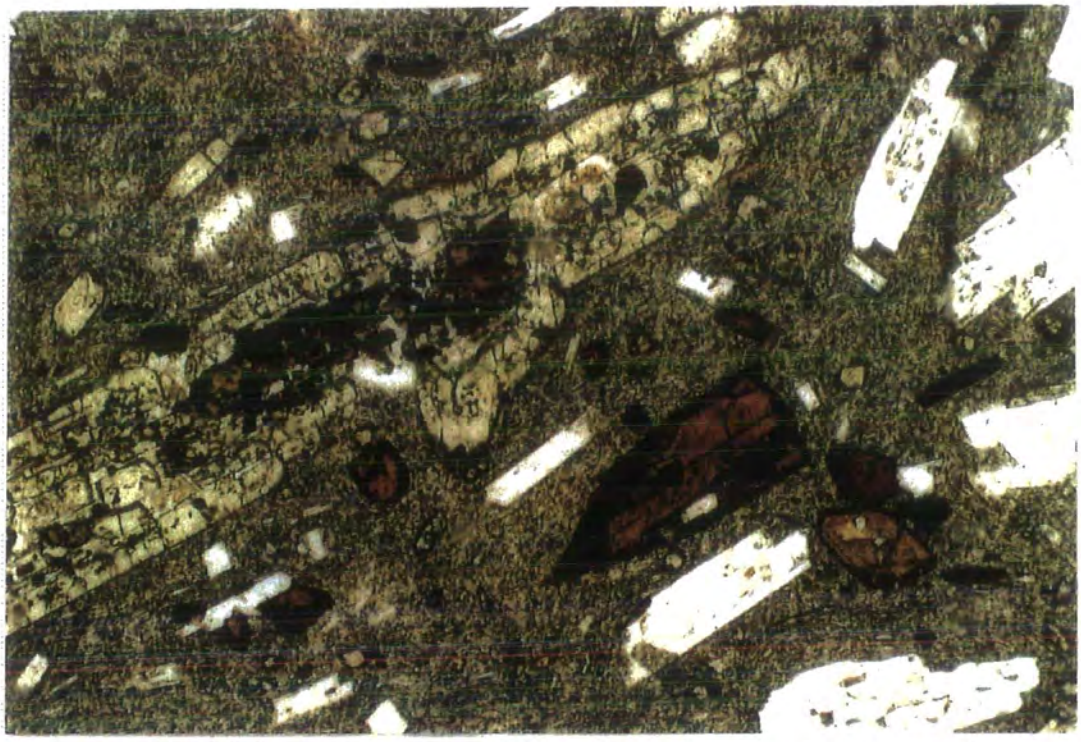

*Photo: 6.4. **Amphibole xenocryst surrounded by the reaction rims of ortho- and clinopyroxene respectively. Sample MK93, dacite, the Dumlu amphibole dacite/andesite. Magnification 4x, PPL.***

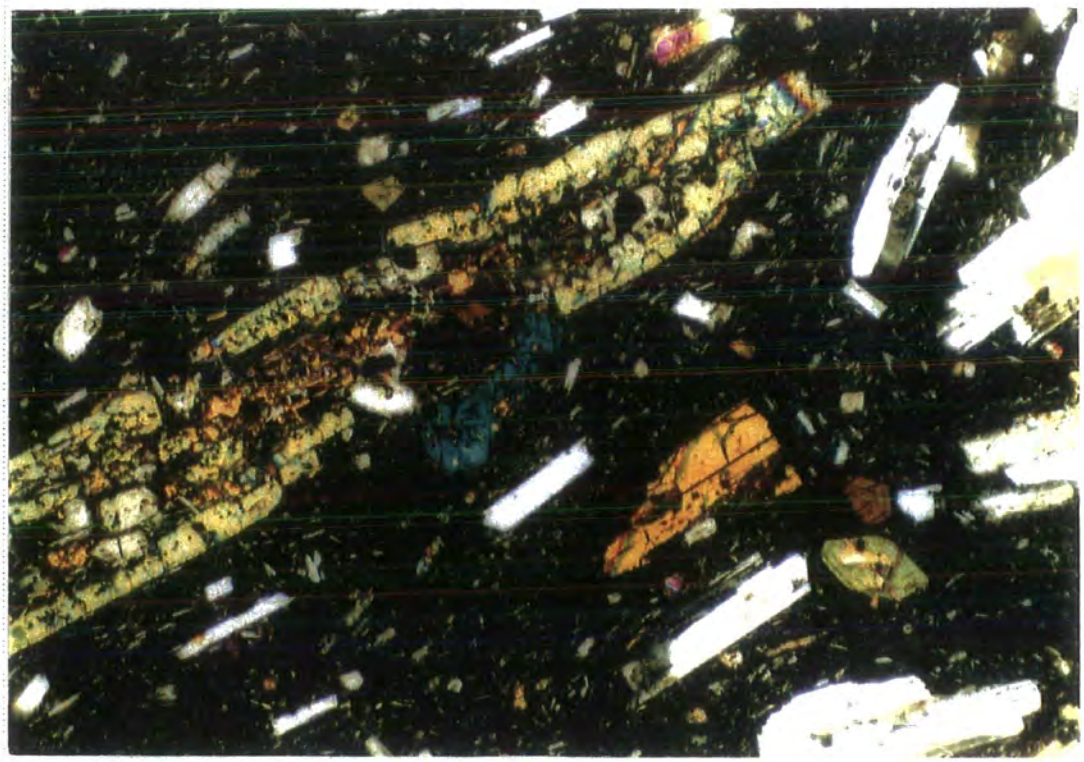

Photo: 6.5. The same view under XPL.

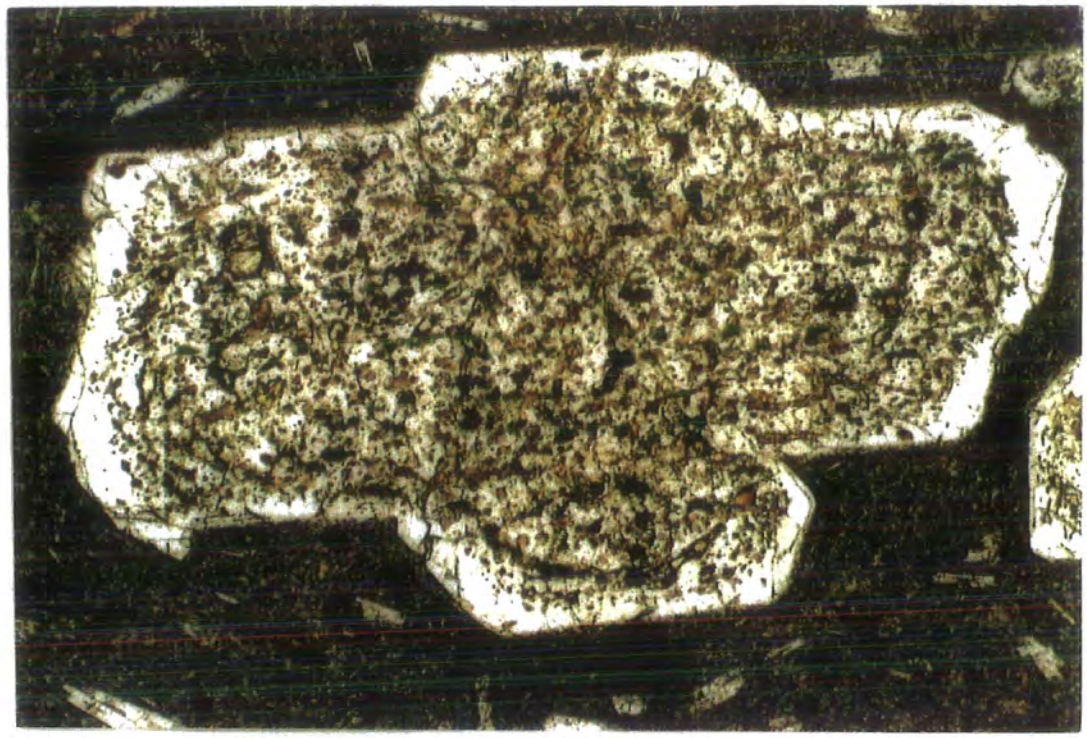

Photo: 6.6. Brownish clear glass inclusions enclosed in a plagioclase megacryst in porphyritic dacite. They partly show a zonal arrangement. Sample MK93, the Dumlu amphibole dacite/andesite unit, Mt. Dumlu. Magnification: 4x, PPL.

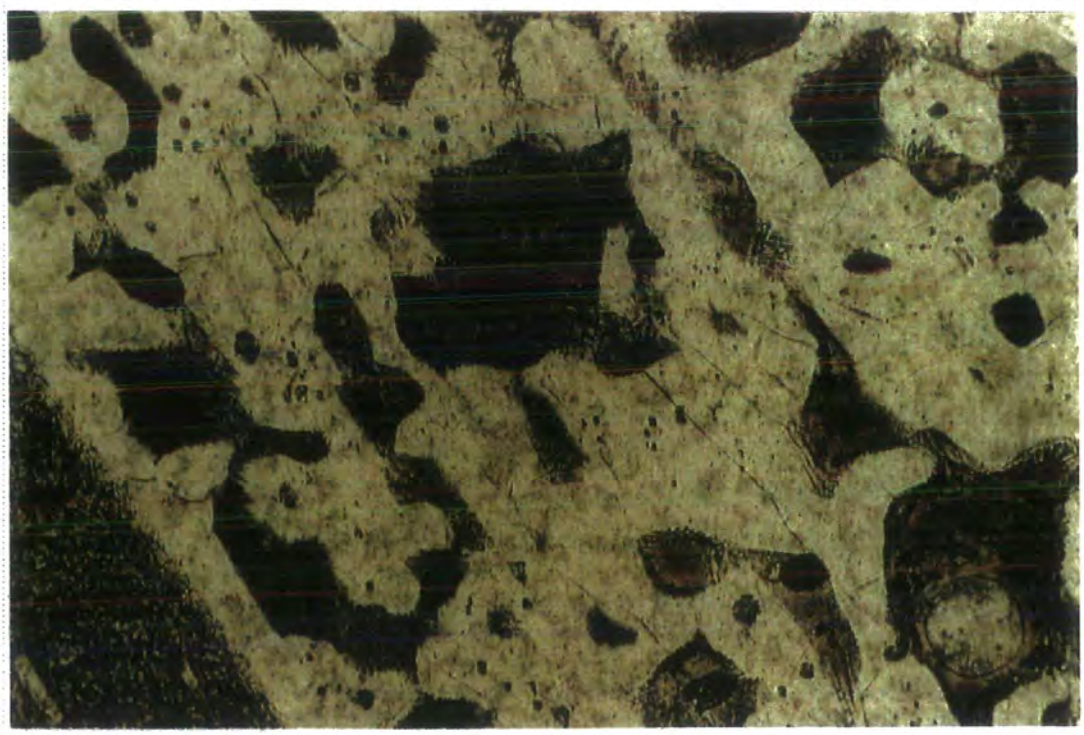

Photo: 6.7. Close-up photograph of glass inclusions in plagioclase. Sample MK21: dacite, the Güngörmez andesite and dacite, Mt. Kargapazarı. In glass inclusions, there are some dendritic crystals which formed possibly as a result of rapid solidification of acid melt, most of which became brownish glass. Magnification 10x, PPL.

6.1.2. Lavas of the high-Y series

Lavas of the high-Y series are subdivided into two main groups on the basis of their mineral content and SiO_2 concentration. These are: (1) basic to intermediate lavas; and (2) acidic domes, pyroclastic fall and flow (ignimbrite) deposits.

6.1.2.1. Basic to intermediate lavas

The basic to intermediate lavas of the high-Y series crop out as relatively thin lavas flows at almost every level of the volcanic succession from base to the top. However, they become abundant at the top of the plateau. They basically consist of plagioclase, clinopyroxene ± olivine phenocrysts all of which are enclosed in a glassy or microlitic groundmass. The plagioclase phenocrysts span a compositional range between bytownite and labradorite. They form lath-shaped or prismatic, commonly euhedral and subhedral phenocrysts and microlites in the groundmass. They are either unzoned or weakly zoned. Most of the olivine phenocrysts are chrysolite in composition with a small group (from the Güngörmez andesite/dacite) classifying as hyalosiderite from the Kargapazarı area (Section 4.1.4). Some olivine phenocrysts have iddingsitic rims formed as a result of alteration while some others display skeletal embayment textures filled with microlitic-glassy groundmass (Photo 6.8). In some plateau lavas, clustered phenocrysts of olivine, clinopyroxene an plagioclase make up cumulophyric texture (Photo 6.9).

The Karapınar basalt which is located close to the base of the volcanic sequence in the Mt. Kargapazarı area display a typical subophitic texture. This is the only unit on the plateau which shows this particular texture. In this unit, labradorite laths together with olivine microcrystals are embedded in several coarse augite crystals. None of the plagioclase laths show zoning (Photos 6.10 and 11). They all display albite twinning.

6.1.2.2. Acidic domes, pyroclastic falls and flow (ignimbrite) deposits

Pyroclastic falls and flow deposits are the most abundant volcanic products on the Erzurum-Kars Plateau. They are predominantly rhyolitic and sometimes rhyodacitic, and almost completely aphyric showing complex flow banding, accretionary lapilli and a variable degree of welding. Acidic domes are rather scarce on the plateau. They form small dome-shaped bodies at different levels on the plateau. These domes contain abundant alkali feldspar (sanidine and anorthoclase) and plagioclase phenocrysts with rare biotite and pyroxenes.

Among other ignimbrites on the plateau, the Black ignimbrite from the Pasinler area has a unique texture and field appearance. In contrast to the other pyroclastic units

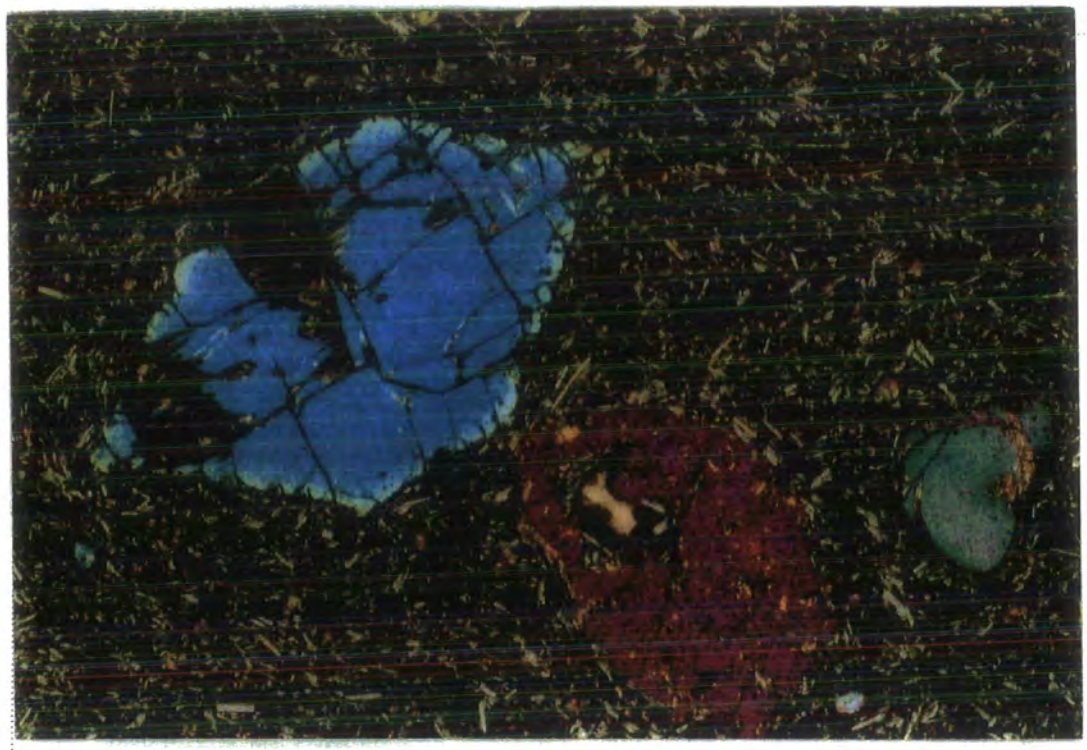

Photo: 6.8. Photograph of olivine basalt from the high-Y series, sample MK144, the Kötek basalt, base of the volcanic succession, north of Horasan. Characteristic six-sided euhedral chrysolite phenocryst, which is enclosed in a hyalopilitic to pilotaxitic groundmass, is partly corroded and contains embayments. Magnification: 4x, XPL.

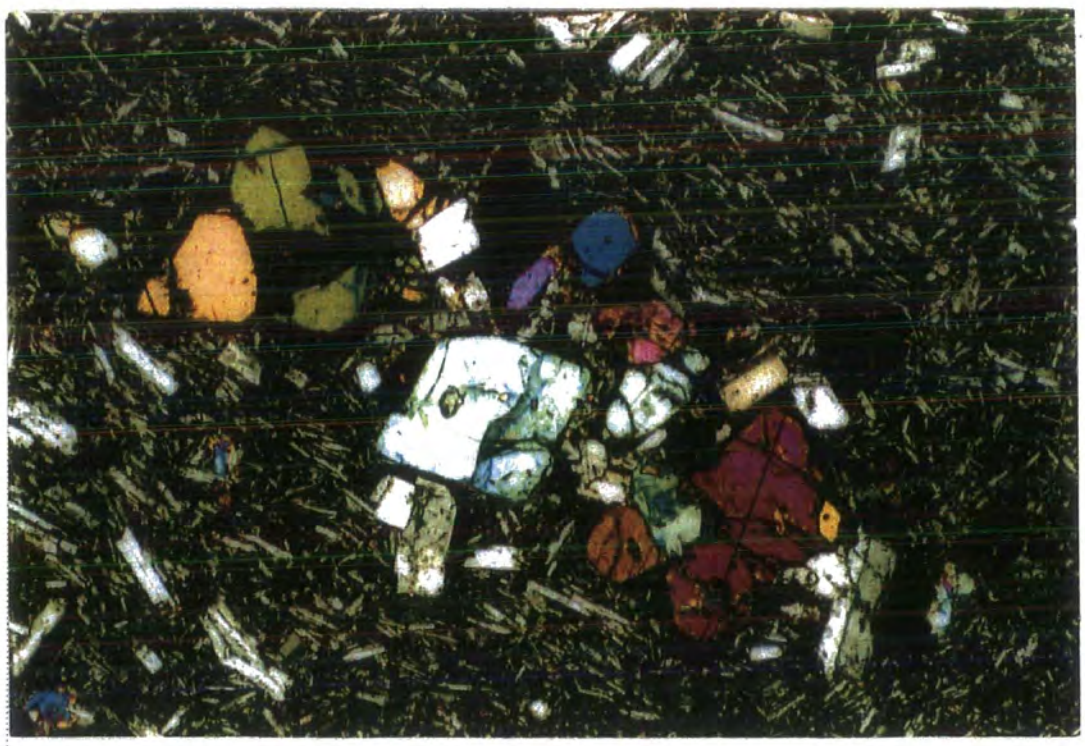

Photo: 6.9. Olivine-bearing andesite from the high-Y series, MK314, the Kargapazarı volcanics in the Pasinler area. Cumulophyric crystal cluster in the centre of the photograph is composed of olivine, plagioclase and clinopyroxene while the groundmass is made up of pilotaxitic plagioclase microlites.

Photo: 6.10. Microphotograph of the subophitic Karapmar basalt, sample MK289, base of the volcanic sequence, Mt. Kargapazarı. Magnification 4x, PPL.

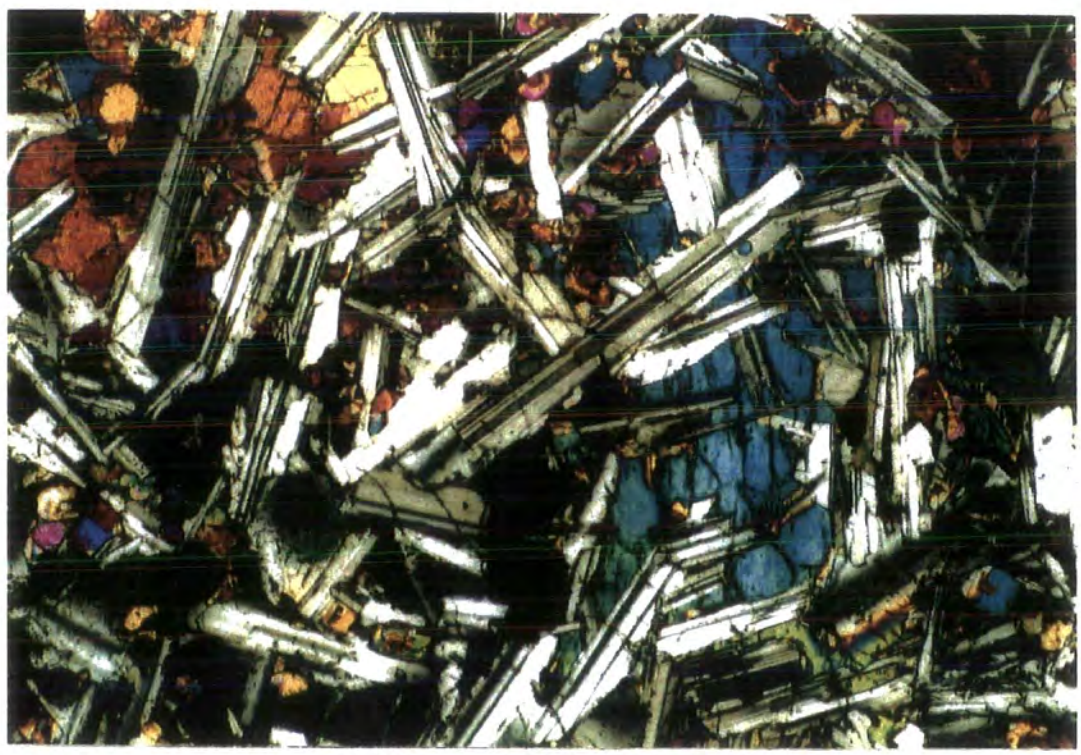

Photo: 6.11. The same photograph under cross-polarised light.

on the plateau, it contains abundant pyrogenetic crystals of plagioclase and less abundant clinopyroxene (Photos 6.12). The black ignimbrite contains abundant glass shards and fiammé. It also displays "eutaxitic texture" formed as a result of regular orientation of flattened lenticles of pumice fragments and obsidian-rich parts.

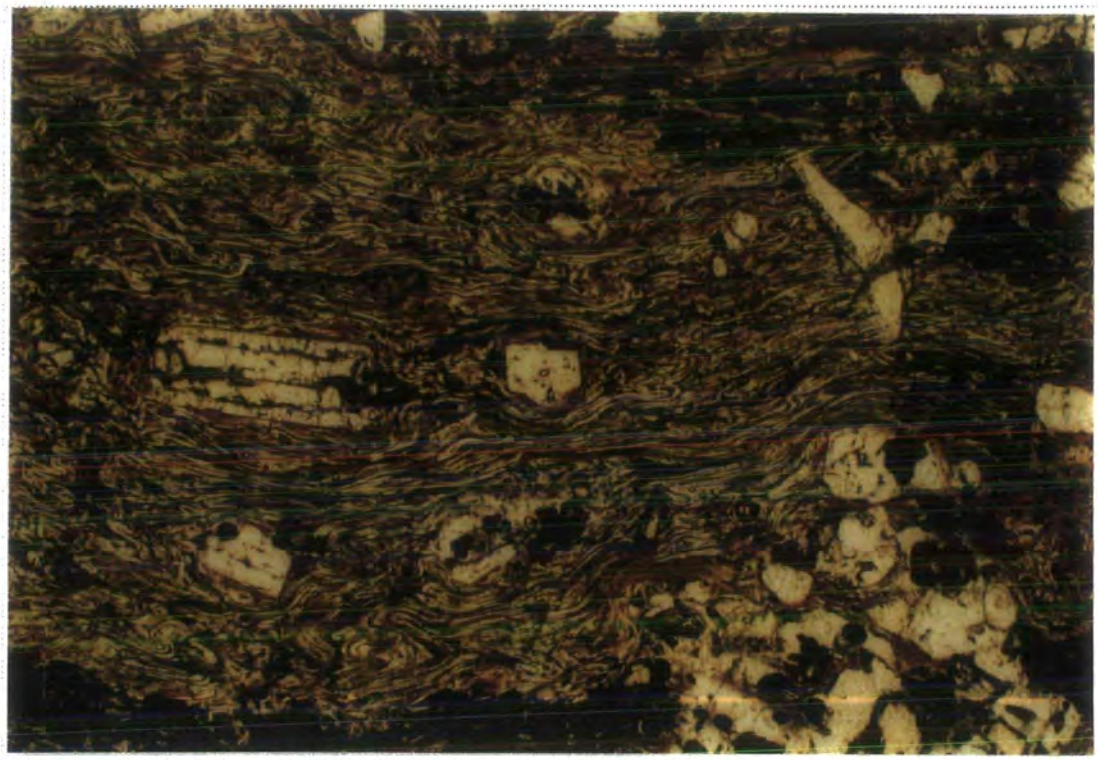

Photo: 6.12. Densely welded Black ignimbrite, sample MK359, from the Pasinler area. Discontinuous lamination is a sign of extreme compaction. Magnification 4x, PPL.

Chapter 7

CONCLUSION AND DISCUSSION

Introduction

In this chapter, a general summary of results reached in previous chapters will be presented with special reference to the plumbing system and extent of magma-crust interaction in the actively-thickening continental crust of Northeastern Anatolia.

7.1. Volcanostratigraphy

The collision related volcanics of the Erzurum-Kars Plateau cover a broad compositional range from basalts to rhyolites. The lavas forming the Erzurum-Kars Plateau chiefly originated from fissures which are believed to be genetically related to post-collisional strike-slip faults and associated localised extensions. These volcanics were formed by three types of eruption:

7.1.1. Lava sheets: these are, in general, andesitic to basaltic in composition and are composed of plateau-forming sheets flows. They are made up of two different lithologies with two different phenocryst assemblages. The first type comprises the most basic lavas on the plateau which contain plagioclase, clinopyroxene and olivine phenocrysts with subordinate orthopyroxene. This type of lava (e.g. the Horasan Plateau unit) covers large areas on the plateau and is relatively thin compared to intermediate to acidic lavas. The second type is composed of intermediate to acidic lavas which are all aphyric or microporphyritic in texture. They have a phenocryst assemblage consisting of plagioclase and two pyroxenes. This second type is the most abundant lithology especially at the base of the succession in the west around Mt. Dumlu.

There are also sporadic scoria or spatter cones on the plateau such as those located to the east of Horasan town, close to Kızıl village and in the Harabedere gorge to the north of Pasinler. The scoria (cinder) or spatter cones form small edifices on the plateau with limited aerial extent. This type of pyroclastic deposit is thought to be the product of hawaiian-strombolian eruptions created by mildly explosive eruption of a near-basaltic magma. They contain abundant scoria breccia, agglutinated lava spatter and volcanic bombs of different shapes.

7.1.2. Pyroclastic deposits: these are made up mainly of pyroclastic flow units and fall deposits. These are the most abundant lithology in the volcanic pile on the central and eastern part of the plateau, especially between the Pasinler and Horasan areas. The pyroclastic fall deposits are the product of plinian type eruptions and composed mainly of pumice-fall deposits. The pyroclastic flows are mainly represented by ignimbrites. They cover the plateau with great lateral extension and variable thickness. The thickness of individual flows reaches up to 100-150 m in places. Most ignimbrites are composed almost completely of volcanic glass and are very poor in phenocryst content. The most common phenocrysts in these units are plagioclase, sanidine and rarely biotite. In some flows, they contain well-developed accretionary lapilli and flow folds. They are often densely vesiculated with abundant accretionary lapilli and, in some zones, changed into perlite. This indicates that they were saturated by volatiles when they erupted. In contrast, the Black ignimbrite in the Pasinler area is exceptionally rich in its phenocryst content. The phenocrysts of this unit are made up predominantly of plagioclase and very rare pyroxene. The Black ignimbrite also contains rare microcrystals of zircon.

7.1.3. Domes: these are represented mainly by two types of lithologies: the amphibole-bearing porphyritic intermediate to acidic lavas (e.g. the Dumlu amphibole dacite/andesite) and the sanidine-bearing acidic lavas. The amphibole-bearing porphyritic domes are abundant in the western and central parts of the plateau, especially in the Mt. Dumlu area, whereas the sanidine-bearing domes dominate the central and eastern part of the Plateau.

There are also some dykes of the Erzurum-Kars Plateau which cut the basement formations and plateau volcanics. They are very rare in the region because most of them are covered by extensive pyroclastic deposits and lavas. They observed in two areas on the plateau: the Büyükdere gorge to the NW of Pasinler and Besikom and Haydarkomları villages in the south of Horasan. Among these, the one located to the south of Horasan has a average thickness of 10-15 m and a length of 6-7 km. All these dykes are either perpendicular or slightly oblique to the direction of compression with approximately E-W strikes. The position of these dykes are thought to have been controlled by localised extension in strike-slip fault zones.

The volcanic units of the plateau can be subdivided into eight series based on their stratigraphic position on the plateau (as also presented in Table 2.1). From the top of the succession (group-8) to the base (group-1) these are:

8. acidic domes and cones on the plateau (e.g. the Odalar rhyolite in Aladağ area)
7. olivine bearing plateau layer (e.g. the Horasan plateau unit)
6. plateau lavas without olivine (the Aladağ andesite)

5. amphibole-bearing porphyritic lavas (e.g. the Dumlu amphibole dacite/andesite)
4. basal intermediate to acidic lavas (the Güngörmez andesite/dacite)
3. black ignimbrite (Pasinler area)
2. pyroclastic basal layer (e.g. the White ignimbrite in Pasinler and Horasan)
1. basal basic lava layer (e.g. the Karapınar basalt in Mt. Kargapazarı)

In the west, around Mt. Dumlu and Mt. Kargapazarı, intermediate to acid lavas make up almost all the volcanic column. Towards the east of the plateau, pyroclastic deposits become abundant and in some places they comprise 40-60 volume % of the succession.

The volcanic succession attains its maximum thickness of about 1000 m in the vicinity of Mt. Dumlu, north of Erzurum and this thickness decreases considerably towards the east.

7.2. Tectonic

The most important structural elements of the Erzurum-Kars Plateau are the strike-slip faults. The palaeotectonic structures such as thrusts and imbrication zones are extensively covered by the volcanic units of the plateau. The strike-slip faults form two major fault zones: the Erzurum-Tbilisi fault zone located between the Mt. Dumlu and Mt. Kargapazarı areas and the Çobandede fault zone in the north of Horasan. There are also numerous individual strike-slip faults on the plateau such as Kağızman fault in the east of Horasan. A part of the Erzurum-Tbilisi strike-slip fault zone has been mapped in this study and presented in Figure 2.10.

The Erzurum-Tbilisi fault zone is composed of several branches of left-lateral strike-slip faults with NNE strikes (Section 2.1). In addition to strike-slip movement these faults display significant normal movement, which complicates the stratigraphic relationships in the volcanic succession. The width of the fault zone is around 20 km. The border between the Karasu basin (also named Erzurum Plain) and the surrounding mountains (Mt. Kargapazarı in the east, Mt. Dumlu in the west and Palandöken mountain chain in the south) is controlled by the sets of strike slip faults.

The Çobandede strike-slip zone consists of left-lateral (named by Koçyiğit, 1985) strike-slip faults and extends between the town of Tekman in the southwest and Çıldır in the northeast. Although left-lateral movement is dominant, there are also some right-lateral, strike-slip conjugate fault-sets present. They also show normal movement; in general, the northwestern blocks of these faults are the upthrown blocks. The Çobandede fault zone runs parallel to the Erzurum-Tbilisi strike-slip fault zone. This may imply that both the Çobandede and the Erzurum-Tbilisi strike-slip fault zones are

the parts of the same tectonic system which is most probably controlled by the strain distribution in the thickening lithosphere by the compressional regime which created the westward tectonic escape of the Central Anatolian block via the East and North Anatolian Transform faults.

The strike-slip faults strongly control the geomorphology of the plateau. For example, the Kargapazarı plateau is bounded by two of these faults: the Kargapazarı fault in the NE and the Karakale-Pertek fault in the SE (Figure 2.10). The plateau tilted to the SE because of the combined effects of normal and lateral movements on these faults. This observation shows that strike-slip faulting has been operational after the formation of volcanics on the plateau.

As in the Karasu basin, the north and south edges of the Pasinler basin are controlled by strike-slip faults (Figure 2.19). The western border of this basin with the Palandöken mountains is also marked by one of these faults. Stratigraphic data obtained from the drill-well logs of the Turkish Petroleum Company (TPAO) (Gedik, 1978) indicates that the thickness of the Erzurum-Kars Plateau volcanics reaches a massive 1250 m close to the middle of the basin with the lithologies dominated by rhyolitic tuff, ignimbrite, obsidian and andesitic lavas (Figure 1.2). On the Pasinler plateau, only a few kilometres away from the location of this drill-well, this thickness decreases considerably down to around 200-350 m. In addition, the lavas and pyroclastic units of the Pasinler Plateau dip southward (~20-30º) as a monoclinal flexure in the north edge of the basin (Photo 2.7). The hinge line of this monoclinal flexure is continuous throughout the southern margin of the Pasinler Plateau with an approximate W-E strike. What these observations suggest is that this depression may have been formed and actively controlled by the strike-slip faults that created a localised extensional system, in other words a pull-apart system. The tectonic activity that gave rise to the formation of this system should have been active throughout the evolution of collision-related volcanic activity on the plateau while the Pasinler basin continuously subsided to form a depression in which pyroclastic units and lavas accumulated. The formation of monoclinal flexure appears to have been controlled also by this subsidence. The Karasu basin in the west seems to have evolved in a similar way to the Pasinler basin. In a narrow zone adjacent to the plain, the volcanic succession of Mt. Kargapazarı area dips to the west towards the basin.

Another striking observation is the parallelism of dykes to the strike-slip faults and also to the main directions of localised extensions created by these faults. The dykes of the Kargapazarı volcanics in the Büyükdere gorge in the NE of Pasinler have strikes of about E-W which are parallel to the hinge line of monoclinal flexure and to

the presumed extensional basin created by the pull-apart system. These dykes are also very close to the hinge line.

7.3. K-Ar dating results

Eighteen K-Ar age determinations were carried out on some key samples at the University of Newcastle on whole rock samples as given in Appendix A. K-Ar dating of these samples indicates the oldest rocks to be about 11 Ma, the youngest about 2.5 Ma (Figure 7.1). The oldest lavas (11.1±0.5 Ma) on the plateau belong to the Kötek basalt in the north of Horasan (Section 2.4.1.2.1) and appear to have erupted immediately after the start of major regional uplift at around 11.8 Ma ago. This is one of the oldest ages obtained from the collision related volcanics in Eastern Anatolia, much older than 8 Ma which has been previously proposed by Pearce et al. (1990). This may significantly change our idea on the timing of the start of volcanism in the region. If the reason for this early plateau volcanism had been the delamination of the

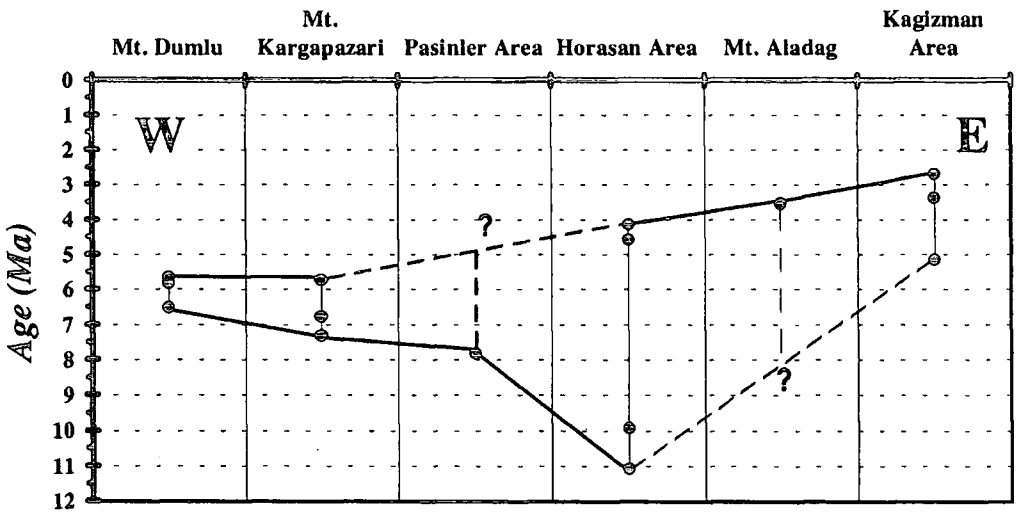

Figure: 7.1. Graph showing K-Ar ages of different parts of the plateau. For more detailed stratigraphic relationship in each section see Figure 5.1.

thickened lithosphere, than delamination could have occurred as early as 11 Ma, almost contemporarily with the regional uplift of Eastern Anatolia. On the other hand, this early volcanism is seen only in the Horasan area on the plateau. Therefore, it can be argued that this early volcanism was a local event controlled probably by localised extension of the crust.

The uplift created a fundamental palaeogeographic, sedimentologic and tectonic change all over Eastern Anatolia. Throughout the region, Serravalian shallow marine (littoral/neritic) sediments gave way to terrestrial sediments patchily deposited in a

wooded, seasonal savannah environment (Dewey et al., 1986). The uplift is documented by the deep dissection of the Miocene-Pliocene erosion surface and the infilling of the resulting valleys by Pliocene lava flows (Şengör and Kidd, 1979; Erinç, 1953). Tanoğlu (1947) and Erinç (1953) argued that the surprising uniformity of timing of uplift and of the elevations attained by the erosion surface is indicative of a block uplift of the entire region rather than a progressive wave of uplift.

England and Houseman (1988) pointed out that if delamination is a catastrophic event, the TBL will be replaced rapidly resulting in a rapid increase in surface elevation. On the basis of new K-Ar dating, it can be argued that delamination is more likely to have been a catastrophic event, as initiation of volcanism on the plateau and the rapid block uplift of the region appear to have occurred simultaneously all over the region. Geochemical and petrographic studies alone are not sufficient to explain presence, timing and nature of such a major, regional tectonic event, so further geophysical and geomorphologic research of the uplift history of the region coupled with the geochemical study is needed to resolve this problem. As seen in Figure 7.1 the Erzurum-Kars Plateau volcanics get younger towards the east (for comparison with the stratigraphic columns see Figure 5.1).

7.4. Results of trace element and isotope systematics

7.4.1. Geochemical characteristics of the volcanism and classification of volcanic units using trace elements

All volcanic units forming the Erzurum-Kars plateau are calc-alkaline in character and show a distinctive subduction signature represented by selective enrichment of the LIL elements (Sr, K, Rb, Ba and Th) and the LREEs (La, Ce and Nd). According to Pearce et al. (1990), this subduction signature is either inherited from pre-collision subduction event which took place during the Upper Cretaceous and Eocene times or can be created by crustal contamination. Another possibility, perhaps a more realistic one, is that both of these processes were operational since there are strong evidence for the assimilation of crust in the evolution of volcanics on the plateau (Chapter 5). The presence of this subduction component is well illustrated on the multi-element patterns (Figure 3.30) and also in Th/Yb versus Ta/Yb bivariate diagram (Figure 3.31) where lavas of the Erzurum-Kars Plateau display a consistent displacement from the mantle metasomatism trend towards higher Th/Yb values.

The behaviour of Y and MREEs and partly HREEs indicate the presence of two distinctly different magma series on the plateau which have experienced two different fractionation histories, one hydrous the other anhydrous (Sections 3.2 and 3.3). The isotopic ratios of these lavas also confirm the presence of these two series. The

difference between these series is best illustrated by their Y content. Therefore, in this study, the lavas forming the Erzurum-Kars Plateau have been divided into two main series, the high-Y and the low-Y series.

7.4.1.1. The low-Y series: the lavas forming this series are unimodal in character and have Y concentrations lower than 20 ppm. They dominate the middle (between 7.5 and 5 Ma) stage of the volcanic activity on the western part of the plateau, probably coinciding with the most intensive period of crustal thickening. Trace element systematics, especially those of Y and MREE to HREEs, indicate that amphibole should have been the dominant mafic phase throughout the fractional crystallisation of this series (Section 3.2). Nb, Ce and La display similar behaviour to that of Y also supporting this idea. The low-Y series is slightly enriched in Sr and depleted in Y, Zr, Th and very slightly in Rb relative to the high-Y series. The low-Y series is composed of two main units: the amphibole-bearing porphyritic lavas and the aphyric lavas.

The amphibole-bearing porphyritic lavas are made up of plagioclase, amphibole and orthopyroxene phenocrysts with subordinate clinopyroxene microlites and microcrystals. They basically form domes on the plateau and are the equivalent of group-5 lavas of the stratigraphic classification. The amphibole-bearing porphyritic lavas are, in general, widespread in the west around Mt. Dumlu, whereas they make up relatively small isolated domes in the Pasinler and Horasan areas to the east. They are almost completely absent in the Kağızman area.

The aphyric lavas consist of plagioclase and two pyroxene microphenocrysts and phenocrysts in a glassy groundmass with variable microlite content. They do not contain amphibole apart from very rare xenocrysts or phenocrysts preserved in glomeroporphyritic phenocryst clusters. Most of these xenocrysts have reaction rims which are mainly represented by ortho- and clinopyroxenes.

7.4.1.2. The high-Y series: lavas of the high-Y series have Y concentrations greater than 20 ppm. They are characterised by a distinct bimodal volcanism (from basalt to rhyolite) in contrast to the low-Y series that comprises an unimodal andesitic volcanism. Trace element characteristics of this series indicate a crystallisation story dominated by anhydrous phases (POAM) including plagioclase, two pyroxenes and rarely olivine. On the basis of their silica content, the high-Y series can be subdivided into two series: basic to intermediate lavas; and acid lavas and ignimbrites.

Basic to intermediate lavas are made up of plagioclase, olivine and clinopyroxene phenocrysts. Even though they are present in every level of the succession as relatively thin flows with variable lateral extension, they become dominant towards the top of the succession forming the erosion-resistant plateau layer especially from Horasan to the east. The Kargapazarı volcanics in Mt. Kargapazarı, the Horasan plateau unit in the

north of Horasan and Kars plateau unit in the north of the Kağızman are of this type. The most distinctive property of these units is that they contain olivine microphenocrysts and phenocrysts. The only exception is the Aladağ andesite which was produced by the central eruptions of Mt. Aladağ volcano. The Aladağ andesite is very similar to the aphyric lavas of the low-Y series in terms of its texture and phenocryst composition, but it is a member of the high-Y series. It does not contain olivine and consists only of plagioclase and two pyroxenes.

Acid lavas and ignimbrites of the high-Y series, which classify as rhyolite, and rarely rhyodacite, with high-silica contents between 73 and 77 SiO_2, are the most abundant volcanic products on the plateau. Acid lavas make up numerous small domes (e.g. the Ardıçlıdağ rhyolite in the Pasinler area and the Saçdağ dacite in the south of Horasan) whereas ignimbrites comprise extensive sheets (e.g. the Black, white and grey ignimbrites in the Pasinler area). Both acid lavas and ignimbrites show a very mild alkaline affinity and classify as alkali-calcic according to Peacock's (1931) scheme.

The isotopic ratios of these two series also show significant differences; the high-Y lavas are always more radiogenic.

7.4.2. The petrologic model for collision related volcanics of the Erzurum-Kars Plateau: magma generation, fractionation and assimilation history

In the following paragraphs, the magmatic evolution of the high- and low-Y series will be described after presenting a short summary of the model for magma genesis, suggested by Pearce et al. (1990), deep in the subcontinental lithosphere in Eastern Anatolia.

7.4.2.1. Model for magma generation

A model for magma genesis in Eastern Anatolia collision zone has been constructed by Pearce et al. (1990) by taking the dry asthenosphere solidus from McKenzie and Bickle (1988) and the solidi for the peridotite-H_2O-CO_2 system from Wyllie (1987). The thickness of rigid, mechanical boundary layer (MBL) was taken around 110 km while that of thermal boundary layer (TBL) was assumed to be 150 km. The geothermal gradient of the mechanical boundary layer has been assumed to be linear and about 9°C km^{-1}. Pearce et al. (1990) presumed the MBL to have been metasomatised by small melt fractions migrating from the asthenosphere to the lithospheric mantle. Based on consideration of mineral stability, they suggested that metasomatised MBL should have been mineralogically zoned from hornblende (garnet

or spinel) lherzolite at shallow depths through hornblende dolomite (garnet, phlogopite) lherzolite to carbonate, garnet, phlogopite lherzolite at the base. They used a simple case of instantaneous homogeneous thickening of the mantle lithosphere by 50% which was deduced from apparent thickness of the region (Figure 7.2). Thickening of the mantle lithosphere by 50% means 50% increase in the thickness of the metasomatised layer and depression of this layer below the amphibole breakdown curve (G point in Figure 7.2). When amphibole breaks down as a result of this perturbation, it changes into garnet and releases water. The water released can react with the wall-rocks to form phlogopite or it can initiate melting.

Pearce et al. (1990) suggested that delamination of TBL would have been a much more effective mechanism for the melting of thickened lithosphere. Thickened TBL is theoretically colder and hence denser than its surroundings. Therefore, it can be partly or completely replaced by asthenosphere by means of delamination and delaminated lower part is foundered into the underlying asthenosphere. In Figure 7.2 the proposed delamination model has been illustrated as a block diagram together with Pearce et al.'s (1990) P-T diagram.

The original concept of delamination was developed by Bird (1978, 1979), Bird and Baumgardner (1981) and Houseman et al. (1981). Recent geophysical research undertaken on active and fossil collision zones strengthened that the lithospheric delamination is both a common and fundamentally important component of collision orogeny (Nelson, 1992). Delamination of a part of lithosphere causes asthenosphere to rise close to the metasomatised lithosphere, resulting in extensive partial melting of this zone. Pearce et al. (1990) argued that this process could have also been accompanied by tectonic mechanisms such as formation of pull-apart basins controlled by strike-slip faults in Eastern Anatolia (Figure 7.2). The geochemical and tectonic data obtained in this study agrees with Pearce et al.'s (1990) proposed model.

7.4.2.2. Fractionation and assimilation history of the volcanics

Trace element systematics indicate the presence of a polybaric crystallisation in the magmatic evolution of the Erzurum-Kars Plateau volcanics. As mentioned above, trace element data suggest two distinctive fractional crystallisation histories: an amphibole dominated crystallisation for the low-Y series and anhydrous crystallisation assemblage (plagioclase, two pyroxene and olivine) for the high-Y series. On the other hand, there is strong evidence of amphibole fractionation for both series at an early stage of crystallisation at depth (Section 3.2).

Figure: 7.2. Block and P-T diagrams showing tectonic elements and conditions of magma generation across Eastern Anatolia.

MBL: mechanical boundary layer
TBL: thermal boundary layer
NATF: the North Anatolian Transform Fault
SATF: the South Anatolian Transform Fault

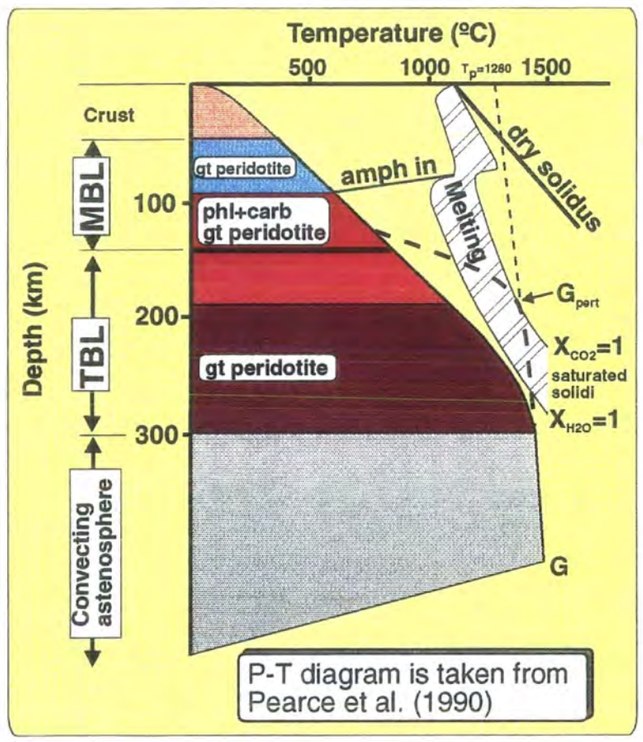

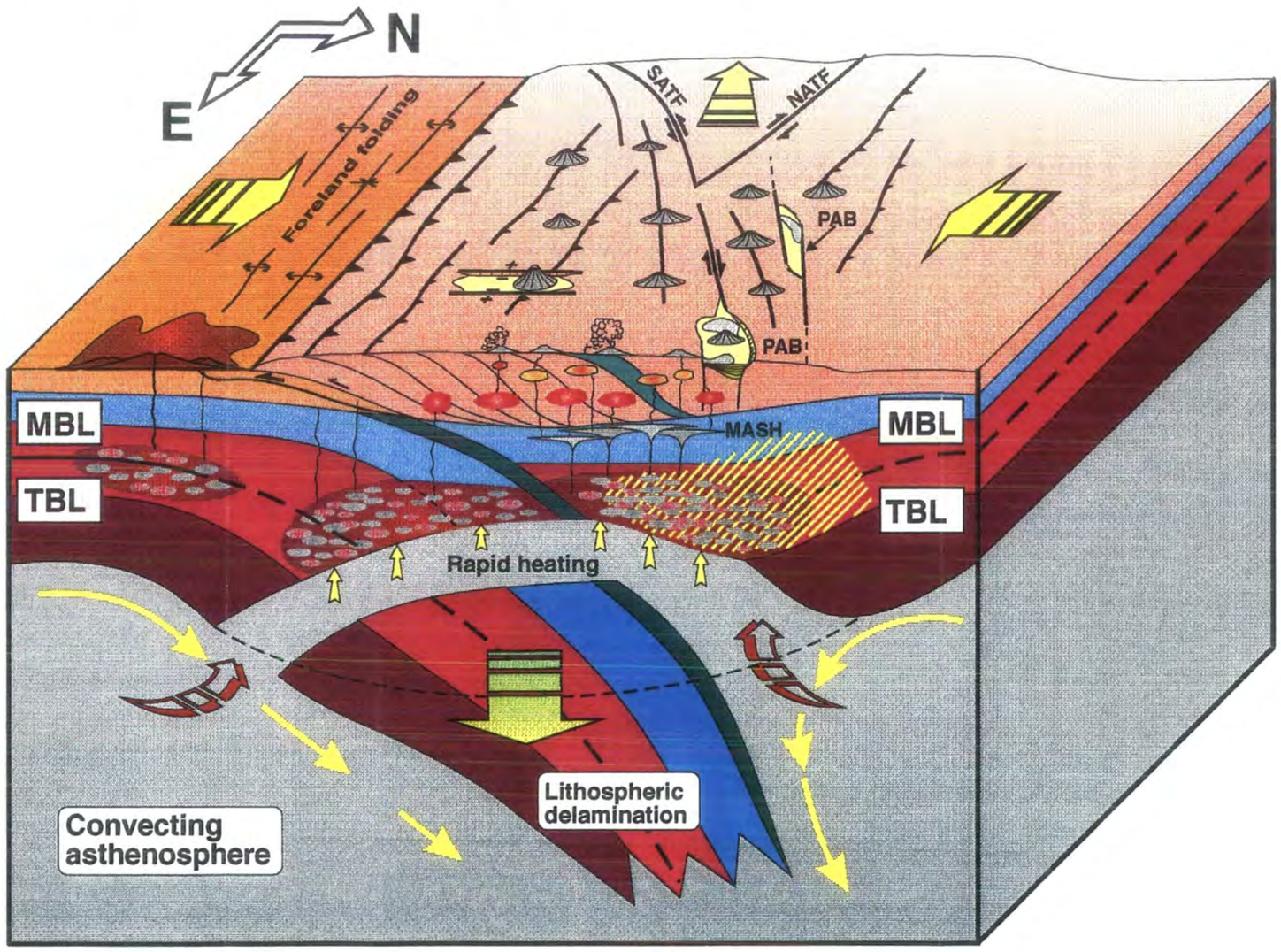

EXPLANATIONS

- Volcanoes
- Thrusts
- Strike-slip faults
- Crustal magma chambers
- Continental crust of Arabian foreland
- Thickened continental crust of Eastern Anatolia
- Cretaceous -Eocene ophiolitic suture
- Eclogitic oceanic crust
- MBL: Garnet peridotite
- MBL: Metasomatised lithosphere Phlogopite, carbonate, garnet peridotite
- TBL: LIL element enriched lithosphere due to metasomatism created by Ctetaceous Eocene arc volcanism.
- TBL: Partial melting zone in metasomatised sub-continental lithosphere
- Garnet peridotite
- Convecting astenosphere

Experimental studies carried out by Gill (1981) and Green (1982) showed that amphibole is a liquidus phase in basaltic to basaltic-andesitic magmas under near water-saturated conditions (>10% H_2O) between depths of 25 and 80 km (under 8-25 kbar pressure). As originally proposed by Lambert et al. (1974) for Mt. Ararat, Pearce et al. (1990) argued that, within the thickened Eastern Anatolian crust at around 25-40 km, crystallisation should initially be amphibole-dominated with subordinate aluminous pyroxenes and magnetite. In shallower depth, the same magma would crystallise two pyroxenes and plagioclase. Since amphibole is not in equilibrium with the magma under shallower conditions, entrained amphibole phenocrysts would be resorbed (Pearce et al., 1990).

In a more recent experimental study, Foden and Green (1992) examined the stability fields of amphibole in the system high-Al basalt-water at pressures from 1 atm to 10 kbar. They summarised their experimental results in the form of a phase diagram for the high-Al basalt system with 5% H_2O. This diagram, which shows possible cooling/ascent paths and the crystallisation products at each stage, is presented in Figure 7.3 together with the cartoon of the proposed petrologic model which displays the general framework of plumbing system in thickened continental crust beneath the Erzurum-Kars Plateau. The depth of proposed magma chambers for the low- and high-Y series have been approximated from the Al-in-hornblende barometer previously calculated in Section 4.2.2.1 assuming that average density of the crust to be around 2700 kgm^{-3}. Since the thickness of upper crust beneath Eastern Anatolia is not well known, it is assumed to be about 25 km, a value close to that of Central Alps (Brown and Musset, 1989), which is also a modern continent-continent convergence zone. Although there is no sufficient information about the total thickness of the crust, it can still be approximated from the average altitude of the plateau (2 km) as about 50-52 km, assuming approximate isostathic balance (Canıtez and Toksöz, 1980; Dewey et al, 1987). The figure is divided roughly into four zones (I to IV) each of which may correspond to one of the unique petrologic domains which displays different type of magma chambers having different compositions, sizes, crystallisation assemblages and wall-rock compositions.

7.4.2.2.1. Zone I: a probable MASH zone

Hildreth and Moorbath (1988) suggested that there is a zone of extensive melting, assimilation, storage and homogenisation (MASH) beneath each large magmatic centre in the Andes. There are some similarities between the Andes and the collision volcanics in Eastern Anatolia such as both of them are calc-alkaline, composed of the same rock types under the influence of AFC and have thick

continental crusts. This zone is located, in general, in the lowermost crust or mantle-crust transition. The magmas reaching to this zone induce local melting, assimilate the wall-rocks and mix with each other. It is also a zone where fractionation takes place before re-establishment of buoyant ascent of these magmas. This fractionation has a critical importance in the establishment of the magma plumbing system, without which the magma would not rise to or near the surface in a situation of perfect gravitational equilibrium as pointed out by Fyfe (1992). According to Hildreth and Moorbath (1988), magmas ascending from such zones all have a base-level isotopic and trace element signature characteristic of that particular MASH domain. They believe in that the MASH process is not simple contamination of basalt but true magma generation in the lower crust or uppermost part of the mantle.

In the actively thickening lithosphere of the Erzurum-Kars Plateau, a MASH zone is assumed to be present. If this it is true, then the base-level isotopic composition of this zone should be similar to that of starting point of AFC arrays (the most primitive end-member: MK130 or 139) presented in Section 5.2.3. Only a small number of samples from the base of the EKPV (MK289: the Karapınar basalt in Mt. Kargapazarı and MK144: Kötek basalt in the north of Horasan) and from the top of the succession in Horasan area (MK139: the Horasan plateau unit), which show very little or no sign of crustal assimilation, may represent the magmas derived from this zone (Figure 5.3, trend III, p. 268). Therefore, there are only very limited data available for the nature and composition of such a zone beneath the plateau. It seems that the proposed MASH zone was not located in the lower crust, because the Pb isotopic ratios of the high-Y series do not show any indication of assimilation of lower crust even though both of the high- and low-Y series may have evolved from the same parental magma. Therefore, the zone appears to have been located in the uppermost part of the mantle, perhaps somewhere close to Moho. Since lavas forming the plateau were derived from the subcontinental lithosphere, possible melting, assimilation and magma mixing events in the MASH zone located also in the subcontinental lithosphere could not create a definable imprint in the isotopic and trace element compositions of these lavas no mater how extensive the contribution of these processes were. In other words, there was probably no contrast between the composition of magma and wall-rocks in terms of their isotopic ratios. The MASH zone was probably the place where the early crystallisation of amphibole took place. This amphibole fractionation should have differentiated the basic melts and performed the function of re-establishing buoyant ascent of magma to form magma chambers higher in the crust having variable depths, sizes and fractionation assemblages.

Based on their experimental studies, Foden and Green (1992) showed that plagioclase is the anhydrous liquidus phase between 1 atm. and 10 kbar but in the

hydrous environment this role is taken by olivine at <7 kbar and then by clinopyroxene at higher pressures. They maintain that, under these conditions, amphibole crystallises only during the closed-system equilibrium crystallisation. This type of crystallisation occurs if the body of magma as a whole remains motionless over a period of time. Under these conditions, magma undergoes extensive convection and mixing, and melt and phenocrysts remain in equilibrium. These conditions seem to be compatible with those can be expected from ponding basaltic magmas in a MASH zone. When the magma body cools, the early formed phenocrysts of clinopyroxene and olivine enter a reaction with magma to produce amphibole. In the Erzurum-Kars Plateau Volcanics, some amphibole phenocrysts which contain low Mg/(Mg+Fe) and also Ti (Figures: 4.13 and 4.14 p.190 and 4.17 p.194) may have been formed by such a reaction i.e. replacement of some of the pyroxenes by amphiboles.

According Foden and Green (1992), this amphibole-out reaction will also operate in more open magmatic systems when the wall-rocks with which the cooling, hydrous basaltic melts are in contact are composed of olivine and pyroxene as in the case of upper mantle or lower crust (point C in Figure 7.2). These anhydrous ferromagnesian phases may be composed of earlier cumulates which were previously emplaced in the lower crust or close to the Moho in the upper lithospheric mantle or they can be peridothitic wall-rock material. In fact, all these prerequisites for the amphibole fractionation could have been available in the proposed MASH zone beneath the Erzurum-Kars Plateau. The presence of this reaction is supported by the observation from several volcanic areas including Api volcano in Indonesia and Adak in Aleutians. In these areas, clinopyroxene-rich xenoliths show pargasitic alteration (Foden and Green, 1992).

The composition of amphiboles which Foden and Green (1992) synthesised in their experiments is mainly pargasitic hornblende. Amphiboles of the Erzurum-Kars Plateau volcanics also classify predominantly as ferroan pargasitic hornblende and ferroan pargasite on Hawthorn's (1981) amphibole classification diagram (Section 4.1.3, Figure 4.13). According to Foden and Green (1992), crystallisation of pargasitic amphibole, which contains very low concentrations of SiO_2 (less than 40 wt. %), from basaltic magmas promotes silica enrichment in derivative liquids, a feature which is also evident in their experimental runs. The composition of their experimental liquids, which is in equilibrium with amphibole, is andesite-like and calc-alkaline.

If the magma is tapped and extracted from the crystalline matrix, the mafic phase will move back into the field of olivine and clinopyroxene (+ plagioclase), because the adiabatic temperature gradient of magma becomes significantly less than the gradient of the amphibole-out reaction. As a result, early-crystallised pargasitic amphiboles

break down via decompressive incongruent melting, eventually forming xenoliths with pyroxene-rich coronas or they are completely resorbed. The resultant magma is relatively low-silica basaltic andesite liquid and a crystalline assemblage dominated by either clinopyroxene or olivine (Foden and Green, 1992). Some amphiboles from the Dumlu and Kargapazarı areas display these sort of reaction textures (Section 6.1.1).

7.4.2.2.2. Zone II: processes in the lower crust and transition between lower and upper crust

Al-in hornblende geobarometer calculations (Section 4.2.2.1) indicate that the lower crust or transition zone between the lower and upper crust (22-28 km) beneath the Eastern Anatolian Collision Zone has been the site of large magma chambers in which crystallisation of amphibole has dominated the mafic crystallising phase associated also with plagioclase and occasional ortho- and clinopyroxene. The lavas originated from these relatively deep chambers are represented in present by the lavas of the low-Y series showing a distinct Y and MREE to HREE depletion which is indicative of amphibole fractionation. Isotopic variations in these lavas indicate that assimilation combined with fractional crystallisation (AFC) was the dominant process throughout the evolution of these magma chambers. Isotopic characteristics, especially those of Pb isotopic ratios, suggest that the magmas in these chambers extensively assimilated a lower crustal material (up to 40%), which is isotopically similar to the granulitic xenoliths from Central Europe (presented in Wilson and Downes, 1991) and from the Pannonian Basin in Hungary. The higher Sr and slightly lower Rb contents of the low-Y series with respect to those of high-Y series also approve contributions from the lower crust because, as Hildreth and Moorbath (1988) pointed out, many lower-crustal mafic granulites are greatly enriched in Sr (as much as 700 to 1800 ppm). Most of the data points are clustered between 30% and 40% on the mixing line. This result may imply that composition of lower crust beneath the Eastern Anatolia region is similar to that of Hungary and Central Europe (B mixing component of Wilson and Downes, 1991). However, $\delta^{18}O$ values of the low-Y series on the Erzurum-Kars Plateau vary between 6.5 and 10, requiring a much more $\delta^{18}O$ enriched source compared to the lower crust beneath Central Europe to create observed variations on the AFC diagrams. There may be two explanations for this:

1. The magma chambers in zone II might have been located in the lower crust and assimilated the lower crustal material which had been previously enriched in $\delta^{18}O$ due to contamination of lower crust by upper crust.

2. Alternatively, these magma chambers might have assimilated a material which is approximately a mixture of 45% lower and 55% upper crust. This composition may

correspond to a transition zone between the lower and upper crust. If the thickness of upper crust is assumed to be around 25 km, which is the case for the Alps (Brown and Musset, 1989), then these magma chambers would be located in the middle of the zone between the lower crust and upper crust. Thrusting of lower crust onto upper crust during collision may have complicated the whole picture, changing the depth and position of the boundary between upper and lower crust. This may also explain why the low-Y magmas evolved in large magma chambers in zone II have relatively high $\delta^{18}O$ values.

Textural evidence from the amphibole-bearing porphyritic lavas of the low-Y series suggests that magma mixing between evolving low-Y andesitic to dacitic magma and fresh and hot high-Y basaltic magma was operational in the magmatic evolution of these series. This evidence includes glass inclusions, sieve texture and complex zoning patterns in plagioclase phenocrysts as presented in Sections 4.1.1.1 and 6.1.1.2. In addition, the distribution of An contents of plagioclase phenocrysts indicates that most phenocrysts are not in equilibrium with their matrix (Fig. 4.7 and 8).

The magma chambers in zone II seem to have been zoned in terms of their phenocryst contents because they produced two texturally diverse lava types with the same geochemistry: amphibole-bearing porphyritic and aphyric lavas. Hildreth (1981) showed that total crystal contents of silicic magma chambers usually increase markedly with depth. The gradients in degree of crystallisation suggest a progressive roofward depression of the liquidus by the upward enrichment of dissolved liquids, because the first magma to escape is poorest in phenocrysts but must normally be closest to the main cooling surface. Mahood (1981) showed that in some eruptions the initially erupted magma is nearly or truly aphyric in others a phenocryst-poor initial volume is followed by an abrupt transition to phenocryst-rich magma. The former is exactly the case for the Mt. Dumlu area where aphyric low-Y lavas (the Güngörmez andesite/dacite) show an abrupt change into phenocryst-rich, amphibole-bearing lava (the Dumlu amphibole dacite/andesite) towards the top of the succession. The presence of occasional lenses of aphyric lava flows in porphyritic units may imply that the phenocryst-poor upper zone was partly re-established during the periods between eruptions.

7.4.2.2.3. Zone III: processes in the upper crustal basic to intermediate magma chambers

This zone includes a slice of upper crust located approximately between 10 and 20 km depth according to amphibole geobarometer results (the Horasan plateau unit in Figure 4.26). The zone appear to have been dominated by the relatively small basaltic

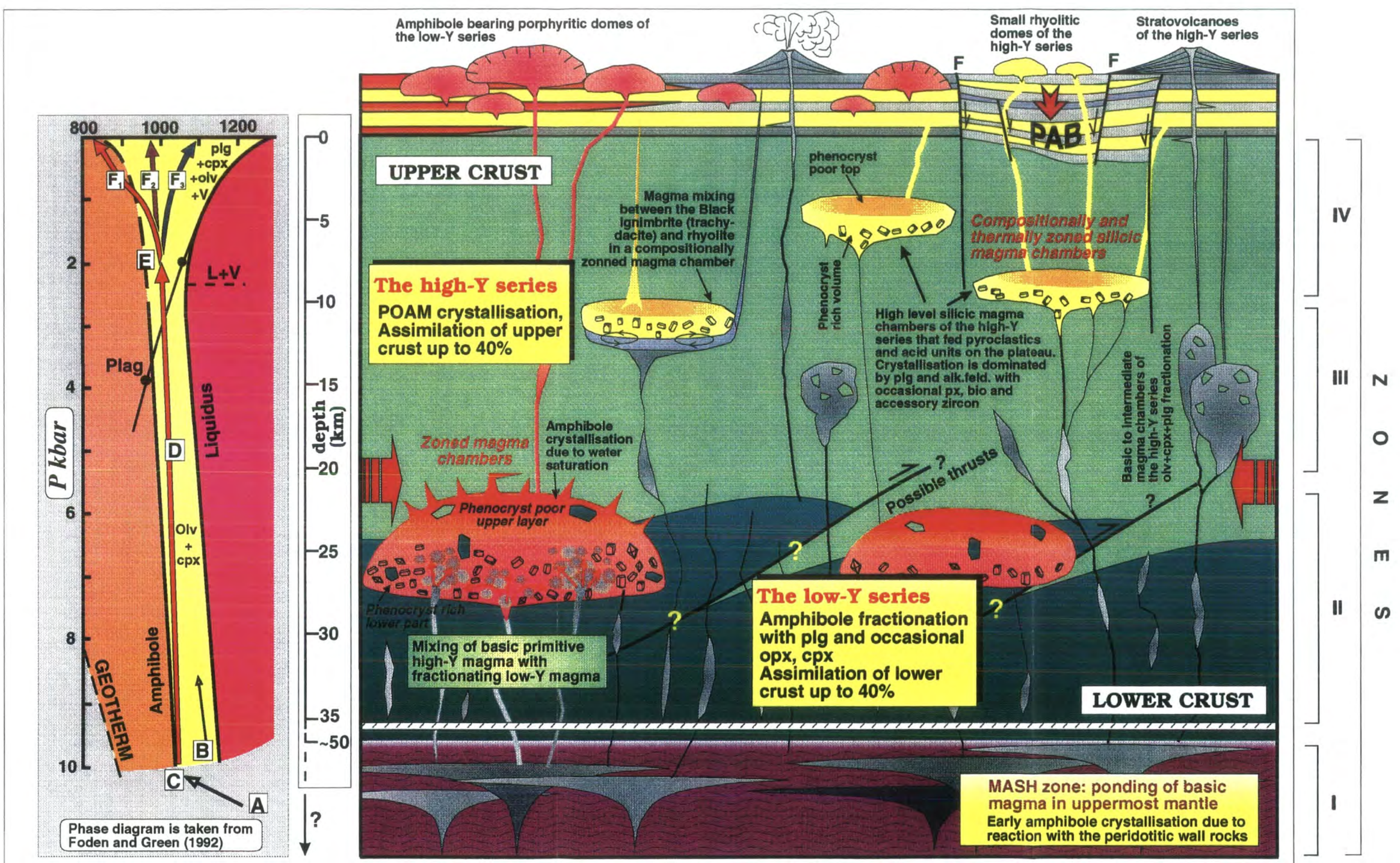

Figure: 7.3. Figure showing a summary of plumbing system of the collision related volcanics on the Erzurum-Kars Plateau, NE Turkey. PAB: Pull Apart Basin, F: strike-slip fault.

to andesitic magma chambers of the high-Y series. Trace element variations and petrographic studies indicate that the magmas in these chambers crystallised anhydrous phases (POAM) such as plagioclase, clinopyroxene with some occasional olivine and orthopyroxene because amphibole was not in equilibrium with the P-T conditions in this zone except for some exceptional cases that crystallised very rare amphibole phenocrysts. The absence of amphibole as a fractionating phase is proven by their higher Y content (>20 ppm). Location of these chambers corresponds to the "D" point in Foden and Green's (1992) phase diagram (Figure 7.3). Isotopic ratios, especially those of Pb isotopes, indicate that the high-Y magmas in these chambers assimilated upper crust up to 40% (Figure 5.9, p. 285). Most of the data points are clustered between 10% and 20%, about 20% less than that of assimilation rate of the low-Y series.

The high-Y lavas do not display any indication of assimilation of lower crust in their isotopic ratios and trace element compositions. Therefore, the magmas evolved in these chambers seem to have been derived directly from the MASH zone (zone I) without stopping within the zone of lower crustal magma chambers (zone II). They should also have been sufficiently hot to have enough energy to melt and assimilate the upper crust extensively. Two pyroxene thermometer calculations following the method of Lindsley and Andersen (1983) gave temperatures in the range of 1050-1200ºC for the basic to intermediate units of the high-Y series, thus supporting this interpretation (Section 4.2.1).

7.4.2.2.4. Zone IV: processes in the shallow level upper crustal silicic magma chambers

This zone is thought to have been located roughly between 10 and 15 km depth and was occupied predominantly by the silicic magma chambers that fed extensive pyroclastic deposits and lavas of the high-Y series on the plateau. The results of the Al-in-amphibole geobarometer (Figure 4.26) indicate crystallisation depths around 10-15 km (e.g. Ardıçlıdağ rhyolite in the Pasinler area) for some of these chambers. Both trace element and major element variations suggest that the magmas in these chambers were experienced a unique fractional crystallisation history. The magmas in these high level chambers appear to have fractionated pyroxenes and olivine in deeper zones (D point), perhaps within the magma chambers of zone III, before ascending to the shallow level (i.e. zone IV) that resulted in their enrichment in normative plagioclase and volatiles. As seen in Figure 3.18, 19 and 20 (Section 3.2.1), data points of the rhyolitic units, which were produced by these chambers, plot away from the general trend of liquid line of descent that is formed by the data points of other units on the plateau. This relationship indicates a unique fractionation history for the acidic units of

the high-Y series. This idea is also strengthened by the absence of transitional samples between these two groups on the plateau (Figures 3.15 to 17 in Chapter 3). The change from basic to acid products is almost always abrupt throughout the region.

On the Erzurum-Kars Plateau, nearly 90% of the total volume of acidic high-Y series is pyroclastic flows and fall deposits which are either very poor in their phenocryst content or completely aphyric. They are predominantly composed of rhyolitic glass. The rest of the series is represented by the rhyolitic and rhyodacitic lavas which contain variable amount of plagioclase and alkali feldspar as main phenocryst phase together with rare biotite. The pyroclastic flows show evidence of extensive water and volatile enrichment such as highly vesiculated zones and well-developed large accretionary lapilli.

Foden and Green (1992) argued that the magmas become normative plagioclase-enriched after fractionation of clinopyroxene and olivine at the "D" point. This point may correspond to the basic to intermediate magma chambers of the high-Y series (zone III) some of which probably fed the high-level magma chambers of zone IV. According to Foden and Green (1992), the magmas are forced to crystallise plagioclase-dominated assemblages in the high level magma chambers, close to "E" point, because of water saturation (Figure 7.3).. On the Erzurum-Kars Plateau, the behaviour of Ba and Sr (Figure 3.25, p. 145) together with the presence of negative Eu anomalies in the acidic units of the high-Y series indicates that the lavas erupted from the magma chambers of zone-IV extensively crystallised plagioclase and alkali feldspar. Crystallisation of these minerals was also accompanied by minor amounts of biotite and accessory zircon.

In the magma chambers of zone-IV, further assimilation of crustal material became very limited, because the rhyolitic magma did not have enough energy to melt the upper crust significantly (as in the case of the study of DePaolo et al., 1992). Eventually, the most important evolutionary process turned out to be crystal fractionation, which produced large volumes of acidic magmas with the same isotopic characteristics as the mafic/intermediate parental magmas. The residual liquids at this stage underwent rapid transition towards dacitic and rhyolitic compositions. As Foden and Green (1992) argued, magma mixing and vapour phase exsolution events probably accompanied the fractional crystallisation (FC) in these chambers. Two feldspar thermometers calculated using Seck's (1971) and Brown and Parsons' (1981) graphical methods gave crystallisation temperatures between 550 and 825ºC, clustering mostly around 650-700ºC for the acidic units of the high-Y series (Figure 4.30 and 31, p. 218). This temperature range is obviously not sufficient for assimilation. In addition, the AFC models presented in Section 5.2.3 show lower "*r*"

values for the acidic members of the high-Y series, which vary predominantly between 5 and 10%, displaying good agreement with this theoretical consideration. On the other hand, Pb isotopic ratios still indicate the presence of a small contribution from the upper crust. This may have occurred deeper in the crust before the magma rose into the high-level chambers, somewhere in the zone III, where the basic to intermediate magmas had still enough energy to assimilate crust in their route to the high-level magma chambers.

Hildreth (1981) argued that the degree of crystallinity decreases toward the cooling surface (especially roofward) of shallow level silicic magma chambers because of the existence of a volatile-rich boundary layer which may be tens of hundreds of meters thick. Degassing of basic additions in the roots of these systems may also provide a flux of volatiles (He, CO_2, S and halogens) (Hildreth, 1981). This layer, which is cooler than the lower levels, caps a dominant magmatic volume which is rich in phenocrysts (i.e. feldspars) forming a compositional and thermal zonation. If the magma erupts, the upper aphyric levels of these chambers will be drained, leaving the phenocryst-rich lower parts undisturbed in most cases. Therefore, the erupted magma will almost always aphyric and volatile saturated, if it does not reach to the phenocryst-rich lower layer, as in the case of the aphyric pyroclastic units of the high-Y series. Unlike the phenocryst-rich domes, pyroclastic flows fed by this upper layer have great aerial distribution due to their low viscosity significantly lowered by their high volatile contents. If the eruptive system drains the phenocryst-rich lower layer, it will erupt phenocryst-rich (in our case anorthoclase, sanidine and plagioclase) magmas. On the Erzurum-Kars Plateau, volcano-stratigraphic and geochemical data suggest that some of the high-level magma chambers beneath the plateau were compositionally and thermally zoned (Figure 3.24, p. 142) as in the case of the Pasinler area (e.g. the Ardıçlıdağ rhyolite, the White/Grey ignimbrites and the Black ignimbrite in the Pasinler area). This mechanism may explain the textural and compositional properties of acidic members of the high-Y lavas and their aerial distribution on the plateau.

Foden and Green (1992) suggested that the cooling paths of ascending magmas shallower than point "E" may follow three different paths. In the first one, the magma develops smaller dP/dT slopes than that of the amphibole-out curve (F_1), resulting in the crystallisation of amphibole in siliceous andesite and dacite (Figure 7.3). The central F_2 path corresponds to a magma fractionating an anhydrous pyroxene-feldspar assemblage as a result of continued adiabatic decompression and cooling. The final (F_3) path demonstrates the possibility of late-stage heating. This could be resulted from one or a set of factors including: (1) magma mixing, (2) the entrainment of hotter mafic magmas by cooler felsic magmas, (3) heating of overlying magma layers by

rising high temperature vapour phases and (4) the release of latent heat of crystallisation during enforced decompressive precipitation of plagioclase (Foden and Green, 1992). The acidic lavas of the high-Y series on the Erzurum-Kars Plateau seem to have followed the second (F_2) and possibly partly the third (F_3) paths because they do not contain amphibole.

To sum up, the isotopic and trace element differences between the high- and low-Y lavas on the Erzurum-Kars Plateau are not significantly dependent upon variations in their source. These differences have been extensively created by the effects of assimilation of lower and upper crust at variable depths combined with fractional crystallisation, both of which had been controlled by the nature and evolution of magma plumbing system in the crust.

7.5. Results of this thesis in comparison with previous studies on the collision-related volcanics of Eastern Anatolia

Lambert et al. (1974)

Results of my thesis from the Erzurum-Kars plateau are in good agreement with Lambert et al.'s (1974) discovery and interpretation of the two Y series. According to these authors, the low-Y series were generated under more hydrous and deeper conditions than the high-Y series. This idea is supported by the al-in-amphibole geobarometry results in this thesis. They maintain that the source of water could be the former subduction zone. This is well seen in multi-element patterns showing a distinctive enrichment in LIL elements and LREEs in this thesis. On the basis of the geotectonic setting of Mt. Ararat, they argued that subduction zone theory could not be applied to this area. They also inferred that, pre-Mesozoic sialic crust could not be a parental material, because Sr isotopic ratios are much lower than that can be expected from the partial fusion of crustal material. The results of this thesis are in good agreement with Lambert and Holland's (1974) interpretation.

Innocenti et al. (1976, 1980, 1982b)

Innocenti et al. (1976, 1980, 1982b) suggested that the earliest volcanism in the Kars-Ararat was calc-alkaline and that this was followed by alkaline volcanism. However, both the results of this thesis and of Pearce et al. (1990) show that this is not true for the collision-related volcanism of Eastern Anatolia. Innocenti et al. (1982a) argued also that, the rare earth elements (REE) and Sr isotope ratios suggested magma genesis by partial melting of mantle anomalously enriched in large ion lithophile

elements (LIL). The data presented in this thesis supports this interpretation. They suggested on the basis of their dating that the andesitic volcanic front migrated northward for 150-200 km during the Pliocene. According to them, this is evidence of the detachment of the subducted slab immediately after continental collision. They also argued that this detachment continued to induce magma generation of progressively lower intensity beneath an area corresponding to the Erzurum-Kars Plateau, located progressively further from the continental suture. The new K-Ar dating results from this thesis, and also from Pearce et al. (1990), show that the oldest eruptions of collision-related volcanism took place in the north, on the Erzurum-Kars Plateau. Furthermore, as Pearce et al. (1990) pointed out, there are no intermediate or deep-focus earthquakes that are indicative of a subducting lithospheric slab.

Gülen (1980)

Gülen (1980) mentioned the presence of systematic variations between isotopic ratios and major and trace element contents of lavas from Mt. Ararat such as that of $^{87}Sr/^{86}Sr$ and MgO. He interpreted his results as an indication of mixing of MORB-type mantle with an alkali-basalt magma in the Mt. Ararat province. According to him, crustal contamination of this mixture generated Süphan volcanics. In my opinion, mixing of MORB-type magma with an alkali basalt magma would not give calc-alkaline lavas of Mt. Ararat. Sr and Nd isotopic ratios would not be sufficient to detect the presence of crustal contribution in Mt. Ararat province if the basement were represented by ophiolitic rocks. The reason for that there may not be a great difference between the ophiolitic basement and the magma in terms of their Sr and Nd isotopic ratios. Even though I have no access to his unpublished database, systematic variations between Mg and Sr isotopic ratio may imply "assimilation combined with fractionation" (AFC) processes in the magmatic evolution of Ararat lavas.

Tokel (1984)

Tokel (1984) suggested that the data from drilling cores in the Eastern Anatolia region indicated the presence of E-W oriented Upper Miocene-Pliocene basins which are bounded by gravity faults and filled by at least 2000 m of limnic and fluvial deposits. On the basis of Turcotte's (1983) mathematical model, he believes that these depressions are related to a rifting event in the region. He proposed that these Upper Miocene to Pliocene basins were filled by voluminous "tholeiitic" and "alkaline" volcanics which are related to the rifting. He claimed that incompatible element (such as Rb, Sr, Nb and Ti) contents of the collision-related volcanics show close resemblance to oceanic tholeiites generated from depleted mantle. Even though the area he studied (Tokel, 1985) overlaps with the area studied in this thesis (between Erzurum and Kars), there are significant differences between the results of his study

and this thesis in terms of the interpretation of geochemical data. First of all, none of the volcanic units shows tholeiitic character in the region. Except for some alkaline volcanic areas located far away in the south around Muş, most collision-related volcanic units in the north are calc-alkaline in character. As it is demonstrated in Chapter 3, Rb, Sr and Nb are not close to MORB (Mid Ocean Ridge Basalts), in contrast they are enriched in the collision related lavas between 2 to 20 times of MORB. Finally, in my opinion, the presence of thick volcano-stratigraphic successions in the intermontane basins in the region can be attributed to the localised extension created by strike-slip fault systems. Both Pasinler and Karasu basins are controlled by strike slip faults and they appear to be pull apart basins, not rifts.

Yılmaz et al. (1987)

Yılmaz et al. (1987) explained the formation of extensive calc-alkaline volcanism in the Eastern Anatolia region by using Dewey et al.'s (1986) model which emphasises possible zones of different rheologic properties in a compressionally deforming continental crust at different levels. Their model involves true crustal magma generation at a zone of detachment around 15 km deep in the crust below which the crust behaves in a ductile manner. They also cited the widespread ignimbritic eruptions as evidence of crustal melting, because, as they described, they represented a water-saturated granitic magma. Yılmaz et al. (1987) also claimed that the Erzurum-Kars region in the north was covered predominantly with alkaline basaltic lavas.

My oxygen and lead isotope database (Chapter 5) shows that except for only one debatable sample from the south of Horasan, none of the samples from the Erzurum-Kars Plateau volcanics has a crustal origin. They all classify as calc-alkaline, not alkaline. Furthermore, there are only three basalt samples among 350 samples collected from 3000 km^2 area of the plateau. The majority of lavas andesitic and dacitic, not predominantly basic. These results are also supported by Pearce et al.'s (1990) database which cover the neovolcanics of the whole of Eastern Anatolia. The extreme water content of the ignimbritic deposits should have been generated by fractional crystallisation (especially plagioclase and alkali feldspar) in the shallow-level magma chambers (Section 7.4.2.2.4, p. 327), and cannot be attributed only to the presence of crustal melting.

Ercan et al. (1990)

Ercan et al. (1990) argued on the basis of their Sr isotopic ratios that the magmas that produced the collision-related volcanism in the Eastern Anatolia region had been contaminated by the Arabian crust which was partly subducted beneath Eastern Anatolia. In their opinion, almost all the volcanic units in the region resemble

the upper crustal composition proposed by Taylor and McClennan (1985) in their Li, V, Sc, Co, Ni, Ba, Ga, Y, Rb, Zr, Hf, Ta and Pb contents. They also argued that the Sr, Nb, Cs, Th, and U contents of these volcanics are similar to that of lower and upper crustal compositions. It seems extremely inappropriate to use most of these elements to deduce the presence of crustal contribution or assimilation, because except for Rb, Zr, Hf, Ta, Th and U, the rest are strongly partitioned into major crystallising phases. For example, Sr, Ba and Pb are partitioned into plagioclase, and Y and to a certain extent Nb into amphibole. If biotite is a crystallising phase in more evolved liquids, then Rb will be affected. Furthermore, crystallisation of even a minor amount of accessory minerals like zircon and apatite in acidic derivatives of these magmas can dramatically modify elements such as Zr, Y and the HREEs.

Pearce et al. (1990)

Pearce et al. (1990) suggested that the character of the neovolcanic activity in the Eastern Anatolia region depended on the tectonic history of the underlying lithosphere and the thermal evolution of the crust. According to them, the calc-alkaline volcanoes of Bingöl, Süphan, Ararat and volcanics of the Erzurum-Kars Plateau were derived from lithosphere carrying a subduction signature associated with pre-collision subduction events. They also maintain that combined assimilation and fractional crystallisation was operational in the thickening continental crust. They argued that there might be two possible mechanisms which could explain the production of great volumes of magmatism: thermal perturbation of metasomatised subcontinental lithosphere and the delamination of the thermal boundary layer. In addition, localised extension could contribute to former mechanisms. Pearce et al. (1990) suggest that the region is characterised by a set of mantle domains running parallel to the collision zone, each of which has yielded magmas of a particular composition since the start of magmatism in the region. Another important inference is that of polybaric crystallisation in the Kars-Mt. Ararat province. In accordance with the Lambert et al.'s (1974) findings from Mt. Ararat, Pearce et al. (1990) demonstrated the presence of extensive amphibole crystallisation on the Erzurum-Kars Plateau during the early stages of fractionation. The work presented in this thesis do support Pearce et al.'s (1990) interpretations for the Erzurum-Kars Plateau.

Tokel and Ercan (1992)

Tokel and Ercan (1992) suggested that "post-collision volcanism" in Anatolia display distinctive geochemical characteristics that do not coincide with the three basic tectonic settings in which magma generation occur and hence this volcanism should be cited in the literature as the type example of post-collision volcanism. They argued

that the main characteristic feature of the collision-related volcanism is the enrichment of high field strength (HFS) elements such as Ti, Nb, Ta and Hf. They claimed that the lavas which have previously been considered as being of the calc-alkaline association are not "true calc-alkalic rocks". They maintained that, moderate concentrations of large ion lithophile (LIL) and light rare earth (LREE) elements cannot be considered as an indicative feature of any of the tectonic settings listed above.

First of all, the term "post-collision volcanism", as they preferred to use, is not appropriate for the collision-related volcanics of Eastern Anatolia, because it is now well established that the collision tectonism has been operational throughout the evolution of neovolcanism in the region and it is still active in present time. In fact, collision itself has been the main tectonic event that gave rise to the magma generation in thickened lithosphere. I do not agree with the idea that the calc-alkaline series are not real calc-alkaline. Extensive database presented in this thesis and also in Pearce et al. (1990) shows that the calc-alkaline volcanics are truly calc-alkaline without any doubt. I agree with the interpretation of Tokel and Ercan (1992) about the existence of a subduction component in the collision-related volcanics of the region. However, this subduction component is best illustrated by enrichment of LIL and LREE elements, not by HFS elements. Finally, the neovolcanism of Eastern Anatolia has already been cited in literature as one of the basic settings of magma generation under the name of "collision volcanism" by Pearce et al. (1990).

REFERENCES

Adam, J., Green, T.H. and Sie, S.H. (1993) Proton microprobe determined partitioning of Rb, Sr, Ba, Y, Zr, Nb and Ta between experimentally produced amphiboles and silicate melts with variable F content, *Chemical Geology*, V. 109, pp. 29-49

Akimasa, M. and Kushiro, I. (1970) Experimental determination of partition coefficients of ten rare earth elements and barium between clinopyroxene and liquid in the synthetic silicate system at 20 kilobar pressure, *Contributions to Mineralogy and Petrology*, V. 26, pp. 42-49

Akkuş, M. F. (1965) Pasinler havzasının 1/25000 ölçekli detay petrol etüdü raporu: M.T.A. Rep., 4087 (unpublished), Ankara-Turkey.

Allègre, C. J. and Minster, J. F. (1978) Quantitative models of trace element behaviour in magmatic process, *Earth Planetary Science Letters*, V. 38, 1.

Anderson, A.T. (1976) Magma mixing: petrological process and volcanological tool, *Journal of Volcanology and Geothermal Research*, V. 1, pp. 3-33

Arpat, A. and Saroglu, F. (1972) The East Anatolian fault system: thougths on its development, *Bull. Miner. Res. Explor. Inst., Turkey,* V. 78, pp. 33-39.

Arth, J.G. (1976) Behaviour of trace elements during magmatic processes -a summary of theoretical models and their applications, *Journal of Res. U.S. Geol. Surv.*, V. 4, 41-47

Arth, J.G. and Barker, F. (1976) Rare-earth partitioning between hornblende and dacitic liquid and implications for the genesis of trondhjemitic-tonalitic magmas, *Geology*, V. 4, pp. 534-536

Bacon, C.R. and Druitt, T.H.(1988) Compositional evolution of the zoned calcalkaline magma chamber of Mounth Mazama, Crater Lake, Oregon, *Contributions to Mineralogy and Petrology*, V. 98, pp. 224-256

Banno, S. (1959) Aegerinnaugites from crystalline schists in Sikoku, *Geol. Soc. Japan J.* V. 65, pp. 652-657

Barth, T.W.F. (1951) The feldspar geological thermometers, *Neues Jahrb Mineral*, V. 82, pp. 143-154

Barth, T.W.F. (1968) Additional data for the two-feldspar geothermometer, *Lithos*, V. 1, pp. 305-306

Baxter, A.N. (1975) Petrology of the Older Series lavas from Mauritius, Indian Ocean, *Geological Society of America Bulletin*, V.86, pp. 1449-1458

Beattie, P., Clifford, F. and Russell, D. (1991) partition coefficients for olivine-melt and orthopyroxene-melt systems, *Contributions to Mineralogy and Petrology*, V. 109, pp. 212-224

Beattie, P., Drake, M., Jones, J., Leeman, W., Longhi, J., McKay, G., Nielsen, R., Palme, H., Shaw, D., Takahashi, E. and Watson, B. (1993) Terminology for trace-element partitioning, *Geochimica et Cosmochimica Acta*, V. 57, pp. 1605-1606

Bell, K. and Powell, J. L. (1969) Strontium isotopic studies of alkali rocks: the potassium rich lavas of the Birunga end Toro-Ankole regions, east and central equatorial Africa, *Journal of Petrology*, V. 10, pp. 536-572

Berlin, R. and Henderson, C.M.B. (1969) The distribution of Sr and Ba between the alkali feldspar, plagioclase and groundmass phases of porphyritic trachytes and phonolites, *Geochimica et Cosmochimica Acta*, V. 33, pp. 247-255

Bird, P. (1978) Initiation of intracontinental subduction in the Himalaya, *Journal of Geophysical Research*, V. 83, p. 4975-4987

Bird, P. (1979) Continental delamination and the Colorado Plateau, *Journal of Geophysical Research*, V. 84, pp. 7561-7571

Bird, P. and Baumgardner, J. (1981) Steady propagation of delamination events, *Journal of Geophysical Research*, V. 86, pp. 4891-4903

Birgili, Ş. (1968) Muş bölgesi 1/25.000 ölçekli Karaköse J48-d_3-d_4 ve Muş K47-b_2 paftalarının detay petrol etüdü hakkında rapor, *M.T.A. Report*, No. 1707 (unpublished), Ankara-Turkey

Blundy, J.D. and Holland, J.B. (1992) "Calcic amphibole equilibria and a new amphibole-plagioclase geothermometer": reply to the comments of Hammarstorm and Zen, and Rutherford and Johnson, *Contributions to Mineralogy and Petrology*, V. 111, pp. 269-272

Blundy, J.D. and Holland, J.B. (1992) "Calcic amphibole equilibria and a new amphibole-plagioclase geothermometer": reply to the comment of Poli and Schmidt, *Contributions to Mineralogy and Petrology*, V. 111, pp. 278-282

Blundy, J.D. and Holland, J.B. (1992) Calcic amphibole equilibria and a new amphibole-plagioclase geothermometer, *Contributions to Mineralogy and Petrology*, V. 104, pp. 208-224

Blundy, J.D. and Wood, B.J. (1991) Crystal-chemical controls on the partitioning of Sr and Ba between plagioclase feldspar, silicate melts, and hydrothermal solutions, *Geochimica et Cosmochimica Acta*, V. 55, pp. 193-209

Bottinga, Y. and Javoy, M. (1975) Oxygen isotope partitioning among the minerals in igneous and metamorphic rocks, *Rev. Geophys. Space Phys.*, V. 13, pp. 401-418

Bowen, N. L. (1956) The evolution of the Igneous Rocks (Dover, New York, N. Y.) reprint of 1928 ed., 332 pp.

Boyd, F. R. (1969) Electron probe study of diopside inclusions from kimberlite, *American Journal of Science*, V. 267-A, pp. 50-69

Boyd, F. R. (1973) A pyroxene geotherm, *Geochimica et Cosmochimica Acta*, V. 37, pp. 2533-2546.

Boynton, W.V. (1984) Geochemistry of the rare earth elements: meteorite studies, in *Rare Earth Element Geochemistry* (P. Hendertson ed.) Elsevier, pp. 63-114

Brenan, J.M. and Watson, E.B. (1991) Partitioning of trace elements between carbonate melt and clinopyroxene and olivine at mantle P-T conditions, *Geochimica et Cosmochimica Acta*, V. 55, pp. 2203-2214

Brinkman, R. (1976) Geology of Turkey, *F. Enke Verlag, Stuttgart*, p.158.

Brooks, C.K., Henderson, P. and Rønsbo, J.G. (1981) Rare-earth partition between allanite and glass in the obsidian of Sandy Braes, Northern Ireland, *Mineralogical Magasine*, V. 44, pp. 157-160

Brown, F.H. and Carmichael, I.S.E. (1971) Quaternary volcanoes of the Lake Rudolf region: II the lavas of North Island, South Island and the Barrier, *Lithos*, V. 4, pp. 305-323

Brown, G.C. and Musset, A.E. (1989) *The Inaccessible Earth*, Unwin Hyman, London, p.235

Brown, W.L. and Parsons, I. (1981) Towards a more practical two-feldspar geothermometer, *Contributions to Mineralogy and Petrology*, V. 76, pp. 369-377

Canıtez, N. And Toksöz, M.N. (1980) Crustal structure beneath Turkey, *EOS Transactions*, American Geophysical Union, V. 61/17, p. 290

Cas, R. A. F. and Wright, J. V. (1993) *Volcanic Successions, Modern and ancient, a geological approach to processes, products and successions*, Chapman & Hall, London, p. 528

Cawthorn, R. G. and Collerson, K. D. (1974) The recalculation of pyroxene end-member parameters and the estimation of ferrous and ferric iron content from electron microprobe analyses. *American Mineralogist*, V. 59, pp. 1203-1208.

Chiba, H., Chacko, T., Clayton, R.N. and Goldsmith, J.R. (1989) Oxygen isotope fractionations involving diopside, forsterite, magnetite and calcite: application to geothermometry, *Geochimica et Cosmochimica Acta*, V. 53, pp. 2985-2995

Colson, R.O. and Gust, D. (1989) Effects of pressure on partitioning of trace elements between low-Ca pyroxene and melt, *American Mineralogist*, V. 74, pp. 31-36

Colson, R.O., McKay, G.A. and Taylor, L.A. (1988) Temperature and composition dependencies of trace element partitioning: olivine/melt and low-Ca pyroxene/melt, *Geochimica et Cosmochimica Acta*, V. 52, pp. 539-553

Colson, R.O., McKay, G.A. and Taylor, L.A. (1989) Change balancing of trivalent trace elements in olivine and low-Ca pyroxene: a test using experimental partitioning data, *Geochimica et Cosmochimica Acta*, V. 53, pp. 643-648

Coryell, C.D., Chase, J.M. and Winchester, J.W. (1963) A procedure for the geochemical interpretation of terrestrial rare-earth abundance pattens, *Journal of Geophysical Research*, V. 68, pp. 559-566

Cox, K.G., Bell, J.D. and Pankhurst, R.J. (1989) *The interpretation of igneous rocks*, sixth edition, Unwin Hyman, London

Currie, K.L. (1991) A simple quantitative calculation of mol fractions of amphibole end-members, *Canadian Mineralogist*, V. 29, pp. 287-299

Deines, P. (1977) On the oxygen isotope distribution among minerals and triplets in igneous and metamorphic rocks, *Geochimica et Cosmochimica Acta*, V. 41, pp. 1709-1730

Demirtaşlı, E. And Pisoni, C. (1965) Ahlat-Adilcevaz bölgesinin jeolojisi (Van gölü kuzeyi), *M.T.A.Bulletin*, V. 64, pp. 22-36, Ankara-Turkey

DePaolo D. J. (1981) Trace element and isotopic effects of combined wall-rock assimilation and fractional crystallisation, *Earth and Planetary Science Letters*, V. 53, pp. 189-202

DePaolo D. J. and Wasserburg, G. J. (1979) Petrogenetic mixing models and Nd-Sr isotopic patterns, *Geochimica Cosmochimica Acta*, V. 43, pp. 615-627

DePaolo D.J., Perry, F.V. and Baldridge, W.S. (1992) Crustal versus mantle sources of granitic magma: a two parameter model based on Nd isotopic studies, *Transections of Royal Society of Edinburg*, V. 83 (1-2), PP. 439-446

Dewey, J.F., Hempton, M.R., Kidd, W.S.F., Şaroğlu, F and Şengör, A.M.C. (1986) Shortening of continental lithosphere: the neotectonics of Eastern Anatolia-a young collision zone, in *Collision Tectonics*, (M.P. Coward and A.C. Ries eds.), Geological Society Special Publication, No: 19, pp. 3-36

Dietrich, H. and Petrakakis, K. (1986) A linear algebraic method for the calculation of pyroxene end member components. *Tschermaks Mineralogische und Petrographische Mitteilungen*, V. 35, pp. 275-282.

Dollase, W. A. and Newman, W (1984) Statistically most probable stoichiometric formulae. *American Mineralogist.* V. 69, pp. 553-556.

Dostal, J., Dupuy, C., Carron, J.P., Le Guen de Kerneizon, M. and Maury, R.C. (1983) Partition coefficients of trace elements: application to volcanic rocks of St. Vincent, West Indies, *Geochimica et Cosmochimica Acta*, V. 47 , pp. 525-533

Downes, H. And Dupuy, C. (1987) Textural, isotopic and REE variations in spinel peridotite xenoliths, Massif Central, France, *Earth and Planetary Science Letters*, V. 82, pp. 121-135

Downes, H. Kempton, P.D., Briot, D., Harmon, R.S. and Leyreloup, A.F. (1991) Pb and O isotope systematics in granulite facies xenoliths, French Massif Central: implications for crustal process, *Earth and Planetary Science Letters*, V. 102, pp. 342-357

Downes, H., Isztin, A.E. and Thirlwall, M.F. (1992) Petrology and Geochemistry of spinel peridotite xenoliths from the western Pannonian Basin (Hungary): evidence for an association between enrichment and texture in the upper mantle, *Contributions to Mineralogy and Petrology*, V. 109, pp. 340-354

Drake, M.J. (1975) The oxidation state of europium as an indicator of oxygen fugacity, *Geochimica et Cosmochimica Acta,* V.39, pp. 55-64

Drake, M.J. and Holloway, J.R. (1977) Partitioning of Sm between plagioclase, clinopyroxene, amphibole, and hydrous silicate liquid at high pressures (abstract). *In papers Presented to the International Conference on Experimental Trace Element Geochemistry*, pp. 21-23

Drake, M.J. and Weill, D.F. (1975) Partition of Sr, Ba, Ca, Y, Eu^{2+}, Eu^{3+}, and other REE between plagioclase feldspar and magmatic liquid: an experimental study, *Geochimica et Cosmochimica Acta,* V. 39, pp. 689-712

Dudas, M.J., Schmitt, R.A. and Harward, M.E. (1971) Trace element partitioning between volcanic plagioclase and dacitic pyroclastic matrix, *Earth and Planetary Science Letters*, V. 11, pp. 440-446

Eichelberger, J.C. (1975) Origin of andesite and dacite: evidence of mixing at Glass Mountain in California and at other circum-Pacific volcanoes, *Geological Society of American Bulletin*, V. 86, pp. 1381-1391

England, P.C. and Houseman, G.A. (1988) The mechanics of the Tibetan Plateau, *Philosophical Transections Royal Society of London*, A326, pp. 523-532

Erakman, B. ad Şahintürk, Ö. (1980) Kars-Ağrı illeri arasıda kalan alanin jeolojisi ve hidrokarbon olanakları, TPAO Arama Grubu Başkanlığı, 4. Bölge Arama Müdürlüğü, unpublished report no: 1508

Ercan, T., Fujitani, T., Matsuda, J.I., Notsu, K., Tokel, S. And Ui, T. (1990) Doğu ve Güneydoğu Anadolu neojen-Kuvaterner volkanitlerine iliskin yeni jeokimyasal, radyometrik ve izotopik verilerin yorumu, publications of M.T.A., pp. 143-164

Erdoğan, T. (1966) Erzurum-Karayazı bölgesi I47-c2, I47-c3, I48-d4 paftalarına ait jeolojik rapor, *M.T.A. Report*, No. 4193 (unpublished), Ankara-Turkey

Erdoğan, T. (1967) Erzurum-Hınıs bölgesi 1/25.000 ölçekli J47-d_1 ve J47-d_2 paftalarının detay petrol etüdü, *M.T.A. Report*, No. 4340 (unpublished), Ankara-Turkey

Erdoğan, T. and Soytürtk, N. (1974) Tekman Baseni jeolojisi ve hidrokarbon imkanları raporu, TPAO Arama Grubu Başkanlığı, Jeoloji Müdürlüğü, unpublished report no: 870

Erentöz, C. And Ketin, İ. (1961) 1/500.000 scale geological map of Turkey, Kars sheet, published by the Institute of Mineral Research and Exploration, Ankara-Turkey

Erinç, S. (1953) *Doğu Anadolu'nun Coğrafyası,* Publication of Istanbul University, no: 572, p. 124

Essene, E. J. and Ffye, W. S. (1967) Omphacite in californian metamorphic rocks, *Contributions Mineral. Petrol.* V. 15, pp. 1-3.

Ewart, A. and Taylor, S.R. (1969) Trace element geochemistry of the rhyolitic volcanic rocks, Central North Island, New Zealand. Phenocryst data, *Contributions to Mineralogy and Petrology,* V. 22, pp. 127-146

Faure G., Bowman, J. r. and Elliot, D. H. (1974) Strontium isotope composition and petrogenesis of the Kirkpatrick Basalt, Queen Alexandra Range, Antarktica, *Contributions to Mineralogy and Petrology.*, V. 3, pp. 153-169

Faure, G. (1986) Principles of isotope geology, second edition, pp. 589, John Wiley & Sons, New York

Ffye, W.S. (1992) Magma underplating of continental crust, *Journal of Volcanology and Geothermal Research*, V. 50, pp. 33-40

Foden, J.D. and Green, D.H. (1992) Possible role of amphibole in the origin of andesite: some experimental and natural evidence, *Contributions to Mineralogy and Petrology*, V. 109, pp. 479-493

Friedman, I. and O'Neil, J.R. (1977) Compilation of stable isotope fractionation factors of geochemical interest, In Data of Geochemistry (M. Fleischer, ed.), sixth edition, Chapter KK, *U.S. Geological Survey Proffesional Papers*, 440KK, 12p.

Fujimaki, H. (1986) Partition coefficients of Hf, Zr, and REE between zircon, apatite, and liquid, *Contributions to Mineralogy and Petrology*, V. 94, pp. 42-45

Fujimaki, H., Tatsumoto, M. and Aoki, K. (1984) Partition coefficients of Hf, Zr and REE between phenocrysts and groundmasses. Proceedings of the fourteenth lunar and planetary science conference, Part 2, Journal of Geophysical Research, V. 89, Suppl. B662-672

Gedik, A. (1978) Doğu Anadolu'da açılan stratigrafik inkişaf (açınsama) sondajları, Yeryuvarı ve İnsan, pp. 31-35.

Gill, J. (1981) *Orogenic andesites and Plate tectonics*, Springer Verlag, Berlin, 390 pp.

Gómez, J. M. C. (1990) A program for pyroxene classification and calculation of end-members. *American Mineralogist*, V. 75, pp. 1426-1427

Gourgaud, A. and Villament, B. (1992) Evolution of magma mixing in an alkaline suit: the Grande Cascade sequence (Monts-Dore, French Massif Central). Geochemical modelling, *Journal of Volcanology and Geothermal Research*, V. 52, pp. 255-275

Graham, C.M. and Powell, R. (1984) A garnet-hornblende geothermometer: calibration, testing, and application to the Pelona Schist, Southern California, *Earth and Planetary Science Letters*, V. 31, pp. 142-152

Green, T.H. (1982) Anatexis of mafic crust and high pressure crystallisation of andesite, In: Orogenic Andesites (R.S. Thorpe, ed.), Wiley, Chichester, U.K., pp. 465-487

Green, T.H. and Pearson, N.J. (1985a) Rare-earth element partitioning between clinopyroxene and silicate liquid at moderate to high pressure, *Contributions to Mineralogy and Petrology*, V. 91, pp. 24-36

Green, T.H. and Pearson, N.J. (1985b) Experimental determination of REE partition coefficients between amphibole and basaltic liquids at high pressure, *Geochimica et Cosmochimica Acta*, V. 49, pp. 1465-1468

Green, T.H. and Pearson, N.J. (1987) An experimental study of Nb and Ta partitioning between Ti-rich minerals and silicate liquids at high pressure and temperature, *Geochimica et Cosmochimica Acta*, V. 51, pp. 55-62

Green, T.H., Sie, S.H., Ryan, C.G. and Cousens, D.R. (1989) Proton microprobe-determined partitioning of Nb, Ta, Zr, Sr and Y between garnet, clinopyroxene and basaltic magma at high pressure and temperature, Chemical geology, V. 74, pp. 201-216

Gülen, L. (1980) Sr, Nd and Pb isotope systematics of Ararat and Suphan volcanoes, Rastern Turkey, *EOS*, V. 63, no. 45, p. 1145

Gülen, L. (1980) Strontium isotope geochemistry of Mount Ararat and Mount Süphan Volcanics, Eastern Turkey, *EOS*, V. 61, no. 17, p. 412

Guo, J. and Green, T.H. (1989) Barium partitioning between alkali feldspar and silicate liquid at high temperature and pressure, *Contributions to Mineralogy and Petrology*, V. 102, pp. 328-335

Hall, A. (1987) *Igneous petrology*, Longman Scientific & Technical, pp. 573

Halsor, S.P. (1989) Large glass inclusions in plagioclase phenocrysts and their bearing on the origin of mixed andesitic lavas at Tolimon Volcano, Guatemala, *Bulletin of Volcanology*, V. 51, pp. 271-280

Hammarstrom, J.M. and Zen, E-an (1986) Aluminium in hornblende: an ampirical igneous geobarometer, *American Mineralogist*, V. 71, pp. 1297-1313

Hammarstrom, J.M. and Zen, E-an (1992) Discussion of Blundy and Holland's (1990) "Calcic amphibole equilibria and a new amphibole-plagioclase geothermometer, *Contributions to Mineralogy and Petrology*, V. 111, pp. 264-266

Hart, S.R. (1984) A large-scale isotopic anomaly in the Southern hemisphere mantle, *Nature*, V. 309, pp. 753-757

Hart, S.R. and Brooks, C. (1974) Clinopyroxene-matrix partitioning of K, Rb, Cs, Sr and Ba, *Geochimica et Cosmochimica Acta*, V. 38, pp. 1799-1806

Hart, S.R. and Dunn, T. (1993) Experimental cpx/melt partitioning of 24 trace elements, *Contributions to Mineralogy and Petrology*, V. 113, pp. 1-8

Hawthorne, F.C. (1981) Crystal chemistry of amphiboles, in *Amphiboles and Other Hydrous Pyroboles-Mineralogy* (D.R. Veblen Ed.), Chelsea, Michigan, U.S.A., pp. 1-95

Hendersen, P. (1990) *Inorganic Geochemistry*, Pergamon Press, p.353, U.K.

Higuchi, H. and Nagasawa, H. (1969) Partition of trace elements between rock-forming minerals and the host volcanic rocks, *Earth and Planetary Science Letters*, V. 7, pp. 281-287

Hildreth, W. (1981) Gradients in silicic magma chambers: implications for lithospheric magmatism, *Journal of Geophysical Research*, V. 86, No: B11, pp. 10153-10192

Hildreth, W. And Moorbath, S. (1988) Crustal contributions to arc magmatism in the Andes of Central Chile, *Contributions to Mineralogy and Petrology.*, V. 98, pp. 455-489

Holland, T.J.B. and Richardson, S.W. (1979) Amphibole zonation in metabasites as a guide to the evolution of metamorphic conditions, *Contribitions to Mineralogy and Petrology*, V. 70, pp. 143-148

Hollister, L.S., Grissom, G.C., Peters, E.K., Stowell, H.H. and Sisson, V.B. (1987) Confirmation of empirical correlation of Al in hornblende with pressure of solidification of calc-alkaline plutons, *American Mineralogist*, V. 72, pp. 231-239

Innocenti, F., Manetti, P., Mazzuoli, R., Pasquaré, G. and Villari, L. (1982a) Anatolia and north-western Iran, in *Andesites*, (R.S. Thorpe ed.), John Wiley & Sons

Innocenti, F., Mazzuoli, R., Pasquaré, G., Radicati di Brozola, F. and Villari, L. (1976) Evolution of volcanism in the area of interaction between the Arabian, Anatolian, and Iranian plates (Lake Van, Eastern Turkey), *Journal of Volcanology and Geothermal Research*, V. 1, pp. 103-112

Innocenti, F., Mazzuoli, R., Pasquaré, G., Radicati di Brozolo, F. and Villari, L. (1982a) Tertiary and Quaternary volcanism of the Erzurum-Kars area (Eastern Turkey): geochronological data and geodynamic evolution, *Journal of Volcanology and Geothermal Research*, V. 13, pp. 223-240

Innocenti, F., Mazzuoli, R., Pasquaré, G., Serri, G. and Villari, L. (1980) Geology ofthe volcanic area north of lake Van (Turkey), Geol. Rundsch., V. 69, pp. 292-322

Irving, A.J. (1978) A review of experimental studies of crystal/liquid trace element partitioning, *Geochimica et Cosmochimica Acta*, V. 42, pp. 743-770

Irving, A.J. and Frey, F.A. (1978) Distribution of trace elements between garnet megacrysts and host volcanic liquidus of kimberkitic to rhyolitic composition, *Geochimica et Cosmochimica Acta*, V. 42, pp. 771-787

Irving, A.J. and Frey, F.A. (1984) Trace element abundances in megacrysts and their host basalts: constraints on partition coefficients and megacryst genesis, *Geochimica et Cosmochimica Acta*, V. , pp. 1201-1221

Isztin, A.E., Downes, H., James, D.E., Upton, B.G.J., Dobosi, G.A., Ingram, G.A., Harmon, R.S. and Scharbert, H.G. (1993) The petrogenensis of Pliocene alkaline volcanic rocks from the Pannonian Basin, Eastern Central Europe, *Journal of Petrology*, V. 34, pp. 317-343

İlker, S. (1966a) Erzurum-Muş bölgesinde Karaköse J48-a_4 ve J48-d_1 paftalarının 1/25000 ölçekli detay petrol etüdü hakkında rapor, *M.T.A. Report*, No. 4177 (unpublished), Ankara-Turkey

İlker, S. (1966b) Erzurum bölgesinde I47-c_1, I47-c_4, I47-d_2 ve I47-d_3 paftalarının detay petrol etüdü hakkında rapor, *M.T.A. Report*, No. 4236 (unpublished), Ankara-Turkey

Johnson, M.C. and Rutherford, M.J. (1989) Experimental calibration of the aluminium-in-hornblende geobarometer with application to Long Valley caldera (California) volcanic rocks, *Geology*, V. 17, pp. 837-841

Kinzler, R.J., Grove, T.L. and Recca, S.I. (1990) An experimental study on the effect of temperature and melt composition of nickel between olivine and silicate melt, *Geochimica et Cosmochimica Acta*, V. 54, pp. 1255-1265

Koçyiğit, A. (1985) Muratbağı-Balabantaş (Horasan) arasında Çobandede fay kuşağının jeotektonik özellikleri ve Horasan-Narman Depremi yüzey kırıkları, *Bulletin of Earth Sciences, The University of Cumhuriyet*, V.2, N. 1, pp. 17-33

Kretz, R. (1982) Transfer and exchange equilibria in a portion of the pyroxene quadrilateral as deduced from natural and experimental data, *Geochimica et Cosmochimica Acta*, V. 46, pp. 411-422.

Kudo, A.M. and Weill, D.F. (1970) An igneous plagioclase thermometer, *Contributions to Mineralogy and Petrology*, V. 25, pp. 52-65

Kuehner, S.M., Laughlin, J.R., Grossman, L., Johnson, M.L. and Burnett, D.S. (1989) Determination of trace element mineral/liquid partition coefficients in melilite and diopside by ion and electron microprobe techniques, *Geochimica et Cosmochimica Acta*, V. 53, pp. 3115-3130

Kuno, H. (1936) Petrological notes on some pyroxene-andesites from Hakone volcano, with special reference to some types with pigeonite phenocrysts, *Japan Journal of Geol. Geogr.*, V. 13, pp. 107-140

Kuno, H. (1950) Petrology of Hakone volcano and the adjacent areas, Japan, *Geological Society of American Bulletin*, V. 61, pp. 957-1019

Kushiro, I. (1962) Clinopyroxene solid solutions. Part 1. The $CaAl_2SiO_6$ component. *Japan J. Geol. Geogr.* V. 33, pp. 213-220

La Tourrette, T.Z., Burnett, D.S. and Bacon, C.R. (1991) Uranium and minor-element partitioning in Fe-Ti oxides and zircon from partially melted granodiorite, Crater Lake, Oregon, *Geochimica et Cosmochimica Acta*, V. 55, pp. 457-469

Lambert, R.S.T., Holland, J.G. and Owen, P.F. (1974) Chemical petrology of a suite of calc-alkaline lavas from Mount Ararat, Turkey, *Journal of Geology*, Vol. 82, pp. 419-438

Larsen, L.M. (1979) Distribution of REE and other trace elements between phenocrysts and peralkaline undersaturated magmas, examplified by rocks from the Gardar igneous province, south Greenland, Lithos, V. 12, pp. 303-315

Leake, B.E. (1978) Nomenculature of amphiboles, *Canadian Mineralogist*, V. 16, pp. 501-520

Leake, B.E. and Winchell, H. (1978) Nomenclature of amphiboles, *American Mineralogist*, V. 63, pp. 1023-1052

Leeman, W.P. and Lindstrom, D.J. (1978) Partitioning of Ni^{2+} between basaltic and synthetic melts and olivines - an experimental study, *Geochimica et Cosmochimica Acta*, V. 42, pp. 801-816

Leeman, W.P. and Phelps, D.W. (1981) Partitioning of rare elements and other trace elements between sanidine and coexisting volcanic glass, Journal of Geophysical Research, V. 86, no. B11, pp. 10193-10199

Lemarchand, F., Villemant, B. and Calas, G. (1987) Trace element distribution coefficients in alkaline series, *Geochimica et Cosmochimica Acta,* V. 51, pp. 1071-1081

Lindsley, D. H. (1983) Pyroxene thermometry, *American Mineralogist.* V. 68, pp. 477-493.

Lindsley, D. H. (1986) Discussion of a linear algebraic method for the calculation of pyroxene end-member components, by Dietrich and Petrakakis. *Tschermaks Mineralogische und Petrographische Mitteilungen*, V. 35, pp. 283-285.

Lindsley, D. H. and Andersen, D. J. (1983) A two pyroxene thermometer: Proceedings of the Thirteenth Lunar and Planetary Science Conference, Part 2, *Journal of Geophysical Research*, V. 88, Supplement, pp. A887-A906.

Lindstrom, D.J. and Weill, D.F. (1978) Partitioning of transition metals between diopside and coexisting silicate liquids, I. nickel, cobalt, and manganese, *Geochimica et Cosmochimica Acta,* V. 42, pp. 817-831

Mahood, G. and Hildreth, W. (1983) Large partition coefficients for trace elements in high-silica rhyolites, *Geochimica et Cosmochimica Acta,* V. , pp. 11-30

Mahood, G.A. (1981) Chemical evolution of a Pliocene rhyolitic center-Sierra La Primavera, Jalisco, Mexico, *Contributions to Mineralogy and Petrology*

Mahood, G.A. and Stimac, J.A. (1990) Trace-element partitioning in pantellerites and trachytes, *Geochimica et Cosmochimica Acta,* V. 54, pp. 2257-2276

Mathez, E.A. (1973) Refinement of the Kudo-Weill plagioclase thermometer and its application to basaltic rocks, *Contributions to Mineralogy and Petrology,* V. 41, pp. 61-72

Matsuhisa, Y. Goldsmith, J.R. and Clayton, R.N. (1979) Oxygen isotopic fractionation in the system quartz-albite-anorthite-water, *Geochimica et Cosmochimica Acta*, V. 43, pp. 1131-1140

Matthews, A., Goldsmith, J.R. and Clayton, R. N. (1983) Oxygen isotope fractionatins involving pyroxenes: the calibration of mineral-pair thermometers, *Geochimica et Cosmochimica Acta*, V. 47, pp. 631-644

McCallum, I.S. and Charette, M.P. (1978) Zr and Nb partition coefficients: implications for the genesis of mare basalts, KREEP and sea floor basalts, *Geochimica et Cosmochimica Acta*, V. 42, pp. 859-869

McHone, J. G. (1987) PCX: an APL program for calculating pyroxene structural formulae and end-members. *Computers & Geosciences*, V. 13, pp. 89-91.

McKay, G., Wagstaff, J. and Yang, S.-R. (1986) Clinopyroxene REE distribution coefficients for shergottites: the REE content of the Shergotty melt, *Geochimica et Cosmochimica Acta*, V. 50, pp. 927-937

McKay, G.A. (1982) Partitioning of REE between olivine, plagioclase, and synthetic melts: implications for the origin of lunar anorthosite, Lunar Planet. Sci., XIII, pp. 493-494

McKay, G.A. (1986) Crystal/liquid partitioning of REE in basaltic systems: extreme fractionation of REE in olivine, *Geochimica et Cosmochimica Acta*, V. 50, pp. 69-79

McKenzie, D. P. (1976) The East Anatolian Fault: a major structure in Eastern Turkey, *Earth. Planet. Sci. Lett.*, V. 29, pp. 189-193

McKenzie, D.P. and Bickle, M.J. (1988) The volume and composition of melt generated by extension of the lithosphere, *Journal of Petrology*, V. 29, pp. 625-679

Mercier, J, -C. C. (1976) Single-pyroxene geothermometry and geobarometry, American Mineralogist, V. 61, pp. 603-615.

Michael, P.J. (1988) Partition coefficients for rare earth elements in mafic minerals of high silica rhyolites: the importance of accessory mineral inclusions, *Geochimica et Cosmochimica Acta*, V. 52 , pp. 275-282

Morimoto, N. (1989) Nomenclature of pyroxenes, *Canadian Mineralogist*, V. 27, pp. 143-156.

Mysen B. O. and Heier, K. S. (1972) Petrogenesis of eclogites in high grade metamorphic gneisses, exemplified by the Hareidland eclogite,

Western Norway, *Contributions to Mineralogy and Petrology,* V. 36, pp. 73-94.

Mysen, B.O. (1978) Experimental determination of rare earth element partitioning between hydrous silicate melt, amphibole and garnet peridotite minerals at upper mantle pressures and temperatures, *Geochimica et Cosmochimica Acta,* V. 42, pp. 1253-1263

Nabelek, C.R. and Lindsley, D.H. (1985) Tetrahedral Al in amphibole: a potential thermometer for some mafic rocks, *Geological Society of America*, Abstracts with Prog., V. 17, p. 673

Nagao, K., Kita, I., Matsuda, J.I. and Ercan, T. (1989) Noble gas and carbon isotopic compositions in quaternary volcanic area in Turkey, *Bulletin of Geomorphology,* V. 17, pp. 101-110, Ankara-Turkey

Nagasawa H. (1971) Partitioning of Eu and Sr between coexisting plagioclase and K-feldspar, *Earth and Planetary Science Letters*, V. 13, pp. 139--144

Nagasawa H. (1973) Rare-earth distribution in alkali rocks from Oki-Dogo Island, Japan, *Contributions to Mineralogy and Petrology*, V. 39, pp. 301-308

Nagasawa, H. (1970) Rare earth concentrations in zircons and apatites and their host dacites and granites, *Earth and Planetary Science Letters*, V. 9, pp. 359-364

Nagasawa, H. and Schnetzler, C.C. (1971) Partitioning of rare earth, alkali and alkaline earth elements between phenocrysts and acidic igneous magma, *Geochimica et Cosmochimica Acta,* V. 35, pp. 953-968

Nakamura, N. (1974) Determination of REE, Ba, Fe, Mg, Na and K in carbonaceous and ordinary chondrites, *Geochimica et Chosmochimica Acta*, V. 38, pp. 757-773

Nash, W.P. and Crecraft, H.R. (1985) Partition coefficients for trace elements in silicic magmas, *Geochimica et Cosmochimica Acta,* V. 49 , pp. 2309-2322

Nelson, K.D. (1992) Are crustal thickness variations in old mountain belts like the Appalachians a consequence of lithospheric delamination, *Geology*, V. 20, pp. 498-502

Nicholls, I.A. and Harris, K.L. (1980) Experimental rare earth element partition coefficients for garnet, clinopyroxene and amphibole coexisting with

andesitic and basaltic liquids, *Geochimica et Cosmochimica Acta*, V. 44, pp. 287-308

Nielsen, R.L., Gallahan, W.E. and Newberger, F. (1992) Experimentally determined mineral-melt partition coefficients for Sc, Y and REE for olivine, orthopyroxene, pigeonite, magnetite and ilmenite, *Contributions to Mineralogy and Petrology*, V. 110, pp. 488-499

Ohtani, E., Kawabe, I., Moriyama, J. and Nagata, Y. (1989) Partitioning of elements between majorite garnet and melt and implications for petrogenesis of komatiite, *Contributions to Mineralogy and Petrology*, V. 103, pp. 263-269

Onuma, N., Higuchi, H., Wakita, H. and Nagasawa, H. (1968) Trace elements partition beween two pyroxenes and the host lava, *Earth and Planetary Science Letters*, V. 5, pp. 47-51

Ota, K. and Dinçel, A. (1975) Volcanic rocks of Turkey, Bull. Geol. Soc of Japan, V. 26, pp. 395-419.

Özcan, A. (1967) Erzurum-Hınıs bölgesinde Erzurum J47-a_3-a_4 paftalarının detay petrol etüdü, *M.T.A. Report*, No. 4128 (unpublished), Ankara-Turkey

Pasquaré, B.G. (1970) Cenozoic volcanics of the Erzurum area, *Geol. Rdsch.*, V. 60, pp. 900-912

Pearce, J.A. (1982) Trace element characteristics of lavas from destructive plate boundries, in *Andesites* (R.S. Thorpe ed.), Wiley, Chichester, pp. 525-548

Pearce, J.A. (1983) Role of the sub-continental litosphere in magma genesis at active continental margins, *In Continental basalts and mantle xenolites* (C.J. Hawkesworth and M.J. Norry, eds), Shiva, Nanthwich, pp. 230-249

Pearce, J.A. and Norry, M.J. (1979) Petrogenetic implications of Ti, Zr, Y, and Nb variations in volcanic rocks, *Contributions to Mineralogy and Petrology*, V. 69, pp. 33-47

Pearce, J.A., Bender, J.F., De Long, S.E., Kidd, W.S.F., Low. P.J., Güner, Y., Şaroğlu, F., Yılmaz, Y., Moorbath, S. And Mitchell, J.G. (1990) Genesis of collision volcanism in Eastern Anatolia, Turkey, *Journal of Volcanology and Geothermal Research*, V. 44, pp. 189-229

Perchuk, L.L. and Ryabchikov, I.D. (1968) Mineral equilibria in the system nepheline-alkali feldspar-plagioclase and their petrological significance, *Journal of Petrology*, V. 9, pp. 123-167

Philpotts, J.A. and Schnetzler, C.C. (1970) Phenocryst-matrix partition coefficients for K, Rb, Sr and Ba, with applications to anorthosite and basalt genesis, *Geochimica et Cosmochimica Acta,* V. 34, pp. 307-322

Phinney, W.C. and Morrison, D.A. (1990) Partition coefficients for calcic plagioclase: implications for Archean anorthosites, *Geochimica et Cosmochimica Acta,* V. 54, pp. 1639-1654

Pinarelly, L., Boriani, A. And Del Moro, A. (1993) The Pb isotopic systematics during crustal contamination of subcrustal magmas: the Herchynian magmatism in the Serie dei Laghi (Southern Alp, Italy), *Lithos*, V. 31, pp. 51-61

Poli, S. and Schmidt, M.W. (1992) A comment on "Calcic amphibole equilibria and a new amphibole-plagioclase geothermometer" by J.D. Blundy and T.J.B. Holland (Contrib Mineral Petrol (1990) 104: 208-224), *Contrib. Mineral. Petrol.* V. 111, pp. 273-282

Powell, R. (1984) Inversion of the assimilation and fractional crystallisation (AFC) equations; characterization of contaminants from isotope and trace element relationships in volcanic suites, *Journal of. Geological. Society of London*, V. 141, pp. 447-452

Powell, R. and Powell, M. (1977) Plagioclase-alkali feldspar geothermometry revisited, *Mineralogy Magasine*, V. 41, pp. 253-256

Rathur, Q. (1966) Pasinler-Horasan (Erzurum) sahasına ait genel jeolojik rapor, *M.T.A. Report*, No. 4168 (unpublished), Ankara-Turkey

Ray, G.L., Shimuzu, N. and Hart, S.R. (1983) An ion microprobe study of the partitioning of trace elements between clinopyroxene and liquid in the system diopside-albite-anorthite, *Geochimica et Cosmochimica Acta,* V. 47, pp. 2131-2140

Richard, L.R. and Clarke, D.B. (1990) AMPHIBOL: a program for calculating structural formulae and for classifying and plotting chemical analyses of amphiboles, *American Mineralogist*, V. 75, pp. 421-423

Ringwood, A.E. (1974) The petrological evolution of island arc system, *J. Geol. Soc. London*, V. 130, pp. 183-204

Rock, N.M.S. and Leake, B.W. (1984) The international Mineralogical Association amphibole nomenclature scheme: computerasation and its consequences, *Mineralogical Magasine*, V. 48, pp. 211-227

Robertson, A.H.F. and Aktaş, (1984) The Maden Complex, SE Turkey: evolution of a neotethyan active margin, In *The Geological Evolution of the Eastern Mediterranean* (AHF. Robertson and J.E. Dixon eds.), Blackwell, Oxford, pp. 375-402

Rollinson, H. (1993) *Using geochemical data: evaluation, presentation, interpretation*, Longman Scientific & Technical, New York, p. 344

Romick, J.D., Kay, S.M. and Kay, R.W. (1992) The influence of amphibole fractionation on the evolution of calc-alkaline andesite and dacite tephra from the central Aleutians, Alaska, *Contributions to Mineralogy and Petrology*, V. 112, pp. 101-118

Ross, M. and Huebner, J. S. (1979) Temperature-composition relationship between naturally occurring augite, pigeonite, and orthopyroxene at one bar pressure, *American Mineralogist*, V. 64, pp. 1133-1155.

Rutherford, M.J. and Johnson, M.C. (1992) Comment on Blundy and Holland's (1990) "Calcic amphibole equilibria an a new amphibole-plagioclase geothermometer", *Contributions to Mineralogy and Petrology*, V. 111, pp. 266-268

Ryerson, F. J. and Hess, P.C. (1978) Implications of liquid-liquid distribution coefficients to mineral-liquid partitioning, *Geochimica et Cosmochimica Acta*, V. 42, pp. 921-932

Salters, V.J.M., Hart, S.R. and Panto, G.Y. (1988) Origin of late Cenozoic volcanic rocks ofthe Carpatian Arc, Hungary, *Ibid.*, pp. 279-292

Saxena, S. K. (1976) Two-pyroxene geothermometer: a model with an approximate solution, *American Mineralogist*, V. 61, pp. 643-652.

Schmidt, W.S (1992) Amphibole composition in tonalite as a function of pressure: an experimental calibration of the Al-in-hornblende barometer, *Contribitions to Mineralogy and Petrology*, V. 110, pp. 304-310

Schnetzler, C.C. and Philpotts, J.A. (1968) Partition coefficients of rare-earth elements an barium between igneous matrix material and rock forming mineral phenocrysts-I. In: *Origin and Distribution of the Elements* (L.H. Ahrens, ed.) pp. 929-938, Oxford: Pergamon.

Schnetzler, C.C. and Philpotts, J.A. (1970) Partition coefficients of rare-earth elements between igneous matrix and rock-forming mineral phenocrysts-II, *Geochimica et Cosmochimica Acta,* V. 34, pp. 331-340

Schock, H.H. (1977) Trace element partitioning between phenocrysts of plagioclase, pyroxenes and magnetite and its host pyroclastic matrix, *J. Rad. Chem.*, V. 38, pp. 974-981

Schock, H.H. (1979) Distribution of rare-earth and other trace elements in magnetites, *Chemical Geology*, V. 26, pp. 119-133

Seck, H.A. (1971) Der Einfluß des Drucks auf die Zusammensetzung koexistierender Alkalifeldspäte und Plagioclase im System $NaAlSi_3O_8$-$KAlSi_3O_8$-$CaAl_2Si_2O_8$-H_2O, *Contributions to Mineralogy and Petrology*, V. 31, pp. 67-86

Seymen, I. (1975) Kelkit vadisi kesiminde Kuzey Anadolu fay zonunun tektonik ozelligi, I.T.U. Maden Fakultesi Yay., pp. 192, Istanbul, Turkey.

Seymen, I. And Aydın, A. (1972) The Bingöl earthquake fault and its relation to North Anatolian Fault Zone, *Bulletion of Mineral Research and Exploration Institute*, Ankara, V. 79, pp. 1-8

Shannon R. D. (1976) Revised effective ionic radii and systematic studies of interatomic distances in halides and chalcogenides, *Acta Cryst.*, A, V. 32, pp. 751-767

Shaw, D.M. et al. (1967) An estimate of the chemical composition of the Canadian Precambrian Shield, *CJES*, V. 4, p. 829

Shelley, D. (1993) Igneous and metamorphic rocks under the microscope; classification, textures, microstructures and mineral preferred orientations, Chapman & Hall, London

Sisson, T.W. (1991) Pyroxene-high rhyolite trace element partition coefficients measured by ion microprobe, *Geochimica et Cosmochimica Acta,* V. 55, pp. 1575-1585

Smith and Leeman (1987)

Sparks, R. S. J. and Walker, G. P. L. (1977) The significance of vitric-enriched air-fall ashes associated with crystal-enriched ignimbrites, *Journal of Volcanology and Geothermal Research*, V. 2, pp. 329-341

Spear, F.S. (1981) An experimental study of hornblende stability and compositional variability in amphibole, *American Journal of Science*, V. 281, pp. 697-734

Stacey, J.S. and Kramers, J.D. (1975) Approximation of terrestrial lead isotope evolution by a two-stage model, *Earth and Planetary Science Letters*, V. 26, pp. 207-221

Stix, J. and Gorton, M.P. (1990) Variations in trace element partition coefficients in sanidine in the Cerro Toledo rhyolite, Jemez Mountains, New Mexico: effects of composition, temperature, and volatiles, *Geochimica et Cosmochimica Acta*, V. 54, pp. 2697-2708

Stormer, J.C. and Carmichael, I.S.E. (1970) The Kundo-Weill plagioclase geothermometer and porphyritic acid glasses, *Contribution to mineralogy and Petrology*, V. 28, pp. 306-309

Stormer, J.C. JR. (1975) A practical two-feldspar geothermometer, *American Mineralogist*, V. 60, pp. 667-674

Sun S. S., Tatsumoto, M. and Schilling, J. -G.(1975) Mantle plume mixing along the Reykjanes Ridge axis: lead isotopic evidence, *Science*, V. 190, pp. 143-149

Sun, C.O., Williams, R.J. and Sun, S.S. (1974) Distribution coefficients of Eu and Sr for plagioclase-liquid and plagioclase-liquid equilibria in oceanic ridge basalt: an experimental study, *Geochimica et Cosmochimica Acta*, V. 38, pp. 1415-1433

Sun, S.S. and Hanson, G.N. (1976) Rare earth element evidence for differentiation of McMurdo Volcanics, Ross Island, Antarctica, *Contribitions to Mineralogy and Petrology*, V. 54, pp. 139-155

Sun, S.S. and McDonough, W.F. (1989) Chemical and isotopic systematics of oceanic basalts: implications for mantle composition and processes: In *Magmatism in Ocean Basins* (A.D. Saunders and M.J. Norry eds.), Geological Society of London Special Publications, V. 42, pp. 313-345

Sungurlu, O. (1967) Erzurum-Hınıs bölgesinin 1/25.000 ölçekli Erzurum J47-b_3-b_4 paftalarına ait jeolojik detay petrol etüdü raporu, *M.T.A. Report*, No. 4176 (unpublished), Ankara-Turkey

Sungurlu, O. (1971) 1/50.000 scale geological maps of NE Anatolia, TPAO's archive, unpublished

Sungurlu, O. (1972) 1/50.000 scale geological maps of NE Anatolia, TPAO's archive, unpublished

Şahintürk, Ö. and Erakman, B. (1978) Kağızman-Tuzluca-Ağrı civarının jeolojisi ve hidrokarbon olanakları ön raporu, TPAO Arama Grubu Başkanlığı, 4. Bölge Arama Müdürlüğü, unpublished report

Şahintürk, Ö. And Kasar, S. (1980) Tercan-Çayırlı baseninin jeolojisi ve hidrokarbon olanakları, TPAO Arama Grubu Başkanlığı, 4. Bölge Arama Müdürlüğü, unpublished report no: 1446

Şaroğlu, F. and Yılmaz, Y. (1987) Geological evolution and basin models during neotectonic episode in Eastern Anatolia, reprinted from *Bulletin of the Mineral Research and Exploration*, No. 107, pp. 62-83, Ankara-Turkey

Şaroğlu, F. and Yılmaz, Y. (1987). Geological evolution and basin models during neotectonic episode in the Eastern Anatolia, Reprinted from Bull. Mineral. Res. Explor. Turkey, 107

Şaroğlu, F., Güner, Y., Kidd. W.S.F. and Şengör, A.M.C. (1980) Neotectonics of Eastern Turkey: new evidence for crustal shortening and thickening in a collision zone, *EOS, Transactions of American Geophysical Union*, V. 61, pp. 360 (Abstract)

Şenalp, M. (1966) Erzurum-Muş bölgesi1/25.000 ölçekli Erzurum J47-a_2, J47-b_1 ve Karaköse J48-c_1, c_2, a_3, c_4, J48-b_3 paftalarının detay petrol etüdü, *M.T.A. Report*, No. 4288 (unpublished), Ankara-Turkey

Şengör, A. M. C. & Yılmaz, Y. (1981) Tethyan evolution of Turkey : a plate tectonic approach, *Tectonophysics*, V. 75, pp. 181-241.

Şengör, A. M. C. (1980) Principles of the Neotechtonism of Turkey, *Publication of DSI*, Ankara

Şengör, A. M. C. and Yılmaz, Y. (1981). Tethyan evolution of Turkey : a plate tectonic approach, *Tectonophysics*, 75, pp. 181-241.

Şengör, A.M.C. and Kidd, W.S.F. (1979) Post-collisional tectonics of the Turkish-Iranian Plateau and a comparison with Tibet, *Tectonophysics*, V. 55, pp. Pp. 361-376

Şengör, A.M.C., Görür, N. and Şaroğlu, F. (1985) Strike-slip faulting and related basin formation in zones of tectonic escape. Turkey as a case study.

In: *Strike-Slip Deformation, Basin Formation and Sedimentation, SEMP Special Publicatios*

Tanoğlu, A. (1947) Zones d'altitute de la Turkuie: détermination et interprétation, Türk Coğrafya Dergisi, V. 3, pp. 37-55

Tanrıverdi, K. (1971) Erzurum (Söylemez) yöresinin jeolojisi ve petrol olanakları, *M.T.A. Report*, No. 6239 (unpublished), Ankara-Turkey

Taylor, H. P. (1980) The effects of assimilation of country rocks by magmas on $^{18}O/^{16}O$ and $^{87}Sr/^{86}Sr$ systematics in igneous rocks, *Earth and Planetary Science Letters*, V. 47, pp. 243-254

Taylor, S.R. and McClennan, S.M. (1985) The continental crust: its composition and evolution, Geoscience Texts, p. 312, *Blackwell Scientific Publications*, London

Tokel, S. (1985) Erzurum-Kars yöresinde Neojen çöküntüsü ile ilgili volkanizmanın incelenmesi, *unpublished thesis for the degree of Associated Proffessorship*, Karadeniz Technical University, 106 p., Trabzon-Turkey

Tokel, S. (1985) Mechanism of crustal deformation and petrogenesis of the Neogene volcanics in East Anatolia, special publication of *Turkiye Jeoloji Kurumu*, Ketin Symposium, (T. Ercan and M.A. Caglayan eds.), pp. 121-130, Ankara-Turkey

Tokel, S. And Ercan, T. (1992) Distinctive geochemical characteristics of post-collision volcanism in Anatolia: slab-mantle interactions, *Abstracts of the 45th Geological Congress of Turkey*, Chambers of Geological Engineers of Turkey (Abstract)

Toker, S. (1965) Erzurum-Hasankale bölgesi, Erzurum I46-b_2, Tortum H46-c_3 paftalarına ait jeolojik rapor, *M.T.A. Report*, No. 4118 (unpublished), Ankara-Turkey

Tourrette, T.Z., Burnett, D.S. and Bacon, C.R. (1991) Uranium and minor-element partitioning in Fe-Ti oxides and zircon from partially melted granodiorite, Crater lake, Oregon, *Geochimica et Cosmochimica Acta*, V. 55, pp. 457-469

Tsuchiyama, A. (1985) Dissolution kinetics of plagioclase in the melt of the system diopside-albite-anorthite, and origin of dusty plagioclase in andesite, *Contribution to Mineralogy and Petrology*, V. 89, pp. 1-16

Turcotte, D.L. (1983) Mechanism of crustal deformation, Journal of Geological Society of London, V. 140, pp. 701-724

Tütüncü, K. (1966) Erzurum ovası kuzey ve güneyinin genel jeolojisi ve petrol imkanları, *M.T.A. Report*, No. 4297 (unpublished), Ankara-Turkey

Tütüncü, K. (1967) 1/25.000 ölçekli Erzurum J47-c_1, c_2, c_3 and c_4 paftalarına ait genel jeoloji ve petrol imkanları, *M.T.A. Report*, No. 4120 (unpublished), Ankara-Turkey

Villemant, B. Jaffrezic, H., Joron, J.L. and Treuil, M. (1981) Distribution coefficients of major and trace elements; fractional crystallisation in the alkali basalt series of Chaine des Puys (Massif Central, France), *Geochimica et Cosmochimica Acta,* V. 45, 1997-2016

Vollmer, R. (1976) Rb-Sr and U-Th-Pb systematics of alkaline rocks: the alkaline rocks from Italy, *Geochim. Cosmochim. Acta*, V. 40, pp. 283-295

Watson, E.B. (1976) Two-liquid partition coefficients: experimental data and geochemical implications, *Contribution to mineralogy and Petrology*, V. 56, pp. 119-134

Watson, E.B. and Harrison, T.M. (1983) Zircon saturation revisited: temperature and composition effects in a variety of crustal magma types, *Earth and Planetary Science Letters*, V. 64, pp. 295-304

Watson, E.B. and Ryerson, F.J. (1986) Partitioning of zirconium between clinopyroxene and magmatic liquids of intermediate composition, *Geochimica et Cosmochimica Acta,* V. 2523-2526

Wells, P. R. A. (1977) Pyroxene thermometry in simple and complex systems. *Contribution to Mineralogy and Petrology*, V. 62, pp. 129-139.

White, A. J. R. (1964) Clinopyroxenes from eclogites and basic granulites. *Am. Mineral.* V. 49, pp. 883-888.

Whittaker, E.J.W. and Muntus, R. (1970) Ionic radii for use in geochemistry, *Geochimica et Cosmochimica Acta,* V. 34, pp. 945-958

Wilson, M. (1989) *Igneous petrogenesis: a global tectonic approach*, Unwin Hymen, London, p. 466

Wilson, M. and Downes, H. (1991) Tertiary-Quaternary extension related alkaline magmatism in Western and Central Europe, *Journal of Petrology*, V. 32, pp. 811-849

Wolff, J.A. (1984) Variation in Nb/Ta during differentiation of phonolitic magma, Tenerife, Canary Islands, *Geochimica et Cosmochimica Acta,* V. 48, pp. 1345-1348

Wood, B. and Banno, S. (1973) Garnet-orthopyroxene and orthopyroxene-clinopyroxene relationship in simple and complex systems, *Contribution to mineralogy and Petrology*, V. 42, pp. 109-124.

Wörner, G., Beusen, J.-M., Duchateau, N., Gijbels, R. and Schmincke, H.-U. (1983) Trace element abundances and mineral-melt distribution coefficients in phonolites from the Laacher See Volcano (Germany), *Contribitions to Mineralogy and Petrology*, V. 84, pp. 152-173

Yılmaz, A., Terlemez, İ. And Uysal, Ş. (1988) Geological characteristics and structural evolution of the ophiolitic units around Sakaltutan Dağı (Erzurum), *METU. Journal of Pure and Applied Sciences*, V. 21, No: 1-3, pp. 221-235

Yılmaz, Y. (1984) Magmatic activity in the geological history of Turkey and its relation to tectonic evolution, special publication of *Turkiye Jeoloji Kurumu*, Ketin Symposium, (T. Ercan and M.A. Caglayan eds.), pp. 63-81, Ankara-Turkey

Yılmaz, Y., Şaroğlu, F. And Güner, Y. (1987) Initiation of the neomagmatism in East Anatolia, *Tectonophysics*, V. 134, pp. 177-199

Yılmaz, Y., Şaroğlu, F. And Güner, Y. (1987). Petrogenetic study of Solhan (Mus) volcanites, Eastern Anatolia, Bull. Earth Sci. Applic. Res. Centre Hacettepe Univ., 14, 133-163.

Yılmaz, Y. (1985). Magmatic activity in the geological history of Turkey and its relation to tectonic evolution, T. J. K. Ketin Symposium.

Yoder, H. S. and Tilley, C. E. (1962) Origin of basalt magmas: an experimental study of natural and synthetic rock systems. *J. Petrol.* V. 3, pp. 342-532.

Zindler, A., Jagoutz, E., Rosenbaum, J. And Rubenstone, L. (1988) Trace element and isotope systematics in mantle minerals, *Geological Society of America Abstracts Denver*, no. 26084, A31

APPENDIX A

Table showing radiometric dating results of samples from the Erzurum-Kars Plateau. These results were obtained from a conventional potassium-argon method by Dr. J. G. Mitchell at the University of Newcastle. For correlation of dating results between sections on the plateau, see Figure 5.1.

	Sample no	Location	Unit	Stratigraphic position	Lithology	K_2O wt.%	Radiogenic ^{40}Ar (mm^3g^{-1})	% Atmos.	Age Ma ±1σ
1	MK29	Mt. Dumlu, Güngörmez village, Dumlusuyu valley	The Güngörmez andesite/dacite	mid	dacite	2.52±0.01	(4.61±0.08).10^{-4}	42.5	5.66±0.10
3	MK50	Mt. Dumlu, Karaçağıl vicinity	The Güngörmez andesite/dacite	mid	dacite	2.45±0.02	(4.65±0.08).10^{-4}	57.0	5.87±0.11
2	MK259	Mt. Dumlu	The Güngörmez andesite/dacite	lower	dacite	2.38±0.02	(5.03±0.10).10^{-4}	52.9	6.54±0.14
5	MK61	Mt. Kargapazarı, N of Haykürt village, Sarıcakaya hill	The Kargapazarı volcanics	top	andesite	2.56±0.01	(4.74±0.18).10^{-4}	89.3	5.73±0.22
6	MK12	Mt. Kargapazarı, Kösk village	The Güngörmez andesite/dacite	base	andesite	2.09±0.01	(4.59±0.14).10^{-4}	72.6	6.79±0.21
4	MK84	Mt. Kargapazarı	The Güngörmez andesite/dacite	base-mid	dacite	2.86±0.04	(6.79±0.15).10^{-4}	35.0	7.34±0.19
9	MK347	NW of Pasinler, Büyükdere gorge	The White ignimbrite	base	rhyolite	4.77±0.02	(8.63±0.16).10^{-4}	69.5	5.60±0.11
7	MK117	NE of Pasinler, Harabedere gorge	The Black dacite	base	andesite	2.45±0.01	(6.20±0.09).10^{-4}	41.7	7.83±0.12
10	MK377	S of Pasinler, S of Ortuzu village	The Miocene Tuzluyolları dacite	basement	dacite	3.19±0.01	(2.38±0.05).10^{-4}	69.8	23.0±0.5
8	MK343	NE of Pasinler, Harabedere gorge	The Eocene Kışlaköy volcanics	basement	BaTracAnd	2.83±0.03	(3.55±0.05).10^{-4}	24.1	38.5±0.7
11	MK134	N of Horasan, Yeniköy village	The Horasan plateau layer	top	dacite	2.52±0.04	(3.37±0.16).10^{-4}	90.1	4.14±0.21
14	MK145	E of Horasan, Uzungazi (Kızıl) village	The Aladağ andesite	top	andesite	2.01±0.01	(2.98±0.12).10^{-4}	86.8	4.59±0.19
12	MK138	N of Horasan, Karaurgan town	The Kötek basalt	base	BaAnd	1.166±0.004	(3.75±0.15).10^{-4}	74.8	9.94±0.40
13	MK144	N of Horasan	The Kötek basalt	base	basalt	0.979±0.005	(3.52±0.15).10^{-4}	83.3	11.1±0.5
15	MK147	Mt. Aladağ, between Kalebaşı and Odalar villages	The Aladağ andesite	top	andesite	2.51±0.02	(2.88±0.10).10^{-4}	72.8	3.55±0.13
17	MK175	NE of Kağızman, N of Örmeli village	The Kars plateau layer	top	BaTracAnd	1.65±0.02	(1.45±0.05).10^{-4}	72.8	2.72±0.10
16	MK162	N of Kağızman, Paslı village	The Kars plateau layer	top	BaAnd	1.321±0.009	(1.45±0.04).10^{-4}	89.3	3.40±0.10
18	MK169	N of Kağızman	The Çukurayva rhyolite	base	TracDac	3.32±0.01	(5.53±0.21).10^{-4}	87.5	5.15±0.20

APPENDIX B: Sample preparation and analytical procedure

APPENDIX B

A. PREPERATION OF THE SAMPLES FOR ANALYSES

1. Powdered sample preparation

Bulk-rock samples were first cut by a diamond-saw into slices, cleaned with water to remove soil and dried with paper towels. Then representative and freshest ones of these slices were selected. After that, their weathered outer surface, some secondary mineral fill and vains and also hammer and saw marks on these slices were carefully trimmed from the samples using the same diamond-saw. After this stage they were cleaned by water and dried with paper towel again. Then they were broken into small pieces which were approximately 1-5 mm in size by using the jaw-crusher (Fritsch Pulverisette jaw crusher; type 01-704). To avoid contamination of the next sample, the jaw-crusher was cleaned by wire brush and alcohol prior to each session of crushing. A fraction of this material was put into the agate-ball grinding mill and powdered for aroun 15-20 minutes. Then powdered samples were put into the bags, labelled and stored in a dry place. Special care was taken in washing and drying the grinding bowls and balls to avoid contamination.

1. Preparation of pressed powder pellets

Before starting the preperation, powdered rock samples were shaked well to homogenise the possible grain fractions e.g. heavy minerals which might differ in density. Previously dried 6-7 g of powdered samples were mixed thoroughly with around 8-11 drops of Mowiol binding agent (2% aqueous solution of PVA) in glass beakers by using a glass rod until an even consistency is obtained. Then they were compressed in a stainless steel mould between a pair of polished steel discs using a hydraulic press at 5-7 tons. After this stage pellets were labelled and finally dried in an oven at 80-100°C prior to analysis.

2. Determination of loss on ignition

4-5 g of the sample powder from each sample was placed in 10 ml glass vial and labelled. These powders were than dried at 110°C for over 1 hour to remove surface water. They are then stored in a dessicator. After cooling plastic snap tops were put on the vials to avoid sample loss through spillage and surface water which might be gained from the atmosphere.

About 4 g from each sample was weighted and put into the porcelain crucibles. Ignitions were performed as batchs of 12 crucibles at 900°C for two hours. After allowing samples to cool in a dessicator they were reweighted and eventually their loss

on ignition was calculated from the difference in the weight. At this stage, the ignited powders were placed in 10 ml glass vials with plastic snap-tops and labelled.

3. Preparation of fused-disks

Before making fusion discs the flux (lithium tetraborate: Johnson Mathey Spectroflux 100B) was dried in the furnace overnight at 600°C to remove any absorbed water or any other volatiles taken up from the atmosphere. Dried flux was stored in a dessicator during the fused disc preparation. Previously ignited samples were dried in the oven at 110°C and just before preparation they were taken from the oven as batches of 4 samples and stored in another dessicator until they were cool. Then 0.45 g of sample and 2.25 g of flux (a proprtion of 1:5) were mixed extensively by using a glass rod and these mixtures were transferred into the 5% Au/Pt crucibles, covered with Pt lids and placed on a silica tray in the furnace at 1050°C. After 20 minutes, samples were poured into the graphite moulds which are surrounded by the stainless steel cylinder on a hot plate at 220°C immediately after swriling molten glass material a few times with a pair of platin tipped tongs to ensure a proper mixing. By carefully inserting a stainless steel plunger (also at 220°C) onto the globule of molten glass, fusion discs were made. After cooling on a cooling block, they were trimmed off any access glass with a pair of small pliers, labelled with self adhesive labels with sample numbers on back of disks (i.e. side in contact with graphite), bagged and stored in a dessicator. Special care was taken in keeping analytical surface of disks clean and cleaning the Pt/Au crucibles in hot 50% HCl for about over 20 minutes after the preparation of each batch to remove any remaining traces of glass to avoid cross contamination.

B. ANALYTICAL WORK

1. XRF ANALYSIS

X-Ray Fluorescence (XRF) analysis was carried out on a Philips PW 1400 Spectrometer with a Rhodium anode tube and an automatic loader at the University of Durham. A total of 350 samples were analysed both on pressed powder pellets and fusion discs for trace (Rb, Sr, Ba, Zr, Y, Nb, Sc, Cr, V, Ni, Zn, Cu, Co, Ga, Ce, Nd, La, Th, Pb) and major elements (SiO_2, TiO_2, Al_2O_3, Fe_2O_3, MnO, MgO, CaO, Na_2O, P_2O_5) respectively. A number of about 30 international standards covering a broad compositional range from basalts to acidic rocks were run and used as calibration standards. Three of these standards and also three samples were run repeatedly as unknowns after every 36 samples throughout analytical work to monitor drift and between run variations. Then analytical accuracy and precision were calculated by

using standards and these samples (Appendix C). Recommended values for the standards were taken from Govindaraju (1989).

2. ICP-MS ANALYSIS

A subset of trace and rare-earth elements including Rb, Sr, Y, Zr, Nb, Cs, Ba, La, Ce, Pr, Nd, Sm, Eu, Gd, Tb, Dy, Ho, Er, Tm, Yb, Lu, Hf, Ta, W, Pb, Th and U was analysed by Inductively Coupled Plasma Mass Specrtometer (ICP-MS) on VG Elemental Plasma Quad device at Industrial Research Laboratories of the University of Durham (UDIRL).

2.1. ICP-MS SAMPLE PREPARATION

Small amount of powdered rock samples were put into the labelled glass containers in an oven at 105°C overnight to dry. Savillex teflon capsules were cleaned by rinsing with deionised water and then leaving them filled with 2 ml Aristar concentrated HNO_3 on the hot plate at 140°C for at least two hours. After following the same procedure twice capsules dried in the oven at 100°C and then numbered. A powder aliquot of 0.1±0.001g was weighed out from each sample and transferred into the capsule. Special care was taken in using anti-static gun to prevent powder sticking to the sides of the capsules and subsequent spillage. In addition to the samples, 6 international standards and also two blanks were prepared. After that, 1 ml Aristar HNO_3 and 4 ml 48% HF were added into the capsules respectively, their caps were closed tightly and the samples were left in the acid on the hot-plate at about 130°C for about two days for complete digestion. At the end of this period the samples were evaporated on the hot-plate to dryness in order to remove HF acid from the system and to allow the formation of nitrate salts. After completing evaporation, 1 ml HNO_3 was edded to the capsules and evaporated again. This procedure was followed twice. Then 2.5 ml HNO_3 and 20 ml deionised water were put into the capsules, their lids were closed and boiled for over one hour to dissolve salts. The solutions were allowed to cool, checked for any solid residue and spiked with 1.25 ml of 2 ppm Rh, Re and Bi internal standard spike solution when they were still in the capsules. After this stage they were transferred into the 50 ml polypropylene volumetric flasks and made up accurately to 50 ml with deionised water. In this case internal standard element concentrations in sample solution became 50 ppb. Finally all the solutions were transferred into the polypropylene containers and kept in a cool and dark place prior to analysis. Two reagent blank samples were prepared with each batch of sample.

The machine was calibrated using solutions of known elemental concentrations. Correction for drift was achieved by analysing a drift monitor every six samples.

3. ANALYTICAL PROCEDURES OF THE ISOTOPE ANALYSIS

Pb, Sr and Nd were extracted on the same dissolution using approximately 100-200 mg of powder of the rock samples. After dissolution using approximately 1 ml of HNO_3 combined with 3 to 5 mls of HF, residues were converted to nitrate and finally chloride; 1 ml of 1M HBr was then added to the residue. Pb was seperated by passing the sample through colums prepared from PVP disposable pipette tips fitted with a 2 mm diameter polyethylene frit and containing Dowex 1 x 8 200-400 mesh resin; completely new colums were prepared for each sample to minimise the Pb blank. The Sr and Nd fractions were collected in 2 mls of 1M HBr and Pb collected in 1 ml of 6M HCl. Sr and Nd were purified using standard one and two-column cation exchange techniques, respectively. Sr and Pb were run as the metal species on single Ta and single Re filaments, respectively, using a Finnegan MAT 262 multicollector mass spectrometer at the NERC Isotope Geosciences Laboratory (NIGL); Nd was run as the metal species on triple Re-Ta filament assemblies using a VG354 multicollector mass spectrometer, also located at NIGL. Blanks for Sr and Pb were less than 800pg and 250pg respectively. Reference standards throughout the course of analysis averaged values of $^{87}Sr/^{86}Sr = 0.710208 \pm 44$ (2σ) for the NBS987 standard, $^{143}Nd/^{144}Nd = 0.511109 \pm 42$ (2σ) for the Johnson Matthey Nd standard. $^{87}Sr/^{86}Sr$ was normalised to $^{86}Sr/^{88}Sr = 0.1194$; $^{143}Nd/^{144}Nd$ was normalised to a value of $^{146}Nd/^{144}Nd = 0.7219$. Pb mass fractionation was 0.09 % per a.m.u. Based on repeated runs of NBS981 common Pb standard, the reproducibility is better than ± 0.1 %. Pb isotopic ratios were corrected relative to the average standard Pb isotopic compositions of Todt et al (1984). Internal errors on individual isotope measurements were always much smaller than the standard reproducibility reported here, and therefore the ability to reproduce the standards should be taken as the imiting factor in interpreting the uncertainity of any given analysis.

UNIV DURHAM

APPENDIX C: Accuracy and precision of analytical data

APPENDIX C-1: Error calculations of XRF major element data

XRF ERROR CALCULATIONS OF MAJOR ELEMENTS

		QLO-1	AGV-1	G-2	W-2	SY-2	G-1	GSP-1	T-1	NIM-S	± standard error
SiO2	*recommended*	**65.55**	**58.79**	**69.08**	**52.44**	**60.05**	**72.44**	**67.15**	**62.7**	**63.63**	*0.57*
	1st. run	65.88	59.72	70.07	52.01	60.21	72.54	66.45	63.71	63.71	
	2nd	66.14	59.71	69.23	51.89	60.08					
	3th	65.86	59.52	69.52	51.71						
	4th	66.24	60.13	69.77	52.35						
	5th	65.67	59.51	69.00	52.57						
	6th	65.39	60.21		52.24						
	7th	65.80	60.02								
	8th	65.73	59.90								
	9th	65.59	59.88								
	10th	65.95	59.96								
	11th	65.53	59.83								
	standard dev.	*0.25*	*0.23*	*0.42*	*0.32*	*0.09*					
TiO2	*recommended*	**0.624**	**1.05**	**0.48**	**1.06**	**0.14**	**0.27**	**0.65**	**0.58**	**0.044**	*0.01*
	1st. run	0.61	1.05	0.50	1.07	0.15	0.26	0.66	0.58	0.06	
	2nd	0.61	1.07	0.48	1.05	0.14					
	3th	0.61	1.06	0.49	1.07						
	4th	0.61	1.06	0.49	1.06						
	5th	0.61	1.07	0.49	1.07						
	6th	0.61	1.08		1.05						
	7th	0.62	1.09								
	8th	0.61	1.07								
	9th	0.61	1.06								
	10th	0.63	1.09								
	11th	0.61	1.07								
	standard dev.	*0.01*	*0.01*	*0.01*	*0.01*	*0.01*					
Al2O3	*recommended*	**16.18**	**17.14**	**15.38**	**15.35**	**12.04**	**14.22**	**15.1**	**16.69**	**17.34**	*0.17*
	1st. run	16.27	17.32	15.82	15.44	12.15	14.39	14.93	16.67	17.35	
	2nd	16.53	17.42	15.42	15.36	12.19					
	3th	16.38	17.16	15.67	15.41						
	4th	16.30	17.57	15.61	15.07						
	5th	16.40	17.36	15.42	15.07						
	6th	16.34	17.35		15.20						
	7th	16.59	17.51								
	8th	16.31	17.42								
	9th	16.37	17.34								
	10th	16.40	17.31								
	11th	16.36	17.38								
	standard dev.	*0.10*	*0.11*	*0.17*	*0.17*	*0.03*					
Fe2O3	*recommended*	**4.287**	**6.726**	**2.676**	**10.661**	**6.346**	**1.927**	**4.324**	**5.878**	**1.4**	*0.05*
	1st. run	4.34	6.81	2.71	10.87	6.34	1.94	4.33	5.98	1.48	
	2nd	4.37	6.91	2.69	10.86	6.32					
	3th	4.36	6.89	2.70	10.89						
	4th	4.37	6.89	2.72	10.87						
	5th	4.37	6.90	2.70	10.87						
	6th	4.37	6.91		10.83						
	7th	4.37	6.90								
	8th	4.36	6.87								
	9th	4.36	6.88								
	10th	4.41	6.98								
	11th	4.36	6.89								
	standard dev.	*0.02*	*0.04*	*0.01*	*0.02*	*0.01*					
MnO	*recommended*	**0.093**	**0.092**	**0.032**	**0.163**	**0.32**	**0.028**	**0.04**	**0.1**	**0.01**	*0.01*
	1st. run	0.09	0.10	0.03	0.17	0.32	0.03	0.04	0.10	0.01	
	2nd	0.09	0.10	0.03	0.17	0.31					
	3th	0.09	0.10	0.03	0.17						
	4th	0.09	0.10	0.03	0.17						
	5th	0.09	0.10	0.03	0.17						
	6th	0.09	0.10		0.17						
	7th	0.09	0.10								
	8th	0.09	0.10								
	9th	0.09	0.10								
	10th	0.09	0.10								
	11th	0.09	0.10								
	standard dev.	*0.00*	*0.00*	*0.00*	*0.00*	*0.01*					

XRF ERROR CALCULATIONS OF MAJOR ELEMENTS

		QLO-1	AGV-1	G-2	W-2	SY-2	G-1	GSP-1	T-1	NIM-S	± standard error
MgO	***recommended***	**1**	**1.53**	**0.75**	**6.37**	**2.69**	**0.36**	**0.96**	**1.89**	**0.46**	***0.08***
	1st. run	1.28	1.76	0.80	6.47	2.77	0.33	0.95	1.88	0.53	
	2nd	1.09	1.64	0.75	6.41	2.72					
	3th	1.06	1.60	0.74	6.51						
	4th	1.09	1.59	0.74	6.35						
	5th	1.05	1.59	0.73	6.30						
	6th	1.08	1.62		6.27						
	7th	1.05	1.58								
	8th	1.03	1.55								
	9th	1.04	1.55								
	10th	1.09	1.57								
	11th	1.03	1.56								
	standard dev.	*0.07*	*0.06*	*0.03*	*0.10*	*0.04*					
CaO	***recommended***	**3.17**	**4.94**	**1.96**	**10.87**	**7.96**	**1.37**	**2.07**	**5.08**	**0.68**	***0.04***
	1st. run	3.21	4.95	2.01	10.97	8.11	1.31	2.04	5.19	0.73	
	2nd	3.26	5.04	1.96	10.91	8.07					
	3th	3.24	5.02	1.97	10.97						
	4th	3.26	5.01	1.99	10.93						
	5th	3.25	5.01	1.98	10.95						
	6th	3.25	5.05		10.89						
	7th	3.26	5.06								
	8th	3.23	4.99								
	9th	3.24	5.01								
	10th	3.18	5.03								
	11th	3.22	5.01								
	standard dev.	*0.03*	*0.03*	*0.02*	*0.03*	*0.03*					
Na2O	***recommended***	**4.2**	**4.26**	**4.08**	**2.14**	**4.31**	**3.33**	**2.8**	**4.39**	**0.43**	***0.10***
	1st. run	4.25	4.45	4.22	2.26	4.33	3.25	2.62	4.50	0.32	
	2nd	4.00	4.27	4.04	2.07	4.31					
	3th	4.01	4.31	4.05	2.14						
	4th	4.15	4.27	4.17	2.11						
	5th	4.10	4.30	4.09	2.10						
	6th	4.09	4.36		2.04						
	7th	4.09	4.31								
	8th	4.05	4.22								
	9th	4.03	4.19								
	10th	4.20	4.25								
	11th	4.02	4.21								
	standard dev.	*0.08*	*0.07*	*0.08*	*0.08*	*0.01*					
K2O	***recommended***	**3.6**	**2.91**	**4.48**	**0.627**	**4.44**	**5.5**	**5.51**	**1.24**	**15.35**	***0.03***
	1st. run	3.59	2.93	4.61	0.63	4.55	5.60	5.56	1.24	15.66	
	2nd	3.66	2.98	4.50	0.62	4.53					
	3th	3.63	2.95	4.51	0.63						
	4th	3.67	2.96	4.56	0.62						
	5th	3.66	2.97	4.54	0.63						
	6th	3.66	2.99		0.62						
	7th	3.66	3.00								
	8th	3.64	2.96								
	9th	3.63	2.96								
	10th	3.71	2.97								
	11th	3.64	2.98								
	standard dev.	*0.03*	*0.02*	*0.04*	*0.01*	*0.01*					
P2O5	***recommended***	**0.254**	**0.49**	**0.14**	**0.131**	**0.43**	**0.083**	**0.28**	**0.14**	**0.12**	***0.01***
	1st. run	0.27	0.50	0.15	0.13	0.42	0.09	0.29	0.16	0.12	
	2nd	0.27	0.50	0.14	0.14	0.43					
	3th	0.27	0.49	0.14	0.13						
	4th	0.26	0.50	0.14	0.13						
	5th	0.26	0.51	0.14	0.13						
	6th	0.27	0.49		0.14						
	7th	0.25	0.49								
	8th	0.27	0.50								
	9th	0.27	0.49								
	10th	0.26	0.50								
	11th	0.26	0.50								
	standard dev.	*0.01*	*0.01*	*0.00*	*0.01*	*0.01*					

APPENDIX C-2: Error calculations of XRF trace element data

XRF ERROR CALCULATIONS OF TRACE ELEMENTS

	Apr-92	QUBS3	DNC-1	W-2	BHVO-1	QUBS5	QUBS5	NIM-N	± standard error (ppm)
Sc	*recommended*	**28.7**	**31**	**35**	**31.8**				*1.97*
	1st. run	30.9	32.3	35.1	32.8				
	2nd. run	28.8	29.3	32.2	32.6				
	3th. run	32.9		36.4					
	standard dev.	*2.05*	*2.12*	*2.15*	*0.14*				
Cr	*recommended*	**569**	**285**	**93**	**289**				*4.17*
	1st. run	555.4	280.5	84.8	288.5				
	2nd. run	565.7	282.2	90.3	288.3				
	3th. run	566.6		88.9					
	standard dev.	*6.22*	*1.20*	*2.86*	*0.14*				
V	*recommended*	**302**	**148**	**262**	**317**				*7.69*
	1st. run	294.9	151.9	270.5	307.1				
	2nd. run	291.9	151.2	260.2	316				
	3th. run	297.6		275.4					
	standard dev.	*2.85*	*0.49*	*7.76*	*6.29*				
Ni	*recommended*	**300**	**247**	**70**	**121**				*6.51*
	1st. run	301.6	241.2	66	110				
	2nd. run	312.8	248.1	77.3	121.4				
	3th. run	300.3		69.3					
	standard dev.	*6.87*	*4.88*	*5.81*	*8.06*				
Ga	*recommended*	**20.36**	**15**	**20**	**21**				*1.32*
	1st. run	20	16.5	19	22.3				
	2nd. run	22.4	16.1	17.7	21.7				
	3th. run	21.2		20.4					
	standard dev.	*1.20*	*0.28*	*1.35*	*0.42*				
Rb	*recommended*	**5.3**	**4.5**	**20**	**11**				*3.52*
	1st. run	-0.8	-0.3	20.5	4.7				
	2nd. run	5.7	2.4	20.8	9.9				
	3th. run	4.8		22.7					
	standard dev.	*3.52*	*1.91*	*1.19*	*3.68*				
Sr	*recommended*	**430**	**145**	**194**	**403**				*2.80*
	1st. run	426.9	142.7	191.7	392.7				
	2nd. run	423.4	144.1	194.2	393.1				
	3th. run	424.9		194.7					
	standard dev.	*1.76*	*0.99*	*1.61*	*0.28*				
Y	*recommended*	**23.05**	**18**	**24**	**27.6**				*1.18*
	1st. run	23.4	17.1	24.7	28.6				
	2nd. run	22.3	18.2	21.8	27.2				
	3th. run	22.5		21.4					
	standard dev.	*0.59*	*0.78*	*1.80*	*0.99*				
Zr	*recommended*	**161.8**	**41**	**94**	**179**				*2.46*
	1st. run	162.1	40.5	93.1	173.2				
	2nd. run	162.5	40.7	93.9	171.8				
	3th. run	161.6		92.2					
	standard dev.	*0.45*	*0.14*	*0.85*	*0.99*				
Nb	*recommended*	**5.25**	**3**	**7.9**	**19**				*0.85*
	1st. run	6.4	4.1	7.9	19.1				
	2nd. run	5.2	4.3	8.5	18				
	3th. run	6		7.3					
	standard dev.	*0.61*	*0.14*	*0.60*	*0.78*				
Ba	*recommended*	**145**	**114**	**182**	**139**	**1376**	**1376**	**100**	*5.43*
	1st. run	145.88	120.32	175.33	134.16	1333.62		105.28	
	2nd. run	144.24				1334.78			
	3th. run								
	standard dev.	*1.16*							
La	*recommended*		**3.8**	**11.4**	**15.8**			**3**	*3.21*
	1st. run		-0.72	10.01	14.04			-1.36	
	2nd. run								
	3th. run								
	standard dev.								
Ce	*recommended*	**26.09**	**10.6**	**24**	**39**	**93.6**	**93.6**	**6**	*4.84*
	1st. run	28.88	15.82	26.22	41.05	83.79		8.85	
	2nd. run	31.48				86.48			
	3th. run								
	standard dev.	*1.84*							
Nd	*recommended*	**20**	**4.9**	**14**	**25.2**	**42.16**	**42.16**	**3**	*2.43*
	1st. run	20.5	1.25	14.57	25.62	44.32		-1.78	
	2nd. run	21.74				44.94			
	3th. run								
	standard dev.	*0.88*							

XRF ERROR CALCULATIONS OF TRACE ELEMENTS

	Oct-92	AGV-1	GSP-1	QUBS-3	RGM-1	G-2	± standard error (ppm)
La	***recommended***	**38**	**184**	**9.3**	**24**	**89**	*1.79*
	1st. run	36.44	180.8	8.22	19.9	88.13	
	2nd. run	37.76	182.43	8.58	21.77		
	3th. run	35.54	182.47	9.16	19.77		
	4th. run	37.88					
	standard dev.	*1.12*	*0.95*	*0.47*	*1.12*		
Ce	***recommended***	**67**	**399**	**26.09**	**47**	**160**	*2.87*
	1st. run	63.62	398.25	28.75	44.56	155.18	
	2nd. run	70.37	403.3	23.36	46.11		
	3th. run	69.56	398.46	26.31	44.47		
	4th. run	64.26					
	standard dev.	*3.50*	*2.86*	*2.70*	*0.92*		
Nd	***recommended***	**33**	**196**	**20**	**19**	**55**	*2.36*
	1st. run	33.46	195.76	19.72	18.98	53.16	
	2nd. run	36.28	201.78	17.52	22.46		
	3th. run	35.36	198.88	17.88	16.52		
	4th. run	35.53					
	standard dev.	*1.20*	*3.01*	*1.18*	*2.98*		

XRF ERROR CALCULATIONS OF TRACE ELEMENTS

	Nov-92	*Andesite* **AGV-1**	*Granite* **GS-N**	*Olv. doler.* **QUBS3**	*Tholeiite* **QUBS4**	**± standard error (ppm)**
Co	***recommended***	**15.3**	**65**	**72.2**	**52**	***1.90***
	1st. run	14.05	65.62	69.38	47.44	
	2nd. run	15.82	62.84	71.35	50.66	
	3th. run	16.63	68.51	69.66	49.25	
	4th. run	15.56	64.72	68.76	48.86	
	5th. run	14.05	66.27	73.39	49.27	
	6th. run			70.59	50.7	
	7th. run			69.34		
	standard dev.	*1.14*	*2.08*	*1.60*	*1.22*	
Cu	***recommended***	**60**	**20**	**106**	**76.3**	***2.01***
	1st. run	61.2	19.41	107.46	75.73	
	2nd. run	61.65	19.4	102.99	73.07	
	3th. run	62.27	20.28	107.63	73.98	
	4th. run	62	20.39	107.07	73.97	
	5th. run	63.7	20.5	108.09	73.27	
	6th. run			104.62	73.36	
	7th. run			106.8		
	standard dev.	*0.95*	*0.55*	*1.87*	*0.97*	
Zn	***recommended***	**88**	**48**	**87.7**	**78.4**	***3.90***
	1st. run	84.94	49.46	94.77	83.54	
	2nd. run	87.74	50.04	93.87	83.22	
	3th. run	85.38	50.11	92.99	83.82	
	4th. run	84.33	50.88	96.83	85.46	
	5th. run	84.16	49.76	90.92	82.68	
	6th. run			95.34	86.62	
	7th. run			93.68		
	standard dev.	*1.44*	*0.53*	*1.87*	*1.50*	
Pb	***recommended***	**36**	**53**	**3.5**	**4.5**	***3.67***
	1st. run	38.84	50.12	3.46	8.21	
	2nd. run	41.81	50.47	3.46	11.63	
	3th. run	39.04	50.47	3.53	11.38	
	4th. run	37.57	51.34	5.08	9.67	
	5th. run	39.83	50.82	5.63	8.62	
	6th. run			5.95	10.17	
	7th. run			3.31		
	standard dev.	*1.56*	*0.46*	*1.16*	*1.40*	
Th	***recommended***	**6.5**	**42**	**3**	**2.7**	***0.99***
	1st. run	7.04	38.56	1.96	2.26	
	2nd. run	8.01	40.45	2.51	3.26	
	3th. run	7.88	40.5	3.5	3.26	
	4th. run	7.5	39.64	4.22	3.79	
	5th. run	7.03	39.81	3.17	3.99	
	6th. run			2.28	3.78	
	7th. run			2.57		
	standard dev.	*0.46*	*0.79*	*0.79*	*0.63*	

APPENDIX C-3: Error calculations of ICP-MS Rare Earth element data

ICP-MS ERROR CALCULATIONS OF RARE EARTH ELEMENTS

	5.4.1993	AGV-1	BCR-1	BHVO-1	BOB-1	FK-N	MRG-1	W-2	X108 Standart error (±)	
Cs	*recommended*	1.3	1.0	0.1		7.0	0.6	1.0	0.6	***0.11***
	1st. run	1.4	0.8	0.2	0.2	6.5	0.6	1.1	0.7	
	2nd. run	1.3	1.0	0.2			0.7	0.9		
	3th. run			0.1			0.6			
La	*recommended*	38.0	24.9	15.8	4.6	1.0	9.8	11.4	0.9	***0.93***
	1st. run	38.5	24.7	15.6	4.8	1.0	8.7	10.5	1.0	
	2nd. run	36.1	26.4	15.3			8.0	10.2		
	3th. run			15.4			9.1			
Ce	*recommended*	67.0	53.7	39.0	13.4	1.0	26.0	24.0	1.7	***1.60***
	1st. run	69.6	51.1	39.5	13.2	1.1	24.9	23.9	1.8	
	2nd. run	65.7	54.8	39.2			22.2	23.1		
	3th. run			36.9			25.8			
Pr	*recommended*	7.6	6.8	5.7	2.0		3.4	5.9	0.3	***1.12***
	1st. run	8.7	6.3	5.6	2.0	0.1	3.7	3.3	0.2	
	2nd. run	8.2	7.2	5.7			3.2	3.0		
	3th. run			5.4			3.6			
Nd	*recommended*	33.0	28.8	25.2	10.1	0.3	19.2	14.0	1.2	***1.09***
	1st. run	33.4	28.3	25.8	10.6	0.3	18.1	13.4	1.2	
	2nd. run	31.7	30.6	25.4			16.6	12.6		
	3th. run			24.3			18.2			
Sr	*recommended*	5.9	6.6	6.2	3.1	0.1	4.5	3.3	0.4	***0.30***
	1st. run	6.0	6.3	6.0	2.8	0.1	4.4	3.4	0.3	
	2nd. run	5.7	6.9	6.0			4.2	3.1		
	3th. run			5.7			4.4			
Eu	*recommended*	1.6	2.0	2.1	1.1	0.4	1.4	1.1	0.1	***0.12***
	1st. run	1.9	1.9	2.1	1.2	0.4	1.4	1.1	0.2	
	2nd. run	1.8	2.2	2.4			1.6	1.1		
	3th. run			2.0			1.4			
Gd	*recommended*	5.0	6.7	6.4	3.9	0.1	4.0	3.6	0.5	***0.35***
	1st. run	5.0	6.9	6.2	3.7	0.1	4.4	3.4	0.4	
	2nd. run	4.7	7.7	5.9			4.2	3.7		
	3th. run			6.2			4.2			
Tb	*recommended*	0.7	1.1	1.0	0.7	0.0	0.5	0.6	0.1	***0.07***
	1st. run	0.6	1.1	0.9	0.6	0.0	0.5	0.7	0.1	
	2nd. run	0.7	1.1	1.0			0.7	0.6		
	3th. run			0.9			0.6			
Dy	*recommended*	3.6	6.3	5.2	4.3	0.1	2.9	3.8	0.6	***0.18***
	1st. run	3.5	6.3	5.2	4.2	0.1	3.0	3.7	0.6	
	2nd. run	3.4	6.9	5.1			2.8	3.9		
	3th. run			5.2			2.8			

	5.4.1993	AGV-1	BCR-1	BHVO-1	BOB-1	FK-N	MRG-1	W-2	X108 Standart error (±)	
Ho	*recommended*	0.7	1.3	1.0	0.9		0.5	0.8	0.1	***0.08***
	1st. run	0.6	1.4	1.0	0.9	0.0	0.5	0.8	0.1	
	2nd. run	0.7	1.5	1.0			0.5	0.8		
	3th. run			1.0			0.5			
Er	*recommended*	1.7	3.6	2.4	2.7	0.0	1.1	2.5	0.5	***0.17***
	1st. run	1.9	3.6	2.4	2.4	0.1	1.2	2.1	0.4	
	2nd. run	1.8	3.8	2.3			1.0	2.1		
	3th. run			2.3			1.0			
Tm	*recommended*	0.3	0.6	0.3	0.4		0.1	0.4	0.1	***0.04***
	1st. run	0.3	0.6	0.4	0.4	0.0	0.1	0.4	0.1	
	2nd. run	0.3	0.6	0.3			0.2	0.3		
	3th. run			0.3			0.1			
Yb	*recommended*	1.7	3.4	2.0	2.6	0.0	0.6	2.1	0.7	***0.17***
	1st. run	1.6	3.7	2.0	2.5	0.1	0.8	2.1	0.6	
	2nd. run	1.7	3.9	2.0			0.8	2.1		
	3th. run			1.9			0.8			
Lu	*recommended*	0.3	0.5	0.3	0.4	0.0	0.1	0.3	0.1	***0.04***
	1st. run	0.3	0.6	0.3	0.4	0.0	0.1	0.4	0.1	
	2nd. run	0.3	0.6	0.3			0.1	0.4		
	3th. run			0.3			0.1			
Hf	*recommended*	5.1	5.0	4.4	2.3	0.1	3.8	2.6	0.7	***0.20***
	1st. run	5.3	5.3	4.4	2.3	0.1	3.7	2.5	0.7	
	2nd. run	4.9	5.4	4.2			3.6	2.3		
	3th. run			4.6			3.6			
Ta	*recommended*	0.9	0.8	1.2	0.6	0.3	0.8	0.5	0.1	***0.07***
	1st. run	1.0	0.7	1.2	0.5	0.3	0.9	0.5	0.1	
	2nd. run	0.9	0.8	1.2			0.9	0.6		
	3th. run			1.2			0.8			
Pb	*recommended*	36.0	13.6	2.6	0.9	240.0	10.0	9.3	1.5	***2.75***
	1st. run	35.0	15.3	2.1	0.9	246.3	4.9	7.2	1.7	
	2nd. run	35.8	14.4	2.2			4.8	7.3		
	3th. run			2.2			4.8			
Th	*recommended*	6.5	6.0	1.1	0.3	0.3	0.9	2.2	0.1	***0.19***
	1st. run	6.3	6.2	1.3	0.4	0.2	0.8	2.1	0.2	
	2nd. run	6.0	6.0	1.1			0.8	2.0		
	3th. run			1.4			0.7			
U	*recommended*	1.9	1.8	0.4	0.1	0.1	0.2	0.5	0.1	***0.07***
	1st. run	2.0	1.7	0.5	0.1	0.1	0.3	0.4	0.2	
	2nd. run	1.8	1.7	0.5			0.2	0.6		
	3th. run			0.4			0.3			

ICP-MS ERROR CALCULATIONS OF RARE EARTH ELEMENTS

		AGV-1	BCR-1	BHVO-1	BOB-1	W-2	X108	Standart error (±)
Cs	*recommended*	1.3	1.0	0.1		1.0	0.6	***0.10***
	1st. run	1.3	1.0	0.1	0.1	0.8	0.6	
	2nd. run			0.1		0.9	0.8	
La	*recommended*	38.0	24.9	15.8	4.6	11.4	0.9	***0.68***
	1st. run	37.4	25.7	16.4	5.3	11.1	1.0	
	2nd. run			16.3		10.2	1.0	
Ce	*recommended*	67.0	53.7	39.0	13.4	24.0	1.7	***0.68***
	1st. run	68.0	53.0	39.1	14.2	23.9	1.8	
	2nd. run			38.4		22.9	1.7	
Pr	*recommended*	7.6	6.8	5.7	2.0	5.9	0.3	***1.34***
	1st. run	8.6	6.9	5.7	2.3	3.1	0.3	
	2nd. run			5.5		3.1	0.3	
Nd	*recommended*	33.0	28.8	25.2	10.1	14.0	1.2	***0.79***
	1st. run	32.0	29.7	26.0	11.1	13.6	1.2	
	2nd. run			24.7		13.1	1.3	
Sm	*recommended*	5.9	6.6	6.2	3.1	3.3	0.4	***0.15***
	1st. run	6.0	6.8	6.2	3.3	3.1	0.3	
	2nd. run			5.9		3.2	0.3	
Eu	*recommended*	1.6	2.0	2.1	1.1	1.1	0.1	***0.12***
	1st. run	1.9	2.1	2.0	1.2	1.1	0.1	
	2nd. run			1.9		1.1	0.1	
Gd	*recommended*	5.0	6.7	6.4	3.9	3.6	0.5	***0.27***
	1st. run	5.3	7.0	6.2	3.8	3.5	0.4	
	2nd. run			5.9		3.6	0.4	
Tb	*recommended*	0.7	1.1	1.0	0.7	0.6	0.1	***0.03***
	1st. run	0.7	1.1	0.9	0.7	0.6	0.1	
	2nd. run			0.9		0.6	0.1	
Dy	*recommended*	3.6	6.3	5.2	4.3	3.8	0.6	***0.15***
	1st. run	3.7	6.5	5.2	4.4	3.7	0.6	
	2nd. run			5.0		3.5	0.6	

		AGV-1	BCR-1	BHVO-1	BOB-1	W-2	X108	Standart error (±)
Ho	*recommended*	0.7	1.3	1.0	0.9	0.8	0.1	***0.04***
	1st. run	0.7	1.3	1.0	0.9	0.8	0.1	
	2nd. run			0.9		0.7	0.2	
Er	*recommended*	1.7	3.6	2.4	2.7	2.5	0.5	***0.19***
	1st. run	1.9	3.6	2.6	2.7	2.3	0.4	
	2nd. run			2.6		2.1	0.5	
Tm	*recommended*	0.3	0.6	0.3	0.4	0.4	0.1	***0.04***
	1st. run	0.3	0.6	0.3	0.4	0.3	0.1	
	2nd. run			0.4		0.3	0.1	
Yb	*recommended*	1.7	3.4	2.0	2.6	2.1	0.7	***0.05***
	1st. run	1.6	3.4	2.0	2.6	2.0	0.7	
	2nd. run			2.1		2.0	0.7	
Lu	*recommended*	0.3	0.5	0.3	0.4	0.3	0.1	***0.03***
	1st. run	0.2	0.5	0.3	0.4	0.3	0.1	
	2nd. run			0.3		0.3	0.1	
Hf	*recommended*	5.1	5.0	4.4	2.3	2.6	0.7	***0.20***
	1st. run	5.0	4.9	4.5	2.5	2.5	0.7	
	2nd. run			4.4		2.1	0.7	
Ta	*recommended*	0.9	0.8	1.2	0.6	0.5	0.1	***0.07***
	1st. run	0.9	0.8	1.3	0.5	0.5	0.0	
	2nd. run			1.3		0.5	0.1	
Pb	*recommended*	36.0	13.6	2.6	0.9	9.3	1.5	***0.81***
	1st. run	36.3	14.1	2.1	1.0	7.7	1.6	
	2nd. run			2.1		8.0	1.7	
Th	*recommended*	6.5	6.0	1.1	0.3	2.2	0.1	***0.12***
	1st. run	6.5	5.9	1.2	0.3	2.3	0.1	
	2nd. run			1.2		2.0	0.1	
U	*recommended*	1.9	1.8	0.4	0.1	0.5	0.1	***0.05***
	1st. run	2.0	1.7	0.4	0.2	0.5	0.1	
	2nd. run			0.5		0.6	0.1	

APPENDIX C-4: Error calculations of Electron Microprobe major element data

ELECTRON MICRO-PROBE ERROR CALCULATIONS

Si	Olivine	Jadeite	Wollastonite	Orthoclase	± *standard error*
recommended	**19.08**	**27.78**	**24.00**	**30.39**	***0.20***
14/7/92	19.09				
15/7/92	19.13	28.16	23.77		
16/7/92	18.92	27.77	24.19		
17/7/92	19.06	27.67	23.88		
20/7/92	19.27	28.14	24.45		
20/7/92	19.27	27.98	23.45		
22/7/92	19.22	27.98	23.81		
23/7/92	19.27	27.92	23.81		
24/7/92	19.30	28.02	23.90		
24/7/92	19.26	27.76	23.79		
28/7/92	19.34	28.25	23.85		
29/7/92	19.12	28.20	23.70		
29/7/92	19.21	27.83	23.98		
30/7/92	19.20	28.17	23.80	30.64	
30/7/92	19.14	27.99	23.97	30.38	
31/7/92	19.18	27.58	23.87	30.58	
31/7/92	19.20	27.94	23.93	30.55	
07/08/92	19.40	28.31	23.99	30.54	
07/08/92	19.25	28.07	23.85	30.26	
10/08/92	19.08	28.00	23.69	30.63	
10/08/92	19.06				
standard dev.	*0.11*	*0.20*	*0.20*	*0.14*	

Al	Jadeite	Orthoclase	± *standard error*
recommended	**13.23**	**9.79**	***0.26***
15/7/92	12.88		
16/7/92	12.79		
17/7/92	12.88		
20/7/92	13.13		
20/7/92	13.05		
22/7/92	13.06		
23/7/92	12.91		
24/7/92	13.07		
24/7/92	12.77		
28/7/92	13.13		
29/7/92	13.16		
29/7/92	13.20		
30/7/92	13.09	9.15	
30/7/92	12.55	9.18	
31/7/92	12.83	9.15	
31/7/92	12.99	9.18	
07/08/92	12.87	9.14	
07/08/92	12.98	9.04	
10/08/92	13.17	9.22	
standard dev.	*0.17*	*0.06*	

Mg	Olivine *standard error*
recommended	**29.45** ***0.15***
14/7/92	29.62
15/7/92	29.43
16/7/92	29.19
17/7/92	29.14
20/7/92	29.48
20/7/92	29.36
22/7/92	29.40
23/7/92	29.30
24/7/92	29.40
24/7/92	29.61
28/7/92	29.36
29/7/92	29.45
29/7/92	29.17
30/7/92	29.35
30/7/92	29.55
31/7/92	29.58
31/7/92	29.54
07/08/92	29.47
07/08/92	29.30
10/08/92	29.19
10/08/92	29.18
standard dev.	*0.15*

Fe	Olivine	Jadeite	Wollastonite	Hematite	± *standard error*
recommended	**7.62**	**0.17**	**0.30**	**69.94**	***0.21***
14/7/92	7.80				
15/7/92	7.59	0.32	0.22		
16/7/92	7.56	0.19	0.28		
17/7/92	7.86	0.00	0.22		
20/7/92	7.48	0.08	0.31		
20/7/92	7.49	0.00	0.13		
22/7/92	7.59	0.09	0.07		
23/7/92	7.60	0.19	0.34		
24/7/92	7.34	0.10	0.31		
24/7/92	7.46	0.12	0.41		
28/7/92	7.50	0.00	0.27		
29/7/92	7.53	0.11	0.33		
29/7/92	7.38	0.20	0.33		
30/7/92	7.30	0.10	0.13	65.86	
30/7/92	7.44	0.53	0.22		
31/7/92	7.32	0.17	0.25		
31/7/92	7.20	0.00	0.08		
07/08/92	7.20	0.10	0.28		
07/08/92	7.40	0.17	0.26		
10/08/92	7.45	0.14	0.26		
10/08/92	7.48				
standard dev.	*0.17*	*0.13*	*0.09*		

ELECTRON MICRO-PROBE ERROR CALCULATIONS

Ca

	Wollastonite	± *standard error*
recommended	**34.32**	***0.43***
15/7/92	34.76	
16/7/92	35.45	
17/7/92	34.32	
20/7/92	35.46	
20/7/92	33.72	
22/7/92	34.48	
23/7/92	34.51	
24/7/92	33.73	
24/7/92	34.22	
28/7/92	34.57	
29/7/92	34.37	
29/7/92	34.58	
30/7/92	34.36	
30/7/92	34.28	
31/7/92	34.56	
31/7/92	34.64	
07/08/92	34.41	
07/08/92	34.59	
10/08/92	34.39	
standard dev.	*0.43*	

Mn

	Olivine	± *standard error*
recommended	**0.09**	***0.08***
14/7/92	0.31	
15/7/92	0.14	
16/7/92	0.19	
17/7/92	0.18	
20/7/92	0.14	
20/7/92	0.03	
22/7/92	0.01	
23/7/92	0.00	
24/7/92	0.10	
24/7/92	0.00	
28/7/92	0.02	
29/7/92	0.11	
29/7/92	0.04	
30/7/92	0.07	
30/7/92	0.10	
31/7/92	0.14	
31/7/92	0.15	
07/08/92	0.07	
07/08/92	0.10	
10/08/92	0.17	
10/08/92	0.20	
standard dev.	*0.08*	

Na

	Jadeite	Orthoclase ± *standard error*	
recommended	**11.34**	**0.40**	***0.12***
15/7/92	10.95		
16/7/92	10.74		
17/7/92	10.92		
20/7/92	11.04		
20/7/92	11.07		
22/7/92	11.04		
23/7/92	11.11		
24/7/92	10.95		
24/7/92	10.79		
28/7/92	11.18		
29/7/92	10.82		
29/7/92	11.13		
30/7/92	10.83	0.36	
30/7/92	10.87	0.29	
31/7/92	10.72	0.42	
31/7/92	11.07	0.36	
07/08/92	11.04	0.34	
07/08/92	11.04	0.49	
10/08/92	10.87	0.36	
standard dev.	*0.14*	*0.06*	

Ni

	Olivine	± *standard error*
recommended	**0.28**	***0.12***
14/7/92	0.23	
15/7/92	0.33	
16/7/92	0.52	
17/7/92	0.38	
20/7/92	0.39	
20/7/92	0.08	
22/7/92	0.19	
23/7/92	0.27	
24/7/92	0.18	
24/7/92	0.10	
28/7/92	0.29	
29/7/92	0.14	
29/7/92	0.23	
30/7/92	0.28	
30/7/92	0.17	
31/7/92	0.18	
31/7/92	0.48	
07/08/92	0.29	
07/08/92	0.22	
10/08/92	0.35	
10/08/92	0.27	
standard dev.	*0.12*	

K

	Orthoclase	± *standard error*
recommended	**13.25**	***0.08***
30/7/92	13.61	
30/7/92	13.51	
31/7/92	13.58	
31/7/92	13.70	
07/08/92	13.57	
07/08/92	13.50	
10/08/92	13.49	
standard dev.	*0.08*	

Ti

	Rutile	± *standard error*
recommended	**59.95**	***0.16***
30/7/92	59.68	
30/7/92	59.86	
31/7/92	59.71	
31/7/92	59.57	
07/08/92	59.49	
07/08/92	59.56	
10/08/92	59.92	
standard dev.	*0.16*	

APPENDIX D: XRF whole-rock major and trace element data-set

APPENDIX D: XRF whole-rock major and trace element data-set

Symbols of Formations

Mt. Dumlu and Mt. Kargapazarı areas

Gad: the Güngörmez andesite/dacite
Gad(Bd): the Güngörmez andesite/dacite (aphyric Black dacite layers)
Amd: the Arzutu amphibole dacite
Dpad: the Dumlu amphibole dacite/andesite
Kb: the Karapınar basalt
Gpd: the Girekösek dacite
Kpa: the Köşk pyroxene andesite
Çpd: the Çobandede dacite
Gpaa: the Göllerdüzü amphibole dacite
Bign(Kp): the Black ignimbrite (Mt. Kargapazarı)
Kv: the Kargapazarı volcanics

Pasinler, Horasan and Kağızman areas

Pasin-1 En1: the Kışlaköy volcanic member of the Eocene Narman group
Pasin-2 Mtd: the Middle Miocene Tuzluyolları dacite
Pasin-3 Baad: the Black andesite/dacite
Pasin-4 Kpd: the Kızılveren amphibole dacite/andesite
Ltl (Gign) Ltl (Gign): the Lower tuff unit (the Grey ignimbrite)
Pasin-5b Ltl (Wign): the Lower tuff unit (the White ignimbrite)
Pasin-5c Ltl (Obsid.): the Lower tuff unit (obsidian)
Pasin-5d Utl (Tuff): the Upper tuff unit
Pasin-6 Bign: the Black ignimbrite
Pasin-7a Kv (Dyke): dykes of the Kargapazarı volcanics
Pasin-7b Kv: the Kargapazarı volcanics
Pasin-8 Ard: the Ardıçlıdağ rhyolite
N.Horas-1 Mad: the Middle Miocene Akveren dacite
N.Horas-2 Köb: the Kötek basalt
N.Horas-3 Pblh (Wign): the Pyroclastic basal unit (the White ignimbrite)
N.Horas-5 Kpad: the Köroğlu amphibole dacite/andesite
N.Horas-6 Hpl: the Horasan plateau unit
S.Horas-1 Sd: the Saçdağ dacite
Aladag-1a Apbl: the Aladağ pyroclastic basal unit
Aladag-1b Apbl (Obsid): the Aladağ pyroclastic basal unit (obsidian)
Aladag-2 Abil: the Aladağ basal intermediate lavas
Aladag-3 Aa (Sc): the Aladağ andesite (spatter cones)
Aladag-4 Aa: the Aladağ andesite
Aladag-5 Orhy: the Odalar rhyolite (acid cones on the plateau)
Kagiz-1 Çr: the Çukurayva rhyolite
Kagiz-2 Ptd: the Paslı trachy-dacite
Kagiz-3 Kpl: the Kars plateau unit

APPENDIX D

XRF analyses of the samples from the Erzurum-Kars Plateau, NE Turkey

Copyright © by Mehmet Keskin

Area	Mt. Dumlu	Mt. Dumlu	Mt. Dumlu	Mt. Dumlu	Mt. Dumlu	Mt. Dumlu	Mt. Dumlu	Mt. Dumlu	Mt. Dumlu	Mt. Dumlu	Mt. Dumlu	Mt. Dumlu	Mt. Dumlu	Mt. Dumlu
Sample no	**MK229**	**MK243**	**MK244**	**MK245**	**MK246**	**MK255**	**MK256**	**MK257**	**MK258**	**MK259**	**MK25**	**MK28**	**MK30**	**MK31**
Unit	Dum-1a	Dum-1a	Dum-1a	Dum-1a	Dum-1a	Dum-1a	Dum-1a	Dum-1a	Dum-1a	Dum-1a	Dum-1b	Dum-1b	Dum-1b	Dum-1b
Symbol	Gad	Gad	Gad	Gad	Gad	Gad	Gad	Gad	Gad	Gad	Gad	Gad	Gad	Gad
Level	Low. lens	Low. lens	Low. lens	Low. lens	Low. lens	Low. lens	Low. lens	Low. lens	Low. lens	Low. lens	Mid	Mid	Mid	Mid
Geoch. desc.	*Dacite*	*Andesite*	*Andesite*	*Andesite*	*Andesite*	*Trac and*	*Trac and*	*Dacite*	*Dacite*	*Dacite*	*Dacite*	*Andesite*	*Dacite*	*Dacite*
SiO2	65.11	57.99	58.28	58.92	59.23	62.26	58.60	69.47	68.13	64.91	64.39	60.27	65.10	64.92
TiO2	0.59	0.92	0.94	0.92	0.95	0.86	1.02	0.43	0.50	0.61	0.70	0.80	0.58	0.58
Al2O3	16.36	17.96	17.92	18.21	17.65	17.12	18.09	15.84	16.17	16.01	16.02	16.69	15.96	15.80
Fe2O3	3.85	6.24	6.27	6.26	6.06	5.58	5.98	2.88	3.09	3.99	4.85	5.70	3.97	3.98
MnO	0.06	0.09	0.08	0.08	0.10	0.08	0.07	0.03	0.05	0.06	0.07	0.09	0.06	0.06
MgO	2.44	3.81	3.39	3.56	3.84	1.49	3.03	1.34	1.66	2.53	2.27	3.25	2.28	2.32
CaO	4.46	6.98	6.84	6.96	6.66	4.43	6.20	3.52	3.78	4.54	5.06	6.16	4.65	4.65
Na2O	4.15	3.88	4.16	4.09	4.07	4.80	4.51	4.24	4.43	4.40	3.95	3.96	3.85	4.13
K2O	2.47	1.83	1.66	1.63	1.69	2.50	2.00	2.59	2.52	2.33	2.65	1.91	2.47	2.41
P2O5	0.24	0.27	0.27	0.28	0.30	0.47	0.38	0.17	0.18	0.25	0.22	0.27	0.25	0.24
L.O.I.	1.56	0.76	0.63	0.77	0.65	0.93	0.65	0.87	0.20	1.24	0.78	1.25	1.12	0.15
Total (LOI free)	99.73	99.98	99.81	100.91	100.53	99.58	99.90	100.51	100.51	99.63	100.18	99.10	99.15	99.08
Sc	21	17	18	17	17	12	15	6	9	8	13	14	10	9
Cr	88	34	29	32	47	1	3	42	24	55	38	46	59	61
V	152	132	147	135	141	100	137	57	67	80	89	112	70	86
Ni	48	16	19	18	26	2	23	41	22	48	38	45	44	41
Co	11	22	19	20	22	12	19	8	9	15	14	19	12	11
Cu	15	16	19	38	14	6	16	12	22	42	12	20	31	30
Zn	60	70	75	72	73	65	68	49	48	63	60	71	58	62
Ga	18	21	22	20	20	20	19	19	18	18	16	17	17	18
Rb	55	41	41	38	37	69	49	82	77	65	71	52	71	72
Sr	432	545	540	547	519	492	642	331	349	451	389	479	417	416
Y	26	17	19	16	16	21	19	11	12	13	13	18	12	9
Zr	197	148	150	143	155	216	167	159	167	178	166	160	167	167
Nb	14	11	11	11	12	17	16	8	10	12	9	11	13	12
Ba	453	407	385	393	424	512	449	475	456	533	503	516	585	567
La	30	26	28	25	26	39	34	23	25	31	27	25	27	26
Ce	54	45	50	49	56	72	68	42	46	57	50	46	49	49
Nd	20	19	20	15	19	25	23	11	13	19	16	18	18	17
Pb	15	11	9	15	11	13	13	16	14	18	13	12	16	16
Th	9	7	6	8	5	9	8	9	9	8	8	8	9	8

APPENDIX D

XRF analyses of the samples from the Erzurum-Kars Plateau, NE Turkey

Copyright © by Mehmet Keskin

Area	Mt. Dumlu	Mt. Dumlu	Mt. Dumlu	Mt. Dumlu	Mt. Dumlu	Mt. Dumlu	Mt. Dumlu	Mt. Dumlu	Mt. Dumlu	Mt. Dumlu	Mt. Dumlu	Mt. Dumlu	Mt. Dumlu	Mt. Dumlu
Sample no	**MK38**	**MK39**	**MK41**	**MK42**	**MK43**	**MK207**	**MK210**	**MK348**	**MK349**	**MK350**	**MK351**	**MK352**	**MK353**	**MK354**
Unit	Dum-1b	Dum-1b	Dum-1b	Dum-1b	Dum-1b	Dum-1b	Dum-1b	Dum-1b	Dum-1b	Dum-1b	Dum-1b	Dum-1b	Dum-1b	Dum-1b
Symbol	Gad	Gad	Gad	Gad	Gad	Gad	Gad	Gad	Gad	Gad	Gad	Gad	Gad	Gad
Level	Mid	Mid	Mid	Mid	Mid	Mid	Mid	Mid	Mid	Mid	Mid	Mid	Mid	Mid
Geoch. desc.	*Andesite*	*Andesite*	*Dacite*	*Andesite*	*Dacite*	*Dacite*	*Dacite*	*Dacite*	*Dacite*	*Dacite*	*Dacite*	*Dacite*	*Dacite*	*Dacite*
SiO2	60.78	60.15	63.52	60.23	64.09	63.64	65.42	63.55	63.82	64.58	63.52	68.76	65.95	66.30
TiO2	0.93	0.96	0.70	0.89	0.71	0.75	0.61	0.76	0.76	0.76	0.76	0.61	0.59	0.60
Al2O3	16.53	16.41	16.13	16.48	16.25	16.81	16.34	17.01	16.99	17.12	16.93	16.64	16.43	16.25
Fe2O3	5.78	6.06	4.50	5.56	4.13	4.34	4.06	4.36	4.37	4.38	4.35	3.40	3.92	4.02
MnO	0.07	0.07	0.08	0.09	0.06	0.06	0.04	0.06	0.06	0.06	0.06	0.03	0.06	0.04
MgO	2.84	2.84	2.42	3.33	2.33	1.74	1.49	1.76	1.79	1.61	1.78	0.66	2.39	1.92
CaO	6.28	6.35	5.28	6.37	4.89	4.50	4.33	4.53	4.54	4.58	4.54	3.71	4.80	4.77
Na2O	3.96	3.99	3.91	3.87	3.74	4.26	4.01	4.11	4.06	4.60	4.32	4.58	4.06	4.13
K2O	1.91	1.91	2.44	1.91	2.61	2.66	2.53	2.96	2.94	2.48	2.79	2.73	2.39	2.52
P2O5	0.35	0.38	0.24	0.33	0.23	0.32	0.24	0.31	0.32	0.31	0.32	0.22	0.25	0.25
L.O.I.	1.18	1.14	1.36	1.57	2.12	0.75	1.07	1.21	1.17	0.63	0.96	0.96	0.82	1.13
Total (LOI free)	99.43	99.12	99.23	99.07	99.05	99.09	99.06	99.40	99.65	100.49	99.36	101.33	100.84	100.80
Sc	14	14	9	15	12	9	11	10	8	7	8	9	10	10
Cr	52	41	42	39	38	1	62	1	4	3	1	2	63	63
V	118	123	96	125	92	90	79	97	87	91	90	75	65	86
Ni	52	60	36	42	29	5	33	6	7	11	6	1	52	48
Co	13	22	17	19	12	9	10	11	12	11	11	7	11	13
Cu	19	39	25	27	10	15	18	17	38	19	15	7	30	24
Zn	70	78	64	71	56	55	57	60	61	59	56	51	59	65
Ga	21	18	18	19	19	19	17	20	19	19	19	19	19	18
Rb	48	49	62	51	61	68	64	69	72	69	72	87	63	70
Sr	564	574	399	537	408	482	409	477	479	483	478	354	427	418
Y	19	20	16	15	18	16	13	15	15	18	15	14	15	14
Zr	175	177	167	172	169	183	180	181	179	181	184	171	168	166
Nb	13	14	11	14	12	13	12	13	14	14	13	10	12	12
Ba	461	618	524	460	793	517	542	509	513	522	513	559	533	506
La	39	37	28	26	29	35	34	34	36	35	32	33	40	33
Ce	58	57	48	55	52	67	50	58	59	63	62	54	58	60
Nd	34	31	15	18	21	20	18	18	20	20	17	19	22	22
Pb	10	13	11	10	13	14	17	14	14	14	12	16	15	13
Th	6	7	8	8	6	8	9	8	8	8	7	10	8	8

APPENDIX D

XRF analyses of the samples from the Erzurum-Kars Plateau, NE Turkey

Copyright © by Mehmet Keskin

Area	Mt. Dumlu	Mt. Dumlu	Mt. Dumlu	Mt. Dumlu	Mt. Dumlu	Mt. Dumlu	Mt. Dumlu	Mt. Dumlu	Mt. Dumlu	Mt. Dumlu	Mt. Dumlu	Mt. Dumlu	Mt. Dumlu	Mt. Dumlu
Sample no	**MK226**	**MK227**	**MK239**	**MK240**	**MK241**	**MK214**	**MK215**	**MK217**	**MK218**	**MK236**	**MK26**	**MK29**	**MK48**	**MK50**
Unit	Dum-1c	Dum-1c	Dum-1c	Dum-1c	Dum-1c	Dum-1d	Dum-1d	Dum-1d	Dum-1d	Dum-1d	Mt.Dum-1e	Mt.Dum-1e	Mt.Dum-1e	Mt.Dum-1e
Symbol	Gad	Gad	Gad	Gad	Gad	Gad	Gad	Gad	Gad	Gad	Gad	Gad(Bd)	Gad(Bd)	Gad(Bd)
Level	Mid. lens	Mid. lens	Mid. lens	Mid. lens	Mid. lens	Upper lens	Upper lens	Upper lens	Upper lens	Upper lens	Upper lens	Mid	Mid	Mid
Geoch. desc.	*Dacite*	*Trac Dac*	*Andesite*	*Trac Dac*	*Trac Dac*	*Andesite*	*Andesite*	*Dacite*	*Dacite*	*Andesite*	*Dacite*	*Dacite*	*Dacite*	*Dacite*
SiO2	63.14	65.33	58.40	62.87	62.72	58.65	58.53	66.64	67.78	59.42	65.06	65.12	63.69	65.13
TiO2	0.69	0.70	0.96	0.97	0.96	0.94	0.94	0.58	0.52	0.95	0.58	0.58	0.76	0.56
Al2O3	16.98	17.41	17.90	16.78	16.66	18.08	18.26	15.74	15.88	17.61	15.91	15.83	16.90	15.85
Fe2O3	4.41	4.21	6.40	5.69	5.49	6.30	6.27	3.99	3.67	6.26	3.97	3.93	4.31	3.93
MnO	0.06	0.03	0.10	0.08	0.08	0.10	0.08	0.06	0.05	0.08	0.06	0.06	0.06	0.06
MgO	2.10	0.53	3.55	1.34	1.51	3.65	3.41	1.65	1.67	3.45	2.34	2.24	1.75	2.30
CaO	4.97	4.06	6.76	4.21	4.19	6.80	6.82	4.30	3.75	6.54	4.66	4.56	4.60	4.61
Na2O	4.24	4.75	4.14	4.92	4.86	4.13	4.14	4.11	4.17	4.14	4.10	4.02	4.29	4.01
K2O	2.23	2.65	1.73	2.69	2.68	1.67	1.67	2.44	2.57	1.77	2.41	2.46	2.56	2.40
P2O5	0.27	0.31	0.30	0.47	0.47	0.27	0.27	0.24	0.20	0.31	0.24	0.24	0.32	0.24
L.O.I.	0.03	1.44	0.43	0.81	0.96	0.64	0.62	1.39	0.86	0.81	0.02	0.04	1.23	0.02
Total (LOI free)	99.10	99.99	100.25	100.00	99.64	100.59	100.39	99.74	100.27	100.54	99.35	99.04	99.22	99.10
Sc	10	6	17	10	12	16	18	10	10	16	9	11	9	10
Cr	0	1	29	3	2	29	25	56	48	44	57	59	0	66
V	93	74	142	81	77	125	141	82	73	141	84	75	91	87
Ni	11	8	21	2	1	18	11	43	34	24	43	39	5	43
Co	12	7	20	10	8	19	18	10	8	17	11	9	10	10
Cu	27	12	5	2	1	14	16	32	41	15	28	30	14	33
Zn	60	59	65	83	76	63	70	64	61	67	60	59	59	60
Ga	19	21	18	21	19	20	19	19	17	19	19	20	18	19
Rb	58	78	43	71	68	43	42	71	81	44	68	71	71	70
Sr	459	439	532	411	410	542	543	382	302	516	419	416	478	411
Y	14	16	18	29	26	17	16	19	14	18	12	12	13	12
Zr	178	197	151	245	245	148	149	184	186	156	168	174	183	177
Nb	12	14	12	16	16	11	11	13	13	12	12	13	14	13
Ba	470	514	390	548	530	397	390	576	500	402	563	521	551	543
La	33	36	26	48	42	29	28	42	28	28	27	26	31	27
Ce	59	62	52	65	70	54	50	65	48	52	53	46	54	48
Nd	23	22	17	29	26	20	21	25	13	23	18	21	17	17
Pb	12	15	12	16	15	11	12	14	22	11	14	13	14	14
Th	7	11	7	9	8	5	6	8	9	7	10	9	9	11

APPENDIX D

XRF analyses of the samples from the Erzurum-Kars Plateau, NE Turkey

Copyright © by Mehmet Keskin

Area	Mt. Dumlu	Mt. Dumlu	Mt. Dumlu	Mt. Dumlu	Mt. Dumlu	Mt. Dumlu	Mt. Dumlu	Mt. Dumlu	Mt. Dumlu	Mt. Dumlu	Mt. Dumlu	Mt. Dumlu	Mt. Dumlu	Mt. Dumlu
Sample no	**MK51**	**MK205**	**MK260**	**MK261**	**MK228**	**MK242**	**MK225**	**MK235**	**MK237**	**MK238**	**MK248**	**MK250**	**MK251**	**MK33a**
Unit	Mt.Dum-1e	Mt.Dum-1e	Dum-2	Dum-2	Dum-3a	Dum-3a	Dum-3b	Dum-3b	Dum-3b	Dum-3b	Dum-3b	Dum-3b	Dum-3b	Dum-3c
Symbol	Gad(Bd)	Gad(Bd)	Amd	Amd	Dpad	Dpad	Dpad	Dpad	Dpad	Dpad	Dpad	Dpad	Dpad	Dpad
Level	Mid	Mid	Base	Base	Lower	Lower	Mid	Mid	Mid	Mid	Mid	Mid	Mid	Top
Geoch. desc.	*Dacite*	*Dacite*	*Dacite*	*Dacite*	*Dacite*	*Dacite*	*Dacite*	*Andesite*	*Ba And*	*Andesite*	*Dacite*	*Dacite*	*Dacite*	*Dacite*
SiO2	65.26	63.69	66.95	64.25	63.43	66.68	64.84	58.14	56.47	57.67	64.29	66.08	65.08	63.40
TiO2	0.57	0.76	0.55	0.73	0.67	0.55	0.72	0.95	0.99	0.94	0.73	0.63	0.70	0.75
Al2O3	15.83	16.99	17.02	16.49	16.52	15.77	17.00	17.80	18.43	17.87	16.64	15.94	16.49	16.23
Fe2O3	3.94	4.28	3.62	4.10	4.39	3.75	4.36	6.27	6.63	6.33	4.70	4.05	4.56	4.69
MnO	0.06	0.06	0.06	0.06	0.07	0.05	0.06	0.08	0.10	0.10	0.09	0.07	0.08	0.07
MgO	2.29	1.74	1.06	2.21	2.39	1.84	1.27	3.37	4.16	3.71	1.85	1.60	2.17	2.50
CaO	4.65	4.57	3.18	4.48	4.78	4.03	4.58	6.82	7.33	6.85	4.88	4.02	4.82	4.84
Na2O	4.01	4.05	4.62	3.89	3.83	3.88	4.37	4.15	3.91	4.12	4.22	4.28	4.21	3.75
K2O	2.38	2.89	2.84	2.74	2.74	2.99	2.46	1.67	1.35	1.68	2.35	2.66	2.35	2.59
P2O5	0.24	0.32	0.25	0.22	0.25	0.22	0.27	0.30	0.30	0.28	0.26	0.23	0.26	0.28
L.O.I.	0.14	0.90	0.66	2.42	1.45	1.63	1.54	0.79	1.40	0.45	1.18	0.94	0.94	1.43
Total (LOI free)	99.24	99.34	100.15	99.19	99.07	99.75	99.93	99.56	99.66	99.54	100.01	99.56	100.72	99.10
Sc	9	10	4	11	11	9	8	17	18	19	10	8	11	11
Cr	63	1	2	14	22	29	16	34	51	30	25	19	26	47
V	91	100	39	88	90	72	86	138	132	112	93	79	85	95
Ni	41	4	9	18	25	22	19	18	22	18	32	24	28	27
Co	11	9	8	12	10	9	12	17	20	21	16	11	15	10
Cu	33	16	3	11	13	7	24	18	16	15	27	21	25	16
Zn	62	59	47	52	61	55	58	71	69	71	67	59	64	63
Ga	19	19	19	17	21	18	20	20	20	21	19	20	19	17
Rb	70	72	67	85	60	75	61	42	20	41	59	69	59	72
Sr	412	482	397	382	445	386	456	543	544	537	450	383	438	423
Y	12	14	15	18	12	10	13	19	17	16	14	15	14	16
Zr	173	183	210	193	167	152	171	148	158	146	169	166	168	182
Nb	12	13	15	14	12	12	12	12	11	12	13	14	12	15
Ba	581	509	660	888	546	598	611	378	495	395	585	628	563	1085
La	26	32	38	26	30	30	33	29	33	28	34	35	33	33
Ce	57	61	63	54	55	52	65	52	49	53	57	61	57	53
Nd	16	17	20	15	16	13	20	19	22	18	16	17	18	25
Pb	15	14	18	15	13	15	14	12	13	10	14	17	13	16
Th	11	9	11	12	8	8	8	6	8	7	9	10	8	10

APPENDIX D

XRF analyses of the samples from the Erzurum-Kars Plateau, NE Turkey

Copyright © by Mehmet Keskin

Area	Mt. Dumlu	Mt. Dumlu	Mt. Dumlu	Mt. Dumlu	Mt. Dumlu	Mt. Dumlu	Mt. Dumlu	Mt. Dumlu	Mt. Dumlu	Mt. Dumlu	Mt. Dumlu	Mt. Dumlu	Mt. Dumlu	Mt. Dumlu
Sample no	**MK34**	**MK35**	**MK36**	**MK37**	**MK44**	**MK45**	**MK46**	**MK47**	**MK49**	**MK52a**	**MK92**	**MK93**	**MK94**	**MK95**
Unit	Dum-3c	Dum-3c	Dum-3c	Dum-3c	Dum-3c	Dum-3c	Dum-3c	Dum-3c	Dum-3c	Dum-3c	Dum-3c	Dum-3c	Dum-3c	Dum-3c
Symbol	Dpad	Dpad	Dpad	Dpad	Dpad	Dpad	Dpad	Dpad	Dpad	Dpad	Dpad	Dpad	Dpad	Dpad
Level	Top	Top	Top	Top	Top	Top	Top	Top	Top	Top	Top	Top	Top	Top
Geoch. desc.	*Dacite*	*Dacite*	*Dacite*	*Andesite*	*Andesite*	*Andesite*	*Trac Dac*	*Rhyolite*	*Dacite*	*Dacite*	*Dacite*	*Dacite*	*Dacite*	*Dacite*
SiO2	63.81	63.63	63.82	57.93	59.84	59.86	68.53	69.14	66.26	63.75	63.12	63.49	65.92	65.13
TiO2	0.75	0.76	0.76	0.94	0.87	0.87	0.40	0.39	0.61	0.75	0.76	0.75	0.59	0.62
Al2O3	16.29	16.37	16.06	18.11	16.60	16.51	16.14	16.33	15.77	16.15	16.20	16.10	15.77	15.87
Fe2O3	4.65	4.68	4.66	6.24	5.72	5.68	2.45	2.40	3.85	4.50	4.74	4.71	3.85	4.02
MnO	0.06	0.08	0.06	0.07	0.08	0.08	0.09	0.08	0.06	0.07	0.07	0.07	0.06	0.06
MgO	2.11	2.03	2.07	3.08	3.78	4.06	0.64	0.17	1.89	2.29	2.55	2.43	1.53	1.85
CaO	4.88	4.88	4.87	7.00	6.35	6.38	1.87	1.81	4.04	4.86	5.00	4.94	4.45	4.25
Na2O	4.18	4.05	4.00	3.96	4.05	3.71	5.23	5.49	3.88	3.80	3.50	3.58	4.01	4.18
K2O	2.51	2.51	2.51	1.66	1.69	1.68	3.48	3.20	2.85	2.70	2.90	2.76	2.61	2.78
P2O5	0.28	0.28	0.28	0.28	0.31	0.30	0.17	0.15	0.19	0.28	0.29	0.29	0.25	0.36
L.O.I.	0.50	0.57	0.53	0.91	1.22	0.66	1.81	0.84	1.89	1.57	1.53	1.60	0.73	1.16
Total (LOI free)	99.52	99.27	99.11	99.27	99.28	99.12	99.00	99.16	99.40	99.15	99.12	99.09	99.06	99.13
Sc	9	11	9	15	14	14	3	4	9	11	14	11	8	9
Cr	35	32	34	29	127	123	1	1	29	35	45	45	28	29
V	97	99	94	132	126	122	4	9	75	93	102	94	73	75
Ni	26	33	26	14	56	52	1	6	18	22	26	29	17	19
Co	12	10	11	14	21	18	1	2	9	11	14	11	9	8
Cu	29	30	28	15	17	13			3	23	13	17	22	11
Zn	65	66	60	67	56	66	55	57	53	62	59	60	54	58
Ga	19	19	20	19	17	20	18	18	18	28	17	18	17	18
Rb	71	72	72	42	38	43	94	88	83	71	70	72	80	81
Sr	426	432	428	556	493	495	266	268	308	419	426	428	383	495
Y	16	18	14	16	14	14	25	25	16	13	15	15	15	14
Zr	182	181	182	143	146	150	385	378	156	180	176	179	178	179
Nb	16	14	15	12	10	10	17	18	9	15	15	15	13	16
Ba	595		544		411	390	680	766	478	528	553	644	530	631
La	32	33	28	24	25	27	42	45	29	39	29	33	27	34
Ce	59	58	61	47	44	49	79	85	38	63	56	53	55	65
Nd	20	24	16	21	19	21	26	31	21	28	17	23	18	20
Pb	15	14	13	10	6	12	16	16	16	14	16	12	16	14
Th	8	6	10	6	7	8	14	12	11	9	8	8	10	9

APPENDIX D

XRF analyses of the samples from the Erzurum-Kars Plateau, NE Turkey

Copyright © by Mehmet Keskin

Area	Mt. Dumlu	Mt. Dumlu	Mt. Dumlu	Mt. Dumlu	Mt. Dumlu	Kargapazarı	Kargapazarı	Kargapazarı	Kargapazarı	Kargapazarı	Kargapazarı	Kargapazarı	Kargapazarı	Kargapazarı
Sample no	**MK96**	**MK97**	**MK216**	**MK223**	**MK232**	**MK1**	**MK3**	**MK4**	**MK5**	**MK6**	**MK7**	**MK8**	**MK10**	**MK12**
Unit	Dum-3c	Dum-3c	Dum-3c	Dum-3c	Dum-3c	Kpzr-1	Kpzr-1	Kpzr-1	Kpzr-1	Kpzr-1	Kpzr-1	Kpzr-1	Kpzr-1	Kpzr-1
Symbol	Dpad	Dpad	Dpad	Dpad	Dpad	Gad	Gad	Gad	Gad	Gad	Gad	Gad	Gad	Gad
Level	Top	Top	Top	Top	Top	Base-Mid	Base-Mid	Base-Mid	Base-Mid	Base-Mid	Base-Mid	Base-Mid	Base-Mid	Base-Mid
Geoch. desc.	*Dacite*	*Dacite*	*Dacite*	*Dacite*	*Dacite*	*Dacite*	*Andesite*	*Rhyolite*	*Dacite*	*Andesite*	*Dacite*	*Andesite*	*Dacite*	*Andesite*
SiO2	65.90	65.98	64.55	64.54	64.56	63.13	57.19	70.22	63.96	57.61	67.95	57.69	64.52	58.98
TiO2	0.60	0.59	0.79	0.75	0.70	0.76	0.91	0.27	0.63	0.93	0.48	0.91	0.63	0.90
Al2O3	15.96	15.90	17.26	16.47	15.82	16.27	16.94	16.46	15.82	16.96	15.85	17.14	16.13	17.45
Fe2O3	3.90	3.87	4.75	4.61	4.41	4.35	6.76	2.02	4.31	6.61	2.83	6.19	3.89	5.51
MnO	0.06	0.06	0.07	0.07	0.07	0.06	0.12	0.02	0.07	0.11	0.05	0.09	0.06	0.08
MgO	1.72	1.75	2.52	2.48	2.47	2.51	3.51	0.19	3.12	4.09	1.37	4.04	3.02	3.35
CaO	4.21	4.21	4.94	4.81	4.70	5.07	7.52	1.54	4.78	7.74	3.34	7.47	4.51	6.79
Na2O	4.01	3.95	4.31	3.88	3.89	3.74	3.96	5.71	3.63	4.08	4.08	4.01	3.45	3.66
K2O	2.62	2.65	2.39	2.72	2.67	2.85	1.87	3.58	2.74	1.85	3.19	1.82	2.66	2.03
P2O5	0.28	0.25	0.29	0.29	0.25	0.27	0.38	0.11	0.21	0.39	0.17	0.39	0.21	0.33
L.O.I.	1.29	1.79	0.69	1.58	1.48	1.88	0.90	1.16	0.94	0.57	2.50	0.56	2.56	1.92
Total (LOI free)	99.26	99.21	101.87	100.60	99.54	99.03	99.16	100.11	99.24	100.37	99.30	99.77	99.08	99.07
Sc	9	7	13	11	11	12	18	3	9	18	6	17	10	14
Cr	23	23	32	31	35	31	102	1	92	100	19	62	89	41
V	72	71	86	96	96	89	159	2	89	156	53	162	91	143
Ni	16	16	25	19	23	36	75	2	78	85	15	46	89	27
Co	14	9	12	14	10	13	22	1	15	24	7	20	14	17
Cu	21	19	22	13	8	12	16	0	40	10	17	17	17	43
Zn	55	54	64	63	58	54	74	49	54	65	43	70	60	68
Ga	18	17	20	18	17	18	19	19	17	19	21	19	17	20
Rb	79	80	53	71	77	78	44	99	75	44	97	42	74	47
Sr	431	395	439	422	360	454	708	189	434	703	305	700	431	651
Y	14	13	14	16	15	14	18	22	12	17	12	18	13	16
Zr	177	176	188	180	180	182	144	355	159	142	165	146	159	151
Nb	14	14	15	14	13	13	14	18	11	14	11	14	13	14
Ba	572	529	576	518	488	470	425	699	466	393	439	434	489	464
La	32	29	31	34	28	28	29	44	20	28	21	30	23	30
Ce	60	52	58	57	55	48	54	69	41	53	38	57	44	49
Nd	21	16	20	21	20	18	25	23	12	18	14	25	16	22
Pb	17	15	17	14	14	14	10	16	11	10	15	10	15	9
Th	7	9	10	8	9	11	5	14	8	4	10	5	8	6

APPENDIX D

XRF analyses of the samples from the Erzurum-Kars Plateau, NE Turkey

Copyright © by Mehmet Keskin

Area	Kargapazarı	Kargapazarı	Kargapazarı	Kargapazarı	Kargapazarı	Kargapazarı	Kargapazarı	Kargapazarı	Kargapazarı	Kargapazarı	Kargapazarı	Kargapazarı	Kargapazarı	Kargapazarı
Sample no	**MK14**	**MK15**	**MK16**	**MK18**	**MK19**	**MK20**	**MK21**	**MK22**	**MK23**	**MK24**	**MK52c**	**MK82**	**MK83**	**MK84**
Unit	Kpzr-1	Kpzr-1	Kpzr-1	Kpzr-1	Kpzr-1	Kpzr-1	Kpzr-1	Kpzr-1	Kpzr-1	Kpzr-1	Kpzr-1	Kpzr-1	Kpzr-1	Kpzr-1
Symbol	Gad	Gad	Gad	Gad	Gad	Gad	Gad	Gad	Gad	Gad	Gad	Gad	Gad	Gad
Level	Base-Mid	Base-Mid	Mid	Mid	Mid	Mid	Mid	Mid	Mid	Mid	Mid	Mid	Mid	Mid
Geoch. desc.	*Andesite*	*Dacite*	*Trac Dac*	*Dacite*	*Dacite*	*Andesite*	*Dacite*	*Andesite*	*Andesite*	*Andesite*	*Andesite*	*Dacite*	*Dacite*	*Dacite*
SiO2	59.57	65.92	67.67	64.57	63.52	61.52	63.28	61.71	62.54	60.59	62.26	64.35	64.26	64.06
TiO2	0.89	0.60	0.52	0.64	0.69	0.77	0.71	0.71	0.74	0.83	0.71	0.67	0.66	0.67
Al2O3	17.63	15.17	15.32	16.14	16.03	15.81	16.08	15.93	16.20	15.92	16.23	16.67	16.68	16.60
Fe2O3	5.13	3.77	3.08	4.04	4.42	5.25	4.50	4.54	4.65	5.41	4.69	4.11	4.08	4.08
MnO	0.08	0.07	0.05	0.06	0.07	0.08	0.07	0.07	0.07	0.08	0.07	0.04	0.06	0.06
MgO	3.07	2.74	1.69	2.32	2.87	3.88	2.97	3.10	3.00	4.30	3.17	1.47	1.99	1.98
CaO	6.81	3.77	2.99	4.37	4.90	5.50	4.97	4.99	5.12	5.93	5.13	4.60	4.63	4.63
Na2O	3.54	3.77	3.83	3.69	3.65	3.70	3.96	3.88	3.97	3.74	3.75	4.25	4.15	3.91
K2O	2.10	3.21	3.90	3.07	2.82	2.49	2.71	2.50	2.66	2.41	2.71	2.63	2.55	2.81
P2O5	0.33	0.15	0.14	0.24	0.24	0.25	0.24	0.23	0.24	0.27	0.23	0.21	0.20	0.21
L.O.I.	2.17	1.73	1.94	1.44	1.45	0.99	0.92	1.06	1.03	1.11	1.19	1.25	0.18	1.04
Total (LOI free)	99.15	99.17	99.19	99.14	99.20	99.24	99.51	97.65	99.19	99.48	98.95	99.02	99.26	99.01
Sc	14	8	5	7	11	14	13	12	12	11	10	9	10	10
Cr	39	86	44	47	62	109	59	62	64	135	72	1	6	5
V	151	67	52	88	91	100	94	95	99	105	92	89	92	91
Ni	30	65	33	56	49	82	51	60	53	103	57	43	39	34
Co	18	12	7	13	12	17	11	13	15	18	14	11	11	14
Cu	48	13	9	13	9	18	14	16	17	29	10	42	38	31
Zn	70	45	43	55	52	59	53	54	56	58	55	55	52	51
Ga	20	17	18	19	17	20	29	18	17	17	19	19	19	20
Rb	47	94	104	77	70	64	75	73	69	58	72	84	78	80
Sr	652	286	268	452	418	421	419	422	425	454	422	389	390	392
Y	17	15	17	14	16	16	15	15	16	16	16	15	15	15
Zr	152	184	198	177	169	162	173	168	172	164	167	185	188	186
Nb	14	12	14	12	13	12	13	13	13	13	13	12	13	13
Ba	443	487	608	547	495	449	492	426	470	625	632	551	511	520
La	27	27	29	27	26	27	26	25	24	22	27	24	23	25
Ce	55	45	46	48	51	45	50	45	46	46	44	46	43	39
Nd	22	18	20	19	23	23	19	17	20	17	20	20	18	16
Pb	13	14	15	15	12	9	13	13	11	14	15	14	11	16
Th	5	10	11	9	8	6	8	8	8	8	8	9	10	12

APPENDIX D

XRF analyses of the samples from the Erzurum-Kars Plateau, NE Turkey

Copyright © by Mehmet Keskin

Area	Kargapazarı	Kargapazarı	Kargapazarı	Kargapazarı	Kargapazarı	Kargapazarı	Kargapazarı	Kargapazarı	Kargapazarı	Kargapazarı	Kargapazarı	Kargapazarı	Kargapazarı	Kargapazarı
Sample no	**MK85**	**MK86**	**MK87**	**MK88**	**MK89**	**MK90**	**MK91**	**MK98**	**MK99**	**MK264**	**MK273**	**MK278**	**MK275**	**MK276**
Unit	Kpzr-1	Kpzr-1	Kpzr-1	Kpzr-1	Kpzr-1	Kpzr-1	Kpzr-1	Kpzr-1	Kpzr-1	Kpzr-1	Kpzr-1	Kpzr-1	Kpzr-1	Kpzr-1
Symbol	Gad	Gad	Gad	Gad	Gad	Gad	Gad	Gad	Gad	Gad	Gad	Gad	Gad	Gad
Level	Mid	Mid	Mid	Mid	Mid	Mid	Mid	Mid	Mid	Mid	Mid	Mid	Top	Top
Geoch. desc.	*Dacite*	*Trac Dac*	*Trac Dac*	*Trac Dac*	*Dacite*	*Dacite*	*Dacite*	*Andesite*	*Andesite*	*Andesite*	*Dacite*	*Trac And*	*Andesite*	*Andesite*
SiO2	64.22	64.48	67.90	66.72	64.99	65.06	63.95	60.16	61.98	58.96	64.06	61.08	61.40	61.11
TiO2	0.67	0.75	0.35	0.54	0.55	0.56	0.51	0.66	0.75	0.90	0.72	0.97	0.79	0.80
Al2O3	16.79	17.08	16.66	16.96	16.37	16.26	16.00	16.73	15.75	17.75	16.42	17.38	15.66	15.96
Fe2O3	4.06	4.96	3.00	3.65	3.63	3.74	3.80	5.18	4.89	5.30	4.41	5.42	5.32	5.23
MnO	0.06	0.06	0.09	0.09	0.06	0.06	0.06	0.06	0.07	0.08	0.05	0.09	0.08	0.07
MgO	1.91	0.38	0.40	0.89	2.49	2.46	3.57	4.31	3.62	3.13	2.16	2.24	3.95	3.71
CaO	4.60	2.91	1.84	2.66	4.49	4.56	5.52	6.59	5.28	6.72	4.75	5.00	5.32	5.58
Na2O	3.88	5.44	5.50	5.04	3.60	3.71	3.23	3.60	3.46	4.08	4.43	4.24	3.92	4.19
K2O	2.89	2.92	3.16	3.54	2.99	2.91	2.28	1.50	2.82	1.96	2.54	2.64	2.45	2.20
P2O5	0.21	0.31	0.13	0.23	0.22	0.21	0.18	0.27	0.26	0.35	0.24	0.28	0.25	0.27
L.O.I.	1.09	2.26	1.86	1.67	1.99	1.99	1.45	1.18	1.25	1.16	1.10	1.12	0.78	0.74
Total (LOI free)	99.29	99.29	99.03	100.32	99.40	99.54	99.08	99.09	98.87	99.24	99.78	99.34	99.16	99.12
Sc	10	7	4	6	9	10	9	14	13	15	10	11	13	12
Cr	0	1	2	1	41	48	130	152	123	11	60	5	111	116
V	87	28	1	5	85	87	90	127	102	155	93	92	100	105
Ni	26	3	4	6	30	34	103	133	82	30	54	12	83	100
Co	11	4	2	5	10	13	17	15	17	18	13	16	19	20
Cu	39	3	-2	-1	30	14	30	20	36	33	27	15	28	38
Zn	51	69	56	58	51	55	50	56	57	74	51	58	56	58
Ga	19	17	19	18	17	19	17	16	19	19	18	18	18	17
Rb	81	79	68	85	73	74	54	41	67	44	73	69	68	62
Sr	386	275	249	312	529	527	531	648	442	676	429	428	411	453
Y	14	31	20	22	10	10	8	10	19	18	22	19	16	17
Zr	185	350	447	363	131	132	89	90	175	156	174	184	172	163
Nb	13	18	15	17	11	11	8	9	13	14	13	14	13	14
Ba	562	592	670	606	644	625	423	424	463	496	487	414	453	439
La	23	27	40	37	22	23	16	22	31	34	45	25	25	25
Ce	51	48	72	71	46	41	31	42	52	62	51	50	45	47
Nd	15	25	26	25	16	14	15	16	24	21	26	20	15	14
Pb	15	13	18	15	15	14	12	9	10	12	14	13	15	14
Th	11	8	13	9	8	9	7	5	7	6	8	6	7	8

APPENDIX D

XRF analyses of the samples from the Erzurum-Kars Plateau, NE Turkey

Copyright © by Mehmet Keskin

Area	Kargapazarı	Kargapazarı	Kargapazarı	Kargapazarı	Kargapazarı	Kargapazarı	Kargapazarı	Kargapazarı	Kargapazarı	Kargapazarı	Kargapazarı	Kargapazarı	Kargapazarı	Kargapazarı
Sample no	**MK277**	**MK280**	**MK281**	**MK290**	**MK53**	**MK54**	**MK55**	**MK57**	**MK58**	**MK289**	**MK293**	**MK387**	**MK265**	**MK266**
Unit	Kpzr-1	Kpzr-1	Kpzr-1	Kpzr-1	Kpzr-1	Kpzr-1	Kpzr-1	Kpzr-1	Kpzr-1	Kpzr-2	Kpzr-3	Kpzr-3	Kpzr-4	Kpzr-4
Symbol	Gad	Gad	Gad	Gad	Gad	Gad	Gad	Gad	Gad	Kb	Gpd	Gpd	Kpa	Kpa
Level	Top	Mid	Mid	Mid	Mid	Mid	Mid	Mid	Mid	Base	Base	Base	Base	Base
Geoch. desc.	*Andesite*	*BaTracAnd*	*Trac And*	*Andesite*	*Andesite*	*Andesite*	*Andesite*	*TracAnd*	*TracAnd*	*Basalt*	*Andesite*	*Dacite*	*Dacite*	*Dacite*
SiO2	60.58	56.14	56.99	62.90	61.45	60.66	61.14	58.40	57.64	49.09	61.35	64.39	63.90	64.14
TiO2	0.80	1.92	1.83	0.72	0.81	0.82	0.80	1.05	1.04	1.26	0.78	0.69	0.61	0.61
Al2O3	15.85	15.97	16.12	15.94	17.32	15.96	17.24	16.12	15.59	16.92	16.73	15.92	15.31	15.55
Fe2O3	5.22	9.22	8.81	4.67	5.10	5.70	5.16	6.55	6.53	10.56	5.28	4.61	4.40	4.42
MnO	0.08	0.14	0.11	0.07	0.07	0.07	0.07	0.09	0.10	0.15	0.09	0.08	0.07	0.06
MgO	4.08	2.72	2.23	3.07	2.18	4.05	2.50	4.49	5.21	7.02	2.84	1.77	3.65	2.97
CaO	6.10	6.31	5.73	5.06	5.63	5.88	5.79	5.95	6.79	10.13	5.33	4.91	4.97	4.89
Na2O	4.11	4.32	4.68	3.85	4.32	3.82	4.15	4.08	3.98	3.11	3.85	4.10	3.53	3.94
K2O	2.18	1.90	2.00	2.58	2.18	1.96	2.13	2.07	2.00	0.51	2.53	2.61	2.73	2.35
P2O5	0.28	0.44	0.45	0.24	0.28	0.27	0.26	0.32	0.32	0.26	0.22	0.22	0.21	0.20
L.O.I.	0.84	1.00	0.97	1.11	1.29	1.04	1.06	1.15	0.97	1.47	0.78	1.32	1.27	1.23
Total (LOI free)	99.28	99.08	99.04	99.10	99.34	99.19	99.24	99.11	99.19	99.01	99.01	99.30	99.38	99.15
Sc	11	23	22	11	12	12	16	14	14	28	11	13	10	11
Cr	116	3	3	66	9	137	17	147	166	261	17	37	120	129
V	99	192	183	100	113	114	128	124	119	163	101	97	89	88
Ni	95	4	3	53	50	103	53	108	119	150	21	31	107	121
Co	21	20	11	15	18	20	17	19	23	47	16	11	18	17
Cu	32	24	20	22	44	63	47	35	30	96	31	26	36	41
Zn	55	79	83	54	63	63	64	69	64	104	64	60	56	56
Ga	20	20	18	18	18	17	18	18	20	20	20	19	17	17
Rb	62	48	52	74	59	55	58	53	51	11	57	66	70	71
Sr	472	415	403	418	553	489	557	522	526	440	407	379	438	439
Y	16	29	31	16	17	15	15	20	18	25	18	15	16	14
Zr	159	203	213	169	157	156	156	185	174	115	172	169	155	152
Nb	13	13	13	13	13	11	12	14	14	7	11	12	12	11
Ba	450	332	335	456	488	446	490	512	455	143	504	519	524	545
La	23	22	24	28	27	22	26	32	25	11	28	30	31	26
Ce	45	49	46	49	46	47	46	57	51	30	50	58	51	48
Nd	11	23	23	18	20	18	19	29	20	16	17	18	18	13
Pb	11	9	9	15	9	12	10	10	10	20	18	15	14	12
Th	6	6	7	7	6	7	7	7	7	1	6	10	7	9

APPENDIX D

XRF analyses of the samples from the Erzurum-Kars Plateau, NE Turkey

Copyright © by Mehmet Keskin

Area	Kargapazarı	Kargapazarı	Kargapazarı	Kargapazarı	Kargapazarı	Kargapazarı	Kargapazarı	Kargapazarı	Kargapazarı	Kargapazarı	Kargapazarı	Kargapazarı	Kargapazarı	Kargapazarı
Sample no	**MK17a**	**MK17b**	**MK52b**	**MK52e**	**MK263**	**MK267**	**MK270**	**MK271**	**MK272**	**MK268**	**MK279**	**MK59**	**MK60**	**MK61**
Unit	Kpzr-5	Kpzr-5	Kpzr-5	Kpzr-5	Kpzr-5	Kpzr-5	Kpzr-5	Kpzr-5	Kpzr-5	Kpzr-6	Kpzr-7	Kpzr-8	Kpzr-8	Kpzr-8
Symbol	Çpd	Çpd	Çpd	Çpd	Çpd	Çpd	Çpd	Çpd	Çpd	Gpaa	Bign(Kp)	Kv	Kv	Kv
Level	Mid	Mid	Mid	Mid	Mid	Mid	Mid	Mid	Mid	Mid	Mid	Plateau	Plateau	Plateau
Geoch. desc.	*Dacite*	*TracDac*	*Andesite*	*Dacite*	*Dacite*	*Dacite*	*Dacite*	*Dacite*	*Dacite*	*Dacite*	*TracDac*	*Andesite*	*Andesite*	*Andesite*
SiO2	66.79	67.95	59.96	63.44	66.48	63.89	66.59	63.42	63.51	65.47	67.55	59.99	59.75	59.69
TiO2	0.57	0.52	0.98	0.71	0.60	0.74	0.61	0.69	0.70	0.63	0.58	0.83	0.83	0.83
Al2O3	15.38	15.32	16.08	15.97	15.48	16.17	15.28	16.31	15.95	15.69	16.10	16.98	17.12	17.03
Fe2O3	3.66	3.08	6.02	4.51	3.86	4.74	3.84	4.45	4.47	3.91	3.33	5.63	5.69	5.66
MnO	0.05	0.06	0.08	0.07	0.06	0.06	0.06	0.07	0.07	0.06	0.08	0.09	0.10	0.10
MgO	1.82	1.66	3.88	2.65	2.82	2.74	2.67	2.92	2.99	2.03	0.51	3.04	3.12	3.34
CaO	3.35	2.86	5.56	4.86	3.95	5.00	3.93	4.97	4.94	3.95	2.01	6.20	6.18	6.35
Na2O	4.20	3.95	4.15	4.16	3.88	4.26	3.90	3.67	3.97	3.92	5.43	3.94	3.92	3.62
K2O	3.13	3.84	2.20	2.50	3.13	2.45	3.24	2.85	2.80	3.27	3.65	2.34	2.32	2.46
P2O5	0.14	0.14	0.30	0.24	0.15	0.26	0.15	0.24	0.24	0.20	0.13	0.25	0.24	0.24
L.O.I.	0.72	1.89	1.51	0.68	1.72	1.08	1.82	1.72	1.07	1.62	0.73	0.67	0.35	1.15
Total (LOI free)	99.08	99.38	99.20	99.10	100.43	100.30	100.27	99.59	99.64	99.14	99.38	99.28	99.28	99.33
Sc	8	5	13	9	8	10	9	11	10	9	7	16	16	17
Cr	85	42	153	59	90	65	84	65	65	30	5	8	8	11
V	57	43	109	86	67	91	75	92	99	70	18	130	126	122
Ni	68	33	119	58	66	66	64	53	54	28	6	23	20	21
Co	8	7	18	12	14	16	11	16	15	10	5	16	19	19
Cu	12	30	14	35	33	34	13	12	12	10	3	35	28	26
Zn	45	43	60	51	54	54	51	51	54	48	62	62	66	66
Ga	18	16	20	17	17	18	15	19	17	16	20	19	18	17
Rb	98	108	55	73	90	72	89	73	75	91	98	67	71	66
Sr	282	257	514	413	294	416	293	421	416	338	197	370	378	375
Y	14	15	20	14	15	17	18	16	16	15	29	24	22	24
Zr	192	201	189	172	179	168	185	170	172	178	323	212	212	208
Nb	13	14	14	14	12	11	13	13	12	14	19	16	16	15
Ba	560	588	505	538	518	496	516	473	486	461	639	710	507	479
La	22	28	31	24	29	29	24	26	30	27	34	28	29	30
Ce	38	50	49	43	44	46	49	51	53	43	59	52	55	59
Nd	16	20	27	20	13	15	15	17	21	15	28	21	26	26
Pb	18	13	10	12	17	15	16	14	14	15	14	12	12	11
Th	9	13	7	8	9	9	9	8	9	9	11	10	11	9

APPENDIX D

XRF analyses of the samples from the Erzurum-Kars Plateau, NE Turkey

Copyright © by Mehmet Keskin

Area	Kargapazarı	Kargapazarı	Kargapazarı	Kargapazarı	Kargapazarı	Kargapazarı	Kargapazarı	Kargapazarı	Kargapazarı	Kargapazarı	Kargapazarı	Kargapazarı	Kargapazarı	Kargapazarı
Sample no	**MK62**	**MK63**	**MK64**	**MK66**	**MK67**	**MK68**	**MK69**	**MK287**	**MK288**	**MK294**	**MK295**	**MK296**	**MK297**	**MK298**
Unit	Kpzr-8	Kpzr-8	Kpzr-8	Kpzr-8	Kpzr-8	Kpzr-8	Kpzr-8	Kpzr-8	Kpzr-8	Kpzr-8	Kpzr-8	Kpzr-8	Kpzr-8	Kpzr-8
Symbol	Kv	Kv	Kv	Kv	Kv	Kv	Kv	Kv	Kv	Kv	Kv	Kv	Kv	Kv
Level	Plateau	Plateau	Plateau	Plateau	Plateau	Plateau	Plateau	Plateau	Plateau	Plateau	Plateau	Plateau	Plateau	Plateau
Geoch. desc.	*BaAnd*	*BaAnd*	*BaAnd*	*BaAnd*	*TracAnd*	*Andesite*	*BaAnd*	*BaAnd*	*Andesite*	*BaAnd*	*BaAnd*	*BaAnd*	*BaAnd*	*BaAnd*
SiO2	55.35	54.39	55.60	56.92	60.24	58.70	56.97	56.28	58.35	55.59	56.78	56.53	56.89	56.55
TiO2	1.04	1.10	1.13	0.95	0.93	0.87	0.98	0.97	0.83	0.96	0.96	0.98	0.98	0.96
Al2O3	16.65	18.58	16.91	16.55	17.10	16.96	16.53	16.84	17.15	16.34	16.97	16.90	16.67	16.60
Fe2O3	7.25	7.52	7.52	6.65	5.87	5.99	6.73	6.69	5.86	6.58	6.59	6.74	6.68	6.65
MnO	0.12	0.13	0.13	0.11	0.09	0.10	0.11	0.12	0.10	0.11	0.11	0.11	0.11	0.11
MgO	5.34	4.87	4.66	4.52	2.26	3.68	4.37	4.55	3.98	4.41	4.35	4.50	4.48	4.51
CaO	8.00	7.72	7.43	7.57	5.49	6.77	7.57	7.89	6.83	7.77	7.63	7.51	7.50	7.92
Na2O	3.33	3.39	3.74	3.61	4.24	3.56	3.75	3.65	3.52	3.69	3.76	3.82	3.86	3.69
K2O	1.76	1.22	1.65	1.91	2.55	2.19	1.81	1.89	2.31	1.94	1.93	1.84	1.87	1.90
P2O5	0.26	0.29	0.24	0.28	0.28	0.26	0.27	0.28	0.24	0.27	0.28	0.28	0.29	0.28
L.O.I.	0.59	4.56	0.58	0.55	1.43	0.86	0.50	0.96	1.26	0.81	0.37	0.47	0.22	0.76
Total (LOI free)	99.10	99.19	99.01	99.08	99.06	99.06	99.10	99.16	99.18	97.66	99.37	99.22	99.33	99.17
Sc	20	22	21	18	17	17	17	18	15	18	17	18	18	18
Cr	147	92	109	91	11	31	100	86	12	83	85	89	93	89
V	156	162	154	141	135	136	147	135	121	143	150	135	142	134
Ni	69	51	46	56	16	37	65	47	39	49	49	53	55	52
Co	28	25	27	24	17	18	22	21	19	23	23	21	24	26
Cu	35	41	27	24	23	22	33	33	18	35	25	29	32	32
Zn	66	73	70	68	69	64	72	59	67	64	65	68	64	70
Ga	19	21	19	20	18	18	17	17	19	17	20	20	19	20
Rb	47	10	37	51	70	62	51	46	62	53	52	48	46	50
Sr	412	499	340	436	366	400	415	440	394	432	433	425	422	426
Y	24	32	30	24	31	24	26	25	21	27	24	22	25	25
Zr	192	222	219	199	243	208	198	194	199	195	196	198	202	195
Nb	13	16	13	15	18	16	14	15	13	15	15	15	14	15
Ba	402	735	382	441	636	465	448	495	482	443	442	441	444	428
La	25	44	28	33	41	30	26	34	29	29	30	28	27	26
Ce	45	57	51	54	62	56	50	51	54	52	53	54	53	51
Nd	19	38	26	27	29	28	23	23	23	20	21	21	15	19
Pb	8	12	11	12	17	13	9	11	13	11	11	12	10	11
Th	9	10	9	7	11	10	8	7	9	9	8	9	8	8

APPENDIX D

XRF analyses of the samples from the Erzurum-Kars Plateau, NE Turkey

Copyright © by Mehmet Keskin

Area	Kargapazarı	Kargapazarı	Kargapazarı	Kargapazarı	Kargapazarı	Kargapazarı	Kargapazarı	Kargapazarı	Standard
Sample no	**MK299**	**MK300**	**MK301**	**MK302**	**MK303**	**MK304**	**MK305**	**MK306**	**error**
Unit	Kpzr-8	Kpzr-8	Kpzr-8	Kpzr-8	Kpzr-8	Kpzr-8	Kpzr-8	Kpzr-8	
Symbol	Kv	Kv	Kv	Kv	Kv	Kv	Kv	Kv	
Level	Plateau	Plateau	Plateau	Plateau	Plateau	Plateau	Plateau	Plateau	
Geoch. desc.	*Andesite*	*BaAnd*	*BaAnd*	*BaAnd*	*BaAnd*	*BaAnd*	*BaAnd*	*BaAnd*	
SiO2	57.07	56.98	56.64	56.75	56.60	56.37	57.02	56.67	±0.57
TiO2	0.97	0.96	0.98	0.97	1.00	0.99	0.97	0.97	±0.01
Al2O3	16.80	16.72	16.88	16.78	16.61	16.57	16.58	16.77	±0.17
Fe2O3	6.64	6.66	6.76	6.68	6.92	6.86	6.63	6.64	±0.05
MnO	0.11	0.11	0.12	0.12	0.12	0.12	0.11	0.11	±0.01
MgO	3.85	4.21	4.30	4.20	4.85	4.75	4.36	4.53	±0.08
CaO	7.56	7.46	7.51	7.55	7.59	7.56	7.50	7.62	±0.04
Na2O	3.88	3.91	3.79	3.84	3.67	3.76	3.86	3.59	±0.10
K2O	1.90	1.87	1.86	1.89	1.90	1.89	1.87	1.98	±0.03
P2O5	0.29	0.29	0.28	0.28	0.29	0.28	0.27	0.28	±0.01
L.O.I.	0.82	0.55	0.43	0.56	0.56	0.34	0.54	0.77	
Total (LOI free)	99.07	99.18	99.13	99.08	99.55	99.15	99.17	99.15	
Sc	21	17	21	18	19	20	19	18	±1.97-2.10
Cr	88	96	94	92	112	106	88	89	±4.17-14.45
V	152	156	133	150	128	139	146	151	±6.64-7.69
Ni	48	68	51	65	69	69	58	56	±4.25-6.51
Co	26	26	27	28	24	27	27	23	±1.9
Cu	31	40	16	31	30	33	34	33	±2.01
Zn	65	71	68	65	68	67	66	67	±3.9
Ga	18	18	21	17	18	18	19	19	±1.32-3.30
Rb	55	52	52	53	50	49	52	46	±1.56-3.52
Sr	432	418	425	422	411	412	424	432	±2.8-5.2
Y	26	23	25	25	24	25	22	25	±1.18-1.2
Zr	197	198	199	197	202	201	197	197	±2.46-6.58
Nb	14	15	15	15	14	14	15	15	±0.85-2.49
Ba	453	434	439	441	417	415	430	442	±5.43
La	30	25	31	31	30	29	30	30	±1.79 (3.21)
Ce	54	50	56	52	53	53	55	55	±2.87 (4.84)
Nd	20	14	21	23	22	22	22	20	±2.36-2.43
Pb	9	11	9	11	12	11	11	11	±3.67
Th	8	9	8	7	7	7	8	7	±0.99

APPENDIX D

XRF analyses of the samples from the Erzurum-Kars Plateau, NE Turkey

Copyright © by Mehmet Keskin

Area	Pasinler	Pasinler	Pasinler	Pasinler	Pasinler	Pasinler	Pasinler	Pasinler	Pasinler	Pasinler	Pasinler	Pasinler	Pasinler
Sample no :	**MK120**	**MK121**	**MK122**	**MK343**	**MK363**	**MK364**	**MK375**	**MK377**	**MK123**	**MK109**	**MK115**	**MK116**	**MK117**
Unit	Pasin-1	Pasin-1	Pasin-1	Pasin-1	Pasin-1	Pasin-1	Pasin-2	Pasin-2	Pasin-3	Pasin-3	Pasin-3	Pasin-3	Pasin-3
Symbol	En1	En1	En1	En1	En1	En1	Mtd	Mtd	Baad	Baad	Baad	Baad	Baad
Level	Basement	Basement	Basement	Basement	Basement	Basement	Basement	Basement	Base	Base	Base	Base	Base
Geoch. desc	*BaTraAnd*	*BasAnd*	*BasAnd*	*BaTrAnd*	*BaAnd*	*BaAnd*	*Dacite*	*Dacite*	*TracAnd*	*Andesite*	*Dacite*	*Andesite*	*Andesite*
SiO2	54.39	54.24	53.61	54.56	55.83	53.81	70.13	69.50	61.55	62.84	63.73	62.35	62.14
TiO2	1.27	1.20	1.35	1.60	1.14	1.01	0.47	0.43	0.71	0.81	0.70	0.90	0.90
Al2O3	18.57	20.60	19.03	17.16	19.53	18.24	14.71	15.43	17.67	16.72	16.88	16.60	16.59
Fe2O3	7.95	7.43	8.63	8.56	7.29	8.54	3.19	3.45	5.37	5.21	4.85	5.70	5.78
MnO	0.13	0.19	0.16	0.08	0.13	0.15	0.03	0.03	0.08	0.08	0.07	0.09	0.09
MgO	3.88	3.17	3.26	2.93	2.70	4.42	0.57	0.38	1.79	1.96	1.44	1.99	1.99
CaO	6.38	7.20	8.42	7.21	7.31	9.45	3.43	3.38	4.83	4.85	4.84	4.91	4.97
Na2O	3.28	3.81	3.37	3.16	3.80	2.87	3.59	3.75	4.15	4.38	4.25	3.79	4.03
K2O	2.77	1.05	1.07	2.85	1.75	1.01	2.92	3.11	2.66	2.15	2.15	2.62	2.34
P2O5	0.46	0.31	0.27	0.60	0.30	0.18	0.16	0.17	0.26	0.20	0.19	0.21	0.20
L.O.I.	3.84	7.14	2.33	3.22	1.78	1.81	0.69	0.63	1.98	0.00	1.25	1.19	0.77
Total (LOI free)	99.08	99.20	99.16	99.11	99.79	99.67	99.20	99.62	99.07	99.20	99.11	99.14	99.04
Sc	18	19	22	16	18	30	9	7	13	15	10	13	16
Cr	12	2	1	28	4	59	6	11	3	9	5	2	3
V	254	193	261	245	184	271	61	59	107	104	96	113	113
Ni	11	1	4	13	7	21	6	11	3	3	12	1	4
Co	19	18	22	20	20	32	5	5	11	12	10	15	18
Cu	184	225	72	246	138	92	8	43	45	27	32	14	29
Zn	81	73	84	89	69	75	25	43	61	63	59	60	63
Ga	18	19	19	19	21	18	16	15	17	19	17	19	19
Rb	46	19	8	55	42	14	67	82	78	57	58	63	59
Sr	430	866	479	359	383	368	357	382	314	379	406	353	357
Y	27	27	25	35	28	22	15	16	24	18	17	21	21
Zr	194	145	162	292	164	98	132	132	244	163	155	169	169
Nb	18	17	21	26	18	9	14	15	12	9	10	10	9
Ba	777	441	349	627	357	274	706	678	486	465	503	480	503
La	31	24	22	45	22	12	22	25	22	17	20	19	17
Ce	60	50	42	79	44	27	51	46	44	33	38	44	43
Nd	31	25	22	39	24	13	15	12	19	15	16	20	16
Pb	15	13	11	25	12	8	16	22	16	13	10	12	14
Th	7	6	4	10	4	2	12	11	8	7	9	9	8

APPENDIX D

XRF analyses of the samples from the Erzurum-Kars Plateau, NE Turkey

Copyright © by Mehmet Keskin

Area	Pasinler	Pasinler	Pasinler	Pasinler	Pasinler	Pasinler	Pasinler	Pasinler	Pasinler	Pasinler	Pasinler	Pasinler	Pasinler
Sample no :	**MK112**	**MK118**	**MK119**	**MK124**	**MK337**	**MK71**	**MK72**	**MK73**	**MK107**	**MK102**	**MK103**	**MK104**	**MK105**
Unit	Pasin-4	Pasin-4	Pasin-4	Pasin-4	Pasin-4	Pasin-5a	Pasin-5a	Pasin-5a	Pasin-5a	Pasin-5a	Pasin-5a	Pasin-5a	Pasin-5a
Symbol	Kpd	Kpd	Kpd	Kpd	Kpd	Ltl (Gign)	Ltl (Gign)	Ltl (Gign)	Ltl (Gign)	Ltl (Gign)	Ltl (Gign)	Ltl (Gign)	Ltl (Gign)
Level	Mid	Mid	Mid	Mid	Mid	Base	Base	Base	Base	Base	Base	Base	Base
Geoch. desc	*Dacite*	*Dacite*	*Dacite*	*Rhyolite*	*Dacite*	*Rhyolite*	*Rhyolite*	*Rhyolite*	*Rhyolite*	*Rhyolite*	*Rhyolite*	*Rhyolite*	*Rhyolite*
SiO2	66.81	66.42	67.02	72.03	66.60	75.45	75.48	75.70	75.91	75.34	75.36	75.79	76.14
TiO2	0.57	0.57	0.55	0.25	0.55	0.10	0.10	0.10	0.10	0.10	0.10	0.10	0.10
Al2O3	15.90	16.56	15.99	14.60	15.97	13.12	13.04	12.92	12.76	13.06	12.87	12.81	13.08
Fe2O3	3.82	3.66	3.72	1.80	3.69	1.23	1.20	1.20	1.21	1.19	1.22	1.18	0.60
MnO	0.06	0.05	0.06	0.04	0.05	0.05	0.05	0.05	0.05	0.04	0.04	0.05	0.01
MgO	1.24	1.24	1.26	0.34	1.23	0.03	0.00	0.02	0.03	0.04	0.02	0.02	0.03
CaO	3.68	4.00	3.66	1.60	3.79	0.43	0.41	0.39	0.40	0.41	0.41	0.41	0.33
Na2O	3.68	3.95	3.57	3.47	3.57	3.38	3.37	3.52	3.64	3.59	3.51	3.75	4.63
K2O	3.26	2.58	3.30	4.71	3.35	5.54	5.46	5.16	5.21	5.25	5.30	4.96	4.28
P2O5	0.16	0.16	0.16	0.08	0.16	0.03	0.02	0.02	0.02	0.02	0.03	0.02	0.02
L.O.I.	1.81	2.02	2.42	2.04	1.94	3.71	3.78	3.34	3.56	3.44	3.64	3.31	0.66
Total (LOI free)	99.17	99.20	99.28	98.91	98.96	99.36	99.12	99.04	99.33	99.04	98.91	99.05	99.16
Sc	8	10	9	5	11	1	2	4	1	3	3	4	2
Cr	5	2	4	3	5	3	6	7	1	3	6	6	3
V	64	74	64	16	64	2	5	2	2	1	0	5	1
Ni	12	0	2	2	5	2	5	6	3	7	8	6	0
Co	8	9	8	1	7	1		1					
Cu	17	16	11	0	48	2	6	1		7	5		
Zn	49	49	47	38	56	42	38	40	40	39	39	40	32
Ga	18	18	18	15	16	16	16	16	16	19	20	16	17
Rb	78	63	77	162	76	173	171	176	176	179	181	179	139
Sr	339	399	341	168	355	8	7	6	7	7	6	6	6
Y	18	11	15	21	17	36	36	35	35	35	36	36	28
Zr	156	142	152	177	150	176	174	173	176	175	173	174	184
Nb	11	11	11	20	11	27	27	26	27	27	27	27	29
Ba	581	500	577	811	523	57	35	27	26	24	23	19	49
La	26	19	20	32	21	45	45	42	47	46	45	46	47
Ce	40	37	40	57	41	90	76	74	81	78	77	79	83
Nd	20	15	13	22	13	38	23	19	24	25	21	25	28
Pb	15	13	15	24	20	24	26	26	25	26	27	28	27
Th	10	9	8	24	8	35	37	37	33	38	38	33	41

APPENDIX D

XRF analyses of the samples from the Erzurum-Kars Plateau, NE Turkey

Copyright © by Mehmet Keskin

Area	Pasinler	Pasinler	Pasinler	Pasinler	Pasinler	Pasinler	Pasinler	Pasinler	Pasinler	Pasinler	Pasinler	Pasinler	Pasinler
Sample no :	**MK75**	**MK76**	**MK77**	**MK309**	**MK347**	**MK355**	**MK70**	**MK74**	**MK345**	**MK110**	**MK111**	**MK78**	**MK79**
Unit	Pasin-5b	Pasin-5b	Pasin-5b	Pasin-5b	Pasin-5b	Pasin-5b	Pasin-5c	Pasin-5c	Pasin-5c	Pasin-5d	Pasin-5d	Pasin-6	Pasin-6
Symbol	Ltl (Wign)	Ltl (Wign)	Ltl (Wign)	Ltl (Wign)	Ltl (Wign)	Ltl (Wign)	Ltl (Obsid.)	Ltl (Obsid.)	Ltl (Obsid.)	Utl (Tuff)	Utl (Tuff)	Bign	Bign
Level	Base	Base	Base	Base	Base	Base	Base	Base	Base	Mid	Mid	Mid	Mid
Geoch. desc	*Rhyolite*	*Rhyolite*	*Rhyolite*	*Rhyolite*	*Rhyolite*	*Rhyolite*	*Rhyolite*	*Rhyolite*	*Rhyolite*	*Rhyolite*	*Rhyolite*	*TracDac*	*TracDac*
SiO2	75.81	71.91	75.32	75.93	75.35	73.97	75.87	75.66	75.33	76.02	69.43	63.09	68.05
TiO2	0.10	0.21	0.11	0.10	0.10	0.14	0.10	0.10	0.10	0.06	0.24	1.08	0.59
Al2O3	12.73	14.66	13.08	12.63	12.98	13.52	12.75	12.86	12.93	13.37	15.76	16.26	16.60
Fe2O3	1.20	1.75	1.23	1.29	1.21	1.43	1.19	1.21	1.21	1.05	2.30	4.93	2.82
MnO	0.04	0.03	0.03	0.03	0.04	0.05	0.05	0.05	0.05	0.04	0.06	0.10	0.07
MgO	0.01	0.05	0.03	0.01	0.03	0.02	0.01	0.01	0.00	0.21	0.12	1.33	0.27
CaO	0.35	0.44	0.35	0.33	0.34	0.38	0.40	0.41	0.40	0.62	1.08	3.20	1.30
Na2O	4.20	4.89	4.18	4.20	4.22	4.52	4.23	3.61	4.28	2.60	4.34	4.69	4.98
K2O	4.69	5.28	4.76	4.75	4.71	4.95	4.73	5.19	4.68	5.46	5.68	4.02	4.37
P2O5	0.02	0.03	0.02	0.03	0.02	0.03	0.02	0.03	0.03	0.02	0.05	0.32	0.10
L.O.I.	0.41	0.71	0.50	0.40	0.39	0.38	0.24	3.91	0.42	11.60	4.87	2.57	1.41
Total (LOI free)	99.13	99.24	99.06	99.28	99.00	99.01	99.36	99.12	99.01	99.46	99.06	99.01	99.15
Sc	3	2	3	3	1	3	1	1	1	2	7	11	5
Cr	5	3	0	2	1	2	1	1	1	4	2	1	3
V	4	6	3	0	1	2	2	2	2		7	58	21
Ni	1	5	6	3	1	2	1	2	3	3	2	8	1
Co					3							4	1
Cu	1				20				20	4	1	3	
Zn	35	41	36	32	44		42	39	48	38	45	71	49
Ga	18	17	19	16	16	19	17	16	17	18	17	18	19
Rb	178	152	178	179	181	168	181	176	176	227	128	92	117
Sr	7	15	8	7	8	10	6	6	6	27	82	270	133
Y	34	29	34	31	30	35	37	35	37	40	31	39	32
Zr	177	377	198	149	171	238	180	175	179	113	308	580	485
Nb	27	27	28	22	27	26	28	27	27	28	21	22	25
Ba	39	108	51	27	27	64	40	52	27	33	626	784	859
La	44	50	48	46	48	56	46	46	50	20	81	50	48
Ce	70	65	75	86	82	87	76	81	89	41	133	91	80
Nd	25	26	31	21	18	23	22	23	21	15	42	44	37
Pb	27	27	25	22	27	0	27	24	30	25	19	23	25
Th	39	32	37	37	34	0	37	37	38	46	27	16	22

APPENDIX D

XRF analyses of the samples from the Erzurum-Kars Plateau, NE Turkey

Copyright © by Mehmet Keskin

Area	Pasinler	Pasinler	Pasinler	Pasinler	Pasinler	Pasinler	Pasinler	Pasinler	Pasinler	Pasinler	Pasinler	Pasinler	Pasinler
Sample no :	**MK80**	**MK106**	**MK113**	**MK114**	**MK315**	**MK318**	**MK319**	**MK321**	**MK356**	**MK358**	**MK359**	**MK362**	**MK307**
Unit	Pasin-6	Pasin-6	Pasin-6	Pasin-6	Pasin-6	Pasin-6	Pasin-6	Pasin-6	Pasin-6	Pasin-6	Pasin-6	Pasin-6	Pasin-7a
Symbol	Bign	Bign	Bign	Bign	Bign	Bign	Bign	Bign	Bign	Bign	Bign	Bign	Kv (Dyke)
Level	Mid	Mid	Mid	Mid	Mid	Mid	Mid	Mid	Mid	Mid	Mid	Mid	Base
Geoch. desc	*Rhyolite*	*TracDac*	*Rhyolite*	*Rhyolite*	*Rhyolite*	*TracDac*	*Rhyolite*	*TracDac*	*Rhyolite*	*TracDac*	*Rhyolite*	*TracDac*	*Andesite*
SiO2	69.62	67.53	69.35	69.02	70.29	65.11	70.72	68.84	69.82	64.90	69.23	68.50	57.06
TiO2	0.42	0.59	0.43	0.43	0.41	0.83	0.42	0.50	0.42	0.87	0.47	0.40	1.05
Al2O3	15.94	16.31	15.74	15.90	15.31	16.15	15.41	15.97	16.16	16.51	15.72	15.59	16.89
Fe2O3	2.03	2.87	2.04	1.99	1.95	3.90	2.01	2.35	2.01	4.06	2.29	1.98	6.59
MnO	0.06	0.08	0.07	0.05	0.07	0.09	0.06	0.08	0.07	0.10	0.07	0.06	0.22
MgO	0.14	0.70	0.33	0.14	0.30	1.13	0.13	0.44	0.32	1.10	0.44	0.20	3.44
CaO	1.04	1.90	1.25	1.67	1.12	2.67	1.01	1.46	1.36	2.64	1.38	1.70	8.49
Na2O	5.16	5.01	4.91	5.35	4.91	4.94	5.19	4.83	5.21	4.67	4.57	5.42	3.50
K2O	4.59	4.30	4.69	4.51	4.96	4.02	4.65	4.85	4.84	4.01	4.88	4.55	1.81
P2O5	0.07	0.12	0.07	0.06	0.07	0.21	0.09	0.11	0.08	0.20	0.09	0.08	0.27
L.O.I.	1.20	2.47	2.82	1.15	2.30	1.61	0.56	3.17	2.35	2.87	2.65	0.81	2.33
Total (LOI free)	99.07	99.40	98.90	99.11	99.40	99.05	99.69	99.41	100.30	99.06	99.15	98.47	99.33
Sc	4	3	5	5	3	5	4	4	5	8	5	4	20
Cr		2	1		4	0	3	2	3	1	1	6	110
V	5	23	5	6	7	43	7	5	4	40	9	4	156
Ni	2	2	2	1	4		1	3	3	3	3	7	48
Co	2	3	2			4	2	2	2	3	2	1	27
Cu						19	3			3			33
Zn	46	53	50	40	52	65	49	50	47	57	44	43	111
Ga	18	17	17	16	17	18	19	18	17	18	17	19	17
Rb	128	111	120	120	127	100	130	115	120	99	128	126	46
Sr	108	170	120	126	100	236	100	135	129	233	124	117	418
Y	34	33	33	30	33	37	35	35	32	36	33	34	31
Zr	457	463	466	473	446	513	449	464	434	506	438	429	189
Nb	26	23	25	25	26	22	26	25	24	23	24	25	13
Ba	799	856	836	699	765	770	722	767	820	786	730	723	363
La	46	45	48	47	51	49	49	49	47	49	47	53	28
Ce	85	81	79	80	88	85	82	88	85	84	86	82	57
Nd	31	31	32	36	30	34	26	28	30	32	28	28	24
Pb	21	20	23	18	46	25	21	22	24	19	21	24	10
Th	23	18	21	22	21	18	21	22	20	19	22	23	7

APPENDIX D

XRF analyses of the samples from the Erzurum-Kars Plateau, NE Turkey

Copyright © by Mehmet Keskin

Area	Pasinler	Pasinler	Pasinler	Pasinler	Pasinler	Pasinler	Pasinler	Pasinler	Pasinler	Pasinler	Pasinler	Pasinler	Pasinler
Sample no :	**MK308**	**MK310**	**MK100**	**MK101**	**MK311**	**MK313**	**MK314**	**MK316**	**MK317**	**MK323**	**MK357**	**MK108**	**MK125**
Unit	Pasin-7a	Pasin-7a	Pasin-7b	Pasin-7b	Pasin-7b	Pasin-7b	Pasin-7b	Pasin-7b	Pasin-7b	Pasin-7b	Pasin-7b	Pasin-8	Pasin-8
Level	Kv (Dyke)	Kv (Dyke)	Kv	Kv	Kv	Kv	Kv	Kv	Kv	Kv	Kv	Ard	Ard
	Base	Base	Top	Top	Top	Top	Top	Top	Top	Top	Top	Top	Top
Geoch. desc	*Andesite*	*Andesite*	*Andesite*	*BaAnd*	*Andesite*	*Andesite*	*Andesite*	*Andesite*	*Andesite*	*TracAnd*	*TracAnd*	*Rhyolite*	*Rhyolite*
SiO2	59.96	61.40	60.43	57.01	58.29	57.24	57.73	61.32	57.12	57.64	57.72	70.08	73.60
TiO2	1.11	0.84	0.83	0.91	0.85	0.88	0.90	0.83	0.93	1.27	1.31	0.24	0.11
Al2O3	18.03	17.25	17.08	16.83	16.84	16.67	16.75	16.93	19.49	17.07	16.74	15.89	13.95
Fe2O3	4.90	5.21	5.45	6.55	6.08	6.42	6.75	5.44	6.37	7.34	7.58	1.75	1.50
MnO	0.05	0.08	0.09	0.11	0.10	0.11	0.09	0.08	0.10	0.09	0.13	0.03	0.06
MgO	2.07	2.58	2.78	4.56	3.75	4.64	3.68	2.47	3.12	2.79	3.41	0.12	0.02
CaO	7.43	5.55	5.85	7.60	6.93	7.48	7.26	5.60	6.25	6.09	6.63	1.01	0.70
Na2O	3.47	3.64	3.85	3.48	3.69	3.47	3.80	4.05	3.86	4.28	4.10	4.73	4.18
K2O	1.80	2.66	2.55	2.00	2.21	2.13	1.95	2.52	1.77	2.20	2.15	5.36	4.99
P2O5	0.27	0.23	0.24	0.27	0.26	0.26	0.26	0.24	0.29	0.31	0.30	0.07	0.02
L.O.I.	3.24	1.61	0.92	1.18	0.81	0.85	1.29	0.67	2.68	1.17	0.49	1.31	2.64
Total (LOI free)	99.09	99.45	99.14	99.33	99.00	99.30	99.18	99.48	99.32	99.08	100.07	99.27	99.13
Sc	22	14	15	17	19	19	19	15	17	21	21	4	4
Cr	144	4	3	78	37	69	71	6	15	27	19	5	3
V	164	127	125	150	136	136	142	123	82	161	177	6	3
Ni	55	13	10	58	43	61	55	19	41	19	13		7
Co	17	16	13	25	21	23	21	18	22	16	19	1	
Cu	38	25	25	24	35	25	29	27	44	49	26	0	
Zn	115	79	64	69	67	66	67	64	77	81	76	48	49
Ga	19	18	24	18	17	17	17	18	19	20	20	18	17
Rb	55	74	72	54	61	56	57	76	18	63	57	122	142
Sr	434	348	347	419	409	420	418	345	388	337	351	92	31
Y	39	27	24	21	22	24	23	23	27	40	31	29	36
Zr	194	217	223	193	198	189	190	223	241	261	251	299	180
Nb	14	15	16	16	16	15	16	16	17	16	16	19	23
Ba	382	496	565	477	490	445	475	506	613	487	567	623	231
La	38	36	31	32	30	29	30	33	39	62	31	83	33
Ce	59	60	59	58	53	52	56	57	64	65	55	131	69
Nd	27	22	27	28	16	22	23	25	26	42	24	43	25
Pb	12	15	14	11	15	11	11	13	15	16	14	19	21
Th	6	12	9	9	9	8	7	11	12	11	9	29	24

APPENDIX D

XRF analyses of the samples from the Erzurum-Kars Plateau, NE Turkey

Copyright © by Mehmet Keskin

Area	Pasinler	Pasinler	Pasinler	Pasinler	Pasinler	Pasinler	Pasinler	Pasinler	Pasinler	Pasinler	N. Horasan	N. Horasan	N. Horasan
Sample no :	**MK320**	**MK324**	**MK327**	**MK328**	**MK331**	**MK332**	**MK334**	**MK338**	**MK342**	**MK360**	**MK127**	**MK128**	**MK129**
Unit	Pasin-8	Pasin-8	Pasin-8	Pasin-8	Pasin-8	Pasin-8	Pasin-8	Pasin-8	Pasin-8	Pasin-8	N.Horas-1	N.Horas-1	N.Horas-1
Level	Ard	Ard	Ard	Ard	Ard	Ard	Ard	Ard	Ard	Ard	Mad	Mad	Mad
	Top	Top	Top	Top	Top	Top	Top	Top	Top	Top	Basement	Basement	Basement
Geoch. desc	*Rhyolite*	*Rhyolite*	*Rhyolite*	*Rhyolite*	*Rhyolite*	*Rhyolite*	*Rhyolite*	*Rhyolite*	*Rhyolite*	*TracDac*	*Dacite*	*Dacite*	*Dacite*
SiO2	72.55	73.83	73.36	73.62	71.27	74.08	71.03	71.00	69.96	68.97	68.78	70.06	66.67
TiO2	0.14	0.11	0.11	0.11	0.18	0.10	0.19	0.17	0.24	0.24	0.35	0.30	0.45
Al2O3	14.49	14.26	13.83	13.93	15.53	13.93	15.37	15.33	16.35	15.89	16.56	16.17	16.84
Fe2O3	1.69	1.52	1.51	1.53	1.96	1.46	1.93	1.92	2.32	2.35	2.81	2.32	3.88
MnO	0.05	0.07	0.06	0.06	0.07	0.05	0.03	0.06	0.07	0.08	0.04	0.03	0.04
MgO	0.03	0.06	0.06	0.08	0.04	0.06	0.08	0.01	0.17	0.19	0.33	0.60	0.71
CaO	0.57	0.70	0.68	1.11	0.75	0.66	0.84	0.66	1.12	1.15	3.24	3.48	3.82
Na2O	4.62	4.08	4.28	4.08	4.43	4.13	4.36	4.51	4.36	4.4	4.35	3.88	3.70
K2O	5.21	5.21	5.10	5.28	5.21	4.69	5.28	5.34	5.42	5.7	2.50	2.04	2.75
P2O5	0.03	0.03	0.03	0.03	0.04	0.02	0.05	0.04	0.06	0.06	0.13	0.10	0.23
L.O.I.	0.35	3.09	2.64	3.32	0.94	2.25	0.84	0.55	1.95	1.64154691	1.49	2.39	3.74
Total (LOI free)	99.37	99.88	99.01	99.83	99.48	99.18	99.16	99.04	100.08	99.04	99.09	98.98	99.11
Sc	5	4	1	3	3	2	6	4	3	3	7	4	10
Cr	1	2	2	3	2	2	3	2	3	2	3	11	20
V	1	1	1	2	4	1	6	2	4	7	23	29	70
Ni	1	2	3	1	2	3	2	3	7	3	4	11	13
Co		1	1		1	1	1		2	0	4	4	8
Cu		1			28		1	4	1	1	12	11	25
Zn	41	48	47	45	52	46	44	45	40	46	47	43	45
Ga	17	17	17	18	16	18	18	17	26	18	19	18	16
Rb	141	139	141	140	129	136	128	133	121	119	63	61	71
Sr	37	34	32	37	57	33	66	48	83	91	500	430	502
Y	30	35	35	36	33	33	40	34	30	34	10	6	12
Zr	202	179	178	175	239	173	243	230	294	317	144	129	127
Nb	21	24	22	24	20	23	17	20	21	19	15	11	14
Ba	302	258	241	229	498	205	527	434	653	741	732	839	923
La	70	37	33	39	70	29	76	70	82	86	21	16	34
Ce	117	72	59	71	127	57	108	125	137	140	38	25	55
Nd	39	25	19	26	37	17	32	37	33	39	12	11	24
Pb	25	24	21	22	23	20	16	21	21	20	18	17	16
Th	26	24	24	24	28	23	27	27	27	25	10	9	15

APPENDIX D

XRF analyses of the samples from the Erzurum-Kars Plateau, NE Turkey

Copyright © by Mehmet Keskin

Area	N. Horasan	N. Horasan	N. Horasan	N. Horasan	N. Horasan	N. Horasan	N. Horasan	N. Horasan	N. Horasan	N. Horasan	N. Horasan	N. Horasan	N. Horasan
Sample no :	**MK141**	**MK142**	**MK138**	**MK144**	**MK126**	**MK136**	**MK137**	**MK132**	**MK133**	**MK140**	**MK130**	**MK131**	**MK134**
Unit	N.Horas-1	N.Horas-1	N.Horas-2	N.Horas-2	N.Horas-3	N.Horas-4	N.Horas-4	N.Horas-5	N.Horas-5	N.Horas-5	N.Horas-6	N.Horas-6	N.Horas-6
Symbol	Mad	Mad	Köb	Köb	Pblh (Wign)	Pblh (Wign)	Pblh (Wign)	Kpad	Kpad	Kpad	Hpl	Hpl	Hpl
Level	Basement	Basement	Base	Base	Base	Base	Base	Mid	Mid	Mid	Plateau	Plateau	Plateau
Geoch. desc.	*Dacite*	*Dacite*	*BaAnd*	*Basalt*	*Rhyolite*	*Rhyolite*	*Rhyolite*	*Dacite*	*Dacite*	*Dacite*	*BaTraAnd*	*BaAnd*	*Dacite*
SiO2	69.93	69.58	53.63	48.76	75.36	75.60	75.78	64.18	68.36	68.62	54.36	56.29	64.01
TiO2	0.42	0.39	1.18	1.34	0.06	0.10	0.10	0.65	0.41	0.39	1.90	1.29	0.71
Al2O3	14.91	15.57	15.81	15.18	14.14	13.04	13.21	16.35	15.91	15.52	15.81	16.68	16.04
Fe2O3	2.78	2.60	8.95	9.10	0.69	0.96	0.88	4.53	2.79	2.87	9.71	8.09	4.80
MnO	0.06	0.03	0.14	0.33	0.05	0.03	0.03	0.06	0.04	0.05	0.18	0.13	0.08
MgO	1.13	0.75	4.93	8.40	0.22	0.00	0.03	1.48	1.11	1.25	4.56	3.86	2.12
CaO	3.29	3.32	9.36	11.40	1.10	0.30	0.32	4.71	3.39	3.53	7.90	7.38	4.80
Na2O	4.08	3.81	3.64	3.29	3.75	4.24	4.38	4.48	3.65	3.84	4.87	3.91	3.86
K2O	2.73	2.78	1.18	1.08	3.42	4.73	4.44	2.44	3.00	2.93	0.99	1.47	2.45
P2O5	0.18	0.16	0.25	0.54	0.03	0.02	0.01	0.31	0.15	0.15	0.33	0.26	0.19
L.O.I.	0.85	1.41	4.32	2.47	2.83	0.79		1.11	2.27	2.05	0.14	2.34	0.18
Total (LOI free)	99.51	98.99	99.08	99.41	98.82	99.01	99.10	99.19	98.83	99.14	100.61	99.37	99.05
Sc	7	6	19	24	2	2	3	11	7	7	26	24	13
Cr	9	13	135	264	2	3	3	22	5	10	11	91	13
V	34	52	149	201	1	1	4	90	55	51	163	162	118
Ni	11	10	78	212	2	4	3	22	8	11	32	51	14
Co	9	5	32	62		0	1	6	5	7	35	22	12
Cu	26	22	22	66				25	11	7	20	35	21
Zn	49	48	77	85	36	48	45	58	48	49	75	76	57
Ga	21	18	18	16	15	18	18	18	18	19	19	18	16
Rb	67	69	22	18	100	161	157	60	80	68	15	27	61
Sr	365	364	441	836	199	12	13	674	362	358	401	385	298
Y	10	10	20	26	7	31	42	15	9	10	33	27	21
Zr	132	136	103	119	43	154	150	174	150	138	214	173	157
Nb	12	12	10	14	18	34	34	17	10	12	7	10	11
Ba	749	793	392	533	960	127	123	790	618	763	175	299	556
La	24	20	18	32	8	21	23	37	22	23	15	16	22
Ce	42	44	33	76	27	45	47	69	43	38	41	39	43
Nd	19	14	19	38	10	18	19	30	17	12	23	20	23
Pb	15	16	5	5	24	27	29	13	14	15	6	7	14
Th	10	12	4	2	9	17	16	12	8	10	3	4	7

APPENDIX D

XRF analyses of the samples from the Erzurum-Kars Plateau, NE Turkey

Copyright © by Mehmet Keskin

Area	N. Horasan	N. Horasan	S. Horasan	S. Horasan	S. Horasan	S. Horasan	S. Horasan	Aladağ	Aladağ	Aladağ	Aladağ	Aladağ	Aladağ
Sample no :	**MK135**	**MK139**	**MK150**	**MK151**	**MK152**	**MK153**	**MK154**	**MK161**	**MK157b**	**MK176**	**MK177**	**MK158**	**MK164**
Unit	N.Horas-6	N.Horas-6	S.Horas-1	S.Horas-1	S.Horas-1	S.Horas-1	S.Horas-1	Aladag-1a	Aladag-1b	Aladag-1b	Aladag-1b	Aladag-2	Aladag-2
Symbol	Hpl	Hpl	Sd	Sd	Sd	Sd	Sd	Apbl	Apbl (Obsid)	Apbl (Obsid)	Apbl (Obsid)	Abil	Abil
Level	Plateau	Plateau	Base	Base	Base	Base	Base	Base	Base	Base	Base	Base	Base
Geoch. desc.	*Basalt*	*Basalt*	*Dacite*	*Dacite*	*Dacite*	*Dacite*	*Dacite*	*Rhyolite*	*Rhyolite*	*Rhyolite*	*Rhyolite*	*TracAnd*	*Dacite*
SiO2	50.02	49.67	64.05	67.64	69.19	66.75	66.91	73.50	75.90	76.09	76.01	61.74	63.57
TiO2	1.79	1.47	0.57	0.37	0.38	0.43	0.42	0.32	0.11	0.10	0.10	1.08	0.67
Al2O3	17.27	17.03	17.26	16.04	16.05	16.51	16.38	14.00	12.98	12.92	13.01	16.67	15.74
Fe2O3	10.96	9.77	3.99	2.91	2.38	3.19	3.17	1.77	0.96	0.89	0.91	5.98	4.88
MnO	0.17	0.15	0.05	0.06	0.03	0.06	0.06	0.01	0.04	0.05	0.04	0.14	0.09
MgO	6.29	7.06	1.81	1.50	0.60	1.57	1.62	0.04	0.02	0.02	0.00	1.41	2.64
CaO	7.96	9.78	4.86	3.64	3.57	3.49	3.68	1.07	0.55	0.50	0.50	4.31	5.17
Na2O	3.96	4.06	4.53	4.31	4.24	4.37	4.41	4.46	3.49	3.97	3.84	4.52	3.66
K2O	0.69	0.73	1.83	2.39	2.41	2.58	2.50	3.94	4.97	4.55	4.52	2.79	2.42
P2O5	0.26	0.31	0.23	0.17	0.17	0.21	0.21	0.08	0.02	0.03	0.02	0.40	0.17
L.O.I.	0.15	0.30	2.28	0.88	1.09	1.63	1.13	0.56	3.30	0.36	0.28	1.35	0.42
Total (LOI free)	99.37	100.03	99.17	99.01	99.02	99.16	99.37	99.11	99.05	99.12	98.97	99.04	99.00
Sc	23	29	12	5	8	6	7	3	0	2	4	13	14
Cr	29	162	11	26	17	14	12	3	6	3	2	3	60
V	161	183	116	62	57	58	58	17	1	2	0	122	106
Ni	44	85	24	14	8	9	12	3	1	3	3	4	35
Co	40	39	12	7	7	8	6	2		1	1	12	19
Cu	9	41	43	20	25	25	17					7	37
Zn	75	75	48	48	41	46	44	54	35	33	33	81	55
Ga	22	22	18	19	18	17	18	17	13	15	16	20	18
Rb	10	9	38	66	65	77	74	60	127	135	132	71	64
Sr	408	489	623	486	495	507	504	74	29	23	25	355	257
Y	30	25	11	9	7	8	9	37	25	23	24	35	25
Zr	191	147	87	106	102	114	106	351	115	100	106	242	188
Nb	7	11	11	13	14	13	14	12	14	16	15	17	10
Ba	166	461	705	896	1054	723	611	2493	626	464	558	692	541
La	13	10	23	22	23	21	25	35	27	19	20	38	20
Ce	32	30	50	46	46	48	46	64	49	37	37	68	46
Nd	22	18	24	17	16	13	18	40	17	11	12	39	15
Pb	8	0	10	20	21	18	15	13	21	23	25	9	14
Th	4	3	5	9	10	12	10	10	15	15	15	10	11

APPENDIX D

XRF analyses of the samples from the Erzurum-Kars Plateau, NE Turkey

Copyright © by Mehmet Keskin

Area	Aladağ	Aladağ	Aladağ	Aladağ	Aladağ	Aladağ	Aladağ	Aladağ	Aladağ	Aladağ	Aladağ	Aladağ	Aladağ
Sample no :	**MK145**	**MK156**	**MK147**	**MK148**	**MK149**	**MK159**	**MK160**	**MK165**	**MK166a**	**MK166b**	**MK168**	**MK146**	**MK171**
Unit	Aladag-3	Aladag-4	Aladag-4	Aladag-4	Aladag-4	Aladag-4	Aladag-4	Aladag-4	Aladag-4	Aladag-4	Aladag-4	Aladag-5	Aladag-5
Symbol	Aa (Sc)	Aa	Aa	Aa	Aa	Aa	Aa	Aa	Aa	Aa	Aa	Orhy	Orhy
Level	Spatter cone	Plateau	Plateau	Plateau	Plateau	Plateau	Plateau	Plateau	Plateau	Plateau	Plateau	Acid cones	Acid cones
Geoch. desc.	*Andesite*	*Andesite*	*Andesite*	*Andesite*	*Andesite*	*Andesite*	*Andesite*	*Dacite*	*Dacite*	*Dacite*	*Andesite*	*Rhyolite*	*Rhyolite*
SiO2	60.33	62.75	62.43	61.90	62.79	60.26	61.76	63.50	63.57	63.52	60.45	69.93	74.52
TiO2	0.68	0.79	0.73	0.84	0.69	1.27	1.06	0.68	0.65	0.66	0.98	0.22	0.15
Al2O3	16.68	15.95	15.53	15.94	15.55	16.34	15.78	16.06	16.01	15.93	16.63	15.35	13.26
Fe2O3	5.43	5.37	5.38	5.71	4.87	7.74	5.74	4.86	4.76	4.80	6.38	2.28	2.08
MnO	0.09	0.08	0.09	0.10	0.08	0.07	0.15	0.08	0.08	0.08	0.10	0.08	0.03
MgO	3.95	2.64	3.43	2.94	3.38	1.83	2.86	2.50	2.69	2.70	3.39	0.23	0.01
CaO	6.71	5.09	5.63	5.27	5.57	5.09	5.33	5.01	5.19	5.21	6.32	1.40	0.46
Na2O	3.56	3.74	3.46	3.62	3.47	4.12	3.87	3.64	3.55	3.60	3.95	4.77	3.72
K2O	2.03	2.42	2.40	2.54	2.49	2.05	2.43	2.71	2.49	2.46	1.77	3.80	4.94
P2O5	0.17	0.21	0.18	0.22	0.18	0.28	0.27	0.18	0.17	0.18	0.21	0.08	0.04
L.O.I.	0.15	0.58	1.16	1.14	1.32	1.41	1.68	1.08	1.13	0.45	0.46	1.83	0.89
Total (LOI free)	99.61	99.04	99.26	99.07	99.08	99.05	99.22	99.22	99.16	99.13	100.18	99.14	99.19
Sc	16	13	17	16	15	22	14	14	15	11	17	3	5
Cr	82	79	126	68	109	22	52	38	60	63	60	5	3
V	134	124	126	125	117	157	136	110	107	111	137	4	1
Ni	75	46	53	31	47	22	34	25	35	34	47	4	6
Co	21	15	13	19	16	18	20	14	14	16	20		1
Cu	37	31	36	34	38	36	36	37	34	30	41		
Zn	59	63	58	67	58	77	66	56	56	56	64	62	48
Ga	20	17	18	18	16	19	19	17	16	17	17	18	19
Rb	59	67	64	66	65	55	62	68	69	70	46	94	77
Sr	332	268	261	275	259	277	283	257	258	259	302	139	8
Y	19	27	26	27	24	32	33	24	25	25	26	32	49
Zr	145	207	185	210	175	258	243	192	184	185	181	278	291
Nb	12	12	11	12	11	12	13	11	11	11	10	18	12
Ba	454	565	542	545	605	508	592	624	560	589	483	672	436
La	19	23	24	27	21	24	28	23	24	21	17	37	71
Ce	37	51	43	47	41	41	61	43	45	44	33	66	113
Nd	18	23	23	28	17	30	31	21	19	15	13	29	58
Pb	10	13	14	15	13	9	10	14	13	15	9	17	15
Th	6	8	9	8	9	7	10	8	8	8	5	14	19

APPENDIX D

XRF analyses of the samples from the Erzurum-Kars Plateau, NE Turkey

Copyright © by Mehmet Keskin

Area	Aladağ	Aladağ	Kagızman	Kagızman	Kagızman	Kagızman	Kagızman	Kagızman	Kagızman	Kagızman	Standard
Sample no :	**MK172**	**MK173**	**MK167a**	**MK167b**	**MK169**	**MK170**	**MK163**	**MK174**	**MK162**	**MK175**	**error**
Unit	Aladag-5	Aladag-5	Kagiz-1	Kagiz-1	Kagiz-1	Kagiz-1	Kagiz-2	Kagiz-2	Kagiz-3	Kagiz-3	
Symbol	Orhy	Orhy	Çr	Çr	Çr	Çr	Ptd	Ptd	Kpl	Kpl	
Level	Acid cones	Acid cones	Base-Mid	Base-Mid	Base-Mid	Base-Mid	Base-Mid	Base-Mid	Plateau	Plateau	
Geoch. desc.	*Rhyolite*	*Rhyolite*	*Rhyolite*	*Rhyolite*	*TracDac*	*TracDac*	*TracDac*	*TracDac*		*BaTraAnd*	
SiO2	74.50	74.60	73.96	74.23	66.80	65.95	67.47	66.48	55.25	53.66	±0.57
TiO2	0.15	0.14	0.21	0.21	0.80	0.80	0.54	0.54	1.13	1.22	±0.01
Al2O3	13.15	13.02	13.60	13.28	16.89	16.92	16.24	15.83	16.90	16.69	±0.17
Fe2O3	2.00	1.95	2.02	1.99	2.84	3.46	3.36	3.96	7.93	8.55	±0.05
MnO	0.06	0.06	0.05	0.05	0.02	0.04	0.08	0.10	0.12	0.14	±0.01
MgO	0.01	0.02	0.03	0.08	0.20	0.32	0.66	0.81	4.79	4.98	±0.08
CaO	0.52	0.57	0.74	0.84	2.98	2.93	2.68	3.18	8.06	7.94	±0.04
Na2O	3.60	3.59	4.08	4.08	5.16	5.09	4.33	4.70	3.47	4.07	±0.10
K2O	5.11	5.13	4.37	4.36	3.36	3.35	3.68	3.16	1.26	1.61	±0.03
P2O5	0.03	0.04	0.04	0.05	0.26	0.26	0.24	0.23	0.25	0.42	±0.01
L.O.I.	0.41	2.43	0.79	0.49	0.98	0.99	2.57	1.10	0.45	0.23	
Total (LOI free)	99.08	99.08	99.10	99.17	99.32	99.11	99.28	98.99	99.17	99.28	
Sc	5	5	2	4	9	11	7	7	18	16	±1.97-2.10
Cr	1	3	1	3	1	89	2	1	88	76	±4.17-14.45
V	1	0	3	5	18	24	20	20	144	169	±6.64-7.69
Ni	5	2	18	1	1	2	7	5	68	79	±4.25-6.51
Co					3	1	5	2	27	30	±1.9
Cu								3	25	19	±2.01
Zn	50	52	40	42	79	64	68	67	70	87	±3.9
Ga	17	17	17	15	20	17	19	19	17	19	±1.32-3.30
Rb	79	74	48	51	92	93	94	77	30	28	±1.56-3.52
Sr	8	8	30	31	277	270	226	229	406	553	±2.8-5.2
Y	43	41	27	31	42	39	37	37	23	28	±1.18-1.2
Zr	293	285	329	321	323	310	315	316	153	200	±2.46-6.58
Nb	14	13	11	10	22	21	20	20	11	19	±0.85-2.49
Ba	405	457	1918	1925	673	723	704	606	329	528	±5.43
La	64	68	38	33	38	40	27	27	19	29	±1.79 (3.21)
Ce	126	127	71	65	75	81	62	65	45	60	±2.87 (4.84)
Nd	56	56	33	34	36	40	26	25	20	23	±2.36-2.43
Pb	14	15	11	12	17	17	15	17	9	7	±3.67
Th	11	13	9	10	10	13	10	13	5	5	±0.99

APPENDIX: E

XRF and ICP-MS results of the samples from the Erzurum-Kars Plateau, NE Turkey

Sample no	MK243	MK237	MK215	MK49	MK93	MK251	MK280	MK281	MK289
Unit	Mt.Dumlu	Mt.Dumlu	Mt.Dumlu	Mt.Dumlu	Mt.Dumlu	Mt.Dumlu	Kargapaz.	Kargapaz.	Kargapaz.
Level	Gad	Gad	Gad	Dpad	Dpad	Dpad	Gad	Gad	Kb
Stra. Posit.	Lower	Mid	Mid	Top	Top	Top	Base	Base	Base
Geoc. Desc.	*Andesite*	*Ba And*	*Andesite*	*Dacite*	*Dacite*	*Dacite*	*Ba And*	*Trac And*	*Basalt*
Age (K-Ar)								*~6.70*	
SiO2	57.99	56.47	58.53	66.26	63.49	65.08	56.14	56.99	49.09
TiO2	0.92	0.99	0.94	0.61	0.75	0.70	1.92	1.83	1.26
Al2O3	17.96	18.43	18.26	15.77	16.10	16.49	15.97	16.12	16.92
Fe2O3	6.24	6.63	6.27	3.85	4.71	4.56	9.22	8.81	10.56
MnO	0.09	0.10	0.08	0.06	0.07	0.08	0.14	0.11	0.15
MgO	3.81	4.16	3.41	1.89	2.43	2.17	2.72	2.23	7.02
CaO	6.98	7.33	6.82	4.04	4.94	4.82	6.31	5.73	10.13
Na2O	3.88	3.91	4.14	3.88	3.58	4.21	4.32	4.68	3.11
K2O	1.83	1.35	1.67	2.85	2.76	2.35	1.90	2.00	0.51
P2O5	0.27	0.30	0.27	0.19	0.29	0.26	0.44	0.45	0.26
L.O.I.	0.76	1.40	0.62	1.89	1.60	0.94	1.00	0.97	1.47
Total	99.98	99.66	100.39	99.40	99.09	100.72	99.08	99.04	99.01
Rb	40.1	18.3	38.9	70.9	65.5	58.2	46.0	54.0	9.4
Sr	554	550	534	299	431	452	413	413	454
Y	17.5	16.8	16.4	17.8	17.3	13.6	30.8	32.8	25.8
Zr	156	163	154	111	200	157	215	211	115
Nb	10.3	10.7	10.5	10.4	14.6	11.8	12.8	13.9	6.6
Cs	1	1	1	4	2	2	2	2	0
Ba	397	489	389	462	596	535	314	331	145
La	27.38	30.06	26.26	33.95	38.46	33.10	24.16	24.74	12.25
Ce	48.22	48.90	47.88	50.80	61.49	57.96	47.28	48.88	26.27
Pr	5.72	5.77	5.34	6.12	6.72	6.03	5.73	5.93	3.37
Nd	21.27	23.03	20.55	20.79	23.89	19.50	23.26	23.63	15.34
Sm	3.73	3.90	3.58	3.78	4.13	3.41	4.83	5.12	3.64
Eu	1.21	1.28	1.14	0.99	1.09	1.10	1.73	1.79	1.34
Gd	3.45	3.55	3.46	3.30	3.26	3.29	5.16	5.43	3.78
Tb	0.49	0.55	0.49	0.51	0.46	0.38	0.79	0.81	0.73
Dy	2.82	3.06	2.74	2.85	2.69	2.09	4.90	4.90	4.32
Ho	0.61	0.58	0.54	0.58	0.49	0.40	1.02	1.03	0.88
Er	1.42	1.62	1.50	1.52	1.39	1.14	2.69	2.92	2.62
Tm	0.24	0.24	0.21	0.22	0.21	0.15	0.46	0.44	0.40
Yb	1.39	1.55	1.38	1.36	1.35	1.04	2.46	2.67	2.61
Lu	0.22	0.25	0.27	0.25	0.20	0.16	0.41	0.41	0.41
Hf	3.11	4.12	3.80	3.26	4.69	3.33	4.37	4.34	3.05
Ta	0.57	0.70	0.63	0.95	0.95	0.67	0.88	0.89	0.47
Pb	9.56	12.64	11.65	13.23	12.97	12.35	9.07	9.01	21.18
Th	4.97	6.67	5.78	11.47	9.94	8.35	5.80	6.55	1.30
U	1.38	1.11	1.40	2.70	2.24	2.01	1.76	1.90	0.41
Chondrite normalised									
La	115.51	126.84	110.80	143.23	162.26	139.68	101.92	104.38	51.69
Ce	78.79	79.90	78.24	83.01	100.47	94.71	77.26	79.87	42.92
Pr	60.22	60.74	56.21	64.45	70.69	63.49	60.37	62.42	35.47
Nd	45.54	49.31	44.00	44.52	51.15	41.76	49.81	50.60	32.85
Sm	24.36	25.49	23.40	24.68	27.02	22.30	31.56	33.48	23.79
Eu	20.87	22.07	19.66	17.02	18.76	18.98	29.81	30.86	23.10
Gd	16.81	17.27	16.84	16.04	15.88	16.03	25.09	26.44	18.39
Tb	12.98	14.71	13.10	13.65	12.31	10.14	21.13	21.56	19.52
Dy	11.12	12.05	10.79	11.23	10.57	8.23	19.30	19.31	17.01
Ho	10.82	10.25	9.54	10.28	8.61	7.02	17.97	18.12	15.55
Er	8.58	9.79	9.06	9.21	8.40	6.91	16.28	17.63	15.83
Tm	9.61	9.41	8.24	8.71	8.09	5.72	17.96	17.41	15.69
Yb	8.20	9.12	8.12	7.98	7.91	6.09	14.46	15.73	15.35
Lu	8.79	9.84	10.63	9.94	8.04	6.12	16.25	16.17	16.14

Copyright © by Mehmet Keskin

APPENDIX: E

XRF and ICP-MS results of the samples from the Erzurum-Kars Plateau, NE Turkey

Sample no	MK265	MK277	MK268	MK63	MK122	MK364	MK375	MK117	MK345
Unit	Kargapaz.	Kargapaz.	Kargapaz.	Kargapaz.	Pasinler	Pasinler	Pasinler	Pasinler	Pasinler
Level	Kpa	Gad	Gpaa	Kv	En1	En1	Mtd	Baad	Ltl
Stra. Posit.	Base	Mid	Mid	Top	Basement	Basement	Basement	Base	Base
Geoc. Desc.	*Dacite*	*Andesite*	*Dacite*	*Ba And*	*Ba And*	*BaAnd*	*Dacite*	*Andesite*	*Obsidian*
Age (K-Ar)				*5.73*			*~23*	*7.83*	
SiO2	63.90	60.58	65.47	54.39	53.61	53.81	70.13	62.14	75.33
TiO2	0.61	0.80	0.63	1.10	1.35	1.01	0.47	0.90	0.10
Al2O3	15.31	15.85	15.69	18.58	19.03	18.24	14.71	16.59	12.93
Fe2O3	4.40	5.22	3.91	7.52	8.63	8.54	3.19	5.78	1.21
MnO	0.07	0.08	0.06	0.13	0.16	0.15	0.03	0.09	0.05
MgO	3.65	4.08	2.03	4.87	3.26	4.42	0.57	1.99	0.00
CaO	4.97	6.10	3.95	7.72	8.42	9.45	3.43	4.97	0.40
Na2O	3.53	4.11	3.92	3.39	3.37	2.87	3.59	4.03	4.28
K2O	2.73	2.18	3.27	1.22	1.07	1.01	2.92	2.34	4.68
P2O5	0.21	0.28	0.20	0.29	0.27	0.18	0.16	0.20	0.03
L.O.I.	1.27	0.84	1.62	4.56	2.33	1.81	0.69	0.77	0.42
Total	99.38	99.28	99.14	99.19	99.16	99.67	99.20	99.04	99.01
Rb	70.3	51.8	88.3	9.1	7.8	14.4	67.2	54.0	182.3
Sr	454	443	342	446	466	386	358	358	1
Y	16.1	15.9	15.7	29.0	25.8	21.9	15.8	20.8	36.3
Zr	148	156	155	210	167	105	116	184	165
Nb	10.1	12.0	12.9	14.7	21.2	9.5	14.2	8.8	28.6
Cs	3	1	4	0	0	0	1	2	6
Ba	499	385	450	631	344	283	681	437	14
La	31.44	28.13	29.23	37.18	21.75	13.32	28.91	19.98	48.73
Ce	45.75	48.57	46.31	57.22	44.18	27.15	48.18	36.66	86.50
Pr	5.52	5.31	5.32	7.79	5.35	3.08	4.90	4.08	8.56
Nd	19.20	19.31	18.11	29.05	21.05	14.31	16.73	15.81	27.02
Sm	3.56	3.48	3.37	5.45	4.07	3.29	3.16	3.05	4.61
Eu	1.09	0.99	1.03	1.69	1.48	1.00	0.99	1.07	0.09
Gd	3.53	2.97	3.41	5.60	4.53	3.39	2.77	3.24	4.88
Tb	0.45	0.47	0.47	0.90	0.64	0.61	0.41	0.51	0.84
Dy	2.42	2.50	2.49	4.91	4.21	3.45	2.41	3.06	5.03
Ho	0.44	0.51	0.48	0.95	0.87	0.74	0.54	0.70	1.10
Er	1.31	1.48	1.35	2.79	2.39	2.19	1.47	1.85	3.37
Tm	0.19	0.24	0.23	0.44	0.35	0.33	0.23	0.33	0.55
Yb	1.14	1.33	1.37	2.79	2.55	2.10	1.53	2.00	3.90
Lu	0.18	0.21	0.19	0.42	0.40	0.35	0.22	0.29	0.62
Hf	3.34	3.83	3.54	4.88	3.73	2.72	2.81	3.95	5.50
Ta	0.61	0.88	0.96	0.99	1.24	0.59	0.98	0.64	2.25
Pb	12.53	11.46	14.65	11.17	9.92	9.55	15.10	12.09	30.23
Th	8.04	7.50	10.59	9.28	3.84	2.73	13.21	6.67	36.97
U	2.19	2.06	3.28	1.93	1.14	0.76	3.55	1.98	11.38
Chondrite normalised									
La	132.67	118.69	123.34	156.88	91.76	56.20	122.00	84.32	205.61
Ce	74.76	79.36	75.68	93.49	72.19	44.36	78.72	59.91	141.35
Pr	58.14	55.90	56.01	82.00	56.36	32.42	51.60	42.97	90.12
Nd	41.10	41.36	38.78	62.20	45.08	30.64	35.84	33.85	57.85
Sm	23.27	22.71	22.05	35.63	26.61	21.52	20.62	19.94	30.16
Eu	18.75	17.11	17.84	29.15	25.53	17.24	17.08	18.43	1.53
Gd	17.15	14.47	16.61	27.26	22.04	16.50	13.48	15.75	23.75
Tb	12.14	12.69	12.56	24.05	17.24	16.31	10.99	13.62	22.47
Dy	9.52	9.84	9.82	19.34	16.56	13.58	9.50	12.06	19.80
Ho	7.77	9.02	8.48	16.87	15.44	13.07	9.46	12.30	19.37
Er	7.94	8.93	8.18	16.88	14.46	13.23	8.86	11.18	20.38
Tm	7.31	9.45	8.99	17.09	13.88	12.94	8.86	12.93	21.68
Yb	6.71	7.81	8.03	16.42	15.01	12.35	9.00	11.77	22.93
Lu	6.90	8.27	7.48	16.62	15.77	13.78	8.75	11.40	24.22

Copyright © by Mehmet Keskin

APPENDIX: E

XRF and ICP-MS results of the samples from the Erzurum-Kars Plateau, NE Turkey

Sample no	MK70	MK112	MK101	MK338	MK144	MK138	MK154	MK132	MK139
Unit	Pasinler	Pasinler	Pasinler	Pasinler	N Horasan	N Horasan	S Horasan	N Horasan	N Horasan
Level	Ltl	Kpd	Kv	Ard	Köb	Köb	Sd	Kpad	Hpl
Stra. Posit.	Base	Mid	Top	Top	Base	Base	Base	Mid	Plateau
Geoc. Desc.	*Obsidian*	*Dacite*	*Ba And*	*Rhyolite*	*Basalt*	*BaAnd*	*Dacite*	*Dacite*	*Basalt*
Age (K-Ar)					*11.10*				
SiO2	75.87	66.81	57.01	71.00	48.76	53.63	66.91	64.18	49.67
TiO2	0.10	0.57	0.91	0.17	1.34	1.18	0.42	0.65	1.47
Al2O3	12.75	15.90	16.83	15.33	15.18	15.81	16.38	16.35	17.03
Fe2O3	1.19	3.82	6.55	1.92	9.10	8.95	3.17	4.53	9.77
MnO	0.05	0.06	0.11	0.06	0.33	0.14	0.06	0.06	0.15
MgO	0.01	1.24	4.56	0.01	8.40	4.93	1.62	1.48	7.06
CaO	0.40	3.68	7.60	0.66	11.40	9.36	3.68	4.71	9.78
Na2O	4.23	3.68	3.48	4.51	3.29	3.64	4.41	4.48	4.06
K2O	4.73	3.26	2.00	5.34	1.08	1.18	2.50	2.44	0.73
P2O5	0.02	0.16	0.27	0.04	0.54	0.25	0.21	0.31	0.31
L.O.I.	0.24	1.81	1.18	0.55	2.47	4.32	1.13	1.11	0.30
Total	99.36	99.17	99.33	99.04	99.41	99.08	99.37	99.19	100.03
Rb	174.1	80.5	50.9	129.5	20.3	24.4	72.8	56.3	9.3
Sr	1	349	437	42	801	459	500	652	520
Y	35.8	18.3	23.1	30.0	25.0	20.5	9.0	15.6	25.5
Zr	168	156	190	52	124	109	42	189	144
Nb	28.6	10.9	14.8	22.0	14.5	10.3	13.4	18.3	10.2
Cs	6	3	1	3	1	0	2	1	0
Ba	14	556	499	425	616	365	648	725	171
La	51.96	31.64	30.15	63.34	30.61	19.48	30.53	39.57	13.46
Ce	87.32	42.40	54.10	119.19	68.85	36.83	51.63	72.67	29.65
Pr	8.70	5.41	5.76	12.05	8.33	4.04	5.39	7.59	3.77
Nd	27.93	18.95	22.85	37.46	33.69	15.89	18.09	27.24	15.77
Sm	4.78	3.65	4.13	6.45	6.14	3.33	3.02	4.28	3.64
Eu	0.09	1.09	1.24	0.80	1.74	1.10	1.00	1.29	1.33
Gd	4.81	3.58	4.22	6.16	5.67	3.70	2.77	3.29	4.14
Tb	0.82	0.50	0.64	0.87	0.71	0.57	0.33	0.48	0.65
Dy	5.37	2.96	3.77	4.82	4.05	3.32	1.51	2.37	4.14
Ho	1.11	0.54	0.79	0.93	0.83	0.62	0.25	0.49	0.80
Er	3.54	1.57	2.15	2.99	2.20	1.82	0.74	1.30	2.46
Tm	0.62	0.26	0.32	0.46	0.32	0.27	0.09	0.21	0.35
Yb	4.02	1.55	2.22	2.72	2.18	1.85	0.60	1.19	2.37
Lu	0.61	0.25	0.34	0.46	0.34	0.29	0.09	0.21	0.35
Hf	6.02	3.50	4.34	1.82	2.79	2.66	1.32	3.80	2.60
Ta	2.36	0.81	0.91	1.62	0.71	0.59	0.83	1.07	0.53
Pb	27.94	15.57	12.59	21.49	5.55	7.36	14.74	13.62	2.56
Th	38.48	9.51	9.88	26.50	3.34	4.96	10.97	10.92	1.65
U	10.94	3.06	2.23	4.02	1.03	1.61	3.05	3.74	0.70
Chondrite normalised							*Copyright © by Mehmet Keskin*		
La	219.25	133.52	127.22	267.26	129.16	82.19	128.81	166.96	56.78
Ce	142.67	69.28	88.40	194.75	112.50	60.18	84.37	118.74	48.44
Pr	91.61	56.97	60.63	126.89	87.68	42.53	56.79	79.95	39.68
Nd	59.80	40.58	48.93	80.21	72.14	34.03	38.74	58.33	33.78
Sm	31.23	23.86	26.99	42.14	40.13	21.76	19.72	27.99	23.77
Eu	1.60	18.85	21.38	13.76	30.00	18.97	17.26	22.30	22.93
Gd	23.40	17.42	20.54	29.99	27.59	18.00	13.46	16.00	20.15
Tb	21.92	13.34	17.11	23.38	18.98	15.24	8.79	12.72	17.28
Dy	21.13	11.65	14.84	18.99	15.94	13.07	5.94	9.33	16.30
Ho	19.70	9.58	13.96	16.45	14.66	10.95	4.35	8.66	14.22
Er	21.36	9.50	12.99	18.05	13.29	11.00	4.50	7.88	14.85
Tm	24.36	10.34	12.55	17.95	12.55	10.59	3.66	8.05	13.68
Yb	23.68	9.14	13.06	16.00	12.82	10.88	3.53	6.99	13.93
Lu	23.95	9.86	13.39	17.97	13.39	11.42	3.58	8.33	13.89

APPENDIX: E

Sample no	MK130	MK135	MK158	MK159	MK174	MK162	MK175
Unit	N Horasan	N Horasan	Mt. Aladag	Mt. Aladag	Kagizman	Kagizman	Kagizman
Level	Hpl	Hpl	Abil	Aa	Ptd	Kpl	Kpl
Stra. Posit.	Plateau	Plateau	Base	Plateau	Base	Plateau	Plateau
Geoc. Desc.	*BaTraAnd*	*Basalt*	*TracAnd*	*Andesite*	*TracDac*	*Ba And*	*BaTraAnd*
Age (K-Ar)	*~4.14*						*2.72*
SiO2	54.36	50.02	61.74	60.26	66.48	55.25	53.66
TiO2	1.90	1.79	1.08	1.27	0.54	1.13	1.22
Al2O3	15.81	17.27	16.67	16.34	15.83	16.90	16.69
Fe2O3	9.71	10.96	5.98	7.74	3.96	7.93	8.55
MnO	0.18	0.17	0.14	0.07	0.10	0.12	0.14
MgO	4.56	6.29	1.41	1.83	0.81	4.79	4.98
CaO	7.90	7.96	4.31	5.09	3.18	8.06	7.94
Na2O	4.87	3.96	4.52	4.12	4.70	3.47	4.07
K2O	0.99	0.69	2.79	2.05	3.16	1.26	1.61
P2O5	0.33	0.26	0.40	0.28	0.23	0.25	0.42
L.O.I.	0.14	0.15	1.35	1.41	1.10	0.45	0.23
Total	100.61	99.37	99.04	99.05	98.99	99.17	99.28
Rb	13.9	8.9	66.7	54.1	74.9	28.4	27.4
Sr	407	403	366	289	230	423	568
Y	31.8	29.5	36.6	32.5	33.5	23.4	29.6
Zr	204	196	235	245	156	167	208
Nb	5.7	5.5	16.8	11.3	21.0	10.2	18.0
Cs	0	0	2	1	2	1	0
Ba	172	137	632	474	631	338	526
La	12.78	11.04	34.22	23.60	28.45	20.17	32.59
Ce	30.17	26.79	62.80	43.95	53.28	38.45	60.47
Pr	4.01	3.95	6.99	5.50	6.48	4.47	6.72
Nd	18.90	16.86	29.94	24.38	24.14	18.23	27.03
Sm	4.48	4.07	5.94	5.24	5.08	3.70	5.05
Eu	1.56	1.63	1.55	1.54	1.61	1.25	1.54
Gd	4.91	4.98	5.90	5.62	5.34	3.74	4.95
Tb	0.90	0.75	0.93	0.92	0.83	0.53	0.79
Dy	5.15	5.01	5.64	5.35	4.98	3.63	4.92
Ho	1.04	0.95	1.16	1.06	1.02	0.70	0.91
Er	3.08	2.81	3.39	3.02	3.08	2.06	2.85
Tm	0.47	0.45	0.55	0.49	0.54	0.31	0.40
Yb	3.05	2.62	3.41	2.97	2.87	1.90	2.93
Lu	0.48	0.44	0.56	0.47	0.42	0.34	0.49
Hf	4.71	4.07	5.48	5.78	3.59	3.65	4.60
Ta	0.45	0.35	1.11	0.80	1.40	0.55	0.93
Pb	5.12	3.47	15.74	11.76	15.70	6.14	9.03
Th	2.52	1.53	10.76	8.63	10.57	4.55	4.41
U	0.67	0.38	2.68	2.46	3.09	1.16	1.00
Chondrite normalised							
La	53.92	46.59	144.39	99.58	120.03	85.10	137.51
Ce	49.30	43.77	102.61	71.81	87.06	62.83	98.81
Pr	42.21	41.58	73.58	57.89	68.21	47.02	70.74
Nd	40.47	36.10	64.11	52.21	51.69	39.03	57.88
Sm	29.28	26.61	38.82	34.25	33.20	24.19	33.01
Eu	26.90	28.12	26.72	26.55	27.82	21.51	26.55
Gd	23.89	24.26	28.71	27.35	25.97	18.22	24.09
Tb	24.06	20.08	24.87	24.60	22.14	14.19	21.12
Dy	20.28	19.72	22.20	21.06	19.59	14.27	19.37
Ho	18.37	16.75	20.49	18.73	18.04	12.42	16.08
Er	18.61	16.95	20.48	18.25	18.59	12.42	17.22
Tm	18.43	17.57	21.57	19.22	21.24	12.11	15.69
Yb	17.94	15.44	20.06	17.47	16.89	11.19	17.24
Lu	18.90	17.26	22.05	18.50	16.57	13.27	19.29

Copyright © by Mehmet Keskin

APPENDIX

MOLE FRACTIONS OF AMPHIBOLES

	Mt. Dumlu area: Dumlu porphyritic amphibole dacite/andesite							
Sample no	MK36-12b	MK36-14c	MK52A-3d	MK52A-4b	MK90-12a	MK90-12c	MK93-8b	MK93-9a
Oxides %								
SiO2	44.18	40.23	45.31	44.92	41.70	42.93	44.15	44.66
TiO2	3.32	3.41	2.88	3.11	2.94	2.97	3.20	3.34
Al2O3	10.64	10.79	10.30	10.51	11.44	11.50	10.23	10.80
Cr2O3	0.10	0.09	0.00	0.00	0.00	0.17	0.00	0.10
FeO	11.70	11.88	12.01	12.08	10.65	11.07	12.12	11.65
MnO	0.13	0.16	0.22	0.17	0.26	0.00	0.07	0.00
MgO	14.76	14.51	14.69	14.60	13.83	13.69	14.45	14.63
CaO	11.57	11.55	11.53	11.47	10.91	10.81	11.51	11.69
Na2O	2.62	2.54	2.29	2.43	2.59	2.52	2.54	2.62
K2O	0.64	0.66	0.61	0.54	0.91	0.86	0.64	0.69
NiO	0.00	0.13	0.02	0.22	0.00	0.11	0.00	0.01
Total	99.66	99.94	99.86	100.05	95.23	96.64	98.90	100.19
Formula								
Si	6.370	6.365	6.502	6.446	6.286	6.363	6.422	6.395
Ti	0.360	0.369	0.311	0.336	0.333	0.331	0.350	0.360
Al	1.808	1.831	1.742	1.778	2.033	2.009	1.753	1.823
Cr	0.011	0.010	0.000	0.000	0.000	0.020	0.000	0.011
Fe	1.410	1.430	1.441	1.449	1.343	1.372	1.474	1.396
Mn	0.016	0.019	0.027	0.020	0.033	0.000	0.009	0.000
Mg	3.173	3.113	3.142	3.123	3.108	3.024	3.133	3.122
Cu	1.788	1.781	1.773	1.764	1.763	1.716	1.794	1.794
Na	0.732	0.710	0.638	0.675	0.756	0.725	0.716	0.727
K	0.117	0.122	0.111	0.100	0.175	0.163	0.118	0.126
Ni	0.000	0.015	0.003	0.026	0.000	0.013	0.000	0.002
No of O atoms	23	23	23	23	23	23	23	23
Total (ions)	15.785	15.765	15.690	15.717	15.830	15.736	15.768	15.755
End Members								
Barroisite			**0.090**	**0.058**		**0.011**		
magnesio-alumino			0.013	0.007		0.003		
magnesio-ferri			0.058	0.039		0.006		
ferro-alumino			0.003	0.002		0.001		
ferro-ferri			0.015	0.010		0.002		
Tschermakite	**0.392**	**0.301**	**0.421**	**0.438**	**0.334**	**0.412**	**0.400**	**0.375**
magnesio-alumino	0.040	0.000	0.060	0.050	0.082	0.113	0.043	0.074
magnesio-ferri	0.268	0.251	0.272	0.296	0.180	0.206	0.264	0.212
ferro-alumino	0.011	0.000	0.016	0.013	0.022	0.033	0.013	0.023
ferro-ferri	0.071	0.048	0.070	0.074	0.048	0.059	0.079	0.066
Edenite	**0.298**		**0.329**	**0.301**	**0.221**	**0.287**	**0.353**	**0.342**
magnesio	0.234		0.260	0.238	0.173	0.223	0.271	0.261
ferro	0.062		0.067	0.059	0.046	0.064	0.081	0.081
A1B4Si5		**0.015**						
magnesio-alumino		0.013						
ferro-alumino		0.002						
A1B4Si6		**0.143**						
Pargasite		0.000						
Fe pargasite		0.000						
hastingsite		0.023						
Mg hastingsite		0.119						
Kaersutite	**0.077**	**0.381**			**0.189**		**0.022**	**0.061**
magnesio-alumino	0.060	0.318			0.148		0.017	0.047
ferro-alumino	0.016	0.060			0.039		0.005	0.015
Taramite	**0.233**	**0.159**	**0.160**	**0.203**	**0.256**	**0.290**	**0.226**	**0.221**
magnesio-alumino	0.024	0.000	0.023	0.023	0.063	0.080	0.024	0.043
magnesio-ferri	0.159	0.133	0.103	0.137	0.138	0.145	0.149	0.125
ferro-alumino	0.006	0.000	0.006	0.006	0.017	0.023	0.007	0.014
ferro-ferri	0.042	0.025	0.027	0.034	0.037	0.041	0.044	0.039

Hornblende barometer of Schmidt (1992)

P (±0.6 kb)	5.6	5.7	5.3	5.5	6.7	6.6	5.3	5.7
Depth (km)	20.0	20.4	18.9	19.5	23.8	23.4	19.1	20.2

Amphibole-plagioclase geothermometer of Blundy and Holland (1990)

T (Kelvin)	1156.0	1155.3	1131.5	1142.5	1110.0	1094.0	1154.0	1155.2
T(°C)	882.8	882.2	858.4	869.4	836.9	820.8	880.9	882.0

	Mt. Dumlu area: Dumlu porphyritic amphibole dacite/andesite							
Sample no	**MK251-1b**	**MK251-2b**	**MK251-3a**	**MK261-1a**	**MK261-2b**	**MK228-1c**	**MK228-2a**	**MK228-3a**
Oxides %								
SiO2	42.40	42.37	43.39	42.59	45.44	41.46	43.06	43.43
TiO2	3.87	3.47	3.26	4.02	2.89	3.94	2.82	2.53
Al2O3	12.56	12.43	11.89	12.01	9.07	12.15	11.67	11.17
Cr2O3	0.04	0.08	0.00	0.05	0.00	0.00	0.00	0.03
FeO	13.39	13.37	13.43	13.07	12.28	12.93	14.02	13.70
MnO	0.00	0.06	0.27	0.17	0.24	0.22	0.28	0.21
MgO	13.28	13.60	13.55	12.92	14.62	13.16	13.54	13.33
CaO	11.03	11.34	11.26	11.17	11.89	11.24	11.18	11.24
Na2O	2.60	2.80	2.61	2.55	2.28	2.50	2.46	2.53
K2O	0.72	0.65	0.65	0.78	0.69	0.66	0.64	0.55
NiO	0.00	0.00	0.01	0.05	0.00	0.00	0.11	0.00
Total	99.88	100.15	100.32	99.38	99.40	98.27	99.78	98.73
Formula								
Si	6.140	6.129	6.253	6.197	6.561	6.112	6.260	6.360
Ti	0.422	0.377	0.354	0.440	0.314	0.437	0.308	0.279
Al	2.143	2.120	2.019	2.060	1.543	2.111	1.999	1.928
Cr	0.005	0.009	0.000	0.005	0.000	0.000	0.000	0.004
Fe	1.621	1.617	1.619	1.590	1.482	1.593	1.705	1.678
Mn	0.000	0.007	0.033	0.021	0.030	0.028	0.035	0.026
Mg	2.865	2.933	2.911	2.803	3.146	2.891	2.935	2.911
Ca	1.712	1.758	1.739	1.743	1.840	1.775	1.742	1.765
Na	0.729	0.785	0.729	0.721	0.638	0.716	0.693	0.719
K	0.132	0.119	0.120	0.145	0.126	0.124	0.118	0.103
Ni	0.000	0.000	0.001	0.006	0.000	0.000	0.013	0.000
No of O atoms	23	23	23	23	23	23	23	23
Total (ions)	15.769	15.853	15.777	15.732	15.681	15.787	15.806	15.772
End Members								
Barroisite					**0.052**			
magnesio-alumino					0.005			
magnesio-ferri					0.034			
ferro-alumino					0.002			
ferro-ferri					0.012			
Tschermakite	**0.464**	**0.376**	**0.450**	**0.419**	**0.358**	**0.420**	**0.495**	**0.451**
magnesio-alumino	0.061	0.041	0.058	0.074	0.032	0.045	0.037	0.064
magnesio-ferri	0.300	0.251	0.288	0.229	0.234	0.276	0.357	0.277
ferro-alumino	0.017	0.012	0.017	0.028	0.011	0.013	0.009	0.020
ferro-ferri	0.086	0.072	0.083	0.085	0.079	0.083	0.086	0.088
Edenite	**0.048**	**0.040**	**0.163**	**0.139**	**0.470**	**0.032**	**0.140**	**0.271**
magnesio	0.037	0.031	0.125	0.101	0.349	0.024	0.111	0.205
ferro	0.011	0.009	0.036	0.037	0.118	0.007	0.027	0.065
A1B4Si5								
magnesio-alumino								
ferro-alumino								
A1B4Si6								
Pargasite								
Fe pargasite								
hastingsite								
Mg hastingsite								
Kaersutite	**0.174**	**0.316**	**0.101**	**0.167**		**0.300**	**0.073**	**0.016**
magnesio-alumino	0.135	0.245	0.077	0.121		0.229	0.058	0.012
ferro-alumino	0.039	0.070	0.022	0.045		0.069	0.014	0.004
Taramite	**0.314**	**0.268**	**0.286**	**0.275**	**0.119**	**0.248**	**0.292**	**0.261**
magnesio-alumino	0.041	0.029	0.037	0.049	0.011	0.026	0.022	0.037
magnesio-ferri	0.203	0.179	0.183	0.150	0.078	0.163	0.210	0.160
ferro-alumino	0.012	0.008	0.011	0.018	0.004	0.008	0.005	0.012
ferro-ferri	0.058	0.051	0.053	0.056	0.026	0.049	0.051	0.051

Hornblende barometer of Schmidt (1992)

P (±0.6 kb)	7.2	7.1	6.6	6.8	4.3	7.0	6.5	6.2
Depth (km)	25.7	25.3	23.6	24.3	15.5	25.1	23.2	22.0

Amphibole-plagioclase geothermometer of Blundy and Holland (1990)

T (Kelvin)	1185.7	1190.7	1166.8	1186.7	1137.2	1197.3	1168.0	1148.5
T(°C)	912.6	917.5	893.6	913.5	864.1	924.1	894.9	875.3

Pasinler area: Kızılveren porphyritic amphibole dacite/andesite

Sample no	MK112-10a	MK112-12a	MK112-16b	MK118-1a	MK118-2a	MK118-2c	MK337-1c	MK337-2c
Oxides %								
SiO2	44.40	44.38	44.45	45.87	44.04	44.22	45.56	44.41
TiO2	2.70	2.39	2.09	1.90	2.59	2.69	1.33	2.40
Al2O3	10.85	10.82	10.86	11.61	11.54	11.75	10.35	10.92
Cr2O3	0.00	0.09	0.17	0.08	0.00	0.00	0.05	0.07
FeO	14.57	13.80	14.67	13.85	13.96	13.98	15.01	14.50
MnO	0.17	0.33	0.19	0.14	0.25	0.29	0.39	0.34
MgO	13.22	13.55	13.06	12.97	12.81	12.90	13.33	13.27
CaO	11.23	11.11	11.24	10.62	10.93	10.54	10.10	11.38
Na2O	2.14	2.13	2.16	2.37	2.52	2.60	2.18	2.33
K2O	0.65	0.56	0.64	0.66	0.60	0.61	0.65	0.51
NiO	0.00	0.00	0.00	0.00	0.03	0.02	0.00	0.00
Total	99.92	99.16	99.54	100.06	99.28	99.58	98.95	100.12
Formula								
Si	6.439	6.463	6.475	6.579	6.413	6.411	6.637	6.422
Ti	0.295	0.261	0.228	0.205	0.284	0.293	0.145	0.261
Al	1.855	1.858	1.864	1.963	1.981	2.008	1.778	1.861
Cr	0.000	0.011	0.020	0.009	0.000	0.000	0.005	0.008
Fe	1.767	1.680	1.787	1.661	1.700	1.695	1.829	1.754
Mn	0.020	0.041	0.024	0.017	0.031	0.035	0.049	0.041
Mg	2.857	2.941	2.837	2.774	2.781	2.788	2.896	2.860
Ca	1.745	1.733	1.754	1.633	1.706	1.638	1.577	1.764
Na	0.601	0.601	0.611	0.658	0.712	0.730	0.616	0.654
K	0.120	0.105	0.119	0.120	0.112	0.112	0.120	0.095
Ni	0.000	0.000	0.000	0.000	0.003	0.002	0.000	0.000
No of O atoms	23	23	23	23	23	23	23	23
Total (ions)	15.699	15.695	15.720	15.619	15.724	15.712	15.651	15.719
End Members								
Barroisite	**0.094**	**0.123**	**0.099**	**0.248**	**0.074**	**0.126**	**0.339**	**0.057**
magnesio-alumino	0.010	0.014	0.013	0.065	0.015	0.023	0.039	0.007
magnesio-ferri	0.060	0.083	0.061	0.121	0.039	0.073	0.244	0.036
ferro-alumino	0.003	0.004	0.004	0.021	0.005	0.007	0.007	0.002
ferro-ferri	0.019	0.021	0.020	0.039	0.014	0.022	0.045	0.012
Tschermakite	**0.483**	**0.485**	**0.462**	**0.378**	**0.435**	**0.437**	**0.406**	**0.472**
magnesio-alumino	0.054	0.056	0.063	0.099	0.088	0.081	0.046	0.055
magnesio-ferri	0.311	0.326	0.283	0.185	0.231	0.252	0.292	0.299
ferro-alumino	0.017	0.014	0.021	0.032	0.031	0.024	0.008	0.017
ferro-ferri	0.098	0.083	0.093	0.060	0.081	0.075	0.054	0.095
Edenite	**0.231**	**0.215**	**0.261**	**0.228**	**0.246**	**0.172**	**0.130**	**0.264**
magnesio	0.175	0.170	0.196	0.171	0.180	0.131	0.108	0.198
ferro	0.055	0.043	0.064	0.056	0.063	0.039	0.020	0.063
A1B4Si5								
magnesio-alumino								
ferro-alumino								
A1B4Si6								
Pargasite								
Fe pargasite								
hastingsite								
Mg hastingsite								
Kaersutite								
magnesio-alumino								
ferro-alumino								
Taramite	**0.192**	**0.177**	**0.178**	**0.146**	**0.246**	**0.265**	**0.124**	**0.207**
magnesio-alumino	0.021	0.021	0.024	0.038	0.050	0.049	0.014	0.024
magnesio-ferri	0.124	0.119	0.109	0.071	0.130	0.153	0.089	0.132
ferro-alumino	0.007	0.005	0.008	0.012	0.017	0.015	0.003	0.008
ferro-ferri	0.039	0.030	0.036	0.023	0.046	0.046	0.016	0.042

Hornblende barometer of Schmidt (1992)

P (±0.6 kb)	5.8	5.8	5.9	6.3	6.4	6.5	5.5	5.8
Depth (km)	20.8	20.8	20.9	22.6	22.9	23.4	19.5	20.9

Amphibole-plagioclase geothermometer of Blundy and Holland (1990)

T (Kelvin)	1101.0	1095.1	1091.9	1045.5	1081.4	1079.7	1095.6	1141.6
T(°C)	827.9	822.0	818.7	772.3	808.2	806.6	822.5	868.4

	Pasinler: Kızılveren porphyritic amphibole dacite/andesite			*Pasinler: Black ignimbrite*				
Sample no	MK337-3a	MK337-4a	MK337-4b	MK106-6b	MK106-6c	MK106-7a	MK106-7b	MK318-2b
Oxides %								
SiO2	43.32	43.20	41.97	44.98	45.15	43.34	43.85	43.71
TiO2	2.34	2.73	2.75	3.52	3.70	4.01	4.21	3.95
Al2O3	10.76	12.76	12.21	10.54	10.47	11.18	11.32	9.73
Cr2O3	0.02	0.11	0.02	0.00	0.01	0.09	0.09	0.00
FeO	15.78	15.19	15.36	10.57	10.66	11.18	11.15	11.95
MnO	0.35	0.22	0.27	0.30	0.29	0.32	0.24	0.40
MgO	12.14	12.48	11.76	14.69	15.08	13.96	14.38	14.29
CaO	10.71	11.13	10.57	11.11	11.04	11.53	11.33	11.29
Na2O	2.10	2.79	2.63	2.65	2.96	2.81	2.91	2.67
K2O	0.64	0.66	0.62	0.80	0.86	0.87	0.79	0.86
NiO	0.00	0.00	0.00	0.08	0.00	0.00	0.07	0.20
Total	98.16	101.25	98.16	99.24	100.22	99.29	100.32	99.06
Formula								
Si	6.430	6.214	6.239	6.468	6.439	6.284	6.279	6.367
Ti	0.261	0.295	0.307	0.381	0.396	0.437	0.453	0.433
Al	1.883	2.164	2.140	1.787	1.760	1.911	1.910	1.671
Cr	0.002	0.013	0.003	0.000	0.001	0.010	0.010	0.000
Fe	1.958	1.827	1.910	1.271	1.272	1.356	1.336	1.456
Mn	0.044	0.027	0.035	0.036	0.035	0.039	0.029	0.050
Mg	2.685	2.676	2.607	3.150	3.206	3.017	3.069	3.102
Ca	1.705	1.715	1.683	1.712	1.687	1.790	1.739	1.762
Na	0.605	0.777	0.758	0.740	0.818	0.790	0.808	0.755
K	0.120	0.121	0.118	0.147	0.157	0.161	0.144	0.161
Ni	0.000	0.000	0.000	0.009	0.000	0.000	0.008	0.023
No of O atoms	23	23	23	23	23	23	23	23
Total (ions)	15.693	15.829	15.799	15.701	15.771	15.794	15.784	15.779
End Members								
Barroisite	**0.126**			**0.071**	**0.036**			
magnesio-alumino	0.012			0.018	0.007			
magnesio-ferri	0.081			0.038	0.022			
ferro-alumino	0.004			0.005	0.002			
ferro-ferri	0.028			0.010	0.006			
Tschermakite	**0.494**	**0.428**	**0.487**	**0.352**	**0.324**	**0.269**	**0.329**	**0.345**
magnesio-alumino	0.046	0.069	0.070	0.087	0.059	0.077	0.062	0.000
magnesio-ferri	0.318	0.241	0.280	0.185	0.195	0.118	0.187	0.259
ferro-alumino	0.016	0.025	0.027	0.024	0.015	0.028	0.019	0.000
ferro-ferri	0.109	0.089	0.106	0.051	0.051	0.044	0.058	0.080
Edenite	**0.176**	**0.113**	**0.127**	**0.347**	**0.349**	**0.258**	**0.233**	**0.318**
magnesio	0.129	0.082	0.091	0.269	0.274	0.186	0.177	0.238
ferro	0.044	0.030	0.035	0.074	0.072	0.069	0.055	0.074
A1B4Si5								
magnesio-alumino								
ferro-alumino								
A1B4Si6								
Pargasite								
Fe pargasite								
hastingsite								
Mg hastingsite								
Kaersutite		**0.147**	**0.039**			**0.257**	**0.163**	**0.086**
magnesio-alumino		0.106	0.028			0.185	0.123	0.064
ferro-alumino		0.039	0.011			0.069	0.038	0.020
Taramite	**0.205**	**0.313**	**0.347**	**0.230**	**0.291**	**0.216**	**0.274**	**0.252**
magnesio-alumino	0.019	0.051	0.050	0.057	0.053	0.062	0.052	0.000
magnesio-ferri	0.132	0.176	0.199	0.121	0.175	0.095	0.156	0.189
ferro-alumino	0.006	0.019	0.019	0.016	0.014	0.023	0.016	0.000
ferro-ferri	0.045	0.065	0.075	0.033	0.046	0.035	0.048	0.058
Hornblende barometer of Schmidt (1992)								
P (±0.6 kb)	6.0	7.3	7.2	5.5	5.4	6.1	6.1	4.9
Depth (km)	21.3	26.0	25.6	19.6	19.2	21.7	21.7	17.7
Amphibole-plagioclase geothermometer of Blundy and Holland (1990)								
T (Kelvin)	1137.8	1169.0	1164.6	1065.8	1074.3	1097.4	1098.7	1081.9
T(°C)	864.7	895.8	891.5	792.7	801.2	824.3	825.5	808.8

	Pasinler: Black ignimbrite						*Pasinler: Ardıçlıdağ rhyolite*	
Sample no	MK318-3b	MK318-4c	MK318-7a	MK319-2b	MK359-3c	MK359-9a	MK125-2a	MK125-3a
Oxides %								
SiO2	43.68	45.94	44.33	45.92	42.58	42.94	43.14	42.84
TiO2	3.96	3.01	3.65	3.17	4.30	3.24	1.99	1.93
Al2O3	10.28	9.00	10.04	9.30	10.44	10.26	8.12	7.68
Cr2O3	0.08	0.00	0.20	0.07	0.00	0.00	0.09	0.00
FeO	12.27	12.24	11.49	14.10	11.85	12.56	27.27	28.13
MnO	0.28	0.36	0.29	0.27	0.34	0.54	1.21	1.55
MgO	14.43	15.09	14.75	12.80	13.88	13.88	5.06	3.79
CaO	11.38	11.35	11.47	10.46	11.54	11.15	9.95	9.53
Na2O	2.75	2.88	2.61	2.51	2.78	2.94	2.25	2.26
K2O	0.87	0.89	0.66	0.92	0.80	0.79	1.00	1.06
NiO	0.05	0.00	0.05	0.00	0.00	0.00	0.17	0.06
Total	100.03	100.77	99.53	99.52	98.50	98.30	100.24	98.83
Formula								
Si	6.305	6.553	6.388	6.651	6.245	6.326	6.671	6.759
Ti	0.429	0.323	0.396	0.346	0.474	0.359	0.232	0.229
Al	1.750	1.513	1.706	1.587	1.806	1.781	1.480	1.428
Cr	0.009	0.000	0.023	0.008	0.000	0.000	0.011	0.000
Fe	1.481	1.460	1.384	1.708	1.453	1.548	3.526	3.712
Mn	0.034	0.044	0.035	0.033	0.042	0.068	0.158	0.208
Mg	3.105	3.209	3.169	2.762	3.035	3.048	1.167	0.892
Ca	1.761	1.735	1.772	1.624	1.813	1.761	1.649	1.611
Na	0.770	0.797	0.730	0.705	0.790	0.840	0.674	0.692
K	0.161	0.162	0.121	0.170	0.150	0.147	0.196	0.212
Ni	0.005	0.000	0.005	0.000	0.000	0.000	0.021	0.008
No of O atoms	23	23	23	23	23	23	23	23
Total (ions)	15.810	15.795	15.730	15.594	15.808	15.878	15.786	15.751
End Members								
Barroisite		**0.054**		**0.256**			**0.226**	**0.293**
magnesio-alumino		0.000		0.047			0.000	0.003
magnesio-ferri		0.041		0.128			0.068	0.063
ferro-alumino		0.000		0.021			0.000	0.010
ferro-ferri		0.012		0.057			0.148	0.201
Tschermakite	**0.335**	**0.273**	**0.400**	**0.265**	**0.258**	**0.279**	**0.304**	**0.236**
magnesio-alumino	0.000	0.002	0.015	0.049	0.009	0.009	0.000	0.003
magnesio-ferri	0.255	0.207	0.296	0.133	0.177	0.199	0.091	0.050
ferro-alumino	0.000	0.000	0.004	0.022	0.003	0.003	0.000	0.008
ferro-ferri	0.076	0.062	0.081	0.059	0.066	0.063	0.199	0.162
Edenite	**0.248**	**0.448**	**0.336**	**0.346**	**0.219**	**0.264**	**0.311**	**0.347**
magnesio	0.189	0.341	0.262	0.238	0.158	0.197	0.093	0.078
ferro	0.056	0.102	0.071	0.106	0.059	0.062	0.204	0.250
A1B4Si5								
magnesio-alumino								
ferro-alumino								
A1B4Si6								
Pargasite								
Fe pargasite								
hastingsite								
Mg hastingsite								
Kaersutite	**0.162**		**0.020**		**0.329**	**0.200**		
magnesio-alumino	0.123		0.016		0.238	0.149		
ferro-alumino	0.037		0.004		0.088	0.047		
Taramite	**0.256**	**0.224**	**0.243**	**0.133**	**0.194**	**0.257**	**0.159**	**0.125**
magnesio-alumino	0.000	0.001	0.009	0.025	0.007	0.009	0.000	0.001
magnesio-ferri	0.195	0.170	0.180	0.067	0.134	0.183	0.047	0.027
ferro-alumino	0.000	0.000	0.003	0.011	0.002	0.003	0.000	0.004
ferro-ferri	0.058	0.051	0.049	0.030	0.050	0.058	0.104	0.085

Hornblende barometer of Schmidt (1992)

P (±0.6 kb)	5.3	4.2	5.1	4.5	5.6	5.5	4.0	3.8
Depth (km)	19.0	15.0	18.3	16.2	19.9	19.5	14.4	13.5

Amphibole-plagioclase geothermometer of Blundy and Holland (1990)

T (Kelvin)	1089.5	1053.2	1074.5	1011.2	1101.3	1085.0	985.7	971.9
T(°C)	816.3	780.0	801.3	738.0	828.2	811.9	712.5	698.7

	Pasinler area :			*North of Horasan:*					
	Ardıçlıdağ rhyolite			*Köroğlu porph dac/and*					
Sample no	MK125-13b	MK330-9b	MK330-9c	MK133-1a	MK133-2c	MK140-1a	MK140-2b	MK140-3a	MK140-4b
Oxides %									
SiO2	43.65	42.51	41.74	44.22	43.09	45.60	45.42	44.57	44.75
TiO2	1.81	1.83	1.82	1.78	2.61	2.25	2.28	2.13	2.34
Al2O3	7.72	8.08	7.97	12.48	12.39	10.58	10.10	10.93	10.35
Cr2O3	0.00	0.00	0.00	0.19	0.09	0.04	0.20	0.00	0.15
FeO	28.51	30.72	29.89	12.65	13.06	13.69	13.70	12.96	13.39
MnO	1.42	1.49	1.86	0.18	0.21	0.13	0.26	0.13	0.32
MgO	4.19	3.46	3.30	14.06	13.16	13.13	14.02	14.28	13.58
CaO	9.62	9.67	9.48	10.97	11.17	11.22	11.49	11.44	11.34
Na2O	2.46	2.52	2.28	2.52	2.50	2.40	1.93	2.24	2.36
K2O	1.11	0.97	1.03	0.50	0.57	0.62	0.47	0.41	0.54
NiO	0.00	0.00	0.00	0.04	0.00	0.14	0.00	0.07	0.04
Total	100.47	101.25	99.38	99.59	98.86	99.80	99.86	99.18	99.16
Formula									
Si	6.767	6.620	6.624	6.371	6.289	6.568	6.540	6.449	6.500
Ti	0.211	0.214	0.217	0.193	0.287	0.243	0.247	0.232	0.256
Al	1.411	1.484	1.490	2.119	2.131	1.798	1.713	1.865	1.773
Cr	0.000	0.000	0.000	0.022	0.011	0.004	0.022	0.000	0.017
Fe	3.696	4.002	3.968	1.524	1.594	1.651	1.650	1.568	1.627
Mn	0.186	0.196	0.250	0.022	0.026	0.016	0.031	0.016	0.039
Mg	0.969	0.804	0.782	3.020	2.863	2.821	3.009	3.081	2.942
Ca	1.598	1.614	1.613	1.694	1.747	1.732	1.773	1.774	1.766
Na	0.738	0.760	0.702	0.704	0.708	0.669	0.539	0.629	0.664
K	0.219	0.192	0.208	0.092	0.106	0.114	0.087	0.076	0.101
Ni	0.000	0.000	0.000	0.005	0.000	0.016	0.000	0.008	0.004
No of O atoms	23	23	23	23	23	23	23	23	23
Total (ions)	15.795	15.886	15.854	15.764	15.761	15.631	15.610	15.697	15.688
End Members									
Barroisite	**0.282**	**0.191**	**0.214**	**0.072**		**0.150**	**0.166**	**0.081**	**0.090**
magnesio-alumino	0.002	0.000	0.000	0.014		0.038	0.016	0.011	0.014
magnesio-ferri	0.066	0.040	0.044	0.046		0.069	0.115	0.055	0.053
ferro-alumino	0.007	0.000	0.000	0.003		0.015	0.004	0.002	0.004
ferro-ferri	0.194	0.141	0.156	0.008		0.027	0.030	0.012	0.017
Tschermakite	**0.207**	**0.304**	**0.326**	**0.491**	**0.479**	**0.356**	**0.476**	**0.482**	**0.411**
magnesio-alumino	0.002	0.000	0.000	0.099	0.104	0.090	0.045	0.066	0.062
magnesio-ferri	0.049	0.064	0.067	0.315	0.263	0.163	0.331	0.326	0.245
ferro-alumino	0.005	0.000	0.000	0.017	0.031	0.036	0.011	0.015	0.020
ferro-ferri	0.142	0.224	0.237	0.055	0.078	0.065	0.085	0.072	0.079
Edenite	**0.362**	**0.271**	**0.246**	**0.167**	**0.194**	**0.361**	**0.268**	**0.262**	**0.333**
magnesio	0.088	0.057	0.051	0.141	0.148	0.256	0.212	0.213	0.249
ferro	0.257	0.200	0.179	0.025	0.044	0.102	0.054	0.047	0.081
A1B4Si5									
magnesio-alumino									
ferro-alumino									
A1B4Si6									
Pargasite									
Fe pargasite									
hastingsite									
Mg hastingsite									
Kaersutite					**0.048**				
magnesio-alumino									
ferro-alumino									
Taramite	**0.149**	**0.234**	**0.214**	**0.270**	**0.280**	**0.133**	**0.091**	**0.175**	**0.166**
magnesio-alumino	0.001	0.000	0.000	0.055	0.061	0.034	0.009	0.024	0.025
magnesio-ferri	0.035	0.049	0.044	0.173	0.154	0.061	0.063	0.118	0.099
ferro-alumino	0.004	0.000	0.000	0.010	0.011	0.013	0.002	0.005	0.008
ferro-ferri	0.102	0.173	0.155	0.030	0.046	0.024	0.016	0.026	0.032

Hornblende barometer of Schmidt (1992)

P (±0.6 kb)	3.7	4.1	4.1	7.1	7.1	5.5	5.1	5.9	5.4
Depth (km)	13.2	14.5	14.6	25.3	25.5	19.8	18.4	20.9	19.4

Amphibole-plagioclase geothermometer of Blundy and Holland (1990)

T (Kelvin)	971.4	1112.9	1111.4	1072.8	1090.4	1113.1	1126.4	1136.7	1131.4
T(°C)	698.3	839.7	838.3	799.7	817.3	839.9	853.2	863.6	858.2

	S of Horasan: Saçdağ dacite		*N of Horasan: Plateau layer*		*Kağızman area: Pasli trachy-dacite*			
Sample no	MK154-5c	MK154-6b	MK134-5a	MK134-11b	MK174-1a	MK174-2d	MK174-3C1	MK174-3R1
Oxides %								
SiO2	43.46	45.27	45.28	45.31	41.36	41.86	42.16	40.48
TiO2	2.27	1.21	2.47	2.60	3.65	3.31	3.44	2.97
Al2O3	12.87	11.40	10.01	9.66	12.44	11.76	11.25	10.83
Cr2O3	0.05	0.07	0.17	0.10	0.00	0.00	0.00	0.04
FeO	14.07	15.17	12.25	11.96	17.76	16.94	16.80	16.21
MnO	0.27	0.27	0.18	0.12	0.31	0.58	0.47	0.45
MgO	12.67	12.93	14.96	15.27	10.92	11.07	11.80	11.21
CaO	11.19	10.99	11.57	11.46	10.70	10.54	10.95	12.74
Na2O	2.50	2.25	2.47	2.27	2.85	2.59	2.72	2.39
K2O	0.63	0.51	0.39	0.53	0.65	0.63	0.57	0.61
NiO	0.00	0.00	0.11	0.10	0.03	0.00	0.00	0.00
Total	99.97	100.08	99.84	99.35	100.67	99.29	100.15	97.93
Formula								
Si	6.293	6.546	6.509	6.535	6.085	6.211	6.203	6.134
Ti	0.247	0.132	0.267	0.282	0.404	0.370	0.380	0.338
Al	2.197	1.942	1.697	1.642	2.156	2.057	1.951	1.934
Cr	0.006	0.008	0.019	0.012	0.000	0.000	0.000	0.005
Fe	1.704	1.835	1.472	1.443	2.186	2.102	2.068	2.054
Mn	0.032	0.033	0.022	0.015	0.038	0.073	0.058	0.058
Mg	2.735	2.787	3.205	3.282	2.393	2.448	2.588	2.532
Ca	1.736	1.702	1.782	1.771	1.687	1.676	1.727	2.068
Na	0.702	0.632	0.688	0.634	0.814	0.745	0.776	0.702
K	0.117	0.094	0.072	0.097	0.122	0.119	0.107	0.118
Ni	0.000	0.000	0.012	0.011	0.004	0.000	0.000	0.000
No of O atoms	23	23	23	23	23	23	23	23
Total (ions)	15.768	15.710	15.746	15.722	15.889	15.802	15.858	15.943
End Members								
Barroisite		**0.182**	**0.076**	**0.111**				
magnesio-alumino		0.033	0.006	0.004				
magnesio-ferri		0.107	0.056	0.089				
ferro-alumino		0.010	0.001	0.001				
ferro-ferri		0.031	0.012	0.017				
Tschermakite	**0.487**	**0.442**	**0.422**	**0.427**	**0.431**	**0.510**	**0.440**	
magnesio-alumino	0.112	0.080	0.032	0.017	0.020	0.033	0.000	
magnesio-ferri	0.249	0.259	0.310	0.340	0.266	0.312	0.304	
ferro-alumino	0.038	0.023	0.007	0.003	0.010	0.015	0.000	
ferro-ferri	0.084	0.076	0.069	0.065	0.130	0.139	0.129	
Edenite	**0.191**	**0.224**	**0.333**	**0.314**		**0.089**	**0.087**	
magnesio	0.142	0.172	0.269	0.261		0.060	0.060	
ferro	0.048	0.051	0.060	0.050		0.027	0.025	
A1B4Si5					**0.038**			
magnesio-alumino					0.025			
ferro-alumino					0.012			
A1B4Si6								
Pargasite								
Fe pargasite								
hastingsite								
Mg hastingsite								
Kaersutite	**0.030**				**0.183**	**0.044**	**0.167**	
magnesio-alumino	0.022				0.122	0.030	0.116	
ferro-alumino	0.007				0.059	0.013	0.049	
Taramite	**0.292**	**0.151**	**0.170**	**0.147**	**0.347**	**0.357**	**0.306**	
magnesio-alumino	0.067	0.027	0.013	0.006	0.016	0.023	0.000	
magnesio-ferri	0.149	0.089	0.125	0.117	0.215	0.219	0.212	
ferro-alumino	0.023	0.008	0.003	0.001	0.008	0.010	0.000	
ferro-ferri	0.050	0.026	0.028	0.022	0.105	0.098	0.089	

Hornblende barometer of Schmidt (1992)

P (±0.6 kb)	7.4	6.2	5.1	4.8	7.3	6.8	6.3	6.2
Depth (km)	26.6	22.3	18.1	17.2	25.9	24.2	22.4	22.1

Amphibole-plagioclase geothermometer of Blundy and Holland (1990)

T (Kelvin)	1063.8	1028.8	1109.3	1107.2	1127.0	1105.2	1115.6	1133.4
T(°C)	790.6	755.6	836.1	834.0	853.8	832.1	842.4	860.2